frontiers | Research Topics

New insights into neurodevelopmental biology and autistic spectrum disorders

Edited by
Hongbao Cao, Michela Candini, Jurgen Germann, Katherine Kuhl-Meltzoff Stavropoulos, Prathibha Karanth, Julia Dallman, Flavia Venetucci Gouveia, Jian-Huan Chen, Edward Quadros, Tongtong Ge and Xingyin Liu

Published in
Frontiers in Neuroscience

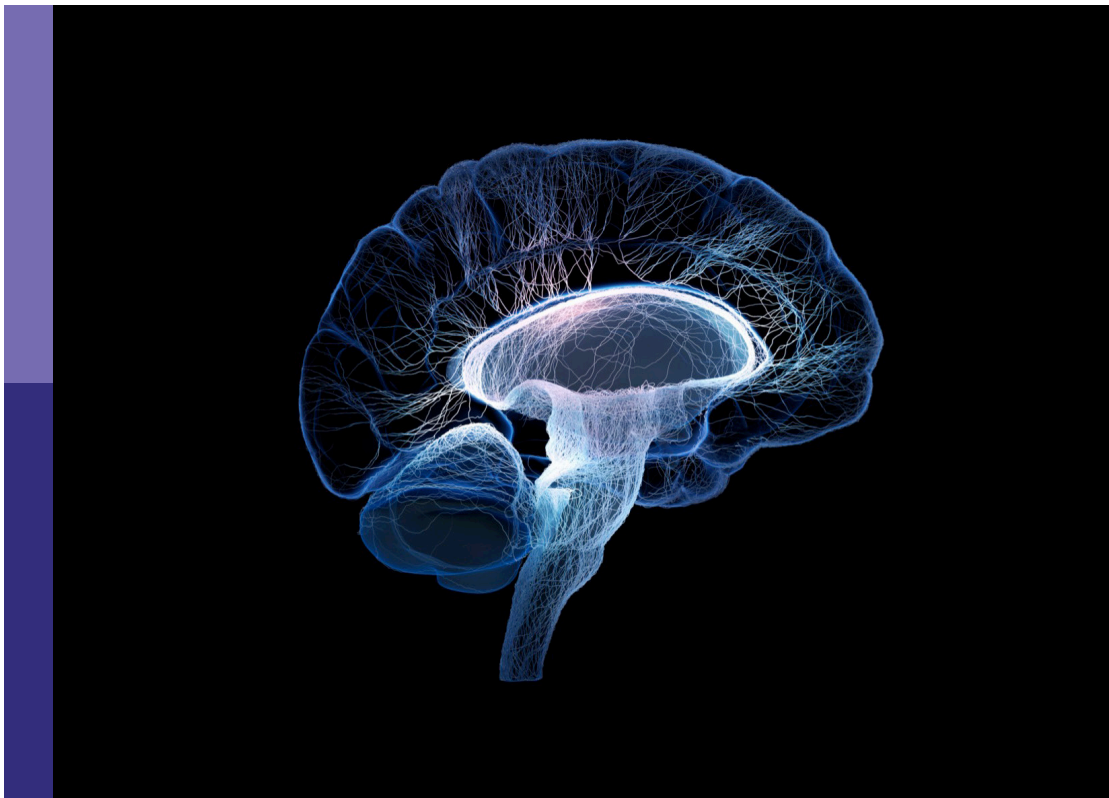

ISSN 1664-8714
ISBN 978-2-8325-3552-3
DOI 10.3389/978-2-8325-3552-3

About Frontiers

Frontiers is more than just an open access publisher of scholarly articles: it is a pioneering approach to the world of academia, radically improving the way scholarly research is managed. The grand vision of Frontiers is a world where all people have an equal opportunity to seek, share and generate knowledge. Frontiers provides immediate and permanent online open access to all its publications, but this alone is not enough to realize our grand goals.

Frontiers journal series

The Frontiers journal series is a multi-tier and interdisciplinary set of open-access, online journals, promising a paradigm shift from the current review, selection and dissemination processes in academic publishing. All Frontiers journals are driven by researchers for researchers; therefore, they constitute a service to the scholarly community. At the same time, the *Frontiers journal series* operates on a revolutionary invention, the tiered publishing system, initially addressing specific communities of scholars, and gradually climbing up to broader public understanding, thus serving the interests of the lay society, too.

Dedication to quality

Each Frontiers article is a landmark of the highest quality, thanks to genuinely collaborative interactions between authors and review editors, who include some of the world's best academicians. Research must be certified by peers before entering a stream of knowledge that may eventually reach the public - and shape society; therefore, Frontiers only applies the most rigorous and unbiased reviews. Frontiers revolutionizes research publishing by freely delivering the most outstanding research, evaluated with no bias from both the academic and social point of view. By applying the most advanced information technologies, Frontiers is catapulting scholarly publishing into a new generation.

What are Frontiers Research Topics?

Frontiers Research Topics are very popular trademarks of the *Frontiers journals series*: they are collections of at least ten articles, all centered on a particular subject. With their unique mix of varied contributions from Original Research to Review Articles, Frontiers Research Topics unify the most influential researchers, the latest key findings and historical advances in a hot research area.

Find out more on how to host your own Frontiers Research Topic or contribute to one as an author by contacting the Frontiers editorial office: frontiersin.org/about/contact

New insights into neurodevelopmental biology and autistic spectrum disorders

Citation

Cao, H., Candini, M., Germann, J., Stavropoulos, K. K.-M., Karanth, P., Dallman, J., Gouveia, F. V., Chen, J.-H., Quadros, E., Ge, T., Liu, X., eds. (2023). *New insights into neurodevelopmental biology and autistic spectrum disorders*. Lausanne: Frontiers Media SA. doi: 10.3389/978-2-8325-3552-3

Table of contents

frontiers | Frontiers in Neuroscience

TYPE Original Research
PUBLISHED 07 September 2022
DOI 10.3389/fnins.2022.957018

OPEN ACCESS

EDITED BY
Julia Dallman,
University of Miami, United States

REVIEWED BY
Kimberly Seifert,
Stanford University, United States
Douglas Dean,
University of Wisconsin-Madison, United States
Cyrus Raji,
Washington University in St. Louis, United States

*CORRESPONDENCE
Seyedmehdi Payabvash
sam.payabvash@yale.edu

SPECIALTY SECTION
This article was submitted to Neurodevelopment, a section of the journal Frontiers in Neuroscience

RECEIVED 30 May 2022
ACCEPTED 08 August 2022
PUBLISHED 07 September 2022

CITATION
Weber CF, Lake EMR, Haider SP, Mozayan A, Mukherjee P, Scheinost D, Bamford NS, Ment L, Constable T and Payabvash S (2022) Age-dependent white matter microstructural disintegrity in autism spectrum disorder.
Front. Neurosci. 16:957018.
doi: 10.3389/fnins.2022.957018

Age-dependent white matter microstructural disintegrity in autism spectrum disorder

Clara F. Weber[1,2], Evelyn M. R. Lake[1], Stefan P. Haider[1,3], Ali Mozayan[1], Pratik Mukherjee[4], Dustin Scheinost[1], Nigel S. Bamford[5], Laura Ment[5], Todd Constable[1] and Seyedmehdi Payabvash[1]*

[1]Department of Radiology and Biomedical Imaging, Yale School of Medicine, New Haven, CT, United States, [2]Social Neuroscience Lab, Department of Psychiatry and Psychotherapy, Lübeck University, Lübeck, Germany, [3]Department of Otorhinolaryngology, University Hospital, Ludwig-Maximilians-Universität München, Munich, Germany, [4]Department of Radiology and Biomedical Imaging, University of California, San Francisco, San Francisco, CA, United States, [5]Departments of Pediatrics, Neurology, Cellular and Molecular Physiology, Yale University, New Haven, CT, United States

There has been increasing evidence of White Matter (WM) microstructural disintegrity and connectome disruption in Autism Spectrum Disorder (ASD). We evaluated the effects of age on WM microstructure by examining Diffusion Tensor Imaging (DTI) metrics and connectome Edge Density (ED) in a large dataset of ASD and control patients from different age cohorts. *N* = 583 subjects from four studies from the National Database of Autism Research were included, representing four different age groups: (1) A Longitudinal MRI Study of Infants at Risk of Autism [infants, median age: 7 (interquartile range 1) months, *n* = 155], (2) Biomarkers of Autism at 12 months [toddlers, 32 (11)m, *n* = 102], (3) Multimodal Developmental Neurogenetics of Females with ASD [adolescents, 13.1 (5.3) years, *n* = 230], (4) Atypical Late Neurodevelopment in Autism [young adults, 19.1 (10.7)y, *n* = 96]. For each subject, we created Fractional Anisotropy (FA), Mean- (MD), Radial- (RD), and Axial Diffusivity (AD) maps as well as ED maps. We performed voxel-wise and tract-based analyses to assess the effects of age, ASD diagnosis and sex on DTI metrics and connectome ED. We also optimized, trained, tested, and validated different combinations of machine learning classifiers and dimensionality reduction algorithms for prediction of ASD diagnoses based on tract-based DTI and ED metrics. There is an age-dependent increase in FA and a decline in MD and RD across WM tracts in all four age cohorts, as well as an ED increase in toddlers and adolescents. After correction for age and sex, we found an ASD-related decrease in FA and ED only in adolescents and young adults, but not in infants or toddlers. While DTI abnormalities were mostly limited to the corpus callosum, connectomes showed a more widespread ASD-related decrease in ED. Finally, the best performing machine-leaning classification model achieved an area under the receiver operating curve of 0.70 in an independent validation cohort. Our results suggest that ASD-related WM microstructural

disintegrity becomes evident in adolescents and young adults—but not in infants and toddlers. The ASD-related decrease in ED demonstrates a more widespread involvement of the connectome than DTI metrics, with the most striking differences being localized in the corpus callosum.

KEYWORDS

autism, age, diffusion tensor imaging, connectome, white matter

Introduction

Autism Spectrum Disorder (ASD) is a neuropsychiatric condition characterized by impairments in communication and social interaction, repetitive behaviors and stereotypical interests (American Psychiatric Association [APA], 2013). ASD prevalence is estimated at 1 in 54 among 8-year-old children in the United States (Maenner et al., 2020). Difficulty of early diagnoses in children, and evidence of incurred benefit due to early and tailored treatment strategies highlight the need for improving diagnostic algorithms and treatment planning. Many etiological and pathophysiological theories of ASD involve genetic and environmental factors (Autism Genome Project Consortium et al., 2007; Chaste and Leboyer, 2012), as well as morphological correlates in the central nervous system. There has been increasing evidence of White Matter (WM) microstructural disintegrity in ASD (Alexander et al., 2007; Aoki et al., 2017; Payabvash et al., 2019b). Previous studies of WM microstructure in children with ASD vary in cohort size (n = 58—n = 213), mostly focus on specific age groups and are therefore limited in their ability to make assumptions of WM changes across the lifespan (Walsh et al., 2021).

In accordance with models emphasizing the abnormal interhemispheric interactions in ASD (Travers et al., 2012), many studies have identified the corpus callosum as the primary location for WM disintegrity in ASD. However, results diverge regarding the particular section within the corpus callosum (Alexander et al., 2007). Findings range from alterations in the whole corpus callosum (Shukla et al., 2010, 2011; Jou et al., 2011) to isolated changes in the splenium or anterior body (Brito et al., 2009; Kumar et al., 2010; Cheon et al., 2011). In addition, many studies have reported more pervasive WM microstructural disintegrity in the frontal and temporal lobes or dominant tracts (Barnea-Goraly et al., 2004; Ameis and Catani, 2015). These inconsistencies could be in part due to age range differences of participants across studies. Moreover, previous evidence is limited as only few studies investigate Diffusion Tensor Imaging (DTI)—the majority of neuroimaging studies have focused on functional and structural MRI and show notable variations in cohort composition, which could mask sex-, age- and ASD-related effects (Walsh et al., 2021).

A more detailed knowledge of age-adjusted microstructural correlates of ASD may improve diagnostic algorithms, facilitate early therapeutic intervention, and provide potential objective biomarkers to monitor treatment response. To draw more robust and meaningful conclusions about age- and ASD-related alterations of WM microstructure, we analyzed diffusivity and tractography among subjects from four different age-group study cohorts in the National Database of Autism Research (NDAR). DTI and T_1-weighted images were used to assess voxel-wise and tract-based differences between ASD patients and typically developing controls (TDC). In addition to conventional DTI-driven measurements, we analyzed edge density (ED) (Owen et al., 2015) as a representation of white matter connectivity. Tract-based metrics were analyzed using both conventional statistical methods as well as combinations of several feature selection algorithms and machine learning classifiers in a multimodal approach.

Materials and methods

Study cohorts

We retrieved all datasets from the National Database of Autism Research (NDAR) that had DTI- and T_1-weighted imaging data available. Subjects from four study cohorts were included, each representing a different age group: (1) A Longitudinal MRI Study of Infants at Risk for Autism (infants) (Piven, 2017); (2) Biomarkers of Autism at 12 months (toddlers) (Courchesne, 2012); (3) Multimodal Developmental Neurogenetics of Females with ASD (adolescents) (Pelphrey, 2017); and (4) Atypical Late Neurodevelopment in Autism: A Longitudinal MRI and DTI Study (young adults) (Lainhart, 2012). We excluded subjects with genetic comorbidities such as fragile X syndrome, insufficient clinical information, evident artefacts on brain scans, and those with failures in image processing, such as coregistration failure. **Figure 1** depicts all inclusion and exclusion criteria in a flowchart. Subjects were allocated to ASD versus typically developing controls (TDC) groups based on the Autism diagnostic schedule (ADOS) diagnosis, which was assessed by age- and development-adjusted

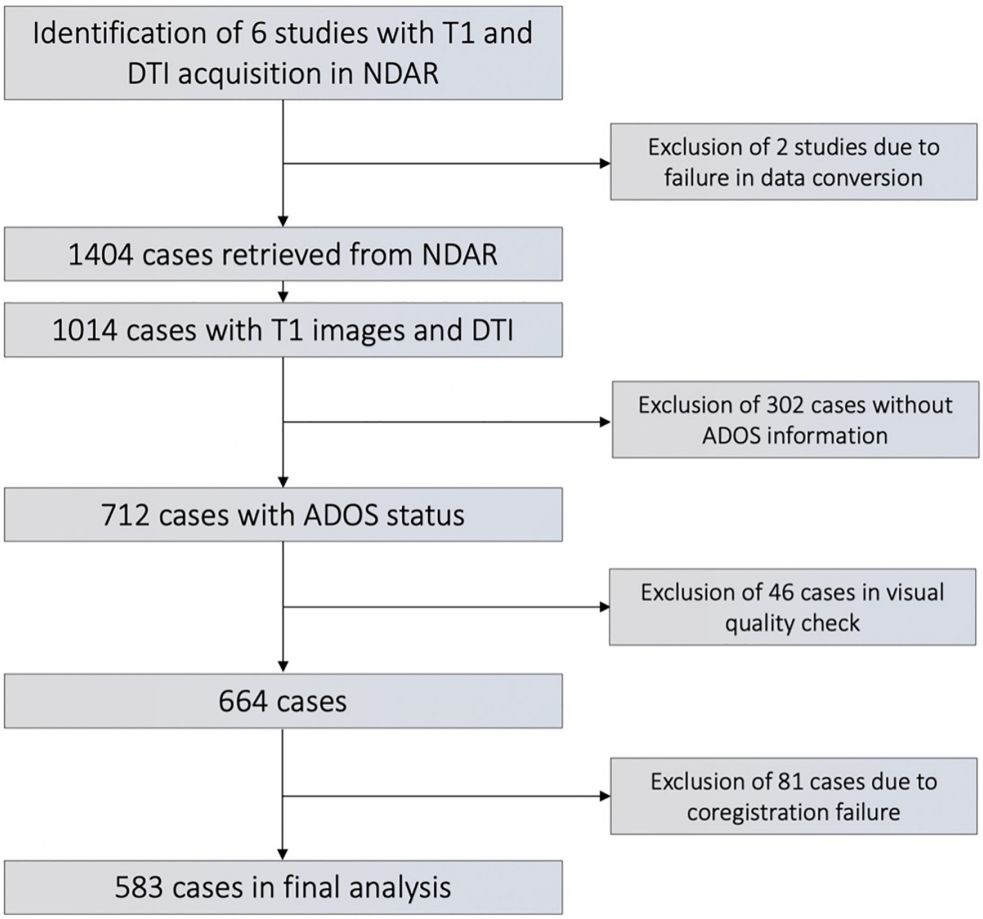

FIGURE 1
Flowchart of subject's inclusion/exclusion.

TABLE 1 Study cohort demographics.

Study	Median age (IQR)	ASD/TDC	Male (%)
Longitudinal MRI study of infants at risk of autism (n = 155)	7 (6–7) months	34/121	65.8%
Biomarkers of autism at 12 months (n = 102)	32 (25–36) months	57/45	73.5%
Multimodal developmental neurogenetics of females with autism (n = 230)	13.1 (5.3) years	106/124	50.9%
Atypical late neurodevelopment in autism (n = 96)	19.1 (10.7) years	67/29	99.0%

ASD, autism spectrum disorder; TDC, typically developing controls. Age is represented as median (interquartile range).

algorithms in the original studies. Detailed information about the age and sex composition of each study cohort is listed in Table 1.

Image acquisition protocols and preprocessing

The acquisition protocols differed across studies. In the infant cohort, T_1-weighted imaging was conducted with a repetition time (TR) of 2400 ms, time to echo (TE) of 3.16 ms, field of view (FOV) of 256, matrix size 224 × 256, and slice thickness 1 mm, diffusion weighted images were acquired in 26 variable b-values between 50 and 1000 s/mm^2 increasing by 200 s/mm^2 at each scan (25 gradient directions and one non-weighted image with b = 0 s/mm^2) image on 3T Siemens Tim Trio, with TR = 12,800–13,300 ms, TE = 102 ms, FOV 190, matrix size 190 × 190, and slice thickness of 2 mm. Toddlers' T_1-weighted imaging was acquired with TR = 6500 ms, TE = 2.8 ms, FOV = 240, matrix size 96 × 96, slice thickness 1.2 mm, DTI included 51 images with b = 1000 s/mm^2 and one non-weighted b = 0 s/mm^2 image acquired on 1.5 T GE Signa

HDxt, TR = 13200 ms, TE = 80.6 ms, FOV 240, matrix size 96 × 96, and slice thickness 2.5 mm. Adolescents' T_1-weighted imaging was acquired with TR = 5300 ms, TE = 3.3 ms, FOV 350, matrix size 192 × 192, slice thickness = 1 mm, DTI included 46 images with $b = 1000$ s/mm^2 and one non-weighted $b = 0$ s/mm^2 image acquired on 3T Siemens Magnetom TrioTim, TR = 13,000 ms, TE = 93 ms, FOV 250, matrix size 192 × 192, and slice thickness 2.5 mm. Adults' T_1-weighted imaging was acquired with TR = 1800, TE = 1.93, FOV 256, matrix size 256 × 240, slice thickness 1 mm, DTI included 4 repetitions of 12 images with $b = 1000$ s/mm^2 and followed by an image with $b = 0$ s/mm^2 acquired on 3T Siemens Magnetom TrioTim, with TR = 7000 ms, TE = 91 ms, FOV = 256, matrix size 128 × 128, and slice thickness 2.5 mm.

All images in DICOM (Digital Imaging and Communication in Medicine) format were converted to Nifti format using *dcm2nii* (Maenner et al., 2020) tool, with extraction of diffusion gradient directions. Images in Medical Imaging NetCDF (MINC) format were converted using *mnc2nii* tool in the FreeSurfer software package (Fischl, 2012), and diffusion gradient direction was extracted from header information.

Diffusion tensor imaging processing pipeline

We preprocessed all DTI images using FSL eddy current correction and brain extraction tool (Smith, 2002; Smith et al., 2004), and subsequently generated fractional anisotropy (FA), mean- (MD), and axial Diffusivity (AD) maps using FSL's diffusion tensor fitting program (DTIFIT). FSLmaths was used to derive radial diffusivity (RD) as the average of the second and third eigenvalues. In order to obtain ED maps, we first applied FSL Bayesian estimation of diffusion parameters obtained using sampling techniques (BEDPOSTX) on FA maps (Behrens et al., 2007), which can overcome limitations of tensor-based representations of diffusivity by identifying crossing fibers. BEDPOSTX results were then fed into probabilistic tractography using FSL PROBTRACKX (Behrens et al., 2003), which was then used for generation of ED maps. We specified seed and waypoint masks as 48 cortical and 7 subcortical nodes per hemisphere as defined in the Harvard-Oxford cortical and subcortical atlas (Frazier et al., 2005; Desikan et al., 2006; Makris et al., 2006; Goldstein et al., 2007) (list provided in **Supplementary Material**; 2.2 Harvard-Oxford Cortical Atlas as well as 2.3 Harvard-Oxford subcortical atlas). These seed and waypoint masks were registered to each individual's native FA space using FSL's linear coregistration tool FLIRT (Smith et al., 2004). The probabilistic tractography-derived ED maps reflect the density of connectome edges (links) between nodes representing the landmark anatomical structures of cerebral gray matter (Owen et al., 2015).

Voxel-wise analysis using tract-based spatial statistics

Voxel-wise analysis of diffusivity metrics was carried out using FSL tract-based spatial statistics (TBSS) (Smith et al., 2006). As described previously (Payabvash et al., 2019b), we coregistered all FA maps to a common space by the standard FSL TBSS pipeline, where all images were non-linearly coregistered to a standard template, in this case the most typical subject in each cohort (-n option). Then, we created a mean skeleton of the highest FAs that represents the center of WM tracts. All FA maps, as well as other diffusivity metrics in respective analyses, were then non-linearly coregistered onto the mean FA skeleton using the FSL non-linear registration tool before performing cross-subject statistics. General linear models (GLM) were used to assess the influence of age, sex and ASD diagnosis. To minimize the effects of data heterogeneity, we conducted analyses for each site separately as acquisition parameters differed between study cohorts. For non-parametric voxel-wise statistics, we applied FSL "randomize" (Winkler et al., 2014) with 5000 permutations and family wise error (FEW) correction of p-values followed by threshold-free cluster enhancement (TFCE) (Smith and Nichols, 2009).

Tract-based analysis

To confirm the results of voxel-wise analysis, we also evaluated the relationship of the averaged diffusion metrics and ED in WM tracts with the age, ASD diagnosis and sex in different study cohorts. We extracted FA, MD, RD, and AD metrics of each of the 48 white matter tracts specified in the John Hopkins University (JHU) white matter tracts labels atlas (Wakana et al., 2007; O'Donnell et al., 2009) by determining the non-zero mean of each individual's image within the respective tract. In order to provide similar analysis to voxel-wise method, for tract-based analysis, measurements were performed in a standard space of MNI-152. A list of all tracts considered is given in **Supplementary Material** (2.1 John Hopkins University White Matter Label Atlas). Given that the brainstem was set as termination mask in fiber tracking for generation of ED maps (Owen et al., 2015), the averaged ED of corticospinal tracts, medial lemnisci and pontine crossing fibers were excluded from tract-based analysis. Tract-based metrics were evaluated for the influence of ASD diagnosis, age, and sex using multiple regression analyses followed by p-value correction using false discovery rate (FDR) in R software (version 4.0.2) (R Core Team, 2020). We conducted analyses for behavioral measures for a subset of adolescents in which ADOS (Lord et al., 2000) scores

(n = 86) were available, as well as in a subset of the adult cohort in which Wechsler Intelligence Quotient (IQ) (Saklofske and Schoenberg, 2011) for 71 individuals (50 ASD, 21 TDC) as well as Social Responsiveness Scale (SRS) (Constantino, 2013) scores for 50 individuals (33 ASD, 17 TDC) were measures. Utilizing a voxel-wise GLM, the influence of aforementioned scores on diffusivity metrics were tested after adjustment for age.

Machine learning

To evaluate the feasibility of machine learning algorithms for the prediction of an ASD diagnosis based on diffusion and connectome-based metrics. Given the results of voxel-wise and tract-based analysis, we included data from the adolescent (n = 176) and adult (n = 74) cohorts (**Table 2**). We applied combinations of six different classifiers and five feature selection algorithms using FA, MD, RD, AD, and ED of white matter tracts separately and combined as input. The diffusion metrics from all WM tracts were included in corresponding analysis pipeline—e.g., the averaged FA from 48 WM tracts were included as input for FA based analysis, and all diffusion metrics were included in combination analyses. The respective feature selection algorithms and classifiers are further detailed in **Supplementary Material** (3. Machine Learning). Machine learning analysis was based on a framework previously described by Haider et al. (2020). Subjects were randomly split into a training/cross-validation set (n = 250) and an independent test set (n = 76) which was completely isolated from training process, with similar ASD-to-TDC-ratio as study cohort distribution. For each combination of classifier and feature selection algorithm, we created a framework of 20 repeats of five-fold cross validation, stratified based on ASD diagnosis, to perform hyperparameter optimization and identify the best performing models. Using Bayesian optimization, the hyperparameters of each machine learning model as well as the number of features included in the model were fine tuned. Upper and lower bounds of each hyperparameter (which was optimized), and the number of tuning repetitions are included in **Supplementary Table 2**. Subsequently, each model's cross validation framework was applied with tuned hyperparameters to evaluate each model's performance based on the mean area under the curve (AUC) of receiver operating characteristics (ROC) across validation folds, which reflects on both the true-positive and false-positive rate and therefore eliminates biases by original case-control distribution. Finally, we trained the optimal model on the whole training/cross-validation cohort (n = 250) with optimized hyperparameters and evaluated the performance in the independent test set (n = 76). We also determined sensitivity and specificity at balanced prediction probability cutoff, using a confusion matrix. All analyses were performed using R (version 4.0.2) (R Core Team, 2020).

Results

Age-dependent alterations of white matter microstructure and connectome edge density imaging

In voxel-wise TBSS analysis, we examined the influence of age on DTI metrics and connectome ED within each study cohort, while correcting for ASD diagnosis as a covariate. There was a pervasive age-related FA increase in infants, toddlers and adolescents (**Figure 2**), as well as a corresponding decline in MD, RD, and AD independent of ASD diagnosis status. In adults, the age-related FA increase was predominantly along the corticospinal tract (**Figure 2**). **Supplementary Figures 3–5** demonstrate the age-dependent changes in DTI metrics among different study cohorts. ED assessment of the brain connectome showed an age-related increase in ED among toddlers and adolescents (**Figure 2**). In toddlers, increasing age was associated with higher ED in commissural tracts as well as frontal, occipital and temporal association tracts. In adolescents, an age-related increase in connectome ED was mainly localized to the posterior corpus callosum. We confirmed findings of voxel-wise analyses in multiple regression analyses of tract-based metrics (**Supplementary Table**: 4 Tract-Based Multiple Regression).

Autism spectrum disorder-related alterations of white matter microstructure and connectome edge density imaging

In voxel-wise analyses, after correcting for age, ASD diagnosis was associated with lower FA in commissural tracts within the corpus callosum among adolescents and adults (**Figure 3**), but not in infants or toddlers. Corresponding increases in MD and RD were found in adults, and a slight decrease of AD was present in adolescents (**Supplementary Figure 6**). Compared to DTI diffusion metrics, ED revealed a more widespread reduction in connectome edges among subjects with ASD in the adolescent and adult cohorts. Among adolescents, ASD was associated with an extensive decrease in the ED of WM tracts—except for the internal capsule—after correction for age and sex as covariates. In the adult cohort, ASD was associated with lower ED within the posterior commissural and paraventricular WM tracts. Infants showed an isolated decrease in ED in the left sagittal stratum which was related to ASD. There were no significant changes in the toddler cohort as assessed in a voxel-wise GLM correcting for age and sex. Tract-based multiple regression analyses confirmed voxel-wise findings with significant ASD-related alterations of white matter diffusion metrics and connectome edges only found among adolescents and adults adjusting for age and sex.

TABLE 2 Distribution of subjects from each cohort among the training/cross-validation versus independent test set, using only data from studies where we found significant ASD-related alterations.

Study	Training			Independent validation		
	No	Age	ASD/TDC	No	Age	ASD/TDC
Multimodal developmental neurogenetics	176	155 (124–182)	82/94	54	162 (119–194)	24/30
Atypical late neurodevelopment in autism	74	242 (194–320)	52/22	22	211 (182–256)	15/7

ASD, autism spectrum disorder; TDC, typically developing children. Age is represented as median (interquartile range) in months.

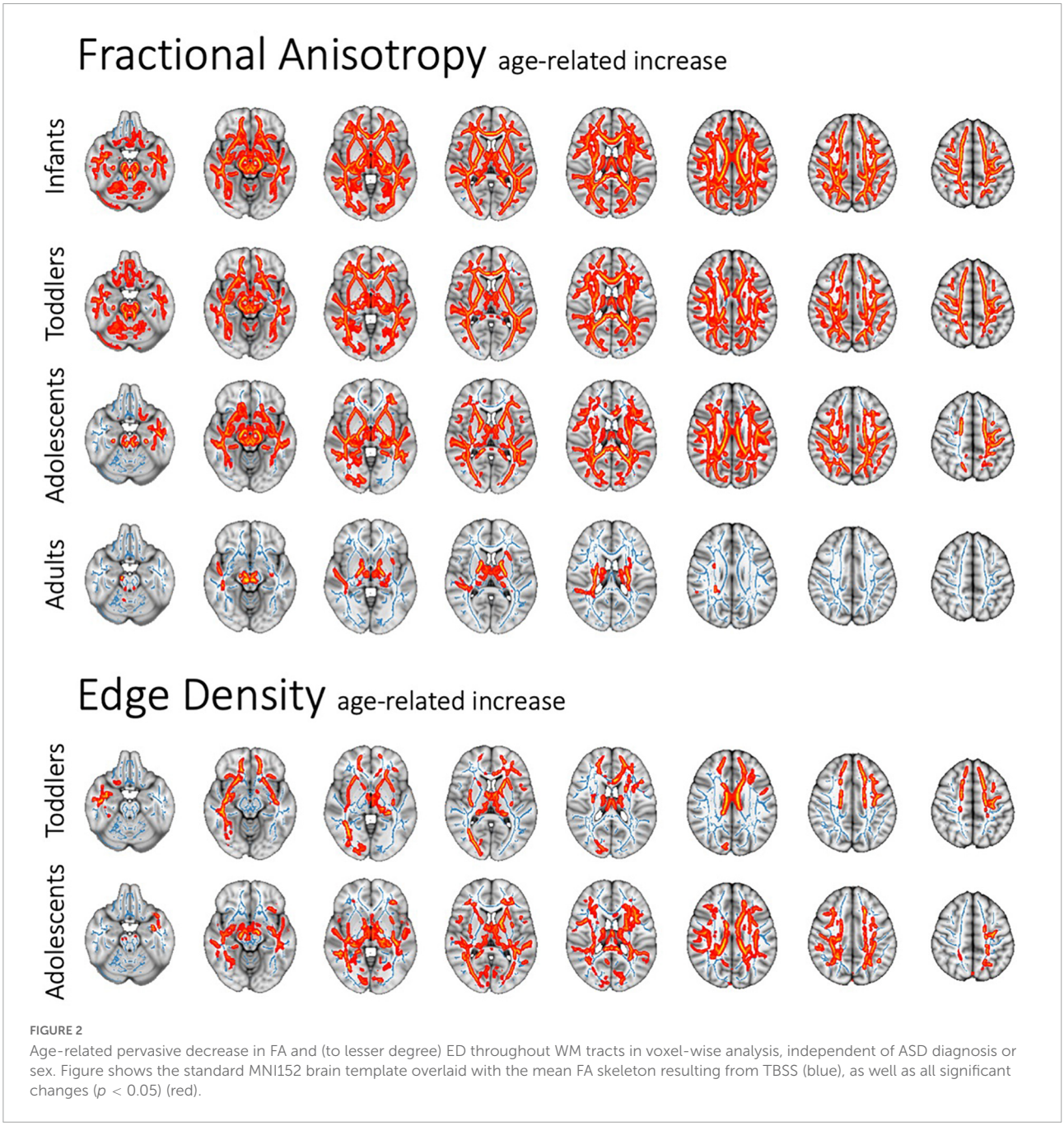

FIGURE 2
Age-related pervasive decrease in FA and (to lesser degree) ED throughout WM tracts in voxel-wise analysis, independent of ASD diagnosis or sex. Figure shows the standard MNI152 brain template overlaid with the mean FA skeleton resulting from TBSS (blue), as well as all significant changes ($p < 0.05$) (red).

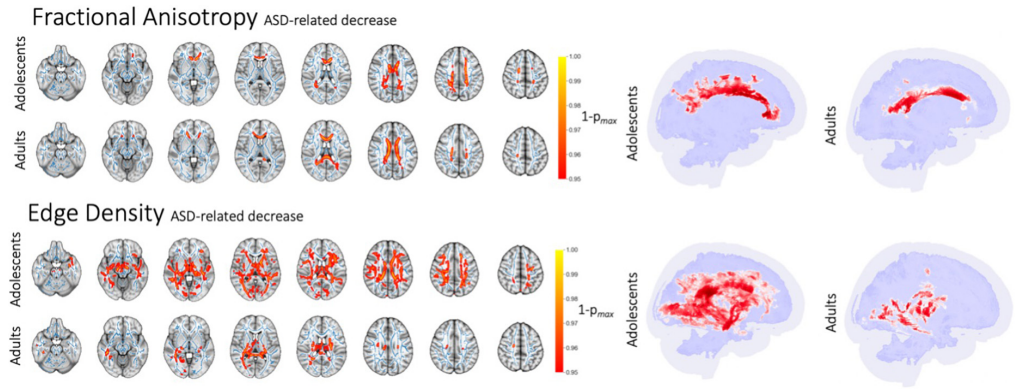

FIGURE 3
ASD-related decrease in FA and ED in voxel-wise analysis after correction for age. Figure shows white matter tracts with significant difference in red ($p < 0.05$) overlaid on the mean FA skeleton resulting from TBSS (blue).

Sex-related changes in white matter microstructure

In the adolescent cohort, there was lower FA along corticospinal tracts in females as compared to males when correcting for ASD diagnosis and age (**Figure 4**). We could not detect corresponding sex-related differences in the MD, RD, and AD of white matter tracts. In the adolescent cohort, ED revealed a more pervasive sex-related reduction in connectome ED among females compared to males. Tract-based multiple regression confirmed the results of voxel-wise analyses. This effect could not be found in younger cohorts after correcting for the covariate of age; the adult cohort only included one female subject and could therefore not be used to assess and make assumptions about sex-specific alterations. Of note, there was no significant difference between males and females regarding ADOS-scores in the adolescent cohort in a two-sided *t*-test (t-statistic 1.46, $p = 0.148$).

Machine learning classifiers predicting autism spectrum disorder diagnosis from tract-based diffusion tensor imaging and connectomics

Figure 5 displays a heatmap demonstrating the mean averaged AUC across validation folds from twenty repeats of five-fold cross validation, considering data from the adolescent and adult cohort (as mentioned above). The average AUC values range from 0.55 to 0.73, with the highest performance achieved using a support vector machine with radial kernel in combination with hierarchical clustering as feature selection applied to MD metrics. This combination model achieved 0.696 AUC (95% Delong CI 0.578–0.800), 63.2% accuracy, 56.1% sensitivity, and 71.4% specificity in the independent validation cohort.

Psychological/cognitive performance and brain microstructure

We found no significant influences of ADOS (Lord et al., 2000) scores on diffusivity metrics. In the adult cohort, there was no significant influence of IQ and SRS scores on diffusivity metrics after correction for age.

Discussion

Using, multicentric data from different age groups, we found an age-related increase in FA and ED, and decrease in MD and RD throughout most WM tracts. After correction for age and sex, ASD diagnosis was associated with WM microstructure disintegrity in adolescent and adult age groups primarily in the corpus callosum. However, ED revealed a more pervasive involvement of the brain's connectome in adolescents and adults with an ASD diagnosis. We also suggest a potential role for applying machine learning classifiers to assist with ASD diagnosis based on tract-based inputs from DTI scans. Limited by the small numbers of female subjects in our study cohorts, we found reduced FA in corticospinal tracts of female adolescents compared with males after correcting for ASD diagnosis and age.

Age-related alterations in diffusivity and anisotropy metrics

We found a pervasive rise in FA with increasing age throughout WM tracts in all study cohorts. In infants

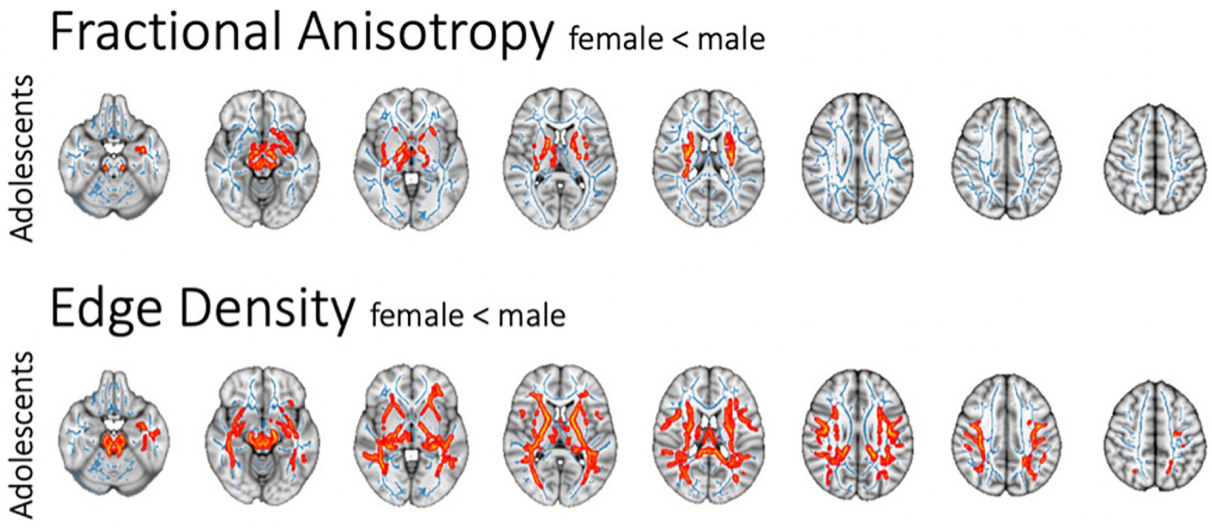

FIGURE 4
Sex-related changes in FA and ED as assessed in voxel-wise analysis after correction for age and ASD diagnosis. The white matter tracts with significant difference are colored red ($p < 0.05$) and overlaid on the mean FA skeleton (blue).

and toddlers, these changes are likely related to increased myelination of axon fibers and the microstructural maturation of WM (Yu et al., 2020). Research about developmental gradients in functional connectivity and WM microstructure suggests that even though most of WM maturation is completed during toddlerhood, further waves of myelination between association cortices with corresponding DTI changes occur in adolescence and adulthood (Sydnor et al., 2021), which may explain our findings among adolescents and older adults. ED can provide further insight into the brain connectome by examining potential fiber tracts between cortical nodes instead of mere assessment of directional water movement by conventional DTI metrics. We found a significant ED increase with age in toddlerhood and adolescence, which aligns with brain maturation in these age groups. Our findings highlight the necessity of adjusting the analysis of ASD-related microstructural changes for a respective subjects' age.

Autism spectrum disorder-related white mater microstructural alterations center in the corpus callosum

Our results suggest that microstructural disintegrity related to ASD is likely more evident in adolescents and young adults, but hardly detectable in younger age groups. These ASD-related changes in WM microstructure are primarily in the anterior and mid corpus callosum (Alexander et al., 2007; Payabvash et al., 2019b). While existing literature presents inconsistent results regarding WM alterations in the particular location within the corpus callosum, our data suggests that DTI abnormalities in the anterior corpus callosum are present in adolescents, become more pronounced and extend to central and posterior commissural tracts with increasing age. Notably, the infants and toddlers age groups included in our analyses are younger than most previous studies (Li et al., 2017). We also found significant ED reductions in central WM tracts related to ASD diagnosis, which were present across most WM tracts in adolescents, but more concentrated to posterior tracts in adults. These findings suggest a more pervasive involvement of the brain connectome compared to what is captured by conventional DTI metrics. Previous studies also show ED alterations in periventricular WM associated with ASD and other neurodevelopmental disorders (Payabvash et al., 2019a,b). In addition, significant changes could be found in a small area within the internal capsule of infants, but not toddlers.

Sex-specific effects

We found significantly lower FA in association and commissural tracts of female adolescents compared to males after correcting for age and ASD diagnosis (**Figure 4**). Previous studies suggested a correlation between sex and diffusivity metrics, as well as sex-related differences in correlation between DTI and behavioral measurements (Waller et al., 2017). A recent review of MRI studies evaluating sex-related effects in ASD also found that DTI metrics differ significantly between male and female subjects (Walsh et al., 2021). The female protective

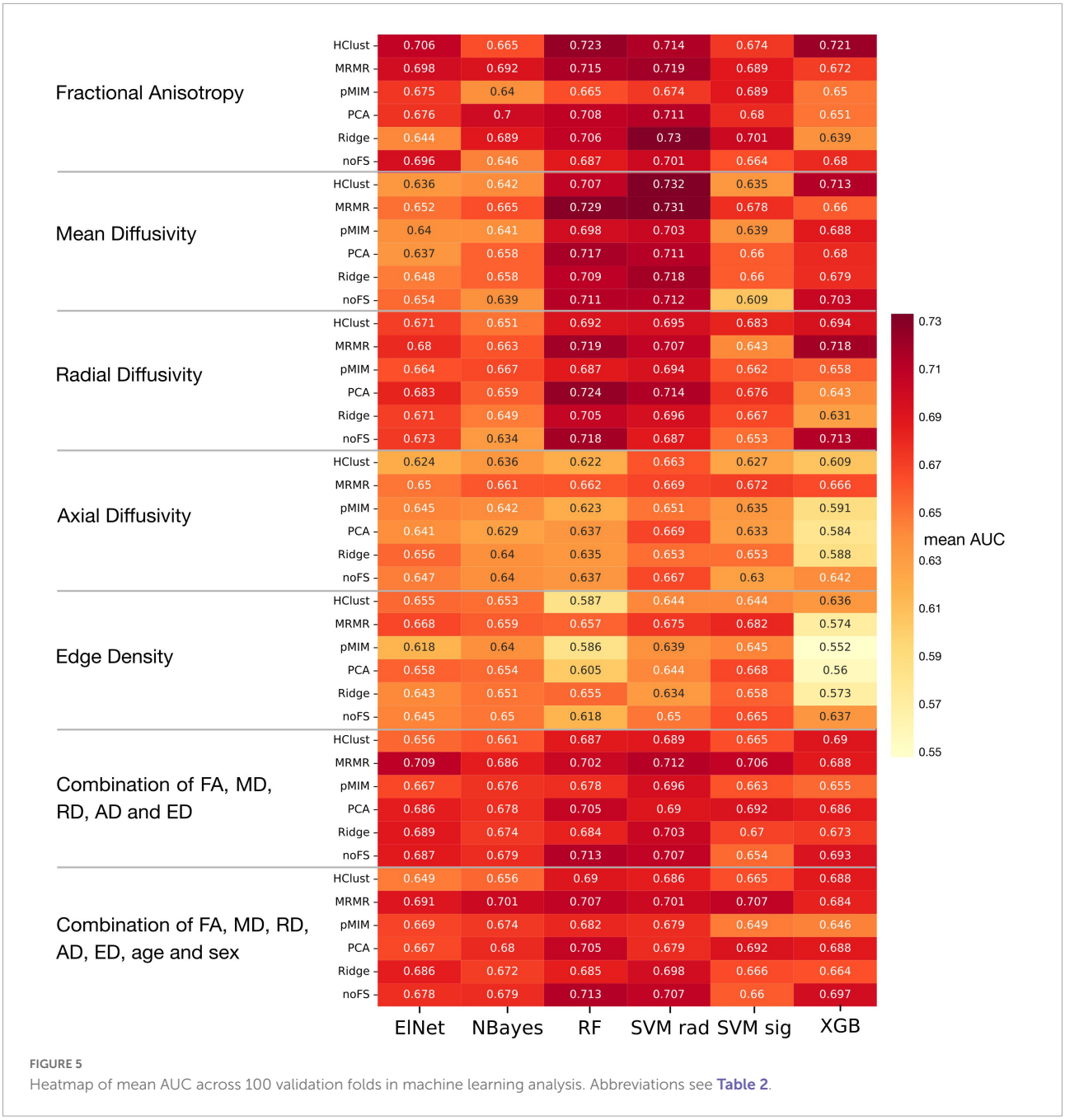

FIGURE 5
Heatmap of mean AUC across 100 validation folds in machine learning analysis. Abbreviations see **Table 2**.

effect and extreme male brain hypothesis suggest that sex-related characteristics of brain organization contribute to ASD symptom severity (Werling and Geschwind, 2015).

There have been extensive discussions about sex-related effects in ASD, as the influence of data assessment bias on hypotheses of etiological aspects is hard to quantify. Bias persists due to later diagnosis of females as stereotypical female behavior aligns better with ASD symptoms and currently used diagnostic algorithms might camouflage ASD diagnosis in females (Ratto et al., 2018). The previously approximated male-to-female ratio of 4:1 has been found to vary between 3:1 and 8:1 depending on quality of ASD assessment, and is nowadays estimated to trend toward a more equal sex distribution (Loomes et al., 2017). We could not find a significant interaction between sex and ASD diagnosis; however, our results underline the importance of considering sex in the investigation of ASD-related alterations.

Machine learning analysis

Machine learning algorithms provide a statistically suitable platform for the analysis of high-dimensional multimodal

neuroimaging data, which may account for the complexity of underlying neurobiological changes better than traditional statistical methods. In this study, we showed the feasibility of machine learning algorithms in assisting with the diagnosis of ASD based on DTI metrics of WM tracts. Using a rigorous cross-validation scheme, we optimized, trained, tested and validated an optimal combination of feature selection model and machine learning classifier to predict ASD diagnosis based on average DTI- and connectome derived metrics of WM tracts among adolescents and adults. Machine learning algorithms can potentially evaluate large amounts of imaging data and give detailed information about the individual's structural connectome. Therefore, algorithms could become a useful tool to consolidate diagnostic algorithms, subsequently improving ASD diagnosis and further differentiate ASD from other neurodevelopmental abnormalities.

Limitations

While analyses of large, multicentric data is a strength of our study, it also poses a limitation due to the heterogeneity of the data and difference in image acquisition techniques. However, given that voxel-wise and tract-based analyses were conducted separately for each site, we minimized the effects of site-specific differences. Of note, harmonization of diffusion MRI has been proposed to mitigate the issue of data acquisition from different scanners and centers (Pinto et al., 2020); but, given that the four cohorts in our study differ in terms of scanner, acquisition method, age of children, female-to-male ratio, and the rate of ASD among subjects, an optimal and fair harmonization technique might not be achieved. Moreover, although we could include 197 female subjects in our analyses (see **Table 1**), the majority of included individuals across different cohorts were male (51–99%), which impairs the generalizability of these results to female patients. We recognize that existing biases in ASD diagnoses extends from original assessments to our analyses. Some inaccuracies also come along with coregistration in TBSS and VBM, especially for pediatric cohorts with high variability in anatomy, motion, and head position. To mitigate these limitations, we excluded all cases with motion artefacts in a visual quality control. Finally, for our subjects, common coregistration templates such as MNI152 are limited in their accuracy, which is why we avoided using generic templates and chose study-specific ones wherever possible. We accounted for possible inaccuracies in voxel-wise analyses by confirming findings in tract-based statistics.

Conclusion

Overall, our results portray a comprehensive assessment of WM microstructure and connectome ED across a wide age range. Based on a large multicentric dataset, we showed age-specific microstructural and connectome abnormalities of WM tracts in ASD. We found a ubiquitous age-related FA increase and diffusivity decrease across different age groups, which highlights the need for age adjusted assessments of ASD-related microstructural alterations. We found an increasing discrepancy between ASD and typically developing individuals with regards to microstructural integrity of anterior commissural tracts starting in adolescents and becoming more pronounced in young adults. ED showed even more extensive involvement of brain connectome in adolescents and young adults with ASD. Additionally, female individuals presented with lower FA values and higher diffusivity in central cerebral white matter after adjustment for age and ASD diagnosis. These findings support previous literature about sex-related effects in DTI metrics and add to sex-related hypotheses in ASD neurobiology. Finally, we showed the feasibility of machine learning classifiers in prediction of ASD diagnosis based on tract-based diffusion and connectome metrics. This creates a foundation for the future application of machine learning in DTI analyses, where such models can integrate multi-modal data to build more robust and generalizable statistical frameworks. Further research is needed to adequately assess the interaction between WM microstructural alterations and symptom severity in ASD.

Data availability statement

Publicly available datasets were analyzed in this study. This data can be found here: https://nda.nih.gov.

Author contributions

CW carried out image processing, analyses, interpreted the findings, wrote, and revised the manuscript. SH assisted in data analysis and in interpretation of findings and revised the manuscript. PM, EL, DS, NB, LM, and TC assisted in interpretation of findings and revised the manuscript. SP designed the study, interpreted findings, and contributed to writing and revision of the manuscript. All authors contributed to the article and approved the submitted version.

Funding

SP received grant support from National Institutes of Health (K23NS118056), Doris Duke Charitable Foundation (2020097), and Foundation of American Society of Neuroradiology.

Conflict of interest

The authors declare that the research was conducted in the absence of any commercial or financial relationships that could be construed as a potential conflict of interest.

Publisher's note

All claims expressed in this article are solely those of the authors and do not necessarily represent those of their affiliated organizations, or those of the publisher, the editors and the reviewers. Any product that may be evaluated in this article, or claim that may be made by its manufacturer, is not guaranteed or endorsed by the publisher.

Supplementary material

The Supplementary Material for this article can be found online at: https://www.frontiersin.org/articles/10.3389/fnins.2022.957018/full#supplementary-material

References

Alexander, A. L., Lee, J. E., Lazar, M., Boudos, R., DuBray, M. B., Oakes, T. R., et al. (2007). Diffusion tensor imaging of the corpus callosum in autism. *Neuroimage* 34, 61–73.

Ameis, S. H., and Catani, M. (2015). Altered white matter connectivity as a neural substrate for social impairment in autism spectrum disorder. *Cortex* 62, 158–181.

American Psychiatric Association [APA] (2013). *Diagnostic And Statistical Manual Of Mental Disorders (Dsm-5§)*. Arlington: American Psychiatric Association.

Aoki, Y., Yoncheva, Y. N., Chen, B., Nath, T., Sharp, D., Lazar, M., et al. (2017). Association of white matter structure with autism spectrum disorder and attention-deficit/hyperactivity disorder. *JAMA Psychiatry* 74, 1120–1128.

Autism Genome Project Consortium, Szatmari, P., Paterson, A. D., Zwaigenbaum, L., Roberts, W., Brian, J., et al. (2007). Mapping autism risk loci using genetic linkage and chromosomal rearrangements. *Nat. Genet.* 39, 319–328. doi: 10.1038/ng1985

Barnea-Goraly, N., Kwon, H., Menon, V., Eliez, S., Lotspeich, L., Reiss, A. L., et al. (2004). White matter structure in autism: Preliminary evidence from diffusion tensor imaging. *Biol. Psychiatry* 55, 323–326.

Behrens, T. E. J., Woolrich, M. W., Jenkinson, M., Johansen-Berg, H., Nunes, R. G., Clare, S., et al. (2003). Characterization and propagation of uncertainty in diffusion-weighted mr imaging. *Magn. Reson. Med.* 50, 1077–1088. doi: 10.1002/mrm.10609

Behrens, T. E., Berg, H. J., Jbabdi, S., Rushworth, M. F., and Woolrich, M. W. (2007). Probabilistic diffusion tractography with multiple fibre orientations: What can we gain? *Neuroimage* 34, 144–155.

Brito, A. R., Vasconcelos, M. M., Domingues, R. C., Hygino Da Cruz, L. C. Jr., Rodrigues, L. D. S., and Gasparetto, E. L. (2009). Diffusion tensor imaging findings in school-aged autistic children. *J. Neuroimaging* 19, 337–343. doi: 10.1111/j.1552-6569.2009.00366.x

Chaste, P., and Leboyer, M. (2012). Autism risk factors: Genes, environment, and gene-environment interactions. *Dialogues Clin. Neurosci.* 14, 281–292.

Cheon, K. A., Kim, Y. S., Oh, S. H., Park, S. Y., Yoon, H. W., Herrington, J., et al. (2011). Involvement of the anterior thalamic radiation in boys with high functioning autism spectrum disorders: A diffusion tensor imaging study. *Brain Res.* 1417, 77–86. doi: 10.1016/j.brainres.2011.08.020

Constantino, J. N. (2013). "Social responsiveness scale," in *Encyclopedia Of Autism Spectrum Disorders*, ed. F. R. Volkmar (New York, NY: Springer), 2919–2929.

Courchesne, E. (2012). *Biomarkers of Autism at 12 Months: From Brain Overgrowth To Genes. 2007-2012*. Cleveland: Grantome.

Desikan, R. S., Ségonne, F., Fischl, B., Quinn, B. T., Dickerson, B. C., Blacker, D., et al. (2006). An automated labeling system for subdividing the human cerebral cortex on mri scans into gyral based regions of interest. *Neuroimage* 31, 968–980. doi: 10.1016/j.neuroimage.2006.01.021

Fischl, B. (2012). Freesurfer. *Neuroimage* 62, 774–781.

Frazier, J. A., Chiu, S., Breeze, J. L., Makris, N., Lange, N., Kennedy, D. N., et al. (2005). Structural brain magnetic resonance imaging of limbic and thalamic volumes in pediatric bipolar disorder. *Am. J. Psychiatry* 162, 1256–1265.

Goldstein, J. M., Seidman, L. J., Makris, N., Ahern, T., O'Brien, L. M., Caviness, V. S. Jr., et al. (2007). Hypothalamic abnormalities in schizophrenia: Sex effects and genetic vulnerability. *Biol. Psychiatry* 61, 935–945.

Haider, S. P., Mahajan, A., Zeevi, T., Baumeister, P., Reichel, C., Sharaf, K., et al. (2020). Pet/ct radiomics signature of human papilloma virus association in oropharyngeal squamous cell carcinoma. *Eur. J. Nucl. Med. Mol. Imaging* 47, 2978–2991. doi: 10.1007/s00259-020-04839-2

Jou, R. J., Jackowski, A. P., Papademetris, X., Rajeevan, N., Staib, L. H., and Volkmar, F. R. (2011). Diffusion tensor imaging in autism spectrum disorders: Preliminary evidence of abnormal neural connectivity. *Aust. N. Z. J. Psychiatry* 45, 153–162.

Kumar, A., Sundaram, S. K., Sivaswamy, L., Behen, M. E., Makki, M. I., Ager, J., et al. (2010). Alterations in frontal lobe tracts and corpus callosum in young children with autism spectrum disorder. *Cereb. Cortex* 20, 2103–2113. doi: 10.1093/cercor/bhp278

Lainhart, J. E. (2012). *Atypical Late Neurodevelopment In Autism: A Longitudinal Mri And Dti Study. 2007-2012*. Cleveland: Grantome.

Li, D., Karnath, H.-O., and Xu, X. (2017). Candidate biomarkers in children with autism spectrum disorder: A review of mri studies. *Neurosci. Bull.* 33, 219–237.

Loomes, R., Hull, L., and Mandy, W. P. L. (2017). What is the male-to-female ratio in autism spectrum disorder? A systematic review and meta-analysis. *J. Am. Acad. Child. Adolesc. Psychiatry* 56, 466–474. doi: 10.1016/j.jaac.2017.03.013

Lord, C., Risi, S., Lambrecht, L., Cook, E. H. Jr., Leventhal, B. L., DiLavore, P. C., et al. (2000). The autism diagnostic observation schedule-generic: A standard measure of social and communication deficits associated with the spectrum of autism. *J. Autism. Dev. Disord.* 30, 205–223.

Maenner, M. J., Shaw, K. A., Baio, J., Washington, A., Patrick, M., Dirienzo, M., et al. (2020). Prevalence of autism spectrum disorder among children aged 8 years — autism and developmental disabilities monitoring network, 11 sites, united states, 2016. *MMWR Surveill. Summ.* 69, 1–12.

Makris, N., Goldstein, J. M., Kennedy, D., Hodge, S. M., Caviness, V. S., Faraone, S. V., et al. (2006). Decreased volume of left and total anterior insular lobule in schizophrenia. *Schizophr. Res.* 83, 155–171.

O'Donnell, L. J., Westin, C. F., and Golby, A. J. (2009). Tract-based morphometry for white matter group analysis. *Neuroimage* 45, 832–844.

Owen, J. P., Chang, Y. S., and Mukherjee, P. (2015). Edge density imaging: Mapping the anatomic embedding of the structural connectome within the white matter of the human brain. *Neuroimage* 109, 402–417. doi: 10.1016/j.neuroimage.2015.01.007

Payabvash, S., Palacios, E. M., Owen, J. P., Wang, M. B., Tavassoli, T., Gerdes, M., et al. (2019b). White matter connectome edge density in children with autism spectrum disorders: Potential imaging biomarkers using machine-learning models. *Brain Connect.* 9, 209–220. doi: 10.1089/brain.2018.0658

Payabvash, S., Palacios, E. M., Owen, J. P., Wang, M. B., Tavassoli, T., Gerdes, M., et al. (2019a). Diffusion tensor tractography in children with sensory processing disorder: Potentials for devising machine learning classifiers. *Neuroimage Clin.* 23:101831. doi: 10.1016/j.nicl.2019.101831

Pelphrey, K. A. (2017). *Multimodal Developmental Neurogenetics Of Females With asd. 2016-2017*. Cleveland: Grantome.

Pinto, M. S., Paolella, R., Billiet, T., Van Dyck, P., Guns, P. J., Jeurissen, B., et al. (2020). Harmonization of brain diffusion mri: Concepts and methods. *Front. Neurosci.* 14:396. doi: 10.3389/fnins.2020.00396

Piven, J. A. (2017). *Longitudinal Mri Study Of Infants At Risk For Autism. 2007-2017*. Cleveland: Grantome.

R Core Team (2020). *R: A Language And Environment For Statistical Computing*. Vienna: R Foundation for Statistical Computing.

Ratto, A. B., Kenworthy, L., Yerys, B. E., Bascom, J., Wieckowski, A. T., White, S. W., et al. (2018). What about the girls? Sex-based differences in autistic traits and adaptive skills. *J. Autism Dev. Disord.* 48, 1698–1711. doi: 10.1007/s10803-017-3413-9

Saklofske, D. H., and Schoenberg, M. R. (2011). "Wechsler adult intelligence scale (all versions)," in *Encyclopedia of Clinical Neuropsychology*, eds J. S. Kreutzer, J. DeLuca, and B. Caplan (New York, NY: Springer), 2675–2680.

Shukla, D. K., Keehn, B., Lincoln, A. J., and Müller, R.-A. (2010). White matter compromise of callosal and subcortical fiber tracts in children with autism spectrum disorder: A diffusion tensor imaging study. *J. Am. Acad. Child Adolesc. Psychiatry* 49, 1269–1278.e2. doi: 10.1016/j.jaac.2010.08.018

Shukla, D. K., Keehn, B., Smylie, D. M., and Muller, R. A. (2011). Microstructural abnormalities of short-distance white matter tracts in autism spectrum disorder. *Neuropsychologia* 49, 1378–1382. doi: 10.1016/j.neuropsychologia.2011.02.022

Smith, S. M. (2002). Fast robust automated brain extraction. *Hum. Brain Mapp.* 17, 143–155.

Smith, S. M., and Nichols, T. E. (2009). Threshold-free cluster enhancement: Addressing problems of smoothing, threshold dependence and localisation in cluster inference. *Neuroimage* 44, 83–98. doi: 10.1016/j.neuroimage.2008.03.061

Smith, S. M., Jenkinson, M., Johansen-Berg, H., Rueckert, D., Nichols, T. E., Mackay, C. E., et al. (2006). Tract-based spatial statistics: Voxelwise analysis of multi-subject diffusion data. *Neuroimage* 31, 1487–1505.

Smith, S. M., Jenkinson, M., Woolrich, M. W., Beckmann, C. F., Behrens, T. E., Johansen-Berg, H., et al. (2004). Advances in functional and structural mr image analysis and implementation as fsl. *Neuroimage* 23, S208–S219. doi: 10.1016/j.neuroimage.2004.07.051

Sydnor, V. J., Larsen, B., Bassett, D. S., Alexander-Bloch, A., Fair, D. A., Liston, C., et al. (2021). Neurodevelopment of the association cortices: Patterns, mechanisms, and implications for psychopathology. *Neuron* 109, 2820–2846.

Travers, B. G., Adluru, N., Ennis, C., Tromp, D. P. M., Destiche, D., Doran, S., et al. (2012). Diffusion tensor imaging in autism spectrum disorder: A review. *Autism Res.* 5, 289–313.

Wakana, S., Caprihan, A., Panzenboeck, M. M., Fallon, J. H., Perry, M., Gollub, R. L., et al. (2007). Reproducibility of quantitative tractography methods applied to cerebral white matter. *Neuroimage* 36, 630–644.

Waller, R., Dotterer, H. L., Murray, L., Maxwell, A. M., and Hyde, L. W. (2017). White-matter tract abnormalities and antisocial behavior: A systematic review of diffusion tensor imaging studies across development. *Neuroimage Clin.* 14, 201–215. doi: 10.1016/j.nicl.2017.01.014

Walsh, M. J. M., Wallace, G. L., Gallegos, S. M., and Braden, B. B. (2021). Brain-based sex differences in autism spectrum disorder across the lifespan: A systematic review of structural mri, fmri, and dti findings. *Neuroimage Clin.* 31:102719. doi: 10.1016/j.nicl.2021.102719

Werling, D. M., and Geschwind, D. H. (2015). Recurrence rates provide evidence for sex-differential, familial genetic liability for autism spectrum disorders in multiplex families and twins. *Mol. Autism* 6:27. doi: 10.1186/s13229-015-0004-5

Winkler, A. M., Ridgway, G. R., Webster, M. A., Smith, S. M., and Nichols, T. E. (2014). Permutation inference for the general linear model. *Neuroimage* 92, 381–397.

Yu, Q., Peng, Y., Kang, H., Peng, Q., Ouyang, M., Slinger, M., et al. (2020). Differential white matter maturation from birth to 8 years of age. *Cereb. Cortex* 30, 2673–2689. doi: 10.1093/cercor/bhz268

frontiers | Frontiers in Neuroscience

TYPE Hypothesis and Theory
PUBLISHED 03 November 2022
DOI 10.3389/fnins.2022.988735

OPEN ACCESS

EDITED BY
Michela Candini,
University of Bologna, Italy

REVIEWED BY
Jessie Poquerusse,
McGill University, Canada
Miguel Ángel García-Cabezas,
Autonomous University of Madrid,
Spain

*CORRESPONDENCE
François Iris
francois.iris@bmsystems.org

SPECIALTY SECTION
This article was submitted to Neurodevelopment, a section of the journal Frontiers in Neuroscience

RECEIVED 07 July 2022
ACCEPTED 10 October 2022
PUBLISHED 03 November 2022

CITATION
Beopoulos A, Géa M, Fasano A and Iris F (2022) Autism spectrum disorders pathogenesis: Toward a comprehensive model based on neuroanatomic and neurodevelopment considerations.
Front. Neurosci. 16:988735.
doi: 10.3389/fnins.2022.988735

Autism spectrum disorders pathogenesis: Toward a comprehensive model based on neuroanatomic and neurodevelopment considerations

Athanasios Beopoulos[1], Manuel Géa[1], Alessio Fasano[2,3] and François Iris[1]*

[1]Bio-Modeling Systems, Paris, France, [2]Division of Pediatric Gastroenterology and Nutrition, Mucosal Immunology and Biology Research Center, Massachusetts General Hospital for Children, Boston, MA, United States, [3]Division of Pediatric Gastroenterology and Nutrition, Center for Celiac Research and Treatment, Massachusetts General Hospital for Children, Boston, MA, United States

Autism spectrum disorder (ASD) involves alterations in neural connectivity affecting cortical network organization and excitation to inhibition ratio. It is characterized by an early increase in brain volume mediated by abnormal cortical overgrowth patterns and by increases in size, spine density, and neuron population in the amygdala and surrounding nuclei. Neuronal expansion is followed by a rapid decline from adolescence to middle age. Since no known neurobiological mechanism in human postnatal life is capable of generating large excesses of frontocortical neurons, this likely occurs due to a dysregulation of layer formation and layer-specific neuronal migration during key early stages of prenatal cerebral cortex development. This leads to the dysregulation of post-natal synaptic pruning and results in a huge variety of forms and degrees of signal-over-noise discrimination losses, accounting for ASD clinical heterogeneities, including autonomic nervous system abnormalities and comorbidities. We postulate that sudden changes in environmental conditions linked to serotonin/kynurenine supply to the developing fetus, throughout the critical GW7 – GW20 (Gestational Week) developmental window, are likely to promote ASD pathogenesis during fetal brain development. This appears to be driven by discrete alterations in

differentiation and patterning mechanisms arising from *in utero* RNA editing, favoring vulnerability outcomes over plasticity outcomes. This paper attempts to provide a comprehensive model of the pathogenesis and progression of ASD neurodevelopmental disorders.

KEYWORDS

autism spectrum disorder (ASD), autonomic nervous system (ANS), neurodevelopment, serotonin, RNA editing, maternal inflammation, kynurenine metabolites, synaptic pruning

Introduction

Autism is not a single disorder, but a spectrum of related disorders with a shared core of symptoms defined by deficits in communication, social reciprocity and repetitive, stereotypic behaviors. While previously thought to present an extreme sex/gender bias (four times more common among males than females) it is now established that this apparent bias is largely due to affected females being more capable of disguising their condition than affected males (Dworzynski et al., 2012; Kreiser and White, 2014; Mandic-Maravic et al., 2015; Hull et al., 2017; Ratto et al., 2018; Young et al., 2018). Currently, autism spectrum disorders (ASD) affects around 1 in 68 children around the world, a 35-fold increase since the earliest epidemiologic studies were conducted in the late 1960s and early 1970s. However, this sharp increase may be also related- to some extent- to diagnostic, specificity, sensitivity or administrative biases (Monteiro et al., 2015; Randall et al., 2018; Ghandour et al., 2019). ASD is characterized by early increases in brain volume and cortical thickness during infancy and the toddler years (2–4 years) in young autistic males and females, followed by an accelerated rate of decline in size, and perhaps degeneration, from adolescence to late middle age in this disorder (Hazlett et al., 2017).

In most cases, this aberrant brain growth does not occur at birth, but rather develops throughout the first 2 years of life after birth. Early post-natal brain overgrowth is then followed by arrest of growth. The sites of regional overgrowth in ASD include frontal and temporal cortices and the amygdala and, in some regions, and individuals, growth arrest may be followed by degeneration (Courchesne et al., 2007). Brain overgrowth follows an important gradient in the cerebrum: greatest in the frontal and temporal cortices, which are most abnormally enlarged, and least in the occipital cortex, with young autistic males presenting a very significant excess of neuron number in the dorsolateral prefrontal cortex (PFC) (Courchesne et al., 2011). Since there is no known neurobiological mechanism in humans capable of generating during postnatal life the large excesses of frontal cortical neurons, the great magnitude of this excess is most probably due to dysregulation of layer formation and layer-specific neuronal differentiation at prenatal developmental stages, rather than to any known postnatal event or mechanism. Therefore, the peak period for detecting and studying the early biological basis of autism is from prenatal life to the first three years postnatally.

Some seasonal cyclicity appears associated with the percentage of children affected by ASD, intellectual disabilities, and learning limitations, with rates being greatest for children conceived in the winter months, and lowest for those conceived during the summer (Mackay et al., 2016). Conception in the winter season is associated with a 6% increased risk of ASD presentation as compared with summer (Zerbo et al., 2011).

Many individuals with ASD have symptoms of associated co-morbidities, including seizures, sleep problems, metabolic conditions, and gastrointestinal (GI) disorders, which have significant health, developmental, social, and educational impacts. The neuroanatomical and biochemical characteristics that have been associated with autism pathogenesis *in utero* (Rossignol and Frye, 2012; Stoner et al., 2014; Zielinski et al., 2014) involve mechanisms that are direct consequences of the effects of low-grade, feverless, systemic inflammatory events (Nankova et al., 2014), while the protective mechanisms against autism pathogenesis have strong anti-inflammatory components (Scumpia et al., 2014). The gut microbiome drives immunoregulation (in particular during the first 3 years of life) and faulty immunoregulation, as well as inflammation, predispose to psychiatric disorders, including autism, while psychological stress drives further inflammation via pathways that involve the gut microbiome (Kostic et al., 2015). Thus, while ASD is significantly associated with subsequent incidence of inflammatory bowel disease (Kim et al., 2022), contrary to many psychological and psychiatric diseases there is a lack of evidence for systemic low-grade inflammation in association with ASD affected individuals (Prosperi et al., 2019).

This paper attempts to explore the most plausible mechanisms involved in the pathogenesis of ASDs and to relate them to the phenotypic and symptomatic manifestations of common characteristics. As our hypothesis paper covers a wide range of different topics and disciplines, we have often tried to include a general description of the mechanisms involved in neurotypical brain development and their respective components (immune regulation, kynurenine pathway, mRNA editing, functional communication between brain areas, etc.) in order to facilitate reading by different specialties and a wider audience.

Materials and methods

The authors conducted an in-depth review of the literature and used a systems biology approach to integrate the complex mechanisms of fetal brain development to then decipher the neurodevelopmental origins encountered in individuals with ASD. Throughout our literature review, we strongly favored studies on human subjects, and in the few cases where this is not the case, it is clearly stated in the text. The analytical procedure implemented (CADI^{TM} : Computer-Assisted Deductive Integration) associates algorithmics and heuristics. The logic behind this model-building approach does not assume functional linearity within biological systems and the components of a model do not incorporate solely what is known. Indeed, since this approach relies upon strict and systematic implementation of negative selection of hypotheses, models arising from this procedure contain elements that have never been described but cannot be refuted by current knowledge and/or available biological data, thereby generating novel understanding. This model-building approach has proven its efficacy in a number of biological research domains, including the discovery of hitherto unsuspected biological mechanisms, pathways, and interactions directly associated with phenotypic transitions *in vivo* (be they pathological or developmental) (Gadal et al., 2003, 2005; Iris et al., 2009; Pouillot et al., 2010; Turck and Iris, 2011; Iris, 2012; Nussbaumer et al., 2016). CADI^{TM} modeling has led to discoveries and patents in the fields of infectious diseases, oncology, neurology, psychiatry, dermatology, immunology, metabolic disorders, innovative bioprocesses for industrial biotech and the creation of new companies exploiting these patents. CADI^{TM} models describe the biological phenomena involved in pathological states and provide novel mechanistic integrations to explain the cause of certain diseases, identify and select predictive biomarkers, and offer new combinations of molecules and new therapeutic strategies. Further information on the Computer-Assisted Deductive Integration method can be found in Iris et al. (2018).

Analysis

The neuro-anatomical specificities of autism

In view of the enormous heterogeneity that characterizes the spectrum of autism, neuroanatomic variations are to be expected. One of the most common disparities in ASD development involves the amygdala, located deep and medially within the temporal lobes of the cerebrum. In typical fetal brain development, the amygdala displays structural connectivity across the cortex, particularly toward frontal and temporal lobes, by gestational week GW13 (Vasung et al., 2010) and a mature structure by 8 months (Vasung et al., 2010). Columns of neuroblasts from the inferior germinal eminence (GE), located ventral to the developing amygdala (Ulfig et al., 2000), migrate along radial glial fibers initiating amygdala development (Müller and O'Rahilly, 1990; Ulfig et al., 2003). As fetal development progresses, the GE shrinks to a small population of cells that surrounds the ventral section of the maturing amygdala. In humans, the paralaminar nucleus (PL) begins to develop during the 8th and 9th gestational month, residing and maturing at the location of the remnant GE (Ulfig et al., 2003), while mature PL still contains subpopulations of immature neurons (Bernier et al., 2000; Yachnis et al., 2000; Fudge and Tucker, 2009; Zhang et al., 2009). PL is a unique subregion of the amygdala, densely innervated by serotonergic fibers with high numbers of receptors for corticotropin releasing hormone and benzodiazepines. It is thought to play key roles in the normal growth and function of the amygdala, especially due to the resident immature cells that appear to confer enhanced neuronal plasticity (deCampo and Fudge, 2012).

Of all the various structural brain abnormalities reported in autism and related to the amygdala (reviewed in Donovan and Basson, 2017), the most consistent seem to be:

- rapid and early increases in the size of the right and left amygdala, which correlate positively with the extent of their deficits in social interaction and communication at age 5 (Ortiz-Mantilla et al., 2010).

- greater amygdala spine density in youths with ASD than in age-matched controls with typical development (TD) (<18 years), but which decreases as they grow older, a pattern not found in TD (Weir et al., 2018).

- initial overabundance of amygdala neurons in young ASD subjects, followed by a reduction in all nuclei during adult years, whereas in TD, there is an increase of mature neurons in the basal and accessory basal nuclei from child to adult, concurrently with a decrease of immature neurons in the PL (Avino et al., 2018).

This is suggestive of a sustained contribution of mature neurons from the PL nucleus toward other nuclei of the neurotypic amygdala, and that this developmental path may be altered in ASD, which may explain the changes in volume seen in ASD and other neurodevelopmental or neuropsychiatric disorders.

The amygdala, stretching from 1 to 4 cm with an average of about 1.8 cm, has a wide range of connections with the brain. The hippocampus, entorhinal cortex, basal ganglia (particularly the striatum), brainstem, thalamus, and hypothalamus are all part of this organization. It is also linked to the limbic system, the associative cortex, the PFC (which controls behavior), the basal forebrain, and other areas. As a result, its stimulation is expected to have a significant impact on the entire brain.

This can be exemplified in one of the amygdala's major functions in humans which is to regulate emotions, particularly fear and anxiety (**Figure 1**), and the behaviors that follow from them. In addition, the amygdala has some memory function

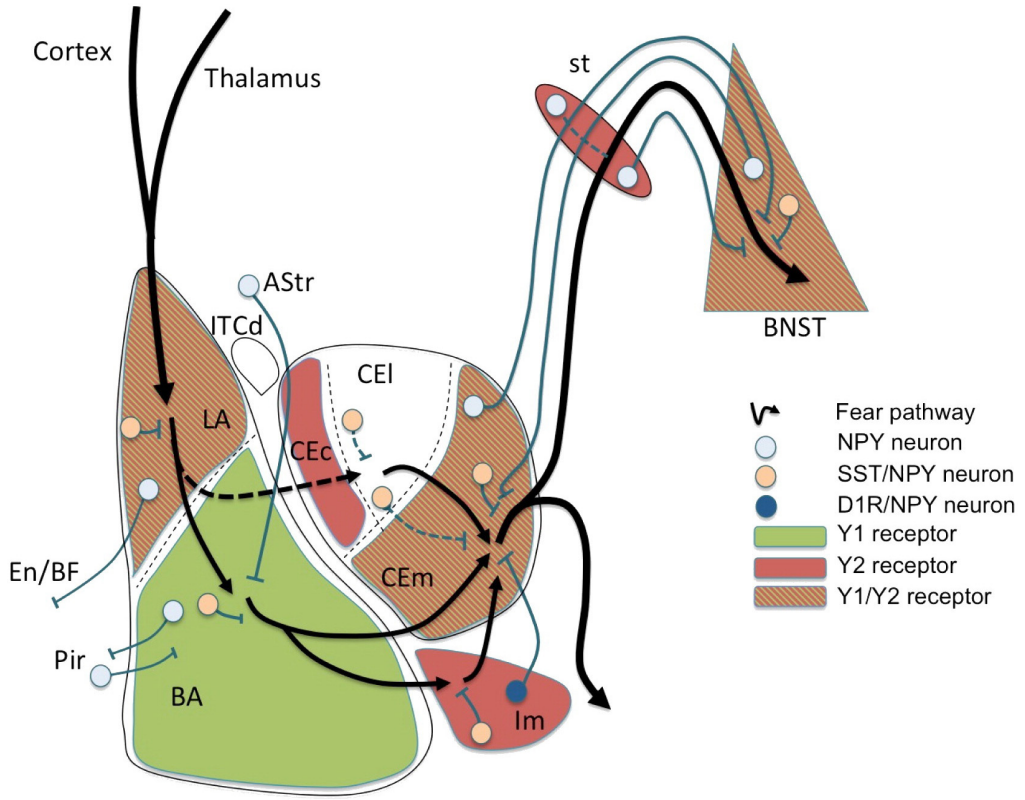

FIGURE 1
Fear circuit in the amygdala. Cortical and thalamic projections conveying somatosensory (US) and auditory (CS) information are targeting the lateral amygdala (LA), a major location of initial synaptic plasticity. Somatostatin (SST)/neuropeptide Y (NPY)/γ-aminobutyric acid (GABA) neurons may inhibit pyramidal neurons by activation of postsynaptic Y1 and presynaptic Y2 receptors reducing CS-related activation and fear learning. Similarly, SST/NPY neurons in the basolateral nucleus (BLA) may have additional Y1 receptor-dependent inhibiting effects. The role of NPYergic afferent and efferent projections of the basolateral complex (LA and BLA) is not yet clear. Fear related stimuli reach the central amygdala (CEA) also via mediodorsal intercalated neurons (ITCd) to the centrolateral subdivision (CEl) or directly via projections from the BLA to the centromedial subdivision (CEm). NPY neurons may modulate afferent and efferent signals locally in the CEl or via inhibitory connections between CEl and CEm, probably by Y2 receptors. However, the main processing occurs in the CEm (expressing Y1 and Y2 receptors) by (1) local inhibitory SST/NPY/GABA neurons, (2) by NPY/GABA afferents originating from the BNST, and (3) by NPY axon terminals originating from neurons of the main intercalated nucleus (Im). The latter projection consisting of NPY/dopamine receptor D1 (D1R)/GABA neurons in the Im is considered to play an essential role in fear extinction by providing a marked increase in feed-forward inhibition from the BLA to the CEm. Lastly, efferents from the CEm may be further modulated by NPY along the stria terminalis (st) or even in the bed nucleus of the stria terminalis (BNST), both by local interneurons and by bi-directional projections connecting the CEm with the BNST. AStr, amygdala-striatal transition zone; En, entorhinal cortex; Pir, piriform cortex; BF, basal forebrain; CEc, capsular subdivision of the central amygdala nucleus. Figure from Tasan et al. (2016), obtained by Elsevier (No. 5410821023270) under a creative commons license 3&4.

toward conditioned learning, which is the remembrance of situations that cause fear and anxiety. Thus, the emotion can be reproduced by stimuli or conditions that are similar to those that caused the initial dread and anxiety.

However, ASD-associated neuro-anatomical alterations aren't limited to the amygdala, and significantly affect the cortex, comprising progressively the six-layer neocortex (I–VI, with the outermost layer I neighboring the pia mater and the innermost layer VI neighboring the white matter), the 5–6 layer mesocortex (lacks or has poorly developed layer IV) and finally the three-layer allocortex. The neocortex takes up 90% of the cortex and mostly involves sensory, motor and associative functions. The mesocortical and allocortical areas form a closed ring at the edge of the hemisphere, forming the limbic areas which are found in the frontal, temporal, parietal, and occipital lobes as well as in the insula (García-Cabezas et al., 2022). Functions of the neocortex rely on a complex architecture of neuronal networks that is key in the excitation/inhibition imbalance observed in several neurodevelopmental disorders, including ASD. The superficial layer 1 (L1), which is consistently affected in autism, mostly comprises local and long-range inputs and sparse inhibitory interneurons that collectively govern brain activities. Its stereotypical organization, generated in early development, where axonal projections synapse onto the dendritic tufts of pyramidal neurons, functions as a crucial integration hub that provides context for sensory

information (i.e., local, thalamocortical, corticocortical, and long-range neuromodulation). As it receives connections from feedback and neuromodulatory pathways during its prolonged development, it plays a crucial role in the development, maturation, and function of the whole cortex. Its maturation continues postnatally with changes related to network affinity refinement affecting the whole cortex. Furthermore, interneurons found in Layer I facilitate disinhibition and thus contribute to plasticity and learning. During its development, it transiently accommodates Cajal-Retzius (CR) cells that regulate neuronal networks formation and migrating interneurons (*see below*). The organization of myelin in the cortex is highly diverse, with the content of intracortical myelin increasing progressively in parallel to laminar architecture elaboration from mesocortical agranular areas to koniocortical areas (García-Cabezas et al., 2020). Myelin sheath densities are representative of the extraordinary spatiotemporal organization of cortical networks (Trutzer et al., 2019; Call and Bergles, 2021; Genescu and Garel, 2021).

The most consistent cortical architecture abnormalities related to ASD appear to be:

- Abnormal patterns of overgrowth (7% increase in cerebrum size, with 5 and 10% increase in total gray and white matters, respectively) beginning before the second year, followed by reduced growth and arrested development at the end of childhood persisting into adolescence (Donovan and Basson, 2017);

- Sites of regional overgrowth that include frontal and temporal cortices (Abot et al., 2018);

- Greater spine densities on pyramidal cells in both the superficial and deep cortical layers of the frontal, temporal, and parietal lobe regions (layer II in each cortical location and within layer V of the temporal lobe) as compared to age-matched control subjects (Hutsler and Zhang, 2010);

- Excessive short to medium distance axons with increased branching in the superficial white matter beneath the anterior cingulate cortex (ACC). This finding is consistent with the hypothesis that prefrontal areas are overconnected in autism and probably explains the increased cortical folding in the frontal lobe in autism. In addition, the decrease in myelin thickness in the orbitofrontal cortex (OFC) observed in ASD may indicate altered relationships between prefrontal areas (Zikopoulos and Barbas, 2010). These areas govern emotion, attentional mechanisms and executive control, processes that are severely affected in autism (Barbas, 2000).

- High spine densities, which are associated with decreased brain weights, are most commonly found in ASD subjects with lower levels of cognitive functions (Hutsler and Zhang, 2010);

- Absence of the decline in cortical surface area that is always present in TD between the ages of 9 and 20 (Mensen et al., 2017);

- Irregular, age-related variations in cortical thickness, with a slower rate of thinning from childhood through adolescence and a faster rate of thinning in late adolescence. In TD, on the other hand, thinning occurs during teen years/early puberty (Nunes et al., 2020).

- In females, the volume and surface area of the temporal and frontal gyri and sulci, as well as the surface area of the left superior frontal and right lateral superior temporal gyri, are reduced. However, there is a tendency for the temporal gyri to thicken, resulting in little change in the volume of these areas (Cauvet et al., 2019), and

- In males, increased volume of the left anterior occipital sulcus and reduced thickness of the right para-hippocampal region of the medial occipito-temporal gyrus are related to autistic traits (Cauvet et al., 2019).

Furthermore, cortical networks in layer 1 are disorganized in autism: autistic children have higher variability in the trajectories and thickness of myelinated axons, whereas adults with autism show a decrease in the relative proportion of thin axons. In contrast, neurotypical controls, from children to adults, demonstrate an increase in the density of myelinated axons. Overall, neuron density decreases with age, as does the density of inhibitory interneurons identified with calbindin (CB), calretinin (CR), and parvalbumin (PV). Cortical activity refinement throughout development of cortical networks involved in cognition is likely aided by neurotypical postnatal alterations in layer 1 of the lateral prefrontal cortex (LPFC). This indicates that it is mostly the disruption of feedback pathways maturation, rather than interneurons in layer 1, that plays a crucial role in the development of autism's excitation-inhibition disequilibrium (Trutzer et al., 2019).

The prominent innervation by serotoninergic neurons and the dense expression of serotonergic receptors in the PFC, which shows overgrowth in ASD children, suggest that serotonin is a major modulator of its function (Wassink et al., 2007; Puig and Gulledge, 2011). Similarly, serotonin prominently promotes amygdala activation in response to emotional stimuli (Bocchio et al., 2016; Sengupta et al., 2017).

It finally should be noted that ASD does not figure among the disorders classified according to the stage of development where cortical elaboration was initially affected [i.e., malformations due to (1) abnormal proliferation/apoptosis; (2) abnormal migration; (3) abnormal late neuronal migration and cortical organization; and (4) cortical development, not otherwise classified; Barkovich et al., 2005]. Rather, ASD has been described as a pathology arising from multiple discrete alterations in brain growth, structure, synaptic organization and modified short- and long-range connectivity in the cortex (Hutsler and Casanova, 2016).

Fetal brain development

Throughout the following discussion, we have adhered to the officially accepted neuromorphological nomenclature

pertaining to fetal brain development. However, interested reader should be made aware of the existence of a new, albeit not yet officially accepted, nomenclature (the Prosomeric Model: Nieuwenhuys and Puelles, 2016; Puelles, 2018, 2021; Watson et al., 2019; Garcia-Calero and Puelles, 2020) with the relation between the classically accepted subdivisions of the neural tube (rhombencephalon, mesencephalon, diencephalon, etc.) and the newly proposed neuromorphological nomenclature being explained in Puelles (2018), Watson et al. (2019), and Garcia-Calero and Puelles (2020).

During embryonic development the ectoderm differentiates to form epithelial and neural tissues. The external (dorsal surface) ectoderm forms the neural plate that folds to generate the neural tube (i.e., the CNS precursor) and the neural crest (multipotent transient lineages that form the paravertebral and prevertebral ganglionic chain and chromaffin tissues). The neural tube generates three primary brain vesicles during GW4–GW5 in human development: the forebrain (prosencephalon) that matures into the cerebrum (telencephalon: cortex and white matter) and the diencephalon (thalamus, hypothalamus, epithalamus, subthalamus, and optical vesicles); the midbrain (mesencephalon: superior and inferior colliculi) and the rhombencephalon that progresses into the metencephalon (the pons and cerebellum) and the myelencephalon (the medulla oblongata). The midbrain and the rhombencephalon (pons, cerebellum, and medulla oblongata) form the brainstem, which begins development around GW6–GW7 and matures in a caudal to rostral arc (**Figure 2A**).

The dorsoventral axis of the telencephalon is further separated, with dorsal (pallial) and ventral (subpallial) domains giving rise to the cerebral cortex and basal ganglia and amygdala, respectively. Furthermore, morphological regions can be classified into auxiliary progenitor domains (prosomeres) based on gene expression (**Figures 2B,C**), that overlap with these anatomic subdivisions.

Arousal, respiration, heart rate, and gross motions of the body and head are all mediated by the medulla, and medullary activities appear before those of the pons, which appear before those of the midbrain. As a result, by GW7–GW9, the fetus is moving spontaneously, starts to "breathe," and by GW25 demonstrates stimulus-induced heart rate accelerations. As the pons, that mediates arousal, body movements, vestibular and vibroacoustic perceptions, takes longer to mature, the fetus only starts responding to vibroacoustic and loud noises coming from the exterior environment with arousal and body movements from GW20 to GW27.

The inferior-auditory colliculus begins its maturation cycle during the 6th week of pregnancy, followed by the superior visual colliculus that begins maturation around the 8th week. However, the development cycle is fairly protracted, as the inferior colliculus does not fully form until about the 17th week, and the superior colliculus takes several weeks longer to establish. Furthermore, midbrain development and myelination are not nearly complete until well after birth. Around GW36, the inferior-auditory colliculus, in collaboration with the lower brainstem, is capable of auditory discriminations and responds to sounds by accelerating the fetal heart rate (FHR), as well as with eye and head movements. The fetus hereafter reacts with reflexive movements when stimulated and is also able to fall asleep with the appearance of rapid eye movements (REM). Therefore, auditory discrimination, FHRs, the wake-sleep cycle, positioning, and protective behaviors appear to be controlled reflexively by the brainstem, which also appears to be engaged in learning processes. These processes have been thoroughly described elsewhere (Huang et al., 2009; Dubois et al., 2014; Seto and Eiraku, 2019).

Neurogenesis and neuronal migration

The different components of the nervous system are developed in distinctive phases going from (1) neurogenesis to (2) neuronal migration to the adequate location, (3) their differentiation along with connection maturation, and (4) the pruning of connections. These developmental phases are governed by hormones, specific proteins and growth factors, which function as traffic cues for the cells or their related processes. These intricate processes have been extensively reviewed (Huang et al., 2009; Lui et al., 2011; Dubois et al., 2014; Kostoviæ et al., 2015; Adnani et al., 2018; Hadders-Algra, 2018a; Lennox et al., 2018; Cadwell et al., 2019; Seto and Eiraku, 2019) and only those aspects that could possibly have relevance to ASD pathogenesis will be explored here. For clarity, **Figure 3** presents a timeline of human brain development.

As stressed above, the cerebral cortex of the adult mammal has a stratified structure made up of different layers, each of which containing a combination of glutamatergic pyramidal neurons, interneurons and projection neurons, and non-pyramidal GABAergic neurons. The great majority of cortical GABAergic cells are extraordinarily varied interneurons that form local connections only, whereas pyramidal neurons account for around 80% of all adult cortical neurons (Wang Y. et al., 2018).

The pallium and subpallium neuroepithelial stem cells (NESCs) multiply extensively by GW5–6 in humans to generate the cerebral vesicles (Bystron et al., 2008). NESCs maturate into radial glia cells, the key progenitor cells in the developing nervous system. Extracerebral microglial cells invade the telencephalon from GW5 onward and regulate the neurogenetic process (Nie et al., 2010). During GW5–7, the first neurons to be generated from the heterologous and transient cell populations of both pallial and subpallial origins are the CR cells and the subplate cells (SP) (Barber and Pierani, 2016).

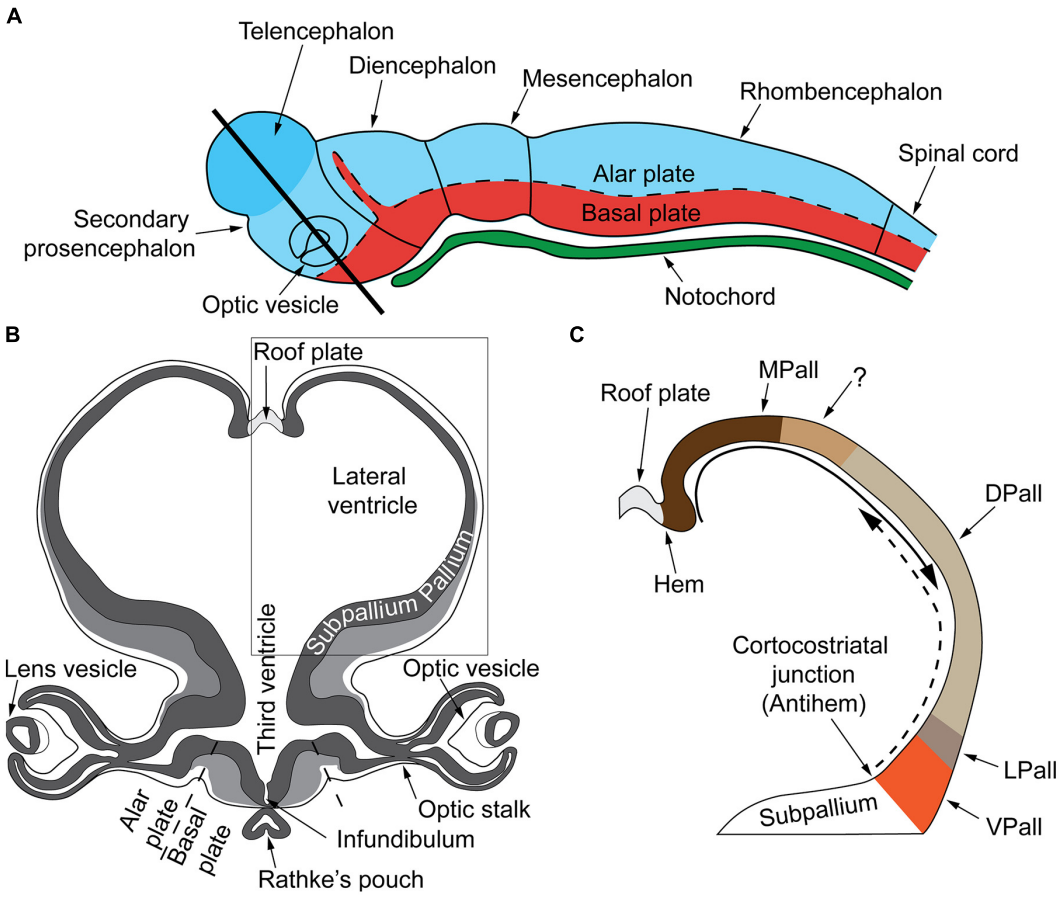

FIGURE 2
(A) Very early cerebral cortex development. Sketch of the mammalian neural tube showing the proneuromeric compartments. The neural tube will develop to form the brain and spinal cord. It is divided to the alar plate (colored in blue) that will later generate neurons associated with sensory functions (somatic and visceral), and the basal plate (red) that will primarily contain motor neurons. The notochord, of mesodermal origin (green) provides directional cues to the surrounding tissues. The telencephalic vesicle (highlighted in darker blue) grows out of the alar plate of the secondary prosencephalon. **(B)** Very early cerebral cortex development. Section through the secondary prosencephalon at the level of the black line in **(A)** shows the optic vesicles and the telencephalic vesicles; the telencephalic vesicles consist of pallial and subpallial territories. **(C)** Two organizers direct the patterning of the pallium: the hem, at the border of the roof plate and the prospective hippocampus, and the antihem, at the corticostriatal junction near the prospective olfactory cortex. The morphogen molecules segregated by these organizers form overlapping gradients (solid and dashed arrows) that pattern the pallium in four sectors: medial, dorsal, lateral, and ventral pallial sectors. The distinction of two parts on the MPall sector corresponding to allocortex (hippocampus) and the adjacent mesocortex (marked with "?") is hypothesized based on architectonic analysis of adult rats and primates. DPall, dorsal pallium; LPall, lateral pallium; MPall, medial pallium; VPall, ventral pallium. Figure from García-Cabezas and Zikopoulos (2019), obtained by Elsevier (No. 5410821023270) under a creative commons license 3&4.

CR cells are a transient cell population that is critical for brain development: these neurons form the preplate (PP) during GW6–7, and are devoid of synapses, communicating through non-synaptic junctions (Kostoviæ et al., 2015). Positioning cues and instructions to the developing cortical neurons and afferents are provided by reelin secreting CR and SP cells (Lakatosova and Ostatnikova, 2012; Barber and Pierani, 2016). The latter regulate migration of developing neurons that will form the thalamocortical connections (Ghosh et al., 1990; Csillik et al., 2002). Through a NMDA receptor-controlled process, reelin secreted by CR cells guides the direction of migration and positioning of neurons (Schaefer et al., 2008; Wang S. et al., 2018). CR cells also play an essential role in corticogenesis by regulating the identity and function of radial glia and the radial glia-to-astrocyte transformation (Super et al., 2000).

Post-mitotic excitatory pyramidal neurons migrate along radial glial (RG) fibers in an inside-out gradient of development (the deepest cellular layers are built first, followed by the ones closest to the surface) from layer VIa to layer II to produce the cortical plate by GW7–20 (**Figure 4**). Pyramidal cells originate from radial glial cells (RGC) at the beginning of cortical plate development (GW7–8), but later, they mostly come from intermediate progenitor cells (IPC) or basal progenitors derived from RGC cells (Kriegstein and Noctor, 2004;

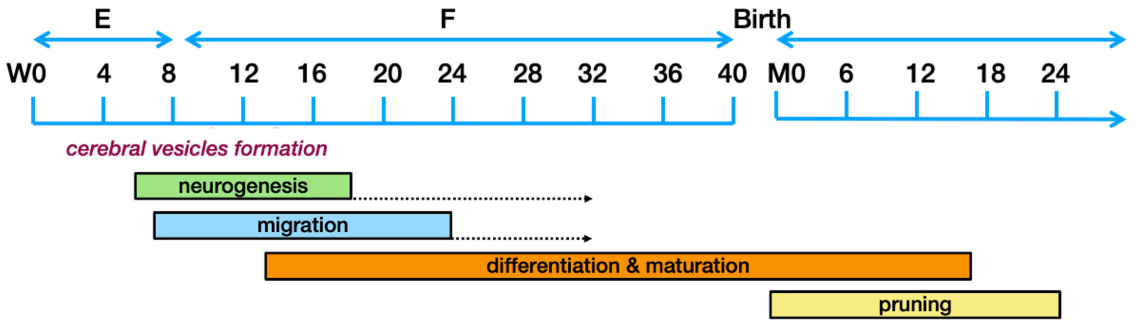

FIGURE 3
Schematic representation of the human brain development timeline. The dotted arrows designate a reduction in the rate of neurogenesis. Figure adapted from Stagni et al. (2015), obtained by Elsevier (No. 5410821023270) under a creative commons license 3&4.

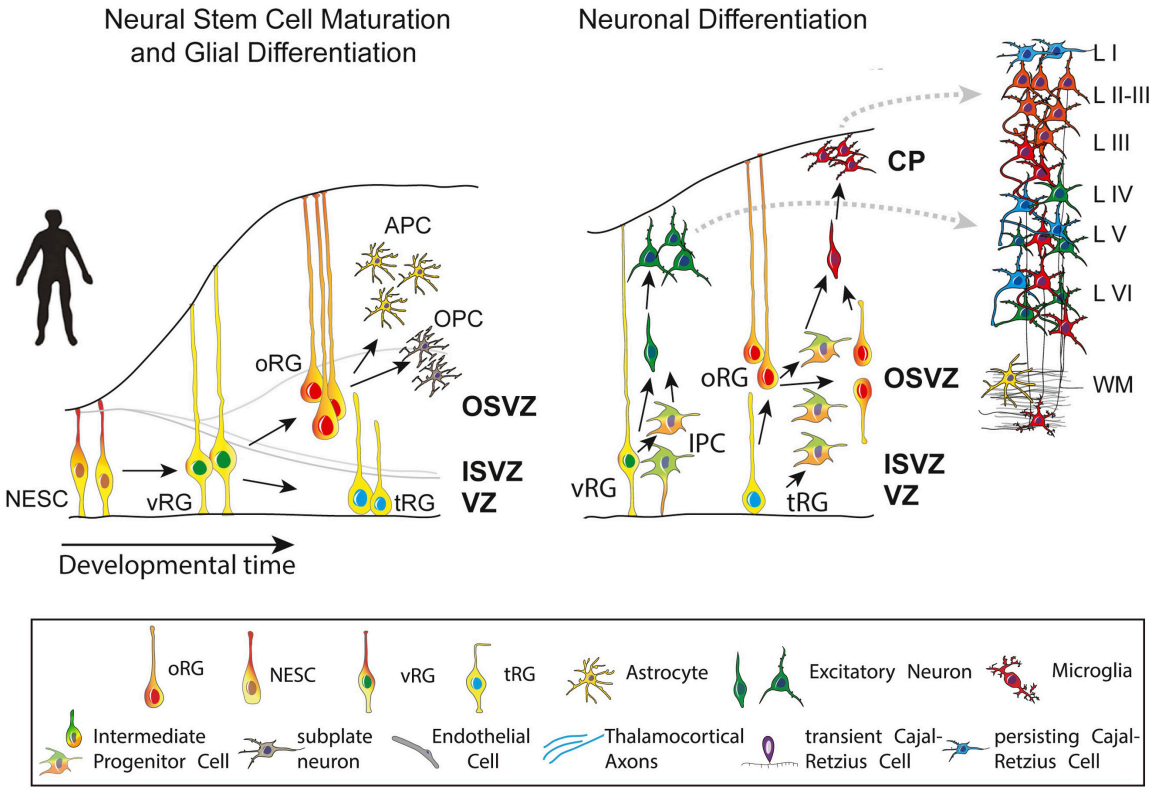

FIGURE 4
Maturation and differentiation in the cortex. **(Left)** Schematic representing radial glia maturation from neuroepithelial stem cells (NESCs), followed by their differentiation into astrocytes. **(Right)** Schematic represents sequential production of cortical layers from radial glia. Human cortical development involves an expanded diversity of radial glia with distinct maturation trajectories **(left)**. Neurogenesis in the human cortex occurs in the ventricular zone early in development and progressively shifts toward the outer subventricular zone (OSVZ). The development of the OSVZ is not homogeneous across prospective cortical areas in human fetuses, but increases from prospective mesocortical to prospective isocortical areas (Barbas and García-Cabezas, 2016). IPCs, intermediate progenitor cells; ISVZ, inner subventricular zone; LI–VI, cortical layer I–VI; NESCs, neuroepithelial stem cells; oRG, outer radial glia; OSVZ, outer subventricular zone; SVZ, subventricular zone; tRG, truncated radial glia; vRG, ventricular radial glia; VZ, ventricular zone; WM, white matter. Figure adapted from Cadwell et al. (2019).

Corbin et al., 2008). The first pyramidal neurons emerge successively from the ventricular zone (VZ) of the cortex, from which they migrate radially to shape a layer within the PP, i.e., the cortical plate (CP), dividing the PP into two zones: the superficial marginal zone (MZ; presumptive layer I containing the CR cells) and the deep SP.

The subventricular zone (SVZ) is a proliferative zone that forms during GW7, while the cortical plate emerges during

GW8, consisting of a cell-dense area with post-migratory neurons that migrate from the VZ along radial glial guides and eventually remain in the CP, arranged in vertical ontogenetic columns. *These columns are characteristically disorganized in the ASD cortex.*

The neocortical anlage is thus constituted of three transient fetal zones: the cell-poor superficial MZ, the cell-dense CP and the plexiform pre-subplate. Early bilaminar synaptogenesis is also found in this neocortical anlage, with synapses present in the MZ and pre-subplate, but absent in the CP. The intermediate zone (IZ) occurs between the neocortical anlage and the periventricular proliferative zones (VZ-SVZ) and comprises early developing afferent fibers emanating from the brain stem (monoaminergic axons), the thalamus (glutamatergic axons) and basal forebrain (cholinergic axons) (Kostoviæ et al., 2015; **Figure 4**). For further details the reader may refer to (Smart et al., 2002; Huang et al., 2009; Lui et al., 2011; Reillo et al., 2011; Martínez-Cerdeño et al., 2012; Dubois et al., 2014; Kostoviæ et al., 2015; Adnani et al., 2018; Hadders-Algra, 2018a; Lennox et al., 2018; Cadwell et al., 2019; Seto and Eiraku, 2019).

Neuronal organization and functionality

The brain undergoes the most substantial changes from the second half of pregnancy to the first three months after birth, particularly in the cortical subplate and cerebellum. From early fetal life to the first trimester post-partum, the transient SP undergoes constant developmental changes and interactions, with clear functional activity. From then on, a second developmental phase becomes distinct, where permanent circuitries dominate the now formed cortical SP (Kostoviæ et al., 2015). The first phase appears to correspond to non-adaptive, exploratory motor behavior and the second to motor behavior integrating environmental restrains (Hadders-Algra, 2018b). *Disruption of SP development is considered to have a great impact in developmental disorders such as schizophrenia, cerebral palsy, ASD and attention deficit hyperactivity disorder (ADHD)* (Hadders-Algra, 2018a).

During the first phase of SP development, SP neurons (SPNs; **Figure 5**) are among the first populations to be generated in the cortex (Kostovic and Rakic, 1980) and to receive synaptic inputs from thalamic axons. These function as a temporary link between thalamic axons and their final target in layer IV (Friauf et al., 1990; Ghosh and Shatz, 1992), that will be invaded and innervated only later in development (Ghosh and Shatz, 1992; Kanold et al., 2003). It is important to note here that the monoamine serotonin (5-HT), a crucial regulator for the formation of neural circuits (*see below*), presynaptically suppresses thalamo-SP afferents via 5HT1B receptors, although without apparently influencing intrinsic SPN properties (Liao and Lee, 2012).

The subplate neurons (SPNs) have a critical function in founding the correct wiring (Casal and Romano, 1978; McConnell et al., 1989) and functional maturation (Kanold et al., 2003) of the cerebral cortex; they then disappear during postnatal development. SPNs appear to be selectively sensitive to injuries (such as hypoxia) that, in humans, are linked to motor and cognitive defects (McQuillen and Ferriero, 2005).

The effects of serotonin on fetal brain development

Higher-order cognitive functions are controlled by cortical circuits, and their operation is heavily reliant on their structure, which evolves during development. The proliferation, migration, and differentiation of neurons and glial cells are among the sequential events that occur primarily during embryonic and early post-natal development and culminate in the establishment of mammalian cortical circuits. While these systems are mostly controlled by genetic programming, they are also affected by a wide range of extrinsic signals (such as hormones, growth factors, guidance cues, cell adhesion molecules, and so on) as well as environmental influences. As hinted before, serotonin (5-HT) is a critical regulator for the development of neuronal circuits (Gaspar et al., 2003; Bonnin and Levitt, 2011). 5-HT influences embryonic development very early, even before serotoninergic neurons appear (Lauder and Krebs, 1978; Shuey et al., 1992; Yavarone et al., 1993; Moiseiwitsch and Lauder, 1995; Whitaker-Azmitia et al., 1996; Buznikov et al., 2001). In the developing embryonic cortex, a number of serotonin receptors are dynamically expressed in a cell-type-and region-specific way. The ionotropic receptor 5-HT3A and the metabotropic receptor 5-HT6 control diverse elements of cortical architecture, such as neuronal migration and dendritic differentiation. Most of the 5-HT reaching the embryo at these early developmental stages originates from maternal or placental sources (**Figure 6** below recapitulates these studies), while increased placental L-tryptophan conversion to 5-HT as a result of maternal inflammation during pregnancy disrupts 5-HT-dependent neurogenic processes during fetal neurodevelopment (Goeden et al., 2016; Williams et al., 2017; Shallie and Naicker, 2019).

Serotonin and neuronal migration

In the mammalian cortex, 5-HT not only regulates the migration of cortical neurons but also triggers the motility of microglia toward the Central Nervous System (CNS) (Krabbe et al., 2012). Secreted or exogenous 5-HT acts at the molecular level as an axon guidance cue to shape neuronal circuit formation during development (Vicenzi et al., 2021).

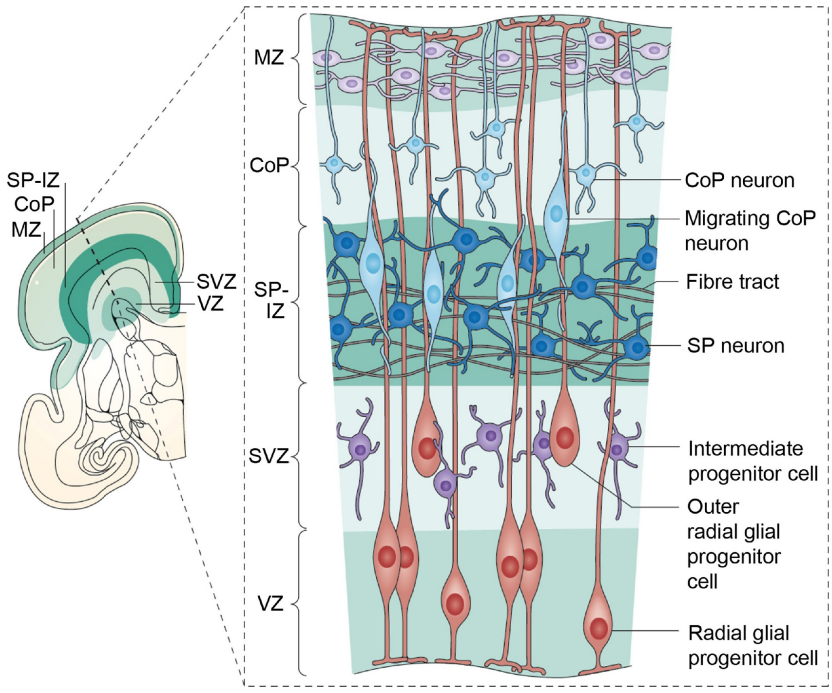

FIGURE 5
The human cerebral cortex at 28 weeks postmenstrual age (PMA; 8 weeks before birth). A coronal section is shown on the left; the inset box on the right provides details of the developmental processes. The ventricular zone (VZ) and subventricular zone (SVZ) constitute the germinal matrices where cell division occurs. The first generations of cells are generated in the VZ, the later generations in the SVZ. The SVZ is a structure that expanded during phylogeny; it is especially large in primates. The radial glial cells span their shafts between the germinal layers and the outer layer of the cortex [marginal zone (MZ)]. The first-generation neurons have migrated to the subplate (SP) and participate in the functional fetal cortex; later generations of neurons migrate to the cortical plate (CoP). Figure from Hadders-Algra (2018a), see Luhmann et al. (2018) for a detailed review, obtained by Elsevier (No. 5410821023270) under a creative commons license 3&4.

5-HT produces concentration-opposite effects: during the late phase of neuronal migration, interneurons expressing 5-HT3A receptors that derive from the caudal ganglionic eminence (CGE) respond increasingly to *low* receptor activation in order to migrate radially toward and integrate into the cortical plate. This type of response increases 5-HT3A positive interneuron motility and enhances radial migration and growth cone activity while defining the positioning of their subpopulations (Murthy et al., 2014). Importantly, it further leads to long-lasting changes in the positioning of reelin positive cortical interneurons (Murthy et al., 2014). Likewise, *ex vivo* application of a high 5-HT concentration on cortical slices decreased the migration rate of both GABA and non-GABAergic neurons (Riccio et al., 2011). High 5-HT further resulted in the retraction of GABAergic neuron migration toward the intermediate zone and cortical plate. This effect was largely mediated by the activation of the cAMP signaling pathway through the 5-HT6 receptor (Riccio et al., 2009) while the same behavior was also reported for glutamatergic neurons (Dayer et al., 2015). In general, increased 5-HT levels modify activity-dependent segregation mechanisms during brain development: KO mice lacking the gene encoding the serotonin transporter (SERT) or the monoamine oxidase A (MAOA) exhibit increased 5-HT levels and the segregation of ipsilateral and contralateral regions in dorsal lateral geniculate nucleus (dLGN) does not occur properly (Upton et al., 1999, 2002; Gaspar et al., 2003; García-Frigola and Herrera, 2010).

Serotonin additionally affects the function of CR cells, which are central regulators of cortical development, and especially of dendritic arborization. Arborization is controlled by the secretion of the glycoprotein reelin (Super et al., 2000; Lakatosova and Ostatnikova, 2012), secretion of which is partly regulated by the quantity of 5-HT present in the area (Vitalis et al., 2013). During embryonic development, CR cells receive serotonergic and noradrenergic synaptic inputs (Janusonis et al., 2004), while the catecholaminergic system projects to the forebrain about the same time as the 5-HT system (E11.5 in mice and approximately GW9 in humans) (Kalsbeek et al., 1988, 1990). Around E15 (approximately GW14 in humans), two streams of tyrosine hydroxylase (TH)-positive axons (i.e., TH is a marker for dopamine, norepinephrine, and catecholamine positive neurons, as it is the rate limiting enzyme for dopamine synthesis) from the rostral section of the ventral tegmental area (VTA) enter the PFC, one in the subplate (SP) and the other in the marginal zone (MZ), where the CR cells reside (Bodea and Blaess, 2015).

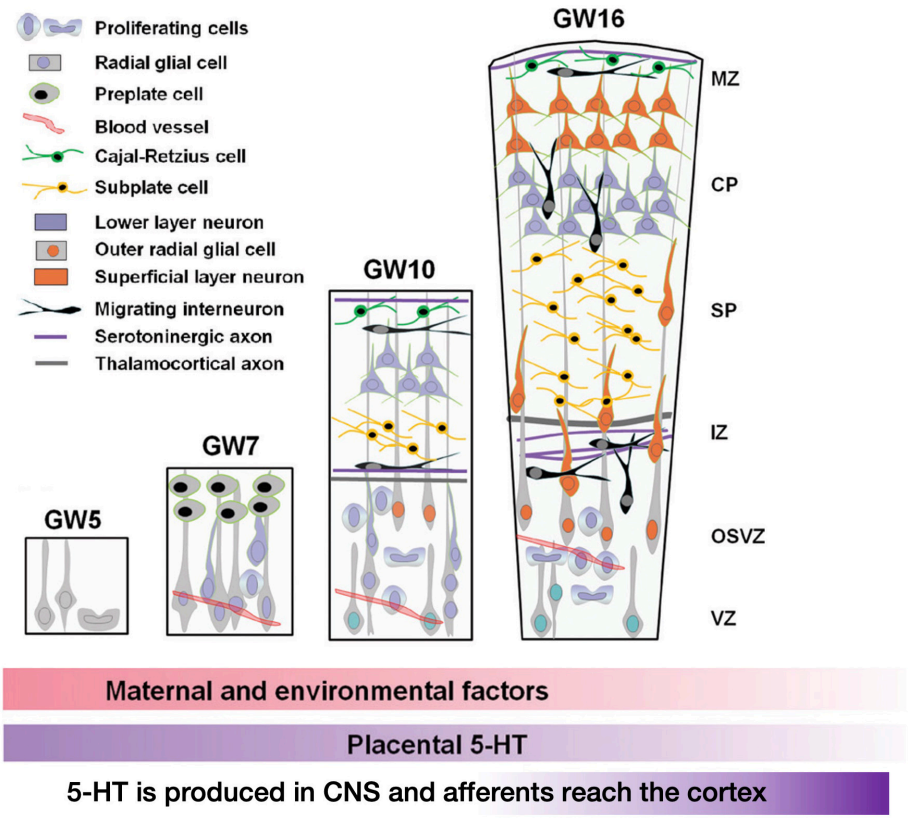

FIGURE 6
Early stages of development of the human cerebral cortex in relation with 5-HT afferents. In human, intense proliferation of the neuroepithelium and formation of the preplate (PP) take place around GW5 and GW6–7, respectively. By GW8–10, PP is split by the migration of the first pyramidal neurons. Cajal-Retzius cells (C-R) will remain in the marginal zone (MZ, presumptive layer I) while sub-plate neurons (SP) will be positioned below the cortical plate (CP). In addition, around GW10, another source of progenitors arises: the outer radial glial (oRG) cells that do not maintain contacts with the apical surface. Monoaminergic axons and thalamo-cortical axons (TC) are already found in the MZ and in the intermediate zone (IZ), respectively. By GW16, SP cells occupy a large proportion of the cortical anlage and oRG are still producing a high number of neurons. Interneurons migrating first tangentially and later radially to the pial surface, incorporate into the CP. The cortical structure is vascularized very early and carries platelets and mast cells that could provide 5-HT to the developing embryo. During the initial phase of cortical development, 5-HT is mainly synthesized in the placenta while later produced by serotonergic neurons of the embryo. The colored lower bars indicate the times at which different factors (maternal and environmental; 5-HT of placental origin, 5-HT produced by the embryo itself) could affect the development (figure from Vitalis and Verney, 2017), obtained by Elsevier (No. 5410821023270) under a creative commons license 3&4.

Within the medial PFC (mPFC), the TH and 5-HT fibers are found in proximity to reelin-secreting CR cells. Altered 5-HT signaling modifies prefrontal cell characteristics, catecholaminergic innervation and cortical integrity (Garcia et al., 2019) suggesting that, during development, there is a functional interplay between 5-HT and catecholaminergic systems that modulates the cellular architecture of the PFC. These two systems have significant structural overlap in the adult brain and appear to receive inputs from each other (Pollak Dorocic et al., 2014). Furthermore, given their active role in higher-order cognitive functioning, there is a clear interplay between the 5-HT and catecholaminergic projections to the PFC (Bortolozzi et al., 2005; Di Giovanni et al., 2008; Niederkofler et al., 2015).

In the mouse, an excess of 5-HT at embryonic day E17.5 (approximately GW17–18 in humans), the period where cortical interneurons and pyramidal neurons migrate to form upper cortical layers, is found to alter their migration in a reversible way (Vitalis et al., 2013). Furthermore, pharmacological perturbation of the 5-HT system by 5-methoxytryptamine, that is a non-selective 5-HT receptor agonist, lowers the levels of reelin that circulate in the blood flow at birth (Janusonis et al., 2004) and results in abnormal microcolumns formation in the presubicular cortex of mice by postnatal day 7. This is a characteristic commonly seen in the brains of ASD patients, along with lower levels of reelin, suggestive of CR cells involvement in the disorder (Fatemi et al., 2005; Lakatosova and Ostatnikova, 2012; Folsom and Fatemi, 2013). Early-life serotonin dysregulation appears to irreversibly impact cortical microcircuit formation and to largely contribute to the occurrence of psychiatric phenotypes.

Serotonin supply to the fetus during the first half of pregnancy mostly relies on exogenous sources, i.e., the placental and maternal platelets that transfer 5-HT from the gut. Serotonin-dependent neurodevelopmental activities, such as corticogenesis and circuitry maturation, coincide with this time frame. As a result, prenatal variables that affect both externally derived and raphe-produced 5-HT content can have a significant impact on the offspring's early brain development (Hanswijk et al., 2020; **Figure 7**). It is interesting to note that the most consistent neurochemical finding reported in ASD affected individuals is a platelet hyperserotonemia, with a 40–70% increase in platelet 5-HT occurring in as many as 30% of autistic subjects (Veenstra-VanderWeele et al., 2002; Janusonis, 2005; Whitaker-Azmitia, 2005; Azmitia et al., 2011).

Maternal inflammation and autism spectrum disorder

Maternal inflammation during pregnancy has an effect on placental function and is linked to an increased risk of neurodevelopmental problems in children. There are indications from epidemiological studies that, during pregnancy, maternal infections by a wide variety of agents, including viruses such as influenza (Shi et al., 2003; Brown et al., 2004) and rubella (Shi et al., 2003; Brown et al., 2004), bacteria (bronchopneumonia; Sørensen et al., 2009), and protozoa (*Toxoplasma gondii*; Brown et al., 2005) increase the risk of schizophrenia or ASD (Grønborg et al., 2013; Zerbo et al., 2015; Meltzer and Van de Water, 2017) in the offspring. This might be reflected in ASD seasonality, associated with a 6% increased risk for children conceived during the winter months (Zerbo et al., 2011).

Moderate immune activation during gestation upregulates tryptophane (TRP) in circulation and its subsequent placental conversion to 5-HT by TRP hydroxylase (TPH). This increases exogenous 5-HT delivery to the fetus and leads to the restriction of 5-HT axonal outgrowth during fetal forebrain development (Goeden et al., 2016). Temperate systemic immune challenge in the mother by the immunostimulant polyriboinosinic-polyribocytidylic acid [Poly (I:C)] (Goeden et al., 2016) rapidly upregulates placental TRP conversion to 5-HT in the mouse, leading to accumulation of exogenous 5-HT within the fetal forebrain, blunting endogenous 5-HT axonal outgrowth specifically (Goeden et al., 2016; Kliman et al., 2018).

Conversely, during intrauterine inflammation, the upregulation of placental indoleamine 2,3-dioxygenase (IDO) shunts tryptophan metabolism away from 5-HT and toward the kynurenine pathway, with neuroactive metabolites being released in fetal circulation (Dharane Neé Ligam et al., 2010). In the fetal brain, kynurenine is converted to kynurenic acid (KA) (Notarangelo et al., 2019), an endogenous antagonist of both NMDA receptors (NMDARs), expressed by SP neurons, and α7-nicotinic receptors expressed by CR cells (Csillik et al., 2002). NMDARs regulate tangential migration in the developing cortex (Ghosh et al., 1990; Csillik et al., 2002) while α7-nicotinic receptors guide the direction of neuronal migration and positioning (Schaefer et al., 2008; Wang S. et al., 2018). In the rabbit, intrauterine inflammation leads to significant upregulation of IDO in the placenta with intense microglial activation and increases in kynurenine acid and quinolinic acid, followed by a significant drop in 5-hydroxyindole acetic acid (a precursor of serotonin) levels in fetal brain's periventricular region at G29 (24 h after treatment) (Williams et al., 2017).

Low grade systemic inflammation is reported to be as high as 25% among US women (Ford et al., 2004), while the gestational period is further subject to maternal inflammation due to numerous phenomena involving fetal genotypes and environmental factors that affect maternal well-being. Maternal infection and/or increased 5-HT supply to the developing fetus during pregnancy, while clearly promoting ASD pathogenesis, is only associated with higher risk of autism and not with overt ASD pathogenesis (Zerbo et al., 2015; Brucato et al., 2017; Guisso et al., 2018). However, it is also clear that increased 5-HT supply to the developing fetus cannot, by itself, be the main inflammatory-associated factor that could be implicated in ASD pathogenesis. Indeed, many other inflammatory mediators, such as the interferons, various interleukins, TGF-β, TNF-α, and β, etc., can reach fetal circulation from the placenta and have been shown to significantly affect brain development during gestation (Wei et al., 2013; Theoharides et al., 2016; Tsivion-Visbord et al., 2020). Furthermore, various studies suggest that the neurodevelopmental consequences of maternal inflammation are depended on the type of the ongoing infection, the gestational time at which the inflammatory reaction starts, its intensity and its duration (for example, see Boksa, 2010). The placenta may react to maternal inflammation with sexually dimorphic consequences for fetal development (Clifton, 2005; Mueller and Bale, 2008) while testosterone surges in newborn males can alter long-term CNS function (Forgie and Stewart, 1993; Wilson and Davies, 2007).

Columnar structure of the neocortex: Typical development versus autism spectrum disorder

As described above, during neurogenesis, newly generated projection neurons migrate along radial glial fibers from the ventricular layers toward the outer, pial surface, giving rise to a modular organization in which cell bodies in the neocortex are 'stacked' on top of one other to construct so-called minicolumns. They consist of vertical chains of approximately 80–100 neurons between cortical layers II–VI, with associated dendrites and

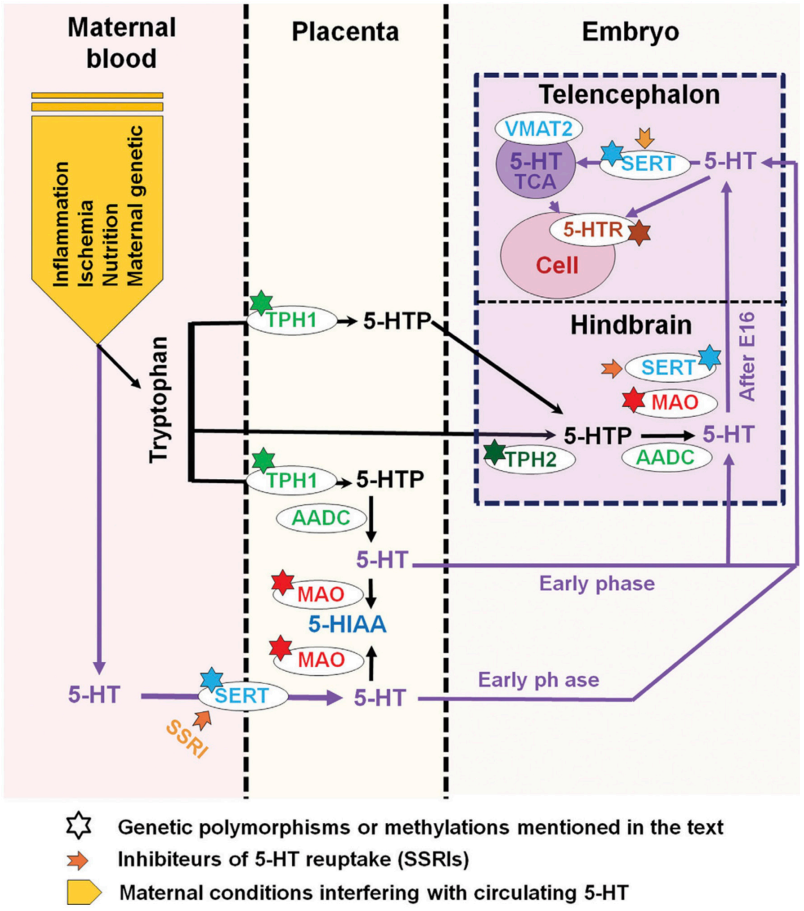

FIGURE 7
Maternal, placental, genetic, and pharmacological conditions determining the amount of serotonin supply to the developing telencephalon. The placenta provides tryptophan to the embryo but can also convert it into 5-HTP (5-hydroxytryptamine) or further into serotonin (5-HT) via various maternal metabolic enzymes. In addition, 5-HT from maternal sources could be taken up by the placenta where the serotonin transporter (SERT) is also expressed. During early embryonic stages, 5-HT could thus be directly delivered to the developing embryo. In the mouse, after E15-E16 (approximately GW 16 in humans), when 5-HT axons of the hindbrain reach the cortex, 5-HT could act on various target cells expressing selected arrays of 5-HT receptors. At this stage, 5-HT could also be taken up and stored by thalamocortical afferents (TC) and released after specific stimulation. In addition, 5-HTP is provided by Tph2 (tryptophan hydroxylase type 2) and AADC (aromatic amino acid decarboxylase) containing neurons that synthetize 5-HT. The large downward arrow on the left in this diagram, adapted from Bonnin and Levitt (2011), points to the maternal conditions that are best known to interfere with 5-HT availability to the embryo. Inhibitors of 5-HT uptake (SSRIs) which affect SERT function at all levels are indicated by a thick orange arrow while known genetic polymorphisms or epigenetic alterations (methylations) which impact serotonin supply are indicated by a star. The major catabolic enzymes of 5-HT are MAO (monoamine oxidases) and tryptophan hydroxylase type 1 (Tph1). Adapted from Bonnin and Levitt (2011) and Vitalis and Verney (2017), obtained by Elsevier (No. 5410821023270) under a creative commons license 3&4.

bundles of myelinated axons. They serve as the basis for cortical information processing by allowing thalamic inputs to be combined with corticocortical processing and thus provide modulatory inputs to incorporate behavioral context into sensory processing (Opris and Casanova, 2014; McKavanagh et al., 2015). The final spacing of these minicolumns is determined by the density of glial scaffolds during development (**Figure 8**).

In ASD affected individuals, there is apparent focal disorganization, with the minicolumns being spaced farther apart with a lower cell density in a given region of cortex (Donovan and Basson, 2017) (**Figure 9**). Although the effect appears to affect higher order association areas most significantly, a 6–10% difference in minicolumn width is observed across all cortical regions (Casanova et al., 2006; McKavanagh et al., 2015; Donovan and Basson, 2017).

This phenomenon suggests anatomical misplacement of the reelin secreting CR cells which provide the positioning cues to the developing cortical neurons and afferents. Hence, while the normotopic position of reelin is important for proper neuronal migration and positioning, leading to their characteristic lamination, it does not affect radial glial elongation (Schaefer et al., 2008; Wang S. et al., 2018). As exposed above, 5-HT regulates the physiology of CR cells through transient synaptic

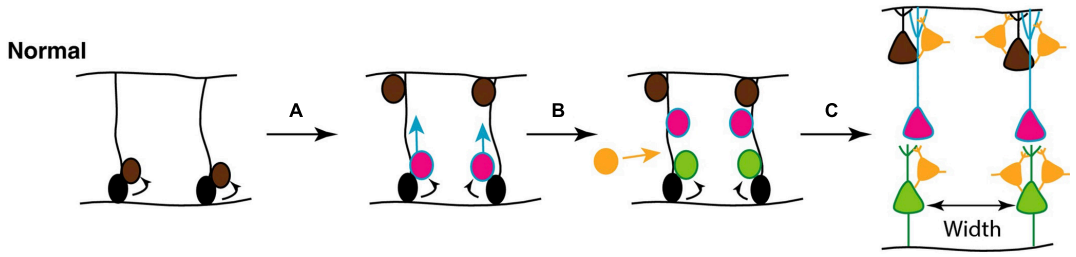

FIGURE 8
(A) Mechanisms underlying focal organization and minicolumn distribution in the cortex. During normal cortical development, radial glial neural stem and progenitor cells (NSCs; black) located in the ventricular zone, with radial processes extending to the pial surface of the neural epithelium, can undergo symmetrical divisions to produce more radial glial NSCs (brown) or asymmetric divisions **(A)** to maintain the NSC pool and generate committed neural progenitors (pink); **(B)** the latter migrate toward the pial surface on the radial scaffold, where they differentiate into projection neurons. This process continues with different classes of neurons (pink, green) being produced in successive waves over developmental time. Hence, different neuronal types are grouped together in different cortical layers **(C)**. GABAergic interneurons (orange) migrate into the neuroepithelium **(B)**, and integrate into the circuitry **(C)**. At the end of this process, projection neurons are organized in radial minicolumns. Figure adapted from Donovan and Basson (2017), obtained by Elsevier (No. 5410821023270) under a creative commons license 3&4.

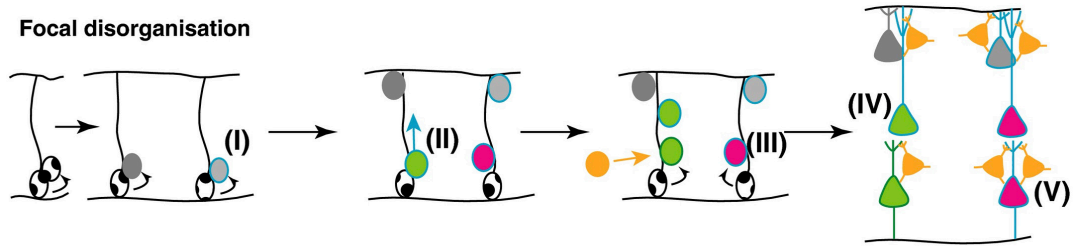

FIGURE 9
Potential mechanisms underlying focal disorganization and altered minicolumn distribution in ASD cortex. Focal disruptions may be the result of a combination of early genetic, epigenetic changes or environmental changes affecting neural stem and progenitor cell such that the resulting neuronal progenitors have defects in **(I)** differentiation **(II)** or migration **(III)** causing them to adopt the wrong fate **(IV)**, or end up in an in appropriate position in the brain **(V)**. The end result is a cortex with apparent disorganization of neuronal cell types and distorted cell densities. Figure adapted from Donovan and Basson (2017), obtained by Elsevier (No. 5410821023270) under a creative commons license 3&4.

contacts with serotoninergic projections, while reelin secretion is regulated in part by the amount of brain 5-HT (Janusonis et al., 2004). Hence, one of the neuroanatomical phenomena that characterize ASD cortical structures, namely disorganized and altered cortical minicolumn distribution, appears to find its roots very early during fetal brain development, possibly as a result of excess 5-HT and/or kynurenine supply to the developing fetus. This may arise subsequently to a sustained low-level maternal inflammatory reaction during a critical developmental window starting around GW9-10 and probably extending to GW20 (see **Figure 9**).

Dendritic and synaptic development

Dendrite development progresses through dendritic arborization and spine growth. The dendrites protrude from the cell body as individual processes. Their development begins prenatally in humans, and continues for about 2 years postnatally, with different phases of synaptic density being detected in the cerebral cortex of primates. The first phases, which occur during early embryonic development, generate low density synapses. Then, synapse number progresses rapidly until nearly the 2nd year of age. Moving forward, the number of synapses reaches a plateau, followed by a rapid synapses elimination phase which continues through adolescence. The last phase is characterized by a new plateau in synapse number in adulthood, followed by a drop through aging. The initial synapse reduction period is acute, dropping to 50% of the number present at 2 years of age through synaptic pruning (**Figure 10**).

Serotonin and post-natal synaptic pruning: Synaptic pruning defects in autism spectrum disorder

Proper synaptic pruning during postnatal development is essential for the development of functional neuronal circuits. When the synaptic pruning process is impaired, the excitatory

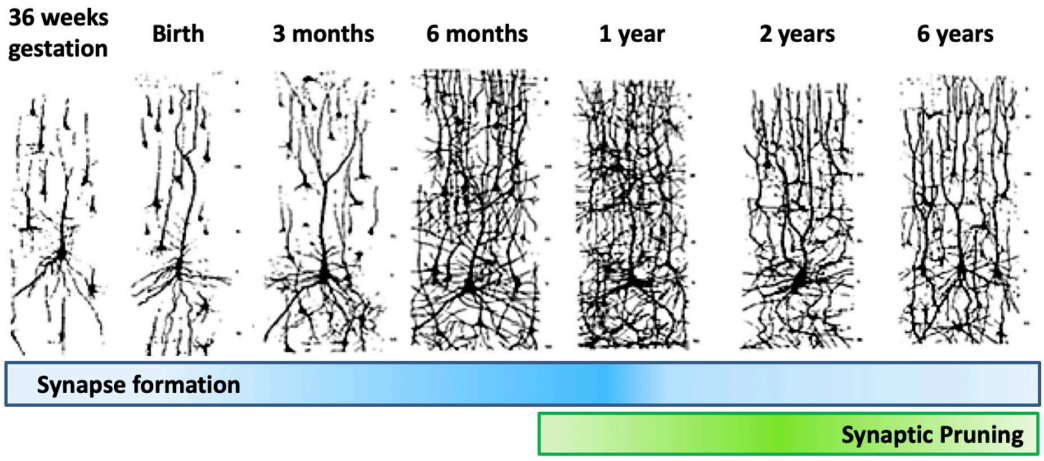

FIGURE 10
Synapse formation and pruning in neurotypical development. Starting from birth until adolescence, the synaptic pruning process, preceded by synaptic overgrowth, optimizes the neurological network by removing redundant and weak connections as defined by the learning process, effectively making the brain more efficient. Adults have been found to have approximately 41% fewer neurons than newborns (Abitz et al., 2007). Figure adapted from Conel (1939), obtained by Elsevier (No. 5410821023270) under a creative commons license 3&4.

versus inhibitory balance (E/I balance) of synapses is disrupted, and this may cause neurodevelopmental disorders such as ASD. The process of synaptic pruning is mostly handled by microglial cells that are -in general- adept to promote neuronal death and clear apoptotic cells (Mallat et al., 2005). During brain development, they are the key players in the elimination of redundant and weak synapses, thus ensuring the proper wiring of neuronal networks. They engulf inappropriate and less active synapses through microglial autophagy, achieving synaptic refinement and neuro-behavioral regulation through selective reshaping of axonal and dendritic arborizations (Paolicelli et al., 2011; Paolicelli and Gross, 2011; Koyama and Ikegaya, 2015). The process appears to involve the neuronal chemokine fractalkine and the CX3CR1 microglial receptor for microglia recruitment and activation (Sheridan and Murphy, 2013). Serotonin is also involved both directly and indirectly in this developmental process (Okado et al., 2001; Serfaty et al., 2008; Penedo et al., 2009; Lesch and Waider, 2012). Activation of 5-HT receptors promotes microglial injury-induced motility but attenuates phagocytic activity (Krabbe et al., 2012). Indeed, postnatal microglia from mice lacking the 5-HT2B receptor ($Htr2B^{-/-}$) are unable to reach serotonergic synaptic boutons, unlike microglia from wild-type mice (Krabbe et al., 2012). This was confirmed prepartum in the *in vivo* developmental model of dLGN synaptic refinement where $Htr2B^{-/-}$ mice had anatomical alterations of retinal projections into the thalamus (Kolodziejczak et al., 2015).

Serotonin also indirectly influences the synaptic pruning process. 5-HT overstimulation during *in utero* development result in misplacement of apical dendrites with respect to the post-natal source of reelin (CR cells) and abnormal cortical microcolumns formation. This culminates in both apical dendrites' exuberance (preservation due to distancing from the source of reelin) and excessive pruning as a consequence of close contact with the source of reelin, depending on the local forms of earlier neuronal migration patterns dysregulations (**Figure 11**).

During the first two decades of life, where synaptic pruning is active, cortical thickness (CT) is likely to represent dendritic arborization. As a result, CT maturational alterations are mostly related to dendritic pruning. However, in autistic individuals, there is a dramatic increase in dendritic growth during the first year of life, while the synaptic pruning process happens to a far lower degree, with a large number of "redundant" connections remaining intact. By 2 years of age, the minicolumns are spaced farther apart with a lower cell density in the cortex. The space between minicolumns is occupied by dendritic bundles and axonal fascicles that extend into multiple layers of the cortex. By late childhood spine density of neurons drops by 50% in TD brain, whereas by only about 16% in ASD brains, negatively impacting signal-to-noise discrimination (Tang et al., 2014; Lieberman et al., 2019). This is reflected by the slower rate of cortical thinning between infancy and adolescence in ASD compared to TD, with an increased thinning in late adolescence, whereas in TD, thinning occurs around puberty and early adulthood (Nunes et al., 2020).

Abnormal pruning is further corroborated by the reduced level of reelin (Reln) and Dab 1 (reelin signal transducer) proteins and mRNA levels in frontal and cerebellar, and non-significantly in parietal, areas of autistic brains compared to control subjects. Accordingly, the mRNA for the reelin receptor (VLDLR) is found significantly elevated in superior frontal and cerebellar areas of autistic brains compared to controls (Fatemi et al., 2005; Kelemenova and Ostatnikova, 2009).

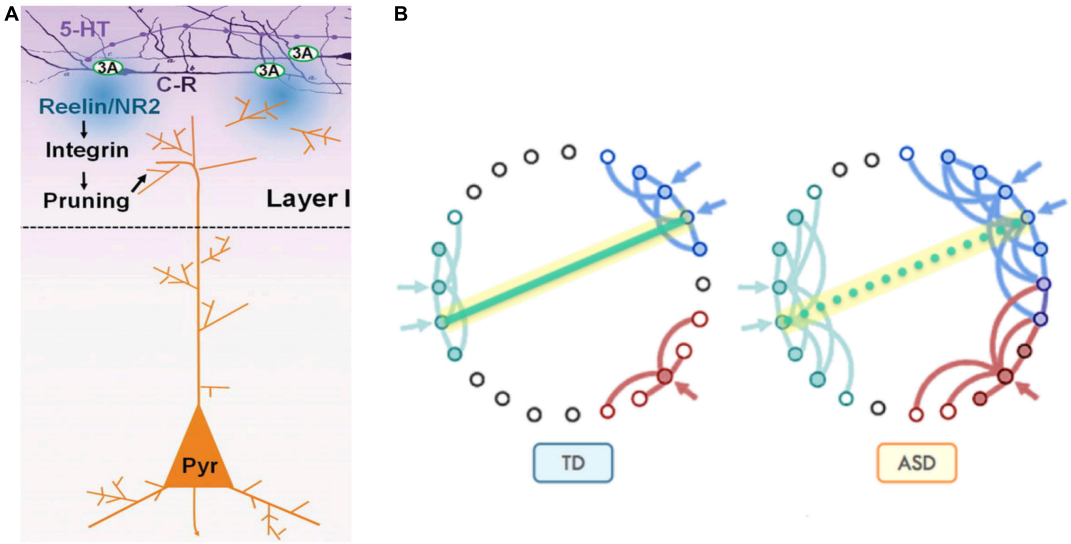

FIGURE 11
(A) Synaptic pruning in brain development serves to refine communication between functional areas by improving the signal-to-noise ratio. At early postnatal stage, Cajal-Retzius cells (C-R) that express 5-HT3A, respond to 5-HT by releasing reelin which, through the activation of the integrin signaling pathway, induces pruning of apical dendrites of pyramidal neurons (Pyr). **(B)** Pruning reduces unnecessary cross-talk with neighboring nodes (blue and red in typical development, Panel TD). However, in the presence of too many overlapping connections, distinct signals from neighboring communities may compete and interfere with each other, effectively creating noise and "confusion" within the network (blue and red in autism spectrum disorder, Panel ASD), while negatively affecting the development of long-distance connectivity, such as those between fronto-parietal regions for higher-order executive functions [adapted from Belmonte et al. (2004), Just et al. (2012), and Vitalis and Verney (2017)], obtained by Elsevier (No. 5410821023270) under a creative commons license 3&4.

Because the cortex is heavily implicated in autistic behaviors, a lack of synaptic pruning in this area will have an impact on the severity of autistic behaviors, as well as on the loss of abilities. Therefore, dysregulation of post-natal synaptic pruning as a result of neuronal migration patterns alterations during the key stages of cerebral cortex early development (between week postnatal WP8 and WP20) stands to result in a huge variety of forms and degrees of signal-over-noise (S/N) discrimination losses, thereby accounting for the enormous clinical heterogeneities encountered in a variety of neurodevelopmental cognitive disorders, prominent amongst which is ASD.

RNA editing mechanisms and epigenetic traits

It is important to stress that while the neuro-anatomical characteristics of ASD may, possibly, be induced by changes in exogenous 5-HT/kynurenine supply, individual susceptibility could be best explained either through epigenetic marking alterations, or dysregulated RNA editing mechanisms. While epigenetic markings may directly affect the relative expression levels of individual genes or groups of genes, they however, require environmental conditions to stay stable long enough to have real physiological effects. Therefore, their relative weight compared to RNA editing mechanisms during brain development is expected to be secondary. RNA editing, in association with both genotypes and environmental conditions, could alter spatiotemporal proteins expression patterns at both quantitative and qualitative levels, in a tissue-specific and context-dependent manner.

As 5-HT signaling is dependent on numerous receptors, transporters, enzymes, other neurotransmitters, and associated genes, a single gene or a cluster of genes cannot account for the consequences related to 5-HT fluctuations. The 5-HT system contains multiple classes of receptors (5-HT1–5-HT7) and related subtypes, some of which present allelic variations that influence receptor function and availability (e.g., 5-HT1A; Parsey et al., 2006), while others are subject to combinatorial mRNA editing, which affects not only receptor and ion channels function and availability, but also expression patterns (e.g., 5-HT2C; Eran et al., 2013). Extensive RNA editing, comprising site-dependent, selective splicing alterations, polyA-tails deadenylation and adenosine-to-inosine (A-to-I) RNA editing (Richter, 2007; Raj and Blencowe, 2015; Behm et al., 2017), takes place in the brain, and a developmentally increasing editing pattern from fetal to adult samples has been reported. This increase in A-to-I editing pattern was associated temporally with the growth of cortical layers and with neuronal maturation (Hwang et al., 2016). Furthermore, allelic variants encoding proteins such as SERT (SLC6A4; transports serotonin from

synaptic spaces into presynaptic neurons and terminates serotonin activity; the S-allele is particularly important for ASD; Brummelte et al., 2017) and CPEB4 (which governs mRNA polyA-tails dynamics) as well as allelic variants of ADAR1 and 2 (which govern A-to-I RNA editing) can significantly affect brain development, both in a positive as well as a negative manner[1]. Indeed, CPEB4 binds to the transcripts of most high-confidence ASD-risk genes (Parras et al., 2018), while A-to-I RNA editing addresses neuronal receptors and channels organization (Streit and Decher, 2011). The latter mostly affects glutamate and voltage-gated ion channels, GABAA and serotonin 2C receptors, filamins and actin organization, while inducing changes in miRNA profiling that affect dendritic spine density, neuronal organization and synaptic transmission by altering the interaction profiles with binding partners (Scadden and Smith, 2001). The detailed results of our work on the impact of RNA editing mechanisms in the pathogenesis of ASD will be the subject of a specific publication.

The likely consequences of defective post-natal synaptic pruning: Focus on the autonomic nervous system

Defects in synaptic pruning may well underlie the variability in S/N, represented by the long-distance underconnectivity and local overconnectivity observed in ASD patients (Courchesne and Pierce, 2005; Anderson et al., 2011; Keown et al., 2013), while also accounting for the large heterogeneity between individuals and age groups.

The exuberance of thin axons that travel short to medium distances in autism, as observed in areas underlying the prefrontal limbic areas, alters the S/N threshold and could 'scramble' long-distance communication signals. This connectivity bias could provide the anatomical basis for the disrupted transmission of emotion signals and help explain why people with autism have difficulty shifting attention and engage in inflexible and repetitive behaviors (Luna et al., 2002; Thakkar et al., 2008; Zikopoulos and Barbas, 2010). Among the areas that appear to be most affected by reduced functional connectivity are the right posterior inferior temporal gyrus, fusiform gyrus and bilateral inferior occipital cortex, which are related to facial recognition, a function often affected in ASD (Long et al., 2016).

Losses in S/N discrimination could also explain the alterations in auditory processing in ASD. Post-mortem studies have revealed that the density of dendritic spines in the temporal lobe is higher in ASDs than in TDs, showing a large age variability within the ASD group (Hutsler and Zhang, 2010). This variability, which probably depends on internal noise levels, both within and between individuals, could be representative of the process of synaptic pruning that relies on prior neuronal migration patterns.

In addition, individuals with ASD are often prone to hyper- or hypo-sensitivity to sound, light and texture, both of which fluctuate from birth to adolescence (Park et al., 2017). This is likely to be reflected in differences in speech-VS-noise discrimination in people with ASD, who are often able to show superior performance in simple psychoacoustic tasks, such as pitch memory and discrimination tasks, while being poor in tasks that require complex auditory processing, such as speech intonation, prosody, and visual-auditory integration (O'Connor, 2012; Dunlop et al., 2016).

Furthermore, ASD-affected individuals exhibit autonomic nervous system (ANS) functioning abnormalities, a common neuro-anatomical alteration underlying ASD. Over-activation of the sympathetic branch of the ANS due to ASD-specific parasympathetic activity deficit, may in turn induce deregulation of the gut-brain axis, thus attenuating intestinal immune and osmotic homeostasis (Beopoulos et al., 2021). The reason for this could be understood in terms of the different connectivity of the two branches of the ANS to the CNS.

The main inputs to the parasympathetic system, which exhibits activity deficit in ASD, originate mainly from limbic forebrain and cortical structures (orbital frontal gyri, cingulate cortex, thalamus, hypothalamus, amygdala, hippocampus). In this system, inputs from nerve X (vagus) connect to cardiac and smooth muscles, to the gastrointestinal tract and to secretory glands in lungs and viscera. In contrast, the main inputs to the sympathetic system, which doesn't exhibit any activity deficit in ASD, originate from thoracic (vertebrae T1-L2) and sacral (vertebrae T1-L2) spinal cord. In this system, inputs from the sacral components connect, via the pelvic nerves, to smooth muscles, secretory glands in the lower gastrointestinal tract and to pelvic viscera.

Dysregulation of post-natal synaptic pruning and the ensuing losses of signal-over-noise discrimination are thus likely to affect the parasympathetic branch more directly and profoundly than the sympathetic branch. This is exemplified in pathological settings such as acute coronary artery disease, where psychological and bio-behavioral factors during the course of daily lives can provoke acute coronary events in individuals who do not fit the traditional high-risk profile for coronary artery disease (Ruberman et al., 1984). During mental stress, subcortical regions related with memory, emotion, and neuro-hormonal sympathetic control are activated. Instead, the frontal evaluative regions, such as the dorsal lateral prefrontal cortex associated with parasympathetic tone, are mostly deactivated.

Here, mental stress-mediated activation of visceral effectors from the CNS promotes parasympathetic withdrawal (HRV) and accentuation of sympathetic tone (norepinephrine) (Soufer et al., 2009) with subsequent β-adrenergic activation maintaining the autonomic imbalance (Brindle et al., 2014).

1 https://databases.lovd.nl/shared/variants/ADAR

The autonomic nervous system and gut homeostasis

The connectivity between the ANS and the immune system play important roles in controlling homeostasis and immune function of the gut. The sympathetic innervation secretes neurotransmitters that influence immune cells and the inflammatory response upon vagus nerve stimulation. By fine-tuning the interaction between the ENS and mucosal immune cells, the gut microbiota plays a role in the response (Bernardazzi et al., 2016; Beopoulos et al., 2021). ANS functioning abnormalities observed in association with ASD (sympathetic over-activation on a background of parasympathetic activity deficits) are very likely to affect neuro-immune interactions, resulting in the decreased secretion of bactericidal peptides and metabolites from Paneth cells, goblet cells and intestinal mucosal surfaces phagocytes, such as macrophages, which coexist with microbial communities (Peck et al., 2017), via an attenuation of autonomically mediated (Furness, 2016) stimulation of exosomal secretion (Fleshner and Crane, 2017) from colonic mucosa (Xu et al., 2016; Willemze et al., 2019), perhaps together with decreased lectins secretion (Pang et al., 2016). This stands to favor the loss of commensal microbial populations while concurrently dysregulating luminal ionic and water homeostasis, thus resulting in the highly heterogeneous and polymorphic dysbiosis concurrently with the unusually high incidences of gastrointestinal dysfunctions observed in association with ASD (Sgritta et al., 2019). These ANS functioning abnormalities apparently develop as a direct consequence of the dysregulations in early brain development and neuroglial migration patterns described above. It could then be maintained by the ensuing losses of signal-over-noise discrimination and subsequent chronic mental stress, as strongly suggested by the typically mental stress -associated comorbidities most frequently associated with autism (anxiety and depressive disorders, sleep problems, etc.). Furthermore, these ANS functioning abnormalities also adequately explain the origins of ASD-associated dysbiosis and the reasons for its persistence through a self-sustaining vicious circle whereby dysbiosis maintains dysregulated gut homeostasis which, in turn, maintains ANS functioning abnormalities which, in turn, maintains dysbiosis (Beopoulos et al., 2021).

It is important to note that defective synaptic pruning is also a hallmark of other neurodevelopmental disorders, although with different outcomes. Excessive pruning in all brain regions is associated with a loss of gray matter volume and is mainly related to schizophrenia, while extensive pruning in certain brain regions is associated with bipolar disorder. In contrast, ASD is mainly associated with defective pruning and increased white and gray matter volume, at least until adolescence. This could indicate differential patterns of neuronal migration occurring in different developmental windows during gestation, which could also depend on sudden changes in environmental conditions, inflammation and RNA editing. It is important to note that while schizophrenia and bipolar disorder are linked to low-grade systemic inflammation, there is no conclusive evidence for systemic inflammation in ASD (Dipasquale et al., 2017; Rosenblat and McIntyre, 2017; Osimo et al., 2018).

Discussion/conclusion

The model presented here is rooted in very early neurogenesis and neuronal migration and, while it does not pretend to incorporate all the likely causes of ASD, it does highlight the conditions and developmental window where alterations in neural development can have major effects on a wide range of symptoms.

Neuronal migration patterns during cerebral cortex formation are largely governed by a combination of genetic, epigenetic and early environmental conditions that may well explain the focal disruption of cortical laminar architecture observed in ASD. The early presence of 5-HT in the brain, as well as its heterologous uptake throughout critical developmental periods, suggest its importance during early steps of brain development and wiring. Maternal low grade systemic inflammation particularly during early and mid-pregnancy, appears to be a major determinant for significantly increased risk of ASD pathogenesis. Sudden changes in environmental conditions, such as an over-supply of serotonin and/or kynurenine to the developing fetus, subsequently to a sustained low-level maternal inflammatory reaction, during a critical developmental window starting between GW8 and GW9 and probably extending to GW20, are likely to promote ASDs pathogenesis during fetal brain development. However, fluctuations in 5-HT are not sufficient to explain the prevalence of ASD, and individual susceptibility is therefore better explained by RNA editing mechanisms than by epigenetic mechanisms that require stable environmental conditions to act. Therefore, in order to provoke the cortical network disorganizations which will give rise to ASD pathogenesis, changes in central 5-HT levels during developmentally sensitive periods of brain development will probably have to occur in conditions where fetal genotypes, such as the S allele for the SLC6A4 gene in combination with CPEB4 and/or ADARs allelic variants would favor vulnerability over plasticity outcomes.

Postnatally, dysregulation of synaptic pruning as a result of neuronal migration patterns alterations during the key stages of cerebral cortex early development (between WP10 and WP30) stands to result in a huge variety of forms and degrees of signal-over-noise discrimination losses, thereby accounting for the enormous clinical heterogeneities encountered in autism, including ANS-associated functioning abnormalities. These are characterized by an over-activation of the sympathetic branch on a background of the parasympathetic activity deficits, which in turn,

induces the deregulation of the gut-brain axis resulting in the maintenance of a persistent dysbiotic state that, in turn can negatively influence the gut-brain axis coordination. These phenomena may very well explain the enormous genetic and symptomatic heterogeneities that are systematically associated with ASD as well as the comorbidities most frequently associated with the pathology (anxiety and depressive disorders, sleep problems, gastrointestinal dysfunctions, etc.).

Data availability statement

The original contributions presented in this study are included in the article/supplementary material, further inquiries can be directed to the corresponding author.

Author contributions

FI: conceptualization and methodology. MG: software and project administration. FI, AB, MG, and AF: validation and resources. FI and AB: formal analysis, investigation, data curation, and writing—original draft preparation. FI, AB, and AF: writing—review and editing. All authors read and agreed to the published version of the manuscript.

Funding

This research was funded by the European Union's Horizon 2020 Research and Innovation Program GEMMA under grant agreement number: 825033. Please see http://www.gemma-project.eu for more information.

Conflict of interest

AB, MG, and FI were employed by the company Bio-Modeling Systems.

The remaining authors declare that the research was conducted in the absence of any commercial or financial relationships that could be construed as a potential conflict of interest.

Publisher's note

References

Abitz, M., Nielsen, R. D., Jones, E. G., Laursen, H., Graem, N., and Pakkenberg, B. (2007). Excess of neurons in the human newborn mediodorsal thalamus compared with that of the adult. *Cereb. Cortex* 17, 2573–2578. doi: 10.1093/cercor/bhl163

Abot, A., Cani, P. D., and Knauf, C. (2018). Impact of intestinal peptides on the enteric nervous system: Novel approaches to control glucose metabolism and food intake. *Front. Endocrinol. (Lausanne)* 9:328. doi: 10.3389/fendo.2018.00328

Adnani, L., Han, S., Li, S., Mattar, P., and Schuurmans, C. (2018). Mechanisms of cortical differentiation. *Int. Rev. Cell Mol. Biol.* 336, 223–320. doi: 10.1016/bs.ircmb.2017.07.005

Anderson, J. S., Druzgal, T. J., Froehlich, A., DuBray, M. B., Lange, N., Alexander, A. L., et al. (2011). Decreased interhemispheric functional connectivity in autism. *Cereb. Cortex* 21, 1134–1146. doi: 10.1093/cercor/bhq190

Avino, T. A., Barger, N., Vargas, M. V., Carlson, E. L., Amaral, D. G., Bauman, M. D., et al. (2018). Neuron numbers increase in the human amygdala from birth to adulthood, but not in autism. *Proc. Natl. Acad. Sci. U.S.A.* 115, 3710–3715. doi: 10.1073/pnas.1801912115

Azmitia, E. C., Singh, J. S., Hou, X. P., and Wegiel, J. (2011). Dystrophic serotonin axons in postmortem brains from young autism patients. *Anat. Rec. (Hoboken)* 294, 1653–1662. doi: 10.1002/ar.21243

Barbas, H. (2000). Complementary roles of prefrontal cortical regions in cognition, memory, and emotion in primates. *Adv. Neurol.* 84, 87–110.

Barbas, H., and García-Cabezas, M. (2016). How the prefrontal executive got its stripes. *Curr. Opin. Neurobiol.* 40, 125–134. doi: 10.1016/j.conb.2016.07.003

Barber, M., and Pierani, A. (2016). Tangential migration of glutamatergic neurons and cortical patterning during development: Lessons from Cajal-Retzius cells. *Dev. Neurobiol.* 76, 847–881. doi: 10.1002/dneu.22363

Barkovich, A. J., Kuzniecky, R. I., Jackson, G. D., Guerrini, R., and Dobyns, W. B. (2005). A developmental and genetic classification for malformations of cortical development. *Neurology* 65, 1873–1887. doi: 10.1212/01.wnl.0000183747.05269.2d

Behm, M., Wahlstedt, H., Widmark, A., Eriksson, M., and Öhman, M. (2017). Accumulation of nuclear ADAR2 regulates adenosine-to-inosine RNA editing during neuronal development. *J. Cell Sci.* 130, 745–753. doi: 10.1242/jcs.200055

Belmonte, M. K., Allen, G., Beckel-Mitchener, A., Boulanger, L. M., Carper, R. A., and Webb, S. J. (2004). Autism and abnormal development of brain connectivity. *J. Neurosci.* 24, 9228–9231. doi: 10.1523/jneurosci.3340-04.2004

Beopoulos, A., Gea, M., Fasano, A., and Iris, F. (2021). Autonomic nervous system neuroanatomical alterations could provoke and maintain gastrointestinal dysbiosis in autism spectrum disorder (ASD): A novel microbiome-host interaction mechanistic hypothesis. *Nutrients* 14:65. doi: 10.3390/nu14010065

Bernardazzi, C., Pego, B., and de Souza, H. S. (2016). Neuroimmunomodulation in the gut: Focus on inflammatory bowel disease. *Mediators Inflamm.* 2016:1363818. doi: 10.1155/2016/1363818

Bernier, P. J., Vinet, J., Cossette, M., and Parent, A. (2000). Characterization of the subventricular zone of the adult human brain: Evidence for the involvement of Bcl-2. *Neurosci. Res.* 37, 67–78. doi: 10.1016/s0168-0102(00)00102-4

Bocchio, M., McHugh, S. B., Bannerman, D. M., Sharp, T., and Capogna, M. (2016). Serotonin, Amygdala and fear: Assembling the puzzle. *Front. Neural Circuits* 10:24. doi: 10.3389/fncir.2016.00024

Bodea, G. O., and Blaess, S. (2015). Establishing diversity in the dopaminergic system. *FEBS Lett.* 589(Pt 24), 3773–3785. doi: 10.1016/j.febslet.2015.09.016

Boksa, P. (2010). Effects of prenatal infection on brain development and behavior: A review of findings from animal models. *Brain Behav. Immun.* 24, 881–897. doi: 10.1016/j.bbi.2010.03.005

Bonnin, A., and Levitt, P. (2011). Fetal, maternal, and placental sources of serotonin and new implications for developmental programming of the brain. *Neuroscience* 197, 1–7. doi: 10.1016/j.neuroscience.2011.10.005

Bortolozzi, A., Díaz-Mataix, L., Scorza, M. C., Celada, P., and Artigas, F. (2005). The activation of 5-HT receptors in prefrontal cortex enhances dopaminergic activity. *J. Neurochem.* 95, 1597–1607. doi: 10.1111/j.1471-4159.2005.03485.x

Brindle, R. C., Ginty, A. T., Phillips, A. C., and Carroll, D. (2014). A tale of two mechanisms: A meta-analytic approach toward understanding the autonomic basis of cardiovascular reactivity to acute psychological stress. *Psychophysiology* 51, 964–976. doi: 10.1111/psyp.12248

Brown, A. S., Begg, M. D., Gravenstein, S., Schaefer, C. A., Wyatt, R. J., Bresnahan, M., et al. (2004). Serologic evidence of prenatal influenza in the etiology of schizophrenia. *Arch. Gen. Psychiatry* 61, 774–780. doi: 10.1001/archpsyc.61.8.774

Brown, A. S., Schaefer, C. A., Quesenberry, C. P. Jr., Liu, L., Babulas, V. P., and Susser, E. S. (2005). Maternal exposure to toxoplasmosis and risk of schizophrenia in adult offspring. *Am. J. Psychiatry* 162, 767–773. doi: 10.1176/appi.ajp.162.4.767

Brucato, M., Ladd-Acosta, C., Li, M., Caruso, D., Hong, X., Kaczaniuk, J., et al. (2017). Prenatal exposure to fever is associated with autism spectrum disorder in the Boston birth cohort. *Autism Res.* 10, 1878–1890. doi: 10.1002/aur.1841

Brummelte, S., Mc Glanaghy, E., Bonnin, A., and Oberlander, T. F. (2017). Developmental changes in serotonin signaling: Implications for early brain function, behavior and adaptation. *Neuroscience* 342, 212–231. doi: 10.1016/j.neuroscience.2016.02.037

Buznikov, G. A., Lambert, H. W., and Lauder, J. M. (2001). Serotonin and serotonin-like substances as regulators of early embryogenesis and morphogenesis. *Cell Tissue Res.* 305, 177–186. doi: 10.1007/s004410100408

Bystron, I., Blakemore, C., and Rakic, P. (2008). Development of the human cerebral cortex: Boulder committee revisited. *Nat. Rev. Neurosci.* 9, 110–122. doi: 10.1038/nrn2252

Cadwell, C. R., Bhaduri, A., Mostajo-Radji, M. A., Keefe, M. G., and Nowakowski, T. J. (2019). Development and arealization of the cerebral cortex. *Neuron* 103, 980–1004. doi: 10.1016/j.neuron.2019.07.009

Call, C. L., and Bergles, D. E. (2021). Cortical neurons exhibit diverse myelination patterns that scale between mouse brain regions and regenerate after demyelination. *Nat. Commun.* 12:4767. doi: 10.1038/s41467-021-25035-2

Casal, M. A., and Romano, S. (1978). [Hydrodynamic and radiologic examination of the common bile duct]. *Acta Gastroenterol. Latinoam.* 8, 109–119.

Casanova, M. F., van Kooten, I. A., Switala, A. E., van Engeland, H., Heinsen, H., Steinbusch, H. W., et al. (2006). Minicolumnar abnormalities in autism. *Acta Neuropathol.* 112, 287–303. doi: 10.1007/s00401-006-0085-5

Cauvet, E., Van't Westeinde, A., Toro, R., Kuja-Halkola, R., Neufeld, J., Mevel, K., et al. (2019). Sex differences along the autism continuum: A twin study of brain structure. *Cereb. Cortex* 29, 1342–1350. doi: 10.1093/cercor/bhy303

Clifton, V. L. (2005). Sexually dimorphic effects of maternal asthma during pregnancy on placental glucocorticoid metabolism and fetal growth. *Cell Tissue Res.* 322, 63–71. doi: 10.1007/s00441-005-1117-5

Conel, J. L. (1939). *The postnatal development of the human cerebral cortex*. Cambridge: Harvard University Press.

Corbin, J. G., Gaiano, N., Juliano, S. L., Poluch, S., Stancik, E., and Haydar, T. F. (2008). Regulation of neural progenitor cell development in the nervous system. *J. Neurochem.* 106, 2272–2287. doi: 10.1111/j.1471-4159.2008.05522.x

Courchesne, E., and Pierce, K. (2005). Why the frontal cortex in autism might be talking only to itself: Local over-connectivity but long-distance disconnection. *Curr. Opin. Neurobiol.* 15, 225–230. doi: 10.1016/j.conb.2005.03.001

Courchesne, E., Campbell, K., and Solso, S. (2011). Brain growth across the life span in autism: Age-specific changes in anatomical pathology. *Brain Res.* 1380, 138–145. doi: 10.1016/j.brainres.2010.09.101

Courchesne, E., Pierce, K., Schumann, C. M., Redcay, E., Buckwalter, J. A., Kennedy, D. P., et al. (2007). Mapping early brain development in autism. *Neuron* 56, 399–413. doi: 10.1016/j.neuron.2007.10.016

Csillik, A. E., Okuno, E., Csillik, B., Knyihár, E., and Vécsei, L. (2002). Expression of kynurenine aminotransferase in the subplate of the rat and its possible role in the regulation of programmed cell death. *Cereb. Cortex* 12, 1193–1201. doi: 10.1093/cercor/12.11.1193

Dayer, A. G., Jacobshagen, M., Chaumont-Dubel, S., and Marin, P. (2015). 5-HT6 receptor: A new player controlling the development of neural circuits. *ACS Chem. Neurosci.* 6, 951–960. doi: 10.1021/cn500326z

deCampo, D. M., and Fudge, J. L. (2012). Where and what is the paralaminar nucleus? A review on a unique and frequently overlooked area of the primate amygdala. *Neurosci. Biobehav. Rev.* 36, 520–535. doi: 10.1016/j.neubiorev.2011.08.007

Dharane Neé Ligam, P., Manuelpillai, U., Wallace, E., and Walker, D. W. (2010). NFκB-dependent increase of kynurenine pathway activity in human placenta: Inhibition by sulfasalazine. *Placenta* 31, 997–1002. doi: 10.1016/j.placenta.2010.09.002

Di Giovanni, G., Di Matteo, V., and Esposito, E. (2008). Serotonin-dopamine interaction: Experimental evidence and therapeutic relevance. Preface. *Prog. Brain Res.* 172:ix. doi: 10.1016/s0079-6123(08)00931-x

Dipasquale, V., Cutrupi, M. C., Colavita, L., Manti, S., Cuppari, C., and Salpietro, C. (2017). Neuroinflammation in autism spectrum disorders: Role of high mobility group box 1 protein. *Int. J. Mol. Cell. Med.* 6, 148–155. doi: 10.22088/acadpub.BUMS.6.3.148

Donovan, A. P., and Basson, M. A. (2017). The neuroanatomy of autism – a developmental perspective. *J. Anat.* 230, 4–15. doi: 10.1111/joa.12542

Dubois, J., Dehaene-Lambertz, G., Kulikova, S., Poupon, C., Hüppi, P. S., and Hertz-Pannier, L. (2014). The early development of brain white matter: A review of imaging studies in fetuses, newborns and infants. *Neuroscience* 276, 48–71. doi: 10.1016/j.neuroscience.2013.12.044

Dunlop, W. A., Enticott, P. G., and Rajan, R. (2016). Speech discrimination difficulties in high-functioning autism spectrum disorder are likely independent of auditory hypersensitivity. *Front. Hum. Neurosci.* 10:401. doi: 10.3389/fnhum.2016.00401

Dworzynski, K., Ronald, A., Bolton, P., and Happé, F. (2012). How different are girls and boys above and below the diagnostic threshold for autism spectrum disorders? *J. Am. Acad. Child Adolesc. Psychiatry* 51, 788–797. doi: 10.1016/j.jaac.2012.05.018

Eran, A., Li, J. B., Vatalaro, K., McCarthy, J., Rahimov, F., Collins, C., et al. (2013). Comparative RNA editing in autistic and neurotypical cerebella. *Mol. Psychiatry* 18, 1041–1048. doi: 10.1038/mp.2012.118

Fatemi, S. H., Snow, A. V., Stary, J. M., Araghi-Niknam, M., Reutiman, T. J., Lee, S., et al. (2005). Reelin signaling is impaired in autism. *Biol. Psychiatry* 57, 777–787. doi: 10.1016/j.biopsych.2004.12.018

Fleshner, M., and Crane, C. R. (2017). Exosomes. DAMPs and miRNA: Features of stress physiology and immune homeostasis. *Trends Immunol.* 38, 768–776. doi: 10.1016/j.it.2017.08.002

Folsom, T. D., and Fatemi, S. H. (2013). The involvement of reelin in neurodevelopmental disorders. *Neuropharmacology* 68, 122–135. doi: 10.1016/j.neuropharm.2012.08.015

Ford, E. S., Giles, W. H., Mokdad, A. H., and Myers, G. L. (2004). Distribution and correlates of C-reactive protein concentrations among adult US women. *Clin. Chem.* 50, 574–581. doi: 10.1373/clinchem.2003.027359

Forgie, M. L., and Stewart, J. (1993). Sex differences in amphetamine-induced locomotor activity in adult rats: Role of testosterone exposure in the neonatal period. *Pharmacol. Biochem. Behav.* 46, 637–645. doi: 10.1016/0091-3057(93)90555-8

Friauf, E., McConnell, S. K., and Shatz, C. J. (1990). Functional synaptic circuits in the subplate during fetal and early postnatal development of cat visual cortex. *J. Neurosci.* 10, 2601–2613. doi: 10.1523/jneurosci.10-08-02601.1990

Fudge, J. L., and Tucker, T. (2009). Amygdala projections to central amygdaloid nucleus subdivisions and transition zones in the primate. *Neuroscience* 159, 819–841. doi: 10.1016/j.neuroscience.2009.01.013

Furness, J. B. (2016). Integrated neural and endocrine control of gastrointestinal function. *Adv. Exp. Med. Biol.* 891, 159–173. doi: 10.1007/978-3-319-27592-5_16

Gadal, F., Bozic, C., Pillot-Brochet, C., Malinge, S., Wagner, S., Le Cam, A., et al. (2003). Integrated transcriptome analysis of the cellular mechanisms associated with Ha-ras-dependent malignant transformation of the human breast epithelial MCF7 cell line. *Nucleic Acids Res.* 31, 5789–5804. doi: 10.1093/nar/gkg762

Gadal, F., Starzec, A., Bozic, C., Pillot-Brochet, C., Malinge, S., Ozanne, V., et al. (2005). Integrative analysis of gene expression patterns predicts specific modulations of defined cell functions by estrogen and tamoxifen in MCF7 breast cancer cells. *J. Mol. Endocrinol.* 34, 61–75. doi: 10.1677/jme.1.01631

Garcia, L. P., Witteveen, J. S., Middelman, A., van Hulten, J. A., Martens, G. J. M., Homberg, J. R., et al. (2019). Perturbed developmental serotonin signaling affects prefrontal catecholaminergic innervation and cortical integrity. *Mol. Neurobiol.* 56, 1405–1420. doi: 10.1007/s12035-018-1105-x

García-Cabezas, M., and Zikopoulos, B. (2019). Evolution, development, and organization of the cortical connectome. *PLoS Biol.* 17:e3000259. doi: 10.1371/journal.pbio.3000259

García-Cabezas, M., Hacker, J. L., and Zikopoulos, B. (2020). A protocol for cortical type analysis of the human neocortex applied on histological samples, the Atlas of Von Economo and Koskinas, and magnetic resonance imaging. *Front. Neuroanat.* 14:576015. doi: 10.3389/fnana.2020.576015

García-Cabezas, M., Hacker, J. L., and Zikopoulos, B. (2022). Homology of neocortical areas in rats and primates based on cortical type analysis: An update of the hypothesis on the dual origin of the neocortex. *Brain Struct. Funct.* doi: 10.1007/s00429-022-02548-0 [Epub ahead of print].

Garcia-Calero, E., and Puelles, L. (2020). Histogenetic radial models as aids to understanding complex brain structures: The amygdalar radial model as a recent example. *Front. Neuroanat.* 14:590011. doi: 10.3389/fnana.2020.590011

García-Frigola, C., and Herrera, E. (2010). Zic2 regulates the expression of sert to modulate eye-specific refinement at the visual targets. *EMBO J.* 29, 3170–3183. doi: 10.1038/emboj.2010.172

Gaspar, P., Cases, O., and Maroteaux, L. (2003). The developmental role of serotonin: News from mouse molecular genetics. *Nat. Rev. Neurosci.* 4, 1002–1012. doi: 10.1038/nrn1256

Genescu, I., and Garel, S. (2021). Being superficial: A developmental viewpoint on cortical layer 1 wiring. *Curr. Opin. Neurobiol.* 66, 125–134. doi: 10.1016/j.conb.2020.10.003

Ghandour, R. M., Sherman, L. J., Vladutiu, C. J., Ali, M. M., Lynch, S. E., Bitsko, R. H., et al. (2019). Prevalence and treatment of depression, anxiety, and conduct problems in US children. *J. Pediatr.* 206, 256–267.e3. doi: 10.1016/j.jpeds.2018.09.021

Ghosh, A., and Shatz, C. J. (1992). Involvement of subplate neurons in the formation of ocular dominance columns. *Science* 255, 1441–1443. doi: 10.1126/science.1542795

Ghosh, A., Antonini, A., McConnell, S. K., and Shatz, C. J. (1990). Requirement for subplate neurons in the formation of thalamocortical connections. *Nature* 347, 179–181. doi: 10.1038/347179a0

Goeden, N., Velasquez, J., Arnold, K. A., Chan, Y., Lund, B. T., Anderson, G. M., et al. (2016). Maternal inflammation disrupts fetal neurodevelopment via increased placental output of serotonin to the fetal brain. *J. Neurosci.* 36, 6041–6049. doi: 10.1523/jneurosci.2534-15.2016

Grønborg, T. K., Schendel, D. E., and Parner, E. T. (2013). Recurrence of autism spectrum disorders in full- and half-siblings and trends over time: A population-based cohort study. *JAMA Pediatr.* 167, 947–953. doi: 10.1001/jamapediatrics.2013.2259

Guisso, D. R., Saadeh, F. S., Saab, D., El Deek, J., Chamseddine, S., Abou-El-Hassan, H., et al. (2018). Correction to: Association of autism with maternal infections. Perinatal and Other Risk Factors: A Case-Control Study. *J. Autism Dev. Disord.* 48:2022. doi: 10.1007/s10803-018-3497-x

Hadders-Algra, M. (2018a). Early human brain development: Starring the subplate. *Neurosci. Biobehav. Rev.* 92, 276–290. doi: 10.1016/j.neubiorev.2018.06.017

Hadders-Algra, M. (2018b). Early human motor development: From variation to the ability to vary and adapt. *Neurosci. Biobehav. Rev.* 90, 411–427. doi: 10.1016/j.neubiorev.2018.05.009

Hanswijk, S. I., Spoelder, M., Shan, L., Verheij, M. M. M., Muilwijk, O. G., Li, W., et al. (2020). Gestational factors throughout fetal neurodevelopment: The serotonin link. *Int. J. Mol. Sci.* 21:5850. doi: 10.3390/ijms21165850

Hazlett, H. C., Gu, H., Munsell, B. C., Kim, S. H., Styner, M., Wolff, J. J., et al. (2017). Early brain development in infants at high risk for autism spectrum disorder. *Nature* 542, 348–351. doi: 10.1038/nature21369

Huang, H., Xue, R., Zhang, J., Ren, T., Richards, L. J., Yarowsky, P., et al. (2009). Anatomical characterization of human fetal brain development with diffusion tensor magnetic resonance imaging. *J. Neurosci.* 29, 4263–4273. doi: 10.1523/jneurosci.2769-08.2009

Hull, L., Mandy, W., and Petrides, K. V. (2017). Behavioural and cognitive sex/gender differences in autism spectrum condition and typically developing males and females. *Autism* 21, 706–727. doi: 10.1177/1362361316669087

Hutsler, J. J., and Casanova, M. F. (2016). Review: Cortical construction in autism spectrum disorder: Columns, connectivity and the subplate. *Neuropathol. Appl. Neurobiol.* 42, 115–134. doi: 10.1111/nan.12227

Hutsler, J. J., and Zhang, H. (2010). Increased dendritic spine densities on cortical projection neurons in autism spectrum disorders. *Brain Res.* 1309, 83–94. doi: 10.1016/j.brainres.2009.09.120

Hwang, T., Park, C. K., Leung, A. K., Gao, Y., Hyde, T. M., Kleinman, J. E., et al. (2016). Dynamic regulation of RNA editing in human brain development and disease. *Nat. Neurosci.* 19, 1093–1099. doi: 10.1038/nn.4337

Iris, F. (2012). Psychiatric systems medicine: Closer at hand than anticipated but not with the expected portrait. *Pharmacopsychiatry* 45(Suppl. 1), S12–S21. doi: 10.1055/s-0032-1309002

Iris, F., Beopoulos, A., and Gea, M. (2018). How scientific literature analysis yields innovative therapeutic hypothesis through integrative iterations. *Curr. Opin. Pharmacol.* 42, 62–70. doi: 10.1016/j.coph.2018.07.005

Iris, F., Gea, M., Lampe, P. H., and Santamaria, P. (2009). [Production and implementation of predictive biological models]. *Med. Sci. (Paris)* 25, 608–616. doi: 10.1051/medsci/2009256-7608

Janusonis, S. (2005). Statistical distribution of blood serotonin as a predictor of early autistic brain abnormalities. *Theor. Biol. Med. Model.* 2:27. doi: 10.1186/1742-4682-2-27

Janusonis, S., Gluncic, V., and Rakic, P. (2004). Early serotonergic projections to Cajal-Retzius cells: Relevance for cortical development. *J. Neurosci.* 24, 1652–1659. doi: 10.1523/jneurosci.4651-03.2004

Just, M. A., Keller, T. A., Malave, V. L., Kana, R. K., and Varma, S. (2012). Autism as a neural systems disorder: A theory of frontal-posterior underconnectivity. *Neurosci. Biobehav. Rev.* 36, 1292–1313. doi: 10.1016/j.neubiorev.2012.02.007

Kalsbeek, A., De Bruin, J. P., Feenstra, M. G., and Uylings, H. B. (1990). Age-dependent effects of lesioning the mesocortical dopamine system upon prefrontal cortex morphometry and PFC-related behaviors. *Prog. Brain Res.* 85, 257–282; discussion 282–253. doi: 10.1016/s0079-6123(08)62684-9

Kalsbeek, A., Voorn, P., Buijs, R. M., Pool, C. W., and Uylings, H. B. (1988). Development of the dopaminergic innervation in the prefrontal cortex of the rat. *J. Comp. Neurol.* 269, 58–72. doi: 10.1002/cne.902690105

Kanold, P. O., Kara, P., Reid, R. C., and Shatz, C. J. (2003). Role of subplate neurons in functional maturation of visual cortical columns. *Science* 301, 521–525. doi: 10.1126/science.1084152

Kelemenova, S., and Ostatnikova, D. (2009). Neuroendocrine pathways altered in autism. Special role of reelin. *Neuro Endocrinol. Lett.* 30, 429–436.

Keown, C. L., Shih, P., Nair, A., Peterson, N., Mulvey, M. E., and Müller, R. A. (2013). Local functional overconnectivity in posterior brain regions is associated with symptom severity in autism spectrum disorders. *Cell Rep.* 5, 567–572. doi: 10.1016/j.celrep.2013.10.003

Kim, J. Y., Choi, M. J., Ha, S., Hwang, J., Koyanagi, A., Dragioti, E., et al. (2022). Association between autism spectrum disorder and inflammatory bowel disease: A systematic review and meta-analysis. *Autism Res.* 15, 340–352. doi: 10.1002/aur.2656

Kliman, H. J., Quaratella, S. B., Setaro, A. C., Siegman, E. C., Subha, Z. T., Tal, R., et al. (2018). Pathway of maternal serotonin to the human embryo and fetus. *Endocrinology* 159, 1609–1629. doi: 10.1210/en.2017-03025

Kolodziejczak, M., Béchade, C., Gervasi, N., Irinopoulou, T., Banas, S. M., Cordier, C., et al. (2015). Serotonin modulates developmental microglia via 5-HT2B receptors: Potential implication during synaptic refinement of retinogeniculate projections. *ACS Chem. Neurosci.* 6, 1219–1230. doi: 10.1021/cn5003489

Kostic, A. D., Gevers, D., Siljander, H., Vatanen, T., Hyötyläinen, T., Hämäläinen, A. M., et al. (2015). The dynamics of the human infant gut microbiome in development and in progression toward type 1 diabetes. *Cell Host Microbe* 17, 260–273. doi: 10.1016/j.chom.2015.01.001

Kostovic, I., and Rakic, P. (1980). Cytology and time of origin of interstitial neurons in the white matter in infant and adult human and monkey telencephalon. *J. Neurocytol.* 9, 219–242. doi: 10.1007/bf01205159

Kostoviæ, I., Sedmak, G., Vukšiæ, M., and Judaš, M. (2015). The relevance of human fetal subplate zone for developmental neuropathology of neuronal migration disorders and cortical dysplasia. *CNS Neurosci. Ther.* 21, 74–82. doi: 10.1111/cns.12333

Koyama, R., and Ikegaya, Y. (2015). Microglia in the pathogenesis of autism spectrum disorders. *Neurosci. Res.* 100, 1–5. doi: 10.1016/j.neures.2015.06.005

Krabbe, G., Matyash, V., Pannasch, U., Mamer, L., Boddeke, H. W., and Kettenmann, H. (2012). Activation of serotonin receptors promotes microglial injury-induced motility but attenuates phagocytic activity. *Brain Behav. Immun.* 26, 419–428. doi: 10.1016/j.bbi.2011.12.002

Kreiser, N. L., and White, S. W. (2014). ASD in females: Are we overstating the gender difference in diagnosis? *Clin. Child Fam. Psychol. Rev.* 17, 67–84. doi: 10.1007/s10567-013-0148-9

Kriegstein, A. R., and Noctor, S. C. (2004). Patterns of neuronal migration in the embryonic cortex. *Trends Neurosci.* 27, 392–399. doi: 10.1016/j.tins.2004.05.001

Lakatosova, S., and Ostatnikova, D. (2012). Reelin and its complex involvement in brain development and function. *Int. J. Biochem. Cell Biol.* 44, 1501–1504. doi: 10.1016/j.biocel.2012.06.002

Lauder, J. M., and Krebs, H. (1978). Serotonin as a differentiation signal in early neurogenesis. *Dev. Neurosci.* 1, 15–30. doi: 10.1159/000112549

Lennox, A. L., Mao, H., and Silver, D. L. (2018). RNA on the brain: Emerging layers of post-transcriptional regulation in cerebral cortex development. *Wiley Interdiscip. Rev. Dev. Biol.* 7:290 doi: 10.1002/wdev.290

Lesch, K. P., and Waider, J. (2012). Serotonin in the modulation of neural plasticity and networks: Implications for neurodevelopmental disorders. *Neuron* 76, 175–191. doi: 10.1016/j.neuron.2012.09.013

Liao, C. C., and Lee, L. J. (2012). Evidence for structural and functional changes of subplate neurons in developing rat barrel cortex. *Brain Struct. Funct.* 217, 275–292. doi: 10.1007/s00429-011-0354-5

Lieberman, O. J., McGuirt, A. F., Tang, G., and Sulzer, D. (2019). Roles for neuronal and glial autophagy in synaptic pruning during development. *Neurobiol. Dis.* 122, 49–63. doi: 10.1016/j.nbd.2018.04.017

Long, Z., Duan, X., Mantini, D., and Chen, H. (2016). Alteration of functional connectivity in autism spectrum disorder: Effect of age and anatomical distance. *Sci. Rep.* 6:26527. doi: 10.1038/srep26527

Luhmann, H. J., Kirischuk, S., and Kilb, W. (2018). The superior function of the subplate in early neocortical development. *Front. Neuroanat.* 12:97. doi: 10.3389/fnana.2018.00097

Lui, J. H., Hansen, D. V., and Kriegstein, A. R. (2011). Development and evolution of the human neocortex. *Cell* 146, 18–36. doi: 10.1016/j.cell.2011.06.030

Luna, B., Minshew, N. J., Garver, K. E., Lazar, N. A., Thulborn, K. R., Eddy, W. F., et al. (2002). Neocortical system abnormalities in autism: An fMRI study of spatial working memory. *Neurology* 59, 834–840. doi: 10.1212/wnl.59.6.834

Mackay, D. F., Smith, G. C., Cooper, S. A., Wood, R., King, A., Clark, D. N., et al. (2016). Month of conception and learning disabilities: A record-linkage study of 801,592 children. *Am. J. Epidemiol.* 184, 485–493. doi: 10.1093/aje/kww096

Mallat, M., Marín-Teva, J. L., and Chéret, C. (2005). Phagocytosis in the developing CNS: More than clearing the corpses. *Curr. Opin. Neurobiol.* 15, 101–107. doi: 10.1016/j.conb.2005.01.006

Mandic-Maravic, V., Pejovic-Milovancevic, M., Mitkovic-Voncina, M., Kostic, M., Aleksic-Hil, O., Radosavljev-Kircanski, J., et al. (2015). Sex differences in autism spectrum disorders: Does sex moderate the pathway from clinical symptoms to adaptive behavior? *Sci. Rep.* 5:10418. doi: 10.1038/srep10418

Martínez-Cerdeño, V., Cunningham, C. L., Camacho, J., Antczak, J. L., Prakash, A. N., Cziep, M. E., et al. (2012). Comparative analysis of the subventricular zone in rat, ferret and macaque: Evidence for an outer subventricular zone in rodents. *PLoS One* 7:e30178. doi: 10.1371/journal.pone.0030178

McConnell, S. K., Ghosh, A., and Shatz, C. J. (1989). Subplate neurons pioneer the first axon pathway from the cerebral cortex. *Science* 245, 978–982. doi: 10.1126/science.2475909

McKavanagh, R., Buckley, E., and Chance, S. A. (2015). Wider minicolumns in autism: A neural basis for altered processing? *Brain* 138(Pt 7), 2034–2045. doi: 10.1093/brain/awv110

McQuillen, P. S., and Ferriero, D. M. (2005). Perinatal subplate neuron injury: Implications for cortical development and plasticity. *Brain Pathol.* 15, 250–260. doi: 10.1111/j.1750-3639.2005.tb00528.x

Meltzer, A., and Van de Water, J. (2017). The role of the immune system in autism spectrum disorder. *Neuropsychopharmacology* 42, 284–298. doi: 10.1038/npp.2016.158

Mensen, V. T., Wierenga, L. M., van Dijk, S., Rijks, Y., Oranje, B., Mandl, R. C., et al. (2017). Development of cortical thickness and surface area in autism spectrum disorder. *Neuroimage Clin.* 13, 215–222. doi: 10.1016/j.nicl.2016.12.003

Moiseiwitsch, J. R., and Lauder, J. M. (1995). Serotonin regulates mouse cranial neural crest migration. *Proc. Natl. Acad. Sci. U.S.A.* 92, 7182–7186. doi: 10.1073/pnas.92.16.7182

Monteiro, S. A., Spinks-Franklin, A., Treadwell-Deering, D., Berry, L., Sellers-Vinson, S., Smith, E., et al. (2015). Prevalence of autism spectrum disorder in children referred for diagnostic autism evaluation. *Clin. Pediatr. (Phila)* 54, 1322–1327. doi: 10.1177/0009922815592607

Mueller, B. R., and Bale, T. L. (2008). Sex-specific programming of offspring emotionality after stress early in pregnancy. *J. Neurosci.* 28, 9055–9065. doi: 10.1523/jneurosci.1424-08.2008

Müller, F., and O'Rahilly, R. (1990). The human brain at stages 21-23, with particular reference to the cerebral cortical plate and to the development of the cerebellum. *Anat. Embryol. (Berl)* 182, 375–400. doi: 10.1007/bf02433497

Murthy, S., Niquille, M., Hurni, N., Limoni, G., Frazer, S., Chameau, P., et al. (2014). Serotonin receptor 3A controls interneuron migration into the neocortex. *Nat. Commun.* 5:5524. doi: 10.1038/ncomms6524

Nankova, B. B., Agarwal, R., MacFabe, D. F., and La Gamma, E. F. (2014). Enteric bacterial metabolites propionic and butyric acid modulate gene expression, including CREB-dependent catecholaminergic neurotransmission, in PC12 cells–possible relevance to autism spectrum disorders. *PLoS One* 9:e103740. doi: 10.1371/journal.pone.0103740

Nie, K., Molnár, Z., and Szele, F. G. (2010). Proliferation but not migration is associated with blood vessels during development of the rostral migratory stream. *Dev. Neurosci.* 32, 163–172. doi: 10.1159/000301135

Niederkofler, V., Asher, T. E., and Dymecki, S. M. (2015). Functional interplay between dopaminergic and serotonergic neuronal systems during development and adulthood. *ACS Chem. Neurosci.* 6, 1055–1070. doi: 10.1021/acschemneuro.5b00021

Nieuwenhuys, R., and Puelles, L. (2016). *Towards a new neuromorphology*. New York, NY: Springer International Publishing.

Notarangelo, F. M., Beggiato, S., and Schwarcz, R. (2019). Assessment of prenatal kynurenine metabolism using tissue slices: Focus on the neosynthesis of kynurenic acid in mice. *Dev. Neurosci.* 41, 102–111. doi: 10.1159/000499736

Nunes, A. S., Vakorin, V. A., Kozhemiako, N., Peatfield, N., Ribary, U., and Doesburg, S. M. (2020). Atypical age-related changes in cortical thickness in autism spectrum disorder. *Sci. Rep.* 10:11067. doi: 10.1038/s41598-020-67507-3

Nussbaumer, M., Asara, J. M., Teplytska, L., Murphy, M. P., Logan, A., Turck, C. W., et al. (2016). Selective mitochondrial targeting exerts anxiolytic effects in vivo. *Neuropsychopharmacology* 41, 1751–1758. doi: 10.1038/npp.2015.341

O'Connor, K. (2012). Auditory processing in autism spectrum disorder: A review. *Neurosci. Biobehav. Rev.* 36, 836–854. doi: 10.1016/j.neubiorev.2011.11.008

Okado, N., Narita, M., and Narita, N. (2001). A biogenic amine-synapse mechanism for mental retardation and developmental disabilities. *Brain Dev.* 23(Suppl. 1), S11–S15. doi: 10.1016/s0387-7604(01)00371-0

Opris, I., and Casanova, M. F. (2014). Prefrontal cortical minicolumn: From executive control to disrupted cognitive processing. *Brain* 137(Pt 7), 1863–1875. doi: 10.1093/brain/awt359

Ortiz-Mantilla, S., Choe, M. S., Flax, J., Grant, P. E., and Benasich, A. A. (2010). Associations between the size of the amygdala in infancy and language abilities during the preschool years in normally developing children. *Neuroimage* 49, 2791–2799. doi: 10.1016/j.neuroimage.2009.10.029

Osimo, E. F., Cardinal, R. N., Jones, P. B., and Khandaker, G. M. (2018). Prevalence and correlates of low-grade systemic inflammation in adult psychiatric inpatients: An electronic health record-based study. *Psychoneuroendocrinology* 91, 226–234. doi: 10.1016/j.psyneuen.2018.02.031

Pang, X., Xiao, X., Liu, Y., Zhang, R., Liu, J., Liu, Q., et al. (2016). Mosquito C-type lectins maintain gut microbiome homeostasis. *Nat. Microbiol.* 1:16023. doi: 10.1038/nmicrobiol.2016.23

Paolicelli, R. C., and Gross, C. T. (2011). Microglia in development: Linking brain wiring to brain environment. *Neuron Glia Biol.* 7, 77–83. doi: 10.1017/s1740925x12000105

Paolicelli, R. C., Bolasco, G., Pagani, F., Maggi, L., Scianni, M., Panzanelli, P., et al. (2011). Synaptic pruning by microglia is necessary for normal brain development. *Science* 333, 1456–1458. doi: 10.1126/science.1202529

Park, W. J., Schauder, K. B., Zhang, R., Bennetto, L., and Tadin, D. (2017). High internal noise and poor external noise filtering characterize perception in autism spectrum disorder. *Sci. Rep.* 7:17584. doi: 10.1038/s41598-017-17676-5

Parras, A., Anta, H., Santos-Galindo, M., Swarup, V., Elorza, A., Nieto-González, J. L., et al. (2018). Autism-like phenotype and risk gene mRNA deadenylation by CPEB4 mis-splicing. *Nature* 560, 441–446. doi: 10.1038/s41586-018-0423-5

Parsey, R. V., Oquendo, M. A., Ogden, R. T., Olvet, D. M., Simpson, N., Huang, Y. Y., et al. (2006). Altered serotonin 1A binding in major depression: A [carbonyl-C-11]WAY100635 positron emission tomography study. *Biol. Psychiatry* 59, 106–113. doi: 10.1016/j.biopsych.2005.06.016

Peck, B. C. E., Shanahan, M. T., Singh, A. P., and Sethupathy, P. (2017). Gut microbial influences on the mammalian intestinal stem cell niche. *Stem Cells Int.* 2017:5604727. doi: 10.1155/2017/5604727

Penedo, L. A., Oliveira-Silva, P., Gonzalez, E. M., Maciel, R., Jurgilas, P. B., Melibeu Ada, C., et al. (2009). Nutritional tryptophan restriction impairs plasticity of retinotectal axons during the critical period. *Exp. Neurol.* 217, 108–115. doi: 10.1016/j.expneurol.2009.01.021

Pollak Dorocic, I., Fürth, D., Xuan, Y., Johansson, Y., Pozzi, L., Silberberg, G., et al. (2014). A whole-brain atlas of inputs to serotonergic neurons of the dorsal and median raphe nuclei. *Neuron* 83, 663–678. doi: 10.1016/j.neuron.2014.07.002

Pouillot, F., Blois, H., and Iris, F. (2010). Genetically engineered virulent phage banks in the detection and control of emergent pathogenic bacteria. *Biosecur. Bioterror.* 8, 155–169. doi: 10.1089/bsp.2009.0057

Prosperi, M., Guiducci, L., Peroni, D. G., Narducci, C., Gaggini, M., Calderoni, S., et al. (2019). Inflammatory biomarkers are correlated with some forms of regressive autism spectrum disorder. *Brain Sci.* 9:366. doi: 10.3390/brainsci9120366

Puelles, L. (2018). Developmental studies of avian brain organization. *Int. J. Dev. Biol.* 62, 207–224. doi: 10.1387/ijdb.170279LP

Puelles, L. (2021). Recollections on the origins and development of the prosomeric model. *Front. Neuroanat.* 15:787913. doi: 10.3389/fnana.2021.787913

Puig, M. V., and Gulledge, A. T. (2011). Serotonin and prefrontal cortex function: Neurons, networks, and circuits. *Mol. Neurobiol.* 44, 449–464. doi: 10.1007/s12035-011-8214-0

Raj, B., and Blencowe, B. J. (2015). Alternative splicing in the mammalian nervous system: Recent insights into mechanisms and functional roles. *Neuron* 87, 14–27. doi: 10.1016/j.neuron.2015.05.004

Randall, M., Egberts, K. J., Samtani, A., Scholten, R. J., Hooft, L., Livingstone, N., et al. (2018). Diagnostic tests for autism spectrum disorder (ASD) in preschool children. *Cochrane Database Syst. Rev.* 7:Cd009044. doi: 10.1002/14651858.CD009044.pub2

Ratto, A. B., Kenworthy, L., Yerys, B. E., Bascom, J., Wieckowski, A. T., White, S. W., et al. (2018). What about the girls? Sex-based differences in autistic traits and adaptive skills. *J. Autism Dev. Disord.* 48, 1698–1711. doi: 10.1007/s10803-017-3413-9

Reillo, I., de Juan Romero, C., García-Cabezas, M., and Borrell, V. (2011). A role for intermediate radial glia in the tangential expansion of the mammalian cerebral cortex. *Cereb. Cortex* 21, 1674–1694. doi: 10.1093/cercor/bhq238

Riccio, O., Jacobshagen, M., Golding, B., Vutskits, L., Jabaudon, D., Hornung, J. P., et al. (2011). Excess of serotonin affects neocortical pyramidal neuron migration. *Transl. Psychiatry* 1:e47. doi: 10.1038/tp.2011.49

Riccio, O., Potter, G., Walzer, C., Vallet, P., Szabo, G., Vutskits, L., et al. (2009). Excess of serotonin affects embryonic interneuron migration through activation of the serotonin receptor 6. *Mol. Psychiatry* 14, 280–290. doi: 10.1038/mp.2008.89

Richter, J. D. (2007). CPEB: A life in translation. *Trends Biochem. Sci.* 32, 279–285. doi: 10.1016/j.tibs.2007.04.004

Rosenblat, J. D., and McIntyre, R. S. (2017). Bipolar disorder and immune dysfunction: Epidemiological findings, proposed pathophysiology and clinical implications. *Brain Sci.* 7:144. doi: 10.3390/brainsci7110144

Rossignol, D. A., and Frye, R. E. (2012). A review of research trends in physiological abnormalities in autism spectrum disorders: Immune dysregulation, inflammation, oxidative stress, mitochondrial dysfunction and environmental toxicant exposures. *Mol. Psychiatry* 17, 389–401. doi: 10.1038/mp.2011.165

Ruberman, W., Weinblatt, E., Goldberg, J. D., and Chaudhary, B. S. (1984). Psychosocial influences on mortality after myocardial infarction. *N. Engl. J. Med.* 311, 552–559. doi: 10.1056/nejm198408303110902

Scadden, A. D., and Smith, C. W. (2001). RNAi is antagonized by A–>I hyper-editing. *EMBO Rep.* 2, 1107–1111. doi: 10.1093/embo-reports/kve244

Schaefer, A., Poluch, S., and Juliano, S. (2008). Reelin is essential for neuronal migration but not for radial glial elongation in neonatal ferret cortex. *Dev. Neurobiol.* 68, 590–604. doi: 10.1002/dneu.20601

Scumpia, P. O., Kelly-Scumpia, K., and Stevens, B. R. (2014). Alpha-lipoic acid effects on brain glial functions accompanying double-stranded RNA antiviral and inflammatory signaling. *Neurochem. Int.* 64, 55–63. doi: 10.1016/j.neuint.2013.11.006

Sengupta, A., Bocchio, M., Bannerman, D. M., Sharp, T., and Capogna, M. (2017). Control of amygdala circuits by 5-HT neurons via 5-HT and glutamate cotransmission. *J. Neurosci.* 37, 1785–1796. doi: 10.1523/jneurosci.2238-16.2016

Serfaty, C. A., Oliveira-Silva, P., Faria Melibeu Ada, C., and Campello-Costa, P. (2008). Nutritional tryptophan restriction and the role of serotonin in development and plasticity of central visual connections. *Neuroimmunomodulation* 15, 170–175. doi: 10.1159/000153421

Seto, Y., and Eiraku, M. (2019). Human brain development and its in vitro recapitulation. *Neurosci. Res.* 138, 33–42. 10.1016/j.neures.2018.09.011

Sgritta, M., Dooling, S. W., Buffington, S. A., Momin, E. N., Francis, M. B., Britton, R. A., et al. (2019). Mechanisms underlying microbial-mediated changes in social behavior in mouse models of autism spectrum disorder. *Neuron* 101, 246–259.e6. doi: 10.1016/j.neuron.2018.11.018

Shallie, P. D., and Naicker, T. (2019). The placenta as a window to the brain: A review on the role of placental markers in prenatal programming of neurodevelopment. *Int. J. Dev. Neurosci.* 73, 41–49. doi: 10.1016/j.ijdevneu.2019.01.003

Sheridan, G. K., and Murphy, K. J. (2013). Neuron-glia crosstalk in health and disease: Fractalkine and CX3CR1 take centre stage. *Open Biol.* 3:130181. doi: 10.1098/rsob.130181

Shi, L., Fatemi, S. H., Sidwell, R. W., and Patterson, P. H. (2003). Maternal influenza infection causes marked behavioral and pharmacological changes in the offspring. *J. Neurosci.* 23, 297–302. 10.1523/jneurosci.23-01-00297.2003

Shuey, D. L., Sadler, T. W., and Lauder, J. M. (1992). Serotonin as a regulator of craniofacial morphogenesis: Site specific malformations following exposure to serotonin uptake inhibitors. *Teratology* 46, 367–378. doi: 10.1002/tera.1420460407

Smart, I. H., Dehay, C., Giroud, P., Berland, M., and Kennedy, H. (2002). Unique morphological features of the proliferative zones and postmitotic compartments of the neural epithelium giving rise to striate and extrastriate cortex in the monkey. *Cereb. Cortex* 12, 37–53. doi: 10.1093/cercor/12.1.37

Sørensen, H. J., Mortensen, E. L., Reinisch, J. M., and Mednick, S. A. (2009). Association between prenatal exposure to bacterial infection and risk of schizophrenia. *Schizophr. Bull.* 35, 631–637. doi: 10.1093/schbul/sbn121

Soufer, R., Jain, H., and Yoon, A. J. (2009). Heart-brain interactions in mental stress-induced myocardial ischemia. *Curr. Cardiol. Rep.* 11, 133–140.

Stagni, F., Giacomini, A., Guidi, S., Ciani, E., and Bartesaghi, R. (2015). Timing of therapies for down syndrome: The sooner, the better. *Front. Behav. Neurosci.* 9:265. doi: 10.3389/fnbeh.2015.00265

Stoner, R., Chow, M. L., Boyle, M. P., Sunkin, S. M., Mouton, P. R., Roy, S., et al. (2014). Patches of disorganization in the neocortex of children with autism. *N. Engl. J. Med.* 370, 1209–1219. doi: 10.1056/NEJMoa1307491

Streit, A. K., and Decher, N. (2011). A-to-I RNA editing modulates the pharmacology of neuronal ion channels and receptors. *Biochemistry (Mosc)* 76, 890–899. doi: 10.1134/s0006297911080049

Super, H., Del Rio, J. A., Martinez, A., Perez-Sust, P., and Soriano, E. (2000). Disruption of neuronal migration and radial glia in the developing cerebral cortex following ablation of Cajal-Retzius cells. *Cereb. Cortex* 10, 602–613. doi: 10.1093/cercor/10.6.602

Tang, G., Gudsnuk, K., Kuo, S. H., Cotrina, M. L., Rosoklija, G., Sosunov, A., et al. (2014). Loss of mTOR-dependent macroautophagy causes autistic-like synaptic pruning deficits. *Neuron* 83, 1131–1143. doi: 10.1016/j.neuron.2014.07.040

Tasan, R. O., Verma, D., Wood, J., Lach, G., Hörmer, B., de Lima, T. C., et al. (2016). The role of neuropeptide Y in fear conditioning and extinction. *Neuropeptides* 55, 111–126. doi: 10.1016/j.npep.2015.09.007

Thakkar, K. N., Polli, F. E., Joseph, R. M., Tuch, D. S., Hadjikhani, N., Barton, J. J., et al. (2008). Response monitoring, repetitive behaviour and anterior cingulate abnormalities in autism spectrum disorders (ASD). *Brain* 131(Pt 9), 2464–2478. doi: 10.1093/brain/awn099

Theoharides, T. C., Tsilioni, I., Patel, A. B., and Doyle, R. (2016). Atopic diseases and inflammation of the brain in the pathogenesis of autism spectrum disorders. *Transl. Psychiatry* 6:e844. doi: 10.1038/tp.2016.77

Trutzer, I. M., García-Cabezas, M., and Zikopoulos, B. (2019). Postnatal development and maturation of layer 1 in the lateral prefrontal cortex and its disruption in autism. *Acta Neuropathol. Commun.* 7:40. doi: 10.1186/s40478-019-0684-8

Tsivion-Visbord, H., Kopel, E., Feiglin, A., Sofer, T., Barzilay, R., Ben-Zur, T., et al. (2020). Increased RNA editing in maternal immune activation model of neurodevelopmental disease. *Nat. Commun.* 11:5236. doi: 10.1038/s41467-020-19048-6

Turck, C. W., and Iris, F. (2011). Proteome-based pathway modelling of psychiatric disorders. *Pharmacopsychiatry* 44(Suppl. 1), S54–S61. doi: 10.1055/s-0031-1271701

Ulfig, N., Neudörfer, F., and Bohl, J. (2000). Transient structures of the human fetal brain: Subplate, thalamic reticular complex, ganglionic eminence. *Histol. Histopathol.* 15, 771–790. doi: 10.14670/hh-15.771

Ulfig, N., Setzer, M., and Bohl, J. (2003). Ontogeny of the human amygdala. *Ann. N Y Acad. Sci.* 985, 22–33. doi: 10.1111/j.1749-6632.2003.tb07068.x

Upton, A. L., Ravary, A., Salichon, N., Moessner, R., Lesch, K. P., Hen, R., et al. (2002). Lack of 5-HT(1B) receptor and of serotonin transporter have different effects on the segregation of retinal axons in the lateral geniculate nucleus

compared to the superior colliculus. *Neuroscience* 111, 597–610. doi: 10.1016/s0306-4522(01)00602-9

Upton, A. L., Salichon, N., Lebrand, C., Ravary, A., Blakely, R., Seif, I., et al. (1999). Excess of serotonin (5-HT) alters the segregation of ispilateral and contralateral retinal projections in monoamine oxidase A knock-out mice: Possible role of 5-HT uptake in retinal ganglion cells during development. *J. Neurosci.* 19, 7007–7024. doi: 10.1523/jneurosci.19-16-07007.1999

Vasung, L., Huang, H., Jovanov-Miloševiæ, N., Pletikos, M., Mori, S., and Kostoviæ, I. (2010). Development of axonal pathways in the human fetal fronto-limbic brain: Histochemical characterization and diffusion tensor imaging. *J. Anat.* 217, 400–417. doi: 10.1111/j.1469-7580.2010.01260.x

Veenstra-VanderWeele, J., Kim, S. J., Lord, C., Courchesne, R., Akshoomoff, N., Leventhal, B. L., et al. (2002). Transmission disequilibrium studies of the serotonin 5-HT2A receptor gene (HTR2A) in autism. *Am. J. Med. Genet.* 114, 277–283. doi: 10.1002/ajmg.10192

Vicenzi, S., Foa, L., and Gasperini, R. J. (2021). Serotonin functions as a bidirectional guidance molecule regulating growth cone motility. *Cell. Mol. Life Sci.* 78, 2247–2262. doi: 10.1007/s00018-020-03628-2

Vitalis, T., and Verney, C. (2017). *Sculpting cerebral cortex with serotonin in rodent and primate*. London: IntechOpen.

Vitalis, T., Ansorge, M. S., and Dayer, A. G. (2013). Serotonin homeostasis and serotonin receptors as actors of cortical construction: Special attention to the 5-HT3A and 5-HT6 receptor subtypes. *Front. Cell. Neurosci.* 7:93. doi: 10.3389/fncel.2013.00093

Wang, Y., Ye, M., Kuang, X., Li, Y., and Hu, S. (2018). A simplified morphological classification scheme for pyramidal cells in six layers of primary somatosensory cortex of juvenile rats. *IBRO Rep.* 5, 74–90. doi: 10.1016/j.ibror.2018.10.001

Wang, S., Brunne, B., Zhao, S., Chai, X., Li, J., Lau, J., et al. (2018). trajectory analysis unveils reelin's role in the directed migration of granule cells in the dentate gyrus. *J. Neurosci.* 38, 137–148. doi: 10.1523/jneurosci.0988-17.2017

Wassink, T. H., Hazlett, H. C., Epping, E. A., Arndt, S., Dager, S. R., Schellenberg, G. D., et al. (2007). Cerebral cortical gray matter overgrowth and functional variation of the serotonin transporter gene in autism. *Arch. Gen. Psychiatry* 64, 709–717. doi: 10.1001/archpsyc.64.6.709

Watson, C., Bartholomaeus, C., and Puelles, L. (2019). Time for radical changes in brain stem nomenclature-applying the lessons from developmental gene patterns. *Front. Neuroanat.* 13:10. doi: 10.3389/fnana.2019.00010

Wei, H., Alberts, I., and Li, X. (2013). Brain IL-6 and autism. *Neuroscience* 252, 320–325. doi: 10.1016/j.neuroscience.2013.08.025

Weir, R. K., Bauman, M. D., Jacobs, B., and Schumann, C. M. (2018). Protracted dendritic growth in the typically developing human amygdala and increased spine density in young ASD brains. *J. Comp. Neurol.* 526, 262–274. doi: 10.1002/cne.24332

Whitaker-Azmitia, P. M. (2005). Behavioral and cellular consequences of increasing serotonergic activity during brain development: A role in autism? *Int. J. Dev. Neurosci.* 23, 75–83. doi: 10.1016/j.ijdevneu.2004.07.022

Whitaker-Azmitia, P. M., Druse, M., Walker, P., and Lauder, J. M. (1996). Serotonin as a developmental signal. *Behav. Brain Res.* 73, 19–29. doi: 10.1016/0166-4328(96)00071-x

Willemze, R. A., Welting, O., van Hamersveld, P., Verseijden, C., Nijhuis, L. E., Hilbers, F. W., et al. (2019). Loss of intestinal sympathetic innervation elicits an innate immune driven colitis. *Mol. Med.* 25:1. doi: 10.1186/s10020-018-0068-8

Williams, M., Zhang, Z., Nance, E., Drewes, J. L., Lesniak, W. G., Singh, S., et al. (2017). Maternal inflammation results in altered tryptophan metabolism in rabbit placenta and fetal brain. *Dev. Neurosci.* 39, 399–412. doi: 10.1159/000471509

Wilson, C. A., and Davies, D. C. (2007). The control of sexual differentiation of the reproductive system and brain. *Reproduction* 133, 331–359. doi: 10.1530/rep-06-0078

Xu, A. T., Lu, J. T., Ran, Z. H., and Zheng, Q. (2016). Exosome in intestinal mucosal immunity. *J. Gastroenterol. Hepatol.* 31, 1694–1699. doi: 10.1111/jgh.13413

Yachnis, A. T., Roper, S. N., Love, A., Fancey, J. T., and Muir, D. (2000). Bcl-2 immunoreactive cells with immature neuronal phenotype exist in the nonepileptic adult human brain. *J. Neuropathol. Exp. Neurol.* 59, 113–119. doi: 10.1093/jnen/59.2.113

Yavarone, M. S., Shuey, D. L., Sadler, T. W., and Lauder, J. M. (1993). Serotonin uptake in the ectoplacental cone and placenta of the mouse. *Placenta* 14, 149–161. doi: 10.1016/s0143-4004(05)80257-7

Young, H., Oreve, M. J., and Speranza, M. (2018). Clinical characteristics and problems diagnosing autism spectrum disorder in girls. *Arch. Pediatr.* 25, 399–403. doi: 10.1016/j.arcped.2018.06.008

Zerbo, O., Iosif, A. M., Delwiche, L., Walker, C., and Hertz-Picciotto, I. (2011). Month of conception and risk of autism. *Epidemiology* 22, 469–475. doi: 10.1097/EDE.0b013e31821d0b53

Zerbo, O., Qian, Y., Yoshida, C., Grether, J. K., Van de Water, J., and Croen, L. A. (2015). Maternal infection during pregnancy and autism spectrum disorders. *J. Autism Dev. Disord.* 45, 4015–4025. doi: 10.1007/s10803-013-2016-3

Zhang, X. M., Cai, Y., Chu, Y., Chen, E. Y., Feng, J. C., Luo, X. G., et al. (2009). Doublecortin-expressing cells persist in the associative cerebral cortex and amygdala in aged nonhuman primates. *Front. Neuroanat.* 3:17. doi: 10.3389/neuro.05.017.2009

Zielinski, B. A., Prigge, M. B., Nielsen, J. A., Froehlich, A. L., Abildskov, T. J., Anderson, J. S., et al. (2014). Longitudinal changes in cortical thickness in autism and typical development. *Brain* 137(Pt 6), 1799–1812. doi: 10.1093/brain/awu083

Zikopoulos, B., and Barbas, H. (2010). Changes in prefrontal axons may disrupt the network in autism. *J. Neurosci.* 30, 14595–14609. doi: 10.1523/jneurosci.2257-10.2010

frontiers | Frontiers in Neuroscience

TYPE Original Research
PUBLISHED 04 January 2023
DOI 10.3389/fnins.2022.1072667

OPEN ACCESS

EDITED BY
Julia Dallman,
University of Miami, United States

REVIEWED BY
Lucas Cheadle,
Cold Spring Harbor Laboratory, United States
Daniel Llano,
University of Illinois at Urbana-Champaign, United States

*CORRESPONDENCE
Mark L. Gabriele
✉ gabrieml@jmu.edu

SPECIALTY SECTION
This article was submitted to Neurodevelopment, a section of the journal Frontiers in Neuroscience

RECEIVED 17 October 2022
ACCEPTED 09 December 2022
PUBLISHED 04 January 2023

CITATION
Carroll JB, Hamidi S and Gabriele ML (2023) Microglial heterogeneity and complement component 3 elimination within emerging multisensory midbrain compartments during an early critical period. *Front. Neurosci.* 16:1072667. doi: 10.3389/fnins.2022.1072667

Microglial heterogeneity and complement component 3 elimination within emerging multisensory midbrain compartments during an early critical period

Julianne B. Carroll, Shaida Hamidi and Mark L. Gabriele *

Department of Biology, James Madison University, Harrisonburg, VA, United States

The lateral cortex of the inferior colliculus (LCIC) is a midbrain shell region that receives multimodal inputs that target discrete zones of its compartmental (modular-matrix) framework. This arrangement emerges perinatally in mice (postnatal day, P0-P12) as somatosensory and auditory inputs segregate into their respective modular and matrix terminal patterns. Microglial cells (MGCs) perform a variety of critical functions in the developing brain, among them identifying areas of active circuit assembly and selectively pruning exuberant or underutilized connections. Recent evidence in other brain structures suggest considerable MGC heterogeneity across the lifespan, particularly during established developmental critical periods. The present study examines the potential involvement of classical complement cascade signaling (C3-CR3/CD11b) in refining early multisensory networks, and identifies several microglial subsets exhibiting distinct molecular signatures within the nascent LCIC. Immunostaining was performed in GAD67-green fluorescent protein (GFP) and CX3CR1-GFP mice throughout and after the defined LCIC critical period. GAD labeling highlights the emerging LCIC modularity, while CX3CR1 labeling depicts MGCs expressing the fractalkine receptor. C3 expression is widespread throughout the LCIC neuropil early on, prior to its conspicuous absence from modular zones at P8, and more global disappearance following critical period closure. CD11b-expressing microglia while homogeneously distributed at birth, are biased to modular fields at P8 and then the surrounding matrix by P12. Temporal and spatial matching of the disappearance of C3 by LCIC compartment (i.e., modules then matrix) with CD11b-positive MGC occupancy implicates complement signaling in the selective refinement of early LCIC connectivity. Multiple-labeling studies for a variety of established MGC markers (CD11b, CX3CR1, Iba1, TMEM119) indicate significant MGC heterogeneity in the LCIC as its compartments and segregated multisensory maps emerge. Marker colocalization was the exception rather than the rule, suggesting that unique MGC subpopulations exist in the LCIC and perhaps

serve distinct developmental roles. Potential mechanisms whereby microglia sculpt early multisensory LCIC maps and how such activity/inactivity may underlie certain neurodevelopmental conditions, including autism spectrum disorder and schizophrenia, are discussed.

KEYWORDS

inferior colliculus, multisensory, C3, CR3/CD11b, development, refinement, pruning

Introduction

Synaptic pruning is an essential component of neurodevelopment that involves selective removal of extraneous or underutilized contacts (Wilton et al., 2019). Microglial cells (MGCs), the resident macrophages of the nervous system, play a pivotal role in this process of network refinement during early critical periods (Paolicelli et al., 2011; Hong et al., 2016; Mosser et al., 2017; Thion and Garel, 2017, 2020). MGCs exhibit various activation states, from highly phagocytic during periods of targeted engulfment of opsonized material, to resting or surveilling states after circuits are established and functionally-tuned (Jurga et al., 2020). Aberrations in MGC pruning behaviors are thought to underlie certain neurodevelopmental conditions (Zhan et al., 2014; Bordeleau et al., 2019; Faust et al., 2021), including autism spectrum disorders (ASD, under-pruning) and schizophrenia (over-pruning).

Recent single-cell RNA sequencing studies reveal microglial heterogeneities throughout the brain, with the most significant diversity exhibited during developmental critical periods (De Biase et al., 2017; Hammond et al., 2019; Li et al., 2019; Masuda et al., 2019, 2020; Tan et al., 2020). Given the differential expression of MGC transcriptional markers observed across the lifespan, various conditions and brain regions, it is reasonable that distinct microglial subsets serve timely roles with unique responsibilities. Two canonical developmental MGC gene clusters involve the expression of fractalkine and classical complement signaling cascade components, each of which include a host of specific markers.

The fractalkine pathway, most typically implicated in microglial recruitment and migration, involves interactions of the neuronally-expressed fractalkine ligand (CX3CL1) with its corresponding receptor (CX3CR1) found exclusively on MGCs (Harrison et al., 1998; Jung et al., 2000; Paolicelli et al., 2014; Arnoux and Audinat, 2015). CX3CL1 can either be membrane-bound, or liberated when cleaved by the metalloproteinase ADAM10 (Gunner et al., 2019). MGC occupancy along with aspects of synaptic pruning/maturation are delayed in developing barrel fields (Hoshiko et al., 2012) and hippocampus (Paolicelli et al., 2011; Pagani et al., 2015) in CX3CR1 mutants, suggesting involvement of MGCs and fractalkine signaling in governing important features of early circuit assembly.

The classical complement cascade, in particular complement component 3 (C3) and its receptor CR3, appear equally involved in MGC-neuronal crosstalk during development and certain disease states (Stevens et al., 2007; Schafer et al., 2012; Stephan et al., 2012). An initiating protein, C1q, produced by MGCs attaches to cells or portions of cells marking them for subsequent removal. C1q tagging ultimately leads to the production of the opsonin C3. MGCs initiate phagocytosis of selectively tagged debris *via* C3 binding with its cognate receptor, complement receptor 3 (CR3) (Stephan et al., 2012). CR3 is a heterodimer of integrin αM (CD11b) and β2 (CD18) subunits, with CD11b being an established marker for CR3-expressing MGCs (Bajic et al., 2013; Vorup-Jensen and Jensen, 2018; Lamers et al., 2021).

To explore potential microglial influences on the assembly of multisensory circuits, the present study focuses on a specific shell region of the midbrain inferior colliculus (IC). The IC consists of three subdivisions; the central nucleus (CNIC), the dorsal cortex (DCIC), and the lateral cortex (LCIC). Though classically described as an auditory relay hub due to its well-documented CNIC, the LCIC exhibits multimodal response properties (Aitkin et al., 1978, 1981; Jain and Shore, 2006; Gruters and Groh, 2012) that emerge from its discretely-mapped, network configuration. In adult mice, somatosensory projections target patchy zones positive for glutamic acid decarboxylase (GAD), termed modules, while auditory inputs terminate throughout the encompassing matrix (Lesicko et al., 2016, 2020). Discontinuous LCIC modular fields span its intermediate layer (layer 2, Chernock et al., 2004) and are completely surrounded by a calretinin-positive matrix (layers 1 and 3; Dillingham et al., 2017; Gay et al., 2018). These and other identified neurochemical and guidance markers reliably label the emerging LCIC compartmental structure and were instrumental in defining an early critical period regarding its characteristic cytoarchitectural organization and interfacing multisensory afferent patterns (from birth to postnatal day 12, P12; Dillingham et al., 2017; Gay et al., 2018; Stinson et al., 2021). Inputs of somatosensory and auditory origin exhibit considerable overlap initially, prior to fully segregating into modality-specific compartments (modular and matrix, respectively; Lamb-Echegaray et al., 2019; Weakley et al., 2022).

Recently, we reported that microglial colonization of the LCIC and timely occupancy of its emerging modules by

CX3CR1-positive MGCs is fractalkine signaling-dependent (Brett et al., 2022). The present study explores the potential role complement signaling may play in refining early LCIC connectivity. Here, developmentally regulated changes in C3 and CD11b expression with respect to emerging LCIC compartments are documented in a series of GAD67-green fluorescent protein (GFP) mice. Additionally, we examine the possibility of molecularly distinct MGC subpopulations in the neonatal LCIC by concurrently labeling for several established MGC markers (CD11b, TMEM119, Iba1) in CX3CR1-GFP mice. The results reveal widespread C3 expression that is subsequently pruned in a compartmental-specific progression (i.e., modules first, then matrix), and that such refinement appears temporally and spatially linked to the presence of CD11b-expressing MGCs. Examined MGC markers were generally non-overlapping, providing evidence for the likelihood of considerable MGC heterogeneity in the developing LCIC.

Materials and methods

Animals

A developmental series of mice spanning the established LCIC critical period (P0, P4, P8, P12; $n \geq 3$ at each age) of two transgenic lines [GAD67-GFP ($n = 46$) and CX3CR1-GFP ($n = 47$)] were used for experimentation. In some instances, an additional developmental timepoint was examined well after critical period closure (P36). GAD67-GFP knock-in mice enabled easy identification of emerging LCIC modules, and thus assessments of various MGC markers in relation to developing LCIC compartments. Previous efforts from our lab verifying the specificity of this mouse line are published elsewhere (Gay et al., 2018). Details regarding the targeting of enhanced GFP to the locus of the GAD gene, breeding strategies, and genotyping sequences have been previously described (Yanagawa et al., 1997; Tamamaki et al., 2003; Ono et al., 2005). Breeding pairs for this line were originally furnished by Dr. Peter Brunjes (University of Virginia School of Medicine) with permission granted from Dr. Yuchio Yanagawa (Gunma University Graduate School of Medicine, Gunma, Japan). CX3CR1-GFP mice (JAX 005582) facilitated visualization of fractalkine-receptor expressing MGCs in heterozygous and homozygous progeny. Similar to wild-type, $CX3CR1^{+/GFP}$ mice are capable of fractalkine signaling, whereas such functionality is compromised in $CX3CR1^{GFP/GFP}$ littermates. In the present study, only heterozygous mice for this line were used and are referred to simply as CX3CR1-GFP hereafter. CX3CR1-GFP mice were used to assess potential MGC heterogeneity and relative colocalization with a variety of other MGC markers. Previous work in our lab confirmed the presence of CX3CR1-expressing MGCs in the nascent LCIC and characterized migratory behaviors that recognize its emerging compartments (Brett et al., 2022) and temporally correlate with peak shaping of its multisensory afferent streams (Lamb-Echegaray et al., 2019; Weakley et al., 2022).

Both strains were bred on a C57BL/6J background (JAX 000664). GAD-GFP breeding consisted of pairing heterozygous males with C57BL/6J females. Progeny were observed with a Dark Reader Spot Lamp and viewing goggles prior to P4 to identify GFP-expressing pups (Clare Chemical Research, Dolores, CO, USA, Cat# SL10S)[1]. CX3CR1-GFP genotyping was outsourced (Transnetyx, Cordova, TN, USA)[2] using probes specific for this JAX line from the provided database. Approximately equal numbers of male and female subjects were used for all experimentation, and no sex-specific differences were observed. All experimental procedures are in accordance with National Institutes of Health guidelines and have been approved by the IACUC of James Madison University (No. 20-1421).

Perfusions and tissue sectioning

In preparation for midbrain sectioning, mice were given an overdose of ketamine (200 mg/kg) and xylazine (20 mg/kg). Brains were transcardially perfused with physiological rinse (0.9% NaCl and 0.5% $NaNO_2$ in dH_2O) followed by 4% paraformaldehyde, and then by a solution of 4% paraformaldehyde and 10% sucrose for cryoprotection. Brains were removed from the skull and stored at 4°C in 4% paraformaldehyde/10% sucrose solution for 24 h, and then were allowed to equilibrate at the same temperature in a solution of 4% paraformaldehyde/30% sucrose. The tissue block was cut in the coronal plane at 50 μm using a sliding freezing microtome and sections throughout the rostrocaudal extent of the midbrain were collected in 0.1 M phosphate-buffered saline (PBS, pH 7.4).

Immunocytochemistry

To begin processing for various markers of interest (see **Table 1** for all relevant antibody information), sections were rinsed in phosphate buffered saline (PBS) three times for five minutes each. Tissue sections were then blocked in 5% normal serum for 30 min (species of normal serum always corresponded to species of secondary antibody production). Blocking was followed immediately by transfer to primary antibody solution at the identified optimal dilution and sections were agitated overnight at 4°C.

For double-immunolabeling experiments, sections were allowed to equilibrate to room temperature the following day for 20 min before rinsing in PBS three times for eight minutes each.

1 www.clarechemical.com

2 https://www.transnetyx.com/

TABLE 1 Antibody information.

Antibody name	Structure of immunogen	Manufacturer info	Concentration used
Anti-C3	Lyophilized powder of IgG fraction to mouse complement C3 and buffer salts	MP Biomedicals, 0855463, goat, RRID:AB_2334481	1:200
Anti-CD11b, clone 5C6	Purified IgG prepared by affinity chromatography on protein G from tissue culture supernatant	Bio-Rad, MCA711G, rat, monoclonal, RRID:AB_323167	1:200
Anti-Iba1	Synthetic peptide that corresponds to the C-terminus of Iba1	Wako Chemicals, 019-19741, rabbit, polyclonal, RRID:AB_839504	1:1000
Anti-TMEM119	Recombinant fragment (GST-tag) within Mouse TMEM119 aa 100 to the C-terminus (intracellular)	Abcam, AB209064, rabbit, monoclonal RRID:AB_2800343	1:150
Alexa Fluor 350 goat anti-rat IgG	IgG recognizes both heavy and light chains from rat	Thermo Fisher Scientific, A21093, RRID:AB_2535748	1:25
Biotinylated horse anti-rabbit IgG	IgG recognizes both heavy and light chains from rabbit	Vector Laboratories, BA-1100, RRID:Ab_2336201	1:600
Biotinylated horse anti-goat IgG	IgG recognizes both heavy and light chains from goat	Vector Laboratories, BA-9500, RRID:AB_2336123	1:600
Biotinylated goat anti-rat IgG	IgG recognizes both heavy and light chains from rat	Vector Laboratories. BA-9401, RRID:AB_2336208	1:600

Tissue was then incubated for 90 min in a directly-conjugated secondary antibody (Alexa Fluor 350). After an additional four PBS rinses of 10 min each, tissue was blocked in the appropriate 5% normal serum prior to incubation in the second primary antibody at 4°C overnight.

On the final day of processing, tissue was once again allowed to return to room temperature, then rinsed three times in PBS. Next, an appropriate biotinylated secondary antibody was applied for 1 h, followed by three additional PBS rinses. Lastly, a streptavidin fluorescent conjugate (DyLight 549 streptavidin, 1:200, Vector Laboratories, Newark, CA, USA, SA-5549, RRID:AB_2336408) was applied for 2 h before three final PBS rinses. Tissue was then mounted onto slides and coverslipped with Prolong Diamond anti-fade mountant (Thermo Fisher Scientific, Waltham, MA, USA, P36970). For single-labeling studies, the biotinylated amplification described above was used in lieu of a directly conjugated secondary approach. For TMEM119 processing, tissue was blocked in 10% instead of 5% normal serum, and all steps beginning with the initial PBS rinses through the biotinylated secondary included 0.5% Triton X-100 (Millipore Sigma, Burlington, MA, USA, TX1568).

Epifluorescent imaging

Wide-field image capturing was performed on a Nikon Eclipse Ti-2 microscope (Nikon, Melville, NY) using a monochrome, Hamamatsu ORCA-Flash 4.0 V3 CMOS camera (Hamamatsu, Bridgewater, NJ) and PlanApo objectives (10x, 20x, 40x; NA = 0.30, 0.75, and 1.30, respectively). Filter sets (Chroma Technology, Bellows Falls, VT) were designed with careful attention to the spectra of the various fluorophores to make certain no bleed through exists between channels. An extended depth of field (EDF) algorithm was used to generate two-dimensional images from acquired Z-stacks (Elements Software; Nikon). The Nikon Elements EDF module facilitates merging of captured Z-stacks into two-dimensional images, using only the focused regions for each optical plane. Separate channels were pseudocolored and lookup tables were adjusted slightly for each image to reduce background noise and best depict labeling observed through the microscope. Images were saved as lossless JPEG2000 files prior to subsequent quantitative analyses. Masking of minimal artifact observed outside section contours in a few instances was performed (Adobe Photoshop, San Jose, CA) to enhance overall figure quality.

LCIC modular identification, C3 brightness profile sampling, and areal coverage assessments

Raw JPEG2000 images were opened in NIS-Elements and exported as uncompressed TIFF files and imported into ImageJ software (NIH, Bethesda, MD, RRID:SCR_003070)[3] in order to generate brightness plot profiles for C3 and GAD channels at P4, P8, and P12. Mid-rostrocaudal sections of the IC where LCIC modularity was most apparent were used. Sampling focused on these ages as qualitative C3 observations appeared to progress from the earliest indications of C3 disappearance (P4), to strikingly discontinuous C3 patterns (P8), to absence

3 https://imagej.net/

of discernible C3 labeling (P12). Merged channels were first separated and converted to grayscale, and then a threshold function was performed to facilitate clear delineation of modular boundaries (for more information see Brett et al., 2022). A freehand tool (line thickness of 100) was used to sample and fully encompass layer 2 GAD-positive modules in a ventral-to-dorsal progression. Once the sampling contour was set, a region of interest (ROI) function was utilized to duplicate and save the exact sampling contour for use in the other channel of the same image. Sampling data for the channels provided brightness profile patterns of the fluorescent markers with respect to one another.

For C3 and CD11b areal coverage comparisons at critical stages (i.e., P4 and P8 for C3, and P8 and P12 for CD11b), extracted GAD and C3 or CD11b channels from 20x digital merges were opened in FIJI (Schindelin et al., 2012). Five sections were taken from three animals for a total of fifteen sections analyzed at each age. In the GAD channel, modular boundaries were identified (Brett et al., 2022), traced with the freehand tool, and combined using the ROI manager. GAD channels were then closed and all subsequent steps were performed exclusively on corresponding C3 or CD11b channels. The entirety of the LCIC in the field of view was outlined next and added to the ROI manager. Selecting both the GAD-defined modular and total LCIC ROIs, the XOR (i.e., exclusive or operator) function was used to create a ROI for just the encompassing matrix. Additionally, a sufficiently large box was drawn in the region of the C3 or CD11b channel containing no tissue to provide a background level. Modular, matrix, and background medians for each of the ROIs were calculated. The following ratio from those median values was used to assess relative areal C3 or CD11b coverage: (module–background)/(matrix–background). Values above one correlate closely to largely modular expression, those near one indicate comparable or homogeneous compartmental expression, while those diminishing below one indicate expression preference for the surrounding matrix.

Results

C3 expression with respect to emerging LCIC compartments

To explore the potential involvement of the complement system on the refinement of segregating LCIC multisensory maps (Weakley et al., 2022), C3 expression was examined in a developmental series of GAD67-GFP mice (**Figure 1**). Timepoints included four equally spaced stages spanning its established critical period (**Figures 1A–L**), as well as one well after its closure (**Figures 1M–O**). C3 expression is strong at birth, dominating the neuropil throughout the LCIC (**Figures 1A–C**). Many of the small lacunae observed in the dense plexus of C3 immunostaining were occupied by GAD-positive cells (**Figure 1C**). Coincident with the first hints of primitive GAD cell clusters at P4 was the earliest indication of similarly patterned and seemingly spatially matched C3 loss (**Figures 1E, F**). By P8, conspicuous intermittent C3-negative patches were now readily apparent within an encompassing plexus of C3-positive matrix (**Figures 1G–I**). Discontinuous LCIC patches lacking C3 expression reliably aligned with the well-established GAD-positive modular zones at this age (**Figure 1I**). LCIC C3 expression tails off by the critical period end at P12 (**Figures 1J–L**) once multimodal afferents have fully segregated. Absence of any noteworthy C3 was consistently observed at P36, confirming the transient nature of its early postnatal expression (**Figures 1M–O**).

C3 quantification at pivotal LCIC timepoints and areal coverage

Representative brightness plot profiles generated from LCIC layer 2 sampling at P4 and P8, and P12 confirm observed changes in C3 expression with respect to developing LCIC compartments (**Figures 2A–F**). Channel-specific waveforms at P4 (**Figures 2A, B**) reveal hints of emerging periodic signal fluctuations in C3 expression (red) relative to the still developing LCIC modularity (green). At P8 (**Figures 2C, D**), consistently out-of-phase waveforms for C3 and GAD are reliably observed, highlighting the fact that C3 voids (i.e., troughs in red signal) precisely align with clearly defined GAD-positive modules (i.e., peaks in green signal). Lack of noteworthy C3 signal at P12 suggests its downregulation or clearance from both LCIC compartments by its critical period closure (**Figures 2E, F**). Median LCIC areal intensity measures (**Figure 2G**) support these qualitative observations. Calculated compartmental C3 ratios (modules/matrix) decrease significantly from P4 to P8 ($p < 0.001$), as C3 modular voids become increasingly apparent (i.e., matrix-only expression by P8).

Spatiotemporal compartmental localization of CD11b-positive MGCs

Similar to the above-mentioned C3 experiments, CR3/CD11b-expressing microglia were examined relative to the developing LCIC modular-matrix framework (**Figure 3**). CD11b expressing MGCs colonize all three IC subdivisions at birth (**Figures 3A–C**). Starting at P4, CD11b becomes noticeably more restricted to the LCIC as compared to the neighboring CNIC (**Figures 3D–F**). By P8, CD11b-positive microglia are even more biased to the LCIC and most heavily concentrated within layer 2, overlapping GAD-defined modular fields (**Figures 3G–I**). A largely complementary pattern is seen at P12 with MGC location now preferential for the surrounding matrix, suggesting that complement signaling microglia first concentrate within modular zones prior to selective occupancy

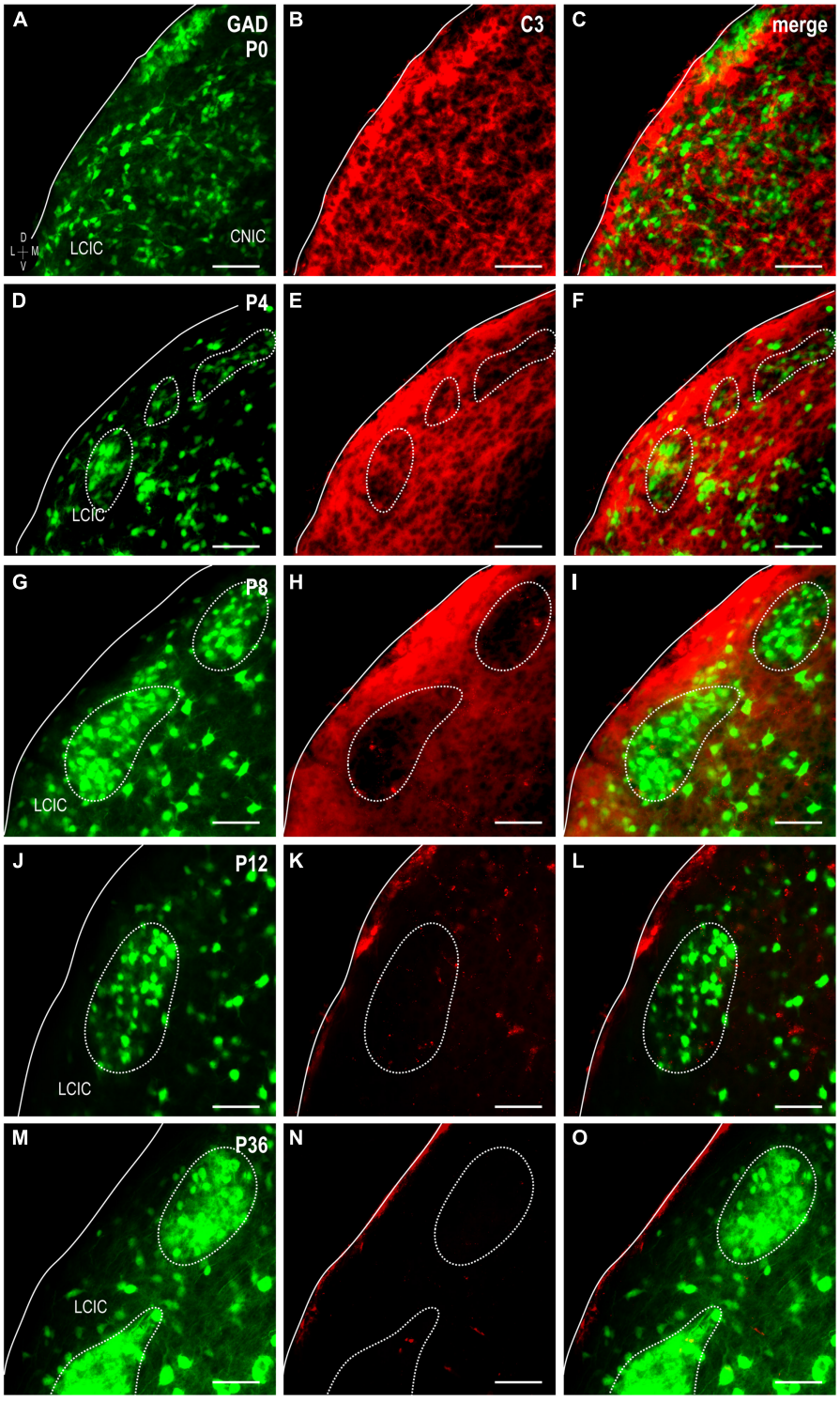

FIGURE 1
Complement component 3 (C3) expression (red) in a developmental series [P0, **(A–C)**; P4, **(D–F)**; P8, **(G–I)**; P12, **(J–L)**; P36, **(M–O)**] of glutamic acid decarboxylase (GAD)-green fluorescent protein (GFP) (green) mice. Hints of GAD-positive lateral cortex of the inferior colliculus (LCIC) modules emerge by P4 and become increasingly apparent with age (*dashed contours*). A diffuse plexus of C3 neuropil expression dominates the LCIC at birth **(B,C)**, with many of its voids occupied by GAD-positive somata. As LCIC modules begin to organize at P4, the slightest indication of C3 loss is observed within these domains **(E,F)**. By P8, C3 expression is completely lacking within GAD-defined modular zones, yet remains strongly concentrated throughout the surrounding matrix **(H,I)**. C3 expression is gone from both LCIC compartments at P12 coincident with its critical period closure **(K,L)**, and remains so thereafter [P36; **(N,O)**]. Scale bars = 50 μm.

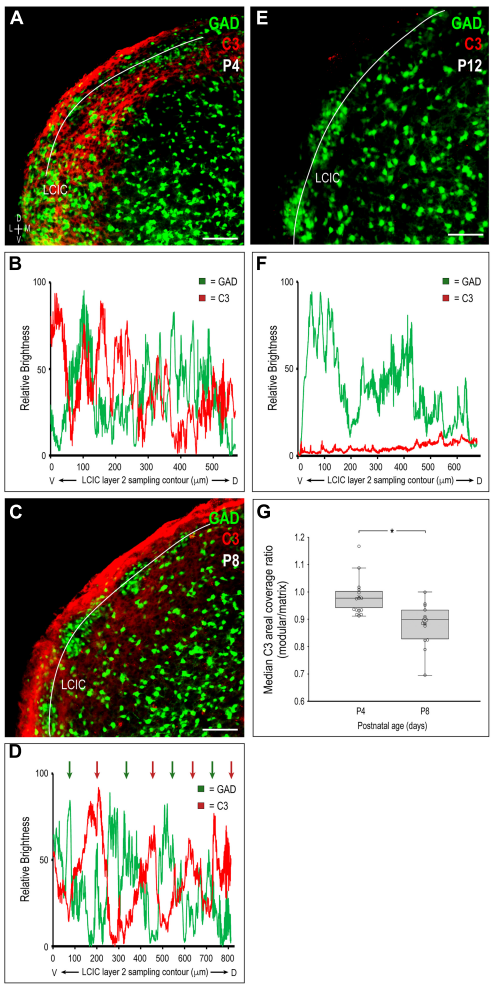

FIGURE 2
Quantification of complement component 3 (C3) expression patterns with respect to the emerging lateral cortex of the inferior colliculus (LCIC) compartmental structure. Multichannel region of interest (ROI) contour sampling of LCIC layer 2 modular fields at P4 **(A)**, P8 **(C)**, and P12 **(E)** with corresponding glutamic acid decarboxylase (GAD) (green) and C3 (red) expression profiles **(B,D,F)**. Although C3 signal fluctuations are evident at P4, they still appear largely unorganized with respect to emerging GAD-positive modules **(B)**. By P8, clear periodicities are observed for both channels with waveforms that are consistently out-of-phase with each other [*green and red arrows* in **(D)**]. Such spatial offset confirms modular-specific C3 loss at this age, with strong expression persisting throughout the encompassing matrix. By LCIC critical period closure at P12, C3 expression is barely detectable **(F)**, suggesting its clearance from both LCIC compartments. Box and whisker plots comparing median compartmental areal coverage ratios at critical period stages P4 and P8 **(G)**. Their vertical separation demonstrates significant differences in modular C3 expression at these ages (*$p < 0.001$). Note that the disjoint P4 and P8 boxes indicate that 3/4 of the P4 ratios are above 3/4 of the P8 ratios. P4 values clustered about or just below 1 suggest a transition at this age from homogeneous C3 LCIC expression seen earlier, to the beginnings of selective C3 disappearance within modular confines. Markedly lower P8 values quantitatively indicate continued modular-specific C3 loss. Horizontal lines within boxes represent medians; X's within boxes represent means. Scale bars in **(A,C,E)** = 100 μm.

of the encompassing matrix (Figures 3J–L). By P36, similar to C3 expression, CD11b-positive microglia are absent throughout the LCIC (Figures 3M–O). Higher magnification imaging highlights preferential clustering within modular confines at P8 (Figure 4A) that shifts to the surrounding matrix by P12 (Figure 4B). Median LCIC CD11b areal intensity measures (Figure 4C) yield ratios at P8 generally above one (i.e. primarily modular) that decrease significantly to generally less than one by P12 (primarily matrix, $p < 0.01$). Taken together, compartment-specific C3 disappearance (first modules, then matrix) follows similarly timed and spatially-matched aggregations of CD11b-expressing microglia. As anticipated, no co-localization between CD11b (microglial) and GAD (neuronal) labeling was observed.

LCIC C3 clearance follows shift in CD11b compartmental expression

Complement component 3 and CD11b were examined together in GAD-67 GFP mice at P8 and P12 to confirm that CD11b-positive MGCs concentrate within GAD modules where C3 expression initially disappears, prior to a similar progression observed in the adjacent matrix (Figure 5). Double-labeling results in GAD-GFP mice reliably show changing CD11b microglial patterns that correlate with age-matched compartmental C3 disappearance, first within layer 2 modules (P8, Figures 5A–D) followed next by the surrounding matrix (P12, Figures 5E–H).

Evidence of LCIC microglial heterogeneity: CX3CR1 and CD11b

The colonization and spatial patterning of fractalkine receptor expressing MGCs (CX3CR1-GFP) in the nascent mouse LCIC has recently been reported by our lab (Brett et al., 2022). Observed CX3CR1 patterns that appeared different from those described here for CD11b prompted further investigations to determine whether distinct MGC subpopulations exist in the LCIC during its early critical period. While present throughout the LCIC at birth, CX3CR1- and CD11b-positive MGCs show little to no noticeable organization and no co-localization (Figure 6A). From P4 to P8, CX3CR1-positive microglia dominate the matrix and ring modular domains that conspicuously lack fractalkine receptor expressing microglia, consistent with that described previously (Brett et al., 2022). CX3CR1 and CD11b continue to label separate MGC subpopulations, with overall spatial patterns that appear equally distinct (matrix vs. modular, respectively; Figures 6B, C). By P12, CX3CR1-positive microglia occupy LCIC modules (delayed in homozygous mice, see Brett et al., 2022), as CD11b-expressing microglia vacate said zones for the encompassing matrix (Figure 6D). Intriguingly, as LCIC

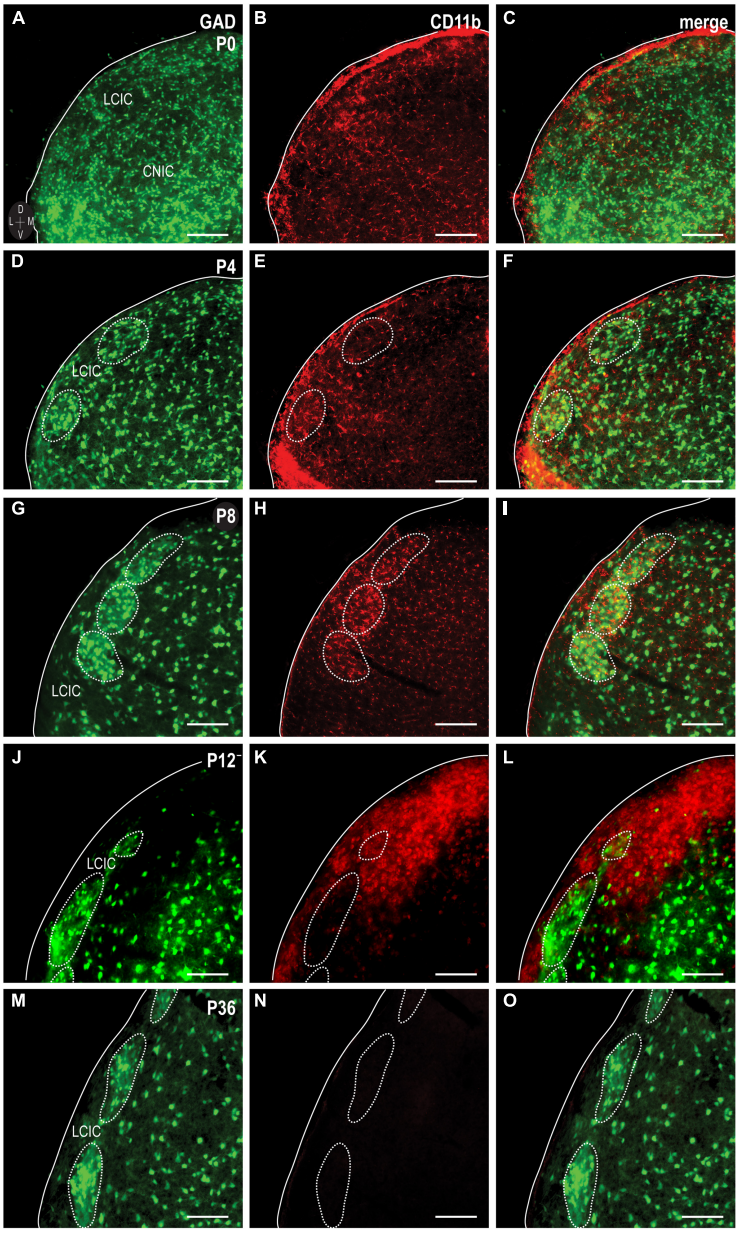

FIGURE 3
Integrin αM (CD11b) expression (red) in a developmental series [P0, **(A–C)**; P4, **(D–F)**; P8, **(G–I)**; P12, **(J–L)**; P36, **(M–O)**] of glutamic acid decarboxylase (GAD)-GFP (green) mice. CD11b expression is apparent and homogeneously distributed throughout IC subdivisions at birth, prior to concentrating more toward the lateral cortex of the inferior colliculus (LCIC) by P4. At P8, CD11b expression localizes most notably within LCIC GAD-defined modular fields. CD11b-expressing microglial cells (MGCs) shift to occupying the surrounding matrix at P12. By P36, CD11b expression is largely undetectable in the LCIC. Scale bars = 100 μm.

modularity emerges from P4 to P12, both populations appear to have changing preferences for different aspects of the developing compartmental framework. CX3CR1-positive microglia appear to congregate in the matrix prior to invasion of the modules, and vice versa for CD11b (Figures 7A–C). Distinct subpopulations for these two microglial markers is best appreciated at higher magnification where lack of any overlap was consistently seen (Figures 7D–F).

Further evidence of LCIC microglial heterogeneity: TMEM119 and Iba1

Lack of CX3CR1 and CD11b colocalization prompted further experimentation utilizing other established microglial markers: TMEM119 and Iba1. TMEM119 is reported to be a highly specific MGC marker in adult mouse, although there is currently no known function for the transmembrane protein

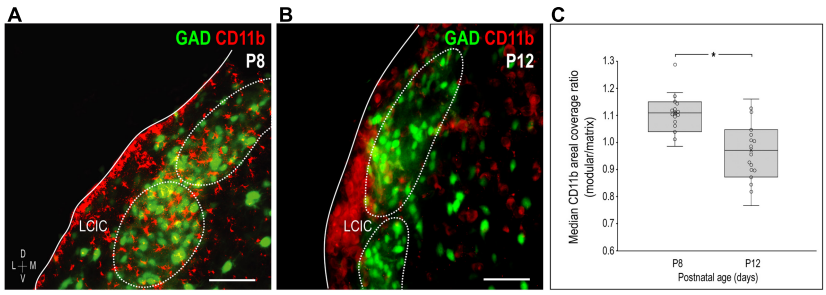

FIGURE 4
Changing compartment-specific integrin αM (CD11b) patterns from P8 to P12. CD11b expression (red) at P8 is concentrated in the lateral cortex of the inferior colliculus (LCIC) and most concentrated within glutamic acid decarboxylase (GAD)-positive modules [green, **(A)**]. CD11b expression at P12 is complementary to that observed at P8, with labeling that now predominates in the surrounding matrix **(B)**. Areal coverage analyses for CD11b **(C)** support qualitative observations, showing significant shifts in CD11b compartmental expression from P8 (primarily modular) to P12 (primarily matrix, $*p < 0.01$). Scale bars in **(A,B)** = 50 μm.

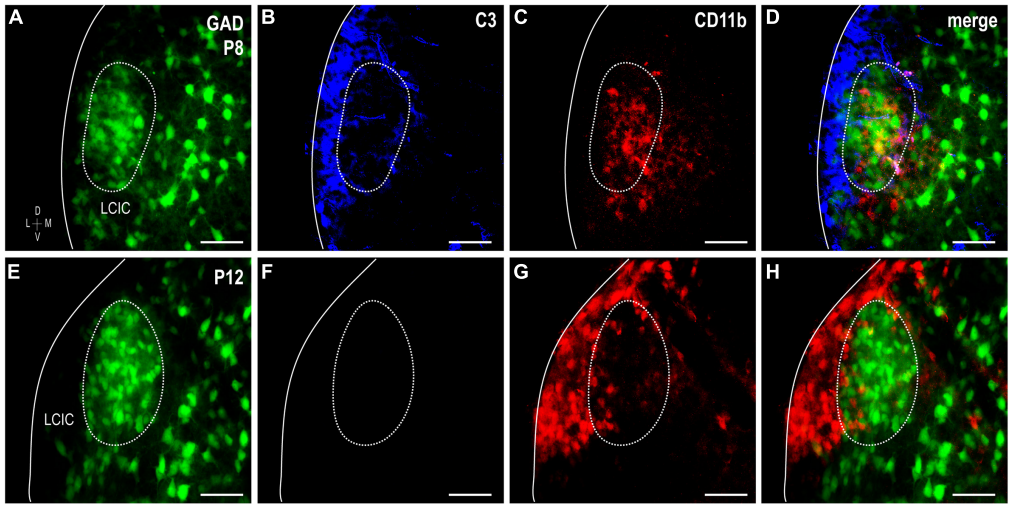

FIGURE 5
Sequential complement component 3 (C3) compartmental clearance follows shift in integrin αM (CD11b)-expressing microglial cell (MGC) location. Double-labeling studies for C3 (blue) and CD11b (red) in glutamic acid decarboxylase (GAD)-GFP (green) mice at P8 **(A–D)** and P12 **(E–H)**. At P8, CD11b-positive microglia occupy GAD-defined modules, where C3 labeling is now weak compared to the surrounding matrix. By P12, CD11b-positive MGCs preferentially congregate in the matrix where C3 expression is now also unremarkable. Scale bars = 50 μm.

(Bennett et al., 2016). TMEM119 immunocytochemistry in a developmental series of CX3CR1-GFP mice (**Figure 8**) shows that while absent at birth, it is detectable thereafter throughout IC, and biased toward LCIC layer 2 modular fields. Again, no significant colocalization was observed at any stage, with the only exception being the very occasional double-labeled cell encountered at P12.

To confirm the relative spatial and cellular patterns observed for the various MGC markers in the same tissue, immunolabeling for both CD11b and TMEM119 was performed in P8 CX3CR1-GFP tissue (**Figure 9**). This timepoint was chosen for further investigation as each marker exhibits LCIC compartmental-specific expression at this age. CX3CR1-positive MGCs occupy the matrix (**Figure 9A**) and ring modules (for more *see* Brett et al., 2022) largely positive for CD11b- and TMEM119-expressing microglia (**Figures 9B, C**). Despite the similar overall preference of CD11b- and TMEM119-positive cells for modular zones at P8, little cellular colocalization was observed (**Figure 9D**), suggesting the presence of multiple distinct MGC subsets that may serve potentially different roles in development.

Iba1 (ionized calcium-binding adapter molecule 1), yet another MGC-specific marker, was investigated at P8 in CX3CR1-GFP mice alongside CD11b (**Figures 9E–H**). No triple-labeled cells were observed, nor were double-labeled cells for CD11b and Iba1. However, all Iba1-positive microglia were also CX3CR1-positive, and there was a distinct population of fractalkine receptor-expressing cells which did not express

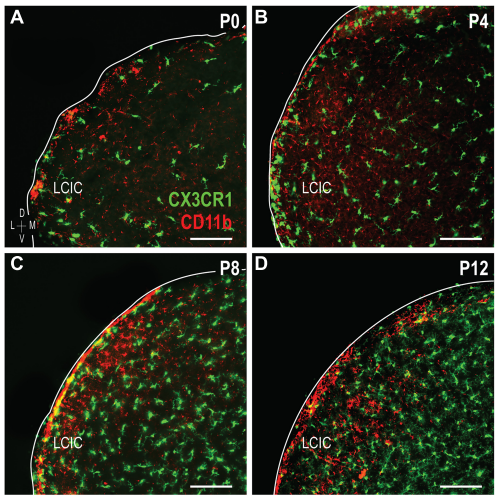

FIGURE 6
Developmental progression of digital merges of integrin αM (CD11b) immunostaining in CX3CR1-GFP heterozygous mice **(A–D)**. Microglial cells (MGCs) expressing the fractalkine receptor (CX3CR1, green) appear to be distinct subpopulations from those expressing CD11b (red) in the lateral cortex of the inferior colliculus (LCIC) throughout its early critical period. CX3CR1 patterns shown here are in keeping with those recently reported Brett et al. (2022), namely with matrix dominated expression that rings modular domains at P4/P8, prior to entering modules at P12. This progression contrasts that for CD11b, which first shows preference for LCIC modules, prior to a later shift into surrounding matrix regions. Scale bars = 100 μm.

Iba1. This particular finding is in keeping with that previously reported (Brett et al., 2022). These results further substantiate the notion that extensive MGC heterogeneity exists within the LCIC during its early postnatal critical period.

Discussion

Results of the present study suggest complement cascade involvement and microglial heterogeneity in the LCIC during its established developmental critical period. C3 and CD11b are transiently expressed as LCIC compartments emerge (Dillingham et al., 2017; Gay et al., 2018; Stinson et al., 2021) and multimodal LCIC afferents segregate accordingly (Lamb-Echegaray et al., 2019; Weakley et al., 2022). Clustering of CD11b-positive MGCs within the modules first and then the matrix, coupled with the sequential disappearance of C3 from said zones, implicate C3-CR3/CD11b signaling as being important for pruning early LCIC multimodal maps. Evidence of heterogenous MGC subpopulations with changing spatial patterns suggests potentially distinct roles and responsibilities for each during early ontogeny. Further classification of these and likely other yet to be identified MGC subsets will be important for providing insights into the mechanisms underlying multisensory circuit assembly, and how aberrant network refinement correlates with certain neurodevelopmental conditions, like ASD and schizophrenia.

Complement signaling and compartmental pruning within the developing LCIC

The temporal and spatial shaping of auditory and somatosensory afferent patterns correlate not only with emerging LCIC compartments, but also with the discretely-organized complement component protein expression reported here. Both C3 and CD11b are transiently expressed or cleared shortly after the LCIC critical period closure. CD11b-positive MGC occupancy that parallels the disappearance of C3 first within the modules followed by the matrix (**Figure 10**), speaks toward the likelihood of complement-dependent LCIC pruning that follows a compartmental-specific progression. Analogous C3 experiments to those performed here in CR3KO mice are needed to further substantiate this claim. If indeed C3-CR3 binding is required for selective LCIC pruning, one might hypothesize the observed sequence of C3 loss would not be seen in mutants with compromised signaling. Additional studies that assess relative MGC engulfment activity (e.g., C3-tagged somatosensory and/or auditory terminals) in various mutant strains at critical developmental stages should provide further insights concerning the specific roles microglia play in aspects of LCIC multisensory circuitry refinement.

Synaptic elimination in other systems appears to be mediated in part by other identified opsonins that may also figure prominently in the refinement of early LCIC networks. Externalized phosphatidylserine (PS) induces phagocytic MGC activity through several of its cognate receptors (e.g., TREM2, GPR56; Li et al., 2020; Scott-Hewitt et al., 2020; Raiders et al., 2021), and also partners with upstream complement components such as C1q to instruct engulfment behaviors (Païdassi et al., 2008; Martin et al., 2012). PS localization in the developing hippocampus and visual thalamus is predominantly presynaptic and is selectively targeted by MGCs during established periods of peak pruning. Similar to C3/CR3 knockouts (Schafer et al., 2012), retinogeniculate connections in C1q mutants are insufficiently pruned and exhibit elevated levels of PS and reduced engulfment of PS-labeled material (Scott-Hewitt et al., 2020). Whether PS and/or C1q are present in the developing LCIC, and whether or not each function independently or may influence other aspects of complement signaling within this structure remains to be determined.

MGC heterogeneity in the nascent LCIC

Multiple LCIC microglial subsets with seemingly unique molecular signatures were demonstrated in the present study.

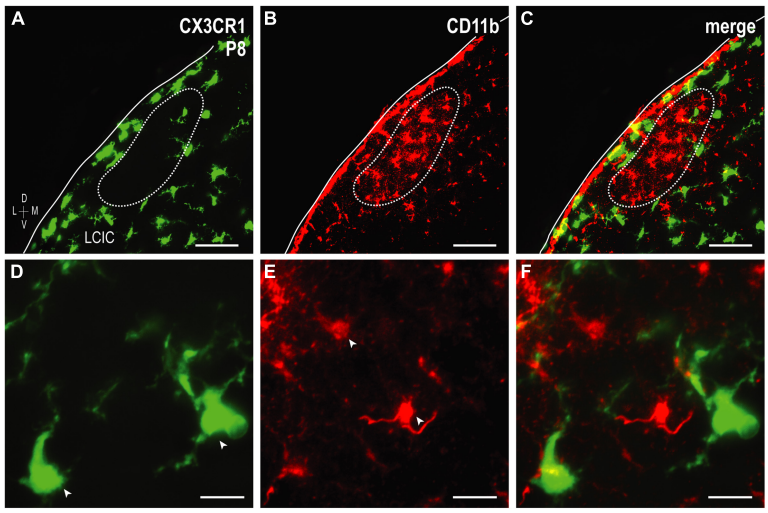

FIGURE 7
Higher magnification series of integrin αM (CD11b) expression in P8 fractalkine receptor (CX3CR1)-GFP tissue showing distinct microglial cell (MGC) subsets. CX3CR1-expressing microglia (green) at P8 surround modules [*dashed contours*, **(A–C)**, for more see Brett et al., 2022] where complement receptor expression (CD11b, red) is most concentrated. At every examined timepoint with notable CD11b expression (i.e., not P36), lateral cortex of the inferior colliculus (LCIC) CX3CR1 **(D)** and CD11b **(E)** expression was non-overlapping **(F)**, providing evidence that supports the notion of different MGC populations with unique molecular signatures. Arrowheads in **(D,E)** indicate unique microglial subpopulations. Scale bars in **(A–C)** = 50 μm; **(D–F)** = 20 μm.

Recent single-cell RNA-seq studies in other brain areas reveal distinct MGC transcriptional clusters across the lifespan and in response to injury/inflammation, with the most marked diversity observed during early critical periods of development (De Biase et al., 2017; Hammond et al., 2019; Li et al., 2019; Masuda et al., 2019, 2020; Tan et al., 2020). The significant lack of co-localization for most of the microglial markers examined here, with any observed overlap being the exception rather than the norm, supports the notion of considerable MGC heterogeneity in the developing LCIC (**Figure 11**). Certainly, there are numerous other established MGC markers (e.g., P2YR12, SIRPα, CD115, etc.; Jurga et al., 2020; Raiders et al., 2021) not explored here that could shed further light on the extent of LCIC MGC heterogeneity. Correlating such immunostaining findings with future RNA-sequencing experiments focused on the nascent LCIC should prove highly informative about the extent of distinct MGC subpopulations, and perhaps the potential responsibilities each have for orchestrating various developmental events.

MGC pruning and neurodevelopmental conditions

In addition to specific opsonins marking underutilized contacts and debris for selective phagocytosis, other tags such as CD47 appear to serve an alternate role, one of protecting connections deemed necessary from potential elimination (Lehrman et al., 2018; Raiders et al., 2021). A balance of "eat me" and "don't eat me" tags is important for ensuring that MGC mediated pruning is sufficient and not overstated in the developing brain. Such under- or over-pruning during especially critical windows are thought to correlate

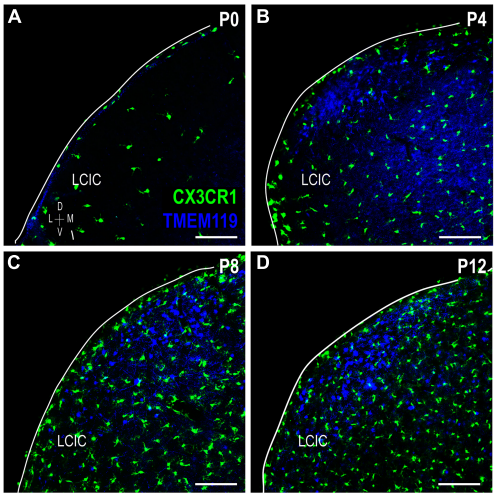

FIGURE 8
Transmembrane protein (TMEM119) expression (blue) in a developmental series **(A–D)** of fractalkine receptor (CX3CR1)-GFP (green) mice. Lateral cortex of the inferior colliculus (LCIC) TMEM119 expression is absent at birth (a) and then largely localized to layer 2 after its appearance at P4 **(B–D)**. Aside from rare double-labeled cells seen at P12 (*data not shown*), no co-localization was observed. Scale bars = 100 μm.

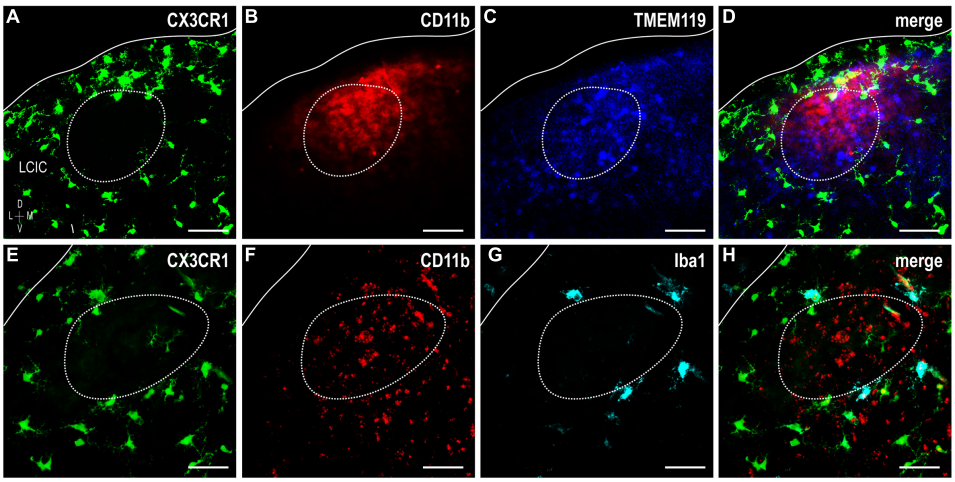

FIGURE 9
Fractalkine receptor (CX3CR1)-GFP (green), integrin αM (CD11b) (red), and transmembrane protein (TMEM119) (blue) or Iba1 (cyan) expression at P8. Significant lack of co-localization of established MGC markers supports considerable lateral cortex of the inferior colliculus (LCIC) microglial diversity during its early critical period. CX3CR1-positive microglial cells (MGCs) occupy the matrix and surround modules (*dashed contours,* for more see Brett et al., 2022) while CD11b and TMEM119 labeling exhibits a complementary modular bias **(A–D)**. Like CX3CR1, Iba1-positive microglia ring LCIC modules at P8, and are distinct from CD11b staining **(E–H)**. While all Iba1-positive cells also express CX3CR1, not all fractalkine receptor expressing cells are positive Iba1. Scale bars = 50 μm.

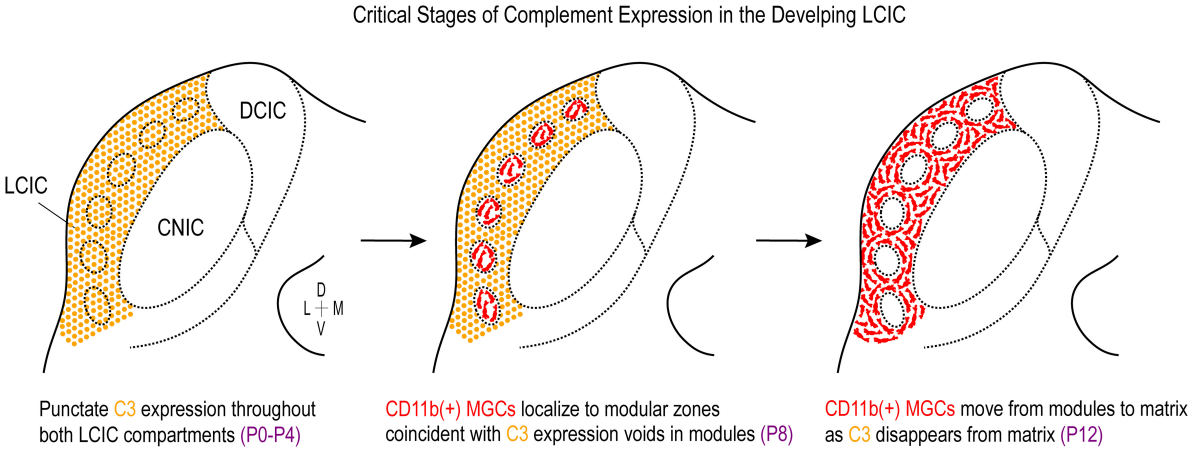

FIGURE 10
Summary schematic of complement cascade expression in the developing lateral cortex of the inferior colliculus (LCIC). Complement component 3 (C3) expression (orange) is prominent throughout both LCIC compartments at the earliest timepoints examined (P0–P4). Integrin αM (CD11b)-positive microglia (red) are present in the LCIC at these stages (not shown), although do not exhibit any compartmental bias yet. At the critical period peak (P8), C3 expression is selectively lost from modular zones which are now occupied by CD11b-positive microglial cells (MGCs). By P12, CD11b-expressing microglia now occupy the encompassing matrix, where C3 expression is no longer apparent. This developmental sequence implicates complement cascade signaling as a potential key player in compartmental-specific pruning in the nascent LCIC.

with common behavioral phenotypes associated with certain neurodevelopmental conditions. Autism spectrum disorders are typically associated with under-pruning and increased dendritic spine densities compared to neurotypical controls (Hustler and Zhang, 2010; Faust et al., 2021). Several ASD-linked genes are known to influence synaptic pruning in mice, with reported decreases in network refinement and altered social behaviors (Voineagu et al., 2011; De Rubeis et al., 2014; Bourgeron, 2015). In contrast to ASD, various models of schizophrenia consistently point toward over-pruning defects, with reduced spine densities in various brain regions (Fromer et al., 2014; Presumey et al., 2017; Johnson and Stevens, 2018; Yilmaz et al., 2021).

Construction and appropriate sculpting of integrative multisensory circuits during development are likely key for

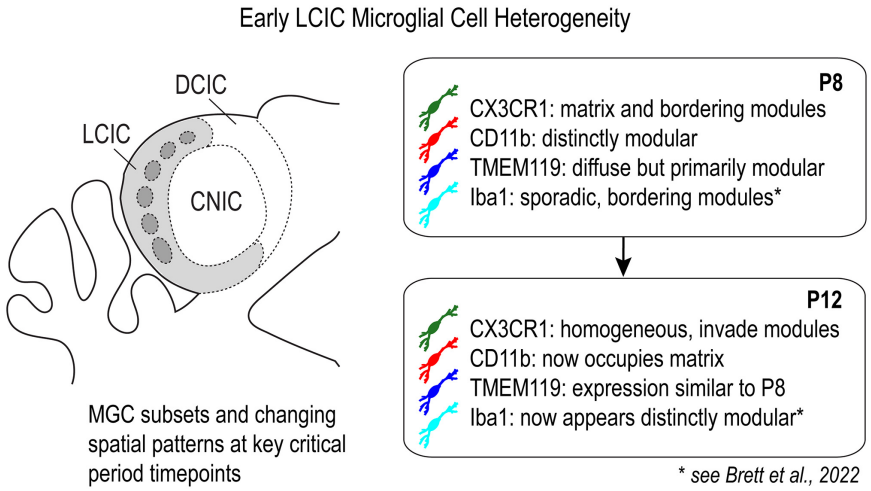

FIGURE 11
Schematic highlighting differential expression of established microglial cell (MGC) markers in the lateral cortex of the inferior colliculus (LCIC) at key critical period timepoints.

realizing early social-communication milestones. Deficits in certain sensory tasks are highly predictive of later onset and severity of cognitive and behavioral symptoms associated with ASD (Brandwein et al., 2015; Robertson and Baron-Cohen, 2017). In addition to unisensory assessments, impairments in multisensory perceptual binding (Kwakye et al., 2011; Collignon et al., 2013; Stevenson et al., 2014a,b,c, 2018) provide perhaps the most relevant diagnostic criteria, as hallmark features of autism (e.g., difficulties with speech, communication, and social interactions) are inherently multisensory processes. The LCIC with its segregated multimodal afferent-efferent systems likely serves as an important staging ground for further sensory integration at next-level structures (Lesicko et al., 2020). In addition, the LCIC figures prominently in the processing of certain reflexive behaviors (e.g., pre-pulse inhibition, PPI, of the acoustic startle response, ASR), and lesioning of the LCIC is known to significantly alter such responses (Groves et al., 1974; Leitner and Cohen, 1985; Parham and Willott, 1990). Changes in LCIC-mediated response behaviors (ASR, PPI) have been reported extensively in individuals with autism and schizophrenia (Kohl et al., 2013; Haß et al., 2017; Takahashi and Kamio, 2018). Further inquiries that build upon our present findings are needed to determine the extent to which developmental pruning programs may go awry in multisensory structures like the LCIC, and the behavioral consequences that manifest as a result in certain neurodevelopmental conditions.

Concluding remarks

This study implicates microglia and complement cascade signaling in the compartmental-specific pruning of early connections within the LCIC. Furthermore, our data suggest significant MGC heterogeneity in multisensory regions of the developing midbrain. The mechanisms that govern the precise expression of its molecular tags (e.g. activity-dependent C3/CD47 expression) and the manner in which specific MGC subpopulations are signaled in the LCIC, however, remain largely unaddressed. Careful mapping of the described regional changes and heterogeneities to future single-cell RNA sequencing and spatial transcriptomic studies of LCIC glial populations should deepen our appreciation for the complexity of multisensory midbrain pruning programs and how each may figure into the pathogenesis of certain neurodevelopmental disorders.

Data availability statement

The raw data supporting the conclusions of this article will be made available by the authors, without undue reservation.

Ethics statement

The animal study was reviewed and approved by the James Madison University's Animal Care and Use Committee (approval number: 20-1421).

Author contributions

JC, SH, and MG contributed to the presented experiments. JC and SH performed the all tissue processing,

associated imaging, and data sampling. JC and MG performed the data quantification. MG prepared the all figures and wrote the manuscript. All authors contributed to the article and approved the submitted version.

Funding

This work was funded by the National Institutes of Health (1R15DC018885-01), the National Science Foundation (DBI-0619207 and DBI-1725855), and the JMU Department of Biology Light Microscopy and Imaging Facility.

Acknowledgments

We would like to thank Dr. Thomas Gabriele for his statistical consultations, Dr. Kristopher Kubow for his microscopy help with areal coverage analysis, and Stephanie Atkins and Sarah Keegan for their invaluable assistance with breeding and maintenance of our mouse colony.

Conflict of interest

The authors declare that the research was conducted in the absence of any commercial or financial relationships that could be construed as a potential conflict of interest.

Publisher's note

References

Aitkin, L. M., Dickhaus, H., Schult, W., and Zimmermann, M. (1978). External nucleus of inferior colliculus: Auditory and spinal somatosensory afferents and their interactions. *J. Neurophysiol.* 41, 837–847. doi: 10.1152/jn.1978.41.4.837

Aitkin, L. M., Kenyon, C. E., and Philpott, P. (1981). The representation of the auditory and somatosensory systems in the external nucleus of the cat inferior colliculus. *J. Comp. Neurol.* 196, 25–40. doi: 10.1002/cne.901960104

Arnoux, I., and Audinat, E. (2015). Fractalkine signaling and microglia functions in the developing brain. *Neural Plast.* 2015:689404. doi: 10.1155/2015/689404

Bajic, G., Yatime, L., Sim, R. B., Vorup-Jensen, T., and Andersen, G. R. (2013). Structural insight on the recognition of surface-bound opsonins by the integrin I domain of complement receptor 3. *Proc. Natl. Acad. Sci. U.S.A.* 110, 16426–16431. doi: 10.1073/pnas.1311261110

Bennett, M. L., Bennett, F. C., Liddelow, S. A., Ajami, B., Zamanian, J. L., Fernhoff, N. B., et al. (2016). New tools for studying microglia in the mouse and human CNS. *Proc. Natl. Acad. Sci. U.S.A.* 113, E1738–E1746. doi: 10.1073/pnas.1525528113

Bordeleau, M., Carrier, M., Luheshi, G. N., and Tremblay, M. É (2019). Microglia along sex lines: From brain colonization, maturation and function, to implication in neurodevelopmental disorders. *Semin. Cell. Dev. Biol* 94, 152–163. doi: 10.1016/j.semcdb.2019.06.001

Brandwein, A. B., Foxe, J. J., Butler, J. S., Frey, H. P., Bates, J. C., Shulman, L. H., et al. (2015). Neurophysiological indices of atypical auditory processing and multisensory integration are associated with symptom severity in autism. *J. Autism Dev. Disord.* 45, 230–244. doi: 10.1007/s10803-014-2212-9

Brett, C. A., Carroll, J. B., and Gabriele, M. L. (2022). Compromised fractalkine signaling delays microglial occupancy of emerging modules in the multisensory midbrain. *Glia* 7, 697–711. doi: 10.1002/glia.24134

Bourgeron, T. (2015). From the genetic architecture to synaptic plasticity in autism spectrum disorder. *Nat. Rev. Neurosci.* 16, 551–563. doi: 10.1038/nrn3992

Chernock, M. L., Larue, D. T., and Winer, J. A. (2004). A periodic network of neurochemical modules in the inferior colliculus. *Hear. Res.* 188, 12–20. doi: 10.1016/S0378-5955(03)00340-X

Collignon, O., Charbonneau, G., Peters, F., Nassim, M., Lassonde, M., Lepore, F., et al. (2013). Reduced multisensory facilitation in persons with autism. *Cortex* 49, 1704–1710. doi: 10.1016/j.cortex.2012.06.001

De Biase, L. M., Schuebel, K. E., Fusfeld, Z. H., Jair, K., Hawes, I. A., Cimbro, R., et al. (2017). Local cues establish and maintain region-specific phenotypes of basal ganglia microglia. *Neuron* 95, 341.e–356.e. doi: 10.1016/j.neuron.2017.06.020

De Rubeis, S., He, X., Goldberg, A. P., Poultney, C. S., Samocha, K., Cicek, A. E., et al. (2014). Synaptic, transcriptional and chromatin genes disrupted in autism. *Nature* 515, 209–215. doi: 10.1038/nature13772

Dillingham, C. H., Gay, S. M., Behrooz, R., and Gabriele, M. L. (2017). Modular-extramodular organization in developing multisensory shell regions of the mouse inferior colliculus. *J. Comp. Neurol.* 525, 3742–3756. doi: 10.1002/cne.24300

Faust, T. E., Gunner, G., and Schafer, D. P. (2021). Mechanisms governing activity-dependent synaptic pruning in the developing mammalian CNS. *Nat. Rev. Neurosci.* 22, 657–673. doi: 10.1038/s41583-021-00507-y

Fromer, M., Pocklington, A. J., Kavanagh, D. H., Williams, H. J., Dwyer, S., Gormley, P., et al. (2014). De novo mutations in schizophrenia implicate synaptic networks. *Nature* 506, 179–184. doi: 10.1038/nature12929

Gay, S. M., Brett, C. A., Stinson, J. P. C., and Gabriele, M. L. (2018). Alignment of EphA4 and ephrin-B2 expression patterns with developing modularity in the lateral cortex of the inferior colliculus. *J. Comp. Neurol.* 526, 2706–2721.

Groves, P. M., Wilson, C. J., and Boyle, R. D. (1974). Brain stem pathways, cortical modulation, and habituation of the acoustic startle response. *Behav. Biol.* 10, 391–418. doi: 10.1016/s0091-6773(74)91975-0

Gruters, K. G., and Groh, J. M. (2012). Sounds and beyond: Multisensory and other non-auditory signals in the inferior colliculus. *Front. Neural Circuits* 6:96. doi: 10.3389/fncir.2012.00096

Gunner, G., Cheadle, L., Johnson, K. M., Ayata, P., Badimon, A., Mondo, E., et al. (2019). Sensory lesioning induces microglial synapse elimination via ADAM10 and fractalkine signaling. *Nat. Neurosci.* 22, 1075–1088. doi: 10.1038/s41593-019-0419-y

Haß, K., Bak, N., Szycik, G. R., Glenthøj, B. Y., and Oranje, B. (2017). Deficient prepulse inhibition of the startle reflex in schizophrenia using a cross-modal paradigm. *Biol. Psychol.* 128, 112–116. doi: 10.1016/j.biopsycho.2017.07.016

Hammond, T. R., Dufort, C., Dissing-Olesen, L., Giera, S., Young, A., Wysoker, A., et al. (2019). Single-cell RNA sequencing of microglia throughout the mouse lifespan and in the injured brain reveals complex cell-state changes. *Immunity* 50, 253.e–271.e. doi: 10.1016/j.immuni.2018.11.004

Harrison, J. K., Jiang, Y., Chen, S., Xia, Y., Maciejewski, D., McNamara, R. K., et al. (1998). Role for neuronally derived fractalkine in mediating interactions

between neurons and CX3CR1-expressing microglia. *Proc. Natl. Acad. Sci. U.S.A.* 95, 10896–10901. doi: 10.1073/pnas.95.18.10896

Hong, S., Dissing-Olesen, L., and Stevens, B. (2016). New insights on the role of microglia in synaptic pruning in health and disease. *Curr. Opin. Neurobiol.* 36, 128–134. doi: 10.1016/j.conb.2015.12.004

Hoshiko, M., Arnoux, I., Avignone, E., Yamamoto, N., and Audinat, E. (2012). Deficiency of the microglial receptor CX3CR1 impairs postnatal functional development of thalamocortical synapses in the barrel cortex. *J. Neurosci.* 32, 15106–15111. doi: 10.1523/jneurosci.1167-12.2012

Hustler, J., and Zhang, H. (2010). Increased dendritic spine densities on cortical projection neurons in autism spectrum disorders. *Brain Res.* 1309, 83–94. doi: 10.1016/j.brainres.2009.09.120

Jain, R., and Shore, S. (2006). External inferior colliculus integrates trigeminal and acoustic information: Unit responses to trigeminal nucleus and acoustic stimulation in the guinea pig. *Neurosci. Lett.* 395, 71–75. doi: 10.1016/j.neulet.2005.10.077

Johnson, M. B., and Stevens, B. (2018). Pruning hypothesis comes of age. *Nature* 554, 438–439. doi: 10.1038/d41586-018-02053-7

Jung, S., Aliberti, J., Graemmel, P., Sunshine, M. J., Kreutzberg, G. W., Sher, A., et al. (2000). Analysis of fractalkine receptor CX(3)CR1 function by targeted deletion and green fluorescent protein reporter gene insertion. *Mol. Cell. Biol.* 20, 4106–4114. doi: 10.1128/MCB.20.11.4106-4114.2000

Jurga, A. M., Paleczna, M., and Kuter, K. Z. (2020). Overview of general and discriminating markers of differential microglia phenotypes. *Front. Cell. Neurosci.* 14:198. doi: 10.3389/fncel.2020.00198

Kohl, S., Heekeren, K., Klosterkötter, J., and Kuhn, J. (2013). Prepulse inhibition in psychiatric disorders–apart from schizophrenia. *J. Psychiatr. Res.* 47, 445–452. doi: 10.1016/j.jpsychires.2012.11.018

Kwakye, L. D., Foss-Feig, J. H., Cascio, C. J., Stone, W. L., and Wallace, M. T. (2011). Altered auditory and multisensory temporal processing in autism spectrum disorders. *Front. Integr. Neurosci.* 4:129. doi: 10.3389/fnint.2010.00129

Lamb-Echegaray, I. D., Noftz, W. A., Stinson, J. P. C., and Gabriele, M. L. (2019). Shaping of discrete auditory inputs to extramodular zones of the lateral cortex of the inferior colliculus. *Brain Struct. Funct.* 224, 3353–3371. doi: 10.1007/s00429-019-01979-6

Lamers, C., Plüss, C. J., and Ricklin, D. (2021). The promiscuous profile of complement receptor 3 in ligand binding, immune modulation, and pathophysiology. *Front. Immunol.* 12:662164. doi: 10.3389/fimmu.2021.662164

Lehrman, E. K., Wilton, D. K., Litvina, E. Y., Welsh, C. A., Chang, S. T., Frouin, A., et al. (2018). CD47 protects synapses from excess microglia-mediated pruning during development. *Neuron* 100, 120.e–134.e. doi: 10.1016/j.neuron.2018.09.017

Leitner, D. S., and Cohen, M. E. (1985). Role of the inferior colliculus in the inhibition of acoustic startle in the rat. *Physiol. Behav.* 34, 65–70. doi: 10.1016/0031-9384(85)90079-4

Lesicko, A. M. H., Hristova, T. S., Maigler, K. C., and Llano, D. A. (2016). Connectional modularity of top-down and bottom-up multimodal inputs to the lateral cortex of the mouse inferior colliculus. *J. Neurosci.* 36, 11037–11050. doi: 10.1523/jneurosci.4134-15.2016

Lesicko, A. M. H., Sons, S. K., and Llano, D. A. (2020). Circuit mechanisms underlying the segregation and integration of parallel processing streams in the inferior colliculus. *J. Neurosci.* 40, 6328–6344. jneurosci.0646-20.2020 doi: 10.1523/

Li, Q., Cheng, Z., Zhou, L., Darmanis, S., Neff, N. F., Okamoto, J., et al. (2019). Developmental heterogeneity of microglia and brain myeloid cells revealed by deep single-cell RNA sequencing. *Neuron* 101, 207.e–223.e. doi: 10.1016/j.neuron.2018.12.006

Li, T., Chiou, B., Gilman, C. K., Luo, R., Koshi, T., Yu, D., et al. (2020). A splicing isoform of GPR56 mediates microglial synaptic refinement via phosphatidylserine binding. *EMBO J.* 39:e104136. doi: 10.15252/embj.2019104136

Martin, M., Leffler, J., and Blom, A. M. (2012). Annexin A2 and A5 serve as new ligands for C1q on apoptotic cells. *J. Biol. Chem.* 287, 33733–33744. doi: 10.1074/jbc.M112.341339

Masuda, T., Sankowski, R., Staszewski, O., Böttcher, C., Amann, L., Sagar, et al. (2019). Spatial and temporal heterogeneity of mouse and human microglia at single-cell resolution. *Nature* 566, 388–392. doi: 10.1038/s41586-019-0924-x

Masuda, T., Sankowski, R., Staszewski, O., and Prinz, M. (2020). Microglia heterogeneity in the single-cell era. *Cell Rep.* 30, 1271–1281. doi: 10.1016/j.celrep.2020.01.010

Mosser, C. A., Baptista, S., Arnoux, I., and Audinat, E. (2017). Microglia in CNS development: Shaping the brain for the future. *Prog. Neurobiol.* 149-150, 1–20. doi: 10.1016/j.pneurobio.2017.01.002

Ono, M., Yanagawa, Y., and Koyano, K. (2005). GABAergic neurons in inferior colliculus of the GAD67-GFP knock-in mouse: Electrophysiological and morphological properties. *Neurosci. Res.* 51, 475–492. doi: 10.1016/j.neures.2004.12.019

Pagani, F., Paolicelli, R. C., Murana, E., Cortese, B., Di Angelantonio, S., Zurolo, E., et al. (2015). Defective microglial development in the hippocampus of Cx3cr1 deficient mice. *Front. Cell. Neurosci.* 9:111. doi: 10.3389/fncel.2015.00111

Parham, K., and Willott, J. F. (1990). Effects of inferior colliculus lesions on the acoustic startle response. *Behav. Neurosci.* 104, 831–840. doi: 10.1037//0735-7044.104.6.831

Paolicelli, R. C., Bisht, K., and Tremblay, M. É (2014). Fractalkine regulation of microglial physiology and consequences on the brain and behavior. *Front. Cell. Neurosci.* 8:129. doi: 10.3389/fncel.2014.00129

Paolicelli, R. C., Bolasco, G., Pagani, F., Maggi, L., Scianni, M., Panzanelli, P., et al. (2011). Synaptic pruning by microglia is necessary for normal brain development. *Science* 333, 1456–1458. doi: 10.1126/science.1202529

Païdassi, H., Tacnet-Delorme, P., Garlatti, V., Darnault, C., Ghebrehiwet, B., Gaboriaud, C., et al. (2008). C1q binds phosphatidylserine and likely acts as a multiligand-bridging molecule in apoptotic cell recognition. *J. Immunol.* 180, 2329–2338. doi: 10.4049/jimmunol.180.4.2329

Presumey, J., Bialas, A. R., and Carroll, M. C. (2017). Complement system in neural synapse elimination in development and disease. *Adv. Immunol.* 135, 53–79. doi: 10.1016/bs.ai.2017.06.004

Raiders, S., Han, T., Scott-Hewitt, N., Kucenas, S., Lew, D., Logan, M. A., et al. (2021). Engulfed by glia: Glial pruning in development, function, and injury across species. *J. Neurosci.* 41, 823–833. doi: 10.1523/jneurosci.1660-20.2020

Robertson, C. E., and Baron-Cohen, S. (2017). Sensory perception in autism. *Nat. Rev. Neurosci.* 18, 671–684. doi: 10.1038/nrn.2017.112

Schafer, D. P., Lehrman, E. K., Kautzman, A. G., Koyama, R., Mardinly, A. R., Yamasaki, R., et al. (2012). Microglia sculpt postnatal neural circuits in an activity and complement-dependent manner. *Neuron* 74, 691–705. doi: 10.1016/j.neuron.2012.03.026

Schindelin, J., Arganda-Carreras, I., Frise, E., Kaynig, V., Longair, M., Pietzsch, T., et al. (2012). Fiji: An open-source platform for biological-image analysis. *Nat. Methods* 9, 676–682. doi: 10.1038/nmeth.2019

Scott-Hewitt, N., Perrucci, F., Morini, R., Erreni, M., Mahoney, M., Witkowska, A., et al. (2020). Local externalization of phosphatidylserine mediates developmental synaptic pruning by microglia. *EMBO J.* 39:e105380. doi: 10.15252/embj.2020105380

Stephan, A. H., Barres, B. A., and Stevens, B. (2012). The complement system: An unexpected role in synaptic pruning during development and disease. *Annu. Rev. Neurosci.* 35, 369–389. doi: 10.1146/annurev-neuro-061010-113810

Stevens, B., Allen, N. J., Vazquez, L. E., Howell, G. R., Christopherson, K. S., Nouri, N., et al. (2007). The classical complement cascade mediates CNS synapse elimination. *Cell* 131, 1164–1178. doi: 10.1016/j.cell.2007.10.036

Stevenson, R. A., Segers, M., Ferber, S., Barense, M. D., and Wallace, M. T. (2014a). The impact of multisensory integration deficits on speech perception in children with autism spectrum disorders. *Front. Psychol.* 5:379. doi: 10.3389/fpsyg.2014.00379

Stevenson, R. A., Siemann, J. K., Schneider, B. C., Eberly, H. E., Woynaroski, T. G., Camarata, S. M., et al. (2014b). Multisensory temporal integration in autism spectrum disorders. *J. Neurosci.* 34, 691–697. doi: 10.1523/jneurosci.3615-13.2014

Stevenson, R. A., Siemann, J. K., Woynaroski, T. G., Schneider, B. C., Eberly, H. E., Camarata, S. M., et al. (2014c). Evidence for diminished multisensory integration in autism spectrum disorders. *J. Autism Dev. Disord.* 44, 3161–3167. doi: 10.1007/s10803-014-2179-6

Stevenson, R. A., Segers, M., Ncube, B. L., Black, K. R., Bebko, J. M., Ferber, S., et al. (2018). The cascading influence of multisensory processing on speech perception in autism. *Autism* 22, 609–624. doi: 10.1177/1362361317704413

Stinson, J. P. C., Brett, C. A., Carroll, J. B., and Gabriele, M. L. (2021). Registry of compartmental ephrin-B3 guidance patterns with respect to emerging multimodal midbrain maps. *Front. Neuroanat.* 15:649478. doi: 10.3389/fnana.2021.649478

Takahashi, H., and Kamio, Y. (2018). Acoustic startle response and its modulation in schizophrenia and autism spectrum disorder in Asian subjects. *Schizophr. Res.* 198, 16–20. doi: 10.1016/j.schres.2017.05.034

Tamamaki, N., Yanagawa, Y., Tomioka, R., Miyazaki, J., Obata, K., and Kaneko, T. (2003). Green fluorescent protein expression and colocalization with calretinin, parvalbumin, and somatostatin in the GAD67-GFP knock-in mouse. *J. Comp. Neurol.* 467, 60–79. doi: 10.1002/cne.10905

Tan, Y. L., Yuan, Y., and Tian, L. (2020). Microglial regional heterogeneity and its role in the brain. *Mol. Psych.* 25, 351–367. doi: 10.1038/s41380-019-0609-8

Thion, M. S., and Garel, S. (2017). On place and time: Microglia in embryonic and perinatal brain development. *Curr. Opin. Neurobiol.* 47, 121–130. doi: 10.1016/j.conb.2017.10.004

Thion, M. S., and Garel, S. (2020). Microglial ontogeny, diversity and neurodevelopmental functions. *Curr. Opin. Genet. Dev.* 65, 186–194.

Voineagu, I., Wang, X., Johnston, P., Lowe, J. K., Tian, Y., Horvath, S., et al. (2011). Transcriptomic analysis of autistic brain reveals convergent molecular pathology. *Nature* 474, 380–384. doi: 10.1038/nature10110

Vorup-Jensen, T., and Jensen, R. K. (2018). Structural immunology of complement receptors 3 and 4. *Front. Immunol.* 9:2716. doi: 10.3389/fimmu.2018.02716

Weakley, J. M., Kavusak, E. K., Carroll, J. B., and Gabriele, M. L. (2022). Segregation of multimodal inputs into discrete midbrain compartments during an early critical period. *Front. Neural Circuits* 16:882485. doi: 10.3389/fncir.2022.882485

Wilton, D. K., Dissing-Olesen, L., and Stevens, B. (2019). Neuron-glia signaling in synapse elimination. *Annu. Rev. Neurosci.* 42, 107–127. doi: 10.1146/annurev-neuro-070918-050306

Yanagawa, Y., Kobayashi, T., Kamei, T., Ishii, K., Nishijima, M., Takaku, A., et al. (1997). Structure and alternative promoters of the mouse glutamic acid decarboxylase 67 gene. *Biochem. J.* 326, 573–578. doi: 10.1042/bj3260573

Yilmaz, M., Yalcin, E., Presumey, J., Aw, E., Ma, M., Whelan, C. W., et al. (2021). Overexpression of schizophrenia susceptibility factor human complement C4A promotes excessive synaptic loss and behavioral changes in mice. *Nat. Neurosci.* 24, 214–224. doi: 10.1038/s41593-020-00763-8

Zhan, Y., Paolicelli, R. C., Sforazzini, F., Weinhard, L., Bolasco, G., Pagani, F., et al. (2014). Deficient neuron-microglia signaling results in impaired functional brain connectivity and social behavior. *Nat. Neurosci.* 17, 400–406. doi: 10.1038/nn.3641

frontiers | Frontiers in Neuroscience

TYPE Original Research
PUBLISHED 06 January 2023
DOI 10.3389/fnins.2022.1086994

OPEN ACCESS

EDITED BY
Flavia Venetucci Gouveia,
University of Toronto, Canada

REVIEWED BY
Ariel Ávila,
Universidad Católica de la Santísima Concepción, Chile
Irmgard Amrein,
ETH Zürich, Switzerland

*CORRESPONDENCE
Geeske M. van Woerden
✉ g.vanwoerden@erasmusmc.nl

SPECIALTY SECTION
This article was submitted to Neurodevelopment, a section of the journal Frontiers in Neuroscience

RECEIVED 01 November 2022
ACCEPTED 07 December 2022
PUBLISHED 06 January 2023

CITATION
Rigter PMF, de Konink C and van Woerden GM (2023) Loss of CAMK2G affects intrinsic and motor behavior but has minimal impact on cognitive behavior. *Front. Neurosci.* 16:1086994. doi: 10.3389/fnins.2022.1086994

Loss of CAMK2G affects intrinsic and motor behavior but has minimal impact on cognitive behavior

Pomme M. F. Rigter[1,2], Charlotte de Konink[2,3] and Geeske M. van Woerden[1,2,3]*

[1]Department of Clinical Genetics, Erasmus Medical Center, Rotterdam, Netherlands, [2]Erfelijke Neuro-Cognitieve Ontwikkelingsstoornissen, Expertise Centre for Neurodevelopmental Disorders, Erasmus Medical Center, Rotterdam, Netherlands, [3]Department of Neuroscience, Erasmus Medical Center, Rotterdam, Netherlands

Introduction: The gamma subunit of calcium/calmodulin-dependent protein kinase 2 (CAMK2G) is expressed throughout the brain and is associated with neurodevelopmental disorders. Research on the role of CAMK2G is limited and attributes different functions to specific cell types.

Methods: To further expand on the role of CAMK2G in brain functioning, we performed extensive phenotypic characterization of a *Camk2g* knockout mouse.

Results: We found different CAMK2G isoforms that show a distinct spatial expression pattern in the brain. Additionally, based on our behavioral characterization, we conclude that CAMK2G plays a minor role in hippocampus-dependent learning and synaptic plasticity. Rather, we show that CAMK2G is required for motor function and that the loss of CAMK2G results in impaired nest-building and marble burying behavior, which are innate behaviors that are associated with impaired neurodevelopment.

Discussion: Taken together, our results provide evidence for a unique function of this specific CAMK2 isozyme in the brain and further support the role of CAMK2G in neurodevelopment.

KEYWORDS

***Camk2g* knockout, behavior, plasticity, isoforms, neurodevelopment**

Introduction

The calcium/calmodulin-dependent protein kinase 2 (CAMK2) family consists of four different isozymes, CAMK2A, CAMK2B, CAMK2G, and CAMK2D, transcribed from individual genes but with high homology as they all consist of the same domains. Of these domains, the linker domain between the regulatory and association domain shows substantial variation between members (Sloutsky and Stratton, 2021). All four isozymes are expressed in the brain, though at different expression levels

(Tobimatsu and Fujisawa, 1989; Bayer et al., 1999; Murray et al., 2003). The role of CAMK2A and CAMK2B in brain functioning has been studied extensively using different mouse models, revealing their critical role in learning and synaptic plasticity (Silva et al., 1992a,b; Giese et al., 1998; Elgersma et al., 2002; van Woerden et al., 2009; Borgesius et al., 2011; Achterberg et al., 2014). This is accentuated by the discovery of mutations in the corresponding genes of patients suffering from neurodevelopmental disorders with intellectual disability (Küry et al., 2017; Akita et al., 2018; Chia et al., 2018; Rizzi et al., 2020; Heiman et al., 2021; Proietti Onori and van Woerden, 2021). Studying the role of CAMK2G in the brain has only recently become a focus of interest, amongst others due to the identification of patients with neurodevelopmental disorders carrying a mutation in the *CAMK2G* gene (de Ligt et al., 2012; Proietti Onori et al., 2018), highlighting the function of CAMK2G in normal brain functioning.

CAMK2G expression can be detected by embryonic day 11.5 (E11.5) in mice, and it is expressed throughout the brain in excitatory neurons, interneurons, and astrocytes (Tobimatsu and Fujisawa, 1989; Sakagami and Kondo, 1993; Bayer et al., 1999; Vallano et al., 2000; Batiuk et al., 2020; Huntley et al., 2020; Kozareva et al., 2021). The highest expression is observed in interneurons, and both global and interneuron-specific loss of CAMK2G results in impaired cognition and plasticity (Cohen et al., 2016, 2018; He et al., 2021, 2022). Different splice variants are expressed by the *Camk2g* gene, one of which contains a nuclear localization signal (NLS) in its variable domain. This specific isoform is shown to shuttle calcium-bound calmodulin to the nucleus in excitatory neurons, potentially playing a role in excitation–transcription coupling (Ma et al., 2014; Cohen et al., 2016). However, in interneurons, CAMK2G is not involved in calmodulin shuttling to the nucleus (Cohen et al., 2016). Additionally, knockdown of *Camk2g* was found to cause abnormal neurite growth in primary neurons, which could be normalized by re-expressing both a CAMK2G isoform with as well as without the NLS (Proietti Onori et al., 2018). Together, these results show that more research is required to get full insight into the role of CAMK2G in neurons and more broadly, in the brain.

Similar to mice, in humans *CAMK2G* is one of the main CAMK2 isozymes expressed during early neurodevelopment (Proietti Onori et al., 2018). The finding that a mutation in this gene causes a neurodevelopmental disorder (Proietti Onori et al., 2018) suggests that CAMK2G plays an important role in neurodevelopment. Patients carrying mutations in *CAMK2G* show, besides intellectual disability, a spectrum of phenotypic traits (Proietti Onori et al., 2018). To provide further insight into the role of CAMK2G in normal brain function, we obtained global *Camk2g* knockout mice and performed an extensive phenotypic characterization. We tested cognitive behavior but also other forms of behavior as patients with *CAMK2G* missense mutations suffer from severe intellectual disability and autism spectrum disorder but also impaired motor skills, hypotonia during infancy, and atypical body growth development (Proietti Onori et al., 2018). Our results indicate that in contrast to CAMK2A and CAMK2B, CAMK2G is not essential for hippocampus-dependent learning or synaptic plasticity, which contradicts previous *Camk2g* knockout mice studies (Cohen et al., 2018; He et al., 2021). Instead, we found that CAMK2G plays a role in motor and innate behavior, further supporting the role of CAMK2G in neurodevelopment.

Materials and methods

Mouse line

We obtained the *Camk2g* knockout mouse by ordering frozen sperm heterozygous for the MGI allele $Camk2g^{TM1a(EUCOMM)Wtsi}$ in a C57BL/6N background from the European Conditional Mouse Mutagenesis Program (EUCOMM). A super ovulating female C57BL/6J mouse was inseminated by IVF, followed by the rederivation of the fertilized eggs to a surrogate C57BL/6J mom. To obtain the experimental groups, heterozygous $Camk2g^{TM1a(EUCOMM)Wtsi}$ mice were crossed and the genotype was determined by PCR. For the experiments, we used male and female adult mice (>8 weeks old). They were group-housed at 22 ± 2°C, except for the nest-building test for which they had to be single-caged, and had food and water available *ad libitum* in a 12/12-h light/dark cycle. Experiments were executed during the light phase by an experimenter blind to the genotypes. All experiments with animals were conducted in accordance with the European Commission Council Directive 2010/63/EU (CCD project license AVD101002017893), and all described experiments and protocols were ethically approved by an independent review board of the Erasmus MC.

Western blot on isolated brain regions

Animals were anesthetized by isoflurane and decapitated. The brain was quickly removed from the skull and the cerebellum and brainstem were separated. The cerebrum was turned upside down, and the hypothalamus was isolated. Next, it was cut in half coronally, and from the anterior part, the striatum was isolated. The leftover tissue, predominantly the anterior cortex, but without the olfactory bulb, was labeled "forebrain." From the posterior cerebrum, the cortex was isolated and collected. Now the oval-shaped hippocampus was visible and isolated. The leftover tissue, predominantly the thalamus, was labeled "diencephalon." As soon as the regions were collected in Eppendorf tubes, they were snap-frozen in liquid nitrogen.

Samples were sonicated in lysis buffer (0.1M Tris–HCl of pH 6.8, 4% SDS) with 1:20 protease inhibitor cocktail (P8340, Sigma, St Louis, MO, United States) and 1:40 phosphatase inhibitor cocktail 2 (P5726, Sigma) and 3 (P0044, Sigma). Protein concentrations were determined by the Pierce™ BCA protein assay (23225, Thermo Fisher Scientific, Waltham, MA, United States), and Bis-Tris SDS PAGE gels (3450124, Bio-rad, Hercules, CA, United States) were loaded with 30 μg protein, denatured by adding Dithiothreitol (DTT, 0.1M) and boiling at 95°C. The gel was transferred using a turbo transfer system (1704150, Bio-Rad) on a nitrocellulose membrane (1704159, Bio-rad). Blots were probed with primary antibodies anti-CAMK2G (HPA040656, Sigma, 1:1000), anti-ACTIN (MAB1501R, Sigma, St Louis, MO, United States, 1:20 000), anti-CAMK2A [NB100-1983 (clone 6G9), Novus Biologicals, Abingdon, United Kingdom, 1:20 000], and anti-CAMK2B (13-9800, Invitrogen, Waltham, MA, United States, 1:10 000) for 2 h at room temperature or overnight at 4°C. Blots were probed with IRDye® secondary antibodies (800CW Goat anti-Mouse, 680LT Goat anti-Rabbit, LI-COR, Lincoln, NE, United States, 1:15 000) for 1 h at room temperature. Blots were developed on an Odyssey® Imager (LI-COR) and quantified with Image Studio™ Lite software (LI-COR).

RNA-seq analysis

To look at the distribution of *Camk2g* splice variants, we utilized an RNA-seq dataset that measured the transcriptome of the forebrain and cerebellum in adult male C57BL/6 mice (GEO: GSE141252; PRJNA592965; Stoeger et al., 2019). We imported raw sequencing data of the two brain regions of 4 mice (mouse number 10, 12, 13, and 25) to the Galaxy web platform (Afgan et al., 2018) and assessed the quality of the reads by FastQC (Galaxy Version 0.73 + galaxy0).[1] Single-end reads were mapped to the mouse reference genome (mm39 Full) using the RNA star algorithm (Galaxy Version 2.7.8a; Dobin et al., 2013). Generated.bam files were opened in Integrative Genomics Viewer (version 2.11.9), and Sashimi plots of the *Camk2g* transcript were analyzed for the number of junctions between exons. Sashimi plots of the *Camk2g* linker domain are shown in **Supplementary Figure 3**. The number of splice junctions was averaged across the 4 mice and compared between the brain regions. To calculate the ratio of splicing, the number of times the exon was spliced out was divided by the average number of times the exon was spliced in; for example, for exon 13, the number of splice junctions from exon 12–14 (exon 13 spliced out) was divided by the average number of splice junctions from exon 12–13 and exon 13–14 (exon 13 spliced in).

1 Babraham Bioinformatics. *FastQC. A quality control tool for high throughput sequence data*. Available online at: https://www.bioinformatics.babraham.ac.uk/projects/fastqc/.

Behavior

Mice were handled by an experimenter blinded to their genotype before the start of experiments. The order of experiments was as follows: rotarod, Morris water maze, and fear conditioning. In a separate cohort: rotarod, open field, marble burying, grip strength, nest building, forced swim, and balance beam test.

Rotarod

Mice were placed on an accelerating cylinder (4–40 rpm; Ugo Basile Biological Research Apparatus, model 7650) for 5 consecutive days with 2 trials per day. A trial lasted for a maximum of 5 min, and the daily trials had a 45–60 min interval. The experimenter manually scored how long a mouse would stay on the rotarod or how long it clung to the cylinder for 3 consecutive rotations without walking. Sample sizes were 19 female and 26 male mice for $Camk2g^{+/+}$ ($n = 45$), and 22 female and 23 male mice for $Camk2g^{-/-}$ ($n = 45$).

Morris water maze

Mice were trained in a circular pool of 1.2 m to find a round platform of 11 cm that was submerged (1 cm) in cloudy water at 25–26°C. The training lasted 5 consecutive days with two trials per day in which the mouse was released at a pseudorandom location and had 60 s to locate the platform. The latency to find the platform was scored manually, and if the mouse did not find the platform within 60 s, it was guided by the experimenter. In between trials, the mouse rested on the platform for 30 s. The probe trial started with placing the mouse on the platform for 30 s, after which the platform was removed and the mouse was tracked using EthoVision® software (Noldus®, Wageningen, Netherlands). The probe trial was executed on day 5. Sample sizes were 6 female and 9 male mice for $Camk2g^{+/+}$ ($n = 15$), and 9 female and 6 male mice for $Camk2g^{-/-}$ ($n = 15$).

Fear conditioning

Mice were placed in a soundproof box (26 cm × 22 cm × 18 cm; San Diego Instruments, San Diego, CA, United States) with a grid floor, white light turned on, and a camera monitoring motor activity. Conditioning consisted of placing the mice in a lightened soundproof box (26 × 22 × 18 cm; San Diego Instruments) and after 150 s presenting them with 85 dB tone for 20 s, followed by a single foot shock of 1.0 mA that lasted 2 s. Contextual memory was tested 24 h later by placing the mice in the same context for 180 s and measuring the amount of freezing by the camera. Again, 24 h later, cued memory was tested by placing the mice in a modified context for 220 s. The modification consisted of making the box dark, placing plexiglass walls in a triangular shape, removing the grid floor, and presenting them with a mild acetone smell. After 120 s,

mice were presented with the conditioned stimulus, i.e., the tone, for 100 s, and the amount of freezing was measured by the camera. Freezing behavior was defined as no activity for 1.00 s and analyzed by Video Freeze® software (Med Associates Inc., Fairfax, VT, United States). Sample sizes were 6 female and 9 male mice for *Camk2g*$^{+/+}$ (n = 15), and 9 female and 6 male mice for *Camk2g*$^{-/-}$ (n = 15). A separate cohort was tested for only contextual fear conditioning that consisted of 7 female and 8 male mice for *Camk2g*$^{+/+}$ (n = 15), and 6 female and 9 male mice for *Camk2g*$^{-/-}$ (n = 15).

Open field

Mice were placed facing the wall in a brightly lit circular open arena of 110 cm in diameter. Their activity was tracked for 10 min using EthoVision® software (Noldus®). Sample sizes were 6 female and 9 male mice for *Camk2g*$^{+/+}$ (n = 15), and 7 female and 8 male mice for *Camk2g*$^{-/-}$ (n = 15).

Grip strength

Mice were placed on the grid of the grip strength test (Bioseb, Vitrolles, France) that was set at an angle of 30°. The grip strength of the fore and hind limbs was simultaneously measured by steadily pulling the tail in a horizontal direction. This was repeated 3 times per mouse. Sample sizes were 6 female and 9 male mice for *Camk2g*$^{+/+}$ (n = 15), and 7 female and 8 male mice for *Camk2g*$^{-/-}$ (n = 15).

Balance beam

Mice were placed on a platform and motivated with the gentle guidance of the hand to cross a beam 1 m long to a second platform that was closed. Beams were 12, 10, or 8 mm wide and were suspended at 50 cm in the air. Mice crossed the beams 3 times on 3 consecutive days; on day 1, mice were tested on beams of 12 and 10 mm, on day 2 mice were tested on beams of 10 and 8 mm, and on day 3 mice were tested on beams of 12, 10, and 8 mm. Videos were recorded and manually analyzed offline for the number of foot slips and latency. The figure reports the results when crossing the specific beam for the second day. Sample sizes were 5 female and 4 male mice for *Camk2g*$^{+/+}$ (n = 9), and 4 female and 5 male mice for *Camk2g*$^{-/-}$ (n = 9).

Marble burying

Mice were placed in an open Makrolon cage (50 cm × 26 cm × 18 cm) containing a 4-cm bedding (Lignocel Hygenic Animal Bedding, JRS) with 20 blue glass marbles equally distributed on top. After 30 min, mice were gently removed from the cages, and the number of marbles buried (>50% covered) was scored manually. Sample sizes were 6 female and 9 male mice for *Camk2g*$^{+/+}$ (n = 15), and 7 female and 8 male mice for *Camk2g*$^{-/-}$ (n = 15).

Nest building

For this experiment, mice were single-caged 5–7 days beforehand. The former nest building material was replaced by extra thick blot filter paper (11 g; 1703969, Bio-rad). Paper that was not used to build a nest was weighed every 24 h for 5 consecutive days. Sample sizes were 6 female and 9 male mice for *Camk2g*$^{+/+}$ (n = 15), and 7 female and 8 male mice for *Camk2g*$^{-/-}$ (n = 15).

Forced swim test

Mice were placed in a glass cylinder (diameter 18 cm and height 27 cm) that was filled with water at 26 ± 1°C up to 15 cm. Trials lasted 6 min, of which the first 2 min were for the mice to get habituated to the situation and the final 4 min were scored manually for immobility, defined as no activity other than that needed for the mice to remain afloat and keep its balance. Sample sizes were 6 female and 9 male mice for *Camk2g*$^{+/+}$ (n = 15), and 7 female and 8 male mice for *Camk2g*$^{-/-}$ (n = 15).

Electrophysiology

Mice were sedated by inhalation of isoflurane and decapitated. The brains were quickly removed and placed in a vibratome (PELCO easiSlicer™, Ted Pella, Inc., Redding, CA, United States) with ice-cold artificial cerebrospinal fluid (ACSF; in mM: 120 NaCl, 3.5 KCl, 2.5 CaCl2, 1.3 MgSO4, 1.25 NaH2PO4, 26 NaHCO3, and 10 D-glucose). Sagittal slices of 400 μm were made from which the hippocampus was isolated and left to recover for 60 min in oxygenated (95%) and carbonated (5%) ACSF at room temperature. Bipolar platinum/iridium stimulating and recording electrodes (FHC; Bowdoin, ME, United States) were placed in the CA3-CA1 Schafer collateral pathway and the slices were left to habituate for 30 min. The input/output paradigm was executed by stimulation of 10, 20, 40, 60, 80, and 100 mA at 0.05 Hz. Paired-pulse facilitation was stimulated at one-third of max field excitatory postsynaptic potential (fEPSP) as assessed by the input/output. Paired pulses were given with an interval of 10, 25, 50, 100, 200, and 400 μs at 0.05 Hz, and this was repeated two times. LTP recordings were at 1 Hz and consisted of a baseline recording of 10 min, followed by LTP induction and subsequent recordings for 60–120 min. Induction of 100 Hz lasted for 1 s and stimulation was done at one-third max fEPSP. Theta induction was done at two-thirds max fEPSP strength with a burst of 4 stimuli at 100 Hz, repeated 10, 3, or 2 times, with an interval of 200 μs between stimulation bursts. Recordings took place in submerged chambers with a flow of 2 ml/min of ACSF at 30°C. Analysis was done in pCLAMP 11 software (Molecular Devices, San Jose, CA, United States), measuring the slope of the fEPSP and normalizing it to the baseline. Recordings that showed an unstable response during baseline were excluded.

Statistical analysis

Statistical analysis was done with GraphPad Prism software. Behavioral data were tested for normality with the D'Agostino-Pearson test. Subsequently, parametric or non-parametric tests were used, and *P*-values of <0.05 were considered significant. Details about the statistical tests used and their exact values are indicated in the figure legends together with the sample sizes.

Results

Camk2g knockout mice (EUCOMM; *Camk2g*$^{-/-}$) were bred in a C57BL/6J background. For all experiments, wild-type littermates (*Camk2g*$^{+/+}$) were used as control. *Camk2g*$^{-/-}$ were viable and appeared healthy, but showed reduced body weight compared with *Camk2g*$^{+/+}$ (**Supplementary Figure 1**). To validate the *Camk2g*$^{-/-}$ mice and assess where CAMK2G is expressed, we isolated 8 brain regions from *Camk2g*$^{-/-}$ and *Camk2g*$^{+/+}$ mice and performed Western blots on forebrain, striatum, hypothalamus, diencephalon, cortex, hippocampus, cerebellum, and brainstem. Probing for CAMK2G revealed three bands, of which the upper two were specific and were absent in the *Camk2g*$^{-/-}$ samples (**Figure 1A**), suggesting different isoforms of CAMK2G are expressed in the brain. In general, CAMK2G is expressed quite consistently throughout the brain, with a trend for the highest expression levels in the cortex (**Figures 1A, B**; for statistics see the legends). As expected, CAMK2G is absent in all brain regions of the *Camk2g*$^{-/-}$ samples, while CAMK2A and CAMK2B expressions were unaltered compared to *Camk2g*$^{+/+}$ (**Figures 1A, D**). The lowest aspecific band of CAMK2G overlapped with CAMK2B (for raw blots see **Supplementary Figure 2**). Interestingly, the two CAMK2G isoforms showed a region-defined expression: in regions from the cerebrum, both isoforms were nearly equally expressed, but in the cerebellum and brainstem, expression of the larger isoform was markedly decreased (**Figures 1A, C**).

To confirm the presence of different CAMK2G isoforms in different brain areas, an online RNA-seq database (GEO accession number: GSE141252; Stoeger et al., 2019 bioRxiv) on the forebrain and cerebellum tissue of adult C57BL/6J mice was used to quantify exon-junctions of the *Camk2g* transcripts. Confirming literature (Takeuchi et al., 2000; Tombes et al., 2003; Kamata et al., 2006; Sloutsky and Stratton, 2021), we found splice variants solely in the linker domain of *Camk2g*, splicing out exon 13, 15, 16, and/or 19 (for numbering of exons see **Supplementary Figure 3**). **Figure 1E** illustrates exons in the linker domain with the amount of transcript reads between exons (for raw data plots, see **Supplementary Figure 4**). Intriguingly, exon 13 showed the largest difference between brain regions and is spliced out more frequently in the cerebellum than in the forebrain (**Figure 1F**), which would translate to a 1.1 kDa decrease in size on protein level, corresponding to our Western blot results (**Figure 1A**). Therefore, the observed different ratio in cerebrum versus cerebellum protein expression is likely due to region-specific CAMK2G isoform distribution.

Having established that our mouse model is indeed lacking CAMK2G expression, we set out to study the role of CAMK2G in learning and plasticity. For spatial memory, we made use of the Morris water maze. Although the *Camk2g*$^{-/-}$ mice show slightly longer latencies to find the platform in the first 2 days compared with *Camk2g*$^{+/+}$ mice, all mice showed a reduction in their latency to find the platform over days, with no differences between genotypes over days (**Figure 2A**). Reduction in latency does not necessarily mean that the mouse shows spatial learning as mice can use different non-hippocampus-dependent strategies to find the platform. Hence, to assess hippocampus-dependent spatial memory, the platform was removed for a probe trial on day 5 and the time spent in the different quadrants of the water maze was analyzed. Both *Camk2g*$^{+/+}$ and *Camk2g*$^{-/-}$ spent significantly more time in the target quadrant (TQ) compared with the other quadrants (**Figures 2B, C**), indicating intact, or at best very moderately impaired, spatial learning in our *Camk2g*$^{-/-}$ mouse model. Additionally, no differences were found in the number of platform crosses (**Figure 2D**) or the swim speed (**Figure 2E**).

We next tested associative learning using contextual and cued fear conditioning. Mice were placed in a context, where after 150 s a tone was presented for 20 s, immediately followed by a foot shock (**Figure 2F**). No significant differences in freezing behavior were observed between the *Camk2g*$^{+/+}$ and *Camk2g*$^{-/-}$ mice during baseline measurement (**Figure 2G**). Surprisingly, *Camk2g*$^{-/-}$ showed significantly more freezing than *Camk2g*$^{+/+}$ in the context condition (**Figure 2H**). Also in the cued condition, *Camk2g*$^{-/-}$ showed significantly more freezing than *Camk2g*$^{+/+}$; however, baseline freezing was already significantly different in the *Camk2g*$^{-/-}$ mice compared with their wild-type littermates. To assess the learning effect, pre-tone freezing levels were subtracted from tone freezing levels, which still revealed significantly higher freezing levels in *Camk2g*$^{-/-}$ than *Camk2g*$^{+/+}$ (**Figure 2I**). Combining the tone and shock strongly activates the amygdala, potentially masking the hippocampus-dependent contribution of this conditioning task. To explicitly test the hippocampal contribution to the phenotype, in a separate cohort we only tested contextual conditioning, omitting the cue. Again, no significant difference was observed in baseline freezing levels (**Figure 2J**). When placed back in the same context 24 h later, similar freezing levels were observed between *Camk2g*$^{+/+}$ and *Camk2g*$^{-/-}$ (**Figure 2K**). Thus, our results suggest that CAMK2G is not necessary for hippocampus-dependent learning and memory, but potentially plays a role in amygdala-dependent associative fear conditioning.

Having assessed hippocampal learning, we set out to investigate hippocampal synaptic plasticity in *Camk2g*$^{-/-}$,

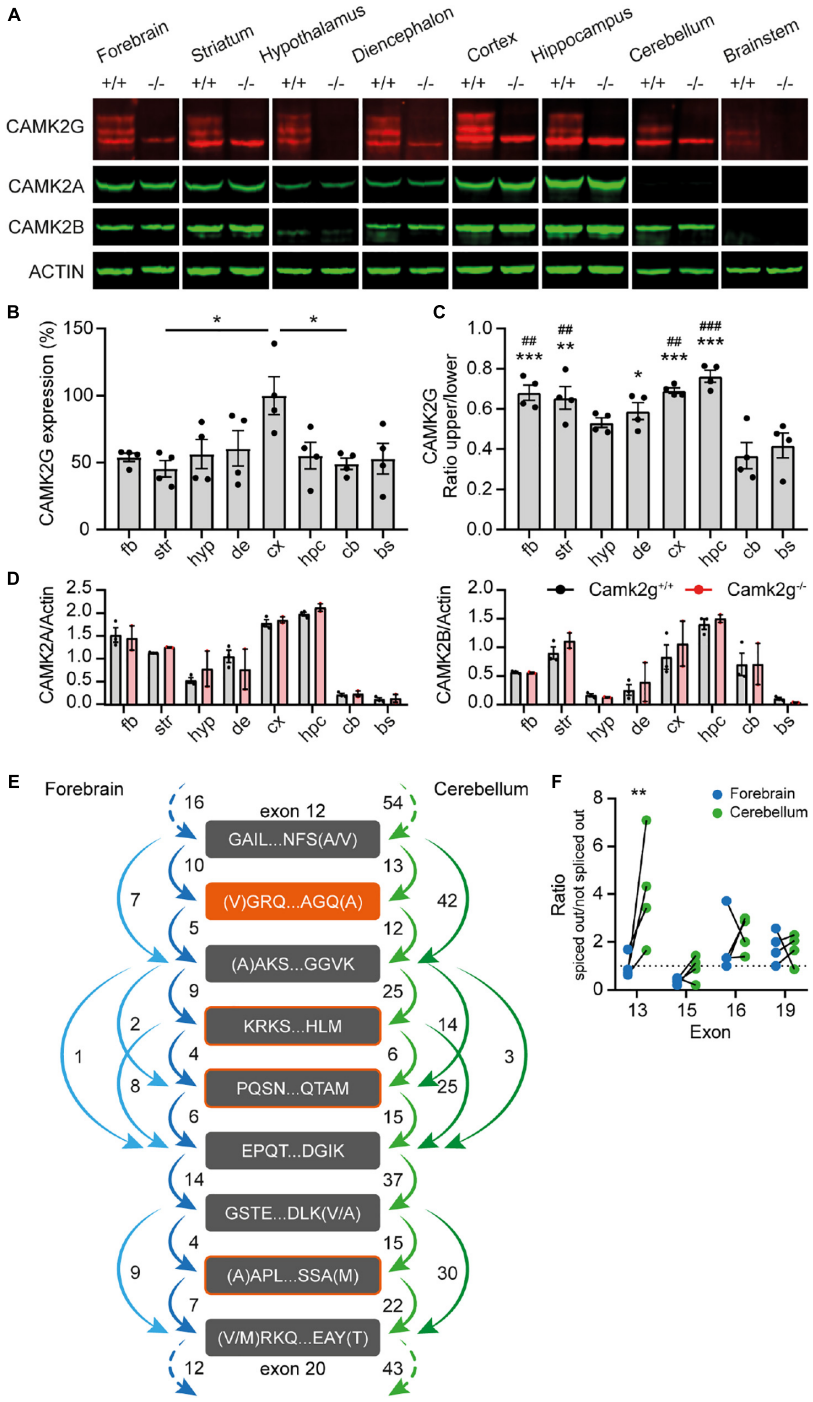

FIGURE 1
CAMK2G expression profile in the brain. **(A)** Immunoblots of different isolated brain regions in *Camk2g* wild type (+/+) and knockout (−/−) mice probed with antibodies against CAMK2G, CAMK2A, CAMK2B, and ACTIN. Note the triple band of CAMK2G, of which 2 are absent in *Camk2g*$^{-/-}$ mice. **(B)** Quantification of CAMK2G expression, normalized to values in the cortex. fb, forebrain; str, striatum; hyp, hypothalamus; de, diencephalon; cx, cortex; hpc, hippocampus; cb, cerebellum; bs, brainstem [one-way ANOVA with Bonferroni's *post hoc* analysis, $F_{(7,24)} = 2.98$, $p = 0.021$; fb vs. str $p > 0.999$, fb vs. hyp $p > 0.999$, fb vs. bg $p > 0.999$, fb vs. cx $p = 0.088$, fb vs. hpc $p > 0.999$, fb vs. cb $p > 0.999$, fb vs. bs $p > 0.999$, str vs. hyp $p > 0.999$, str vs. bg $p > 0.999$, str vs. cx $p = 0.019$, str vs. hpc $p > 0.999$, str vs. cb $p > 0.999$, str vs. bs $p > 0.999$, hyp vs. bg $p > 0.999$, hyp vs. cx $p = 0.134$, hyp vs. hpc $p > 0.999$, hyp vs. cb $p > 0.999$, hyp vs. bs $p > 0.999$, bg vs. cx $p = 0.272$, bg vs. hpc $p > 0.999$, bg vs. cb $p > 0.999$, bg vs. bs $p > 0.999$, cx vs. hpc $p = 0.109$, cx vs. cb $p = 0.037$, cx vs. bs $p = 0.073$, hpc vs. cb $p > 0.999$, hpc vs. bs $p > 0.999$, cb vs. bs $p > 0.999$; $n = 4$]. **(C)** Ratio of the specific CAMK2G bands. The lower band shows higher expression levels throughout the brain, but

(Continued)

FIGURE 1 (Continued)
exceptionally so in cerebellum and brainstem, *indicates significance compared to cerebellum and # compared to brainstem [one-way ANOVA with Bonferroni's post-hoc analysis compared to Cb and Bs, $F_{(7,24)} = 9.57$, $p < 0.001$; fb vs. cb $p < 0.001$, fb vs. bs $p = 0.003$, str vs. cb $p = 0.001$, str vs. bs $p = 0.008$, hyp vs. cb $p = 0.115$, hyp vs. bs $p = 0.615$, de vs. cb $p = 0.013$, de vs. bs $p = 0.090$, cx vs. cb $p < 0.001$, cx vs. bs $p = 0.002$, hpc vs. cb $p < 0.001$, hpc vs. bs $p < 0.001$, and cb vs. bs $p > 0.999$]. **(D)** CAMK2A (left) and CAMK2B (right) expression differs between brain regions, but importantly does not differ between *Camk2g*$^{+/+}$ and *Camk2g*$^{-/-}$ [two-way Anova, CAMK2A $F_{(7,24)} = 0.245$, $p = 0.625$; CAMK2B $F_{(7,24)} = 0.809$, $p = 0.378$; $n = 2–3$]. **(E)** Average amount of reads between exons of *Camk2g* in RNA-seq database on the forebrain (blue) and the cerebellum (green). The start and end of the amino acid sequence are indicated for the exons. Splice variants only occur on exons 13 (orange), 15, 16, and 19 (outlined in orange). **(F)** Ratio of when the exon is spliced out versus not spliced out in the forebrain and the cerebellum, lines indicate quantifications within mice. Only exon 13 shows a significant ratio difference between the forebrain and the cerebellum, with exon 13 more often spliced out in the cerebellum [two-way ANOVA with Bonferroni's *post hoc* analysis on exon splicing, interaction: $F_{(3,24)} = 3.86$, $p = 0.022$; exon 13 $p = 0.001$, exon 15, 16, and 19 $p > 0.999$; $n = 4$]. Data represents mean ± SEM; *, #$p < 0.05$, **, ##$p < 0.01$, and ***, ###$p < 0.001$.

which could potentially still reveal a mild phenotype. We performed extracellular field recordings in the CA1 to CA3 Shaffer collateral pathway and detected no differences in baseline synaptic transmission since the presynaptic fiber volley and the field excitatory postsynaptic potential (fEPSP) increased equally between *Camk2g*$^{+/+}$ and *Camk2g*$^{-/-}$ mice with increasing stimulus strength (**Figure 3A**). We detected a significant decrease in the paired-pulse facilitation in *Camk2g*$^{-/-}$ compared with *Camk2g*$^{+/+}$, but this was only apparent at the 10- and 50-ms intervals (**Figure 3B**). Induction of long-term potentiation (LTP) using a 100-Hz induction protocol resulted in LTP in both *Camk2g*$^{+/+}$ and *Camk2g*$^{-/-}$, with no significant difference neither after 60 min nor after 120 min recording between the two groups (**Figure 3C** and **Supplementary Figure 5**). As the classical 100-Hz stimulation is very strong, it is possible that a plasticity phenotype is masked, hence, milder LTP induction protocols were tested. No differences in LTP were found between Camk2g$^{+/+}$ and Camk2g$^{-/-}$ in the 10-theta condition; however, Camk2g$^{-/-}$ showed significantly impaired LTP compared to Camk2g$^{+/+}$ in the 3-theta induction condition (**Figures 3D, E**). Surprisingly, this difference was lost in the 2-theta condition (**Figure 3F**). These results suggest that if there is a role for CAMK2G in synaptic plasticity at the CA3-CA1 synapse, it is very mild.

To further study the effect of the absence of CAMK2G on behavior and brain function, we expanded our tests to include other forms of behavior such as motor and innate behavior. We tested locomotor activity in the open field and found a trend toward decreased activity in *Camk2g*$^{-/-}$ compared with *Camk2g*$^{+/+}$, though not significant (**Figure 4A**). We further challenged their motor performance as well as their motor learning using the accelerating rotarod. Although both the *Camk2g*$^{-/-}$ and *Camk2g*$^{+/+}$ mice showed motor learning over days, the *Camk2g*$^{-/-}$ performed significantly poorer at all time points measured (**Figure 4B**). Also, on the balance beam, sensitive to balance and fine motor coordination, *Camk2g*$^{-/-}$ consistently showed more foot slips crossing beams of varying widths (**Figure 4C**). Since *CAMK2G* patients show developmental hypotonia (Proietti Onori et al., 2018), we tested if reduced muscle strength could play a role in the reduced motor performance seen in *Camk2g*$^{-/-}$ mice, but this was not the case as grip strength was equal between the groups (**Figure 4D**). Finally, we assessed some innate behaviors of the *Camk2g*$^{-/-}$ using the nest building, marble burying, and forced swim test. Compared with *Camk2g*$^{+/+}$, *Camk2g*$^{-/-}$ used significantly less material to build a nest over days (**Figure 5A**) and showed impaired burying behavior (**Figure 5B**). No significant differences were observed between *Camk2g*$^{-/-}$ and *Camk2g*$^{+/+}$ mice in floating behavior in the forced swim test (**Figure 5C**).

Discussion

With the identification of patients suffering from *CAMK2G*-associated neurodevelopmental disorder (de Ligt et al., 2012; Proietti Onori et al., 2018), the interest to study the role of CAMK2G in normal brain functioning significantly increased. Here, we set out to expand the knowledge on the role of CAMK2G in neuronal functioning through the characterization of a novel *Camk2g*$^{-/-}$ mouse model. We provide evidence for differential expression of different CAMK2G isoforms depending on the brain area, where we speculate that this is due to differential splicing of exon 13. At the behavioral level, our results suggest that CAMK2G has a minor role in hippocampus-dependent spatial learning and memory, as well as synaptic plasticity, but does affect amygdala-dependent fear learning. Finally, we find clear phenotypes in fine motor performance and intrinsic behaviors, as measured using the nest-building and marble-burying assays.

The expression levels of CAMK2G throughout the brain were assessed by isolating different brain regions of *Camk2g*$^{+/+}$ and *Camk2g*$^{-/-}$ mice. Isolation of brain regions was validated by CAMK2A expression, which was highest in the hippocampus and the cortex and lowest in the cerebellum and the brainstem, and CAMK2B expression, also highest in the hippocampus and dominant in the cerebellum yet nearly absent in the brainstem (Cook et al., 2018). Total levels of CAMK2G did not differ much between the different brain areas. Interestingly, in brain areas where CAMK2B and CAMK2A showed little

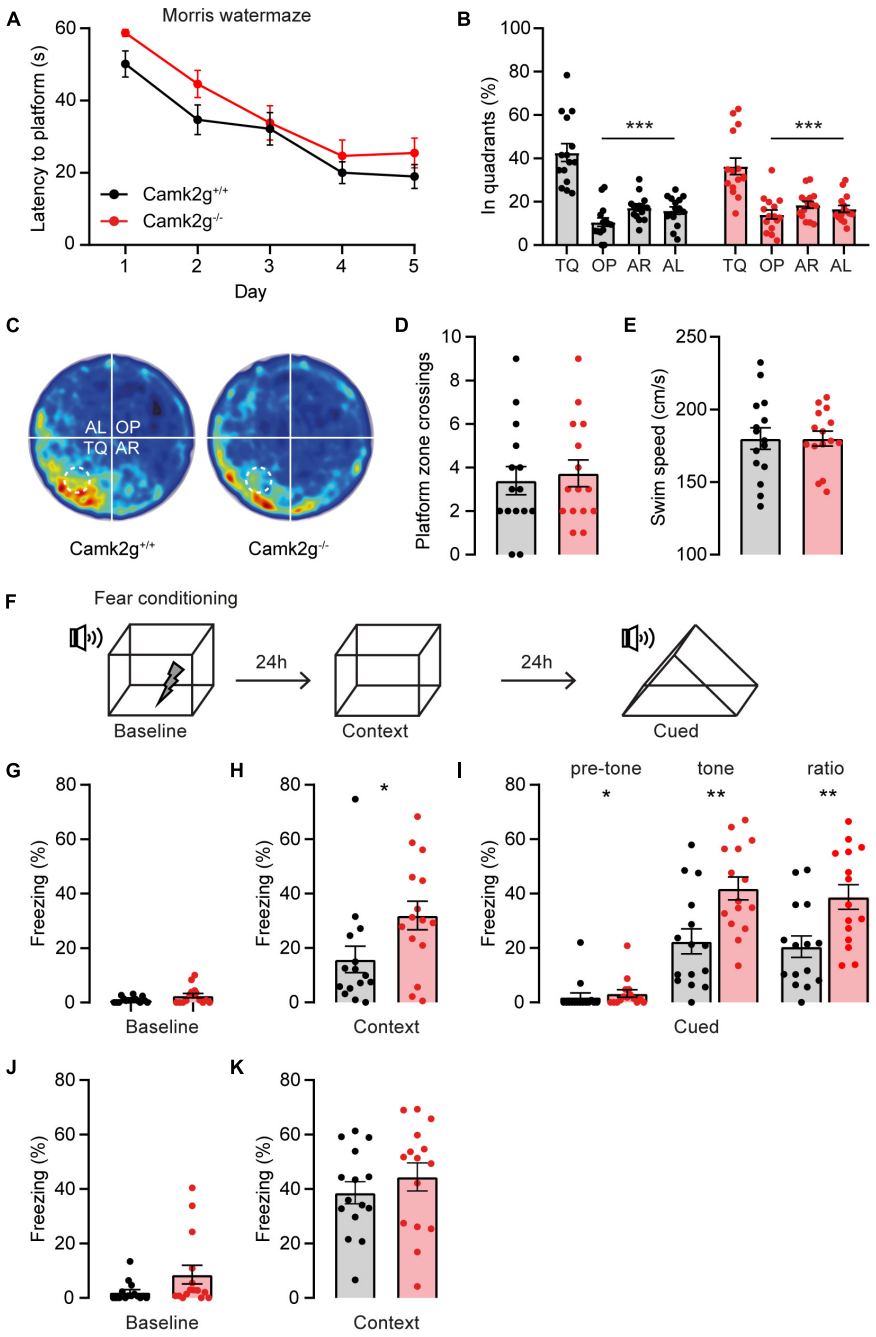

FIGURE 2

CAMK2G in cognitive behavior. **(A)** *Camk2g*$^{+/+}$ and *Camk2g*$^{-/-}$ mice similarly showed reduced latencies to find the platform over days [two-way repeated measures ANOVA; interaction: $F_{(4,112)} = 0.41$, $p = 0.804$]. **(B)** Both groups spent significantly more time in the target quadrant (TQ) compared with other quadrants in the probe trial on day 5 [one-way ANOVA with Bonferroni's *post hoc* analysis. *Camk2*$^{+/+}$: $F_{(3,56)} = 31.61$, $p < 0.001$, TQ vs. OP $p < 0.001$, TQ vs. AR $p < 0.001$, TQ vs. AL $p < 0.001$; *Camk2*$^{-/-}$: itF$_{(3,56)} = 17.04$, $p < 0.001$, TQ vs. OP $p < 0.001$, TQ vs. AR $p < 0.001$, TQ vs. AL $p < 0.001$]. TQ, target quadrant; OP, opposite; AR, adjacent right; AL, adjacent left. **(C)** Heat map of the probe trial, the arena is divided into four quadrants and the location where the platform was located during learning is indicated with a dashed line. **(D)** During the probe trial, mice crossed the zone where the platform was situated during learning with a similar frequency [unpaired *t*-test, $t_{(28)} = 0.37$, $p = 0.711$]. **(E)** Swim speed velocity was similar between groups during the probe trial [unpaired *t*-test, $t_{(28)} = 0.0018$, $p = 0.999$]. **(F)** Schematic representation of the fear conditioning test. **(G)** Freezing behavior at baseline showed no significant difference between *Camk2g*$^{+/+}$ and *Camk2g*$^{-/-}$ (Mann–Whitney *U* test, $U = 84.5$, $p = 0.245$). **(H)** When placed in the same context, *Camk2g*$^{-/-}$ showed significantly more freezing (Mann–Whitney *U* test, $U = 60$, $p = 0.030$). **(I)** When put in a different context, *Camk2g*$^{-/-}$ already showed more freezing than *Camk2g*$^{+/+}$ pretone (Mann–Whitney *U* test, $U = 64$, $p = 0.026$). Upon exposure to the tone, *Camk2g*$^{-/-}$ again showed significantly more

(Continued)

FIGURE 2 (Continued)
freezing than *Camk2g*$^{+/+}$ [unpaired *t*-test, $t_{(28)}$ = 3.13, p = 0.004]. The ratio was calculated by subtracting pre-tone from tone freezing levels and still showed significantly more freezing in *Camk2g*$^{-/-}$ than *Camk2g*$^{+/+}$ [unpaired *t*-test, $t_{(28)}$ = 3.02, p = 0.005]. **(J)** In a separate cohort, mice were tested exclusively for contextual fear conditioning and showed no differences in freezing behavior at baseline (Mann–Whitney *U* test, U = 71, p = 0.083). **(K)** When put in the same context 24 h later, *Camk2g*$^{-/-}$showed no differences in freezing compared to *Camk2g*$^{+/+}$ [unpaired *t*-test, $t_{(28)}$ = 0.885, p = 0.384]. Data represents mean ± SEM (n = 15); * $p < 0.05$, ** $p < 0.01$, *** $p < 0.001$.

expression, such as the hypothalamus, CAMK2G appeared to be one of the more dominating CAMK2 isozymes. However, we have to be careful in drawing such conclusion as we did not use a pan-CAMK2 antibody to directly compare expression levels between CAMK2s. Even though the CAMK2G antibody also recognized CAMK2B (see raw blots in **Supplementary Figure 2**), which runs at the height of the lowest band, it is interesting to see that in the hypothalamus and the brainstem, the lowest band can still be seen in the WT but no longer in the knockout samples. As CAMK2B is hardly detectable in these brain areas and this lowest band disappears in *Camk2g*$^{-/-}$ samples, these findings could suggest the expression of a third smaller isoform of CAMK2G. A more specific antibody that does not cross-react with CAMK2B would be necessary to substantiate this conclusion. For the upper two CAMK2G bands, we find evidence for differential expression of different CAMK2G isoforms. Based on RNA-seq data, the different isoforms correspond with differential splicing of exon 13. Our data suggest that the isoform containing this exon is expressed in the cerebrum but hardly in the cerebellum. Interestingly, the most common transcript found in the human hippocampus does not contain this exon as the number of transcripts with exon 13 detected was <1% (Sloutsky et al., 2020). Whether CAMK2G in the human brain shows region-specific isoforms or whether this differential expression of isoforms is species-specific remains to be studied. A homolog of exon 13 is expressed by CAMK2B, sharing 55% similarity with exon 13 in CAMK2G on the amino acid level, and encompasses the binding region for F-Actin (O'leary et al., 2006). Future research will have to show whether this exon in CAMK2G also mediates binding to F-Actin.

Our conclusion that CAMK2G has a minor role in hippocampal learning, memory, and cognition is in contrast with previous findings. The first study on a global *Camk2g*$^{-/-}$ mouse model showed impaired long-term (24 h) memory, as well as reduced late-phase LTP in *Camk2g*$^{-/-}$ (Cohen et al., 2018). Furthermore, they show that the deletion of CAMK2G solely in forebrain excitatory neurons is sufficient to cause the deficits seen in the global *Camk2g*$^{-/-}$ mice (Cohen et al., 2018). Interestingly, the following study showed that CAMK2G is mainly expressed in interneurons and that the deletion of CAMK2G specifically in parvalbumin-positive interneurons is sufficient to induce deficits in synaptic plasticity in these interneurons as well as in behavioral long-term (24 h) memory (He et al., 2021). It is challenging to explain the differences in findings between the different labs. One of the possible explanations is the differences in mouse strains used. The mice we used for our experiments were kept in the C57BL/6J background, whereas the original mice used in the other studies were in a 29SvEv/C57BL6/CD1 mixed background (Backs et al., 2010; Cohen et al., 2018; He et al., 2021). Indeed, it has been shown for other mouse models that mouse strain can make a significant difference in behavioral phenotypes (Born et al., 2017; Sonzogni et al., 2018). However, to test whether this is indeed the case for CAMK2G, the different mouse strains would need to be assessed side by side.

It might not be surprising that CAMK2G only has a minor role in hippocampus-dependent learning and plasticity. CAMK2A and CAMK2B, the two most abundant CAMK2 isozymes expressed in the brain, have both been shown to be essential for hippocampal plasticity and learning (Silva et al., 1992a,b; Elgersma et al., 2002; Borgesius et al., 2011), and the deletion of *Camk2a* and *Camk2b* simultaneously results in the complete absence of NMDA-receptor dependent LTP (Kool et al., 2019). If CAMK2G were to play a role in these processes as well, it should (partially) compensate for the lack of CAMK2A and CAMK2B, which it does not. Especially considering that CAMK2G is one of the earliest CAMK2 isozymes to be expressed during development; it can be detected already as early as E11.5, whereas CAMK2B starts to be expressed at E14.5 and CAMK2A around P1 (Bayer et al., 1999).

On the other hand, it is possible that CAMK2G affects different intracellular pathways than CAMK2A and/or CAMK2B, having a unique role in plasticity. For example, CAMK2G plays a role in the excitation–transcription coupling in excitatory neurons, shuttling calmodulin to the nucleus upon excitation (Ma et al., 2014; Cohen et al., 2016). This specific excitation–transcription shuttling could explain why the previous study in *Camk2g*$^{-/-}$ mice only found a difference in late-phase LTP and not in the early phase (Cohen et al., 2018). However, when testing late-LTP in our mouse model, we did not find a deficit (**Supplementary Figure 5**). The discrepancy in findings could be due to different induction protocols. We used a 1 × 100 Hz for 1 s induction protocol, whereas Cohen et al. (2018) used a stronger induction protocol: 3 × 100 Hz for 1 s with 5 min interstimulus interval. Whether these differences in induction protocols could result in differences in excitation–transcription coupling remains to be studied. The difference in mouse strains used is likely a better explanation for the discrepancy in findings between labs. Indeed, strain

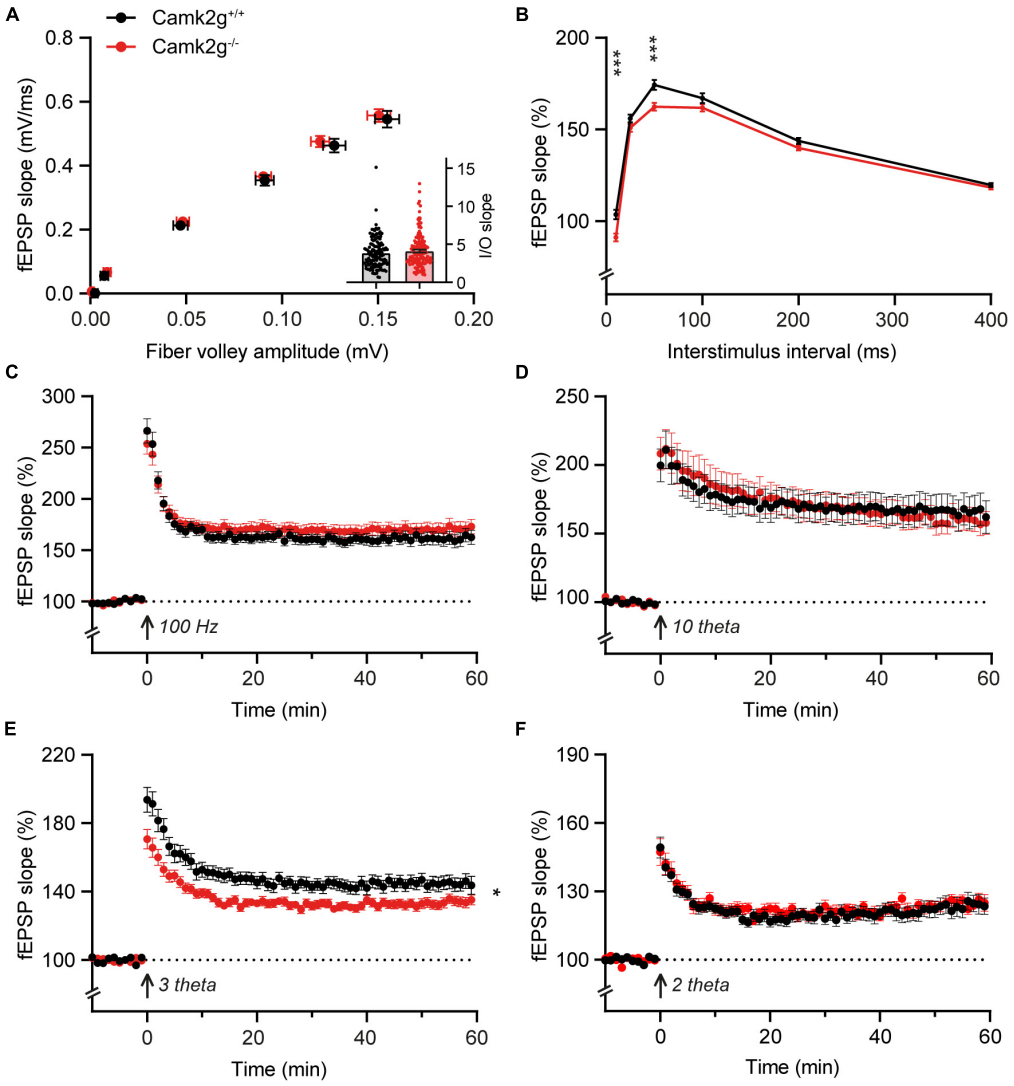

FIGURE 3
CAMK2G in synaptic plasticity. **(A)** Field recordings were done in the Schaffer-collateral-CA1 synapses of the hippocampus. At baseline synaptic transmission, mice did not show differences in the input/output (I/O) between the presynaptic fiber volley and postsynaptic fEPSP with increasing stimulus strength [unpaired *t*-test on slopes of curve (inset), $t_{(268)} = 1.01$, $p = 0.314$. Fiber volley $n = 126/21$ slices/mice for *Camk2g*$^{+/+}$ and $n = 144/24$ for *Camk2g*$^{-/-}$; fEPSP $n = 144/21$ for *Camk2g*$^{+/+}$ and $n = 162/24$ for *Camk2g*$^{-/-}$]. **(B)** We tested presynaptic short-term plasticity with paired-pulse facilitation and showed differences between *Camk2g*$^{+/+}$ and *Camk2g*$^{-/-}$ mice at interstimulus intervals of 10 and 50 ms [unpaired *t*-tests, 10 ms: $t_{(197)} = 3.70$, $p < 0.001$; 25 ms: $t_{(197)} = 1.65$, $p = 0.101$; 50 ms: $t_{(197)} = 3.45$, $p < 0.001$; 100 ms: $t_{(197)} = 1.54$, $p = 0.125$; 200 ms: $t_{(197)} = 1.82$, $p = 0.071$; 400 ms: $t_{(197)} = 0.94$, $p = 0.352$; $n = 95/15$ for *Camk2g*$^{+/+}$ and $n = 104/17$ for *Camk2g*$^{-/-}$]. **(C)** No differences were found in LTP elicited by stimulation at 100-Hz for 1 s [two-way repeated measures ANOVA on final 10 min, genotype: $F_{(1,77)} = 1.01$, $p = 0.318$; $n = 37/7$ for *Camk2g*$^{+/+}$ and $n = 42/8$ for *Camk2g*$^{-/-}$]. **(D)** No differences were found in LTP elicited by 10-theta stimulation [two-way repeated measures ANOVA on final 10 min, genotype: $F_{(1,35)} = 0.25$, $p = 0.622$; $n = 19/5$ for *Camk2g*$^{+/+}$ and $n = 18/5$ for *Camk2g*$^{-/-}$]. **(E)** *Camk2g*$^{-/-}$ mice showed reduced post-tetanic potentiation and LTP elicited by 3-theta stimulation [two-way repeated measures ANOVA on final 10 min, genotype: $F_{(1,80)} = 7.02$, $p = 0.010$; $n = 41/11$ for *Camk2g*$^{+/+}$ and $n = 42/12$ for *Camk2g*$^{-/-}$]. **(F)** No differences were found in LTP elicited by 2-theta stimulation [two-way repeated measures ANOVA on final 10 min, genotype: $F_{(1,59)} = 0.12$, $p = 0.734$; $n = 28/9$ for *Camk2g*$^{+/+}$ and $n = 33/10$ for *Camk2g*$^{-/-}$]. Data represents mean ± SEM; * $p < 0.05$, *** $p < 0.001$.

differences have been shown both for hippocampal learning and LTP (Nguyen et al., 2000). Finally, CAMK2G is not the only CAMK2 isozyme containing a nuclear localization signal (NLS), as this has also been shown for a CAMK2A isoform found in the midbrain/diencephalon regions (Brocke et al., 1995), and for CAMK2D (Srinivasan et al., 1994; Shioda et al., 2015). However, the exact role of the nuclear translocation of these isozymes remains to be elucidated.

There are several piles of evidence that suggest a role for CAMK2G in neurodevelopment: (1) the expression onset of *CAMK2G* is already very early in neurodevelopment, and at that developmental timepoint, CAMK2G and CAMK2D

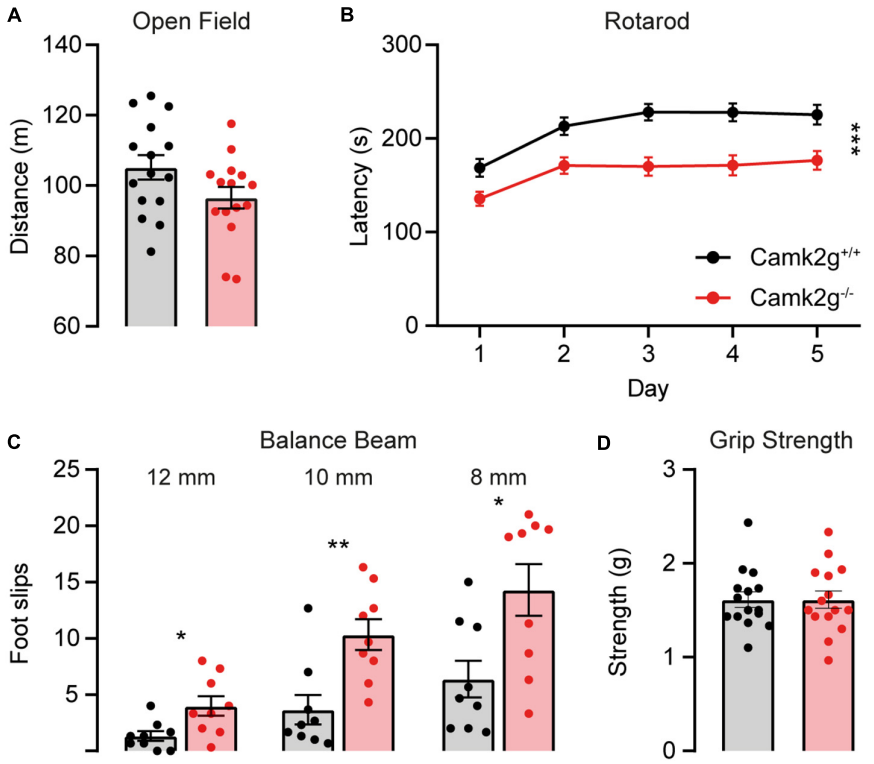

FIGURE 4
CAMK2G in motor behavior. **(A)** No differences were found in the distance traveled in the open field [unpaired *t*-test, $t_{(28)} = 1.85$, $p = 0.076$; $n = 15$]. **(B)** *Camk2g*$^{-/-}$ mice showed reduced latency to fall of the accelerating rotarod [two-way repeated measures ANOVA; interaction: $F_{(4,352)} = 1.51$, $p = 0.200$; genotype: $F_{(1,88)} = 18.40$, $p < 0.001$; $n = 45$]. **(C)** *Camk2g*$^{-/-}$ mice consistently slipped more often when crossing beams that were 12, 10, and 8 mm wide [unpaired *t*-test or Mann–Whitney *U* test; 12 mm: $t_{(28)} = 2.75$, $p = 0.014$; 10 mm: $U = 8.5$, $p = 0.003$; 8 mm: $t_{(28)} = 2.81$, $p = 0.013$; $n = 9$]. **(D)** Grip strength was unaltered between *Camk2g*$^{+/+}$ and *Camk2g*$^{-/-}$ mice [Mann–Whitney *U* test, $U = 111$, $p = 0.959$; $n = 15$]. Data represents mean ± SEM; * $p < 0.05$, ** $p < 0.01$, *** $p < 0.001$.

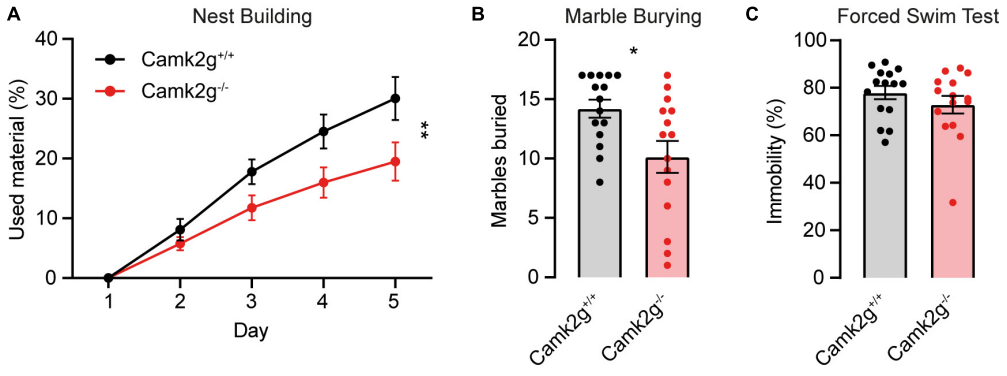

FIGURE 5
CAMK2G in intrinsic behavior. **(A)** *Camk2g*$^{-/-}$ mice used less material to build nests than *Camk2g*$^{+/+}$ mice [two-way repeated measures ANOVA; interaction: $F_{(4,112)} = 4.55$, $p = 0.002$]. **(B)** *Camk2g*$^{-/-}$ mice buried less marbles than *Camk2g*$^{+/+}$ mice [unpaired *t*-test, $t_{(28)} = 2.65$, $p = 0.013$]. **(C)** No differences were found in the amount of time the mice spent immobile in the forced swim test (Mann–Whitney *U* test, $U = 90.5$, $p = 0.372$). Data represent mean ± SEM ($n = 15$); * $p < 0.05$, ** $p < 0.01$.

are the most abundant CAMK2 isozymes expressed in the brain (Proietti Onori et al., 2018); (2) CAMK2G is necessary for proper neurite formation during neuronal development *in vitro* (Proietti Onori et al., 2018; Xi et al., 2019), and (3) a pathogenic mutation in CAMK2G has been shown to cause a neurodevelopmental disorder in children (de Ligt et al., 2012; Proietti Onori et al., 2018). Our findings that CAMK2G plays an important role in motor and innate behavior further support the

neurodevelopmental role for CAMK2G. Indeed, the behavioral tests assessed here, especially marble burying and rotarod, have been shown by us and others to have critical developmental periods, for example, in *Ube3a* and *Shank3* knockout mice (Silva-Santos et al., 2015; Mei et al., 2016; Rotaru et al., 2020; Sonzogni et al., 2020). Not only does adult *Ube3a* or *Shank3* gene reinstatement fail to rescue the marble burying or rotarod phenotypes but adult deletion of Ube3a also fails to induce phenotypes in these behavioral assays (Sonzogni et al., 2019). Another evidence for a neurodevelopmental origin for motor behavior comes from the inducible *Camk2b* knockout mouse. Deletion of *Camk2b* from the germline causes severe impairment in rotarod performance, whereas in mice where deletion of *Camk2b* is induced in adulthood, this phenotype is much milder (Kool et al., 2016). This is in stark contrast to cognitive behavior as, for example, tested in a conditional *Camk2a* mouse model. Deletion of *Camk2a* in adult mice is as detrimental for hippocampal learning and plasticity as germline deletion (Achterberg et al., 2014), and adult reinstatement rescues all cognitive behavior (Rigter et al., 2022). One important aspect here is the onset of expression. Whereas CAMK2G, CAMK2B, and UBE3A already have their expression onset prenatally, CAMK2A starts to be expressed postnatally; hence, early neurodevelopment is unaltered (Bayer et al., 1999; Judson et al., 2014).

Overall, our results reinforce previous literature suggesting that CAMK2G plays a critical role in normal brain functioning, albeit not in hippocampus-dependent memory, and further support the role of CAMK2G in neurodevelopment.

Data availability statement

The original contributions presented in this study are included in the article/**Supplementary material**, further inquiries can be directed to the corresponding author.

Ethics statement

The animal study was reviewed and approved in accordance with the European Commission Council Directive 2010/63/EU (CCD project license AVD101002017893), by an Independent Review Board (IRB) of the Erasmus MC.

Author contributions

PR performed the experiments, analyzed the data, and wrote the manuscript. CK performed the experiments and was responsible for the mouse breedings and genotyping. GW designed the study and wrote the manuscript. All authors contributed to the article and approved the submitted version.

Funding

This research was supported by the NWO-VIDI (016.Vidi.188.014 to GW).

Acknowledgments

We would like to thank Ype Elgersma for insightful discussions and critical reading of the manuscript, and Eva Niggl and Armando Schoonbrood for technical assistance.

Conflict of interest

The authors declare that the research was conducted in the absence of any commercial or financial relationships that could be construed as a potential conflict of interest.

Publisher's note

Supplementary material

The Supplementary Material for this article can be found online at: https://www.frontiersin.org/articles/10.3389/fnins.2022.1086994/full#supplementary-material

References

Achterberg, K., Buitendijk, G., Kool, M., Goorden, S., Post, L., Slump, D., et al. (2014). Temporal and region-specific requirements of αCaMKII in spatial and contextual learning. *J. Neurosci.* 34, 11180–11187. doi: 10.1523/JNEUROSCI.0640-14.2014

Afgan, E., Baker, D., Batut, B., van den Beek, M., Bouvier, D., Cech, M., et al. (2018). The Galaxy platform for accessible, reproducible and collaborative biomedical analyses: 2018 update. *Nucleic Acids Res.* 46, W537–W544. doi: 10.1093/NAR/GKY379

Akita, T., Aoto, K., Kato, M., Shiina, M., Mutoh, H., Nakashima, M., et al. (2018). De novo variants in CAMK2A and CAMK2B cause neurodevelopmental disorders. *Ann. Clin. Transl. Neurol.* 5, 280–296. doi: 10.1002/acn3.528

Backs, J., Stein, P., Backs, T., Duncan, F., Grueter, C., McAnally, J., et al. (2010). The gamma isoform of CaM kinase II controls mouse egg activation by regulating cell cycle resumption. *Proc. Natl. Acad. Sci. U. S. A.* 107, 81–86. doi: 10.1073/pnas.0912658106

Batiuk, M., Martirosyan, A., Wahis, J., de Vin, F., Marneffe, C., Kusserow, C., et al. (2020). Identification of region-specific astrocyte subtypes at single cell resolution. *Nat. Commun.* 11:1220. doi: 10.1038/s41467-019-14198-8

Bayer, K., Löhler, J., Schulman, H., and Harbers, K. (1999). Developmental expression of the CaM kinase II isoforms: Ubiquitous γ- and δ-CaM kinase II are the early isoforms and most abundant in the developing nervous system. *Mol. Brain Res.* 70, 147–154. doi: 10.1016/S0169-328X(99)00131-X

Borgesius, N. Z., van Woerden, G. M., Buitendijk, G. H., Keijzer, N., Jaarsma, D., Hoogenraad, C. C. (2011). βCaMKII plays a nonenzymatic role in hippocampal synaptic plasticity and learning by targeting αCaMKII to synapses. *J. Neurosci.* 31, 10141–10148. doi: 10.1523/JNEUROSCI.5105-10.2011

Born, H. A., Dao, A., Levine, A., Lee, W., Mehta, N., Mehra, S., et al. (2017). Strain-dependence of the angelman syndrome phenotypes in Ube3a maternal deficiency mice. *Sci. Rep.* 7:8451. doi: 10.1038/s41598-017-08825-x

Brocke, L., Srinivasan, M., and Schulman, H. (1995). Developmental and regional expression of multifunctional Ca^{2+}/calmodulin-dependent protein kinase isoforms in rat brain. *J. Neurosci.* 15, 6797–6808. doi: 10.1523/jneurosci.15-10-06797.1995

Chia, P., Zhong, F., Niwa, S., Bonnard, C., Utami, K., Zeng, R., et al. (2018). A homozygous loss-of-function CAMK2A mutation causes growth delay, frequent seizures and severe intellectual disability. *Elife* 7:e32451. doi: 10.7554/eLife.32451

Cohen, S. M., Suutari, B., He, X., Wang, Y., Sanchez, S., Tirko, N., et al. (2018). Calmodulin shuttling mediates cytonuclear signaling to trigger experience-dependent transcription and memory. *Nat. Commun.* 9:2451. doi: 10.1038/s41467-018-04705-8

Cohen, S., Ma, H., Kuchibhotla, K., Watson, B., Buzsáki, G., Froemke, R., et al. (2016). Excitation-transcription coupling in parvalbumin-positive interneurons employs a novel CaM Kinase-dependent pathway distinct from excitatory neurons. *Neuron* 90, 292–307. doi: 10.1016/j.neuron.2016.03.001

Cook, S., Bourke, A., O'Leary, H., Zaegel, V., Lasda, E., Mize-Berge, J., et al. (2018). Analysis of the CaMKIIα and β splice-variant distribution among brain regions reveals isoform-specific differences in holoenzyme formation. *Sci. Rep.* 8:5448. doi: 10.1038/s41598-018-23779-4

de Ligt, J., Willemsen, M., van Bon, B., Kleefstra, T., Yntema, H., Kroes, T., et al. (2012). Diagnostic exome sequencing in persons with severe intellectual disability. *N. Engl. J. Med.* 367, 1921–1929. doi: 10.1056/nejmoa1206524

Dobin, A., Davis, C., Schlesinger, F., Drenkow, J., Zaleski, C., Jha, S., et al. (2013). Star: Ultrafast universal RNA-seq aligner. *Bioinformatics* 29, 15–21. doi: 10.1093/BIOINFORMATICS/BTS635

Elgersma, Y., Fedorov, N., Ikonen, S., Choi, E., Elgersma, M., Carvalho, O., et al. (2002). Inhibitory autophosphorylation of CaMKII controls PSD association, plasticity, and learning. *Neuron* 36, 493–505. doi: 10.1016/S0896-6273(02)01007-3

Giese, K., Fedorov, N., Filipkowski, R., and Silva, A. (1998). Autophosphorylation at Thr286 of the α calcium-calmodulin kinase II in LTP and learning. *Science* 279, 870–873. doi: 10.1126/science.279.5352.870

He, X., Li, J., Zhou, G., Yang, J., McKenzie, S., Li, Y., et al. (2021). Gating of hippocampal rhythms and memory by synaptic plasticity in inhibitory interneurons. *Neuron* 109, 1013–1028.e9. doi: 10.1016/j.neuron.2021.01.014

He, X., Wang, Y., Zhou, G., Yang, J., Li, J., Li, T., et al. (2022). A critical role for γCaMKII in decoding NMDA signaling to regulate AMPA receptors in putative inhibitory interneurons. *Neurosci. Bull.* 38, 916–926. doi: 10.1007/S12264-022-00840-X

Heiman, P., Drewes, S., and Ghaloul-Gonzalez, L. (2021). A familial case of CAMK2B mutation with variable expressivity. *Sage Open Med. Case Rep.* 9:2050313X21990982. doi: 10.1177/2050313X21990982

Huntley, M., Srinivasan, K., Friedman, B., Wang, T., Yee, A., Wang, Y., et al. (2020). Genome-wide analysis of differential gene expression and splicing in excitatory neurons and interneuron subtypes. *J. Neurosci.* 40, 958–973. doi: 10.1523/JNEUROSCI.1615-19.2019

Judson, M., Sosa-Pagan, J., Del Cid, W., Han, J., and Philpot, B. (2014). Allelic specificity of Ube3a expression in the mouse brain during postnatal development. *J. Comp. Neurol.* 522, 1874–1896. doi: 10.1002/CNE.23507

Kamata, A., Takeuchi, Y., and Fukunaga, K. (2006). Identification of the isoforms of Ca^{2+}/calmodulin-dependent protein kinase II and expression of brain-derived neurotrophic factor mRNAs in the substantia nigra. *J. Neurochem.* 96, 195–203. doi: 10.1111/J.1471-4159.2005.03531.X

Kool, M. J., Onori, M., Borgesius, N., van de Bree, J., Elgersma-Hooisma, M., Nio, E., et al. (2019). CAMK2-dependent signaling in neurons is essential for survival. *J. Neurosci.* 39, 5424–5439. doi: 10.1523/JNEUROSCI.1341-18.2019

Kool, M., van de Bree, J., Bodde, H., Elgersma, Y., and van Woerden, G. (2016). The molecular, temporal and region-specific requirements of the beta isoform of Calcium/Calmodulin-dependent protein kinase type 2 (CAMK2B) in mouse locomotion. *Sci. Rep.* 6:26989. doi: 10.1038/srep26989

Kozareva, V., Martin, C., Osorno, T., Rudolph, S., Guo, C., Vanderburg, C., et al. (2021). A transcriptomic atlas of mouse cerebellar cortex comprehensively defines cell types. *Nature* 598, 214–219. doi: 10.1038/s41586-021-03220-z

Küry, S., van Woerden, G., Besnard, T., Proietti Onori, M., Latypova, X., Towne, M., et al. (2017). De novo mutations in protein kinase genes CAMK2A and CAMK2B cause intellectual disability. *Am. J. Hum. Genet.* 101, 768–788. doi: 10.1016/j.ajhg.2017.10.003

Ma, H., Groth, R., Cohen, S., Emery, J., Li, B., Hoedt, E., et al. (2014). γCaMKII shuttles Ca^{2+}/CaM to the nucleus to trigger CREB phosphorylation and gene expression. *Cell* 159, 281–294. doi: 10.1016/j.cell.2014.09.019

Mei, Y., Monteiro, P., Zhou, Y., Kim, J., Gao, X., Fu, Z., et al. (2016). Adult restoration of Shank3 expression rescues selective autistic-like phenotypes. *Nature* 530, 481–484. doi: 10.1038/nature16971

Murray, K. D., Isackson, P. J., and Jones, E. G. (2003). N-methyl-d-aspartate receptor dependent transcriptional regulation of two calcium/calmodulin-dependent protein kinase type II isoforms in rodent cerebral cortex. *Neuroscience* 122, 407–420. doi: 10.1016/J.NEUROSCIENCE.2003.07.015

Nguyen, P., Abel, T., Kandel, E., and Bourtchouladze, R. (2000). Strain-dependent differences in LTP and hippocampus-dependent memory in inbred mice. *Learn. Mem.* 7, 170–179. doi: 10.1101/lm.7.3.170

O'leary, H., Lasda, E., and Ulrich Bayer, K. (2006). CaMKII association with the actin cytoskeleton is regulated by alternative splicing. *Mol. Biol. Cell* 17, 4656–4665. doi: 10.1091/mbc.E06

Proietti Onori, M., and van Woerden, G. M. (2021). Role of calcium/calmodulin-dependent kinase 2 in neurodevelopmental disorders. *Brain Res. Bull.* 171, 209–220. doi: 10.1016/j.brainresbull.2021.03.014

Proietti Onori, M., Koopal, B., Everman, D., Worthington, J., Jones, J., Ploeg, M., et al. (2018). The intellectual disability-associated CAMK2G p.Arg292Pro mutation acts as a pathogenic gain-of-function. *Hum. Mutat.* 39, 2008–2024. doi: 10.1002/humu.23647

Rigter, P., Wallaard, I., Aghadavoud Jolfaei, M., Kingma, J., Post, L., and Elgersma, M. (2022). Adult Camk2a gene reinstatement restores the learning and plasticity deficits of Camk2a knockout mice. *Iscience* 25:105303. doi: 10.1016/j.isci.2022.105303

Rizzi, S., Spagnoli, C., Salerno, G., Frattini, D., Caraffi, S., Trimarchi, G., et al. (2020). Severe intellectual disability, absence of language, epilepsy, microcephaly and progressive cerebellar atrophy related to the recurrent de novo variant p.(P139L) of the CAMK2B gene: A case report and brief review. *Am. J. Med. Genet. Part A* 182, 2675–2679. doi: 10.1002/AJMG.A.61803

Rotaru, D. C., Mientjes, E. J., and Elgersma, Y. (2020). Angelman Syndrome: From Mouse Models to Therapy. *Neuroscience* 445, 172–189. doi: 10.1016/J.NEUROSCIENCE.2020.02.017

Sakagami, H., and Kondo, H. (1993). Differential expression of mRNAs encoding γ and δ subunits of CA^{2+}/calmodulin-dependent protein kinase type II (CaM kinase II) in the mature and postnatally developing rat brain. *Mol. Brain Res.* 20, 51–63. doi: 10.1016/0169-328X(93)90109-3

Shioda, N., Sawai, M., Ishizuka, Y., Shirao, T., and Fukunaga, K. (2015). Nuclear translocation of calcium/calmodulin-dependent protein kinase IIδ3 promoted by protein phosphatase-1 enhances brain-derived neurotrophic factor expression in dopaminergic neurons. *J. Biol. Chem.* 290, 21663–21675. doi: 10.1074/JBC.M115.664920

Silva, A., Paylor, R., Wehner, J., and Tonegawa, S. (1992b). Impaired spatial learning in α-calcium-calmodulin kinase II mutant mice. *Science* 257, 206–211. doi: 10.1126/science.1321493

Silva, A., Stevens, C. F., Tonegawa, S., and Wang, Y. (1992a). Deficient hippocampal long-term potentiation in α-calcium-calmodulin kinase II mutant mice. *Science* 257, 201–206. doi: 10.1126/science.1378648

Silva-Santos, S., van Woerden, G., Bruinsma, C., Mientjes, E., Jolfaei, M., Distel, B., et al. (2015). Ube3a reinstatement identifies distinct developmental windows in a murine Angelman syndrome model. *J. Clin. Investig.* 125, 2069–2076. doi: 10.1172/JCI80554

Sloutsky, R., and Stratton, M. M. (2021). Functional implications of CaMKII alternative splicing. *Eur. J. Neurosci.* 54, 6780–6794. doi: 10.1111/EJN.14761

Sloutsky, R., Dziedzic, N., Dunn, M., Bates, R., Torres-Ocampo, A., Boopathy, S., et al. (2020). Heterogeneity in human hippocampal CaMKII transcripts reveals allosteric hub-dependent regulation. *Sci. Signal.* 13:eaaz0240. doi: 10.1126/scisignal.aaz0240

Sonzogni, M., Hakonen, J., Bernabé Kleijn, M., Silva-Santos, S., Judson, M., Philpot, B., et al. (2019). Delayed loss of UBE3A reduces the expression of angelman syndrome-associated phenotypes. *Mol. Autism* 10:23. doi: 10.1186/s13229-019-0277-1

Sonzogni, M., Wallaard, I., Silva Santos, S., Kingma, J., du Mee, D., van Woerden, G., et al. (2018). A behavioral test battery for mouse models of angelman syndrome: A powerful tool for testing drugs and novel Ube3a mutants. *Mol. Autism* 9:47. doi: 10.1186/s13229-018-0231-7

Sonzogni, M., Zhai, P., Mientjes, E., van Woerden, G., and Elgersma, Y. (2020). Assessing the requirements of prenatal UBE3A expression for rescue of behavioral phenotypes in a mouse model for angelman syndrome. *Mol. Autism* 11:70.

Srinivasan, M., Edman, C. F., and Schulman, H. (1994). Alternative splicing introduces a nuclear localization signal that targets multifunctional CaM Kinase to the nucleus. *J. Cell Biol.* 126, 839–852. doi: 10.1083/jcb.126.4.839

Stoeger, T., Grant, R., McQuattie-Pimentel, A., Anekalla, K., Liu, S., Tejedor-Navarro, H., et al. (2019). Aging is associated with a systemic length-driven transcriptome imbalance. *Biorxiv* [Preprint]. doi: 10.1101/691154

Takeuchi, Y., Yamamoto, H., Fukunaga, K., Miyakawa, T., and Miyamoto, E. (2000). Identification of the isoforms of Ca^{2+}/calmodulin-dependent protein Kinase II in rat astrocytes and their subcellular localization. *J. Neurochem.* 74, 2557–2567. doi: 10.1046/J.1471-4159.2000.0742557.X

Tobimatsu, T., and Fujisawa, H. (1989). Tissue-specific expression of four types of rat calmodulin-dependent protein kinase II mRNAs. *J. Biol. Chem.* 264, 17907–17912.

Tombes, R. M., Faison, M. O., and Turbeville, J. M. (2003). Organization and evolution of multifunctional Ca^{2+}/CaM-dependent protein kinase genes. *Gene* 322, 17–31. doi: 10.1016/j.gene.2003.08.023

Vallano, M., Beaman-Hall, C., Mathur, A., and Chen, Q. (2000). Astrocytes express specific variants of CaM KII δ and γ, but not α and β, that determine their cellular localizations. *Glia* 30, 154–164. doi: 10.1002/(SICI)1098-1136(200004)30:2

van Woerden, G., Hoebeek, F., Gao, Z., Nagaraja, R., Hoogenraad, C., Kushner, S., et al. (2009). BCaMKII controls the direction of plasticity at parallel fiber-purkinje cell synapses. *Nat. Neurosci.* 12, 823–825. doi: 10.1038/nn.2329

Xi, F., Xu, R., Xu, J., Ma, J., Wang, W., Wang, F., et al. (2019). Calcium/calmodulin-dependent protein kinase II regulates mammalian axon growth by affecting F-actin length in growth cone. *J. Cell. Physiol.* 234, 23053–23065. doi: 10.1002/jcp.28867

frontiers | Frontiers in Neuroscience

TYPE Original Research
PUBLISHED 25 January 2023
DOI 10.3389/fnins.2022.1077908

OPEN ACCESS

EDITED BY
Flavia Venetucci Gouveia,
University of Toronto, Canada

REVIEWED BY
Jia Wang,
Harbin Medical University, China
Bo Rao,
Zhongnan Hospital, Wuhan University, China

*CORRESPONDENCE
Mingmin Ning
✉ 2018203030023@whu.edu.cn
Ximing Wang
✉ wxming369@163.com

SPECIALTY SECTION
This article was submitted to Neurodevelopment, a section of the journal Frontiers in Neuroscience

RECEIVED 23 October 2022
ACCEPTED 30 December 2022
PUBLISHED 25 January 2023

CITATION
Li C, Chen W, Li X, Li T, Chen Y, Zhang C, Ning M and Wang X (2023) Gray matter asymmetry atypical patterns in subgrouping minors with autism based on core symptoms. *Front. Neurosci.* 16:1077908. doi: 10.3389/fnins.2022.1077908

Gray matter asymmetry atypical patterns in subgrouping minors with autism based on core symptoms

Cuicui Li[1], Wenxiong Chen[2], Xiaojing Li[2], Tong Li[1], Ying Chen[3], Chunling Zhang[3], Mingmin Ning[2]* and Ximing Wang[1]*

[1]Shandong Provincial Hospital Affiliated to Shandong First Medical University, Jinan, China, [2]Guangzhou Women and Children's Medical Center, Guangzhou, China, [3]Central Hospital Affiliated to Shandong First Medical University, Jinan, China

Abnormal gray matter (GM) asymmetry has been verified in autism spectrum disorder (ASD), which is characterized by high heterogeneity. ASD is distinguished by three core symptom domains. Previous neuroimaging studies have offered support for divergent neural substrates of different core symptom domains in ASD. However, no previous study has explored GM asymmetry alterations underlying different core symptom domains. This study sought to clarify atypical GM asymmetry patterns underlying three core symptom domains in ASD with a large sample of 230 minors with ASD (ages 7–18 years) and 274 matched TD controls from the Autism Brain Imaging Data Exchange I (ABIDE I) repository. To this end, the scores of the revised autism diagnostic interview (ADI-R) subscales were normalized for grouping ASD into three core-symptom-defined subgroups: social interaction (SI), verbal communication (VA), and restricted repetitive behaviors (RRB). We investigated core-symptom-related GM asymmetry alterations in ASD resulting from advanced voxel-based morphometry (VBM) by general linear models. We also examined the relationship between GM asymmetry and age and between GM asymmetry and symptom severity assessed by the Autism Diagnostic Observation Schedule (ADOS). We found unique GM asymmetry alterations underlying three core-symptom-defined subgroups in ASD: more rightward asymmetry in the thalamus for SI, less rightward asymmetry in the superior temporal gyrus, anterior cingulate and caudate for VA, and less rightward asymmetry in the middle and inferior frontal gyrus for RRB. Furthermore, the asymmetry indexes in the thalamus were negatively associated with ADOS_SOCIAL scores in the general ASD group. We also showed significant correlations between GM asymmetry and age in ASD and TD individuals. Our results support the theory that each core symptom domain of ASD may have independent etiological and neurobiological underpinnings, which is essential for the interpretation of heterogeneity and the future diagnosis and treatment of ASD.

KEYWORDS

autism, gray matter asymmetry, minors, core symptom domains, brain-behavior relationships

1. Introduction

Autism spectrum disorder (ASD) encompasses a group of pervasive neurodevelopmental disorders characterized by three core symptom domains: social interaction deficits (SI), verbal communication abnormalities (VA), and restricted repetitive behaviors (RRB) (Shulman et al., 2020). All three core symptom domains encompass various behaviors that manifest diversely across the disease, making ASD a condition with complex behaviors. While ASD is a common neurodevelopmental condition and has been investigated in numerous studies, it is also remarkably heterogeneous, complicating its diagnosis and neuroimaging findings. Over the past 30 years, the definition of autism has undergone a constant transformation, leading to the current autism spectrum (Shulman et al., 2020).

Identifying neuroimaging is vital to understanding the etiology and pathophysiology of ASD patients. Such markers can lead to early diagnosis and better treatment (Loth et al., 2016), particularly early in life, when interventions can have the greatest effect on patients with ASD. Although the exact neuroimaging changes in patients with ASD remain unknown, some brain structural alterations seem to be involved. These changes include decreased cortical thickness in the right pre- and postcentral gyrus and increased cortical thickness in the superior temporal sulcus, cingulate gyrus, and fusiform gyrus (Hardan et al., 2006; Hyde et al., 2010); greater gray matter (GM) volume in the amygdala, bilateral superior temporal gyrus, and precuneus and lower GM volume in the right inferior temporal gyrus in children with ASD (Retico et al., 2016; Lucibello et al., 2019); atypical cortical thickness development with accelerated expansion followed by accelerated thinning and atypical cortical volume development with increased cortical total volume (especially in the frontal and temporal lobes) in young ASD children (Li et al., 2017; Rommelse et al., 2017); and altered brain structure asymmetry with significantly increased rightward asymmetry in the posterior superior temporal gyrus, inferior parietal lobule, and auditory cortex and reduced rightward asymmetry in the parahippocampal gyrus, fusiform- and inferior temporal thickness (Gage et al., 2009; Floris et al., 2016; Postema et al., 2019).

Brain asymmetry is thought to be an evolutionary adaptation ensuring more efficient transcortical information integration and avoiding redundancy in cognitive processing (Hugdahl, 2011). Alterations in brain asymmetry have been shown to influence a variety of neurological and psychotic disorders, especially ASD (Prior and Bradshaw, 1979). ASD patients exhibit deficits in left hemisphere skills, such as language and motor skills, while right hemisphere skills remain relatively unaffected (McCann, 1982). This pattern in ASD has spawned theories that attempt to reconcile its complex clinical features with atypical brain asymmetry. However, there are mixed findings on brain structural asymmetry alterations in patients with ASD (Postema et al., 2019). For instance, a study showed increased leftward asymmetry of GM volume in the language-association areas in ASD (Hazlett et al., 2006). However, research by De Fossé et al. (2004) found rightward asymmetry of GM volume in the language-related cortex in ASD.

Untangling the heterogeneity of brain structural asymmetry may lead to the improvement of accurate diagnoses and elaborate clinical subgrouping and may help in developing targeted treatment plans for patients with ASD. Regarding heterogeneity, most studies focus on ex-factors, such as age, comorbidities, medication use, and methodological differences (Hobson and Petty, 2021). However, Haar et al. (2016) found that differences between the ASD group and the control group were overshadowed by considerable within-group variability. Happé et al. (2006) demonstrated that each core symptom domain of ASD has independent etiological and neurobiological underpinnings. Ronald et al. (2006) studied the genetic etiology of autistic traits in 3,419 normal child twin pairs and found that unique genetic variance was associated with each of the three core symptom domains. As such, individuals will vary within a huge permutation network, unavoidably leading to a highly heterogeneous population. Additionally, previous neuroimaging studies of ASD have offered support for the divergent neural substrates of different core symptom domains, which are mediated by partially distinct brain regions. For instance, social cognition mainly relies on certain social brain regions, such as the fusiform face area, amygdala, medial prefrontal cortex, anterior cingulate cortex, superior temporal sulcus, and inferior frontal gyrus, RRB has been linked to abnormalities in motor regions, and reduced activation in the right parahippocampal gyrus, cerebellum, left anterior cingulate, and bilateral cingulate in face-processing social tasks has been reported in patients with ASD (Spencer et al., 2011; Patriquin et al., 2016; Duret et al., 2018; Wilkes and Lewis, 2018). In addition, our previous research showed that atypical gyrification patterns encode changes in the symptom dimensions of ASD (Ning et al., 2021). The analysis is complicated by likely distinct symptom clusters or subgroups that exist among patients with ASD (Lenroot and Yeung, 2013). Significant intra- and interindividual variabilities in patients with ASD make it challenging to reliably determine the neural mechanisms of the disorder. Therefore, it is necessary to subcategorize patients with ASD according to core symptoms to explore their brain structural asymmetry. However, no previous study thus far has explored this issue.

Based on the above research, we hypothesize that subgroups dominated by different core symptom domains may have unique brain structural asymmetry alterations because each subgroup has differential clinical manifestations and neurobiological underpinnings. However, we also assumed that there would be shared brain structural asymmetry alterations because these subgroups are on the same disease spectrum and have partly similar pathological mechanisms. For this, an advanced voxel-based morphometry (VBM) method established by Kurth et al. (2015) and a large sample (230 minors with ASD, 274 control subjects) from the Autism Brain Imaging Data Exchange I (ABIDE I) repository was used to clarify GM asymmetry atypical patterns underlying three core symptom domains and to further explore the relationship between GM asymmetry and age and between abnormal GM asymmetry and symptom severity measured by the Autism Diagnostic Observation Schedule (ADOS).

2. Participants and methods

2.1. Participant recruitment

A total of 230 minors with ASD (ages 7–18 years) and 274 matched typically developing (TD) controls were examined from ABIDE I: a consortium with 539 individuals with ASD and 573 TD controls (ages 7–64 years) collected from 17 sites. Our data were aggregated across right sites that included at least five individuals with ASD and five age-, gender-, and site-matched TD controls who met our inclusion criteria. Briefly, we selected individuals aged 7–18

(the ages most represented in ABIDE I sites) with good quality T1-weighted images that can be preprocessed successfully, with complete revised autism diagnostic interview (ADI-R) scores.

To investigate whether GM asymmetry differs across ASD dominated by different core symptom domains, we divided minors with ASD into three subgroups, SI, VA, and RRB based on the ADI-R (Bokadia et al., 2020). The ADI-R is a semistructured scale that evaluates and scores the condition mainly through interviews with patients' parents, including the ADI-R-SOCIAL-TOTAL-A (corresponding to SI), ADI-R-VERBAL-TOTAL-BV (corresponding to VA), and ADI-R-RRB-TOTAL-C (corresponding to RRB) subscales. First, we used the corresponding maximal values to normalize the scores of three ADI-R subscales according to the following formula and then obtained three values between 0 and 1, denoted as S, V, and R, respectively (Bokadia et al., 2020).

$$X' = \frac{X}{X\_MAX}$$

Finally, minors with ASD were assigned to three subgroups according to the normalized scores: subjects with S as the largest value were included in the SI subgroup; subjects with V as the largest value were included in the VA subgroup; subjects with R as the largest value were included in the RRB subgroup. If S = V or S = R or V = R, he would be excluded. TD controls were randomly selected to form age-, gender- and site-matched TD groups. To maximize the sample size, each TD control was matched four times, meaning that some controls may have appeared in multiple subgroups. Ultimately, 230,146, 43, and 41 patients were included in the general ASD, SI, VA, and RRB subgroups, respectively, and 264, 249, 127, and 111 controls were included in the corresponding TD subgroups.

The ADI-R was from the parents' assessment, which lacked an assessor's objective evaluation of clinical symptoms. To prevent any influence of subjective parents' assessment on the subgroup, we conducted subgroups based on ADOS with the same methodology. ADOS is a semistructured standard diagnostic tool employing a play-based approach to detect autistic symptoms. Ultimately, 148,19, and 0 patients were included in the SI_2, VA_2, and RRB_2 subgroups based on ADOS, respectively, and 225, 55, and 0 controls were included in the corresponding TD subgroups.

All data were anonymized and collected by studies approved by the regional Institutional Review Boards.

2.2. MRI data acquisition

Whole-brain high-resolution T1-weighted anatomical images of all participants in our study were acquired in ABIDE I, and detailed parameters and acquisition protocols used at each site can be seen at http://fcon_1000.projects.nitrc.org/indi/abide/.

2.3. Image analysis

2.3.1. Image preprocessing

In our study, we preprocessed 3D T1-weighted images using VBM[1] toolbox for Statistical Parametric Mapping (SPM8[2]) software. Before preprocessing, visual checks were performed for all images. (1) Segment tissue: the symmetrical tissue probability map downloaded from the internet[3] was used to perform tissue segmentation on 3D T1-weighted images to obtain GM, white matter (WM) and cerebrospinal fluid segments, and quality inspection was performed. (2) Flip tissue segments: the GM and WM segments obtained in the last step were flipped with the midline of the brain as the axis to create new images with reversed left and right brain hemispheres. (3) Generate a symmetrical template: the flipped images obtained in step 2 and the original versions obtained in step 1 were used to generate a symmetrical Diffeomorphic Anatomical Registration Lie (DARTEL) template. (4) Warp images: unflipped and flipped GM images obtained in steps 1 and 2, respectively, were warped to the symmetric DARTEL template obtained in step 3. (5) Generate the right-hemisphere mask: a right-hemisphere mask was generated in MRIcron[4] using the DARTEL template obtained in step 3 to limit further analysis to the right hemisphere.

2.3.2. Estimation of the asymmetry index (AI)

All warped original GM versions and their corresponding warped flipped GM segments (both generated in step 4) and the right-hemispheric mask (obtained in step 5) were selected to calculate the voxel-wise GM asymmetry following the optimized protocol by Kurth et al. (2015). In this step, the left hemispheres were discarded for all original and flipped GM versions of all subjects during the masking procedure. As a result, the original and flipped GM segments yielded the right and left hemispheres, respectively (Kurth et al., 2015). Then, the masked asymmetry index (AI) images of each participant were generated according to the following formula: AI = ((i1−i2)/((i1+i2).*0.5)).*i3, in which i1 and i2 are original and flipped GM warped images, respectively, and i3 is the right-hemispheric mask image (Kurth et al., 2015). The resulting AI images were then spatially smoothed with an 8 mm Gaussian kernel. In the results, positive and negative AI values indicate rightward and leftward asymmetry, respectively.

2.4. Statistical analyses

Differences in gender between each subgroup pair were tested using the chi-square test in SPSS software (IBM Corp, Armonk, NY), and other variables were tested using the independent two-sample *t*-test. At an uncorrected threshold of $P < 0.05$, the results were considered statistically significant. For demographic differences among the three subgroups, the nonparametric test was used for ADI-R subscores, and $P < 0.05$ was considered statistically significant after Bonferroni correction by SPSS software.

To explore which brain regions exhibited differences in GM asymmetry between the ASD/SA/VI/RRB group and corresponding TD groups, general linear models were evaluated, with age, gender, and site as covariates in SPM8. When the participants belong to site 1, site 1 was recorded as 1 and other sites were recorded as 0 (other sites = 0, site 1 = 1). The same was true for the other sites. In the Data Preprocessing Assistant for rs-fMRI software (DPARSF[5]; Yan et al.,

1 http://dbm.neuro.uni-jena.de/vbm8

2 http://www.fil.ion.ucl.ac.uk/spm

3 http://dbm.neuro.uni-jena.de/vbm8/TPM_symmetric.nii

4 https://www.nitrc.org/frs/?group_id=152

5 http://rfmri.org/dpabi

2016), brain clusters with significant differences in between-group comparisons were saved as masks.

In addition, to test the relationship between symptom severity measured by ADOS subscores and AIs in the general ASD group, multiple regression analyses were implemented, with age, gender, and site as covariates in SPM8. Scatter plots describing the linear relation between the clinical severity and AIs were conducted in SPSS. Because few ASD participants were using ADOS in three subgroups based on ADI-R, we performed regression analyses only in the general ASD group; ultimately, 129 ASD patients in the general ASD group were used for regression analyses. Similarly, to explore the relationship between AIs and age in patients with ASD and TD controls, multiple regression analyses were implemented, with gender and site as covariates. Scatter plots describing the linear relation between age and AIs were generated in SPSS. Importantly, multiple regression analyses concentrated on masks saved in the above between-group comparisons.

In all general linear models and multiple regression analyses, the results were corrected for multiple comparisons using the Gaussian random field (GRF) procedure with the voxel level of P-value < 0.005 and the cluster level of $P < 0.05$ implemented by DPARSF (Deng and Wang, 2021).

3. Results

3.1. Demographic and clinical details

Descriptive statistics are presented in **Tables 1**, **2** and **Supplementary Table 1**. There were no significant differences between each subgroup pair in age and gender ($P > 0.05$). Three subgroups significantly differed in ADI-R subscale scores ($P < 0.05$).

3.2. Differences in GM asymmetry between general ASD and TD controls

As shown in **Figure 1A** and **Table 3**, specific brain regions showed significant differences between general ASD and TD controls: ASD patients had more leftward asymmetry in Cluster A1 (inferior temporal/middle temporal gyrus), Cluster A2 (parahippocampal gyrus), Cluster A3 (superior temporal gyrus), and Cluster A6 (precuneus) and had more rightward asymmetry in Cluster A4 (thalamus), Cluster A5 (medial frontal gyrus) and Cluster A7 (postcentral/precentral gyrus).

3.3. Differences in GM asymmetry between ASD subgroups and TD controls

Differences in GM asymmetry between the SI/VA/RRB group and corresponding TD groups were then assessed (**Figures 1B–D** and **Table 3**). In particular, relative to the TD group, the SI subgroup showed significantly more rightward asymmetry in Cluster S2 (thalamus) and Cluster S4 (postcentral/precentral gyrus) and less rightward asymmetry in Cluster S1 (middle temporal gyrus) and Cluster S3 (precuneus). The VA subgroup showed significantly less rightward asymmetry than the TD group in Cluster V1 (inferior temporal gyrus), Cluster V2 (middle temporal/superior temporal gyrus), Cluster V3 (anterior cingulate/caudate), and Cluster V4 (precuneus/postcentral gyrus). Relative to the TD group, the RRB subgroup showed significantly more rightward asymmetry in Cluster R4 (precentral/postcentral gyrus) and less rightward asymmetry in Cluster R1 (middle temporal gyrus), Cluster R2 (inferior frontal/middle frontal gyrus), Cluster R3 (inferior temporal/fusiform gyrus), and Cluster R5 (precuneus).

3.4. GM asymmetry results validation

GM asymmetry results between ADOS-based ASD subgroups and TD controls overlapped in main brain areas with GM asymmetry findings based on ADI-R, suggesting that our subgrouping based on ADI-R was robust (**Supplementary Figure 1** and **Supplementary Table 2**).

3.5. Brain-behavior relationships

The multiple regression analyses using clinical severity measured by ADOS as the independent predictor of AI showed significant negative associations: AIs of Cluster A4 were negatively associated with social scores measured by the ADOS in the general ASD group ($r = -0.187$, $P = 0.032$; **Figure 2**).

3.6. The effect of age

Multiple regression analyses were calculated between AIs and age in patients with ASD and TD controls: Cluster V1 exhibited increased leftward asymmetry from age 7 to 18 in the VA subgroup ($r = -0.361$, $P = 0.017$), Cluster A5 presented increased rightward asymmetry with age in the general ASD group ($r = 0.155$, $P = 0.019$), and Cluster A2 showed increased rightward asymmetry over time in the TD group ($r = 0.162$, $P = 0.008$; **Figure 3**).

4. Discussion

In this study, we attempted to explore atypical GM asymmetry patterns and subcategorize the neuroimaging of ASD based on its core symptoms in a large brain imaging database (ABIDE I). We found unique and elaborate GM asymmetry patterns among the three ASD subgroups.

4.1. The atypical pattern of GM asymmetry in the general ASD group

Abnormal structural asymmetries in patients with ASD have been reported to be widely distributed across various brain regions (Maximo et al., 2014). Examples include significantly increased rightward asymmetry in the inferior parietal lobule, auditory cortex (Floris et al., 2016), posterior superior temporal gyrus (Gage et al., 2009), and lateral orbitofrontal surface area (Postema et al., 2019) and reduced rightward asymmetry in the medial orbitofrontal surface

TABLE 1 Participant demographics.

	Variables		NYU	UCLA	UM	KKI	PITT	STANFORD	TRINITY	YALE	Total
ASD and TD	Subjects (N)	ASD (TD)	56 (65)	52 (45)	65 (62)	14 (25)	7 (9)	14 (20)	9 (14)	13 (24)	230 (264)
	Age (years)	ASD	11.23 ± 2.62	13.04 ± 2.50	13.00 ± 2.34	10.26 ± 1.46	12.80 ± 1.00	9.86 ± 1.63	14.62 ± 1.75	12.45 ± 2.97	12.25 ± 2.61
		TD	12.06 ± 2.79	12.96 ± 1.92	13.69 ± 2.59	10.37 ± 1.31	13.32 ± 1.00	9.95 ± 1.60	14.33 ± 1.63	12.52 ± 2.57	12.48 ± 2.58
	Gender M (F)	ASD	56 (10)	47 (5)	55 (10)	13 (1)	4 (3)	11 (3)	9 (0)	10 (3)	199 (31)
		TD	50 (13)	39 (6)	50 (12)	24 (1)	7 (2)	16 (4)	14 (0)	17 (7)	219 (45)
	Statistics	Age	$t = -1.69$, $p = 0.09$	$t = 0.33$, $p = 0.57$	$t = -1.56$, $p = 0.12$	$t = -0.25$, $p = 0.80$	$t = -1.03$, $p = 0.32$	$t = -0.12$, $p = 0.90$	$t = 0.41$, $p = 0.69$	$t = -0.73$, $p = 0.94$	$t = -1.00$, $p = 0.32$
		Gender	$X^2 = 0.40$, $p = 0.53$	$X^2 = 0.17$, $p = 0.87$	$X^2 = 0.35$, $p = 0.56$	$X^2 = 0.18$, $p = 0.67$	$X^2 = 0.78$, $p = 0.38$	$X^2 = 0.01$, $p = 0.92$	–	$X^2 = 0.16$, $p = 0.69$	$X^2 = 1.20$, $p = 0.27$
SI and TD	Subjects (N)	SI (TD)	30 (58)	16 (34)	16 (44)	14 (25)	7 (9)	14 (20)	9 (14)	13 (24)	146 (249)
	Age (years)	SI	11.69 ± 2.67	12.80 ± 2.55	12.68 ± 2.30	10.26 ± 1.46	12.80 ± 1.00	9.89 ± 1.63	14.62 ± 1.75	12.45 ± 2.97	12.25 ± 2.56
		TD	12.59 ± 2.82	13.03 ± 1.73	13.19 ± 2.46	10.37 ± 1.31	13.31 ± 1.00	9.95 ± 1.60	14.33 ± 1.63	12.52 ± 2.57	12.49 ± 2.47
	Gender M (F)	SI	28 (2)	15 (1)	15 (1)	13 (1)	4 (3)	11 (3)	9 (0)	10 (3)	124 (22)
		TD	54 (4)	29 (5)	43 (1)	24 (1)	7 (2)	16 (4)	14 (0)	17 (7)	213 (36)
	Statistics	Age	$t = -1.44$, $p = 0.15$	$t = -0.37$, $p = 0.71$	$t = -0.72$, $p = 0.48$	$t = -0.25$, $p = 0.80$	$t = -1.03$, $p = 0.32$	$t = -0.12$, $p = 0.90$	$t = 0.41$, $p = 0.69$	$t = -0.93$, $p = 0.36$	$t = -0.49$, $p = 0.62$
		Gender	$X^2 = 0.002$, $p = 0.97$	$X^2 = 0.74$, $p = 0.39$	$X^2 = 0.58$, $p = 0.45$	$X^2 = 0.18$, $p = 0.67$	$X^2 = 0.78$, $p = 0.38$	$X^2 = 0.01$, $p = 0.92$	–	$X^2 = 0.16$, $p = 0.69$	$X^2 = 0.03$, $p = 0.87$

(Continued)

10.3389/fnins.2022.1077908

TABLE 1 (Continued)

	Variables		NYU	UCLA	UM	Total
RRB and TD	Subjects (N)	RRB (TD)	10 (33)	15 (34)	16 (44)	41 (111)
	Age (years)	RRB	11.14 ± 2.59	12.70 ± 2.60	12.45 ± 2.13	12.22 ± 2.45
		TD	11.90 ± 2.06	13.02 ± 1.73	13.19 ± 2.46	12.75 ± 2.19
	Gender M (F)	RRB	10 (0)	14 (1)	15 (1)	39 (2)
		TD	33 (0)	29 (5)	43 (1)	106 (5)
	Statistics	Age	$t = -0.96$, $p = 0.34$	$t = -0.49$, $p = 0.62$	$t = -1.06$, $p = 0.29$	$t = -1.28$, $p = 0.20$
		Gender	–	$X^2 = 0.30$, $p = 0.59$	$X^2 = 0.58$, $p = 0.45$	$X^2 = 0.01$, $p = 0.92$
VA and TD	Subjects (N)	VA (TD)	16 (48)	10 (35)	17 (44)	43 (127)
	Age (years)	VA	10.42 ± 2.47	13.00 ± 2.75	13.42 ± 2.73	12.21 ± 2.93
		TD	11.16 ± 2.40	13.00 ± 2.10	14.66 ± 2.67	12.88 ± 2.83
	Gender M (F)	VA	12 (4)	8 (2)	16 (1)	36 (7)
		TD	33 (15)	31 (4)	43 (1)	107 (20)
	Statistics	Age	$t = -1.06$, $p = 0.29$	$t = 0.00$, $p = 1$	$t = -1.60$, $p = 0.12$	$t = -1.34$, $p = 0.18$
		Gender	$X^2 = 0.23$, $p = 0.64$	$X^2 = 0.50$, $p = 0.48$	$X^2 = 0.50$, $p = 0.48$	$X^2 = 0.07$, $p = 0.93$

ASD, autism spectrum disorder; TD, typically developing; SI, subgroup dominated by social interaction deficits; VA, subgroup dominated by verbal communication abnormalities; RRB, subgroup dominated by restricted repetitive behaviors; KKI, Kennedy Krieger Institute; NYU, New York University Langone Medical Center; UCLA, University of California-Los Angeles; UM, University of Michigan; YALE, Yale Child Study Center; STANFORD: Stanford University; TRINITY, Trinity Centre for Health Sciences; PITT, University of Pittsburgh School of Medicine.

10.3389/fnins.2022.1077908

TABLE 2 Differences in the three ADI-R subscales among the three ASD subgroups.

Variables	Std. Test Statistic	*P*-value*	Std. Test Statistic	*P*-value*	Std. Test Statistic	*P*-value*
	SI vs. VA		SI vs. RRB		VA vs. RRB	
ADI-R-SOCIAL	−4.295	< 0.0001	3.727	< 0.0001	0.607	1.000
ADI-R-VERBAL	−2.666	0.023	0.512	1.000	−4.759	< 0.0001
ADI-R-RRB	−0.524	1.000	6.909	< 0.0001	5.178	< 0.0001

ADI-R-SOCIAL, social subscore of autism diagnostic interview-revised (ADI-R); ADI-R-VERBAL, verbal subscore of ADI-R; ADI-R-RRB, restricted repetitive behaviors subscore of ADI-R; SI, subgroup dominated by social interaction deficits; VA, subgroup dominated by verbal communication abnormalities; RRB, subgroup dominated by restricted repetitive behaviors.
*Bonferroni corrected *p*-values.

area, putamen volume, and the parahippocampal gyrus (Postema et al., 2019; Li et al., 2021). The reported multiregional asymmetry alterations are consistent with the notion that laterality is easily disrupted in patients with ASD (Maximo et al., 2014). In our study, the results showed that various GM asymmetry alterations were located in several clusters in the general ASD group, predominantly involving the temporal, frontal, and parahippocampal gyrus, which part overlapped with findings in previous studies, such as the parahippocampal gyrus having more leftward asymmetry (Li et al., 2021). However, in the postcentral gyrus, general ASD showed more rightward asymmetry; previous studies by Hau et al. (2022) reported leftward asymmetry of the postcentral gyrus volume in ASD patients relative to the TD group. Interestingly, we found that this brain region exhibited more rightward asymmetry in the SI and RRB subgroups but leftward asymmetry in the VA subgroup. Furthermore, our analysis revealed additional GM asymmetry alterations, including the anterior cingulate, caudate, inferior frontal gyrus, middle frontal gyrus, and fusiform, that were present only in ASD subgroups but not in the general ASD group. Our results further suggested the neuroimaging heterogeneity of ASD. Such heterogeneity would result in the truth being offset or inaccurate if ASD is considered as a whole.

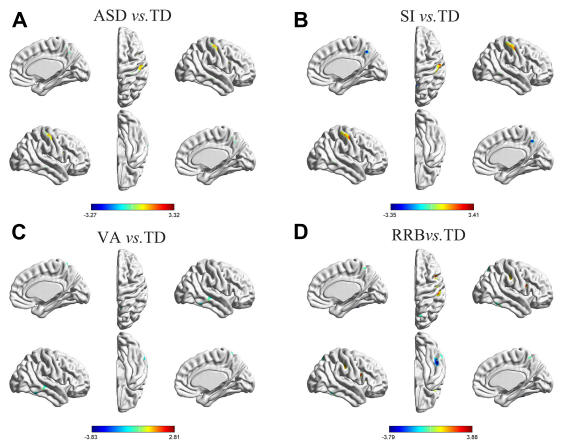

FIGURE 1
Differences in GM asymmetry in between-group comparisons. **(A)** General ASD vs. TD controls: seven clusters with significant differences between general ASD and TD controls. **(B)** SI vs. TD: four clusters with significant differences between SI and TD controls. **(C)** VA vs. TD: four clusters with significant differences between VA and TD controls. **(D)** RRB vs. TD: five clusters with significant differences between RRB and TD controls; the red color indicates the general ASD/SI/VA/RRB group with more rightward asymmetry, and the blue color indicates more leftward asymmetry. The results were corrected for multiple comparisons using the Gaussian random field procedure with the voxel level *P*-value < 0.005 and the cluster level of $P < 0.05$. GM, gray matter; ASD, autism spectrum disorder; TD, typically developing; SI, subgroup dominated by social interaction deficits; VA, subgroup dominated by verbal communication abnormalities; RRB, subgroup dominated by restricted repetitive behaviors.

4.2. Divergent GM asymmetry patterns in ASD subgroups

Different GM asymmetry alterations were presented across three core-symptom-defined ASD subgroups in our study, consistent with previous notions that brain structure and function alterations are associated with specific clinical symptoms in ASD. For instance, social cognition mainly relies upon certain social brain regions (Patriquin et al., 2016). The results of our study indicated that different clinical phenotypes defined by divergent core-symptom domains would result in heterogeneity in neuroimaging.

Specifically, there was more rightward asymmetry in the thalamus for SI, less rightward asymmetry in the superior temporal gyrus, anterior cingulate, and caudate for VA, and less rightward asymmetry in the middle and inferior frontal gyrus for RRB.

The thalamus, known as the subcortical-cortical relay, is related to social deficits and is thought to be a vital region in ASD (Schuetze et al., 2016). Although MRI cannot provide cellular-level evidence for changed thalamic volume asymmetry, alterations in thalamic volume may be concerned with changes in myelination or other properties of WM axons innervating the region or changes in dendritic or neuropil compartments (Schuetze et al., 2016). Structurally, the rightward asymmetry of thalamic volume modulated the correlation between parental alienation and the social abilities of children with social anxiety disorder (Zhang et al., 2020). On the functional level, hypoconnectivity between the posterior thalamus and parieto-occipital cortex has been found in ASD (Nair et al., 2013), and the pulvinar nucleus has been shown to have significant connections with the prefrontal and parieto-occipital cortices in studies on humans (Arcaro et al., 2015). The occipital abnormalities have been related to social reciprocity deficits in ASD (Amaral et al., 2008). Our results indicate that thalamic volume properties at the structural level may result in alterations in these functional connectivities, which, in turn, influence social interaction in ASD.

The superior temporal gyrus (STG) is one of the language-functional regions in normally developed and language-impaired subjects. During embryologic and early postnatal development, the right STG is equally capable of language processing as the left STG (Kertesz et al., 1992). Nevertheless, this equivalent capacity starts to vary during later development, with the left STG showing a clear advantage in language processing (Kertesz et al., 1992). Reports on language-association area asymmetry in ASD have had inconsistent

TABLE 3 Coordinates of clusters with significant differences in between-group comparisons.

	Cluster	Location	MNI coordinates			voxels	*t*-value
			x	y	z		
ASD vs. TD	A1	Inferior Temporal Gyrus/Middle Temporal Gyrus	67.5	−34.5	−22.5	268/126	−3.271
	A2	ParaHippocampal	13.5	1.5	−24	69	−3.170
	A3	Superior Temporal Gyrus	42	10.5	−16.5	41	−2.810
	A4	Thalamus	19.5	−18	12	127	3.169
	A5	Medial Frontal Gyrus	12	37.5	25.5	5	2.739
	A6	Precuneus	3	−60	45	106	−2.998
	A7	Postcentral Gyrus/Precentral Gyrus	55.5	−24	60	233/145	3.053
SI vs. TD	S1	Middle Temporal Gyrus	60	−24	−9	67	−2.986
	S2	Thalamus	19.5	−18	12	65	2.955
	S3	Precuneus	3	−58.5	46.5	182	−3.355
	S4	Postcentral/Precentral Gyrus	55.5	−25.5	60	456/172	3.411
VA vs. TD	V1	Inferior Temporal Gyrus	66	−48	−19.5	78	−3.829
	V2	Middle Temporal/Superior Temporal Gyrus	45	−27	−1.5	133/102	−3.310
	V3	Anterior Cingulate/Caudate	9	22.5	−3	75/56	−3.055
	V4	Precuneus/Postcentral	9	−58.5	67.5	146/75	−2.973
RRB vs. TD	R1	Middle Temporal Gyrus	57	6	−24	42	−2.678
	R2	Inferior Frontal/Middle Frontal Gyrus	25.5	31.5	−25.5	81/60	−2.869
	R3	Inferior Temporal Gyrus/Fusiform	48	−40.5	−25.5	607/245	−3.794
	R4	Postcentral/Precentral	48	9	22.5	536/204	3.877
	R5	Precuneus	16.5	−72	57	103	−3.017

ASD, autism spectrum disorder; TD, typically developing; SI, subgroup dominated by social interaction deficits; VA, subgroup dominated by verbal communication abnormalities; RRB, subgroup dominated by restricted repetitive behaviors.

results, with research showing increased leftward asymmetry of fusiform- and inferior temporal thickness (Postema et al., 2019), study reporting increased leftward asymmetry of GM volume in the language-association areas (Hazlett et al., 2006), lack of planum temporale leftward asymmetry (Rojas et al., 2005), or investigation exhibiting rightward asymmetry of GM volume in language-related cortex in ASD (De Fossé et al., 2004). The fact that patients in the VA subgroup in our study exhibited less rightward asymmetry again provides evidence for atypical GM asymmetry in ASD, albeit admittedly in a different pattern than much of the prior literature.

The frontostriatal system plays a key role in social motivation, which is thought to be the basis of abnormities in verbal communication in ASD (Delmonte et al., 2013). A previous study showed that the mechanisms controlling the number and volume of neurons and the total volume of the caudate nucleus are dysregulated in ASD (Hollander et al., 2005). These cellular alterations result in different volumes of the bilateral caudate (i.e., abnormal caudate asymmetry) in ASD. Abnormal caudate asymmetry underlies the disruption of structural and functional connectivities between the frontal cortex (including anterior cingulate) and striatum (Delmonte et al., 2013), which may potentially explain the link between the leftward asymmetry of the caudate and anterior cingulate and verbal communication deficits in ASD in our study.

It was reported that response inhibition is consistently associated with the inferior and middle frontal gyrus, which may relate to the severity of core deficits in ASD (Voorhies et al., 2018). Functionally, during the inhibition condition task, the ASD initially engaged the right rather than the left frontal cortex (typically developing first recruited the left middle frontal gyrus) and had reduced recruitment of non-frontal regions, which is related to their difficulty in executing top-down control (Vara et al., 2014). In our study, increased rightward asymmetry of GM volume in the inferior and middle frontal gyrus was found in the RRB subgroup. Alterations in structural asymmetry may have functional consequences. Our results may explain the first recruitment of the right frontal cortex in ASD. The increased structural rightward asymmetry may be the foundation of long-range functional hypoconnectivity and local hyperconnectivity in the frontal cortex, which are the underlying deficits of RRB in ASD.

Unique GM asymmetry alterations in each subgroup underline that core-symptom-specific analyses of structural asymmetry are well motivated. For the reason of dividing the heterogeneous ASD subjects into symptom-related subgroups would increase the specificity and accuracy of neuroimaging findings.

4.3. Brain-behavior relationships

By multiple regression analysis, we found that the AIs in Cluster A4 (thalamus) were negatively associated with social scores measured by ADOS. The reduced social score (i.e., lower symptom severity) provides preliminary proof that increased rightward asymmetry in Cluster A4 might have a compensatory effect in regulating social deficits. Although ASD patients have inactive responses to social stimuli, in some cases this low interaction may be improved by early intervention (Cohen et al., 2018). The data here suggest that

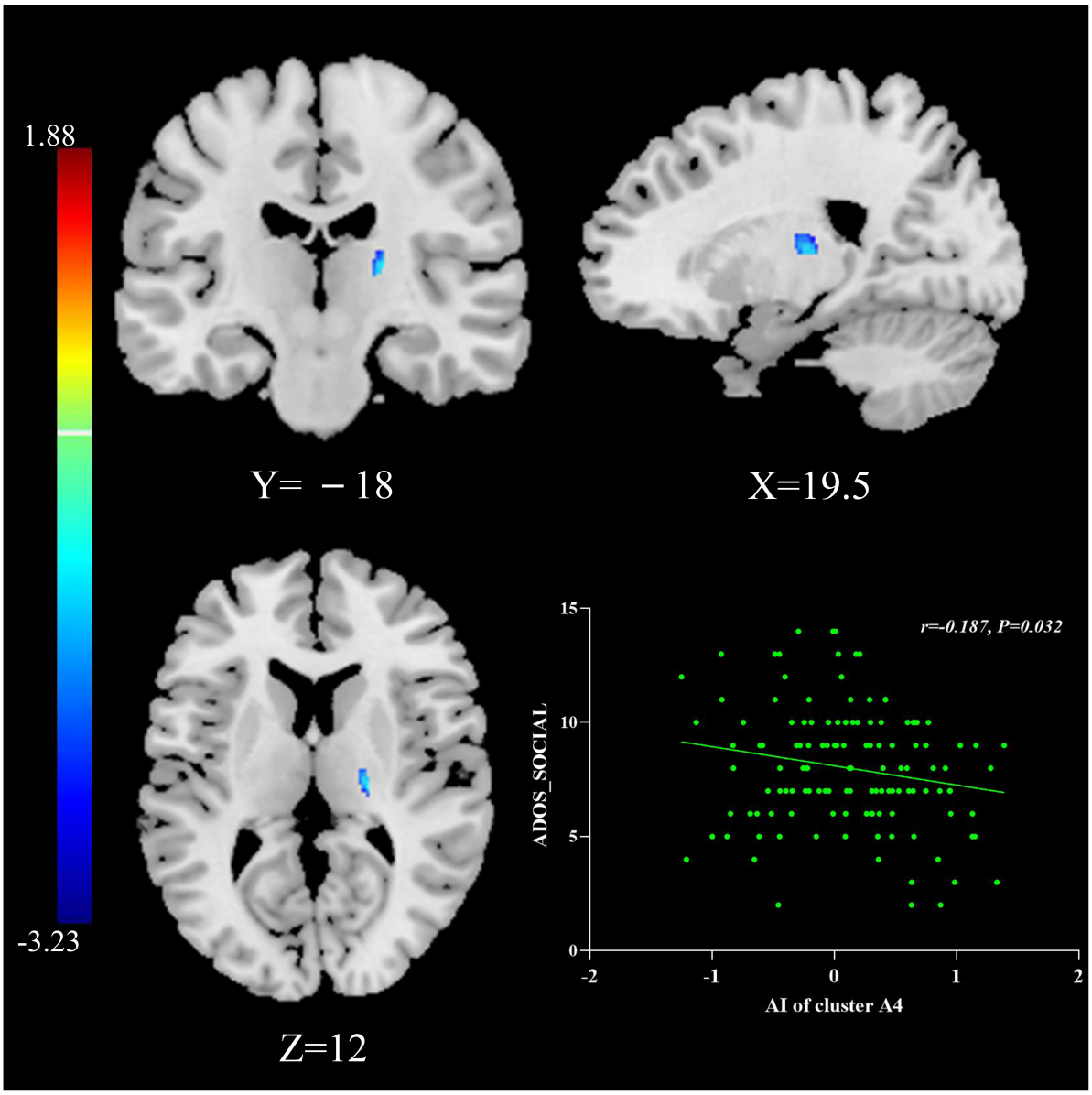

FIGURE 2
The relationship between AIs and symptom severity. AIs of Cluster A4 were negatively associated with social scores measured by the ADOS in the general ASD group. The results were corrected for multiple comparisons using the Gaussian random field procedure with the voxel level P-value < 0.005 and the cluster level of $P < 0.05$. ASD, autism spectrum disorder; AI, asymmetry index; ADOS, Autism Diagnostic Observation Schedule.

atypical rightward asymmetry of the thalamus may indeed be the anatomic basis of social interaction deficits in ASD, and timely and effective interventions may exert their effect through recombination and functional balance of social-cognitive brain networks (Cohen et al., 2018), including the thalamus. This effect may provide novel ideas and new targets for the future treatment of ASD. However, more reproducible studies are needed to confirm this relationship.

4.4. Common GM asymmetry patterns in the general ASD group and ASD subgroups

The general ASD group and three subgroups showed consistent changes in the middle temporal and precuneus gyrus. Both brain regions overlap with the default mode network (DMN), which may be the cocircuit responsible for three core symptom domains. In the DSM-5, only two domains are included, achieved by merging the first two domains indicated in the DSM-IV-TR (social interaction and communication domains) into the social communication domain (Shulman et al., 2020). The model indicates convergence of social interaction and communication deficits, but not with RRB. The potential effect of the new criteria has received extensive attention, with some studies inspecting the sensitivity and specificity of the revision (Guthrie et al., 2013). However, no study has examined brain structural alterations related to the revised diagnostic domains. In our study, it should be noted that although there were overlapping brain regions between the SI subgroup and VA subgroup, there were even more differences in asymmetry alterations, including different brain regions and varying directions (i.e., the postcentral gyrus). Therefore, we believe that it is more reasonable to divide general

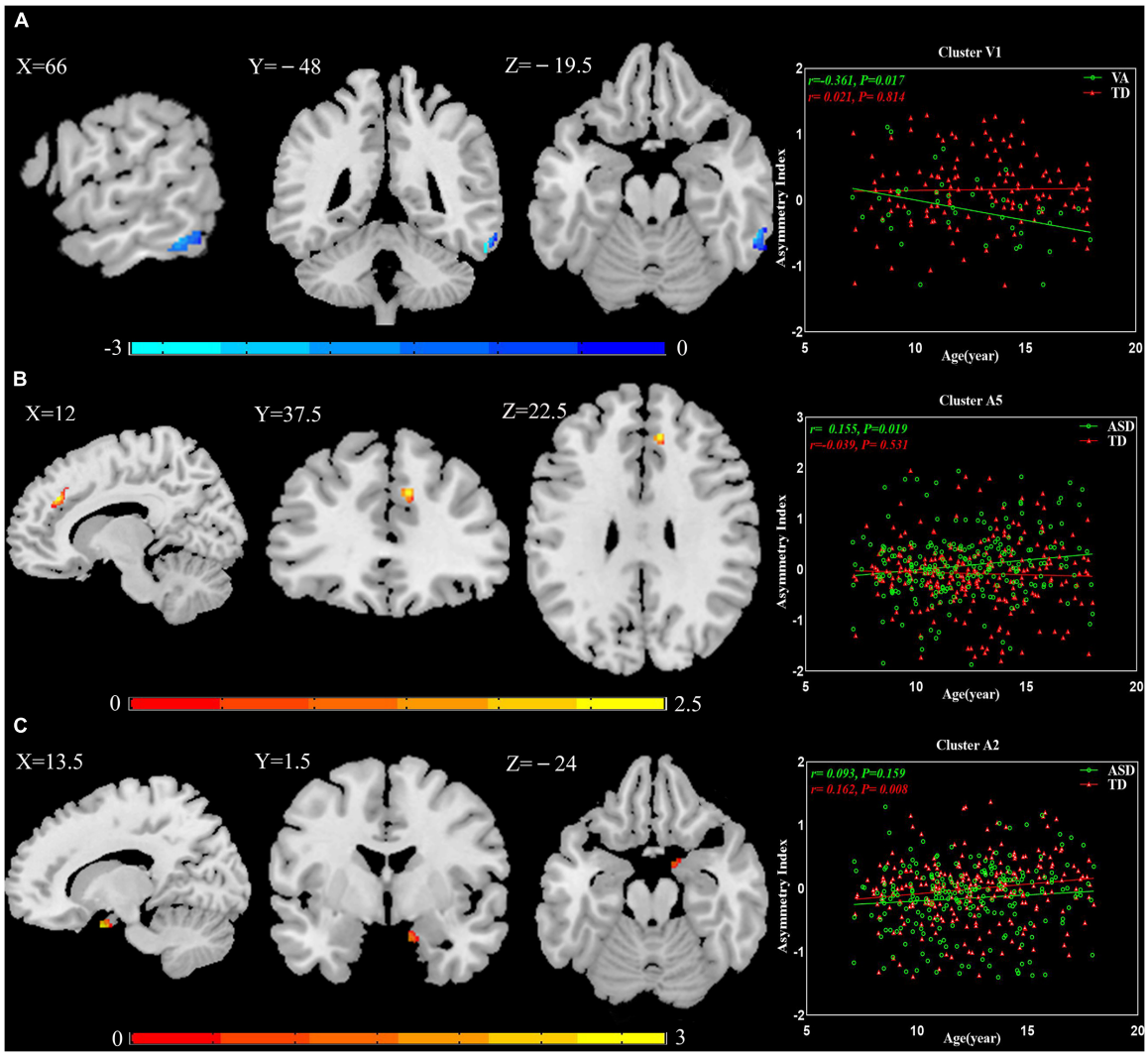

FIGURE 3
The relationship between AIs and age. **(A)** Cluster V1 exhibited increased leftward asymmetry from age 7 to 18 in the VA subgroup. **(B)** Cluster A5 presented increased rightward asymmetry with age in the general ASD group. **(C)** Cluster A2 showed increased rightward asymmetry over time in the TD group. The results were corrected for multiple comparisons using the Gaussian random field procedure with the voxel level P-value < 0.005 and the cluster level of $P < 0.05$. AI, asymmetry index; ASD, autism spectrum disorder; TD, typically developing; VA, subgroup dominated by verbal communication abnormalities.

ASD patients into three core-symptom-related subgroups in brain structural research.

4.5. The effect of age

The results of the multiple regression analyses between AIs and age suggested that GM asymmetry may not be constant in minors. In TD controls, this manifested as increased rightward asymmetry from age 7 to 18 in Cluster A2. In patients with ASD, the abnormal GM asymmetry changed with age: Cluster V1 had more leftward asymmetry, and Cluster A5 had more rightward asymmetry. In corresponding TD controls, both clusters showed reverse asymmetry. This demonstrates that degrees of abnormality in Cluster V1 and Cluster A5 were increased. Whether these GM asymmetry alterations are caused by genetics, the environment, or both is unknown. Prior studies have shown that there are structural asymmetries present even before birth (Hepper et al., 1991; McCartney and Hepper, 1999). Autopsy histological studies have indicated that genetic factors contribute to brain lateralization (Karlebach and Francks, 2015). Our observations further illustrate the importance of early intervention for ASD. This is a key field for future study and warrants further longitudinal analysis.

4.6. Limitations

We examined the relationship between abnormal GM asymmetry and age but did not conduct longitudinal comparisons between the age effect and GM asymmetry due to the limitation of the sample size. To investigate the longitudinal change in GM asymmetry in each subgroup, it is necessary to employ the current grouping pattern and explore the effect of age on GM asymmetry using a higher-power approach with longitudinal tracking and a larger

number of participants. Data in our study were screened from the ABIDE I database and collected from eight sites around the world, which resulted in additional variabilities, including differences in scanning equipment and parameters, clinical behavioral evaluation, and participant selection. However, the bias of the site was minimized by using this effect as a covariate when conducting statistical analyses.

5. Conclusion

To identify the neural substrates underlying different core symptom domains, we explored the core-symptom-related alterations in GM asymmetry in ASD. We found unique GM asymmetry changes in three ASD subgroups and some specific alterations across subgroups were greatly overshadowed in the general ASD group. These findings emphasize the role of core symptoms in exploring ASD-related neuroimaging alterations and provide a clear characterization of core-symptom-related differences in neurobiology. Furthermore, abnormal GM asymmetries increase in degree with age, illustrating the importance of early intervention and treatment. In addition, the compensatory effect of Cluster A4 in regulating social deficits may provide novel ideas and new targets for the future treatment of ASD. In conclusion, our results further support the theory that each core symptom domain of ASD may have independent etiological and neurobiological underpinnings, which is crucial to the future diagnosis and treatment of ASD.

Data availability statement

The datasets presented in this study can be found in online repositories. The names of the repository/repositories and accession number(s) can be found in the article/**Supplementary material**.

Ethics statement

Ethical review and approval were not required for the study on human participants in accordance with the local legislation and institutional requirements. Written informed consent from the participant's legal guardian/next of kin was not required to participate in this study in accordance with the national legislation and institutional requirements.

Author contributions

CL and MN conceived and designed the experiments. CL, MN, WC, XL, TL, YC, CZ, and XW analyzed the data. CL and MN wrote the manuscript. All authors contributed to the article and approved the submitted version.

Acknowledgments

We would like to express our sincere appreciation to the data donors and organizers and participants who participated in this study and to Dr. Gao Lei from Zhongnan Hospital of Wuhan University for his guidance on image processing technology.

Conflict of interest

The authors declare that the research was conducted in the absence of any commercial or financial relationships that could be construed as a potential conflict of interest.

Publisher's note

All claims expressed in this article are solely those of the authors and do not necessarily represent those of their affiliated organizations, or those of the publisher, the editors and the reviewers. Any product that may be evaluated in this article, or claim that may be made by its manufacturer, is not guaranteed or endorsed by the publisher.

Supplementary material

The Supplementary Material for this article can be found online at: https://www.frontiersin.org/articles/10.3389/fnins.2022.1077908/full#supplementary-material

SUPPLEMENTARY FIGURE 1
Differences in GM asymmetry in between-group comparisons based on ADOS. **(A)** SI_2 vs. TD: 3 clusters with significant differences between SI_2 and TD controls. **(B)** VA_2 vs. TD: 3 clusters with significant differences between VA_2 and TD controls. The red color indicates SI_2/VA_2 with more rightward asymmetry, and the blue color indicates more leftward asymmetry. The results were corrected for multiple comparisons using the Gaussian random field procedure with the voxel level P-value < 0.005 and the cluster level of $P < 0.05$. GM, gray matter; ADOS, Autism Diagnostic Observation Schedule; SI_2, subgroup dominated by social interaction deficits based on ADOS; VA_2, subgroup dominated by verbal communication abnormalities based on ADOS.

References

Amaral, D. G., Schumann, C. M., and Nordahl, C. W. (2008). Neuroanatomy of autism. *Trends Neurosci.* 31, 137–145. doi: 10.1016/j.tins.2007.12.005

Arcaro, M. J., Pinsk, M. A., and Kastner, S. (2015). The anatomical and functional organization of the human visual pulvinar. *J. Neurosci.* 35, 9848–9871. doi: 10.1523/JNEUROSCI.1575-14.2015

Bokadia, H., Rai, R., and Torres, E. B. (2020). Digitized Autism Observation Diagnostic Schedule: Social Interactions beyond the Limits of the Naked Eye. *J. Pers. Med.* 10:159. doi: 10.3390/jpm10040159

Cohen, Jd, Smith, T., Thompson, K., Collins, A., Knaus, T., and Tager-Flusberg, H. (2018). Altered anterior insular asymmetry in pre-teen and adolescent youth with

autism spectrum disorder. *Ann. Behav. Neurosci.* 1, 24–35. doi: 10.18314/abne.v1i1.1120

De Fossé, L., Hodge, S. M., Makris, N., Kennedy, D. N., Caviness, V. S., McGrath, L., et al. (2004). Language-association cortex asymmetry in autism and specific language impairment. *Ann. Neurol.* 56, 757–766. doi: 10.1002/ana.20275

Delmonte, S., Gallagher, L., O'Hanlon, E., McGrath, J., and Balsters, J. H. (2013). Functional and structural connectivity of frontostriatal circuitry in Autism Spectrum Disorder. *Front. Hum. Neurosci.* 7:430. doi: 10.3389/fnhum.2013.00430

Deng, Z., and Wang, S. (2021). Sex differentiation of brain structures in autism: Findings from a gray matter asymmetry study. *Autism Res.* 14, 1115–1126. doi: 10.1002/aur.2506

Duret, P., Samson, F., Pinsard, B., Barbeau, E., Boré, A., Soulières, I., et al. (2018). Gyrification changes are related to cognitive strengths in autism. *Neuroimage Clin.* 20, 415–423. doi: 10.1016/j.nicl.2018.04.036

Floris, D. L., Lai, M. C., Auer, T., Lombardo, M. V., Ecker, C., Chakrabarti, B., et al. (2016). Atypically rightward cerebral asymmetry in male adults with autism stratifies individuals with and without language delay. *Hum. Brain Mapp.* 37, 230–253. doi: 10.1002/hbm.23023

Gage, N. M., Juranek, J., Filipek, P. A., Osann, K., Flodman, P., Isenberg, A. L., et al. (2009). Rightward hemispheric asymmetries in auditory language cortex in children with autistic disorder: an MRI investigation. *J. Neurodev. Disord.* 1, 205–214. doi: 10.1007/s11689-009-9010-2

Guthrie, W., Swineford, L. B., Wetherby, A. M., and Lord, C. (2013). Comparison of DSM-IV and DSM-5 factor structure models for toddlers with autism spectrum disorder. *J. Am. Acad. Child Adolesc. Psychiatry* 52:e792. doi: 10.1016/j.jaac.2013.05.004

Haar, S., Berman, S., Behrmann, M., and Dinstein, I. (2016). Anatomical abnormalities in autism? *Cereb. Cortex* 26, 1440–1452. doi: 10.1093/cercor/bhu242

Happé, F., Ronald, A., and Plomin, R. (2006). Time to give up on a single explanation for autism. *Nat. Neurosci.* 9, 1218–1220. doi: 10.1038/nn1770

Hardan, A. Y., Muddasani, S., Vemulapalli, M., Keshavan, M. S., and Minshew, N. J. (2006). An MRI study of increased cortical thickness in autism. *Am. J. Psychiatry* 163, 1290–1292. doi: 10.1176/ajp.2006.163.7.1290

Hau, J., Baker, A., Chaaban, C., Kohli, J. S., Keehn, R. J. J., Linke, A. C., et al. (2022). Reduced asymmetry of the hand knob area and decreased sensorimotor u-fiber connectivity in middle-aged adults with autism. *Cortex* 153, 110–125. doi: 10.1016/j.cortex.2022.04.004

Hazlett, H. C., Poe, M. D., Gerig, G., Smith, R. G., and Piven, J. (2006). Cortical gray and white brain tissue volume in adolescents and adults with autism. *Biol. Psychiatry* 59, 1–6. doi: 10.1016/j.biopsych.2005.06.015

Hepper, P. G., Shahidullah, S., and White, R. (1991). Handedness in the human fetus. *Neuropsychologia* 29, 1107–1111. doi: 10.1016/0028-3932(91)90080-r

Hobson, H., and Petty, S. (2021). Moving forwards not backwards: heterogeneity in autism spectrum disorders. *Mol. Psychiatry* 26, 7100–7101. doi: 10.1038/s41380-021-01226-7

Hollander, E., Anagnostou, E., Chaplin, W., Esposito, K., Haznedar, M. M., Licalzi, E., et al. (2005). Striatal volume on magnetic resonance imaging and repetitive behaviors in autism. *Biol. Psychiatry* 58, 226–232. doi: 10.1016/j.biopsych.2005.03.040

Hugdahl, K. (2011). Fifty years of dichotic listening research - still going and going and. . .. *Brain Cogn.* 76, 211–213. doi: 10.1016/j.bandc.2011.03.006

Hyde, K. L., Samson, F., Evans, A. C., and Mottron, L. (2010). Neuroanatomical differences in brain areas implicated in perceptual and other core features of autism revealed by cortical thickness analysis and voxel-based morphometry. *Hum. Brain Mapp.* 31, 556–566. doi: 10.1002/hbm.20887

Karlebach, G., and Francks, C. (2015). Lateralization of gene expression in human language cortex. *Cortex* 67, 30–36. doi: 10.1016/j.cortex.2015.03.003

Kertesz, A., Polk, M., Black, S. E., and Howell, J. (1992). Anatomical asymmetries and functional laterality. *Brain* 115(Pt 2), 589–605. doi: 10.1093/brain/115.2.589

Kurth, F., Gaser, C., and Luders, E. (2015). A 12-step user guide for analyzing voxel-wise gray matter asymmetries in statistical parametric mapping (SPM). *Nat. Protoc.* 10, 293–304. doi: 10.1038/nprot.2015.014

Lenroot, R. K., and Yeung, P. K. (2013). Heterogeneity within autism spectrum disorders: what have we learned from neuroimaging studies? *Front. Hum. Neurosci.* 7:733. doi: 10.3389/fnhum.2013.00733

Li, C., Ning, M., Fang, P., and Xu, H. (2021). Sex differences in structural brain asymmetry of children with autism spectrum disorders. *J. Integr. Neurosci.* 20, 331–340. doi: 10.31083/j.jin2002032

Li, D., Karnath, H.-O., and Xu, X. (2017). Candidate biomarkers in children with autism spectrum disorder: a review of MRI studies. *Neurosci. Bull.* 33, 219–237. doi: 10.1007/s12264-017-0118-1

Loth, E., Murphy, D. G., and Spooren, W. (2016). Defining precision medicine approaches to autism spectrum disorders: concepts and challenges. *Front. Psychiatry* 7:188. doi: 10.3389/fpsyt.2016.00188

Lucibello, S., Verdolotti, T., Giordano, F., Lapenta, L., Infante, A., Piludu, F., et al. (2019). Brain morphometry of preschool age children affected by autism spectrum disorder: correlation with clinical findings. *Clin. Anat.* 32, 143–150. doi: 10.1002/ca.23252

Maximo, J. O., Cadena, E. J., and Kana, R. K. (2014). The implications of brain connectivity in the neuropsychology of autism. *Neuropsychol. Rev.* 24, 16–31. doi: 10.1007/s11065-014-9250-0

McCann, B. S. (1982). Hemispheric asymmetries and early infantile autism. *J. Autism. Dev. Disord.* 11, 401–411. doi: 10.1007/BF01531615

McCartney, G., and Hepper, P. (1999). Development of lateralized behaviour in the human fetus from 12 to 27 weeks' gestation. *Dev. Med. Child. Neurol.* 41, 83–86. doi: 10.1017/s0012162299000183

Nair, A., Treiber, J. M., Shukla, D. K., Shih, P., and Muller, R. A. (2013). Impaired thalamocortical connectivity in autism spectrum disorder: a study of functional and anatomical connectivity. *Brain* 136, 1942–1955. doi: 10.1093/brain/awt079

Ning, M., Li, C., Gao, L., and Fan, J. (2021). Core-Symptom-Defined cortical gyrification differences in autism spectrum disorder. *Front. Psychiatry* 12:619367. doi: 10.3389/fpsyt.2021.619367

Patriquin, M. A., DeRamus, T., Libero, L. E., Laird, A., and Kana, R. K. (2016). Neuroanatomical and neurofunctional markers of social cognition in autism spectrum disorder. *Hum. Brain Mapp.* 37, 3957–3978. doi: 10.1002/hbm.23288

Postema, M. C., Van Rooij, D., Anagnostou, E., Arango, C., Auzias, G., Behrmann, M., et al. (2019). Altered structural brain asymmetry in autism spectrum disorder in a study of 54 datasets. *Nat. Commun.* 10, 1–12. doi: 10.1038/s41467-019-13005-8

Prior, M. R., and Bradshaw, J. L. (1979). Hemisphere functioning in autistic children. *Cortex* 15, 73–81. doi: 10.1016/s0010-9452(79)80008-8

Retico, A., Giuliano, A., Tancredi, R., Cosenza, A., Apicella, F., Narzisi, A., et al. (2016). The effect of gender on the neuroanatomy of children with autism spectrum disorders: a support vector machine case-control study. *Mol. Autism.* 7, 1–20. doi: 10.1186/s13229-015-0067-3

Rojas, D. C., Camou, S. L., Reite, M. L., and Rogers, S. J. (2005). Planum temporale volume in children and adolescents with autism. *J. Autism Dev. Disord.* 35, 479–486. doi: 10.1007/s10803-005-5038-7

Rommelse, N., Buitelaar, J. K., and Hartman, C. A. (2017). Structural brain imaging correlates of ASD and ADHD across the lifespan: a hypothesis-generating review on developmental ASD–ADHD subtypes. *J. Neural. Transm.* 124, 259–271. doi: 10.1007/s00702-016-1651-1

Ronald, A., Happé, F., Bolton, P., Butcher, L. M., Price, T. S., Wheelwright, S., et al. (2006). Genetic heterogeneity between the three components of the autism spectrum: a twin study. *J. Am. Acad. Child. Adolesc. Psychiatry* 45, 691–699. doi: 10.1097/01.chi.0000215325.13058.9d

Schuetze, M., Park, M. T., Cho, I. Y., MacMaster, F. P., Chakravarty, M. M., and Bray, S. L. (2016). Morphological alterations in the thalamus, striatum, and pallidum in autism spectrum disorder. *Neuropsychopharmacology* 41, 2627–2637. doi: 10.1038/npp.2016.64

Shulman, C., Esler, A., Morrier, M. J., and Rice, C. E. (2020). Diagnosis of autism spectrum disorder across the lifespan. 29, 253–273. *Child Adolesc. Psychiatr. Clin. N. Am.* doi: 10.1016/j.chc.2020.01.001

Spencer, M., Holt, R., Chura, L., Suckling, J., Calder, A., Bullmore, E., et al. (2011). A novel functional brain imaging endophenotype of autism: the neural response to facial expression of emotion. *Transl. Psychiatry* 1, e19–e19. doi: 10.1038/tp.2011.18

Vara, A. S., Pang, E. W., Doyle-Thomas, K. A., Vidal, J., Taylor, M. J., and Anagnostou, E. (2014). Is inhibitory control a 'no-go' in adolescents with autism spectrum disorder? *Mol. Autism* 5:6. doi: 10.1186/2040-2392-5-6

Voorhies, W., Dajani, D. R., Vij, S. G., Shankar, S., Turan, T. O., and Uddin, L. Q. (2018). Aberrant functional connectivity of inhibitory control networks in children with autism spectrum disorder. *Autism Res.* 11, 1468–1478. doi: 10.1002/aur.2014

Wilkes, B., and Lewis, M. (2018). The neural circuitry of restricted repetitive behavior: Magnetic resonance imaging in neurodevelopmental disorders and animal models. *Neurosci. Biobehav. Rev.* 92, 152–171. doi: 10.1016/j.neubiorev.2018.05.022

Yan, C. G., Wang, X. D., Zuo, X. N., and Zang, Y. F. (2016). DPABI: Data processing & analysis for (resting-state) brain imaging. *Neuroinformatics* 14, 339–351. doi: 10.1007/s12021-016-9299-4

Zhang, Y., Liu, W., Lebowitz, E. R., Zhang, F., Hu, Y., Liu, Z., et al. (2020). Abnormal asymmetry of thalamic volume moderates stress from parents and anxiety symptoms in children and adolescents with social anxiety disorder. *Neuropharmacology* 180:108301. doi: 10.1016/j.neuropharm.2020.108301

frontiers | Frontiers in Neuroscience

TYPE Hypothesis and Theory
PUBLISHED 16 February 2023
DOI 10.3389/fnins.2023.1101422

OPEN ACCESS

EDITED BY
Michela Candini,
University of Bologna, Italy

REVIEWED BY
Frederic Bilan,
Université de Poitiers, France
Sofia Lizarraga,
University of South Carolina, United States

*CORRESPONDENCE
François Iris
✉ francois.iris@bmsystems.org

SPECIALTY SECTION
This article was submitted to Neurodevelopment, a section of the journal Frontiers in Neuroscience

RECEIVED 17 November 2022
ACCEPTED 31 January 2023
PUBLISHED 16 February 2023

CITATION
Beopoulos A, Géa M, Fasano A and Iris F (2023) RNA epitranscriptomics dysregulation: A major determinant for significantly increased risk of ASD pathogenesis. *Front. Neurosci.* 17:1101422. doi: 10.3389/fnins.2023.1101422

RNA epitranscriptomics dysregulation: A major determinant for significantly increased risk of ASD pathogenesis

Athanasios Beopoulos[1], Manuel Géa[1], Alessio Fasano[2] and François Iris[1]*

[1]Bio-Modeling Systems, Tour CIT, Paris, France, [2]Division of Pediatric Gastroenterology and Nutrition, Mucosal Immunology and Biology Research Center, Center for Celiac Research and Treatment, Massachusetts General Hospital for Children, Boston, MA, United States

Autism spectrum disorders (ASDs) are perhaps the most severe, intractable and challenging child psychiatric disorders. They are complex, pervasive and highly heterogeneous and depend on multifactorial neurodevelopmental conditions. Although the pathogenesis of autism remains unclear, it revolves around altered neurodevelopmental patterns and their implications for brain function, although these cannot be specifically linked to symptoms. While these affect neuronal migration and connectivity, little is known about the processes that lead to the disruption of specific laminar excitatory and inhibitory cortical circuits, a key feature of ASD. It is evident that ASD has multiple underlying causes and this multigenic condition has been considered to also dependent on epigenetic effects, although the exact nature of the factors that could be involved remains unclear. However, besides the possibility for differential epigenetic markings directly affecting the relative expression levels of individual genes or groups of genes, there are at least three mRNA epitranscriptomic mechanisms, which function cooperatively and could, in association with both genotypes and environmental conditions, alter spatiotemporal proteins expression patterns during brain development, at both quantitative and qualitative levels, in a tissue-specific, and context-dependent manner. As we have already postulated, sudden changes in environmental conditions, such as those conferred by maternal inflammation/immune activation, influence RNA epitranscriptomic mechanisms, with the combination of these processes altering fetal brain development. Herein, we explore the postulate whereby, in ASD pathogenesis, RNA epitranscriptomics might take precedence over epigenetic modifications. RNA epitranscriptomics affects real-time differential expression of receptor and channel proteins isoforms, playing a prominent role in central nervous system (CNS) development and functions, but also RNAi which, in turn, impact the spatiotemporal expression of receptors, channels and regulatory proteins irrespective of isoforms. Slight dysregulations in few early components of brain development, could, depending upon their extent, snowball into a huge variety of

pathological cerebral alterations a few years after birth. This may very well explain the enormous genetic, neuropathological and symptomatic heterogeneities that are systematically associated with ASD and psychiatric disorders at large.

KEYWORDS

Autism spectrum disorder (ASD), maternal inflammation, mRNA alternative splicing, mRNA poly(A)-tail modulation, adenosine-to-inosine RNA editing, RNA epitranscriptomics

1. Introduction

Among the psychiatric disorders that develop in children, Autism spectrum disorder (ASD) is perhaps the most severe, persistent and difficult to treat, mainly due to its multifactorial neurodevelopmental origin, which results in great heterogeneity across the spectrum of the condition (Faras et al., 2010). Diagnosis is based on behavioral observation, pointing to deficiencies in social interaction and communication, as well as constrained and repetitive behavioral patterns of activities and interests. As the name implies, there is inherent heterogeneity in ASD, with frequent psychiatric and medical comorbidities such as attention deficit/hyperactivity disorder, intellectual disability, anxiety disorder, and oppositional defiant disorder (Masi et al., 2017).

While the mechanisms underlying ASD remain poorly understood, they focus on alterations in CNS development and their implications for brain function (Watts, 2008). ASD is thus largely defined as a developmental disorder affecting neural connectivity, which affects the organization of the cortical network and the ratio of neural excitation to inhibition. However, little progress has been made toward the causes for laminar-specific excitatory and inhibitory cortical circuits disruption (Watts, 2008; Prem et al., 2020). Recent genetic studies have also identified that risk genes substantially converge in the development of the cortex between the 8 and 24th week of gestation (GW8-24) (Courchesne et al., 2019; Beopoulos et al., 2022). However, the majority of animal studies on ASD focus primarily on postnatal development and defects in synaptic transmission, rather than on early developmental processes guiding central nervous system (CNS) formation, such as cell differentiation, proliferation, migration, and arborization. Instead, it is assumed that the multigenic state of ASD is dependent on epigenetic effects, without however being able to pinpoint such factors (Eshraghi et al., 2018; Prem et al., 2020). Indeed, monozygotic (MZ) twins with different phenotypic traits exhibit considerable epigenetic variation as well as differentially methylated ASD-related gene loci (Kaminsky et al., 2009; Gordon et al., 2012).

Nevertheless, besides the possibility for differential epigenetic markings directly affecting the relative expression levels of individual genes or groups of genes, there are at least three mRNA epitranscriptomic mechanisms, which function cooperatively and could, in association with both genotypes and environmental conditions, alter spatiotemporal proteins expression patterns during brain development, at both quantitative and qualitative levels, in a tissue-specific, and context-dependent manner. These are differential mRNAs alternative splicing (Vuong et al., 2016; Stark et al., 2019), cytoplasmic-shortening or elongation of mRNAs poly(A)-tails (Eckmann et al., 2011; Weill et al., 2012) and adenosine-to-inosine (A-to-I) RNA editing (Slotkin and Nishikura, 2013; Liu et al., 2014) which addresses not only mRNAs but also RNA interference pathways (RNAi). All three mechanisms are known to function cooperatively and produce an enormous diversity of protein isoforms endowing the CNS with considerable phenotypic plasticity and functional adaptability (Gommans et al., 2009).

Here, we explore the postulate whereby, in the pathogenesis of ASD, RNA epitranscriptomics might probably take precedence over differential epigenetic (methylation/acetylation) modifications which require environmental conditions to stay stable long enough to have real physiological effects. Indeed, RNA epitranscriptomics affect not only real-time differential expression of receptor and channel proteins isoforms, playing a prominent role in CNS development and functions, but also similarly affect RNAi which, in turn, impact the expression of receptor and channel proteins irrespective of isoforms. This may very well explain the enormous genetic and symptomatic heterogeneities that are systematically associated with psychiatric disorders at large and not only with ASD.

2. Materials and methods

The authors conducted an in-depth review of the literature and used a systems biology approach to integrate the complex mechanisms of fetal brain development to then decipher the most probable origins of the neurodevelopmental alterations encountered in individuals with ASD. Throughout our literature review, we strongly favored studies on human subjects, and in the few instances where this was not possible, this is clearly stated in the text. The analytical procedure implemented (CADI^{TM}: Computer-Assisted Deductive Integration, BM-Systems, Paris, France) associates algorithmics and heuristics. The logic behind this model-building approach does not assume functional linearity within biological systems and the components of a model do not incorporate solely what is known. Indeed, since this approach relies upon strict and systematic implementation of negative selection of hypotheses, models arising from this procedure contain elements that have never been described but cannot be refuted by current knowledge and/or available biological data, thereby generating novel understanding. This model-building approach has proven its efficacy in a number of biological research domains, including

the discovery of hitherto unsuspected biological mechanisms, pathways, and interactions directly associated with phenotypic transitions *in vivo* (be they pathological or developmental) (Gadal et al., 2003, 2005; Iris et al., 2009; Pouillot et al., 2010; Turck and Iris, 2011; Iris, 2012; Nussbaumer et al., 2016). CADI™ modeling has led to discoveries and patents in the fields of infectious diseases, oncology, neurology, psychiatry, dermatology, immunology, metabolic disorders, innovative bioprocesses for industrial biotech and the creation of new companies exploiting these patents. CADI™ models describe the biological phenomena involved in pathological states and provide novel mechanistic integrations to explain the cause of certain diseases, identify and select predictive biomarkers, and offer new combinations of molecules and new therapeutic strategies. Further information on the CADI method can be found in Iris et al. (2018).

3. Analysis

3.1. The genetic and epigenetics of increased risks in ASD pathogenesis

Genetic factors undeniably contribute to the risk for ASD (Abrahams and Geschwind, 2008). However, the genetics of autism are extremely complex and there are currently at least 1034 genes known to confer risk of ASD[1], while as yet undefined environmental factors, in conjunction with genotype, play a prominent role in the etiology of ASD. Most of the 126 genes strongly predisposing to autism, in the context of a syndromic (e.g., fragile X syndrome) as well as idiopathic disorder, in addition to most of the 194 genes identified as significant predisposition candidates, bear rare single gene mutations, each of which, should they also be causal, would have a plethora of deleterious physiological consequences far beyond autism *per se*. Thus, genomic variants at risk for ASD may be rare, *de novo* and high effect variants, independently or in combination with common or inherited low effect variants (Gratten et al., 2014). However, previous studies have revealed that ASD-risk genes exhibit a huge range of spatiotemporal expression patterns in human brain (Ben-David and Shifman, 2013; Parikshak et al., 2013; Willsey et al., 2013; Chang et al., 2015) and only a small percentage of probands can be explained by identified ASD risk-genes (De Rubeis et al., 2014; Sanders et al., 2015). Indeed, sequencing of the whole genome of 85 families of ASD quartets (parents and two affected siblings) showed that while 42% of individuals with ASD had ASD-relevant mutations, only 31% of sibling pairs carried the same variants, highlighting the genetic heterogeneity occurring within families (Yuen et al., 2015).

This suggests that although the combination of specific interactions between different genes appears necessary to cause ASD, environmental factors, post-translational modifications (PTMs), and epigenetics should contribute to the manifestation of ASD-related specificities (Muhle et al., 2004). However, among the few studies that assessed epigenetic features in individuals with ASD, it appears that even if differential methylated variants at specific CpGs are identified, they have a very small-magnitude effect [< 10% absolute difference; reviewed in: (Siu and Weksberg, 2017; Waye and Cheng, 2018; Wiśniowiecka-Kowalnik and Nowakowska, 2019)].

In this context, it is important to note that environmental factors such as maternal psychological stress and prenatal infections (rubella, influenza, cytomegalovirus, etc.) influence epigenetic mechanisms, such as DNA and/or histones methylation, histones acetylation, and microRNA expression (Alegria-Torres et al., 2011; Barua and Junaid, 2015), which can then affect fetal endocrine programming and brain development (Babenko et al., 2015; Vaiserman, 2015). Hence, environmental factors act in a synergistic manner with genetic factors to influence inter-individual DNA methylation differences. Furthermore, these individual differences in methylation not only vary between cell types (Nardone et al., 2017) but are also not stable over time (Wong et al., 2010; Vogel Ciernia and LaSalle, 2016). It is worth to consider that chromatin regulatory genes are among high-risk variants associated with ASD (Walker et al., 2019). Changes in the chromatin environment can also alter RNA splicing mechanisms and this could be an indirect way in which mutations in chromatin regulatory genes could affect RNA epitranscriptomic mechanisms. This however, is unlikely to affect entire networks (Voineagu et al., 2011), so as to then lead to focal disorganization and altered minicolumn distribution typical to ASD cortex (Donovan and Basson, 2017).

Therefore, besides the possibility for differential epigenetic markings directly affecting the relative expression levels of individual genes or groups of genes, RNA epitranscriptomic mechanisms also could, in association with both genotypes and environmental conditions, alter spatiotemporal proteins expression patterns at both quantitative and qualitative levels, in a tissue-specific and context-dependent manner. Indeed, differential mRNAs alternative splicing, cytoplasmic-shortening or -elongation of mRNAs poly(A)-tails and adenosine-to-inosine (A- to -I) RNA editing, which are known to function cooperatively, alter gene expression and function in multiple ways. Among these, the amino acid (AA) sequence of proteins and their expression can be altered due to codon change during mRNA translation, pre-mRNA splicing, alteration of RNA stability by modification of nuclease recognition sites, or through changes in miRNA production and targeting, as well as alteration of RNA-protein interactions (Christofi and Zaravinos, 2019; Licht et al., 2019). About 3,817 differentially edited sites, addressing 943 target transcripts, have been identified in specific association with autism as compared to schizophrenia and genetic amyotrophic lateral sclerosis (Karagianni et al., 2022). Furthermore, 30–40% of brain-specific microexon splicing processes are found disrupted in over a third of ASD affected individuals (Irimia et al., 2014). The differentially edited transcripts are involved in molecular processes that include synaptic transmission, hypoxic conditions, endosome/lysosome function, cytoskeleton rearrangements, apoptosis, protein, and RNA processing.

3.2. The RNA epitranscriptomic mechanisms

3.2.1. mRNA alternative splicing

The majority of mammalian multi-exon genes, through changes in splice site selection, generate multiple mRNA isoforms

1 https://gene.sfari.org/database/gene-scoring/

that give rise to proteins of different function and structure, or alter mRNA stability, translation, and localization. Exons and introns can be selected from the precursor mRNA and the translation product can give rise to isoforms with conflicting functions, or differential temporal and/or spatial expression patterns, resulting in considerable plasticity, and adaptability (Wang et al., 2015).

Nearly 95% of human gene transcripts are subject to alternative splicing (AS) (Pan Q. et al., 2008; Wang et al., 2008; Johnson et al., 2009). Splicing regulation is extensively used in the mammalian nervous system to generate specific protein isoforms that influence every aspect of neurodevelopment and function (Zheng and Black, 2013; Raj and Blencowe, 2015) with splicing defects being strongly associated with neurological and neurodegenerative diseases. Recent genome-wide studies of AS in mice have emphasized its occurrence throughout development within several regions of the nervous system (Dillman et al., 2013; Yan et al., 2015). In particular, AS is involved in cell fate decisions during cortical neurogenesis (Linares et al., 2015; Zhang et al., 2016), synaptogenesis and synaptic plasticity [reviewed in Raj and Blencowe (2015) and Vuong et al. (2016)]. AS events are considerably regulated by *cis*-regulatory RNA sequences and *trans*-acting splicing factors (Wang and Burge, 2008; Kornblihtt et al., 2013). Numerous AS topologies have been documented, comprising interchange among alternative 5′ or 3′ splice sites, alternative 5′ or 3′ terminal exons (A5E and A3E), cassette exons, mutually exclusive exons, intron retention (IR), and a range of arrangements among these options (Wang and Burge, 2008). For most groups of splicing events, several splicing sites will be present concomitantly on the nascent pre-mRNA. In addition, a large proportion of AS events take place in the 5′ and 3′ untranslated regions (UTR) of the mRNA bordering the open reading frame (ORF). Even if this has no effect on the polypeptide sequence, it can modulate other features of the mRNA performance. Furthermore, many AS-mediated alterations in the ORF sequence have been shown to affect mRNA stability, subcellular localization and translational activity (**Figure 1**; Braunschweig et al., 2013;

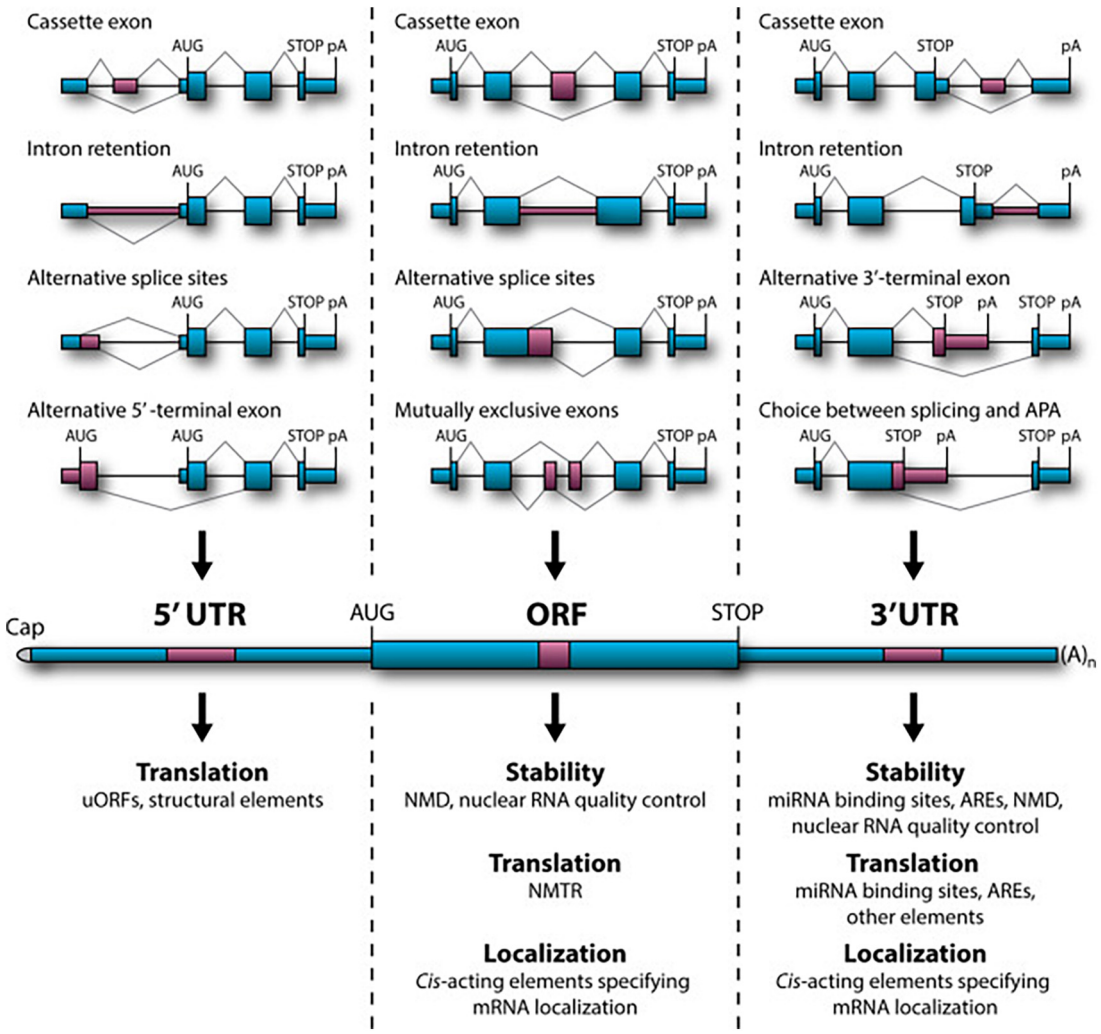

FIGURE 1
Role of alternative splicing (AS) in mRNA stability, translational activity and subcellular localization. **(Top)** Examples of relevant AS topologies; mid: mature mRNA containing 5′ and 3′UTRs flanking the protein-coding ORF; **(bottom)** downstream regulation outcomes of AS events in the corresponding regions. APA, alternative cleavage and polyadenylation; ARE, AU-rich element; NMD, nonsense-mediated decay; NMTR, nonsense-mediated translational repression; uORF, upstream open reading frame (ORF). Figure obtained from Mockenhaupt and Makeyev (2015) under a creative commons license 3 and 4.

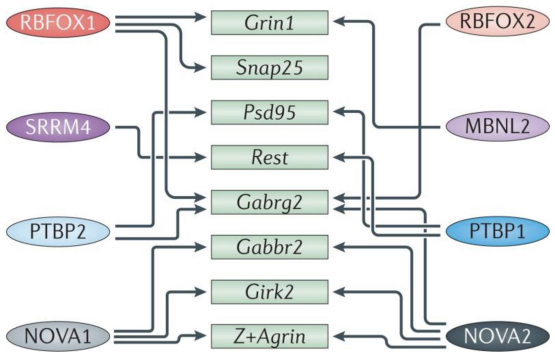

FIGURE 2
Diagram representing some of the splicing mechanisms in the brain. Numerous transcripts important in brain and neurological development (green boxes) are cross-regulated (indicated by arrows) by multiple RNA-binding proteins (RBPs; colored ovals on the **left** and **right**). Girk2, inwardly rectifying potassium channel Kir3.2; Gabrg2, GABAA receptor subunit gamma 2; Gabbr2, GABAB receptor 2; MBNL, muscleblind-like; NOVA, neuro-oncological ventral antigen; Psd95, postsynaptic density protein 95; PTBP, polypyrimidine tract binding protein; Rest, repressor element 1-silencing transcription factor; RBFOX, RNA-binding protein fox 1 homolog; Snap25, synaptosome-associated protein 25; SRRM4, serine/arginine repetitive matrix protein 4. Figure from Vuong et al. (2016) obtained by Springer Nature under license No 5430810425823.

Hamid and Makeyev, 2014; Sibley, 2014). AS should therefore not be seen as a binary "splice or not" event, determined by the intrinsic properties of the splice site in question. Rather, it is a context-specific competition in which the splicing machinery must discriminate and choose between multiple splice sites.

Specialized pre-mRNA binding proteins control alternative splicing patterns by altering spliceosome assembly at specific splice locations [for review, see (Fu and Ares, 2014; Matera and Wang, 2014; Lee and Rio, 2015)]. These proteins differ in structure and depending on their binding position, interactions with cofactors and signaling pathway modification, can have a variety of impacts on a target transcript. While certain splicing regulators are found throughout the brain, others are only found in certain tissues. The hindbrain and ventral spinal cord express NOVA1, while the forebrain and dorsal spinal cord express NOVA2, with considerable overlap in the midbrain and hindbrain (Yang et al., 1998). In addition, different neuronal cell types exhibit unique maturation susceptibility through the expression of different combinations of regulators [reviewed in Li et al. (2007)] which also affect different, often overlapping, alternative splicing programs, as each transcript is typically targeted by several regulators (**Figure 2**).

As cells move along the neural lineage, their alternative splicing patterns vary substantially. They are induced by modification in the expression of certain RNA-binding proteins, such as the polypyrimidine tract binding proteins 1 and 2 (PTBP1, 2) and serine/arginine repetitive matrix protein 4 (SRRM4; known as nSR100). PTBP1 depletion from cultured fibroblasts is found to induce their *trans*-differentiation into neurons (Xue et al., 2013), whereas PTB1 loss in mice mutants causes precocious neurogenesis and depletion of neural stem cells, diminishing the population of ependymal cells that ascend from radial glia. Mice depleted for PTBP2 resulted in altered stem cell positioning and proliferation (Poduri et al., 2013). Furthermore, loss of splicing regulators like NOVA2 and RNA-binding protein fox-1 homolog 2 (RBFOX2), which regulate alternative splicing of components of the Reelin signaling system, cause abnormalities in cortical, and cerebellar lamination (Yano et al., 2010). For instance, mis-splicing of the Reelin component disabled 1 (Dab1) causes multiple types of layer II/III and IV neurons to migrate improperly (Poduri et al., 2013).

Many aspects of synaptic function are also influenced by alternative splicing factors, including synapse specificity *via* the KH domain-containing, RNA-binding, signal transduction-associated (KHDRBS) family, regulation of inhibitory synapses *via* NOVA2, and splicing of synaptic components and ion channels and *via* Muscleblind-like 2 (MBNL2), the sodium channel modifier 1 (SCNM1), and the neuronal ELAV-like (nELAVL) proteins (SCNM1) RBFOX1 and RBFOX2 (Vuong et al., 2016; **Figure 3**).

One of the alternative splicing targets of KHDRBS, are the neurexins (Nrxn), encoding presynaptic cell surface proteins that form a heterophilic adhesion complex with neuroligins at neuronal synapses. They promote synaptogenesis through *trans*-synaptic signaling by organizing pre- and postsynaptic compartments in a bidirectional manner. The synapse-specific functions of neurexins variants are conferred through extensive alternative splicing and controlled by various genes and promoters (Craig and Kang, 2007). To give an order of magnitude, pre-mRNAs from the three Nrxn genes produce more than 2,000 protein isoforms by alternative splicing (Baudouin and Scheiffele, 2010). Mutations in neuroligin and neurexin genes are associated with neurodevelopmental disorders, including ASD (Wang et al., 2018).

The role of neurexins in the regulation of synaptogenesis is reminiscent of an adhesive program that depends on the affinity of the generated variants for post-synaptic, cell type-specific ligands. To illustrate, alternative splicing at exon 20 generates the NRX4 + protein variants with a 30 AA insertion (Ex4 +), whereas omission of exon 20 results in the NRX4- variant (ΔEx4). Here, the inclusion of exon 20 is negatively regulated by KHDRBS (Craig and Kang, 2007). The NRX Ex4 + and ΔEx4 variants show differential interactions with neuroligins, leucine-rich repeat proteins (LRRTMs), and the Cbln1-GluD2 complex that are critical mediators of synaptogenesis (Uemura et al., 2010). ΔEx4 isoforms are found to preferentially bind neuroligin 1B that is abundantly found at glutamatergic synapses, whereas Ex4 + isoforms favorably bind neuroligin-2 (NLGN2A) at GABAergic and glycinergic synapses (Chih et al., 2006).

Additionally, alternative splicing is both spatially and temporally controlled. In mice, neuronal activity induces changes in Nrxn1 splice isoform selection through calcium/calmodulin-dependent kinase IV (CAMKIV) signaling. The KH-domain RNA-binding protein SAM68 associates with RNA response elements in the Nrxn1 pre-RNA and regulates the incorporation of exon 20, and this also varies between brain regions. In the developing cortex, Nrxn ΔEx4 mRNAs decrease in accordance with the developmental evolution (post-natal days 0–21) of granule cell's resting potential (−25 to −55 mV) (Rossi et al., 1998). In parallel, depolarization results in an activity-dependent change between Ex4 (+) and ΔEx4 mRNAs, increasing the expression of the latter by t10-fold, while decreasing Ex4 (+) variants and total

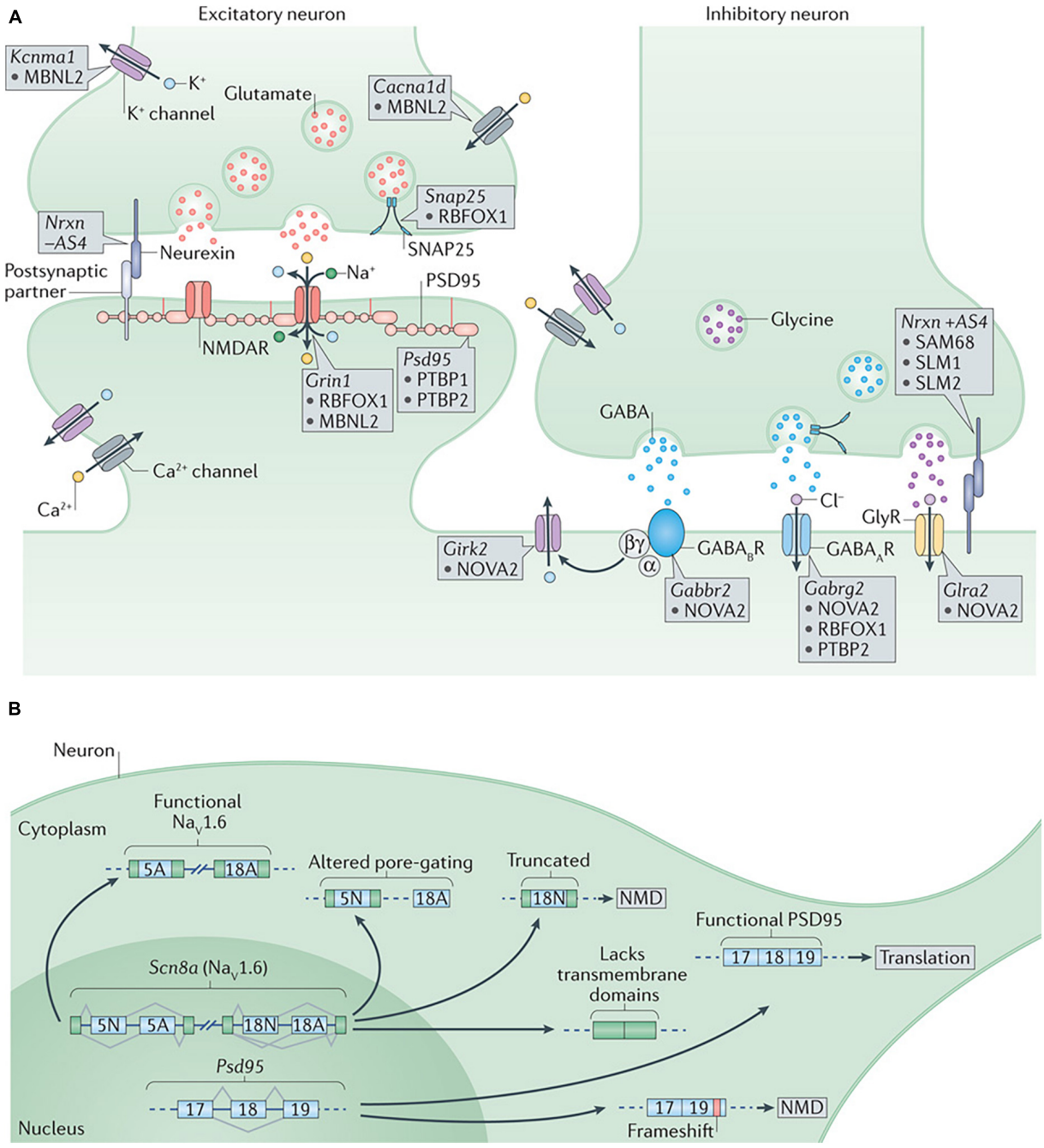

FIGURE 3

(A) Alternative splicing regulation of synaptogenesis and synaptic function. At the presynaptic terminal, alternative splicing of synaptosomal-associated protein 25 (Snap25) by RNA-binding protein fox 1 homolog 1 (RBFOX1/A2BP1) and of the calcium-activated potassium channel subunit alpha 1 (Kcnma1) by muscleblind-like 2 (MBNL2) are important to control neurotransmitter release. Differential splicing of the presynaptic neurexins (Nrxns) at AS4 by KHDRBS proteins (SAM68, SLM1, and SLM2) controls targeting to postsynaptic partners. At excitatory synapses, alternative splicing of the transcript encoding the NMDA receptor subunit GluN1, Grin1, is regulated by RBFOX1 (A2BP1) and MBNL2, whereas the polypyrimidine tract binding proteins (PTBPs) control productive splicing of the scaffold protein, postsynaptic density protein 95 (Psd95). Splicing of the transcripts encoding L-type voltage-gated calcium channels, such as the pore-forming subunit Cav1.3 (encoded by Cacna1d), by MBNL2 may allow the voltage sensitivity, conductance, or other properties to be tuned as synapses differentiate. At inhibitory synapses, neuro-oncological ventral antigen 2 (NOVA2) mediates alternative splicing of the transcripts encoding many postsynaptic components such as the metabotropic GABAB receptor (Gabbr2), the inwardly rectifying potassium channel Kir3.2 (Girk2) and the glycine receptor alpha 2 (Glra2). Splicing of the GABAA receptor subunit transcript (Gabrg2) is controlled by multiple splicing regulators including NOVA2, RBFOX1 (A2BP1) and PTBP2.
(B) Alternative splicing regulation of synaptogenesis and synaptic function. Alternative splicing controls the expression and function of many synaptic components. Expression of PSD95 is repressed by PTBP-controlled exclusion of exon 18 until late in neuronal maturation when it is required for synaptogenesis. The gene encoding the voltage-gated sodium channel Nav1.6, Scn8a, has multiple alternative exons (such as 5N, 5A, 18N, and 18A as shown in the figure) that can change its gating properties, determine its localization or alter its overall function. GABAAR, GABAA receptor; GABABR, GABAB receptor; GlyR, glycine receptor; NMD, nonsense-mediated decay; NMDAR, NMDA receptor; SAM68, SRC-associated in mitosis 68 kDa protein. Figure from Vuong et al. (2016) obtained by Springer Nature under license No 5430810425823.

Nrxn1 transcripts. This is suggestive of a depolarization-induced change (and thus cell type specific) in the turnover of pre-existing Nrx1 mRNA (Iijima et al., 2011). Dysfunction of SAM68 binding results in motor coordination deficits in mice (Iijima et al., 2011).

Another consequence of altered early developmental programs specific to ASD is the deregulation of layer formation and layer-specific neuronal migration in prenatal cerebral cortex development (Beopoulos et al., 2022). Moreover, the gene expression profiles that, in neurotypical development (ND), distinguish the frontal from the temporal cortex are significantly attenuated (Johnson et al., 2009), implying that transcriptional and splicing dysregulation are among the underlying mechanisms of neuronal dysfunction in this disorder. Furthermore, in ASD brains, lower cognitive functioning is associated with higher densities of apical pyramidal cell dendrites along layer II and within the cortical lobe of layer IV (Hutsler and Zhang, 2010). Concomitantly, ASD brains display considerably dysregulated splicing of the ataxin-2 binding protein 1 A2BP1 (RBFOX1)-dependent alternative exons (Voineagu et al., 2011; **Figure 4**).

Concurrently, while nuclear A2BP1 regulates the alternative splicing of a variety of neuronal transcripts, it is itself alternatively spliced to produce cytoplasmic isoforms that regulate mRNA stability and translation. Cytoplasmic Rbfox1 binds to 3′-UTR of mRNA targets, increasing their abundance and in particular those associated with cortical development and autism (Lee et al., 2016). CLIP-seq from ASD-like mice brains show enrichment in Rbfox1 targets involved in the regulation of brain development and in particular in the control of synaptic activity and calcium signaling (Weyn-Vanhentenryck et al., 2014). In parallel, Rbfox1 nuclear downregulation is found to alter neuronal positioning during corticogenesis (embryonic day 14.5) in mice. The defects were found to occur during radial migration and terminal translocation (Hamada et al., 2016). Furthermore, A2BP1, along with MBNL2 which also mediates pre-mRNA alternative splicing regulation, controls the splicing of GRIN1 (NMDA-type ionotropic glutamate receptor subunit 1 -NMDAR1) (Vuong et al., 2016). GRIN1 exon five skipping prolongs the time course of excitatory NMDAR postsynaptic currents (EPSCs) at thalamic relay synapses and increases spine density along apical dendrites of pyramidal neurons in layer V (Liu et al., 2019).

However, A2BP1 (RBFOX1) is not the only alternative splicing factor dysregulated in human ASD brains. SRRM4 (nSR100) is only expressed in the CNS (Calarco et al., 2009), and is found downregulated in autism (Irimia et al., 2014). SRRM4 alters neuronal destiny and differentiation (Makeyev et al., 2007; Raj et al., 2011) by promoting alternative splicing and inclusion of neural-specific exons in target mRNAs (Calarco et al., 2009). Depletion of SRRM4 in mice results in abnormal cortical lamination by halting neurogenesis of upper-layer neurons and causing accumulation of progenitor cells in lower-layer neurons (Poduri et al., 2013). The most characteristic class of nSR100-regulated exons are microexons, which are largely conserved, frame-preserving, neurally enriched cassette exons ranging from 3 to 27 bp in length (Irimia et al., 2014). Microexons are significantly enriched in genes with crucial involvement in synaptic biology and genetic links to ASD, and they typically encode residues of surface of proteins, affecting protein-protein interactions (Irimia et al., 2014; Li et al., 2015). Microexon processing-related splicing defects are associated with ASD. Comparisons between large cohorts of autism and control brain samples showed disrupted splicing of 30–40% brain-specific microexons in over a third of individuals with ASD (Irimia et al., 2014).

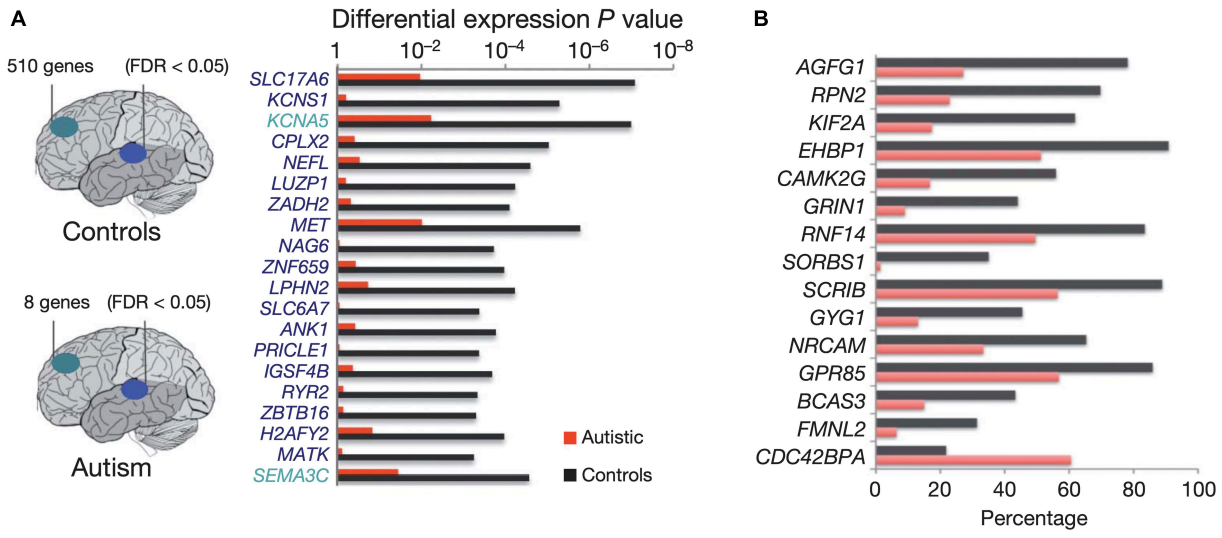

FIGURE 4
Diagram depicting the number of genes showing significant expression differences between frontal and temporal cortex in control samples (top) and autism samples (bottom). **(A)** Top 20 genes differentially expressed between frontal and temporal cortex in control samples. All of the genes shown are also differentially expressed between frontal and temporal cortex in fetal mid-gestation brain, but show no significant expression differences between frontal and temporal cortex in autism. The horizontal bars depict *p* values for differential expression between frontal and temporal cortex in the autism and control groups. **(B)** Top A2BP1 (RBFOX1) -specific differential splicing (DS) events. DS events showing the most significant differences in alternative splicing between low-A2BP1 autism cases and controls as well as DS differences consistent with the A2BP1 binding site position. The horizontal axis depicts the percentage of transcripts including the alternative exon. Red-autism samples, black-control samples Figure modified from Voineagu et al. (2011) obtained by Springer Nature under license No 5430811097703 and 5431300363740.

3.2.2. mRNA-specific poly(A)-tail modulation

Following gene transcription in eukaryotic cells, the newly formed mRNA matures by processing of both ends. Nuclear polyadenylation of the 3′ end by poly-A polymerase adds a poly(A) tail to the mRNA molecule, contributing to the translational regulation of the transcript by increasing its stability and allowing its export from the nucleus [reviewed in Di Giammartino et al. (2011)]. With the exception of replication-dependent histone mRNAs, that instead of a poly(A) tail end in a histone downstream element (a stem-loop structure followed by a purine-rich sequence), all other mRNAs acquire around 250–300 adenosine residues (Siianova et al., 1990; Marzluff et al., 2002). However, the exact 3′ polyadenylation position is tightly regulated and defines the regulatory susceptibility of the mature transcript. In addition, the exact length of the poly(A) tail is also closely regulated in both nucleus and the cytoplasm and defines the transport, translation and recycling rate of the mature transcripts [reviewed in Zhang et al. (2010), Eckmann et al. (2011), and Weill et al. (2012)]. When the mRNA reaches the cytoplasm, the poly(A) tail, along with the 5′ cap, stabilize the closed loop that is formed by the attachment of the cap structure to the translation initiation factor 4F (eIF4F) complex, and thus contribute to the initiation of the translation process (Kahvejian et al., 2005). The structure and integrity of the newly circularized mRNA becomes the target of non-mRNA-specific translation regulatory elements (Dever, 2002; Beilharz et al., 2010), while transcript-specific translational control is made possible by *cis*-acting regulatory sequences (Abaza and Gebauer, 2008). These regulatory elements typically reside in the 3′UTR, although they can be also present in the 5′ UTR or the coding sequence, and assemble mRNA specific ribonucleoprotein complexes (mRNPs), deadenylation mRNPs and cytoplasmic polyadenylation complexes that dynamically modulate the length of the poly(A) tail (Piqué et al., 2008; Chekulaeva et al., 2011), which, in turn, defines the extent of mRNA translation (Beilharz and Preiss, 2007). Silent mRNPs localize and accumulate in specific cell regions to be reactivated by cytoplasmic poly(A) elongation when and where the encoded proteins are needed. The acquisition of the poly(A) tail and the subsequent modification of its length, can be thus seen as a dynamic process that regulates gene expression in time and space. In general, ASD cortices, as shown by post mortem studies, present a global poly(A)-tail shortening pattern that remarkably impacts several high confidence ASD-risk genes (Parras et al., 2018).

To give an illustrative example, alternative polyadenylation of the serotonin transporter SLC6A4/SERT1 leads to symptoms of anxiety and depression with impaired retention of fear extinction memory, mimicking the phenotype of SERT1 KO mice (Battersby et al., 1999; Gyawali et al., 2010). The mouse SLC6A4 gene yields two AS products with 123 bp differences that lead to a polyadenylation polymorphism. The human gene contains a single T/G nucleotide polymorphism (rs3813034) in the more distal of the two polyadenylation signals, influencing the forms of polyadenylation that occur in the brain (Battersby et al., 1999; Gyawali et al., 2010). In both mice and humans, impaired retention of fear extinction memory is selectively impaired in homozygous carriers of the G allele (Wellman et al., 2007; Narayanan et al., 2011), which is associated with a lower distal polyadenylated fraction, as the T allele results in greater utilization of the polyadenylation site. Functionally, the distal polyadenylation sequence element is positively correlated with the equilibrium level of SERT1 mRNA (Gyawali et al., 2010) and is located next to a microRNA (miR-16) binding site (Baudry et al., 2010), implying that binding of regulatory proteins to the distal sequence element could regulate miR-16 binding (Shanmugam et al., 2008) and modify SIRT1 translation (Baudry et al., 2010; Hartley et al., 2012). This establishes a clear link between SERT1-mediated activity and the use of polyadenylation in the amygdala-prefrontal cortex network. The distal polyadenylated fraction of SERT1 in brain tissue of men is significantly higher than that of women, independent of rs3813034 genotype. Panic disorder is a female-predominant condition, with an approximately twofold higher prevalence in women than in men. Therefore, the G allele of SERT1 rs3813034 appears to be the risk allele in women (Gyawali et al., 2010). Developmental hyperserotonin (DHS) is the most consistent neurochemical finding reported in autism and has been implicated in the pathophysiology of ASD (Hough and Segal, 2016).

Furthermore, with respect to ASD susceptibility, cytoplasmic polyadenylation element-binding proteins 1-4 (CPEB1-4) bind to mRNAs containing CPE sequences, and activate or repress translation by inducing cytoplasmic elongation or shortening of their poly(A) tails (Ivshina et al., 2014). In the developing brain, and in response to environmental embryonic cues, CPEBs regulate mRNA transcription of cell communication mediators, such as hormones, that are involved in memory formation and learning, through modulation of synaptic plasticity (Si et al., 2003; Sarkissian et al., 2004; Ivshina et al., 2014; Fioriti et al., 2015). Synaptic plasticity is further achieved by activity-dependent local translation of dendritic mRNAs. In early mice development, CPEB resides at synaptic sites of hippocampal neurons. Polyadenylation at synapses is mediated by the N-methyl-D-aspartate receptor (NMDAR)-related activation of Aurora, one of the kinases that phosphorylates CPEB (Huang et al., 2002; **Figure 5**). In the mammalian adult brain, CPEB is localized in postsynaptic densities of the dendritic layers of the hippocampus (Wu et al., 1998). While CPEB KO mice exhibit deficits in synaptic plasticity and memory formation, FMR1/CPEB1 double-knockout (KO) rescues the fragile X-like phenotype of FMR1-KO mice (Zukin et al., 2009). The fragile X syndrome (FXS) is the most common-known genetic cause of autism and is characterized by the loss of fragile X mental retardation 1 protein (FMRP).

Memory consolidation uses a similar mechanism (**Figure 6**): αCaMKII, which is also found at the dendrites of hippocampal neurons, contains CPEs in its 3′ UTR, and in the rat brain is polyadenylated by CPEB1 when stimulated by light (Wu et al., 1998). In addition, αCaMKII phosphorylates and activates CPEB1 (Atkins et al., 2005; Weill et al., 2012), creating a positive feedback loop that stabilizes synaptic inputs (Aslam et al., 2009). Mice expressing CamKII lacking the 3′UTR, have reduced protein levels, severely affecting late-phase long-term potentiation, spatial and long-term memory (Miller et al., 2002).

Comparison of transcript levels from the cortices of 43 post-mortem idiopathic ASDs and 63 NT controls showed no change in CPEB1 and 2 levels, whereas CPEB3 and CPEB4 were found slightly decreased and increased, respectively. However, at the protein level, CPEB4 was significantly decreased, obeying the ASD-specific trend of poly(A) tail shortening, and showed an isoform

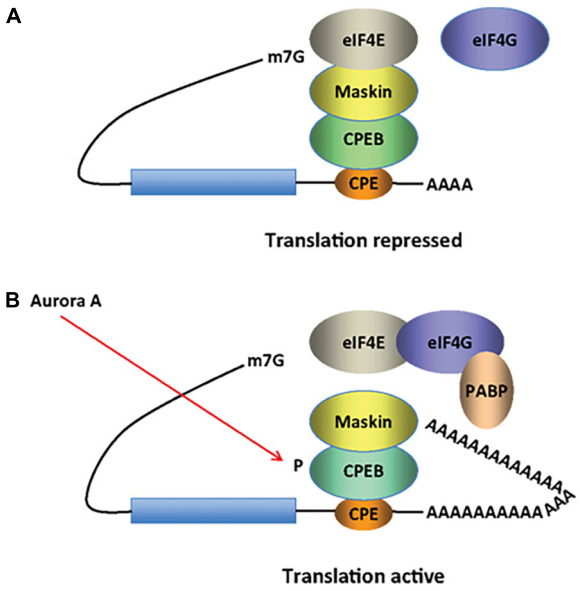

FIGURE 5
CPEB activity in inducing cytoplasmic shortening or elongation of poly(A)-tails. Some mRNAs contain a cytoplasmic polyadenylation element (CPE), which is bound by CPEB. **(A)** CPEB also interacts with Maskin (or Neuroguidin, a functionally related protein), which in turn interacts with the cap (m7G) binding protein eIF4E. Such mRNAs are translationally inactive because Maskin inhibits the association of eIF4E and eIF4G, another initiation factor that helps recruit the 40S ribosomal subunit to the 5′ end of the mRNA. **(B)** Cues such as NMDA receptor activation stimulate the kinase Aurora A, which phosphorylates CPEB, an event that causes poly(A) tail elongation. poly(A) binding protein (PABP) binds the newly elongated poly(A) tail and recruits eIF4G. The PABP-eIF4G dimer helps to displace Maskin from eIF4E, allowing eIF4G to bind eIF4E and initiate translation [figure modified from Zukin et al. (2009), obtained under a creative commons license 3 and 4].

imbalance due to a reduced inclusion of the neuron-specific micro-exon 4 (ΔEx4 > Ex4 +) (Theis et al., 2003; Parras et al., 2018). This micro-exon encodes the eight amino acid "'B region" that inserts motifs for PTMs, such as phosphorylation by S6K, AKT, PKA, or PKC (Theis et al., 2003). Of note, most transcripts of high-risk ASD genes are linked by CPEB4 and over 40 of them, including Dyrk1a, FOXP1, and WAC SFARI database (see text footnote 1), show reduced poly(A) tails as well as reduced protein levels. When mice are exposed to an equivalent imbalance of CPEB isoforms, their levels of CPEB transcript-dependent proteins are reduced and they exhibit ASD-like behavioral, neuroanatomical, and electrophysiological phenotypes (Parras et al., 2018). Another epitranscriptomic mechanism, with major implications for brain function across lifespan, including early brain development, is adenosine-to-inosine RNA editing, the effects of which may contribute to the development of the neuroanatomical and behavioral characteristics of ASD.

3.2.3. Adenosine-to-inosine RNA editing

Eukaryotes use RNA editing, where an RNA molecule is chemically modified at the nucleotide base, as a posttranscriptional mechanism that greatly increases transcript diversity from a limited size genome. In the CNS, the predominant form of RNA editing is the deamination of adenosine (A) to form inosine (I), that is then recognized as guanosine (G) during translation. A-to-I editing is biologically significant in both translated and UTR of RNA, with consequences ranging from trivial to critical, affecting molecular stability, gene expression and function. When editing occurs in the coding sequence, it is referred to as a "recoding event" which can also alter splice sites and base pairing, thus affecting the secondary structure of the RNA. It further changes the binding specificities with other molecules such as mi/siRNAs and proteins. The results of most editing events are still unknown (Yang et al., 2021), with recent research suggesting that the majority of pre-mRNAs are edited (Franzen et al., 2018).

The reaction is carried out by the "Adenosine Deaminases that Act on RNA" enzyme family (ADAR 1, 2, and 3 enzymes in vertebrates) (Bass, 2002; Slotkin and Nishikura, 2013). ADAR1 and ADAR2 are expressed throughout the body, although they are more prevalent in the CNS (Palladino et al., 2000; Nishikura, 2010), whereas ADAR3 localizes exclusively in the brain and is considered catalytically inactive. According to current knowledge, ADAR1 is associated with hyper-editing, being the major editor of repetitive sites, ADAR2 with site-selective editing, being the major editor of non-repetitive coding sites, while ADAR3 may act as an inhibitor of editing by competing with ADAR1 and 2 for RNA binding (Tan et al., 2017). ADAR1 is ubiquitously expressed from two different promoters, one being constitutively active, giving rise to the nuclear p110 isoform (cADAR1), and the other being interferon induced (p150), resulting in a version of the ADAR1 enzyme (iADAR1) that is partially localized to the cytoplasm (Veno et al., 2012; **Figure 7**).

The extent of RNA editing by ADAR proteins is vast, with millions of sites already identified in the human genome (Tariq and Jantsch, 2012; Bazak et al., 2014; Picardi et al., 2017). It has major implications for nervous system function throughout life (Savva et al., 2012), and a review of A-to-I editing rates in the brains of six different age groups (fetus, infant, child, adolescent, middle-aged, and elderly) revealed 748 sites with significant differences in editing rates between all groups, with 742 of these sites showing an increasing pattern of editing during development from fetal to adult samples. This increase in the A-to-I editing pattern is associated with cortical layer growth and neuronal maturation (Hwang et al., 2016).

Proteins derived from edited pre-mRNAs vary considerably in function and most often affect receptors and ion channels widely expressed in the brain. In addition, proteins involved in cytoskeletal remodeling, thereby contributing to neuronal growth and plasticity, are strongly affected by RNA editing. In general, editing of protein-coding RNAs leads to the generation of protein isoforms and diversification of protein functions (Tariq and Jantsch, 2012; **Figure 8**).

A global bias for A-to-I hypo-editing in ASD brains, with the number of downregulated RNA editing sites across brain regions in ASD far exceeding those that were upregulated, involving many synaptic genes, has recently been reported. The fragile-X protein, FMRP, interacts with ADAR1 and ADAR2 in an RNA-independent manner, whereas FXR1P interacts only with ADAR1. FXR1 and FMR1 showed a negative (inhibitory) and positive (enhancing) correlation with termination changes, respectively. Furthermore, there is a converging pattern of RNA editing alterations in ASD and fragile X syndrome, providing a molecular bridge between these related disorders (Tran et al., 2019).

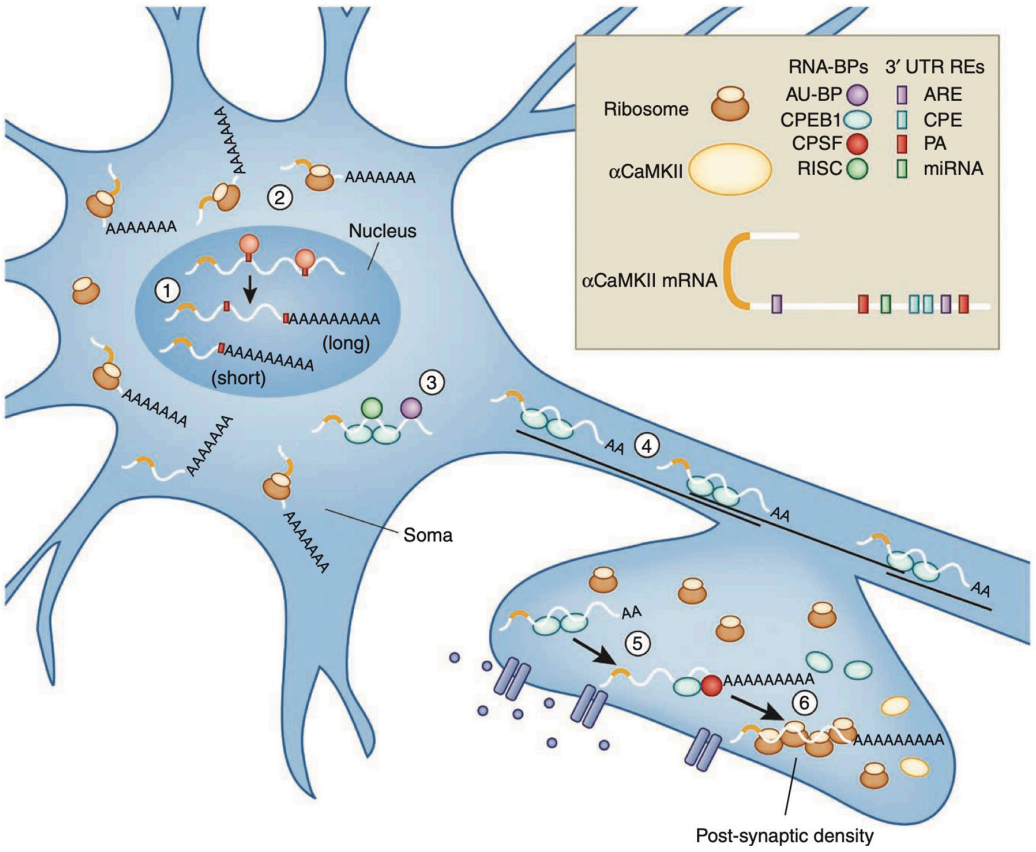

FIGURE 6
Recycling of αCaMKII mRNA in neurons. Alternative polyadenylation (APA) of αCaMKII mRNA generates two transcripts with 3′ UTRs of different lengths (1). Both transcripts are polyadenylated in the nucleus, but the composition of the *cis*-elements in their 3′ UTR modifies their cytoplasmic fates. The short isoform is translated mainly in the soma (2), whereas miRNA binding sites, AU-rich elements (AREs) and cytoplasmic polyadenylation elements (CPEs) mediate deadenylation, repression (3) and transport (4) of the long transcript to dendrites. Upon neuronal stimulation in the post-synaptic densities (PSD), CPEB1 promotes αCaMKII mRNA polyadenylation (5), and αCAMKII local translation (6). Figure from Weill et al. (2012), obtained by Springer Nature under license No 5430811375131.

3.2.3.1. Brain proteins significantly affected by adenosine-to-inosine mRNA editing

3.2.3.1.1. Glutamate-gated ion channels

Five subunits of the ionotropic glutamate ion channel (AMKA) GRIA (GluA2, GluA3, GluA4, GluK1, and GluK2) undergo RNA editing in their coding regions by ADAR (Bass, 2002). Four editing sites where an AA substitution occurs have been identified, specifically arginine to glycine (R/G), glutamine to arginine (Q/R), tyrosine to cysteine (Y/C), and isoleucine to valine (I/V). In GluA2 (GRIA2), the Q/R substitution (CAG to CIG) plays a critical role in the function of the ion channel, as it is located in the pore loop domain, rendering the channel impermeable to Ca^{2+}. GluA2 subunits are edited in almost 100% of all transcripts at the Q/R site (Daniel et al., 2017). The consequences of (sub) editing are critical, as ADAR2 KO homozygous mice die within weeks of birth due to repetitive seizures caused by excessive Ca^{2+} influx. However, the mice can be rescued by introducing the $GRIA2^{R}$ mutation that carries the Q/R substitution (Higuchi et al., 2000; Greger et al., 2006).

In GluA2 and 3, the c-terminal domain binds to the PDZ domains 4–6 of the neuronal scaffolding proteins GRIP1 and 2 (glutamate receptor interacting proteins 1 and 2; 7 PDZ domains in total). Loss of Grip expression in mice results in delayed recycling of GluA2 and increases sociability. Adversely, gain-of-function mutations in Grip proteins (GRIP1 to PDZ4-6), observed in ASD patients contribute to reduced social interactions (Han et al., 2017).

Both GRIP1 and GRIP2 (glutamate receptor-interacting proteins) exist in different splice isoforms, with GRIP1b/2b isoforms including an alternative 18 amino acid domain, excluded form GRIP1a/2a, at their extreme N-terminus, that determines the palmitoylation fate of the protein. For instance, GRIP1a (non-palmitoylated) and GRIP1b (palmitoylated) splice variants inhibit and increase NMDA-induced AMPAR internalization in cultured hippocampal neurons respectively (Hanley and Henley, 2010). Hence, up- regulated GRIP1/2 alternative splicing, due to decreased mRNA A-to-I editing, increases GRIP1a/2a isoforms availability, and could promote decreased sociability and social interactions.

However, AMPA receptors are associated with a large network of proteins (at least 14 members), many of which have multiple alternatively spliced isoforms, that play important roles in receptor membrane trafficking, by guiding the receptor from the cell body to the synapse and by possibly regulating the downstream signal transduction pathway (Song and Huganir, 2002; Santos et al., 2009). In addition, AMPAR subunits are subject to numerous PTMs that

give rise to various combinatorial effects. For example, GluA1 undergoes 11 PTMs that can occur independently and reversibly (seven phosphorylations, two palmitoylations, one ubiquitination, and one S-nitrosylation), resulting in 2^{11} potential GluA1 variants, each of which is expected to exhibit slightly altered properties. This number will be further increased by considering the heteromeric nature of AMPARs (Diering and Huganir, 2018).

3.2.3.1.2. $GABA_A$ receptors

The ligand gated chloride channel receptors $GABA_A$ are comprised of five subunits: 2 α sub-units, 2 β subunits, and either a γ or a δ subunit (Hevers and Luddens, 1998). Additionally, there exist 6 α, 3 β, 3 γ, and 4 δ sub-units allowing for even greater generation and assembly diversification of stoichiometries. Furthermore, the α3 subunit can be edited at position 343, resulting in an isoleucine (I: AUA) to methionine (M: AUI) codon change (Ohlson et al., 2007; Tian et al., 2011). The I/M change results in delayed currents and faster inhibition upon GABA stimulation (Rula et al., 2008), apparently due to decreased subunit stability and overall receptor trafficking, probably by altering α and γ subunits, or ligand, interaction, thereby reducing its cell surface expression (Daniel et al., 2011; Tariq and Jantsch, 2012). Editing of the α3 subunit is developmentally regulated, with its pre-mRNA going from unedited at embryonic day 15 to over 80% edited at postnatal day 7 (Ohlson et al., 2007; Rula et al., 2008). The expression of the unedited α3 GABA receptor during development is crucial for synapse formation (Ben-Ari et al., 2007) and its overall expression decreases with age concomitantly with the increase of the expression of the α1 subunit (Hutcheon et al., 2004).

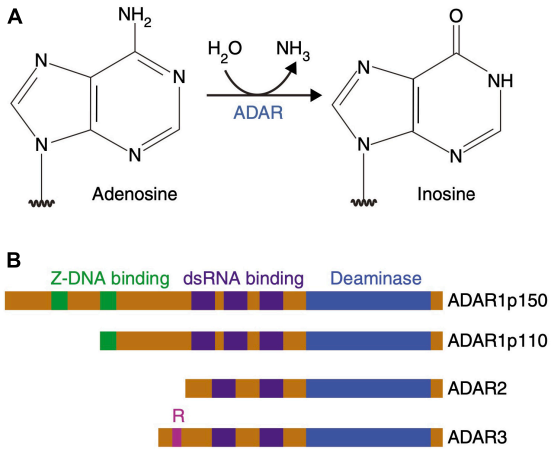

FIGURE 7
Adenosine deamination and the ADAR enzyme family. **(A)** ADAR enzymes catalyze the A-to-I hydrolytic deamination reaction, by which an adenosine loses an amine group and is converted to inosine. **(B)** There are four main proteins of the ADAR enzyme family: two isoforms of ADAR1 (p110 and p150), ADAR2 and ADAR3. All of these enzymes contain a conserved deaminase domain, shown in blue. The double-stranded (ds) RNA-binding domains, shown in purple, determine substrate specificity. The two ADAR1 isoforms differ in their Z-DNA-binding domains, shown in green. ADAR3 contains an arginine-rich domain, shown in pink, which binds single-stranded RNA. Figure from Slotkin and Nishikura (2013), obtained by Springer Nature under license No 5431360984026.

Molecular genetics and pharmacological data designate α1-containing $GABA_A$ receptors as "sedative" subtype(s) and α2 and/or α3-containing receptors as "anxiolytic" subtype(s) while agonists of the α5-containing receptors, such as diazepam, impair cognition (Atack, 2011a,b). systemic decrease in $GABA_AR$ signaling, reduced sociability and attention, while blocking cortical $GABA_AR$ impaired social behavior and attention. Since the effects of specific-receptor ligands are marginal, α5-containing $GABA_A$ receptors could be involved in attention deficits but do not appear to contribute to reduced sociability (Paine et al., 2020), thus potentially increasing the weight of α3 subtype hypo-editing on ASD-related social behavior.

3.2.3.1.3. Serotonin 2C receptor

Similarly, the serotonin 2C receptor (5-HT2CR) is subject to combinatorial editing at five sites [referred to as A, B, C' (E), C, and D sites] found within the G protein coupling domain (second intracellular loop), which plays a key role in mammalian cerebral cortex development and is targeted by the only FDA-approved drugs to treat autistic symptoms, risperidone and aripiprazole.

Cortical circuit development is a complex process that involves the differentiation, proliferation, and migration of epithelial, glial, and neural cell subtypes, followed by synapse formation and curation of redundant connections through synaptic pruning. While these processes are largely controlled by genetic programming, they are further regulated by a wide range of extrinsic signals (such as hormones, growth factors, guidance signals, cell adhesion molecules, etc.) as well as environmental influences. Serotonin (5-HT) is a key regulator of neural circuit development by modulating neuronal proliferation, migration and differentiation. Most of its effects are mediated by the 14 5-HT receptors, all of which are G protein-coupled, with the exception of the ionotropic 5-HT type 3A receptor (5-HT3A) which is responsible for rapid neuronal activation (Takumi et al., 2020; Beopoulos et al., 2022). Dysregulation of the 5-HT system is involved in the development of several neuropsychiatric disorders, including intellectual disability, autism, depression and anxiety (Kinast et al., 2013; Brummelte et al., 2017; Velasquez et al., 2017).

In mammals, during early cortical development and up to 16 weeks of gestation (GW16), 5-HT is of maternal and/or placental origin (Cote et al., 2007; Bonnin and Levitt, 2011; Beopoulos et al., 2022), whereas later, serotonergic afferents invade the cortex and the developing fetus initiates its own 5-HT production (Gaspar et al., 2003; Vitalis and Rossier, 2011; Budday et al., 2015; Nowakowski et al., 2016; Beopoulos et al., 2022). Importantly, 5-HT signaling is influenced by numerous epigenetic and genetic factors, as well as by perinatal stress (Papaioannou et al., 2002; Provenzi et al., 2016), infection and inflammation (Winter et al., 2009; Gupta et al., 2015), 5-HT metabolism and storage, (Popa et al., 2008) and genetic alterations (Pluess et al., 2010; Karg et al., 2011). 5-HT2CRs are known for their prevalent role in anxiety, with their editing converting the amino acids INI to VSV, VGV, or VNV. Mice possessing only the fully edited VGV isoform of 5-HT2CR, which thereby overexpress brain 5-HT2CR, notably at isoforms diversity and neurotrophic expression levels, are strikingly predisposed to post-traumatic stress-like disorder (PTSD), a trauma- and stress-related disorder characterized by dysregulated fear responses and neurobiological impairments (Martin et al., 2013; Regue et al., 2019; **Figure 9**).

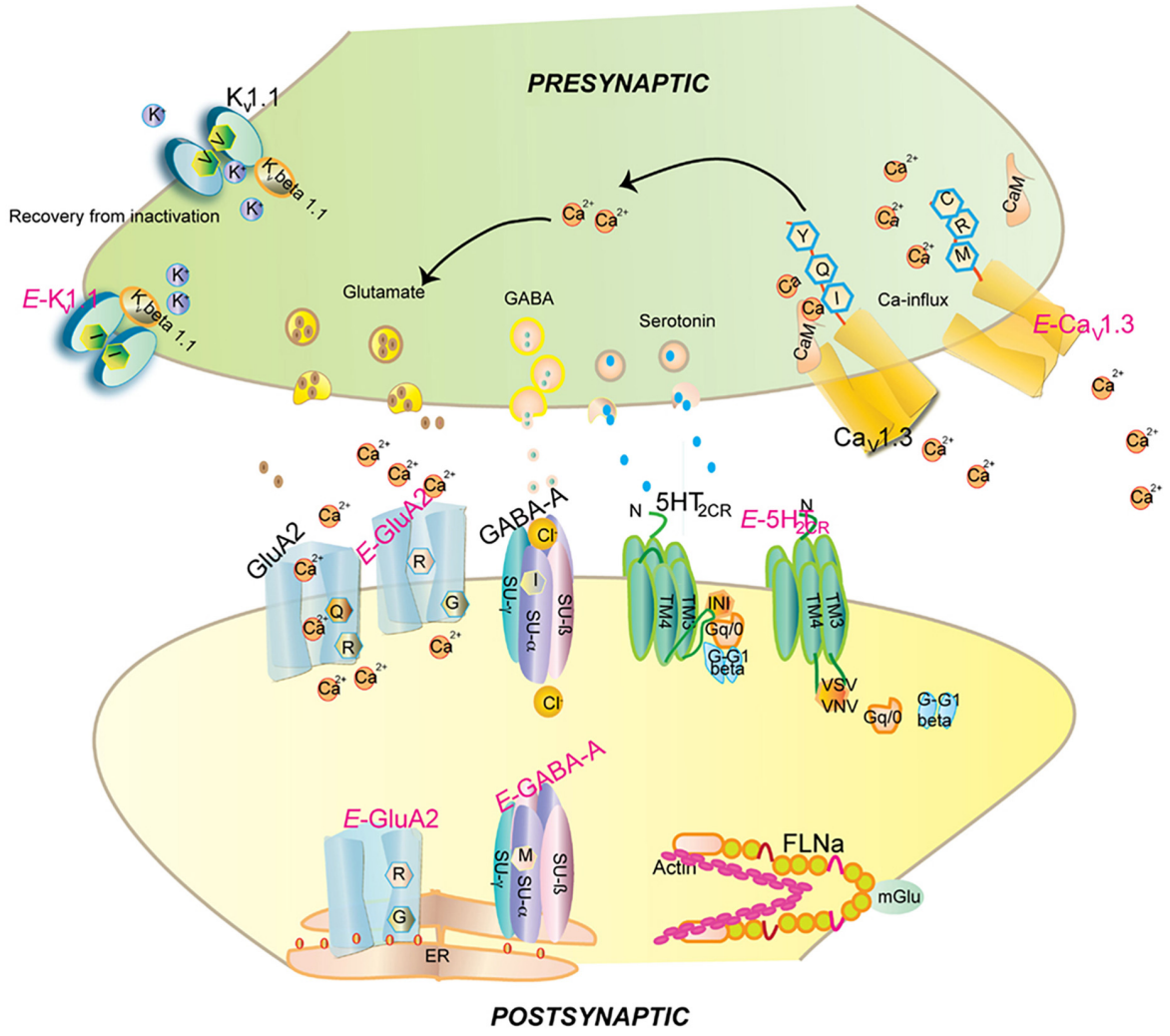

FIGURE 8
Impact of editing on selected neuronal receptors and proteins. Shown are several receptors and channels in their unedited (labeled in black) and edited (E, labeled in pink) versions. Editing at the Q/R site of ionotropic glutamate receptor GRIA2 (GluA2) subunit decreases Ca2 + permeability and endoplasmic reticulum exit efficiency. Membrane trafficking of the $GABA_A$ receptor is reduced by editing of I to M in the alpha3 subunit. Editing of the serotonin 5-HT2c receptor converts the amino acids I-N-I to V-S-V, V-G-V, or V-N-V. This reduces G-protein coupling in the receptor. The editing-induced I to V exchange in the potassium voltage-gated channel KCNA1 (Kv1.1) alters the interaction with KCNB1. Editing of the IQ motif in voltage-gated calcium channel CACNA1D (Cav1.3) to MR abolishes calmodulin binding. Filamin-α (FLNA) is edited in a region that is known to interact with metabotropic glutamate receptor GRM7 (mGlu7) and some of its relatives. Figure from Tariq and Jantsch (2012), obtained under a creative commons license 3 and 4.

Editing of the five sites in the G protein-coupling domain of 5-HT2CR changes three codons [AAU (asparagine), AUA (isoleucine) and AUU (isoleucine), i.e., 157-IRNPI-161 at I, N and I] (Bezanilla, 2004), leading to a possible six different 5-HT2CR isoforms. Overall, up to 24 receptor isoforms are expressed with considerably modified G protein–coupling functions, impacting 5-HT effectiveness and ligand-binding affinity (Nishikura, 2010). Extensively edited receptor isoforms, as the fully edited VGV, activate G protein less efficiently than non-edited (i.e., INI) receptors (Schmauss, 2003).

Furthermore, although studies in mice have shown that 5-HT2C pre-mRNA editing is regulated in a 5HT-dependent manner, the efficacies of the hallucinogenic drug lysergic acid diethylamide (LSD) and other serotonergic drugs are also regulated by RNA editing. This suggests that modification of the editing efficiencies or patterns generates populations of 5-HT2CRs that respond differentially to serotonergic drugs (Niswender et al., 2001), while simultaneously RNA editing efficiency is also influenced by the drugs themselves (Gurevich et al., 2002). Taken together, the data from transgenic mice strongly indicate that the editing status of the 5-HT2CRs can directly influence behavior, highlighting the significance of RNA editing in the etiology and development of psychiatric disorders.

In the human prefrontal cortex (PFC), the most abundant 5-HT2C mRNA sequences originate from the editing of the A site, or from the editing arrangements AC'C, ABCD, and ABD. While there are no appreciable differences in the 5-HT2CR RNA editing efficiencies in the prefrontal cortex of schizophrenia or major depressive disorder patients compared to controls, the

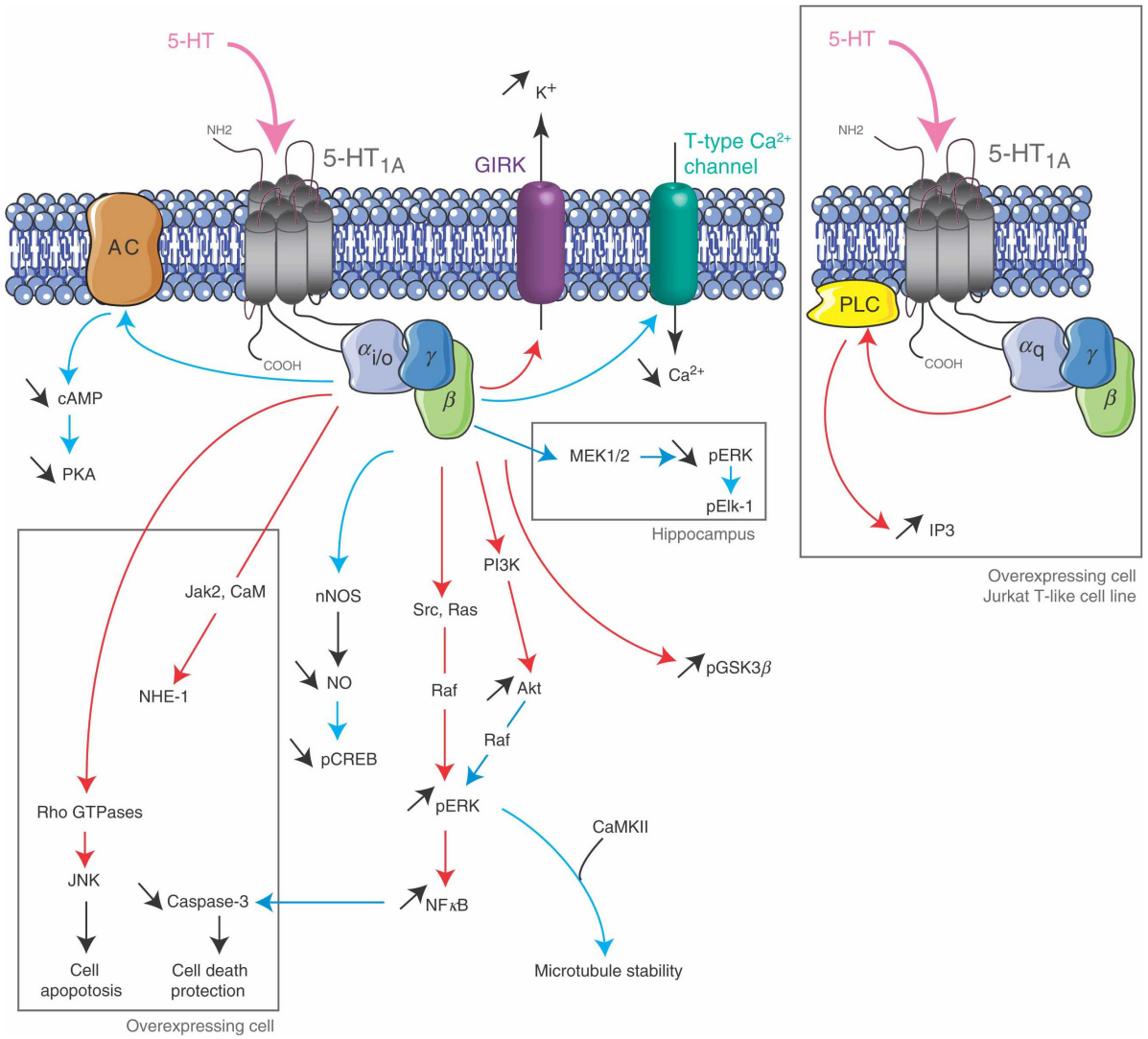

FIGURE 9
5-HT2C receptor signaling pathways. The 5-HT2CR is coupled to PLC in neurons and choroid plexus, and its activation leads to an accumulation of IP3. It inhibits K + conductance in both neurons and choroid plexus and stimulates an apical Cl- conductance in choroid plexus. It may also be coupled to PLD in transfected cells and choroid plexus. Figure from Masson et al. (2012), obtained under a creative commons license 3 and 4.

editing pattern of 5-HT2CR mRNA is significantly different in the prefrontal cortex of depressed suicide victims (Niswender et al., 2001; Gurevich et al., 2002; Schmauss, 2003). Here, C' site editing is considerably amplified, D site editing is significantly reduced, and the C site shows a tendency toward increased editing. When mice were treated with the antidepressant drug fluoxetine (Prozac) changes in C', C, and D site editing were induced, that were the exact opposite of those observed in suicide victims (Gurevich et al., 2002). The comparison of relative isoform frequencies between ASD individuals and controls revealed considerable differences, with the most significant in MNV, IDV, and ISI isoforms, all under-represented in ASD brains (Eran et al., 2013).

3.2.3.1.4. Voltage-gated calcium channels

The core sequence of the calmodulin-binding IQ domain of the of the pore-forming α1 subunit (CACNA1D) of the low voltage activated (LVA) L-type calcium channels Cav1.3 is also subject to A-to-I editing, although only in the brain (Huang et al., 2012). LVA channels are involved in multiple process such as neurotransmitter secretion, synaptic transmission, neuronal pace-making and modulation of other ion channels (Singh et al., 2008). LVA are Ca^{2+} influx channels and are subject to voltage depended inhibition (VDI) and Ca^{2+} depended inhibition (CDI).

The α1 subunit that forms the pore is composed by four domains (I–IV), and each domain has six transmembrane regions (S1–S6) (Catterall et al., 2005), with S1-S4 constituting the voltage sensitive domain and S5- S6 forming the central pore. S6 covers and blocks the inner surface of the pore. Upon activation, the S4 segment moves outward displacing the S6 domain and opens the pore (Swartz, 2004). Calmodulin (CaM) binds to C-terminus of the α1 subunit through its IQ domain with the Ca2 + -CaM complex formation resulting in CDI (Tadross et al., 2008). Ca^{2+} binding to the N- and C-terminal CaM

lobes/hotspots, further regulates channel function (Dick et al., 2008).

The IQ domain of CACNA1D includes the ADAR-2 editable IQDY amino acid sequence. Editing generates multiple isoforms such as MQDY, MQDC, IRDY, MRDC, MRDY, and IQDC. The MQ and IR edits display weakened CDI, while MR edits show up to 50% reduced CDI with faster recovery upon inactivation. Reduced CDI increases repetitive action potentials and calcium spikes (**Figure 10**). Editing patterns are developmentally regulated, being absent in mice before embryonic day 14 (E14) while becoming prominent after postnatal day 4 (P4). Editing is spatially distributed along the brain, with the highest editing patterns found at the frontal cortex and hippocampus (Huang et al., 2012).

As noted above, edited CaV1.3s exhibit reduced CDI, and in neurotypical development, neurons in the suprachiasmatic nucleus display particularly reduced CDI, along with higher repetitive action potential frequencies, and calcium spike activity (Huang et al., 2012). The suprachiasmatic nucleus is the seat of the brain's circadian clock (Gillette and Tischkau, 1999) and autism is frequently associated with co-morbidities such as disturbed sleep patterns and altered circadian rhythms which, in turn often result in impaired vigilance, learning, and memory abilities, and abnormal anxiety responses (Won et al., 2017; Zuculo et al., 2017).

Genetic studies have pointed to alterations in voltage-gated calcium channels as ASD-specific candidates, with mutations in most of the pore-forming and auxiliary subunits being present in autistic individuals (Breitenkamp et al., 2015). The most prominent among them, are those affecting the loci encoding the α subunits such as CACNA1D, CACNA1A, CACNA1B, CACNA1C, CACNA1G, CACNA1E, CACNA1F, CACNA1H, and CACNA1I along with those affecting their accessory subunits CACNA2D3, CACNB2, and CACNA2D4 (Liao and Li, 2020).

3.2.3.1.5. Voltage-gated potassium channels

Voltage-gated potassium Kv1.1 neuronal channels are consisted of a pore forming tetramer of α-subunits, together with 4 β-subunits and accessory subunits. Through the opening and closing of the potassium selective pore, they regulate action potential and neuronal excitability. The human Kv1.1 (KCNA1) gene lacks introns and is susceptible to A-to-I RNA editing, resulting in an exchange of isoleucine for valine at the sixth transmembrane segment (S6, amino acid 400), positioned within the ion conducting pore (Bhalla et al., 2004). Kv1.1 channels in medulla, thalamus and spinal cord are edited up to 65–80% (Decher et al., 2010).

In the ER, Kv1.1 associates with the redox sensor Kvb1 (Pan Y. et al., 2008). Kvb1 contains an inactivation domain at its N-terminal region, which regulates Kv1.1's lag time and inactivation. In comparison to the unedited form of the channel, the edited Kv1.1 recovers from Kvb1-mediated inactivation 20 times faster (Bezanilla, 2004; Bhalla et al., 2004; **Figure 11**). It has been further demonstrated that while the Kv channel blocker 4-aminopyridine (4-AP) causes epileptic seizures in the unedited channels, the edited channels are rendered insensitive to 4-AP by severing the connection between the pore lining and the channel blocker (Streit et al., 2011). Arachidonic acid has been shown to have a similar lack of sensitivity toward edited channels (Decher et al., 2010).

3.2.3.1.6. Filamins and actin organization

Homo- and heterodimers of FLNA and FLNB filamin proteins mediate orthogonal branching of actin filaments (Sheen et al., 2002; Popowicz et al., 2006), thereby participating in actin reorganization and vesicular trafficking, a process essential for, among others, cell motility, migration, dendritic spine, and synapse formation (Dillon and Goda, 2005; Popowicz et al., 2006). FLNA or FLNB depletion leads to defects in cardiovascular and bone development, with FLNA depletion ultimately causing embryonic death (Feng et al., 2006; Hart et al., 2006; Zhou et al., 2007).

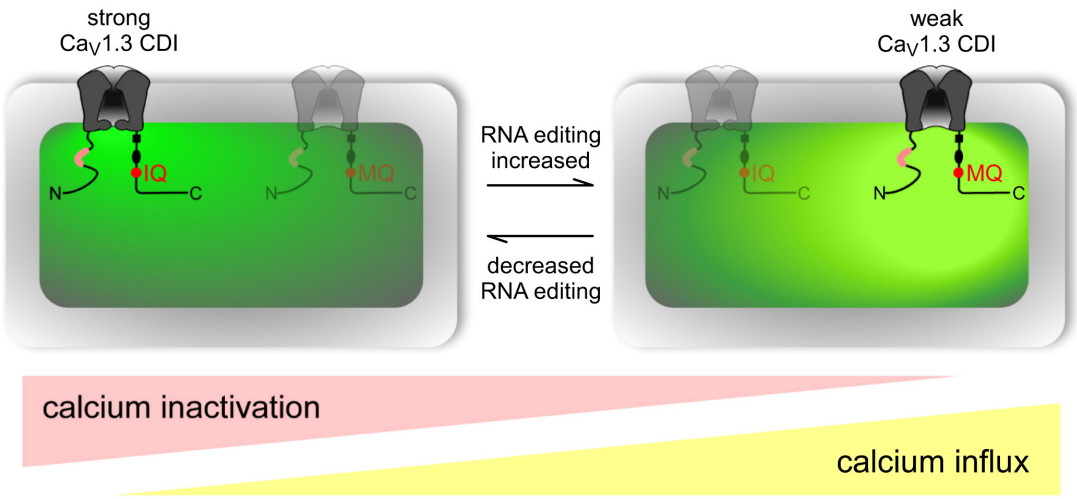

FIGURE 10
Overview of RNA editing effects on CaV1.3 Ca2 + -dependent inactivation (CDI) and calcium load in neurons. Channel schematic as defined in Figure above. Increased RNA editing **(right scenario)** favors channels with MQ and other edited versions of the IQ domain, decreasing overall CDI and presumably increasing cellular Ca2 + load (intense yellow-green coloration). Decreased editing **(left scenario)** favors default channels with IQ version of IQ domain, increasing overall CDI and potentially decreasing cellular Ca2 + load (weak yellow-green coloration). Actual neurons reside on a continuum between these two extremes, as represented by ramp schematics at bottom. Figure from Huang et al. (2012), obtained by Elsevier under license No 5430820583951.

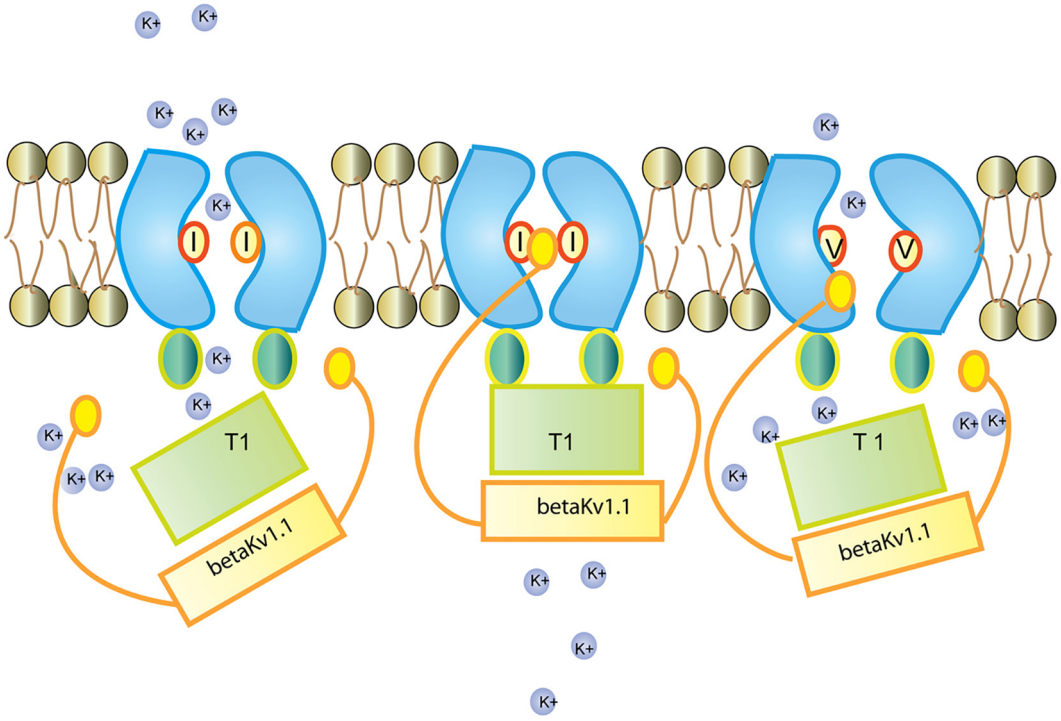

FIGURE 11
Regulation of the Kv1.1 (KCNA1) channel by Kvb1.1 (KCNE5). Kvb1.1 has an inactivation gate which interacts with the unedited (I) form of the Kv1.1 receptor. Editing of Kv1.1 changes the isoleucine to valine (V). This reduces the affinity for Kvb1.1 and enhances recovery from inactivation. While all Kv channels (voltage-gated) function along the same principles (Grizel et al., 2014), different Kv channel subtypes show very different responses to short stimulation (Cameron et al., 2017). Figure from Tariq and Jantsch (2012), obtained under a creative commons license 3 and 4.

Both FLNA and FLNB are subject to developmentally regulated editing that leads to glutamine (Q) to arginine (R) codon exchange in the highly conserved repeat 22 (Li et al., 2009; Wahlstedt et al., 2009), which is part of the 21–24 repeats, involved in the interaction with multiple proteins (Enz, 2002; Popowicz et al., 2006). Editing regulates the interaction of FLNA with glutamate receptors GRIA5a, 5b, 7b, 8a, and GRIA4a and 7a through their C-terminus. It also regulates its interaction with β-integrins and migfilin, an adaptor protein present at cell-cell and cell-extracellular matrix adhesion sites, linking the cytoskeleton to filamin. FLNA repeat 21 interacts with β-integrins, only if repeat 20 disassociates from it, with the efficiency of the association depending on the interactions between repeats 21–24 (Lad et al., 2007, 2008). Editing thus affects competition between different filamin ligands for common binding sites on FLN repeat domains with consequences for cell-cell interactions and signaling. Two β-integrins (ITGB3 and ITGB7) as well as at least one integrins-binding partner (CIB2), involved in the regulation of Ca^{2+}-dependent mechano-transduction, are amongst the genes clearly associated with increased ASD risks in the SFARI Gene database (see text footnote 1).

The potassium channel KCND2 (Kv4.2) and FLNA also interact at filopodial roots, and FLNA is expressed in both cortical and hippocampus neurons. This interaction, which once more involves FLNA repeats 21–24, depends on a "PTPP" amino acid motif in Kv4.2 (AA601-604). Co-expression of filamin in heterologous cells through correct introduction of functional KV4.2 channels at the cell surface, increases the entire cell current density by around 2.7-fold (Petrecca et al., 2000).

Hence, FLNA editing is likely to change neuronal receptors and channels organization as well as synaptic transmission by altering the interaction profiles with binding partners. Furthermore, miRNAs are also the object of A-to-I RNA editing which, in turn, impacts the spatiotemporal expression of receptors, channels and regulatory proteins irrespective of isoforms.

3.2.3.2. Brain-specific miRNAs subject to adenosine-to-inosine RNA editing

A probable key evolutionary function of A-to-I RNA editing might be the modulation of RNA interference (RNAi) efficacy, and this by competing for shared double-stranded RNA (dsRNA) substrates with the microRNA/small interfering RNA (miRNA/siRNA) pathway (Yang et al., 2005; Nishikura, 2006).

RNA interference (RNAi) is the specific suppression of gene expression by means of miRNA and/or siRNA. The siRNA inhibits the expression of a specific target mRNA with the process being initiated by the enzyme Dicer, which cleaves long dsRNA molecules into short dsRNAs. Following RNA separation into single strands, the sense strand will be cleaved by the protein Ago2 and incorporated into the structure of the RNA-induced silencing complex (RISC), which can now bind complementarily to its target mRNA and degrade it. miRNAs are non-coding genomic or exogenous RNAs that are instead involved in the regulation of several mRNAs. miRNAs are derived from a long RNA coding sequence (pri-miRNA) that is processed in the cell nucleus by the

RNaseIII Drosha, aided by the dsRNA-binding protein DGCR8, to generate a 70-nucleotide stem-loop structure (pre-miRNA). The dsRNA portion of the pre-miRNA then undergoes the same downstream processing as the siRNA (initiated by Dicer) to form the mature miRNA molecule that can be incorporated into the RISC complex.

Dicer appears to discriminate between dsRNAs with I-U wobble base pairs and those with only Watson-Crick base pairs. The synthesis of siRNAs and miRNAs by Dicer is progressively decreased as ADARs deaminate dsRNAs. In fact, Dicer cannot cleave *in vitro* dsRNAs that have been significantly edited (50% of adenosines changed to inosines) by ADARs (Zamore et al., 2000; Scadden and Smith, 2001; Yang et al., 2005). Therefore, even minimal siRNA/miRNA editing can affect both mRNA targeting and miRNA/siRNA efficiency. miRNAs are found to be deregulated as a whole in patients with ASD, with no specific miRNAs being systematically altered among individuals (Abu-Elneel et al., 2008; Anitha and Thanseem, 2015).

Additionally, adenosine residues in UAG triplets may be modified more frequently, according to a wide analysis of previously established pri-miRNA editing sites. Among 209 pri-miRNAs containing UAG triplets, 43 UAG editing sites and 43 non-UAG editing sites in 47 pri-miRNAs were highly modified in the human brain. *In vitro* miRNA processing by recombinant Drosha-DGCR8 and Dicer-TRBP (TRBP: the RNA-binding cofactor of Dicer) complexes showed that the majority of pri-miRNA editing interferes with miRNA processing steps (**Figure 12**) and that editing generated new types of miRNAs. miRNA editing could have a significant impact on RNAi gene silencing, as approximately 16%

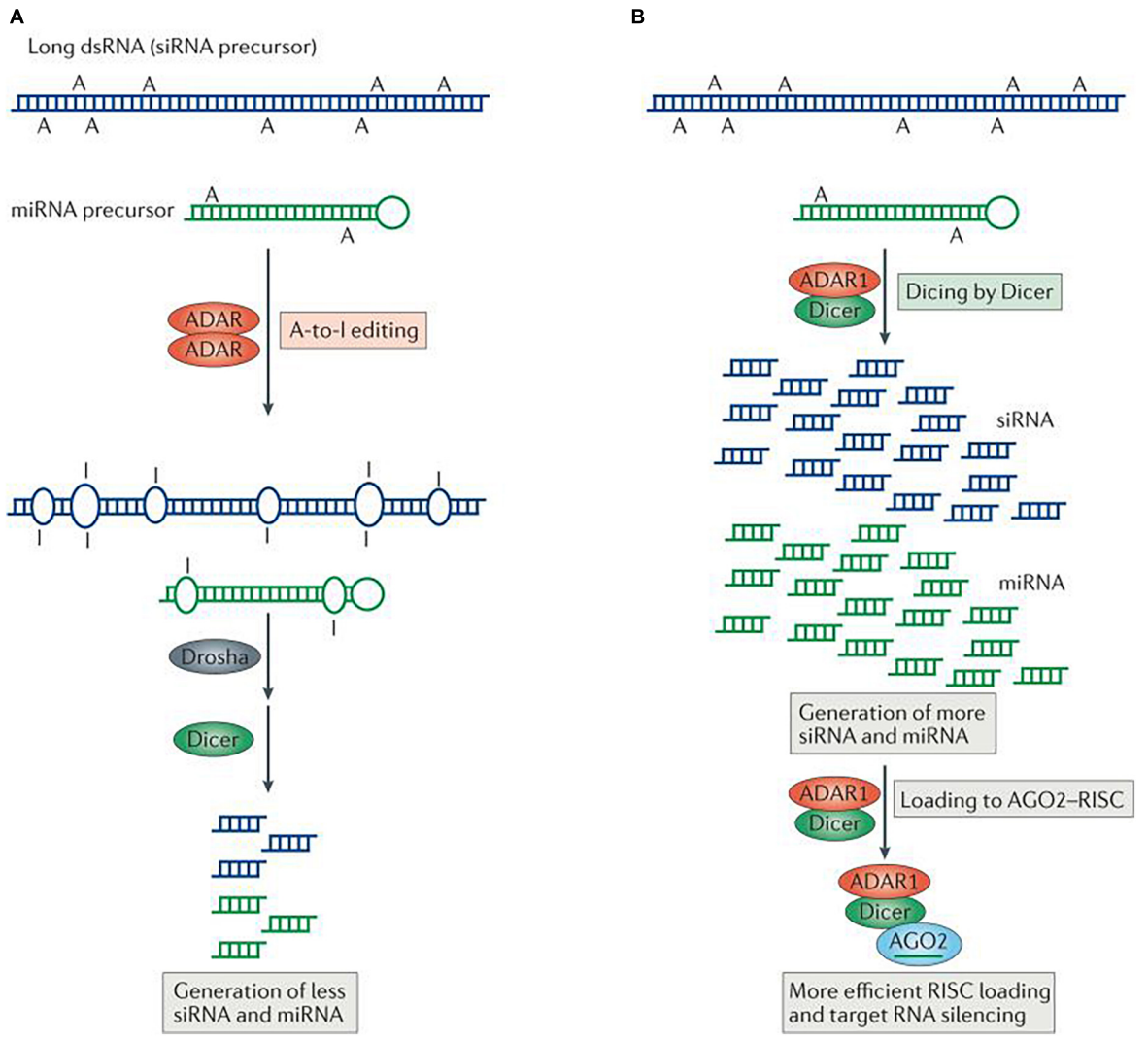

FIGURE 12
Regulation of RNA interference (RNAi) by adenosine deaminases acting on RNA (ADARs). Two different types of interaction between RNA-editing and RNAi pathways are known, one antagonistic and the other stimulative. **(A)** In antagonistic interactions, ADAR–ADAR homodimers edit long double-stranded RNA (dsRNA) and certain microRNA (miRNA) precursors. Editing changes the dsRNA structure and makes it less accessible to Drosha and/or Dicer, consequently decreasing the efficacy of RNAi by reducing the production of short interfering RNAs (siRNAs) and miRNAs. **(B)** In the case of stimulative interactions, ADAR1, as part of a Dicer–ADAR1 heterodimer, promotes RNAi by increasing the Dicer cleavage reaction rate, thereby generating more siRNAs and miRNAs and enhancing RISC (RNA-induced silencing complex) loading and target mRNA silencing. AGO2, Argonaute 2. Figure from Nishikura (2016), obtained by Springer Nature under license No 5430820144326.

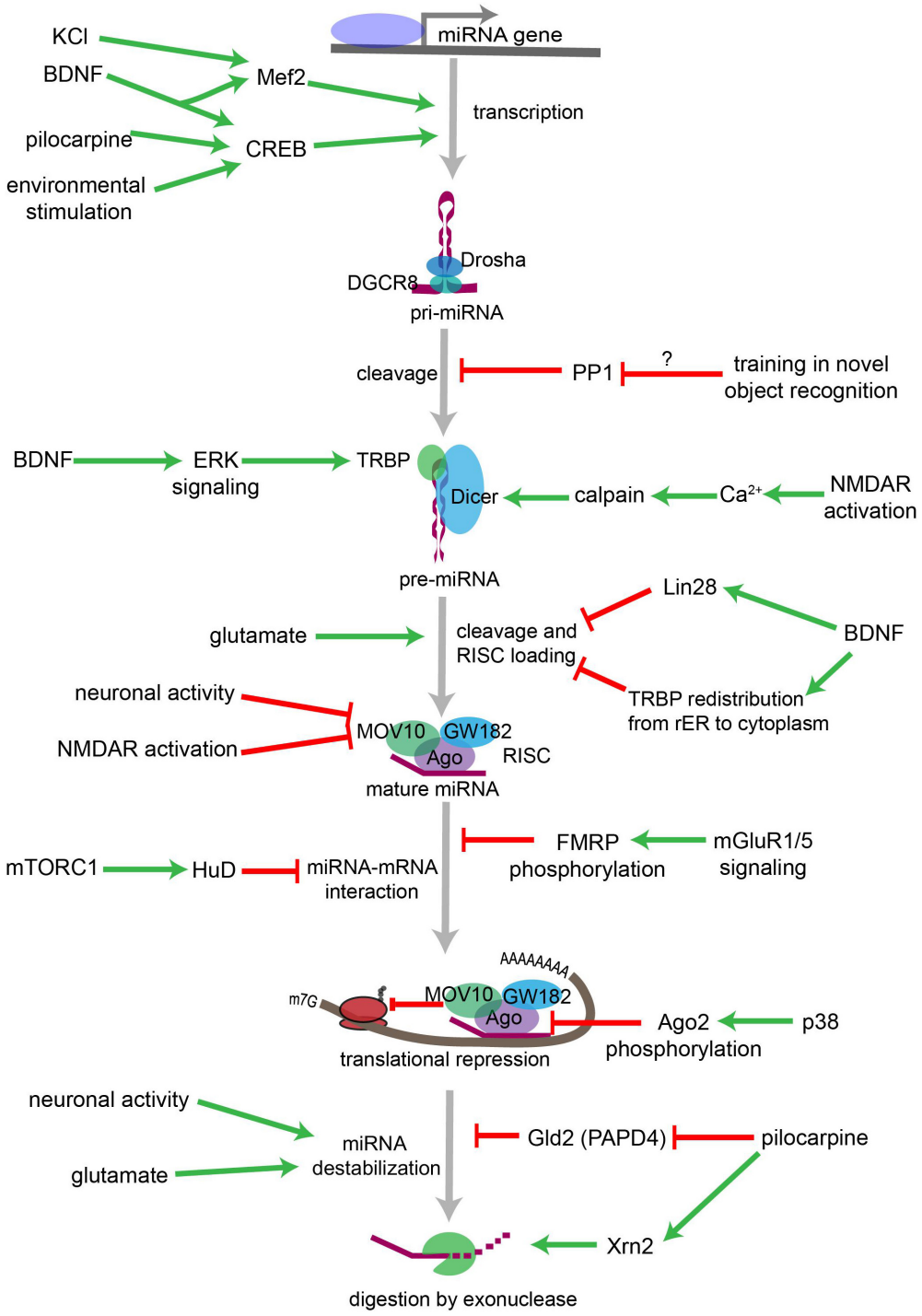

FIGURE 13
Overview of neuronal signaling events that influence miRNA biogenesis, activity, and degradation. Each step within the miRNA biogenesis pathway may be stimulated (green arrow) or inhibited (red bar) by intra- and extracellular signaling events. Pri-miRNA levels increase when BDNF or other signals activate transcription factors that stimulate the transcription of miRNA-encoding genes. Pri-miRNA cleavage by the Microprocessor is influenced by the activity of proteins, such as PP1 which inhibits Microprocessor activity. Pre-miRNA cleavage by Dicer is increased in response to glutamate, BDNF signaling, or NMDA receptor activation. BDNF can also inhibit Dicer's ability to cleave some pre-miRNAs by inducing Lin28 binding to the pre-miRNA terminal loop or by promoting TRBP redistribution and dissociation from Dicer. Neuronal activity and NMDA receptor activation inhibit RISC activity by promoting the degradation of the RISC component Mov10. miRNA interactions with target mRNAs are also influenced by RNA binding proteins such as FMRP or HuD neuron-specific HuD and HuB are subject to adenosine-to-inosine RNA editing at five editing sites each (Enstero et al., 2010), which are regulated by mGluRs (GRMs) and mTORC1 signaling, respectively. P38-induced phosphorylation of Ago2 stimulates mRNA translation by causing the RISC to release its bound miRNA. miRNAs may also be destabilized by increases in neuronal activity, by glutamatergic signaling, or by pilocarpine-induced inhibition of the miRNA stabilizing protein Gld2. Pilocarpine may also stimulate miRNA degradation by increasing expression of the exonuclease Xrn2. Figure from Thomas et al. (2018), obtained under a creative commons license 3 and 4.

of human pri-miRNAs are subject to A to I deamination (Kawahara et al., 2008).

In the brain, CNS signaling events alter miRNA levels and activities, adjusting the response of individual neurons to changing cellular contexts (**Figure 13**). Conversely, miRNAs control the synthesis of proteins that govern synaptic transmission and other types of neuronal signaling, which in turn shapes neuronal communication. Regulation of axonal and dendritic growth, spine development and synaptogenesis by a number of miRNAs has been shown to be critical to brain development. During early development, miRNAs principally foster neuronal differentiation, whereas at later stages, they primarily serve as molecular brakes throughout synaptic development and plasticity (Bicker et al., 2014). Neurological deficits in humans have been associated with defects in miRNA production, and significant changes in miRNA levels occur in traumatic brain injury, epilepsy and in response to less serious brain insults in rodent models (Thomas et al., 2018). The representation and development of some of these diseases in mouse models can also be modified by manipulating specific miRNAs (Thomas et al., 2018).

In cultures of young primary hippocampal neurons at different developmental stages (stage 2–4), the expression of most neuronal miRNAs remains low during early development but increases consistently over the course of neuronal differentiation. A specific subset of 14 miRNAs displayed decreased expression at stage 3, and sustained expression when axonal growth was observed. In mature hippocampal neurons after 21 days of culture, 210 miRNAs were expressed, with 114 at high levels. Following induction of neuronal activity, 51 miRNAs, comprising miR-134, miR-146, miR-181, miR-185, miR- 191, and miR-200a demonstrated altered expression patterns after NMDA receptor-dependent plasticity, and 31 miRNAs, including miR-107, miR-134, miR-470, and miR-546 were upregulated by homeostatic plasticity protocols (van Spronsen et al., 2013).

The miR-134 gene is a negative regulator of dendritic spine size. miR-134 localizes to the postsynaptic compartment in cultured neurons and controls translation of the kinase Limk1, which is essential for the development of dendritic spines, by phosphorylating and inactivating the actin depolymerizing factor Cofilin. This causes a reorganization of the actin cytoskeleton. Dendritic spine size is decreased by miR-134 overexpression, whereas Limk1 restoration rescues spine morphology (Schratt et al., 2006). Therefore, miR-134 regulates neuronal excitability and dendritic spine morphology by preventing Limk1 mRNA

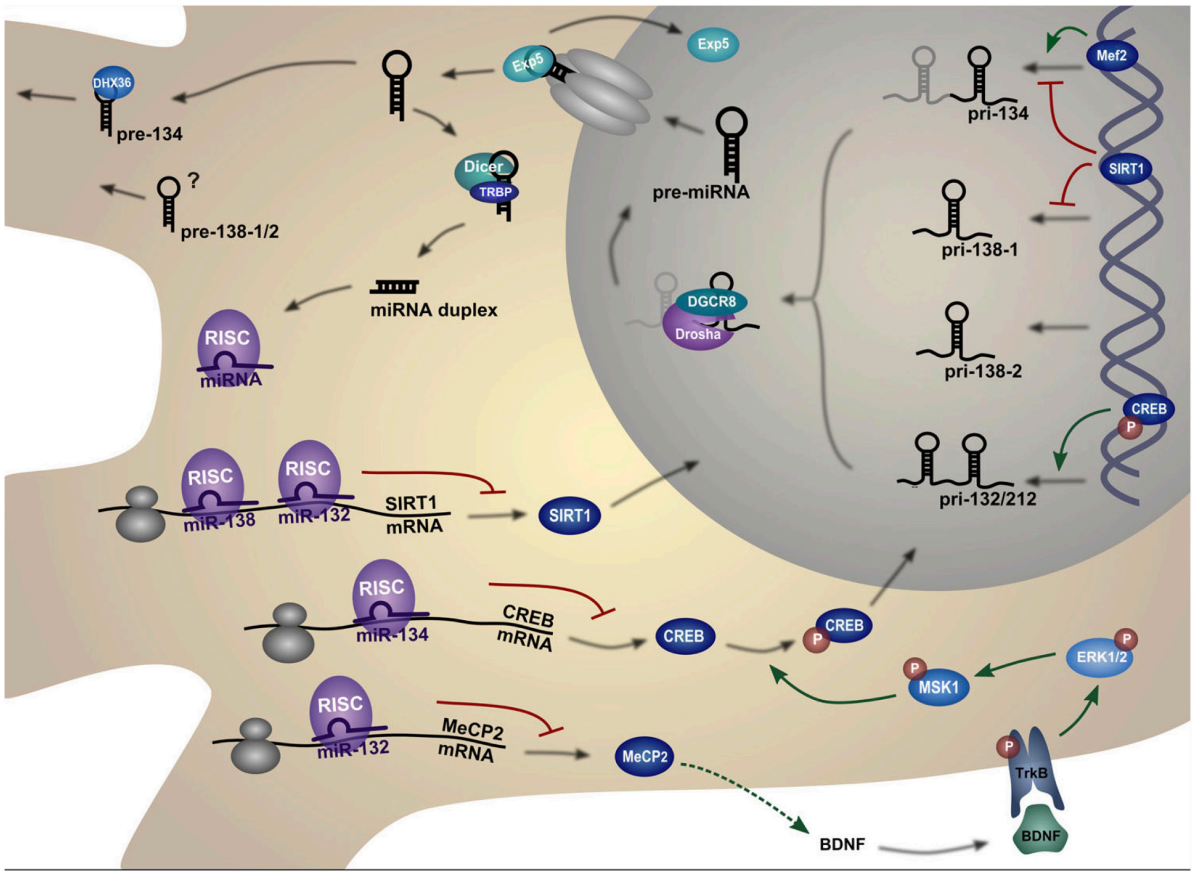

FIGURE 14
Biogenesis and regulation pathways of dendritic miRNAs. The miRNA gene is transcribed into a primary miRNA transcript (pri-mRNA) which is cleaved by Drosha to generate a hairpin miRNA precursor (pre-miRNA). After nuclear export, the pre-miRNA is cleaved by Dicer to form the double-stranded miRNA duplex. One strand of this duplex, the mature miRNA, is then incorporated into the miRNA-induced silencing complex (miRISC). The miRISC complex can bind to complementary target mRNAs, thereby repressing their translation. The figure depicts those targets that are in turn regulating miRNA expression in neurons. Figure from Bicker et al. (2014), obtained by Springer Nature under license No 5430820320321.

from being translated, which restricts the size of dendritic spines (Jimenez-Mateos et al., 2015; **Figure 14**).

Recent studies have linked ASD, intellectual disability, and schizophrenia to microdeletions encompassing MIR137HG, the host gene that encodes miR-137 part of the miR-379-410 cluster, which includes 39 miRNAs, located in the DLK1-GTL2 paternally imprinted locus in mice (DLK1-DIO3 region in humans). The miR-137 appears to regulate many types of synaptic plasticity as well as signaling cascades that are thought to be abnormal in schizophrenia, acting upstream in many important neurodevelopmental pathways. In addition, miR-137, which has over 1300 predicted targets, regulates adult neurogenesis, synaptic plasticity, and glutamatergic signaling (Pacheco et al., 2019).

These studies illustrate the ability of miRNAs to affect the human brain by shaping neuronal communication and offer a mechanism by which miRNA deregulation may contribute to the development of psychiatric disorders (**Figure 15**).

Abnormal expression levels of miRNAs, including miR-132, miR-23a, miR-93 and miRNA-148b upregulation and miR-106b, miR-146b downregulation, were observed in the cerebellar cortex of autistic patients (Abu-Elneel et al., 2008). Similar dysregulation of miRNA expression was also observed in serum and lymphoblastoid cells of autistic patients (Talebizadeh et al., 2008; Sarachana et al., 2010; Mundalil Vasu et al., 2014), while increased levels of miR134-5p and miR138-5p were also reported (Hirsch et al., 2018).

In the SFARI database[2], miR-137 also is one of the 202 genes deemed to present suggestive evidence of predisposition to autism and shows clear genetic association with ASD (Mahmoudi and Cairns, 2017). Individuals with ASD (Carter et al., 2011), intellectual disability (Willemsen et al., 2011), and syndromic obesity (D'Angelo et al., 2015; Tucci et al., 2016) had

2 https://gene.sfari.org

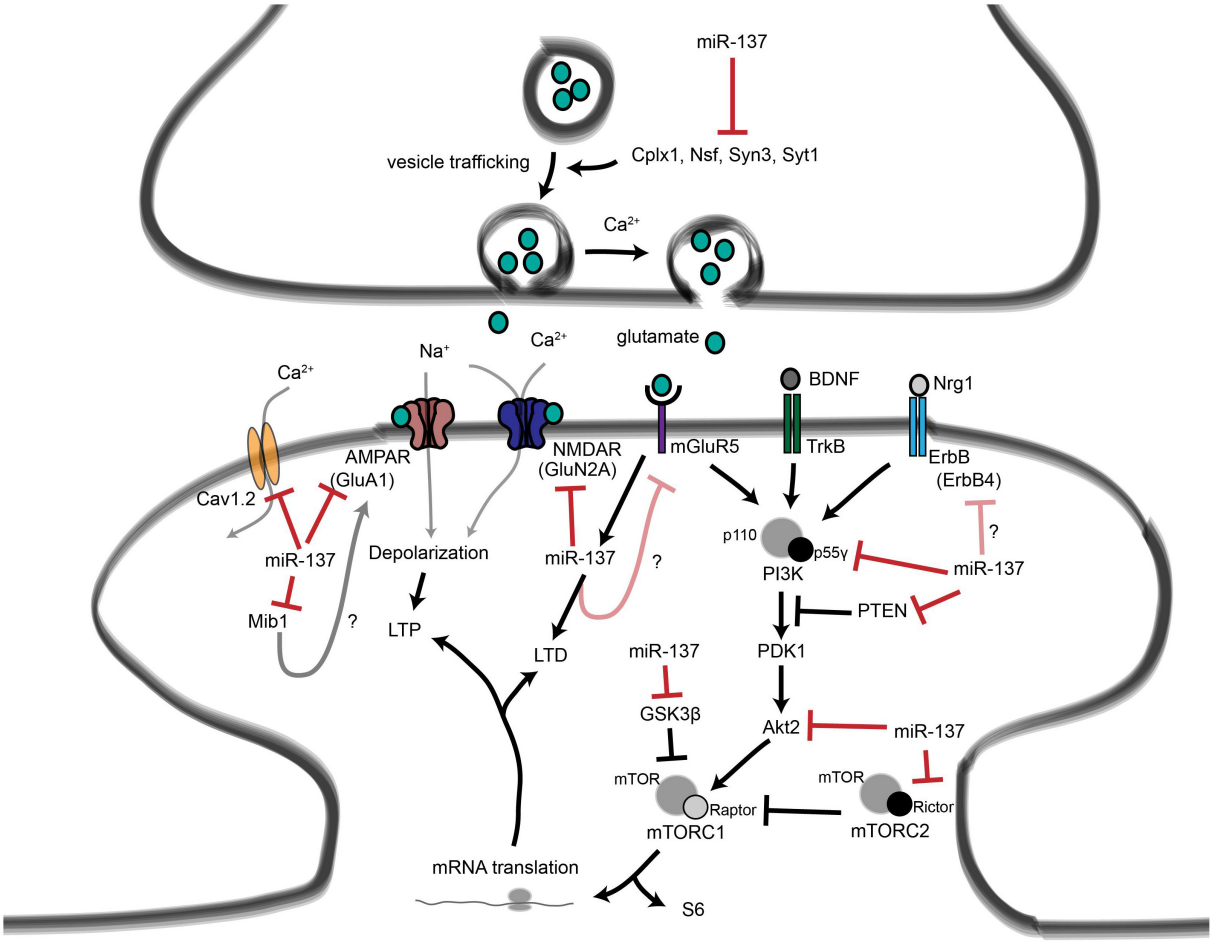

FIGURE 15
Roles for miR-137 at the glutamatergic synapse. This figure summarizes the findings of Kwon et al. (2013), Zhao et al. (2013), Olde Loohuis et al. (2015), Siegert et al. (2015), and Thomas et al. (2017). miR-137 regulates presynaptic signaling by regulating vesicle trafficking in the axon terminal. miR-137 also targets the mRNA that encodes the L-type calcium channel subunit Cav1.2 (CACNA1C), which has also been linked to schizophrenia with genome-wide significance. Postsynaptically, miR-137 regulates the levels of glutamatergic receptor subunits GluA1 (GRIA1) and GluN2A (GRIN2A), and bioinformatic predictions suggest that miR-137 may target the metabotropic glutamate receptor mGluR5 (GRM5) as well as ErbB4, which regulates the strength of glutamatergic synapses. mGluR5 signaling, in turn, increases miR-137 levels. miR-137 also regulates proteins within the PI3K-Akt-mTOR pathway, e.g., p55g, to regulate neuronal responses to BDNF and Nrg1 signaling. miR-137 may regulate PI3K-Akt-mTOR signaling downstream of mGluR receptors as well. Figure from Thomas et al. (2018), obtained under a creative commons license 3 and 4.

microdeletions on chromosome 1 at position p21.3, impacting MIR137. When several genome-wide association studies were combined, meta-analyses revealed that MIR137 was strongly related with schizophrenia. In the region 3.6 kb upstream of MIR137 (1:g.98515539A > T), an uncommon functional enhancer variant was discovered to be connected to schizophrenia and bipolar disorder (Duan et al., 2014). In heterozygous conditional-knockout mice, partial loss of MIR137 led to dysregulated synaptic plasticity, repetitive behavior, and decreased learning and social behavior; treatment with papaverine, an inhibitor of PDE10A, or PDE10A knockdown alleviated these impairments (Cheng et al., 2018).

4. Conclusion

In our previous work (Beopoulos et al., 2022), we had explored the possible impacts of increased placental release of serotonin, subsequent to sustained maternal low-grade inflammation in early to mid-pregnancy, upon the probability of ASD pathogenesis in the offspring and found strongly corroborating evidence in a multiplicity of reports. Hence, although subject to numerous caveats involving fetal genotypes and environmental factors affecting maternal wellbeing, maternal low-grade systemic inflammation, reported be about 25% in a sample of adult US women (Ford et al., 2004), particularly during early and mid-pregnancy, seems to be a major determinant for significantly increased risk of ASD pathogenesis.

The increased 5-HT supply to the growing fetus cannot, however, be the only inflammatory-associated component that is implicated in the pathophysiology of ASD. Indeed, a number of additional inflammation-related factors, including interferons, other interleukins, TGFβ, TNFα and β, etc., can incorporate the fetal blood through the placenta and have been proven to have a major impact on *in utero* fetal brain development (Wei et al., 2013; Theoharides et al., 2016; Tsivion-Visbord et al., 2020). Additionally, a comparison of results from several studies reveals that the type of causal immunogen, the gestational stage at which the maternal inflammatory reaction starts, its severity, and its duration might all have an impact on how maternal inflammation affects neurodevelopment [for example, see (Boksa, 2010)]. The inflammatory response of the placenta during pregnancy can have sexually dimorphic consequences on fetal development (Clifton, 2005; Mueller and Bale, 2008), and the postpartum increase in neonatal testosterone in males can affect long-term CNS function (Forgie and Stewart, 1993; Wilson and Davies, 2007). This led us to postulate that in the pathogenesis of ASD, RNA epitranscriptomic dysregulations might probably take precedence over differential epigenetic (methylation/acetylation) modifications and to investigate the dynamic mechanisms most likely to be affected.

The link between maternal inflammation/immune activation, RNA epitranscriptomics and neurodevelopment has been demonstrated in studies in which mice were treated prenatally with the inflammatory mediator poly (I:C) or LPS on day 9 of gestation (E9). Offspring treated prenatally with LPS showed increased neuronal density at postnatal day (PD)14 but no changes were observed in arborization mediators such as reelin. However, prenatal poly(I:C)-treated mice had fewer reelin-positive cells in the dorsal stratum oriens at PD28, whereas increased expression of GAD67 (catalyzes GABA production from L-glutamic acid) in the ventral stratum oriens was observed in prenatal LPS-treated male mice and prenatal poly(I:C) during the prenatal period (Harvey and Boksa, 2012).

In another study, the offspring of mice treated with poly (I:C) at E9 showed marked behavioral deficits at PD24 with the brains of the fetuses increasing A-to-I RNA editing levels, independently of mRNA expression levels, affecting genetic pathways related to brain development (Tsivion-Visbord et al., 2020). DACT3, COG3, and GRIA2 were amongst the mRNAs presenting the greatest increases in A-to-I editing. Dact3 plays a crucial role in the mouse central nervous system's embryonic development (Fisher et al., 2006), and COG3, a component of the COG complex, interacts with BLOC-1, which, along with the AP-3 complex, is necessary to direct membrane protein cargos into vesicles assembled at cell bodies for delivery into neurites and nerve terminals (Lee et al., 2012). Neurite extension is another function of the BLOC-1 complex that relies on its association with SNARE proteins (Setty et al., 2007). Although there are intriguing mechanistic differences between rodent and the corresponding human regional brain development patterns (Lim and Alvarez-Buylla, 2016), the above reports clearly establish mechanistic links between maternal immune activation during early pregnancy and brain development alterations together with long-term behavioral deficits in the offspring.

According to the present work, the neuroanatomic characteristics of ASD are found to be better explained through dysregulated RNA epitranscriptomic mechanisms occurring early during brain development than through differential epigenetic markings alone. Among such mechanisms, dysregulated mRNA-specific poly(A)-tail modulation is strongly correlated with genetic factors and high-risk genes associated with ASD pathogenesis; alterations in mRNA alternative splicing concurrently with dysregulated A-to-I RNA editing, correlates with the functional characteristics of neuronal receptors and channels organizations. The latter primarily influences GABAA and serotonin 2C receptors, glutamate and voltage-gated ion channels, filamins and actin organization, and eventually synaptic structures and plasticity. A-to-I RNA editing also induces changes in mi/siRNA profiling that impact neuronal organization, dendritic spine density and synaptic transmission by changing the interaction affinities with binding partners while also affecting neuronal migration, glial differentiation and regional brain patterning. RNA epitranscriptomics may well account for the enormous genetic and symptomatic heterogeneities that are systematically associated with psychiatric disorders at large and not with ASD only (Gandal et al., 2018; Walker et al., 2019).

Data availability statement

The original contributions presented in this study are included in this article/supplementary material, further inquiries can be directed to the corresponding author.

Author contributions

FI: conceptualization and methodology. MG: software. FI, AB, MG, and AF: validation and resources. FI and AB: formal analysis, data curation, and writing—original draft preparation. FI, AB, and AF: writing—review and editing. MG: project administration. All authors have read and agreed to the published version of the manuscript.

Funding

This research was funded by the European Union's Horizon 2020 Research and Innovation Program GEMMA under grant agreement number 825033. Please see http://www.gemma-project.eu for more information.

Conflict of interest

The authors declare that the research was conducted in the absence of any commercial or financial relationships that could be construed as a potential conflict of interest.

Publisher's note

References

Abaza, I., and Gebauer, F. (2008). Trading translation with RNA-binding proteins. *RNA* 14, 404–409. doi: 10.1261/rna.848208

Abrahams, B. S., and Geschwind, D. H. (2008). Advances in autism genetics: on the threshold of a new neurobiology. *Nat. Rev. Genet.* 9, 341–355. doi: 10.1038/nrg2346

Abu-Elneel, K., Liu, T., Gazzaniga, F. S., Nishimura, Y., Wall, D. P., Geschwind, D. H., et al. (2008). Heterogeneous dysregulation of microRNAs across the autism spectrum. *Neurogenetics* 9, 153–161. doi: 10.1007/s10048-008-0133-5

Alegria-Torres, J. A., Baccarelli, A., and Bollati, V. (2011). Epigenetics and lifestyle. *Epigenomics* 3, 267–277. doi: 10.2217/epi.11.22

Anitha, A., and Thanseem, I. (2015). microRNA and Autism. *Adv. Exp. Med. Biol.* 888, 71–83. doi: 10.1007/978-3-319-22671-2_5

Aslam, N., Kubota, Y., Wells, D., and Shouval, H. Z. (2009). Translational switch for long-term maintenance of synaptic plasticity. *Mol. Syst. Biol.* 5:284. doi: 10.1038/msb.2009.38

Atack, J. R. (2011a). GABAA receptor subtype-selective modulators. I. α2/α3-selective agonists as non-sedating anxiolytics. *Curr. Top. Med. Chem.* 11, 1176–1202. doi: 10.2174/156802611795371350

Atack, J. R. (2011b). GABAA receptor subtype-selective modulators. II. α5-selective inverse agonists for cognition enhancement. *Curr. Top. Med. Chem.* 11, 1203–1214. doi: 10.2174/156802611795371314

Atkins, C. M., Davare, M. A., Oh, M. C., Derkach, V., and Soderling, T. R. (2005). Bidirectional regulation of cytoplasmic polyadenylation element-binding protein phosphorylation by Ca2+/calmodulin-dependent protein kinase II and protein phosphatase 1 during hippocampal long-term potentiation. *J. Neurosci.* 25, 5604–5610. doi: 10.1523/jneurosci.5051-04.2005

Babenko, O., Kovalchuk, I., and Metz, G. A. (2015). Stress-induced perinatal and transgenerational epigenetic programming of brain development and mental health. *Neurosci. Biobehav. Rev.* 48, 70–91. doi: 10.1016/j.neubiorev.2014.11.013

Barua, S., and Junaid, M. A. (2015). Lifestyle, pregnancy and epigenetic effects. *Epigenomics* 7, 85–102. doi: 10.2217/epi.14.71

Bass, B. L. (2002). RNA editing by adenosine deaminases that act on RNA. *Annu. Rev. Biochem.* 71, 817–846. doi: 10.1146/annurev.biochem.71.110601.135501

Battersby, S., Ogilvie, A. D., Blackwood, D. H., Shen, S., Muqit, M. M., Muir, W. J., et al. (1999). Presence of multiple functional polyadenylation signals and a single nucleotide polymorphism in the 3′ untranslated region of the human serotonin transporter gene. *J. Neurochem.* 72, 1384–1388. doi: 10.1046/j.1471-4159.1999.721384.x

Baudouin, S., and Scheiffele, P. (2010). SnapShot: Neuroligin-neurexin complexes. *Cell* 141, 908, 908.e1. doi: 10.1016/j.cell.2010.05.024

Baudry, A., Mouillet-Richard, S., Schneider, B., Launay, J. M., and Kellermann, O. (2010). miR-16 targets the serotonin transporter: a new facet for adaptive responses to antidepressants. *Science* 329, 1537–1541. doi: 10.1126/science.1193692

Bazak, L., Haviv, A., Barak, M., Jacob-Hirsch, J., Deng, P., Zhang, R., et al. (2014). A-to-I RNA editing occurs at over a hundred million genomic sites, located in a majority of human genes. *Genome Res.* 24, 365–376. doi: 10.1101/gr.164749.113

Beilharz, T. H., Humphreys, D. T., and Preiss, T. (2010). miRNA Effects on mRNA closed-loop formation during translation initiation. *Prog. Mol. Subcell Biol.* 50, 99–112. doi: 10.1007/978-3-642-03103-8_7

Beilharz, T. H., and Preiss, T. (2007). Widespread use of poly(A) tail length control to accentuate expression of the yeast transcriptome. *RNA* 13, 982–997. doi: 10.1261/rna.569407

Ben-Ari, Y., Gaiarsa, J. L., Tyzio, R., and Khazipov, R. (2007). GABA: a pioneer transmitter that excites immature neurons and generates primitive oscillations. *Physiol. Rev.* 87, 1215–1284. doi: 10.1152/physrev.00017.2006

Ben-David, E., and Shifman, S. (2013). Combined analysis of exome sequencing points toward a major role for transcription regulation during brain development in autism. *Mol. Psychiatry* 18, 1054–1056. doi: 10.1038/mp.2012.148

Beopoulos, A., Géa, M., Fasano, A., and Iris, F. (2022). Autism spectrum disorders pathogenesis: Toward a comprehensive model based on neuroanatomic and neurodevelopment considerations. *Front. Neurosci.* 16:988735. doi: 10.3389/fnins.2022.988735

Bezanilla, F. (2004). RNA editing of a human potassium channel modifies its inactivation. *Nat. Struct. Mol. Biol.* 11, 915–916. doi: 10.1038/nsmb1004-915

Bhalla, T., Rosenthal, J. J., Holmgren, M., and Reenan, R. (2004). Control of human potassium channel inactivation by editing of a small mRNA hairpin. *Nat. Struct. Mol. Biol.* 11, 950–956. doi: 10.1038/nsmb825

Bicker, S., Lackinger, M., Weiss, K., and Schratt, G. (2014). MicroRNA-132, -134, and -138: a microRNA troika rules in neuronal dendrites. *Cell Mol. Life Sci.* 71, 3987–4005. doi: 10.1007/s00018-014-1671-7

Boksa, P. (2010). Effects of prenatal infection on brain development and behavior: a review of findings from animal models. *Brain Behav. Immun.* 24, 881–897. doi: 10.1016/j.bbi.2010.03.005

Bonnin, A., and Levitt, P. (2011). Fetal, maternal, and placental sources of serotonin and new implications for developmental programming of the brain. *Neuroscience* 197, 1–7. doi: 10.1016/j.neuroscience.2011.10.005

Braunschweig, U., Gueroussov, S., Plocik, A. M., Graveley, B. R., and Blencowe, B. J. (2013). Dynamic integration of splicing within gene regulatory pathways. *Cell* 152, 1252–1269. doi: 10.1016/j.cell.2013.02.034

Breitenkamp, A. F., Matthes, J., and Herzig, S. (2015). Voltage-gated Calcium Channels and Autism Spectrum Disorders. *Curr. Mol. Pharmacol.* 8, 123–132. doi: 10.2174/1874467208666150507105235

Brummelte, S., Mc Glanaghy, E., Bonnin, A., and Oberlander, T. F. (2017). Developmental changes in serotonin signaling: Implications for early brain function, behavior and adaptation. *Neuroscience* 342, 212–231. doi: 10.1016/j.neuroscience.2016.02.037

Budday, S., Steinmann, P., and Kuhl, E. (2015). Physical biology of human brain development. *Front. Cell Neurosci.* 9:257. doi: 10.3389/fncel.2015.00257

Calarco, J. A., Superina, S., O'Hanlon, D., Gabut, M., Raj, B., Pan, Q., et al. (2009). Regulation of vertebrate nervous system alternative splicing and development by an SR-related protein. *Cell* 138, 898–910. doi: 10.1016/j.cell.2009.06.012

Cameron, M. A., Al Abed, A., Buskila, Y., Dokos, S., Lovell, N. H., and Morley, J. W. (2017). Differential effect of brief electrical stimulation on voltage-gated potassium channels. *J. Neurophysiol.* 117, 2014–2024. doi: 10.1152/jn.00915.2016

Carter, M. T., Nikkel, S. M., Fernandez, B. A., Marshall, C. R., Noor, A., Lionel, A. C., et al. (2011). Hemizygous deletions on chromosome 1p21.3 involving the DPYD gene in individuals with autism spectrum disorder. *Clin. Genet.* 80, 435–443. doi: 10.1111/j.1399-0004.2010.01578.x

Catterall, W. A., Perez-Reyes, E., Snutch, T. P., and Striessnig, J. (2005). International Union of Pharmacology. XLVIII. Nomenclature and structure-function relationships of voltage-gated calcium channels. *Pharmacol. Rev.* 57, 411–425. doi: 10.1124/pr.57.4.5

Chang, J., Gilman, S. R., Chiang, A. H., Sanders, S. J., and Vitkup, D. (2015). Genotype to phenotype relationships in autism spectrum disorders. *Nat. Neurosci.* 18, 191–198. doi: 10.1038/nn.3907

Chekulaeva, M., Mathys, H., Zipprich, J. T., Attig, J., Colic, M., Parker, R., et al. (2011). miRNA repression involves GW182-mediated recruitment of CCR4-NOT through conserved W-containing motifs. *Nat. Struct. Mol. Biol.* 18, 1218–1226. doi: 10.1038/nsmb.2166

Cheng, Y., Wang, Z. M., Tan, W., Wang, X., Li, Y., Bai, B., et al. (2018). Partial loss of psychiatric risk gene Mir137 in mice causes repetitive behavior and impairs sociability and learning via increased Pde10a. *Nat. Neurosci.* 21, 1689–1703. doi: 10.1038/s41593-018-0261-7

Chih, B., Gollan, L., and Scheiffele, P. (2006). Alternative splicing controls selective trans-synaptic interactions of the neuroligin-neurexin complex. *Neuron* 51, 171–178. doi: 10.1016/j.neuron.2006.06.005

Christofi, T., and Zaravinos, A. (2019). RNA editing in the forefront of epitranscriptomics and human health. *J. Transl. Med.* 17, 319. doi: 10.1186/s12967-019-2071-4

Clifton, V. L. (2005). Sexually dimorphic effects of maternal asthma during pregnancy on placental glucocorticoid metabolism and fetal growth. *Cell Tissue Res.* 322, 63–71. doi: 10.1007/s00441-005-1117-5

Cote, F., Fligny, C., Bayard, E., Launay, J. M., Gershon, M. D., Mallet, J., et al. (2007). Maternal serotonin is crucial for murine embryonic development. *Proc. Natl. Acad. Sci. U.S.A.* 104, 329–334. doi: 10.1073/pnas.0606722104

Courchesne, E., Pramparo, T., Gazestani, V. H., Lombardo, M. V., Pierce, K., and Lewis, N. E. (2019). The ASD Living Biology: from cell proliferation to clinical phenotype. *Mol. Psychiatry* 24, 88–107. doi: 10.1038/s41380-018-0056-y

Craig, A. M., and Kang, Y. (2007). Neurexin-neuroligin signaling in synapse development. *Curr. Opin. Neurobiol.* 17, 43–52. doi: 10.1016/j.conb.2007.01.011

D'Angelo, C. S., Moller Dos Santos, M. F., Alonso, L. G., and Koiffmann, C. P. (2015). Two new cases of 1p21.3 deletions and an unbalanced translocation t(8;12) among individuals with syndromic obesity. *Mol. Syndromol.* 6, 63–70. doi: 10.1159/000371600

Daniel, C., Wahlstedt, H., Ohlson, J., Bjork, P., and Ohman, M. (2011). Adenosine-to-inosine RNA editing affects trafficking of the gamma-aminobutyric acid type A (GABA(A)) receptor. *J. Biol. Chem.* 286, 2031–2040. doi: 10.1074/jbc.M110.130096

Daniel, C., Widmark, A., Rigardt, D., and Öhman, M. (2017). Editing inducer elements increases A-to-I editing efficiency in the mammalian transcriptome. *Genome Biol.* 18:195. doi: 10.1186/s13059-017-1324-x

De Rubeis, S., He, X., Goldberg, A. P., Poultney, C. S., Samocha, K., Cicek, A. E., et al. (2014). Synaptic, transcriptional and chromatin genes disrupted in autism. *Nature* 515, 209–215. doi: 10.1038/nature13772

Decher, N., Streit, A. K., Rapedius, M., Netter, M. F., Marzian, S., Ehling, P., et al. (2010). RNA editing modulates the binding of drugs and highly unsaturated fatty acids to the open pore of Kv potassium channels. *EMBO J.* 29, 2101–2113. doi: 10.1038/emboj.2010.88

Dever, T. E. (2002). Gene-specific regulation by general translation factors. *Cell* 108, 545–556. doi: 10.1016/s0092-8674(02)00642-6

Di Giammartino, D. C., Nishida, K., and Manley, J. L. (2011). Mechanisms and consequences of alternative polyadenylation. *Mol. Cell* 43, 853–866. doi: 10.1016/j.molcel.2011.08.017

Dick, I. E., Tadross, M. R., Liang, H., Tay, L. H., Yang, W., and Yue, D. T. (2008). A modular switch for spatial Ca2+ selectivity in the calmodulin regulation of CaV channels. *Nature* 451, 830–834. doi: 10.1038/nature06529

Diering, G. H., and Huganir, R. L. (2018). The AMPA receptor code of synaptic plasticity. *Neuron* 100, 314–329. doi: 10.1016/j.neuron.2018.10.018

Dillman, A. A., Hauser, D. N., Gibbs, J. R., Nalls, M. A., McCoy, M. K., Rudenko, I. N., et al. (2013). mRNA expression, splicing and editing in the embryonic and adult mouse cerebral cortex. *Nat. Neurosci.* 16, 499–506. doi: 10.1038/nn.3332

Dillon, C., and Goda, Y. (2005). The actin cytoskeleton: integrating form and function at the synapse. *Annu. Rev. Neurosci.* 28, 25–55. doi: 10.1146/annurev.neuro.28.061604.135757

Donovan, A. P., and Basson, M. A. (2017). The neuroanatomy of autism - a developmental perspective. *J. Anat.* 230, 4–15. doi: 10.1111/joa.12542

Duan, J., Shi, J., Fiorentino, A., Leites, C., Chen, X., Moy, W., et al. (2014). A rare functional noncoding variant at the GWAS-implicated MIR137/MIR2682 locus might confer risk to schizophrenia and bipolar disorder. *Am. J. Hum. Genet.* 95, 744–753. doi: 10.1016/j.ajhg.2014.11.001

Eckmann, C. R., Rammelt, C., and Wahle, E. (2011). Control of poly(A) tail length. *Wiley Interdiscip. Rev. RNA* 2, 348–361. doi: 10.1002/wrna.56

Enstero, M., Akerborg, O., Lundin, D., Wang, B., Furey, T. S., Ohman, M., et al. (2010). A computational screen for site selective A-to-I editing detects novel sites in neuron specific Hu proteins. *BMC Bioinform.* 11:6. doi: 10.1186/1471-2105-11-6

Enz, R. (2002). The actin-binding protein Filamin-A interacts with the metabotropic glutamate receptor type 7. *FEBS Lett.* 514, 184–188.

Eran, A., Li, J. B., Vatalaro, K., McCarthy, J., Rahimov, F., Collins, C., et al. (2013). Comparative RNA editing in autistic and neurotypical cerebella. *Mol. Psychiatry* 18, 1041–1048. doi: 10.1038/mp.2012.118

Eshraghi, A. A., Liu, G., Kay, S. S., Eshraghi, R. S., Mittal, J., Moshiree, B., et al. (2018). Epigenetics and autism spectrum disorder: is there a correlation? *Front. Cell Neurosci.* 12:78. doi: 10.3389/fncel.2018.00078

Faras, H., Al Ateeqi, N., and Tidmarsh, L. (2010). Autism spectrum disorders. *Ann. Saudi. Med.* 30, 295–300. doi: 10.4103/0256-4947.65261

Feng, Y., Chen, M. H., Moskowitz, I. P., Mendonza, A. M., Vidali, L., Nakamura, F., et al. (2006). Filamin A (FLNA) is required for cell-cell contact in vascular development and cardiac morphogenesis. *Proc. Natl. Acad. Sci. U.S.A.* 103, 19836–19841. doi: 10.1073/pnas.0609628104

Fioriti, L., Myers, C., Huang, Y. Y., Li, X., Stephan, J. S., Trifilieff, P., et al. (2015). The persistence of hippocampal-based memory requires protein synthesis mediated by the prion-like protein CPEB3. *Neuron* 86, 1433–1448. doi: 10.1016/j.neuron.2015.05.021

Fisher, D. A., Kivimäe, S., Hoshino, J., Suriben, R., Martin, P. M., Baxter, N., et al. (2006). Three Dact gene family members are expressed during embryonic development and in the adult brains of mice. *Dev. Dyn.* 235, 2620–2630. doi: 10.1002/dvdy.20917

Ford, E. S., Giles, W. H., Mokdad, A. H., and Myers, G. L. (2004). Distribution and correlates of C-reactive protein concentrations among adult US women. *Clin. Chem.* 50, 574–581. doi: 10.1373/clinchem.2003.027359

Forgie, M. L., and Stewart, J. (1993). Sex differences in amphetamine-induced locomotor activity in adult rats: role of testosterone exposure in the neonatal period. *Pharmacol. Biochem. Behav.* 46, 637–645. doi: 10.1016/0091-3057(93)90555-8

Franzen, O., Ermel, R., Sukhavasi, K., Jain, R., Jain, A., Betsholtz, C., et al. (2018). Global analysis of A-to-I RNA editing reveals association with common disease variants. *PeerJ* 6:e4466. doi: 10.7717/peerj.4466

Fu, X. D., and Ares, M. Jr. (2014). Context-dependent control of alternative splicing by RNA-binding proteins. *Nat. Rev. Genet.* 15, 689–701. doi: 10.1038/nrg3778

Gadal, F., Bozic, C., Pillot-Brochet, C., Malinge, S., Wagner, S., Le Cam, A., et al. (2003). Integrated transcriptome analysis of the cellular mechanisms associated with Ha-ras-dependent malignant transformation of the human breast epithelial MCF7 cell line. *Nucleic Acids Res.* 31, 5789–5804. doi: 10.1093/nar/gkg762

Gadal, F., Starzec, A., Bozic, C., Pillot-Brochet, C., Malinge, S., Ozanne, V., et al. (2005). Integrative analysis of gene expression patterns predicts specific modulations of defined cell functions by estrogen and tamoxifen in MCF7 breast cancer cells. *J. Mol. Endocrinol.* 34, 61–75. doi: 10.1677/jme.1.01631

Gandal, M. J., Haney, J. R., Parikshak, N. N., Leppa, V., Ramaswami, G., Hartl, C., et al. (2018). Shared molecular neuropathology across major psychiatric disorders parallels polygenic overlap. *Science* 359, 693–697. doi: 10.1126/science.aad6469

Gaspar, P., Cases, O., and Maroteaux, L. (2003). The developmental role of serotonin: news from mouse molecular genetics. *Nat. Rev. Neurosci.* 4, 1002–1012. doi: 10.1038/nrn1256

Gillette, M. U., and Tischkau, S. A. (1999). Suprachiasmatic nucleus: the brain's circadian clock. *Recent. Prog. Horm. Res.* 54, 33–58.

Gommans, W. M., Mullen, S. P., and Maas, S. (2009). RNA editing: a driving force for adaptive evolution? *Bioessays* 31, 1137–1145. doi: 10.1002/bies.200900045

Gordon, L., Joo, J. E., Powell, J. E., Ollikainen, M., Novakovic, B., Li, X., et al. (2012). Neonatal DNA methylation profile in human twins is specified by a complex interplay between intrauterine environmental and genetic factors, subject to tissue-specific influence. *Genome Res.* 22, 1395–1406. doi: 10.1101/gr.136598.111

Gratten, J., Wray, N. R., Keller, M. C., and Visscher, P. M. (2014). Large-scale genomics unveils the genetic architecture of psychiatric disorders. *Nat. Neurosci.* 17, 782–790. doi: 10.1038/nn.3708

Greger, I. H., Akamine, P., Khatri, L., and Ziff, E. B. (2006). Developmentally regulated, combinatorial RNA processing modulates AMPA receptor biogenesis. *Neuron* 51, 85–97. doi: 10.1016/j.neuron.2006.05.020

Grizel, A. V., Glukhov, G. S., and Sokolova, O. S. (2014). Mechanisms of activation of voltage-gated potassium channels. *Acta Nat.* 6, 10–26.

Gupta, V., Khan, A. A., Sasi, B. K., and Mahapatra, N. R. (2015). Molecular mechanism of monoamine oxidase A gene regulation under inflammation and ischemia-like conditions: key roles of the transcription factors GATA2, Sp1 and TBP. *J. Neurochem.* 134, 21–38. doi: 10.1111/jnc.13099

Gurevich, I., Tamir, H., Arango, V., Dwork, A. J., Mann, J. J., and Schmauss, C. (2002). Altered editing of serotonin 2C receptor pre-mRNA in the prefrontal cortex of depressed suicide victims. *Neuron* 34, 349–356.

Gyawali, S., Subaran, R., Weissman, M. M., Hershkowitz, D., McKenna, M. C., Talati, A., et al. (2010). Association of a polyadenylation polymorphism in the serotonin transporter and panic disorder. *Biol. Psychiatry* 67, 331–338. doi: 10.1016/j.biopsych.2009.10.015

Hamada, N., Ito, H., Nishijo, T., Iwamoto, I., Morishita, R., Tabata, H., et al. (2016). Essential role of the nuclear isoform of RBFOX1, a candidate gene for autism spectrum disorders, in the brain development. *Sci. Rep.* 6:30805. doi: 10.1038/srep30805

Hamid, F. M., and Makeyev, E. V. (2014). Emerging functions of alternative splicing coupled with nonsense-mediated decay. *Biochem. Soc. Trans.* 42, 1168–1173. doi: 10.1042/bst20140066

Han, M., Mejias, R., Chiu, S. L., Rose, R., Adamczyk, A., Huganir, R., et al. (2017). Mice lacking GRIP1/2 show increased social interactions and enhanced phosphorylation at GluA2-S880. *Behav. Brain Res.* 321, 176–184. doi: 10.1016/j.bbr.2016.12.042

Hanley, L. J., and Henley, J. M. (2010). Differential roles of GRIP1a and GRIP1b in AMPA receptor trafficking. *Neurosci. Lett.* 485, 167–172. doi: 10.1016/j.neulet.2010.09.003

Hart, A. W., Morgan, J. E., Schneider, J., West, K., McKie, L., Bhattacharya, S., et al. (2006). Cardiac malformations and midline skeletal defects in mice lacking filamin A. *Hum. Mol. Genet.* 15, 2457–2467. doi: 10.1093/hmg/ddl168

Hartley, C. A., McKenna, M. C., Salman, R., Holmes, A., Casey, B. J., Phelps, E. A., et al. (2012). Serotonin transporter polyadenylation polymorphism modulates the retention of fear extinction memory. *Proc. Natl. Acad. Sci. U.S.A.* 109, 5493–5498. doi: 10.1073/pnas.1202044109

Harvey, L., and Boksa, P. (2012). A stereological comparison of GAD67 and reelin expression in the hippocampal stratum oriens of offspring from two mouse models of maternal inflammation during pregnancy. *Neuropharmacology* 62, 1767–1776. doi: 10.1016/j.neuropharm.2011.11.022

Hevers, W., and Luddens, H. (1998). The diversity of GABAA receptors. Pharmacological and electrophysiological properties of GABAA channel subtypes. *Mol. Neurobiol.* 18, 35–86. doi: 10.1007/bf02741459

Higuchi, M., Maas, S., Single, F. N., Hartner, J., Rozov, A., Burnashev, N., et al. (2000). Point mutation in an AMPA receptor gene rescues lethality in mice deficient in the RNA-editing enzyme ADAR2. *Nature* 406, 78–81. doi: 10.1038/35017558

Hirsch, M. M., Deckmann, I., Fontes-Dutra, M., Bauer-Negrini, G., Della-Flora Nunes, G., Nunes, W., et al. (2018). Behavioral alterations in autism model induced by valproic acid and translational analysis of circulating microRNA. *Food Chem. Toxicol.* 115, 336–343. doi: 10.1016/j.fct.2018.02.061

Hough, L. H., and Segal, S. (2016). Effects of developmental hyperserotonemia on the morphology of rat dentate nuclear neurons. *Neuroscience* 322, 178–194. doi: 10.1016/j.neuroscience.2016.02.021

Huang, H., Tan, B. Z., Shen, Y., Tao, J., Jiang, F., Sung, Y. Y., et al. (2012). RNA editing of the IQ domain in Ca(v)1.3 channels modulates their Ca(2)(+)-dependent inactivation. *Neuron* 73, 304–316. doi: 10.1016/j.neuron.2011.11.022

Huang, Y. S., Jung, M. Y., Sarkissian, M., and Richter, J. D. (2002). N-methyl-D-aspartate receptor signaling results in Aurora kinase-catalyzed CPEB phosphorylation and alpha CaMKII mRNA polyadenylation at synapses. *EMBO J.* 21, 2139–2148. doi: 10.1093/emboj/21.9.2139

Hutcheon, B., Fritschy, J. M., and Poulter, M. O. (2004). Organization of GABA receptor alpha-subunit clustering in the developing rat neocortex and hippocampus. *Eur. J. Neurosci.* 19, 2475–2487. doi: 10.1111/j.0953-816X.2004.03349.x

Hutsler, J. J., and Zhang, H. (2010). Increased dendritic spine densities on cortical projection neurons in autism spectrum disorders. *Brain Res.* 1309, 83–94. doi: 10.1016/j.brainres.2009.09.120

Hwang, T., Park, C. K., Leung, A. K., Gao, Y., Hyde, T. M., Kleinman, J. E., et al. (2016). Dynamic regulation of RNA editing in human brain development and disease. *Nat. Neurosci.* 19, 1093–1099. doi: 10.1038/nn.4337

Iijima, T., Wu, K., Witte, H., Hanno-Iijima, Y., Glatter, T., Richard, S., et al. (2011). SAM68 regulates neuronal activity-dependent alternative splicing of neurexin-1. *Cell* 147, 1601–1614. doi: 10.1016/j.cell.2011.11.028

Irimia, M., Weatheritt, R. J., Ellis, J. D., Parikshak, N. N., Gonatopoulos-Pournatzis, T., Babor, M., et al. (2014). A highly conserved program of neuronal microexons is misregulated in autistic brains. *Cell* 159, 1511–1523. doi: 10.1016/j.cell.2014.11.035

Iris, F. (2012). Psychiatric systems medicine: closer at hand than anticipated but not with the expected portrait. *Pharmacopsychiatry* 45(Suppl. 1), S12–S21. doi: 10.1055/s-0032-1309002

Iris, F., Beopoulos, A., and Gea, M. (2018). How scientific literature analysis yields innovative therapeutic hypothesis through integrative iterations. *Curr. Opin. Pharmacol.* 42, 62–70. doi: 10.1016/j.coph.2018.07.005

Iris, F., Gea, M., Lampe, P. H., and Santamaria, P. (2009). [Production and implementation of predictive biological models]. *Med. Sci.* 25, 608–616. doi: 10.1051/medsci/2009256-7608

Ivshina, M., Lasko, P., and Richter, J. D. (2014). Cytoplasmic polyadenylation element binding proteins in development, health, and disease. *Annu. Rev. Cell Dev. Biol/* 30, 393–415. doi: 10.1146/annurev-cellbio-101011-155831

Jimenez-Mateos, E. M., Engel, T., Merino-Serrais, P., Fernaud-Espinosa, I., Rodriguez-Alvarez, N., Reynolds, J., et al. (2015). Antagomirs targeting microRNA-134 increase hippocampal pyramidal neuron spine volume in vivo and protect against pilocarpine-induced status epilepticus. *Brain Struct. Funct.* 220, 2387–2399. doi: 10.1007/s00429-014-0798-5

Johnson, M. B., Kawasawa, Y. I., Mason, C. E., Krsnik, Z., Coppola, G., Bogdanović, D., et al. (2009). Functional and evolutionary insights into human brain development through global transcriptome analysis. *Neuron* 62, 494–509. doi: 10.1016/j.neuron.2009.03.027

Kahvejian, A., Svitkin, Y. V., Sukarieh, R., M'Boutchou, M. N., and Sonenberg, N. (2005). Mammalian poly(A)-binding protein is a eukaryotic translation initiation factor, which acts via multiple mechanisms. *Genes Dev.* 19, 104–113. doi: 10.1101/gad.1262905

Kaminsky, Z. A., Tang, T., Wang, S. C., Ptak, C., Oh, G. H., Wong, A. H., et al. (2009). DNA methylation profiles in monozygotic and dizygotic twins. *Nat. Genet.* 41, 240–245. doi: 10.1038/ng.286

Karagianni, K., Pettas, S., Christoforidou, G., Kanata, E., Bekas, N., Xanthopoulos, K., et al. (2022). A systematic review of common and brain-disease-specific RNA editing alterations providing novel insights into neurological and neurodegenerative disease manifestations. *Biomolecules* 12:465. doi: 10.3390/biom12030465

Karg, K., Burmeister, M., Shedden, K., and Sen, S. (2011). The serotonin transporter promoter variant (5-HTTLPR), stress, and depression meta-analysis revisited: evidence of genetic moderation. *Arch. Gen. Psychiatry* 68, 444–454. doi: 10.1001/archgenpsychiatry.2010.189

Kawahara, Y., Megraw, M., Kreider, E., Iizasa, H., Valente, L., Hatzigeorgiou, A. G., et al. (2008). Frequency and fate of microRNA editing in human brain. *Nucleic Acids Res.* 36, 5270–5280. doi: 10.1093/nar/gkn479

Kinast, K., Peeters, D., Kolk, S. M., Schubert, D., and Homberg, J. R. (2013). Genetic and pharmacological manipulations of the serotonergic system in early life: neurodevelopmental underpinnings of autism-related behavior. *Front. Cell Neurosci.* 7:72. doi: 10.3389/fncel.2013.00072

Kornblihtt, A. R., Schor, I. E., Alló, M., Dujardin, G., Petrillo, E., and Muñoz, M. J. (2013). Alternative splicing: a pivotal step between eukaryotic transcription and translation. *Nat. Rev. Mol. Cell Biol.* 14, 153–165. doi: 10.1038/nrm3525

Kwon, E., Wang, W., and Tsai, L. H. (2013). Validation of schizophrenia-associated genes CSMD1, C10orf26, CACNA1C and TCF4 as miR-137 targets. *Mol. Psychiatry* 18, 11–12. doi: 10.1038/mp.2011.170

Lad, Y., Jiang, P., Ruskamo, S., Harburger, D. S., Ylanne, J., Campbell, I. D., et al. (2008). Structural basis of the migfilin-filamin interaction and competition with integrin beta tails. *J. Biol. Chem.* 283, 35154–35163. doi: 10.1074/jbc.M802592200

Lad, Y., Kiema, T., Jiang, P., Pentikainen, O. T., Coles, C. H., Campbell, I. D., et al. (2007). Structure of three tandem filamin domains reveals auto-inhibition of ligand binding. *EMBO J.* 26, 3993–4004. doi: 10.1038/sj.emboj.7601827

Lee, H. H., Nemecek, D., Schindler, C., Smith, W. J., Ghirlando, R., Steven, A. C., et al. (2012). Assembly and architecture of biogenesis of lysosome-related organelles complex-1 (BLOC-1). *J. Biol. Chem.* 287, 5882–5890. doi: 10.1074/jbc.M111.325746

Lee, J. A., Damianov, A., Lin, C. H., Fontes, M., Parikshak, N. N., Anderson, E. S., et al. (2016). Cytoplasmic Rbfox1 regulates the expression of synaptic and autism-related genes. *Neuron* 89, 113–128. doi: 10.1016/j.neuron.2015.11.025

Lee, Y., and Rio, D. C. (2015). Mechanisms and regulation of alternative pre-mRNA splicing. *Annu. Rev. Biochem.* 84, 291–323. doi: 10.1146/annurev-biochem-060614-034316

Li, J. B., Levanon, E. Y., Yoon, J. K., Aach, J., Xie, B., Leproust, E., et al. (2009). Genome-wide identification of human RNA editing sites by parallel DNA capturing and sequencing. *Science* 324, 1210–1213. doi: 10.1126/science.1170995

Li, Q., Lee, J. A., and Black, D. L. (2007). Neuronal regulation of alternative pre-mRNA splicing. *Nat. Rev. Neurosci.* 8, 819–831. doi: 10.1038/nrn2237

Li, Y. I., Sanchez-Pulido, L., Haerty, W., and Ponting, C. P. (2015). RBFOX and PTBP1 proteins regulate the alternative splicing of micro-exons in human brain transcripts. *Genome Res.* 25, 1–13. doi: 10.1101/gr.181990.114

Liao, X., and Li, Y. (2020). Genetic associations between voltage-gated calcium channels and autism spectrum disorder: a systematic review. *Mol. Brain* 13:96. doi: 10.1186/s13041-020-00634-0

Licht, K., Kapoor, U., Amman, F., Picardi, E., Martin, D., Bajad, P., et al. (2019). A high resolution A-to-I editing map in the mouse identifies editing events controlled by pre-mRNA splicing. *Genome Res.* 29, 1453–1463. doi: 10.1101/gr.242636.118

Lim, D. A., and Alvarez-Buylla, A. (2016). The Adult Ventricular-Subventricular Zone (V-SVZ) and Olfactory Bulb (OB) Neurogenesis. *Cold Spring Harb. Perspect. Biol.* 8:a018820. doi: 10.1101/cshperspect.a018820

Linares, A. J., Lin, C. H., Damianov, A., Adams, K. L., Novitch, B. G., and Black, D. L. (2015). The splicing regulator PTBP1 controls the activity of the transcription factor Pbx1 during neuronal differentiation. *eLife* 4:e09268. doi: 10.7554/eLife.09268

Liu, H., Ma, C. P., Chen, Y. T., Schuyler, S. C., Chang, K. P., and Tan, B. C. (2014). Functional Impact of RNA editing and ADARs on regulation of gene expression: perspectives from deep sequencing studies. *Cell Biosci.* 4:44. doi: 10.1186/2045-3701-4-44

Liu, H., Wang, H., Peterson, M., Zhang, W., Hou, G., and Zhang, Z. W. (2019). N-terminal alternative splicing of GluN1 regulates the maturation of excitatory synapses and seizure susceptibility. *Proc. Natl. Acad. Sci. U.S.A.* 116, 21207–21212. doi: 10.1073/pnas.1905721116

Mahmoudi, E., and Cairns, M. J. (2017). MiR-137: an important player in neural development and neoplastic transformation. *Mol. Psychiatry* 22, 44–55. doi: 10.1038/mp.2016.150

Makeyev, E. V., Zhang, J., Carrasco, M. A., and Maniatis, T. (2007). The MicroRNA miR-124 promotes neuronal differentiation by triggering brain-specific alternative pre-mRNA splicing. *Mol. Cell* 27, 435–448. doi: 10.1016/j.molcel.2007.07.015

Martin, C. B., Ramond, F., Farrington, D. T., Aguiar, A. S. Jr., Chevarin, C., Berthiau, A. S., et al. (2013). RNA splicing and editing modulation of 5-HT(2C) receptor function: relevance to anxiety and aggression in VGV mice. *Mol. Psychiatry* 18, 656–665. doi: 10.1038/mp.2012.171

Marzluff, W. F., Gongidi, P., Woods, K. R., Jin, J., and Maltais, L. J. (2002). The human and mouse replication-dependent histone genes. *Genomics* 80, 487–498.

Masi, A., DeMayo, M. M., Glozier, N., and Guastella, A. J. (2017). An overview of autism spectrum disorder, heterogeneity and treatment options. *Neurosci. Bull.* 33, 183–193. doi: 10.1007/s12264-017-0100-y

Masson, J., Emerit, M. B., Hamon, M., and Darmon, M. (2012). Serotonergic signaling: multiple effectors and pleiotropic effects. *Wiley Interdiscipl. Rev.* 1, 685–713. doi: 10.1002/wmts.50

Matera, A. G., and Wang, Z. (2014). A day in the life of the spliceosome. *Nat. Rev. Mol. Cell Biol.* 15, 108–121. doi: 10.1038/nrm3742

Miller, S., Yasuda, M., Coats, J. K., Jones, Y., Martone, M. E., and Mayford, M. (2002). Disruption of dendritic translation of CaMKIIalpha impairs stabilization of synaptic plasticity and memory consolidation. *Neuron* 36, 507–519. doi: 10.1016/s0896-6273(02)00978-9

Mockenhaupt, S., and Makeyev, E. V. (2015). Non-coding functions of alternative pre-mRNA splicing in development. *Semin. Cell Dev. Biol.* 4, 32–39. doi: 10.1016/j.semcdb.2015.10.018

Mueller, B. R., and Bale, T. L. (2008). Sex-specific programming of offspring emotionality after stress early in pregnancy. *J. Neurosci.* 28, 9055–9065. doi: 10.1523/jneurosci.1424-08.2008

Muhle, R., Trentacoste, S. V., and Rapin, I. (2004). The genetics of autism. *Pediatrics* 113, e472–e486.

Mundalil Vasu, M., Anitha, A., Thanseem, I., Suzuki, K., Yamada, K., Takahashi, T., et al. (2014). Serum microRNA profiles in children with autism. *Mol. Autism.* 5:40. doi: 10.1186/2040-2392-5-40

Narayanan, V., Heiming, R. S., Jansen, F., Lesting, J., Sachser, N., Pape, H. C., et al. (2011). Social defeat: impact on fear extinction and amygdala-prefrontal cortical theta synchrony in 5-HTT deficient mice. *PLoS One* 6:e22600. doi: 10.1371/journal.pone.0022600

Nardone, S., Sams, D. S., Zito, A., Reuveni, E., and Elliott, E. (2017). Dysregulation of cortical neuron DNA methylation profile in autism spectrum disorder. *Cereb. Cortex* 27, 5739–5754. doi: 10.1093/cercor/bhx250

Nishikura, K. (2006). Editor meets silencer: crosstalk between RNA editing and RNA interference. *Nat. Rev. Mol. Cell Biol.* 7, 919–931. doi: 10.1038/nrm2061

Nishikura, K. (2010). Functions and regulation of RNA editing by ADAR deaminases. *Annu. Rev. Biochem.* 79, 321–349. doi: 10.1146/annurev-biochem-060208-105251

Nishikura, K. (2016). A-to-I editing of coding and non-coding RNAs by ADARs. *Nat. Rev. Mol. Cell Biol.* 17, 83–96. doi: 10.1038/nrm.2015.4

Niswender, C. M., Herrick-Davis, K., Dilley, G. E., Meltzer, H. Y., Overholser, J. C., Stockmeier, C. A., et al. (2001). RNA editing of the human serotonin 5-HT2C receptor. alterations in suicide and implications for serotonergic pharmacotherapy. *Neuropsychopharmacology* 24, 478–491. doi: 10.1016/s0893-133x(00)00223-2

Nowakowski, T. J., Pollen, A. A., Sandoval-Espinosa, C., and Kriegstein, A. R. (2016). Transformation of the radial glia scaffold demarcates two stages of human cerebral cortex development. *Neuron* 91, 1219–1227. doi: 10.1016/j.neuron.2016.09.005

Nussbaumer, M., Asara, J. M., Teplytska, L., Murphy, M. P., Logan, A., Turck, C. W., et al. (2016). Selective Mitochondrial Targeting Exerts Anxiolytic Effects In Vivo. *Neuropsychopharmacology* 41, 1751–1758. doi: 10.1038/npp.2015.341

Ohlson, J., Pedersen, J. S., Haussler, D., and Ohman, M. (2007). Editing modifies the GABA(A) receptor subunit alpha3. *RNA* 13, 698–703. doi: 10.1261/rna.349107

Olde Loohuis, N. F., Ba, W., Stoerchel, P. H., Kos, A., Jager, A., Schratt, G., et al. (2015). MicroRNA-137 Controls AMPA-Receptor-Mediated Transmission and mGluR-Dependent LTD. *Cell Rep.* 11, 1876–1884. doi: 10.1016/j.celrep.2015.05.040

Pacheco, A., Berger, R., Freedman, R., and Law, A. J. (2019). A VNTR regulates miR-137 expression through novel alternative splicing and contributes to risk for schizophrenia. *Sci. Rep.* 9:11793. doi: 10.1038/s41598-019-48141-0

Paine, T. A., Chang, S., and Poyle, R. (2020). Contribution of GABA(A) receptor subunits to attention and social behavior. *Behav. Brain Res.* 378:112261. doi: 10.1016/j.bbr.2019.112261

Palladino, M. J., Keegan, L. P., O'Connell, M. A., and Reenan, R. A. (2000). A-to-I pre-mRNA editing in Drosophila is primarily involved in adult nervous system function and integrity. *Cell* 102, 437–449. doi: 10.1016/s0092-8674(00)00049-0

Pan, Q., Shai, O., Lee, L. J., Frey, B. J., and Blencowe, B. J. (2008). Deep surveying of alternative splicing complexity in the human transcriptome by high-throughput sequencing. *Nat. Genet.* 40, 1413–1415. doi: 10.1038/ng.259

Pan, Y., Weng, J., Cao, Y., Bhosle, R. C., and Zhou, M. (2008). Functional coupling between the Kv1.1 channel and aldoketoreductase Kvbeta1. *J. Biol. Chem.* 283, 8634–8642. doi: 10.1074/jbc.M709304200

Papaioannou, A., Gerozissis, K., Prokopiou, A., Bolaris, S., and Stylianopoulou, F. (2002). Sex differences in the effects of neonatal handling on the animal's response to stress and the vulnerability for depressive behaviour. *Behav. Brain Res.* 129, 131–139. doi: 10.1016/s0166-4328(01)00334-5

Parikshak, N. N., Luo, R., Zhang, A., Won, H., Lowe, J. K., Chandran, V., et al. (2013). Integrative functional genomic analyses implicate specific molecular pathways and circuits in autism. *Cell* 155, 1008–1021. doi: 10.1016/j.cell.2013.10.031

Parras, A., Anta, H., Santos-Galindo, M., Swarup, V., Elorza, A., Nieto-Gonzalez, J. L., et al. (2018). Autism-like phenotype and risk gene mRNA deadenylation by CPEB4 mis-splicing. *Nature* 560, 441–446. doi: 10.1038/s41586-018-0423-5

Petrecca, K., Miller, D. M., and Shrier, A. (2000). Localization and enhanced current density of the Kv4.2 potassium channel by interaction with the actin-binding protein filamin. *J. Neurosci.* 20, 8736–8744. doi: 10.1523/jneurosci.20-23-08736.2000

Picardi, E., D'Erchia, A. M., Lo Giudice, C., and Pesole, G. (2017). REDIportal: a comprehensive database of A-to-I RNA editing events in humans. *Nucleic Acids Res.* 45, D750–D757. doi: 10.1093/nar/gkw767

Piqué, M., López, J. M., Foissac, S., Guigó, R., and Méndez, R. (2008). A combinatorial code for CPE-mediated translational control. *Cell* 132, 434–448. doi: 10.1016/j.cell.2007.12.038

Pluess, M., Belsky, J., Way, B. M., and Taylor, S. E. (2010). 5-HTTLPR moderates effects of current life events on neuroticism: differential susceptibility to environmental influences. *Prog. Neuropsychopharmacol. Biol. Psychiatry* 34, 1070–1074. doi: 10.1016/j.pnpbp.2010.05.028

Poduri, A., Evrony, G. D., Cai, X., and Walsh, C. A. (2013). Somatic mutation, genomic variation, and neurological disease. *Science* 341:1237758. doi: 10.1126/science.1237758

Popa, D., Lena, C., Alexandre, C., and Adrien, J. (2008). Lasting syndrome of depression produced by reduction in serotonin uptake during postnatal development: evidence from sleep, stress, and behavior. *J. Neurosci.* 28, 3546–3554. doi: 10.1523/jneurosci.4006-07.2008

Popowicz, G. M., Schleicher, M., Noegel, A. A., and Holak, T. A. (2006). Filamins: promiscuous organizers of the cytoskeleton. *Trends Biochem. Sci.* 31, 411–419. doi: 10.1016/j.tibs.2006.05.006

Pouillot, F., Blois, H., and Iris, F. (2010). Genetically engineered virulent phage banks in the detection and control of emergent pathogenic bacteria. *Biosecur. Bioterror.* 8, 155–169. doi: 10.1089/bsp.2009.0057

Prem, S., Millonig, J. H., and DiCicco-Bloom, E. (2020). Dysregulation of neurite outgrowth and cell migration in autism and other neurodevelopmental disorders. *Adv. Neurobiol.* 25, 109–153. doi: 10.1007/978-3-030-45493-7_5

Provenzi, L., Giorda, R., Beri, S., and Montirosso, R. (2016). SLC6A4 methylation as an epigenetic marker of life adversity exposures in humans: A systematic review of literature. *Neurosci. Biobehav. Rev.* 71, 7–20. doi: 10.1016/j.neubiorev.2016.08.021

Raj, B., and Blencowe, B. J. (2015). Alternative splicing in the mammalian nervous system: recent insights into mechanisms and functional roles. *Neuron* 87, 14–27. doi: 10.1016/j.neuron.2015.05.004

Raj, B., O'Hanlon, D., Vessey, J. P., Pan, Q., Ray, D., Buckley, N. J., et al. (2011). Cross-regulation between an alternative splicing activator and a transcription repressor controls neurogenesis. *Mol. Cell* 43, 843–850. doi: 10.1016/j.molcel.2011.08.014

Regue, M., Poilbout, C., Martin, V., Franc, B., Lanfumey, L., and Mongeau, R. (2019). Increased 5-HT2C receptor editing predisposes to PTSD-like behaviors and alters BDNF and cytokines signaling. *Transl. Psychiatry* 9:100. doi: 10.1038/s41398-019-0431-8

Rossi, P., De Filippi, G., Armano, S., Taglietti, V., and D'Angelo, E. (1998). The weaver mutation causes a loss of inward rectifier current regulation in premigratory granule cells of the mouse cerebellum. *J. Neurosci.* 18, 3537–3547. doi: 10.1523/jneurosci.18-10-03537.1998

Rula, E. Y., Lagrange, A. H., Jacobs, M. M., Hu, N., Macdonald, R. L., and Emeson, R. B. (2008). Developmental modulation of GABA(A) receptor function by RNA editing. *J. Neurosci.* 28, 6196–6201. doi: 10.1523/jneurosci.0443-08.2008

Sanders, S. J., He, X., Willsey, A. J., Ercan-Sencicek, A. G., Samocha, K. E., Cicek, A. E., et al. (2015). Insights into autism spectrum disorder genomic architecture and biology from 71 risk loci. *Neuron* 87, 1215–1233. doi: 10.1016/j.neuron.2015.09.016

Santos, S. D., Carvalho, A. L., Caldeira, M. V., and Duarte, C. B. (2009). Regulation of AMPA receptors and synaptic plasticity. *Neuroscience* 158, 105–125. doi: 10.1016/j.neuroscience.2008.02.037

Sarachana, T., Zhou, R., Chen, G., Manji, H. K., and Hu, V. W. (2010). Investigation of post-transcriptional gene regulatory networks associated with autism spectrum disorders by microRNA expression profiling of lymphoblastoid cell lines. *Genome Med.* 2:23. doi: 10.1186/gm144

Sarkissian, M., Mendez, R., and Richter, J. D. (2004). Progesterone and insulin stimulation of CPEB-dependent polyadenylation is regulated by Aurora A and glycogen synthase kinase-3. *Genes Dev.* 18, 48–61. doi: 10.1101/gad.1136004

Savva, Y. A., Rieder, L. E., and Reenan, R. A. (2012). The ADAR protein family. *Genome Biol.* 13:252. doi: 10.1186/gb-2012-13-12-252

Scadden, A. D., and Smith, C. W. (2001). RNAi is antagonized by A–>I hyper-editing. *EMBO Rep.* 2, 1107–1111. doi: 10.1093/embo-reports/kve244

Schmauss, C. (2003). Serotonin 2C receptors: suicide, serotonin, and runaway RNA editing. *Neuroscientist* 9, 237–242. doi: 10.1177/1073858403253669

Schratt, G. M., Tuebing, F., Nigh, E. A., Kane, C. G., Sabatini, M. E., Kiebler, M., et al. (2006). A brain-specific microRNA regulates dendritic spine development. *Nature* 439, 283–289. doi: 10.1038/nature04367

Setty, S. R., Tenza, D., Truschel, S. T., Chou, E., Sviderskaya, E. V., Theos, A. C., et al. (2007). BLOC-1 is required for cargo-specific sorting from vacuolar early endosomes toward lysosome-related organelles. *Mol. Biol. Cell* 18, 768–780. doi: 10.1091/mbc.e06-12-1066

Shanmugam, N., Reddy, M. A., and Natarajan, R. (2008). Distinct roles of heterogeneous nuclear ribonuclear protein K and microRNA-16 in cyclooxygenase-2 RNA stability induced by S100b, a ligand of the receptor for advanced glycation end products. *J. Biol. Chem.* 283, 36221–36233. doi: 10.1074/jbc.M806322200

Sheen, V. L., Feng, Y., Graham, D., Takafuta, T., Shapiro, S. S., and Walsh, C. A. (2002). Filamin A and Filamin B are co-expressed within neurons during periods of neuronal migration and can physically interact. *Hum. Mol. Genet.* 11, 2845–2854. doi: 10.1093/hmg/11.23.2845

Si, K., Giustetto, M., Etkin, A., Hsu, R., Janisiewicz, A. M., Miniaci, M. C., et al. (2003). A neuronal isoform of CPEB regulates local protein synthesis and stabilizes synapse-specific long-term facilitation in aplysia. *Cell* 115, 893–904. doi: 10.1016/s0092-8674(03)01021-3

Sibley, C. R. (2014). Regulation of gene expression through production of unstable mRNA isoforms. *Biochem. Soc. Trans.* 42, 1196–1205. doi: 10.1042/bst20140102

Siegert, S., Seo, J., Kwon, E. J., Rudenko, A., Cho, S., Wang, W., et al. (2015). The schizophrenia risk gene product miR-137 alters presynaptic plasticity. *Nat. Neurosci.* 18, 1008–1016. doi: 10.1038/nn.4023

Siianova, E., Lukashev, V. A., Blinov, V. M., and Troianovskii, S. M. (1990). [The determination and analysis of the primary sequence of the human laminin-binding protein]. *Dokl. Akad. Nauk. SSSR* 313, 227–231.

Singh, A., Gebhart, M., Fritsch, R., Sinnegger-Brauns, M. J., Poggiani, C., Hoda, J. C., et al. (2008). Modulation of voltage- and Ca2+-dependent gating of CaV1.3 L-type calcium channels by alternative splicing of a C-terminal regulatory domain. *J. Biol. Chem.* 283, 20733–20744. doi: 10.1074/jbc.M802254200

Siu, M. T., and Weksberg, R. (2017). Epigenetics of autism spectrum disorder. *Adv. Exp. Med. Biol.* 978, 63–90. doi: 10.1007/978-3-319-53889-1_4

Slotkin, W., and Nishikura, K. (2013). Adenosine-to-inosine RNA editing and human disease. *Genome Med.* 5:105. doi: 10.1186/gm508

Song, I., and Huganir, R. L. (2002). Regulation of AMPA receptors during synaptic plasticity. *Trends Neurosci.* 25, 578–588. doi: 10.1016/s0166-2236(02)02270-1

Stark, R., Grzelak, M., and Hadfield, J. (2019). RNA sequencing: the teenage years. *Nat. Rev. Genet.* 20, 631–656. doi: 10.1038/s41576-019-0150-2

Streit, A. K., Derst, C., Wegner, S., Heinemann, U., Zahn, R. K., and Decher, N. (2011). RNA editing of Kv1.1 channels may account for reduced ictogenic potential of 4-aminopyridine in chronic epileptic rats. *Epilepsia* 52, 645–648. doi: 10.1111/j.1528-1167.2011.02986.x

Swartz, K. J. (2004). Towards a structural view of gating in potassium channels. *Nat. Rev. Neurosci.* 5, 905–916. doi: 10.1038/nrn1559

Tadross, M. R., Dick, I. E., and Yue, D. T. (2008). Mechanism of local and global Ca2+ sensing by calmodulin in complex with a Ca2+ channel. *Cell* 133, 1228–1240. doi: 10.1016/j.cell.2008.05.025

Takumi, T., Tamada, K., Hatanaka, F., Nakai, N., and Bolton, P. F. (2020). Behavioral neuroscience of autism. *Neurosci. Biobehav. Rev.* 110, 60–76. doi: 10.1016/j.neubiorev.2019.04.012

Talebizadeh, Z., Butler, M. G., and Theodoro, M. F. (2008). Feasibility and relevance of examining lymphoblastoid cell lines to study role of microRNAs in autism. *Autism Res.* 1, 240–250. doi: 10.1002/aur.33

Tan, M. H., Li, Q., Shanmugam, R., Piskol, R., Kohler, J., Young, A. N., et al. (2017). Dynamic landscape and regulation of RNA editing in mammals. *Nature* 550, 249–254. doi: 10.1038/nature24041

Tariq, A., and Jantsch, M. F. (2012). Transcript diversification in the nervous system: a to I RNA editing in CNS function and disease development. *Front. Neurosci.* 6:99. doi: 10.3389/fnins.2012.00099

Theis, M., Si, K., and Kandel, E. R. (2003). Two previously undescribed members of the mouse CPEB family of genes and their inducible expression in the principal cell layers of the hippocampus. *Proc. Natl. Acad. Sci. U.S.A.* 100, 9602–9607. doi: 10.1073/pnas.1133424100

Theoharides, T. C., Tsilioni, I., Patel, A. B., and Doyle, R. (2016). Atopic diseases and inflammation of the brain in the pathogenesis of autism spectrum disorders. *Transl. Psychiatry* 6:e844. doi: 10.1038/tp.2016.77

Thomas, K. T., Anderson, B. R., Shah, N., Zimmer, S. E., Hawkins, D., Valdez, A. N., et al. (2017). Inhibition of the Schizophrenia-Associated MicroRNA miR-137 Disrupts Nrg1alpha neurodevelopmental signal transduction. *Cell Rep.* 20, 1–12. doi: 10.1016/j.celrep.2017.06.038

Thomas, K. T., Gross, C., and Bassell, G. J. (2018). microRNAs sculpt neuronal communication in a tight balance that is lost in neurological disease. *Front. Mol. Neurosci.* 11:455. doi: 10.3389/fnmol.2018.00455

Tian, N., Yang, Y., Sachsenmaier, N., Muggenhumer, D., Bi, J., Waldsich, C., et al. (2011). A structural determinant required for RNA editing. *Nucleic Acids Res.* 39, 5669–5681. doi: 10.1093/nar/gkr144

Tran, S. S., Jun, H. I., Bahn, J. H., Azghadi, A., Ramaswami, G., Van Nostrand, E. L., et al. (2019). Widespread RNA editing dysregulation in brains from autistic individuals. *Nat. Neurosci.* 22, 25–36. doi: 10.1038/s41593-018-0287-x

Tsivion-Visbord, H., Kopel, E., Feiglin, A., Sofer, T., Barzilay, R., Ben-Zur, T., et al. (2020). Increased RNA editing in maternal immune activation model of neurodevelopmental disease. *Nat. Commun.* 11:5236. doi: 10.1038/s41467-020-19048-6

Tucci, A., Ciaccio, C., Scuvera, G., Esposito, S., and Milani, D. (2016). MIR137 is the key gene mediator of the syndromic obesity phenotype of patients with 1p21.3 microdeletions. *Mol. Cytogenet.* 9:80. doi: 10.1186/s13039-016-0289-x

Turck, C. W., and Iris, F. (2011). Proteome-based pathway modelling of psychiatric disorders. *Pharmacopsychiatry* 44(Suppl. 1), S54–S61. doi: 10.1055/s-0031-1271701

Uemura, T., Lee, S. J., Yasumura, M., Takeuchi, T., Yoshida, T., Ra, M., et al. (2010). Trans-synaptic interaction of GluRdelta2 and Neurexin through Cbln1 mediates synapse formation in the cerebellum. *Cell* 141, 1068–1079. doi: 10.1016/j.cell.2010.04.035

Vaiserman, A. M. (2015). Epigenetic programming by early-life stress: Evidence from human populations. *Dev. Dyn.* 244, 254–265. doi: 10.1002/dvdy.24211

van Spronsen, M., van Battum, E. Y., Kuijpers, M., Vangoor, V. R., Rietman, M. L., Pothof, J., et al. (2013). Developmental and activity-dependent miRNA expression profiling in primary hippocampal neuron cultures. *PLoS One* 8:e74907. doi: 10.1371/journal.pone.0074907

Velasquez, F., Wiggins, J. L., Mattson, W. I., Martin, D. M., Lord, C., and Monk, C. S. (2017). The influence of 5-HTTLPR transporter genotype on amygdala-subgenual anterior cingulate cortex connectivity in autism spectrum disorder. *Dev. Cogn. Neurosci.* 24, 12–20. doi: 10.1016/j.dcn.2016.12.002

Veno, M. T., Bramsen, J. B., Bendixen, C., Panitz, F., Holm, I. E., Ohman, M., et al. (2012). Spatio-temporal regulation of ADAR editing during development in porcine neural tissues. *RNA Biol.* 9, 1054–1065. doi: 10.4161/rna.21082

Vitalis, T., and Rossier, J. (2011). New insights into cortical interneurons development and classification: contribution of developmental studies. *Dev. Neurobiol.* 71, 34–44. doi: 10.1002/dneu.20810

Vogel Ciernia, A., and LaSalle, J. (2016). The landscape of DNA methylation amid a perfect storm of autism aetiologies. *Nat. Rev. Neurosci.* 17, 411–423. doi: 10.1038/nrn.2016.41

Voineagu, I., Wang, X., Johnston, P., Lowe, J. K., Tian, Y., Horvath, S., et al. (2011). Transcriptomic analysis of autistic brain reveals convergent molecular pathology. *Nature* 474, 380–384. doi: 10.1038/nature10110

Vuong, C. K., Black, D. L., and Zheng, S. (2016). The neurogenetics of alternative splicing. *Nat. Rev. Neurosci.* 17, 265–281. doi: 10.1038/nrn.2016.27

Wahlstedt, H., Daniel, C., Enstërö, M., and Ohman, M. (2009). Large-scale mRNA sequencing determines global regulation of RNA editing during brain development. *Genome Res.* 19, 978–986. doi: 10.1101/gr.089409.108

Walker, R. L., Ramaswami, G., Hartl, C., Mancuso, N., Gandal, M. J., de la Torre-Ubieta, L., et al. (2019). Genetic control of expression and splicing in developing human brain informs disease mechanisms. *Cell* 179, 750-771.e722. doi: 10.1016/j.cell.2019.09.021

Wang, E. T., Sandberg, R., Luo, S., Khrebtukova, I., Zhang, L., Mayr, C., et al. (2008). Alternative isoform regulation in human tissue transcriptomes. *Nature* 456, 470–476. doi: 10.1038/nature07509

Wang, E. T., Ward, A. J., Cherone, J. M., Giudice, J., Wang, T. T., Treacy, D. J., et al. (2015). Antagonistic regulation of mRNA expression and splicing by CELF and MBNL proteins. *Genome Res.* 25, 858–871. doi: 10.1101/gr.184390.114

Wang, J., Gong, J., Li, L., Chen, Y., Liu, L., Gu, H., et al. (2018). Neurexin gene family variants as risk factors for autism spectrum disorder. *Autism Res.* 11, 37–43. doi: 10.1002/aur.1881

Wang, Z., and Burge, C. B. (2008). Splicing regulation: from a parts list of regulatory elements to an integrated splicing code. *RNA* 14, 802–813. doi: 10.1261/rna.876308

Watts, T. J. (2008). The pathogenesis of autism. *Clin. Med. Pathol.* 1, 99–103. doi: 10.4137/cpath.s1143

Waye, M. M. Y., and Cheng, H. Y. (2018). Genetics and epigenetics of autism: a review. *Psychiatry Clin. Neurosci.* 72, 228–244. doi: 10.1111/pcn.12606

Wei, H., Alberts, I., and Li, X. (2013). Brain IL-6 and autism. *Neuroscience* 252, 320–325. doi: 10.1016/j.neuroscience.2013.08.025

Weill, L., Belloc, E., Bava, F. A., and Méndez, R. (2012). Translational control by changes in poly(A) tail length: recycling mRNAs. *Nat. Struct. Mol. Biol.* 19, 577–585. doi: 10.1038/nsmb.2311

Wellman, C. L., Izquierdo, A., Garrett, J. E., Martin, K. P., Carroll, J., Millstein, R., et al. (2007). Impaired stress-coping and fear extinction and abnormal corticolimbic morphology in serotonin transporter knock-out mice. *J. Neurosci.* 27, 684–691. doi: 10.1523/jneurosci.4595-06.2007

Weyn-Vanhentenryck, S. M., Mele, A., Yan, Q., Sun, S., Farny, N., Zhang, Z., et al. (2014). HITS-CLIP and integrative modeling define the Rbfox splicing-regulatory network linked to brain development and autism. *Cell Rep.* 6, 1139–1152. doi: 10.1016/j.celrep.2014.02.005

Willemsen, M. H., Valles, A., Kirkels, L. A., Mastebroek, M., Olde Loohuis, N., Kos, A., et al. (2011). Chromosome 1p21.3 microdeletions comprising DPYD and MIR137 are associated with intellectual disability. *J. Med. Genet.* 48, 810–818. doi: 10.1136/jmedgenet-2011-100294

Willsey, A. J., Sanders, S. J., Li, M., Dong, S., Tebbenkamp, A. T., Muhle, R. A., et al. (2013). Coexpression networks implicate human midfetal deep cortical projection neurons in the pathogenesis of autism. *Cell* 155, 997–1007. doi: 10.1016/j.cell.2013.10.020

Wilson, C. A., and Davies, D. C. (2007). The control of sexual differentiation of the reproductive system and brain. *Reproduction* 133, 331–359. doi: 10.1530/rep-06-0078

Winter, C., Djodari-Irani, A., Sohr, R., Morgenstern, R., Feldon, J., Juckel, G., et al. (2009). Prenatal immune activation leads to multiple changes in basal neurotransmitter levels in the adult brain: implications for brain disorders of neurodevelopmental origin such as schizophrenia. *Int. J. Neuropsychopharmacol.* 12, 513–524. doi: 10.1017/s1461145708009206

Wiśniowiecka-Kowalnik, B., and Nowakowska, B. A. (2019). Genetics and epigenetics of autism spectrum disorder-current evidence in the field. *J. Appl. Genet.* 60, 37–47. doi: 10.1007/s13353-018-00480-w

Won, J., Jin, Y., Choi, J., Park, S., Lee, T. H., Lee, S. R., et al. (2017). Melatonin as a novel interventional candidate for fragile X syndrome with autism spectrum disorder in humans. *Int. J. Mol. Sci.* 18:1314. doi: 10.3390/ijms18061314

Wong, C. C., Caspi, A., Williams, B., Craig, I. W., Houts, R., Ambler, A., et al. (2010). A longitudinal study of epigenetic variation in twins. *Epigenetics* 5, 516–526. doi: 10.4161/epi.5.6.12226

Wu, L., Wells, D., Tay, J., Mendis, D., Abbott, M. A., Barnitt, A., et al. (1998). CPEB-mediated cytoplasmic polyadenylation and the regulation of experience-dependent translation of alpha-CaMKII mRNA at synapses. *Neuron* 21, 1129–1139. doi: 10.1016/s0896-6273(00)80630-3

Xue, Y., Ouyang, K., Huang, J., Zhou, Y., Ouyang, H., Li, H., et al. (2013). Direct conversion of fibroblasts to neurons by reprogramming PTB-regulated microRNA circuits. *Cell* 152, 82–96. doi: 10.1016/j.cell.2012.11.045

Yan, Q., Weyn-Vanhentenryck, S. M., Wu, J., Sloan, S. A., Zhang, Y., Chen, K., et al. (2015). Systematic discovery of regulated and conserved alternative exons in the mammalian brain reveals NMD modulating chromatin regulators. *Proc. Natl. Acad. Sci. U.S.A.* 112, 3445–3450. doi: 10.1073/pnas.1502849112

Yang, W., Wang, Q., Howell, K. L., Lee, J. T., Cho, D. S., Murray, J. M., et al. (2005). ADAR1 RNA deaminase limits short interfering RNA efficacy in mammalian cells. *J. Biol. Chem.* 280, 3946–3953. doi: 10.1074/jbc.M407876200

Yang, Y., Okada, S., and Sakurai, M. (2021). Adenosine-to-inosine RNA editing in neurological development and disease. *RNA Biol.* 18, 999–1013. doi: 10.1080/15476286.2020.1867797

Yang, Y. Y., Yin, G. L., and Darnell, R. B. (1998). The neuronal RNA-binding protein Nova-2 is implicated as the autoantigen targeted in POMA patients with dementia. *Proc. Natl. Acad. Sci. U.S.A.* 95, 13254–13259. doi: 10.1073/pnas.95.22.13254

Yano, M., Hayakawa-Yano, Y., Mele, A., and Darnell, R. B. (2010). Nova2 regulates neuronal migration through an RNA switch in disabled-1 signaling. *Neuron* 66, 848–858. doi: 10.1016/j.neuron.2010.05.007

Yuen, R. K., Thiruvahindrapuram, B., Merico, D., Walker, S., Tammimies, K., Hoang, N., et al. (2015). Whole-genome sequencing of quartet families with autism spectrum disorder. *Nat. Med.* 21, 185–191. doi: 10.1038/nm.3792

Zamore, P. D., Tuschl, T., Sharp, P. A., and Bartel, D. P. (2000). RNAi: double-stranded RNA directs the ATP-dependent cleavage of mRNA at 21 to 23 nucleotide intervals. *Cell* 101, 25–33. doi: 10.1016/s0092-8674(00)80620-0

Zhang, X., Chen, M. H., Wu, X., Kodani, A., Fan, J., Doan, R., et al. (2016). Cell-type-specific alternative splicing governs cell fate in the developing cerebral cortex. *Cell* 166, 1147-1162.e1115. doi: 10.1016/j.cell.2016.07.025

Zhang, X., Virtanen, A., and Kleiman, F. E. (2010). To polyadenylate or to deadenylate: that is the question. *Cell Cycle* 9, 4437–4449. doi: 10.4161/cc.9.22.13887

Zhao, L., Li, H., Guo, R., Ma, T., Hou, R., Ma, X., et al. (2013). miR-137, a new target for post-stroke depression? *Neural Regen. Res.* 8, 2441–2448. doi: 10.3969/j.issn.1673-5374.2013.26.005

Zheng, S., and Black, D. L. (2013). Alternative pre-mRNA splicing in neurons: growing up and extending its reach. *Trends Genet.* 29, 442–448. doi: 10.1016/j.tig.2013.04.003

Zhou, X., Tian, F., Sandzen, J., Cao, R., Flaberg, E., Szekely, L., et al. (2007). Filamin B deficiency in mice results in skeletal malformations and impaired microvascular development. *Proc. Natl. Acad. Sci. U.S.A.* 104, 3919–3924. doi: 10.1073/pnas.0608360104

Zuculo, G. M., Goncalves, B. S. B., Brittes, C., Menna-Barreto, L., and Pinato, L. (2017). Melatonin and circadian rhythms in autism: Case report. *Chronobiol. Int.* 34, 527–530. doi: 10.1080/07420528.2017.1308375

Zukin, R. S., Richter, J. D., and Bagni, C. (2009). Signals, synapses, and synthesis: how new proteins control plasticity. *Front. Neural Circ.* 3:14. doi: 10.3389/neuro.04.014.2009

frontiers | Frontiers in Neuroscience

TYPE Review
PUBLISHED 20 March 2023
DOI 10.3389/fnins.2023.1125428

OPEN ACCESS

EDITED BY
Jian-Huan Chen,
Jiangnan University,
China

REVIEWED BY
Norazlin Kamal Nor,
Universiti Kebangsaan Malaysia Medical Center,
Malaysia
Theoharis Constantin Theoharides,
Tufts University,
United States

*CORRESPONDENCE
Yingbo Li
liyingbo@cqmu.edu.cn

†These authors have contributed equally to this work and share first authorship

SPECIALTY SECTION
This article was submitted to Neurodevelopment, a section of the journal Frontiers in Neuroscience

RECEIVED 16 December 2022
ACCEPTED 03 March 2023
PUBLISHED 20 March 2023

CITATION
Xiong Y, Chen J and Li Y (2023) Microglia and astrocytes underlie neuroinflammation and synaptic susceptibility in autism spectrum disorder.
Front. Neurosci. 17:1125428.
doi: 10.3389/fnins.2023.1125428

Microglia and astrocytes underlie neuroinflammation and synaptic susceptibility in autism spectrum disorder

Yue Xiong†, Jianhui Chen† and Yingbo Li*

Cerebrovascular Diseases Laboratory, Institute of Neuroscience, Chongqing Medical University, Chongqing, China

Autism spectrum disorder (ASD) is a common neurodevelopmental disorder with onset in childhood. The mechanisms underlying ASD are unclear. In recent years, the role of microglia and astrocytes in ASD has received increasing attention. Microglia prune the synapses or respond to injury by sequestrating the injury site and expressing inflammatory cytokines. Astrocytes maintain homeostasis in the brain microenvironment through the uptake of ions and neurotransmitters. However, the molecular link between ASD and microglia and, or astrocytes remains unknown. Previous research has shown the significant role of microglia and astrocytes in ASD, with reports of increased numbers of reactive microglia and astrocytes in postmortem tissues and animal models of ASD. Therefore, an enhanced understanding of the roles of microglia and astrocytes in ASD is essential for developing effective therapies. This review aimed to summarize the functions of microglia and astrocytes and their contributions to ASD.

KEYWORDS

autism spectrum disorders, microglia, astrocytes, neuroinflammation, synaptic pruning, mitochondria, methylation

1. Introduction

Autism spectrum disorder (ASD) is a common neurodevelopmental disorder, characterized by impaired social interaction, communication deficits, repetitive behavior, and narrow and intense interests (Kim et al., 2017). Autistic symptoms emerge in childhood and persist throughout life (Christensen et al., 2016). Although the precise etiologies of ASD are complex, recent evidence points to a contribution of glial cells in the pathophysiology of ASD. "Neuroglia" or "glia" include neuro-epithelial cells [oligodendrocytes (OLGs), astrocytes, oligodendrocyte progenitors, and ependymal cells], neural crest cells (peripheral glia), and myeloid cells (microglia) (Escartin et al., 2021). A recent study suggested that the activation of glial cells may contribute to the cognitive and behavioral impairments of ASD (Petrelli et al., 2016). Glial cells not only have neuronal "gluing" roles but are also involved in neurogenesis, synaptogenesis, inflammation, proper glutamate handling, and many other processes (Gzielo and Nikiforuk, 2021).

Microglia, as the resident macrophages in the central nervous system (CNS), act as the first main form of active immune defense in the brain and spinal cord (Kern et al., 2016; Umpierre and Wu, 2021). As the most abundant glial cells in the CNS, astrocytes play important brain functions in early development and adulthood, such as neurogenesis, synaptic development, synaptic transmission and plasticity, and regulate behavior under physiological and pathological conditions (Wang et al., 2021). Some transcriptions support an essential role in glial cell pathophysiology in the autistic brains. Gliosis and increased glial cell proliferation have been

found in human postmortem brain samples (Petrelli et al., 2016). Moreover, glial abnormalities were found using animal models of ASD, such as Rett syndrome (RTT), Fragile X syndrome, and a mouse model of tuberous sclerosis.

This review discussed how microglia and astrocytes regulate the pathogenesis of ASD. In addition, the interaction between microglia and astrocytes in ASD was discussed. Finally, we describe the possible involvement of the mitochondria and methylation in regulating ASD by microglia.

2. Microglia contribute to neuroinflammation in ASD by releasing cytokines to prune synapses

As resident immune cells in the CNS, microglia, which express Iba1, Cx3cr1, CD11b, and F4/80, are the primary mediators of neuroinflammation (Cowan and Petri, 2018; Hickman et al., 2018). They appear on embryonic day eight and mature 2–3 weeks after birth. Their morphology could change from immature amoebae to mature ramify, maintain tissue homeostasis, and exert innate immune functions through their multiple unique phenotypes and ability to transfer functions (Gzielo and Nikiforuk, 2021). Reactive microglia have neuroinflammatory and neuroprotective properties (Voet et al., 2019). Mediators derived from mast cells could activate microglia, causing localized inflammation and leading to symptoms of ASD (Zhang et al., 2012; Skaper et al., 2017; Kempuraj et al., 2019). Microglia could be divided into two activation states: M1 type (classical activation) and M2 type (alternative activation) (Orihuela et al., 2016; Liao et al., 2020). The M1 phenotype microglia produce inflammatory cytokines and reactive oxygen species (ROS), and the M2 phenotype microglia produce anti-inflammatory cytokines and neurotrophins. Microglia rely on CSF1 and transcription factors, such as interleukin (IL)-34 and IRF8 for survival and maintenance (Hickman et al., 2018). They also induce the expression of target inflammatory genes through different signaling pathways, such as JNK, JAK/STAT, ERK1/2, NF-kB, and p38 (Zhang et al., 2012; Skaper et al., 2017; Kempuraj et al., 2019; Voet et al., 2019).

Microglia are indispensable regulators of inflammatory responses in the CNS (Kwon and Koh, 2020). Under physiological circumstances, microglia exert highly efficient surveillance mechanisms to clear invading pathogens and promote tissue repair. Under pathological conditions, the developing brain is very sensitive to environmental stimuli, and it produces a robust inflammatory response that leads to neuroinflammation, in which microglia react (gliosis), proliferates, and recruits peripheral blood white blood cells, thereby amplifying the initial tissue damage, meanwhile, reactive gliosis may exacerbate the inflammatory state caused by immune activation involved in the pathogenesis of ASD (Petrelli et al., 2016). In the present study, the association between reactive microglia and neuroinflammatory responses in ASD was discussed.

2.1. Cytokines and chemokines released by microglia regulate neuroinflammation

Microglia are activated in multiple brain regions of young adults with ASD by functional positron emission tomography (PET) imaging (Petrelli et al., 2016). Increased pro-inflammatory cytokines in blood and cerebrospinal fluid (CSF) and increased microglia number and activation in the postmortem dorsolateral prefrontal cortex (DLPFC) provide strong evidence of neuroinflammation in ASD (Zantomio et al., 2015). In addition, changes were observed in the expression levels of pro-inflammatory (CD68 and IL-1β) and anti-inflammatory genes (IGF1 and IGF1R) in gray- and white-matter tissues of ACC in males with ASD (Sciara et al., 2020). Current studies have shown that the gene expression of anti-inflammatory cytokine IL-37 and pro-inflammatory cytokines IL-18 and TNF increases in the amygdala and dorsolateral prefrontal cortex of children with ASD (Tsilioni et al., 2019). In addition, IL-38 is decreased in the amygdala of children with ASD (Tsilioni et al., 2020).

Chemokines, as a subset of cytokines that guide cell migration, are mainly divided into two categories: CXC chemokines and CC chemokines (including CCL2 (MCP-1), CCL3 (MIP-1α), CCL4 (MIP-1β), CCL5 (RANTES), CCL11 (Eotaxin)). CCL2 is conformably elevated in the brain and blood of individuals with autism and has been extensively studied. CCL2 is produced by microglia and astrocytes in the CNS, and in turn, CCL2 regulates the reactivity, migration, and proliferation of microglia (Matta et al., 2019; Ye et al., 2021). In the offspring of maternal exposure to CAF (cafeteria diet) diet or Poly (I: C) inoculation, CCL2 signaling disrupts social behavior by microglia morphology (Maldonado-Ruiz et al., 2022). Flavonoid methoxy luteolin, a peptide neurotensin (NT) inhibitor, reduced the gene expression and release of proinflammatory cytokines IL-1β, CCL2, and CCL5 in human microglia (Patel et al., 2016). All data support cytokines and chemokines as essential mediators in neuroinflammation and autism-like behaviors (Table 1).

2.2. Microglia prune synapses by phagocytosis and elimination

Microglia are involved in the development of excitatory circuits through engulfing and eliminating of synapses, called "pruning" (Lewis, 2021). ASD is often accompanied by abnormalities in synapses. Evidence showed increased density of dendritic spines and abnormal synaptic structure in the brains of ASD model mice (Kim

TABLE 1 Variations of cytokine and chemokines in ASD.

	Factor	CSF	Whole blood serum
Cytokine			
	TNF-α	Increased	Increased
	IL-6	Increased	Increased
	IL-17	Increased	Increased
	IL-1β	Increased	Increased
Chemokines			
	CCL2	Increased	Not reported
	CCL3	Not reported	Not reported
	CCL4	Not reported	Not reported
	CCL5	Not reported	Not reported
	CCL11	Not reported	Not reported

CSF, cerebrospinal fluid.

et al., 2017). Microglia shape synaptic function and plasticity through dynamic morphological and functional properties (Ben Achour and Pascual, 2010). Synaptic phagocytosis by microglia is one of the most intensively studied methods to regulate synaptic plasticity. Presynaptic and postsynaptic components within microglial lysosomes have been identified by electron microscopy and high-resolution *in vivo* imaging (Paolicelli et al., 2011; Sancho et al., 2021). The complement cascade is one of the classical phagocytosis pathways mediated by microglia, in which complement component 1q (C1q) initiates C3 on neurons to bind complement receptor 3 (CR3) on microglia to target phagocytic synapses (Sancho et al., 2021). In addition, microglia could remove synapses by phagocytosis *via* the CX3C chemokine receptor 1 (CX3CR1) and CR3 pathways (Li et al., 2020). However, microglia could shape neuronal connectivity though non-phagocytic mechanisms. Postsynaptic calcium elevation increases the likelihood of dendritic spine formation due to microglial contact with dendrites. Conversely, microglial contact with dendritic spines could also increase the possibility of spine retraction by modifying the local extracellular matrix and reducing synaptic stability. Dendritic spine dynamics and synaptic AMPAR transport could be influenced by BDNF and TNFα, respectively, secreted by microglia, which perform their function of partially encapsulating synapses rather than engulfing them (Blagburn-Blanco et al., 2022).

In particular, microglia clustered around neurons in the dorsolateral PFC of patients with ASD due to alterations in the spatial structure of microglia (Varghese et al., 2017). On the one hand, microglia constantly palpate the neuronal surface (Bal-Price and Brown, 2001). In a mouse model of PTEN localization in the cytoplasm (Ptenm3m4/m3m4), evidence of cross-communication between neurons and microglia was found, with Ptenm3m4/m3m4 neurons inducing enhanced pruning from naturally activated microglia (Sarn et al., 2021). In primary cultures of rat microglia and neurons, carbon monoxide exerts antineuroinflammatory and neurotrophic effects by regulating microglia–neuron communication (Soares et al., 2022). On the other hand, microglia could cause the death of phagocytosed cells by engulfing live neurons and neuronal progenitors. Changes in the activation state of microglia affect brain development, possibly through the uptake of neural precursor cells by phagocytosis (Brown and Neher, 2014). The phenomenon is mainly divided into "eat-me" and "do not-eat-me." When microglia detect exposed "eat-me" signals, they rapidly recognize and phagocytose neurons or parts of neurons exposed to the signal. In performing phagocytosis, the "do not-eat-me" signal occurs when inhibitory neuron cell surface signals are absent or removed. Phospholipid phosphatic glycerine is a key "eat-me" signal for microglia to phagocytize dead and surviving neurons. Plasminogen activator inhibitor type 1 (PAI1) acts as a "do not-eat-me" signal on neutrophils, inducing microglial migration but also inhibiting VNR-mediated microglial phagocytosis (Brown and Neher, 2014). *In vitro*, microglial inflammation is activated by TNF-α, Toll-like receptor ligand (TLR), or amyloid-β. Upon activation, microglia release sublethal amounts of reactive nitrogen (RNS) and ROS, leading to reversible phosphatidylserine orientation on neurons and thus triggering microglial phagocytosis of them. When agents are not enough to kill neurons directly, they may induce exposure and, or release molecules (UDP, phosphatidylserine, and calreticulin) by exerting sufficient stress on neurons, triggering microglia phagocytosis in stressed but surviving neurons and eventually leading to cell death by phagocytosis (Fricker et al., 2018).

Microglia play a role in ASD by participating in synaptic pruning. Some animal studies provide strong proof. For example, germline mutations in the tumor suppressor gene *PTEN* are one of the monogenic risk cases for ASD. By generating a nuclear-predominant PtenY68H/+ mouse model, prominent reactive microglia were found, accompanied by enhanced phagocytosis (Sarn et al., 2021). Furthermore, deletion of atg7 was shown to cause autism-like behavior in a myeloid cell-specific lysozyme M-Cre mouse model. Then, co-culture with AtG7-deficient microglia impaired synaptosome degradation and increased immature dendritic filopodia (Kim et al., 2017).

TREM2 is involved in the phagocytosis of excess synapses in the CA1 region of the mouse hippocampus during development (Sancho et al., 2021). TREM2$^{-/-}$ mouse models typically displayed altered sociability and repetitive behavior. TREM2 protein levels were often negatively correlated with the severity of symptoms in patients with ASD (Filipello et al., 2018). Neuronal defects caused by Hoxb8-microglial defects and mutations in synaptic components could cause mice to exhibit autism-like behavior (Nagarajan et al., 2018). A mouse model lacking CX3CR1 showed a transient decrease in microglia and a consequent defect in synaptic pruning during the early postnatal period. In a mouse model of microglial Tmem59 deletion, deletion of microglial Tmem59 impaired synaptic phagocytosis, leading to autism-like behavior (Meng et al., 2022). In autism models, a transient decrease in microglia is followed by a synaptic pruning defect, strongly associated with autistic behaviors such as social deficits. These findings further confirmed that disrupted synaptic pruning mediated by microglia might contribute to ASD (Zhan et al., 2014). Microglia play a unique role in establishing and maintaining the delicate balance of excitatory and inhibitory synapses. Dysfunctional social and cognitive behavior was demonstrated to be associated with alterations in excitatory and inhibitory synaptic connections in the mPFC in ASD. In addition, reductions in mPFC spine density have been described in mouse models of ASD. More importantly, inhibitory neuronal function and synapses are modulated by specific ASD risk genes. For example, most of the behavioral features of RTT were reproducible when the risk MECP2 gene was deleted from all GABAergic interneurons (Blagburn-Blanco et al., 2022).

2.3. Microglia modulate the excitatory/inhibition balance in ASD by pruning synapses

Evidence showed that glial cell function is related to an imbalance between excitatory and inhibitory synaptic function (Andoh et al., 2019a,b). The structural and functional breakdown of the balance between E/I synapses is the pathogenesis of CNS diseases. After aberrant synaptic pruning in microglia was discussed, microglial synaptic pruning resulting in synaptic excitatory to inhibitory (E/I) imbalance was explored (Andoh et al., 2019a,b). Neurons receive excitatory and inhibitory inputs and maintain a balance between the two, known as the E/I balance. If the E/I balance is disrupted, such as increased levels of excitatory input, associated with autism, it could affect brain function and social behavior (Pretzsch and Floris, 2020). To date, studies on microglia-mediated synaptic pruning have focused on excitatory synapses (Favuzzi et al., 2021). Microglia participate in glutamate signaling through the Xc system, and the Xc transporter in the Xc system is a chloride-dependent antiporter that could carry

glutamate out of the cell. Microglia produce ROS, which induces glutathione (GSH) deficiency and initiates the TLR4 signaling pathway, causing an increase in Xc expression and resulting in glutamate efflux. The ROS, IL-1β, and TNF-α secreted by microglia impair EAAT function and increase extracellular glutamate levels. In summary, reactive microglia actively interfere with neurotransmission through the impaired glutamate uptake; release of excitotoxins, such as glutamate, D-serine, and ATP; and alteration of glial transmitter release from astrocytes (Kim et al., 2020). Whether microglia also actively shape the developing inhibitory circuit is not known. However, during development, GABA-receptive microglia selectively prune inhibitory synapses, presenting behavioral abnormalities due to disruption of microglial responses, thus highlighting a critical function of microglia-mediated inhibitory synaptic pruning (Favuzzi et al., 2021).

The autism-like phenotype could be altered by altering the excitation–inhibition balance between microglia and astrocytes. Collectively, the present study demonstrated associations between changes in microglia and E/I balance in ASD.

2.4. Sex differences in microglia may underlie ASD susceptibility

The salience network (SN), central executive network (CEN), and default mode network (DMN) are central to ASD symptomatology. Gender differences exist in the functional connectivity of SN, CEN, and DMN in adolescents with ASD. Therefore, sex-specific biological factors should be considered when investigating the neural mechanisms of ASD (Lawrence et al., 2020). ASD is well known to be approximately four times more common in males than in females. The mechanisms underlying this sex-differential risk are not fully understood, making it more difficult to study the mechanisms behind the risk of gender differences in ASD.

Microglia play an important role in the sex difference in ASDs (Schwarz and Bilbo, 2012; Andoh et al., 2019a,b). For example, high expression levels of microglia markers were observed in males (Werling et al., 2016). In a model of exposure to low lead concentrations during pregnancy, increased glial cells proliferation in the cerebellum of lead-exposed male pups led to an increased incidence of autism-like behavior, suggesting that sex-dependent glial cells influence the incidence of autism-like behavior (Choi et al., 2022). Further evidence regarding sex-specific differences in microglia could be found. For example, a genome-wide association study (GWAS) provided evidence of the upregulation of genes, including microglia markers found in the postmortem brains of male patients with ASD (Werling et al., 2016). In addition, one study showed that exaggerated translation of only microglia caused autism-like behavior in male mice (Xu et al., 2020). In conclusion, sex differences in microglia may underlie vulnerabilities to ASD.

3. Neurotransmitter and ion channels expressed by astrocytes facilitate communication between astrocytes and synapses

The immune function of astrocytes is similar to that of microglia (Sofroniew, 2015). From postnatal day 14 to postnatal day 30, astrocytes develop from initial maturation to full maturation (Gzielo and Nikiforuk, 2021). Astrocytes become reactive astrocytes after injury (Kim and Son, 2021). Reactive astrocytes establish immune responses through morphological changes and proliferation. The process achieved is through extension and hypertrophy, distinct from the microglial contraction process. Astrocytes are divided into A1 neurotoxic phenotype and A2 neuroprotective phenotype (Escartin et al., 2021). The A1 astrocyte phenotype is generated by microglia stimulated by lipopolysaccharide (LPS) *via* TNF, IL-1α, and C1q (Giovannoni and Quintana, 2020). In addition, a soluble neurotoxin secreted by A1 astrocytes could quickly kill neurons and mature OLGs. By contrast, A2 astrocytes have repair functions and could upregulate neurotrophic or anti-inflammatory genes to promote neuronal survival and growth. The most generally commonly used specific markers for A1 and A2 astrocytes were C3, S100a10, and PTX3 (Li et al., 2020; Fan and Huo, 2021). Reactive astrocytes have not only harmful effects of aggravating neuro-inflammation and hindering synaptic sprouting or axon growth but also beneficial effects of anti-inflammation, neuroprotection, and blood–brain barrier repair (Hickman et al., 2018; Fan and Huo, 2021).

Sixty-five percent of the 46 most significant autism-associated genes are expressed in astrocytes, according to a recent GWAS analysis (Yu et al., 2013). Astrocytes are found to be activated in those with ASD diagnosis. The expression of a glial fibrillary acidic protein (GFAP) is upregulated when astrocytes are hypertrophic and proliferate, and in children diagnosed with ASD, GFAP levels were found to be three times higher than controls in the brain and CSF (Kern et al., 2016). In addition, the number of GFAP-positive cells changed in a VPA and poly (I: C) model (Zhao et al., 2019; Gzielo and Nikiforuk, 2021). In a 35-day-old VPA rat model, studies have shown that GFAP immunostaining levels were increased in the medial prefrontal cortex and hippocampus (Mony et al., 2018). In addition to GFAP, samples of patients with ASD showed abnormal expression of astrocyte markers AQP4 and CX43 (Sloan and Barres, 2014).

Astrocytes cannot only regulate inflammation but also maintain homeostasis within the brain by modulating synaptic function and plasticity (Matta et al., 2019). In addition, A1 reactive astrocytes induced the formation of fewer synapses than synapses generated by healthy quiescent astrocytes (Liddelow et al., 2017). Microglia have brief periodic contact with synapses, and astrocytes are conversely warped around pre- and post-synapses as part of the tripartite synapse (Matta et al., 2019; Gzielo and Nikiforuk, 2021). A large number of receptors, adhesion molecules, and ion channels are distributed around astrocyte synapses, and they are essential for maintaining synaptic function (Gzielo and Nikiforuk, 2021).

3.1. Astrocytes regulate neurotransmitter homeostasis in ASD

E/I neurotransmission imbalance is involved in the pathogenesis of ASD, mainly by altering glutamatergic and GABAergic neurotransmission (Canitano and Palumbi, 2021). Astrocytes regulate neurotransmitter homeostasis in the CNS by uptaking synaptically released neurotransmitters, such as glutamate, glycine, and γ-aminobutyric acid (GABA), and releasing their precursors back to neurons after metabolism (Sofroniew and Vinters, 2010).

Glutamate is one of the most prevalent universal neurotransmitters released by excitatory neurons in the CNS (Doughty et al., 2020). Astrocytes maintain glutamate homeostasis and prevent glutamate excitotoxicity by controlling the balance of glutamate release and uptake (Mahmoud et al., 2019). The main pathway of glutamate uptake is achieved by two glutamate transporters: Na^+-dependent and -independent transporters (Anderson and Swanson, 2000; Mahmoud et al., 2019). Several studies have provided evidence of changes in astrocyte glutamate in ASD. In a VPA-induced ASD rat model, an increase in glutamate uptake was found at postnatal day 120 (Bristot Silvestrin et al., 2013). In a ^{1}H-MRS model of children with ASD, abnormalities of glutamate metabolites in the anterior cingulate cortex (ACC) were observed through brain functional magnetic resonance imaging (Jiménez-Espinoza et al., 2021). Selective loss of astrocyte-specific Fmr1 knockout mice (i-Astro-Fmr1-cKO) and repair mice (i-Astro-Fmr1-cON) resulted in dysregulation of the glutamate transporter GLT1 and impaired extracellular glutamate uptake. Enhanced cortical neuronal excitability was also found in astrocyte-specific cKO mice (Higashimori et al., 2016). The glutamate transporter GLT1 is vital for regulating the E/I ratio in astrocytes. In an astrocyte-specific GLT1 knockout mouse model, the mice exhibited excessive repetitive behavior (Aida et al., 2015). However, in addition to the glutamate transport described above, glutamine synthetase (GS) also supports the amino acid neurotransmitter cycle. The glutamine used by neurons is dependent on the GS conversion of glutamate. Studies have shown that GABAergic neurons are more dependent on astrocyte glutamine than excitatory neurons, so the lack of astrocyte GS may lead to altered inhibitory neuronal function (Gzielo and Nikiforuk, 2021).

GABA, as a highly representative inhibitory neurotransmitter, regulates the overall functions controlled by the brain, such as the regulation of learning and memory functions. Impaired GABA transmission may be one of the pathological evidence of E/I imbalance. Astrocytes express GABA receptors (GABAR), mainly ionic GABAA and metabolic GABAB receptors, and GABA transporters (GATs), including GAT-1 and GAT-3. Previous studies have reported reductions in GABAergic interneurons and transmission in mouse models of ASD (Kim et al., 2020). Furthermore, in a model of maternal lead exposure, astrogliosis was able to prevent behavioral changes by ensuring high GABA levels (Choi et al., 2022). Meanwhile, inhibition of abnormally elevated GABAergic synaptic transmission in the hippocampal CA1 region has been shown to restore E/I balance and rescue autism-like behavior (Chen et al., 2022). Furthermore, attention was improved, and behavioral hyperactivity was alleviated in mice due to the inhibition of the astrocyte GABAB-Gi pathway in the striatum (Nagai et al., 2021).

3.2. Astrocytes regulate ion channels in ASD

Astrocytes are activated by ion (calcium, sodium, and potassium) transport and are not electrically excited (Gzielo and Nikiforuk, 2021). One of the critical functions of astrocytes is ion homeostasis. Fluctuations in intracellular ion concentration could mediate astrocyte excitability (Kirischuk et al., 2012). Glutamate release from astrocytes is achieved by the elevation of $[Ca^{2+}]i$ in astrocytes (Parpura et al., 1994; Bezzi et al., 1998). Ca^{2+} signaling is thought to underlie essential physiological functions of astrocytes in various species, such as worms, flies, zebrafish, mice, and possibly humans (Yu et al., 2020). Elevations in astrocytes' Ca^{2+} could cause the release of gliotransmitters, glutamate, GABA, adenosine triphosphate (ATP), and D-serine, which could all modulate postsynaptic neuronal activity and act on presynaptic receptors. Ca^{2+} waves could propagate vasoactive messengers to the soma and its vascular endfeet through astrocytes (Bazargani and Attwell, 2016). In inflammation, the disruption of astrocyte calcium signaling is important (Allen et al., 2022). However, whether astrocytes play a mechanistic role in ASD through Ca^{2+} signaling remains unclear. In astrocyte-specific inositol 1,4,5-triphosphate six receptor type 2 (IP3R2) knockout mice and IP3R2-null mutant mice, IP3R2 led to astrocyte activation through the release of intracellular Ca^{2+} stores. The results suggested that astrocyte dysfunction by Ca^{2+} ions is associated with ASD-like phenotypes (Wang et al., 2021). In addition, astrocytes from individuals with ASD alter behavior and disrupt neuronal activity through abnormal Ca^{2+} signaling (Allen et al., 2022). All the evidence provides that Ca^{2+} signaling has critical physiological functions in ASD. Therefore, calcium signaling-induced changes in astrocytes could be an essential target for intervention in ASD.

Recent studies have shown that perisynaptic astrocyte cytosolic Na^+ concentration ($[Na^+]i$) could be triggered by neuronal activity, resulting in a transient increase. Na^+-permeable channels and Na^+-dependent transporters control $[Na^+]i$ transients, and astrocyte homeostasis responses are dynamically counter-regulated by $[Na^+]i$. For example, $[Na^+]i$ transients dynamically regulate the transmembrane transport of neurotransmitters, the metabolism/signal utilization of lactate and glutamate, and K^+ buffering (Kirischuk et al., 2012). Neurotransmitters, ion transport, amino acids, and many other molecules across the plasma membrane and inner membrane provide energy through an inwardly directed large sodium (+) gradient that puts sodium homeostasis at a central stage in astrocyte physiology. Na(+)/K(+)-ATPase (NKA), as the primary energy consumer of the brain, mediates Na(+) efflux from astrocytes, thereby maintaining Na(+) homeostasis (Rose and Verkhratsky, 2016). Available sodium channels and astrocyte expression have been confirmed by patch-clamp recordings. Importantly, Voltage-dependent sodium currents have been detected in astrocytes within the spinal cord and hippocampal slices (Pappalardo et al., 2016). Astrocytes buffer K^+ by inward rectifying potassium channels (Kir) and aquaporin 4 (Aqp4) and regulating the flow of water and K^+ between the extracellular space and neuronal cells, resulting in an imbalance between neuronal excitation and inhibition (Iliff et al., 2012; Gzielo and Nikiforuk, 2021). For example, impaired astrocyte K^+ buffering, which results in increased neuronal excitation, is due to a loss of water channels, such as Aqp4, which underlies much of autism (Gzielo and Nikiforuk, 2021). In addition, riluzole, a sodium channel blocker, could effectively increase the inhibition index and normalize PFC functional connectivity in ASD (Sohal and Rubenstein, 2019). All the evidence shows the essential physiological functions of Na(+)/K(+) in ASD. Therefore, Na(+)/K(+) signaling-induced changes in astrocytes could be an essential target for intervention

in ASD. In conclusion, astrocytes maintain the balance of cellular E/I ratio, thus promoting homeostasis in the CNS in ASD.

3.3. Astrocytes pruning synapses by expressing neurotransmitter receptors and transporters

Many neurotransmitter receptors and transporters expressed by astrocytes facilitate communication between astrocytes and synapses. For example, astrocytes could modulate synaptic transmission by inhibiting glutamate release from presynaptic neurons and altering receptor expression on postsynaptic neurons. They also trigger the phagocytic pathway through the expressing multiple epidermal growth factor-like domain protein 10 (MEGF10) and MER tyrosine-protein kinase (MERTK), thereby promoting synapse elimination. In addition, astrocytes indirectly trigger synapse elimination by secreting TGF-β, which induces C1q expression in retinal neurons to initiate microglia-mediated phagocytosis.

These findings suggested that astrocyte function may be relevant to the pathophysiology of ASD, such as its ability to influence neuronal circuits that are highly dynamic and plastic in the adult brain (Matta et al., 2019). Recent studies have found that astrocyte complement component 4 (C4) was significantly expressed in the anterior part of the human brain, the sub-ependymal zone (SVZ), and the surrounding area. Alternatively, the C4 protein was localized to neuronal cell bodies and synapses, suggesting that astrocytes may exert synaptic elimination effects through the C4 pathway (Mou et al., 2022).

Some evidence indicated reciprocal communication between astrocytes and neurons in -vitro and -vivo experiments. In a mutant RTT mouse model, the typical morphology of wild-type or mutant hippocampal neurons was disrupted by a vitro co-culture system of astrocytes (Ballas et al., 2009). Using pluripotent stem cells derived from non-syndromic ASD individuals, ASD-derived astrocytes were found to interfere with normal neuronal development through co-culture experiments (Russo et al., 2018). These findings further suggested that neuronal function may be affected by the inflammation of astrocytes (Lee et al., 2020).

4. The co-ordination of microglia and astrocyte modulates inflammation by the inflammatory mediator and secretion of multiple cytokines

Bidirectional communication exists between microglia and astrocytes, and it modulates CNS inflammation through the inflammatory mediator and secretion of multiple cytokines. In conclusion, the basis of neuronal function and dysfunction is microglia–astrocyte crosstalk (Jha et al., 2019). LPS-activated microglia induce reactive astrocytes (Liu et al., 2020), and, in turn, microglia are further activated by ATP released from reactive astrocytes (Traetta et al., 2021). LPS-activated microglia also induce a neurotoxic phenotype in reactive astrocytes. For example, recent studies have found that micro1glial cells secreting interleukins and chemokines, macrophage colony-stimulating factor (M-CSF), monocyte chemoattractant protein-1 (MCP-1), macrophage inflammatory protein-1α/β (MIP-α/β), TNF-α, and C1q could induce a transcriptional response in astrocytes, activating a neurotoxic factor that reduces the expression of neurotrophic factors (Zhang et al., 2010; Linnerbauer et al., 2020). In addition, microglia and astrocytes could be polarized into M2-type microglia and A2-type astrocytes, respectively, by *in-vitro* crosstalk (Kim and Son, 2021).

ORM2, a member of the lipocalin family expressed by astrocytes, regulates microglial activation in response to inflammatory stimuli. Astrocytic ORM2 could bind to the microglial C-C chemokine receptor type 5 (CCR5) and affect microglial activation by blocking the chemokine C-X-C motif ligand (CXCL)-4-CCR5 interaction, indicating the role of ORM2 in astrocyte–microglia interaction (Jo et al., 2017). In microglia–astrocyte co-cultures from VPA animals, microglia exhibited reactivity and exacerbated astrocyte reactivity (Traetta et al., 2021). Thus, the present study highlighted microglia–astrocyte communication as a novel mechanism of neuro-inflammation in ASD. Therefore, this crosstalk could be considered a potential target for intervention in ASD.

5. Mitochondria and methylation may be involved in the regulation of ASD by microglia

Mitochondria are dynamic organelles that undergo rapid changes in their structure and intracellular localization in the face of the needs of different cells (Ho and Theiss, 2022). One of the most common metabolic disorders in patients with ASD is abnormal mitochondrial function. In the latest study, PM2.5 exposure mediated through the mitochondria during gestation and early life could increase the risk of developing ASD (Frye et al., 2021a,b). Clinical epidemiological studies have demonstrated mitochondrial dysfunction in neurodevelopmental disorders (Thangaraj et al., 2018). Evidence suggests that mitochondrial DNA (mtDNA) is a major activator of inflammation when it leaks from stressed mitochondria (Zhong et al., 2019). Moreover, mtDNA escaping stressed mitochondria provokes inflammation *via* cGAS-STING pathway activation, and when oxidized (Ox-mtDNA), it binds to cytosolic NLRP3, thereby triggering inflammasome activation (Xian et al., 2022). In patients with myalgic encephalomyelitis/chronic fatigue syndrome (ME/CFS), who manifests with fatigue, malaise, sleep disorders, and cognitive problems, the exosome-associated mtDNA could stimulate human microglia to release IL-1β (Tsilioni et al., 2022). Moreover, mtDNA is significantly increased in the serum of children with ASD (Theoharides et al., 2013). In addition, FOXP1 syndrome, caused by haploinsufficiency of the forkhead box P1 (FOXP1) gene, is a neurodevelopmental disorder that manifests as motor dysfunction, intellectual disability, language impairment, and autism. Emerging evidence of mitochondrial dysfunction in $FOXP1^{+/-}$ mice suggested that inadequate energy supply and excessive oxidative stress underlie cognitive and motor impairments caused by FOXP1 deficiency (Wang et al., 2022). In addition, odor identification impairment in ASD may be associated with mitochondrial dysfunction (Yang et al., 2022). The mitochondria are involved in astrocyte maturation and synapse formation. The microglia from embryonic ischemic cortical rats could proliferate by transplanting hamster mitochondria (Gyllenhammer et al., 2022). Therefore, mitochondrial dysfunction may play an important role in inducing glial abnormalities in autism.

DNA methylation has become an area of particular interest in ASD (Williams and LaSalle, 2022). Children with autism exhibit impaired methylation (Deth et al., 2008). Impaired methylation and epigenetic disruption contribute to the immune dysfunction commonly seen in autism (Deth et al., 2008). A study found that differentially methylated regions were enriched for transcription factor binding sites related to regulating microglial inflammation and microglial development (Vogel Ciernia et al., 2018). In brain cells, Methyl CpG binding protein-2 (MeCP2) isoforms (E1 and E2) are an important epigenetic regulator. MeCP2 loss- or gain-of-function mutation causes neurodevelopmental disorders, including ASD, MECP2 duplication syndrome, and RTT (Lioy et al., 2011; Liyanage et al., 2019). Studies from animal models of RTT and *MECP2* could explain the malfunction of epigenetic mechanisms in microglia. MeCP2 participates in the regulation of gene transcription by binding to methylated CG sites. A major study showed an RTT-like phenotype in microglia-specific MECP2 knockout mice that could be reversed by supplementation with wild-type microglia. In addition, the deletion of MECP2 in microglia was demonstrated to cause abnormalities in extracellular glutamate levels and neuronal dendrites. These studies suggested that MeCP2 influences mouse behavior by regulating the epigenetic machinery in microglia. Subsequently, other genes associated with ASD, OXTR, MAGEL2, SNRPN, RELN, and GAD1, were found to have hypermethylated transcription start sites in ASD brains, resulting in reduced expression of gene products (Tremblay and Jiang, 2019). While the exact role of microglia is not completely defined, much evidence could suggest that the epigenetic regulation of microglia plays a vital part in the etiology of ASD (Nardone and Elliott, 2016).

6. Conclusion

The roles of microglia and astrocytes in ASD were reviewed (Figure 1). Until recently, the role of glial cells was not appreciated in ASD pathogenesis, so neuro-pharmacological strategies to treat symptoms were almost exclusively targeted at neuronal activity and synaptic transmission. First, this review proposes that glial cells could regulate inflammation, synaptic function, and plasticity. In addition, altered neurotransmitters create an abnormal imbalance caused by changes in receptor and transporter expression levels, modification of released glial transmitters, and dysfunction of uptake. Then, the data suggest that glial cell interactions are at least partially involved in the pathogenesis of ASD and that future pharmacological studies should consider improving glial cell functions. In the end, the epigenetics of glial cells should also be considered in the pathogenesis of ASD,

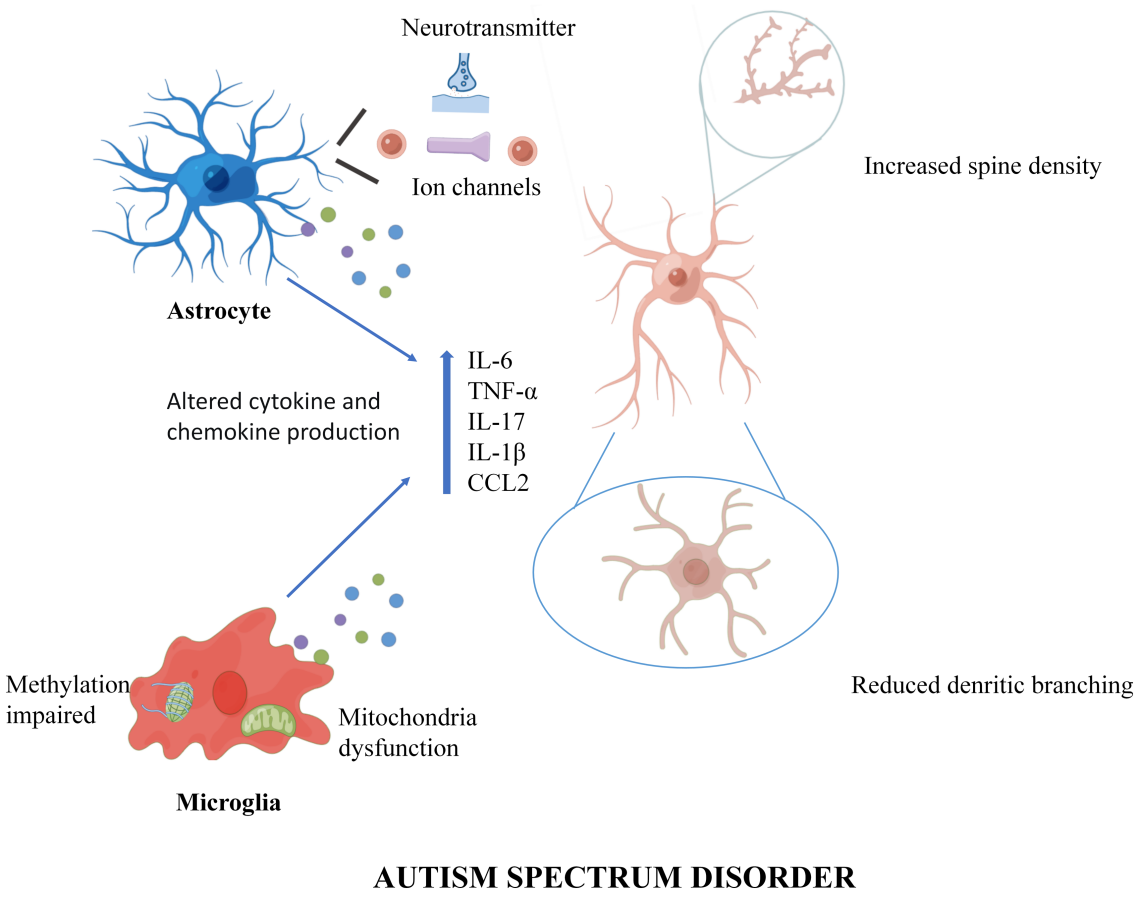

FIGURE 1
A working model of Microglia and Astrocytes underlie neuroinflammation and synaptic susceptibility in Autism Spectrum Disorder. In ASD, astrocytes enhance synaptic pruning through ion channels and neurotransmitters, while microglia trim synapses through intracellular methylation and mitochondrial alterations. In addition, both microglia and astrocytes can cause neuroinflammation and synaptic changes by releasing inflammatory cytokines and chemokines. Figures were created by Figdraw (www.figdraw.com).

suggesting that the study of glial cells may help develop new therapeutic targets for ASD.

Author contributions

YX and JC designed the study and wrote the manuscript. YL contributed to revising the manuscript. All authors contributed to the article and approved the submitted version.

Funding

This study was supported by the Natural Science Foundation of Chongqing (No. cstc2021jcyj-msxmX0065).

Conflict of interest

The authors declare that the research was conducted in the absence of any commercial or financial relationships that could be construed as a potential conflict of interest.

Publisher's note

All claims expressed in this article are solely those of the authors and do not necessarily represent those of their affiliated organizations, or those of the publisher, the editors and the reviewers. Any product that may be evaluated in this article, or claim that may be made by its manufacturer, is not guaranteed or endorsed by the publisher.

References

Aida, T., Yoshida, J., Nomura, M., Tanimura, A., Iino, Y., Soma, M., et al. (2015). Astroglial glutamate transporter deficiency increases synaptic excitability and leads to pathological repetitive behaviors in mice. *Neuropsychopharmacology* 40, 1569–1579. doi: 10.1038/npp.2015.26

Allen, M., Huang, B. S., Notaras, M. J., Lodhi, A., Barrio-Alonso, E., Lituma, P. J., et al. (2022). Astrocytes derived from ASD individuals alter behavior and destabilize neuronal activity through aberrant Ca2+ signaling. *Mol. Psychiatry* 27, 2470–2484. doi: 10.1038/s41380-022-01486-x

Anderson, C. M., and Swanson, R. A. (2000). Astrocyte glutamate transport: review of properties, regulation, and physiological functions. *Glia* 32, 1–14. doi: 10.1002/1098-1136(200010)32:1<1::AID-GLIA10>3.0.CO;2-W

Andoh, M., Ikegaya, Y., and Koyama, R. (2019a). Microglia as possible therapeutic targets for autism spectrum disorders. *Prog. Mol. Biol. Transl. Sci.* 167, 223–245. doi: 10.1016/bs.pmbts.2019.06.012

Andoh, M., Ikegaya, Y., and Koyama, R. (2019b). Synaptic pruning by microglia in epilepsy. *J. Clin. Med.* 8:2170. doi: 10.3390/jcm8122170

Ballas, N., Lioy, D. T., Grunseich, C., and Mandel, G. (2009). Non-cell autonomous influence of MeCP2-deficient glia on neuronal dendritic morphology. *Nat. Neurosci.* 12, 311–317. doi: 10.1038/nn.2275

Bal-Price, A., and Brown, G. C. (2001). Inflammatory neurodegeneration mediated by nitric oxide from activated glia-inhibiting neuronal respiration, causing glutamate release and excitotoxicity. *J. Neurosci.* 21, 6480–6491. doi: 10.1523/JNEUROSCI.21-17-06480.2001

Bazargani, N., and Attwell, D. (2016). Astrocyte calcium signaling: the third wave. *Nat. Neurosci.* 19, 182–189. doi: 10.1038/nn.4201

Ben Achour, S., and Pascual, O. (2010). Glia: the many ways to modulate synaptic plasticity. *Neurochem. Int.* 57, 440–445. doi: 10.1016/j.neuint.2010.02.013

Bezzi, P., Carmignoto, G., Pasti, L., Vesce, S., Rossi, D., Rizzini, B. L., et al. (1998). Prostaglandins stimulate calcium-dependent glutamate release in astrocytes. *Nature* 391, 281–285. doi: 10.1038/34651

Blagburn-Blanco, S. V., Chappell, M. S., De Biase, L. M., and DeNardo, L. A. (2022). Synapse-specific roles for microglia in development: new horizons in the prefrontal cortex. *Front. Mol. Neurosci.* 15:965756. doi: 10.3389/fnmol.2022.965756

Bristot Silvestrin, R., Bambini-Junior, V., Galland, F., Daniele Bobermim, L., Quincozes-Santos, A., Torres Abib, R., et al. (2013). Animal model of autism induced by prenatal exposure to valproate: altered glutamate metabolism in the hippocampus. *Brain Res.* 1495, 52–60. doi: 10.1016/j.brainres.2012.11.048

Brown, G. C., and Neher, J. J. (2014). Microglial phagocytosis of live neurons. *Nat. Rev. Neurosci.* 15, 209–216. doi: 10.1038/nrn3710

Canitano, R., and Palumbi, R. (2021). Excitation/inhibition modulators in autism spectrum disorder: current clinical research. *Front. Neurosci.* 15:753274. doi: 10.3389/fnins.2021.753274

Chen, J., Ma, X. L., Zhao, H., Wang, X. Y., Xu, M. X., Wang, H., et al. (2022). Increasing astrogenesis in the developing hippocampus induces autistic-like behavior in mice via enhancing inhibitory synaptic transmission. *Glia* 70, 106–122. doi: 10.1002/glia.24091

Choi, J., Kim, Y. S., Kim, M. H., Kim, H. J., and Yoon, B. E. (2022). Maternal lead exposure induces sex-dependent cerebellar glial alterations and repetitive behaviors. *Front. Cell. Neurosci.* 16:954807. doi: 10.3389/fncel.2022.954807

Christensen, D. L., Bilder, D. A., Zahorodny, W., Pettygrove, S., Durkin, M. S., Fitzgerald, R. T., et al. (2016). Prevalence and characteristics of autism Spectrum disorder among 4-year-old children in the autism and developmental disabilities monitoring network. *J. Dev. Behav. Pediatr.* 37, 1–8. doi: 10.1097/DBP.0000000000000235

Cowan, M., and Petri, W. A. Jr. (2018). Microglia: immune regulators of neurodevelopment. *Front. Immunol.* 9:2576. doi: 10.3389/fimmu.2018.02576

Deth, R., Muratore, C., Benzecry, J., Power-Charnitsky, V. A., and Waly, M. (2008). How environmental and genetic factors combine to cause autism: a redox/methylation hypothesis. *Neurotoxicology* 29, 190–201. doi: 10.1016/j.neuro.2007.09.010

Doughty, P. T., Hossain, I., Gong, C., Ponder, K. A., Pati, S., Arumugam, P. U., et al. (2020). Novel microwire-based biosensor probe for simultaneous real-time measurement of glutamate and GABA dynamics in vitro and in vivo. *Sci. Rep.* 10:12777. doi: 10.1038/s41598-020-69636-1

Escartin, C., Galea, E., Lakatos, A., O'Callaghan, J. P., Petzold, G. C., Serrano-Pozo, A., et al. (2021). Reactive astrocyte nomenclature, definitions, and future directions. *Nat. Neurosci.* 24, 312–325. doi: 10.1038/s41593-020-00783-4

Fan, Y. Y., and Huo, J. (2021). A1/A2 astrocytes in central nervous system injuries and diseases: angels or devils? *Neurochem. Int.* 148:105080. doi: 10.1016/j.neuint.2021.105080

Favuzzi, E., Huang, S., Saldi, G. A., Binan, L., Ibrahim, L. A., Fernández-Otero, M., et al. (2021). GABA-receptive microglia selectively sculpt developing inhibitory circuits. *Cells* 184, 4048–4063.e32. doi: 10.1016/j.cell.2021.06.018

Filipello, F., Morini, R., Corradini, I., Zerbi, V., Canzi, A., Michalski, B., et al. (2018). The microglial innate immune receptor TREM2 is required for synapse elimination and Normal brain connectivity. *Immunity* 48, 979–991.e8. doi: 10.1016/j.immuni.2018.04.016

Fricker, M., Tolkovsky, A. M., Borutaite, V., Coleman, M., and Brown, G. C. (2018). Neuronal cell death. *Physiol. Rev.* 98, 813–880. doi: 10.1152/physrev.00011.2017

Frye, R. E., Cakir, J., Rose, S., Delhey, L., Bennuri, S. C., Tippett, M., et al. (2021a). Prenatal air pollution influences neurodevelopment and behavior in autism spectrum disorder by modulating mitochondrial physiology. *Mol. Psychiatry* 26, 1561–1577. doi: 10.1038/s41380-020-00885-2

Frye, R. E., Cakir, J., Rose, S., Palmer, R. F., Austin, C., Curtin, P., et al. (2021b). Mitochondria may mediate prenatal environmental influences in autism Spectrum disorder. *J Pers Med.* 11:218. doi: 10.3390/jpm11030218

Giovannoni, F., and Quintana, F. J. (2020). The role of astrocytes in CNS inflammation. *Trends Immunol.* 41, 805–819. doi: 10.1016/j.it.2020.07.007

Gyllenhammer, L. E., Rasmussen, J. M., Bertele, N., Halbing, A., Entringer, S., Wadhwa, P. D., et al. (2022). Maternal inflammation during pregnancy and offspring brain development: the role of mitochondria. *Biol. Psychiatry Cogn. Neurosci. Neuroimag.* 7, 498–509. doi: 10.1016/j.bpsc.2021.11.003

Gzielo, K., and Nikiforuk, A. (2021). Astroglia in autism spectrum disorder. *Int. J. Mol. Sci.* 22:11544. doi: 10.3390/ijms222111544

Hickman, S., Izzy, S., Sen, P., Morsett, L., and El Khoury, J. (2018). Microglia in neurodegeneration. *Nat. Neurosci.* 21, 1359–1369. doi: 10.1038/s41593-018-0242-x

Higashimori, H., Schin, C. S., Chiang, M. S., Morel, L., Shoneye, T. A., Nelson, D. L., et al. (2016). Selective deletion of astroglial FMRP dysregulates glutamate transporter GLT1 and contributes to fragile X syndrome phenotypes in vivo. *J. Neurosci.* 36, 7079–7094. doi: 10.1523/JNEUROSCI.1069-16.2016

Ho, G. T., and Theiss, A. L. (2022). Mitochondria and inflammatory bowel diseases: toward a stratified therapeutic intervention. *Annu. Rev. Physiol.* 84, 435–459. doi: 10.1146/annurev-physiol-060821-083306

Iliff, J. J., Wang, M., Liao, Y., Plogg, B. A., Peng, W., Gundersen, G. A., et al. (2012). A paravascular pathway facilitates CSF flow through the brain parenchyma and the

clearance of interstitial solutes, including amyloid β. *Sci. Transl. Med.* 4:147ra111. doi: 10.1126/scitranslmed.3003748

Jha, M. K., Jo, M., Kim, J. H., and Suk, K. (2019). Microglia-astrocyte crosstalk: an intimate molecular conversation. *Neuroscientist* 25, 227–240. doi: 10.1177/1073858418783959

Jiménez-Espinoza, C., Marcano Serrano, F., and González-Mora, J. L. (2021). N-acetylaspartyl-glutamate metabolism in the cingulated cortices as a biomarker of the etiology in ASD: a 1H-MRS model. *Molecules* 26:675. doi: 10.3390/molecules26030675

Jo, M., Kim, J. H., Song, G. J., Seo, M., Hwang, E. M., and Suk, K. (2017). Astrocytic orosomucoid-2 modulates microglial activation and neuroinflammation. *J. Neurosci.* 37, 2878–2894. doi: 10.1523/JNEUROSCI.2534-16.2017

Kempuraj, D., Thangavel, R., Selvakumar, G. P., Ahmed, M. E., Zaheer, S., Raikwar, S. P., et al. (2019). Mast cell proteases activate astrocytes and glia-neurons and release Interleukin-33 by activating p38 and ERK1/2 MAPKs and NF-κB. *Mol. Neurobiol.* 56, 1681–1693. doi: 10.1007/s12035-018-1177-7

Kern, J. K., Geier, D. A., Sykes, L. K., and Geier, M. R. (2016). Relevance of neuroinflammation and encephalitis in autism. *Front. Cell. Neurosci.* 9:519. doi: 10.3389/fncel.2015.00519

Kim, H. J., Cho, M. H., Shim, W. H., Kim, J. K., Jeon, E. Y., Kim, D. H., et al. (2017). Deficient autophagy in microglia impairs synaptic pruning and causes social behavioral defects. *Mol. Psychiatry* 22, 1576–1584. doi: 10.1038/mp.2016.103

Kim, Y. S., Choi, J., and Yoon, B. E. (2020). Neuron-glia interactions in neurodevelopmental disorders. *Cells* 9:2176. doi: 10.3390/cells9102176

Kim, S., and Son, Y. (2021). Astrocytes stimulate microglial proliferation and M2 polarization in vitro through crosstalk between astrocytes and microglia. *Int. J. Mol. Sci.* 22:8800. doi: 10.3390/ijms22168800

Kirischuk, S., Parpura, V., and Verkhratsky, A. (2012). Sodium dynamics: another key to astroglial excitability? *Trends Neurosci.* 35, 497–506. doi: 10.1016/j.tins.2012.04.003

Kwon, H. S., and Koh, S. H. (2020). Neuroinflammation in neurodegenerative disorders: the roles of microglia and astrocytes. *Transl. Neurodegener.* 9:42. doi: 10.1186/s40035-020-00221-2

Lawrence, K. E., Hernandez, L. M., Bowman, H. C., Padgaonkar, N. T., Fuster, E., Jack, A., et al. (2020). Sex differences in functional connectivity of the salience, default mode, and central executive networks in youth with ASD. *Cereb. Cortex* 30, 5107–5120. doi: 10.1093/cercor/bhaa105

Lee, K. M., Hawi, Z. H., Parkington, H. C., Parish, C. L., Kumar, P. V., Polo, J. M., et al. (2020). The application of human pluripotent stem cells to model the neuronal and glial components of neurodevelopmental disorders. *Mol. Psychiatry* 25, 368–378. doi: 10.1038/s41380-019-0495-0

Lewis, S. (2021). Microglia prune inhibitory synapses, too. *Nat. Rev. Neurosci.* 22:517. doi: 10.1038/s41583-021-00504-1

Li, T., Liu, T., Chen, X., Li, L., Feng, M., Zhang, Y., et al. (2020). Microglia induce the transformation of A1/A2 reactive astrocytes via the CXCR7/PI3K/Akt pathway in chronic post-surgical pain. *J. Neuroinflammat.* 17:211. doi: 10.1186/s12974-020-01891-5

Liao, X., Yang, J., Wang, H., and Li, Y. (2020). Microglia mediated neuroinflammation in autism spectrum disorder. *J. Psychiatr. Res.* 130, 167–176. doi: 10.1016/j.jpsychires.2020.07.013

Liddelow, S. A., Guttenplan, K. A., Clarke, L. E., Bennett, F. C., Bohlen, C. J., Schirmer, L., et al. (2017). Neurotoxic reactive astrocytes are induced by activated microglia. *Nature* 541, 481–487. doi: 10.1038/nature21029

Linnerbauer, M., Wheeler, M. A., and Quintana, F. J. (2020). Astrocyte crosstalk in CNS inflammation. *Neuron* 108, 608–622. doi: 10.1016/j.neuron.2020.08.012

Lioy, D. T., Garg, S. K., Monaghan, C. E., Raber, J., Foust, K. D., Kaspar, B. K., et al. (2011). A role for glia in the progression of Rett's syndrome. *Nature* 475, 497–500. doi: 10.1038/nature10214

Liu, L. R., Liu, J. C., Bao, J. S., Bai, Q. Q., and Wang, G. Q. (2020). Interaction of microglia and astrocytes in the neurovascular unit. *Front. Immunol.* 11:1024. doi: 10.3389/fimmu.2020.01024

Liyanage, V. R. B., Olson, C. O., Zachariah, R. M., Davie, J. R., and Rastegar, M. (2019). DNA methylation contributes to the differential expression levels of Mecp2 in male mice neurons and astrocytes. *Int. J. Mol. Sci.* 20:1845. doi: 10.3390/ijms20081845

Mahmoud, S., Gharagozloo, M., Simard, C., and Gris, D. (2019). Astrocytes maintain glutamate homeostasis in the CNS by controlling the balance between glutamate uptake and release. *Cells* 8:184. doi: 10.3390/cells8020184

Maldonado-Ruiz, R., Trujillo-Villarreal, L. A., Montalvo-Martínez, L., Mercado-Gómez, O. F., Arriaga-Ávila, V., Garza-Ocañas, L., et al. (2022). MCP-1 signaling disrupts social behavior by modulating brain volumetric changes and microglia morphology. *Mol. Neurobiol.* 59, 932–949. doi: 10.1007/s12035-021-02649-7

Matta, S. M., Hill-Yardin, E. L., and Crack, P. J. (2019). The influence of neuroinflammation in autism Spectrum disorder. *Brain Behav. Immun.* 79, 75–90. doi: 10.1016/j.bbi.2019.04.037

Meng, J., Han, L., Zheng, N., Wang, T., Xu, H., Jiang, Y., et al. (2022). Microglial Tmem59 deficiency impairs phagocytosis of synapse and leads to autism-like behaviors in mice. *J. Neurosci.* 42, 4958–4979. doi: 10.1523/JNEUROSCI.1644-21.2022

Mony, T. J., Lee, J. W., Kim, S. S., Chun, W., and Lee, H. J. (2018). Early postnatal valproic acid exposure increase the protein level of astrocyte markers in frontal cortex of rat. *Clin. Psychopharmacol. Neurosci.* 16, 214–217. doi: 10.9758/cpn.2018.16.2.214

Mou, T. M., Lane, M. V., Ireland, D. D. C., Verthelyi, D., Tonelli, L. H., and Clark, S. M. (2022). Association of complement component 4 with neuroimmune abnormalities in the subventricular zone in schizophrenia and autism spectrum disorders. *Neurobiol. Dis.* 173:105840. doi: 10.1016/j.nbd.2022.105840

Nagai, J., Yu, X., Papouin, T., Cheong, E., Freeman, M. R., Monk, K. R., et al. (2021). Behaviorally consequential astrocytic regulation of neural circuits. *Neuron* 109, 576–596. doi: 10.1016/j.neuron.2020.12.008

Nagarajan, N., Jones, B. W., West, P. J., Marc, R. E., and Capecchi, M. R. (2018). Corticostriatal circuit defects in Hoxb8 mutant mice. *Mol. Psychiatry* 23, 1868–1877. doi: 10.1038/mp.2017.180

Nardone, S., and Elliott, E. (2016). The interaction between the immune system and epigenetics in the etiology of autism Spectrum disorders. *Front. Neurosci.* 10:329. doi: 10.3389/fnins.2016.00329

Orihuela, R., McPherson, C. A., and Harry, G. J. (2016). Microglial M1/M2 polarization and metabolic states. *Br. J. Pharmacol.* 173, 649–665. doi: 10.1111/bph.13139

Paolicelli, R. C., Bolasco, G., Pagani, F., Maggi, L., Scianni, M., Panzanelli, P., et al. (2011). Synaptic pruning by microglia is necessary for normal brain development. *Science* 333, 1456–1458. doi: 10.1126/science.1202529

Pappalardo, L. W., Black, J. A., and Waxman, S. G. (2016). Sodium channels in astroglia and microglia. *Glia* 64, 1628–1645. doi: 10.1002/glia.22967

Parpura, V., Basarsky, T. A., Liu, F., Jeftinija, K., Jeftinija, S., and Haydon, P. G. (1994). Glutamate-mediated astrocyte-neuron signalling. *Nature* 369, 744–747. doi: 10.1038/369744a0

Patel, A. B., Tsilioni, I., Leeman, S. E., and Theoharides, T. C. (2016). Neurotensin stimulates sortilin and mTOR in human microglia inhibitable by methoxyluteolin, a potential therapeutic target for autism. *Proc. Natl. Acad. Sci. U. S. A.* 113, E7049–E7058. doi: 10.1073/pnas.1604992113

Petrelli, F., Pucci, L., and Bezzi, P. (2016). Astrocytes and microglia and their potential link with autism Spectrum disorders. *Front. Cell. Neurosci.* 10:21. doi: 10.3389/fncel.2016.00021

Pretzsch, C. M., and Floris, D. L. (2020). Balancing excitation and inhibition in the autistic brain. *elife* 9:e60584. doi: 10.7554/eLife.60584

Rose, C. R., and Verkhratsky, A. (2016). Principles of sodium homeostasis and sodium signalling in astroglia. *Glia* 64, 1611–1627. doi: 10.1002/glia.22964

Russo, F. B., Freitas, B. C., Pignatari, G. C., Fernandes, I. R., Sebat, J., Muotri, A. R., et al. (2018). Modeling the interplay between neurons and astrocytes in autism using human induced pluripotent stem cells. *Biol. Psychiatry* 83, 569–578. doi: 10.1016/j.biopsych.2017.09.021

Sancho, L., Contreras, M., and Allen, N. J. (2021). Glia as sculptors of synaptic plasticity. *Neurosci. Res.* 167, 17–29. doi: 10.1016/j.neures.2020.11.005

Sarn, N., Thacker, S., Lee, H., and Eng, C. (2021). Germline nuclear-predominant Pten murine model exhibits impaired social and perseverative behavior, microglial activation, and increased oxytocinergic activity. *Mol. Autism.* 12:41. doi: 10.1186/s13229-021-00448-4

Schwarz, J. M., and Bilbo, S. D. (2012). Sex, glia, and development: interactions in health and disease. *Horm. Behav.* 62, 243–253. doi: 10.1016/j.yhbeh.2012.02.018

Sciara, A. N., Beasley, B., Crawford, J. D., Anderson, E. P., Carrasco, T., Zheng, S., et al. (2020). Neuroinflammatory gene expression alterations in anterior cingulate cortical white and gray matter of males with autism Spectrum disorder. *Autism Res.* 13, 870–884. doi: 10.1002/aur.2284

Skaper, S. D., Facci, L., Zusso, M., and Giusti, P. (2017). Neuroinflammation, mast cells, and glia: dangerous liaisons. *Neuroscientist* 23, 478–498. doi: 10.1177/1073858416687249

Sloan, S. A., and Barres, B. A. (2014). Mechanisms of astrocyte development and their contributions to neurodevelopmental disorders. *Curr. Opin. Neurobiol.* 27, 75–81. doi: 10.1016/j.conb.2014.03.005

Soares, N. L., Paiva, I., Bravo, J., Queiroga, C. S. F., Melo, B. F., Conde, S. V., et al. (2022). Carbon monoxide modulation of microglia-neuron communication: anti-neuroinflammatory and Neurotrophic role. *Mol. Neurobiol.* 59, 872–889. doi: 10.1007/s12035-021-02643-z

Sofroniew, M. V. (2015). Astrocyte barriers to neurotoxic inflammation. *Nat. Rev. Neurosci.* 16, 249–263. doi: 10.1038/nrn3898

Sofroniew, M. V., and Vinters, H. V. (2010). Astrocytes: biology and pathology. *Acta Neuropathol.* 119, 7–35. doi: 10.1007/s00401-009-0619-8

Sohal, V. S., and Rubenstein, J. L. R. (2019). Excitation-inhibition balance as a framework for investigating mechanisms in neuropsychiatric disorders. *Mol. Psychiatry* 24, 1248–1257. doi: 10.1038/s41380-019-0426-0

Thangaraj, A., Periyasamy, P., Liao, K., Bendi, V. S., Callen, S., Pendyala, G., et al. (2018). HIV-1 TAT-mediated microglial activation: role of mitochondrial dysfunction and defective mitophagy. *Autophagy* 14, 1596–1619. doi: 10.1080/15548627.2018.1476810

Theoharides, T. C., Asadi, S., and Patel, A. B. (2013). Focal brain inflammation and autism. *J. Neuroinflammation* 10:46. doi: 10.1186/1742-2094-10-46

Traetta, M. E., Uccelli, N. A., Zárate, S. C., Gómez Cuautle, D., Ramos, A. J., and Reinés, A. (2021). Long-lasting changes in glial cells isolated from rats subjected to the valproic acid model of autism spectrum disorder. *Front. Pharmacol.* 12:707859. doi: 10.3389/fphar.2021.707859

Tremblay, M. W., and Jiang, Y. H. (2019). DNA methylation and susceptibility to autism spectrum disorder. *Annu. Rev. Med.* 70, 151–166. doi: 10.1146/annurev-med-120417-091431

Tsilioni, I., Natelson, B., and Theoharides, T. C. (2022). Exosome-associated mitochondrial DNA from patients with myalgic encephalomyelitis/chronic fatigue syndrome stimulates human microglia to release IL-1β. *Eur. J. Neurosci.* 56, 5784–5794. doi: 10.1111/ejn.15828

Tsilioni, I., Pantazopoulos, H., Conti, P., Leeman, S. E., and Theoharides, T. C. (2020). IL-38 inhibits microglial inflammatory mediators and is decreased in amygdala of children with autism spectrum disorder. *Proc. Natl. Acad. Sci. U. S. A.* 117, 16475–16480. doi: 10.1073/pnas.2004666117

Tsilioni, I., Patel, A. B., Pantazopoulos, H., Berretta, S., Conti, P., Leeman, S. E., et al. (2019). IL-37 is increased in brains of children with autism spectrum disorder and inhibits human microglia stimulated by neurotensin. *Proc. Natl. Acad. Sci. U. S. A.* 116, 21659–21665. doi: 10.1073/pnas.1906817116

Umpierre, A. D., and Wu, L. J. (2021). How microglia sense and regulate neuronal activity. *Glia* 69, 1637–1653. doi: 10.1002/glia.23961

Varghese, M., Keshav, N., Jacot-Descombes, S., Warda, T., Wicinski, B., Dickstein, D. L., et al. (2017). Autism spectrum disorder: neuropathology and animal models. *Acta Neuropathol.* 134, 537–566. doi: 10.1007/s00401-017-1736-4

Voet, S., Prinz, M., and van Loo, G. (2019). Microglia in central nervous system inflammation and multiple sclerosis pathology. *Trends Mol. Med.* 25, 112–123. doi: 10.1016/j.molmed.2018.11.005

Vogel Ciernia, A., Careaga, M., LaSalle, J. M., and Ashwood, P. (2018). Microglia from offspring of dams with allergic asthma exhibit epigenomic alterations in genes dysregulated in autism. *Glia* 66, 505–521. doi: 10.1002/glia.23261

Wang, J., Fröhlich, H., Torres, F. B., Silva, R. L., Poschet, G., Agarwal, A., et al. (2022). Mitochondrial dysfunction and oxidative stress contribute to cognitive and motor impairment in FOXP1 syndrome. *Proc. Natl. Acad. Sci. U. S. A.* 119:e2112852119. doi: 10.1073/pnas.2112852119

Wang, Q., Kong, Y., Wu, D. Y., Liu, J. H., Jie, W., You, Q. L., et al. (2021). Impaired calcium signaling in astrocytes modulates autism spectrum disorder-like behaviors in mice. *Nat. Commun.* 12:3321. doi: 10.1038/s41467-021-23843-0

Werling, D. M., Parikshak, N. N., and Geschwind, D. H. (2016). Gene expression in human brain implicates sexually dimorphic pathways in autism spectrum disorders. *Nat. Commun.* 7:10717. doi: 10.1038/ncomms10717

Williams, L. A., and LaSalle, J. M. (2022). Future prospects for epigenetics in autism Spectrum disorder. *Mol. Diagn. Ther.* 26, 569–579. doi: 10.1007/s40291-022-00608-z

Xian, H., Watari, K., Sanchez-Lopez, E., Offenberger, J., Onyuru, J., Sampath, H., et al. (2022). Oxidized DNA fragments exit mitochondria via mPTP- and VDAC-dependent channels to activate NLRP3 inflammasome and interferon signaling. *Immunity* 55, 1370–1385.e8. doi: 10.1016/j.immuni.2022.06.007

Xu, Z. X., Kim, G. H., Tan, J. W., Riso, A. E., Sun, Y., Xu, E. Y., et al. (2020). Elevated protein synthesis in microglia causes autism-like synaptic and behavioral aberrations. *Nat. Commun.* 11:1797. doi: 10.1038/s41467-020-15530-3

Yang, R., Zhang, G., Shen, Y., Ou, J., Liu, Y., Huang, L., et al. (2022). Odor identification impairment in autism spectrum disorder might be associated with mitochondrial dysfunction. *Asian J. Psychiatr.* 72:103072. doi: 10.1016/j.ajp.2022.103072

Ye, J., Wang, H., Cui, L., Chu, S., and Chen, N. (2021). The progress of chemokines and chemokine receptors in autism spectrum disorders. *Brain Res. Bull.* 174, 268–280. doi: 10.1016/j.brainresbull.2021.05.024

Yu, T. W., Chahrour, M. H., Coulter, M. E., Jiralerspong, S., Okamura-Ikeda, K., Ataman, B., et al. (2013). Using whole-exome sequencing to identify inherited causes of autism. *Neuron* 77, 259–273. doi: 10.1016/j.neuron.2012.11.002

Yu, X., Nagai, J., and Khakh, B. S. (2020). Improved tools to study astrocytes. *Nat. Rev. Neurosci.* 21, 121–138. doi: 10.1038/s41583-020-0264-8

Zantomio, D., Chana, G., Laskaris, L., Testa, R., Everall, I., Pantelis, C., et al. (2015). Convergent evidence for mGluR5 in synaptic and neuroinflammatory pathways implicated in ASD. *Neurosci. Biobehav. Rev.* 52, 172–177. doi: 10.1016/j.neubiorev.2015.02.006

Zhan, Y., Paolicelli, R. C., Sforazzini, F., Weinhard, L., Bolasco, G., Pagani, F., et al. (2014). Deficient neuron-microglia signaling results in impaired functional brain connectivity and social behavior. *Nat. Neurosci.* 17, 400–406. doi: 10.1038/nn.3641

Zhang, D., Hu, X., Qian, L., O'Callaghan, J. P., and Hong, J. S. (2010). Astrogliosis in CNS pathologies: is there a role for microglia? *Mol. Neurobiol.* 41, 232–241. doi: 10.1007/s12035-010-8098-4

Zhang, S., Zeng, X., Yang, H., Hu, G., and He, S. (2012). Mast cell tryptase induces microglia activation via protease-activated receptor 2 signaling. *Cell. Physiol. Biochem.* 29, 931–940. doi: 10.1159/000171029

Zhao, Q., Wang, Q., Wang, J., Tang, M., Huang, S., Peng, K., et al. (2019). Maternal immune activation-induced PPARγ-dependent dysfunction of microglia associated with neurogenic impairment and aberrant postnatal behaviors in offspring. *Neurobiol. Dis.* 125, 1–13. doi: 10.1016/j.nbd.2019.01.005

Zhong, F., Liang, S., and Zhong, Z. (2019). Emerging role of mitochondrial DNA as a major driver of inflammation and disease progression. *Trends Immunol.* 40, 1120–1133. doi: 10.1016/j.it.2019.10.008

frontiers | Frontiers in Neuroscience

TYPE Original Research
PUBLISHED 17 April 2023
DOI 10.3389/fnins.2023.1088052

OPEN ACCESS

EDITED BY
Jian-Huan Chen,
Jiangnan University,
China

REVIEWED BY
Joshua Shimony,
Washington University in St. Louis,
United States
Tami Bar-Shalita,
Tel Aviv University,
Israel

*CORRESPONDENCE
Elysa J. Marco
✉ emarco@corticacare.com
Pratik Mukherjee
✉ pratik.mukherjee@ucsf.edu

SPECIALTY SECTION
This article was submitted to Neurodevelopment, a section of the journal Frontiers in Neuroscience

RECEIVED 02 November 2022
ACCEPTED 28 March 2023
PUBLISHED 17 April 2023

CITATION
Parekh SA, Wren-Jarvis J, Lazerwitz M, Rowe MA, Powers R, Bourla I, Cai LT, Chu R, Trimarchi K, Garcia R, Marco EJ and Mukherjee P (2023) Hemispheric lateralization of white matter microstructure in children and its potential role in sensory processing dysfunction.
Front. Neurosci. 17:1088052.
doi: 10.3389/fnins.2023.1088052

Hemispheric lateralization of white matter microstructure in children and its potential role in sensory processing dysfunction

Shalin A. Parekh[1], Jamie Wren-Jarvis[1], Maia Lazerwitz[1,2], Mikaela A. Rowe[3], Rachel Powers[1,2], Ioanna Bourla[1], Lanya T. Cai[1], Robyn Chu[2], Kaitlyn Trimarchi[2], Rafael Garcia[2], Elysa J. Marco[2]* and Pratik Mukherjee[1]*

[1]Department of Radiology and Biomedical Imaging, University of California–San Francisco, San Francisco, CA, United States, [2]Cortica Healthcare, San Rafael, CA, United States, [3]Department of Psychology and Neuroscience, University of Colorado Boulder, Boulder, CO, United States

Diffusion tensor imaging (DTI) studies have demonstrated white matter microstructural differences between the left and right hemispheres of the brain. However, the basis of these hemispheric asymmetries is not yet understood in terms of the biophysical properties of white matter microstructure, especially in children. There are reports of altered hemispheric white matter lateralization in ASD; however, this has not been studied in other related neurodevelopmental disorders such as sensory processing disorder (SPD). Firstly, we postulate that biophysical compartment modeling of diffusion MRI (dMRI), such as Neurite Orientation Dispersion and Density Imaging (NODDI), can elucidate the hemispheric microstructural asymmetries observed from DTI in children with neurodevelopmental concerns. Secondly, we hypothesize that sensory over-responsivity (SOR), a common type of SPD, will show altered hemispheric lateralization relative to children without SOR. Eighty-seven children (29 females, 58 males), ages 8–12years, presenting at a community-based neurodevelopmental clinic were enrolled, 48 with SOR and 39 without. Participants were evaluated using the Sensory Processing 3 Dimensions (SP3D). Whole brain 3T multi-shell multiband dMRI (b=0, 1,000, 2,500s/mm^2) was performed. Tract Based Spatial Statistics were used to extract DTI and NODDI metrics from 20 bilateral tracts of the Johns Hopkins University White-Matter Tractography Atlas and the lateralization Index (LI) was calculated for each left–right tract pair. With DTI metrics, 12 of 20 tracts were left lateralized for fractional anisotropy and 17/20 tracts were right lateralized for axial diffusivity. These hemispheric asymmetries could be explained by NODDI metrics, including neurite density index (18/20 tracts left lateralized), orientation dispersion index (15/20 tracts left lateralized) and free water fraction (16/20 tracts lateralized). Children with SOR served as a test case of the utility of studying LI in neurodevelopmental disorders. Our data demonstrated increased lateralization in several tracts for both DTI and NODDI metrics in children with SOR, which were distinct for males versus females, when compared to children without SOR. Biophysical properties from NODDI can explain the hemispheric lateralization of white matter microstructure in children. As a patient-specific ratio, the lateralization index can eliminate scanner-related and inter-individual sources of variability and thus potentially serve as a clinically useful imaging biomarker for neurodevelopmental disorders.

KEYWORDS

sensory processing disorder, lateralization, sensory over-responsivity, neurite orientation dispersion and density imaging, microstructure

Introduction

Diffusion tensor imaging (DTI) studies have shown inherent microstructural asymmetries in the human brain (Ocklenburg et al., 2016). White matter tracts such as the cingulum bundle, posterior limb of the internal capsule, corticospinal tract, superior cerebellar peduncle and arcuate fasciculus are known to be left lateralized while tracts like the inferior longitudinal fasciculus, parts of the superior longitudinal fasciculus, the anterior limb of the internal capsule and the uncinate fasciculus have been shown to be right lateralized on diffusion anisotropy in the human brain (Park et al., 2004; Gong et al., 2005; Yasmin et al., 2009; Takao et al., 2011; Madsen et al., 2012; Takao et al., 2013; DeRosse et al., 2015). It is believed that such hemispheric asymmetries reflect the functional lateralization of the human brain. The most well-known example of functional lateralization is that of language to the left cerebral hemisphere and visuospatial processing to the right cerebral hemisphere (Gotts et al., 2013).

Altered hemispheric lateralization on DTI has been seen in neurodevelopmental disorders like autistic spectrum disorder (ASD), schizophrenia and dyslexia (Fletcher et al., 2010; Lange et al., 2010; Lo et al., 2011; Ocklenburg et al., 2016; Postema et al., 2019; Andica et al., 2021; Floris et al., 2021). While a number of studies have shown loss of normal left lateralization in large association tracts and temporal lobes in autistic children and adolescents (Lo et al., 2011) some studies have shown increased left lateralization (Leisman et al., 2022). The variation in results is likely due to heterogeneity in the autism group with different subjects showing differing symptoms and having different underlying etiologies. For example, Floris et al. (2021) showed that language delay in autistic children corelated with a rightward pattern while core autism symptoms severity correlated with a leftward pattern. A recent study has shown that it is difficult to discriminate imaging biomarkers of autism due to group and individual heterogeneity of phenotypic components or symptoms of autism (Xu et al., 2021). Due to this heterogeneity, it is important to study the individual phenotypic components that make up this heterogeneity in neurodevelopmental disorders (Chang et al., 2014). One such phenotypic component is sensory dysfunction (Chang et al., 2014). Children with autism have difficulties in sensory processing, which is now considered a diagnostic hallmark of autism. As per the Diagnostic and Statistical Manual-5 (DSM-5) hyper- and hypo-reactivity to sensory input (characteristic of sensory modulation) is a core criterion for ASD. This has now resulted in interest in learning the pathophysiological basis of sensory processing and sensory dysfunction and changes in brain microstructure associated with sensory processing dysfunction.

Sensory processing dysfunction (SPD) is difficulty in interpreting the sensory world in an adaptive way. There are different types of SPD including sensory modulation disorder, sensory discrimination disorder and sensory motor control disorder (Miller et al., 2012). These often coexist with each other. Sensory modulation is a core criterion in ASD. Sensory modulation can be further categorized as sensory over responsivity (SOR), sensory under responsivity and sensory craving (Miller et al., 2012). Sensory over responsivity is manifest as exaggerated response to normal sensory stimuli with ordinary sensory stimulation leading to distress (Marco et al., 2011). These sensory stimuli can be auditory tactile or visual. Hemispheric lateralization has not yet been explored in children with SPD.

Brain microstructure has been studied using diffusion MRI (Ocklenburg et al., 2016). Traditional DTI is sensitive to changes in tissue microstructure but lacks specificity for individual tissue microstructural features. More recently, non-gaussian models with biophysical compartment modeling of brain microstructure are being used. One such model, Neurite Orientation Dispersion and Density Imaging (NODDI), enables the quantification of the intracellular volume fraction, also known as the neurite density index (NDI), as well as the axonal fiber orientation dispersion index (ODI) and the free water fraction (FISO). These compartment models are both sensitive and specific and provide more biologically meaningful measures of white matter microstructure than traditional DTI metrics, including for childhood white matter development (Chang et al., 2015) and for many neurological disorders such as traumatic brain injury (Palacios et al., 2020). The NODDI model has been shown to bear excellent correlation to brain microstructure on pathology specimens (Zhang et al., 2012). In adults with autism, the NODDI model has shown better accuracy and specificity than standard diffusion tensor metrics (Andica et al., 2021). There are limited studies of brain microstructural lateralization using the NODDI model in children. A recent study in adults found substantial asymmetries in gray matter microstructure using NODDI reflecting histopathological asymmetries. There were no effects of sex or handedness on these asymmetries (Schmitz et al., 2019). The excellent sensitivity and specificity of the NODDI model would also allow for in-depth understanding of potential signatures of white matter microstructural lateralization differences in children with SOR versus other forms of SPD.

Here, we evaluate lateralization of white matter microstructure using NODDI and conventional DTI parameters in children with neurodevelopmental concerns (NDC) between 8 and 12 years of age. First, we characterize white matter tract hemispheric lateralization in school age children with NDC using NODDI compared to DTI, postulating that the more biophysically meaningful NODDI metrics will help explain the direction of asymmetry observed from the DTI metrics. Then, we directly compare white matter tract hemispheric asymmetry for those children with versus without sensory over-responsivity. Children with and without SOR serve as a test case in the study of lateralization for neurodevelopmental disorders. Our exploratory hypothesis is that children with SOR will have altered regional hemispheric lateralization in white matter microstructure relative to children without SOR (non-SOR) using both DTI and NODDI.

Methods

We prospectively enrolled children, ages 8–12 years, who presented at a community-based neurodevelopmental clinic (Cortica San Rafael, California) using a research protocol approved by the institutional review board at our medical center with written informed consent obtained from the parents or legal guardians and assent obtained from the study participants. Each study participant was recruited following medical intake at Cortica Healthcare. Each participant underwent a thorough review of their history, a general and neurodevelopmental physical examination, and record review by their physician and research coordinator. Children were screened for eligibility in part through the ESSENCE-Q-REV, a 12-question caregiver screener for ESSENCE disorders, including ASD, attention deficit hyperactivity disorder (ADHD), developmental coordination disorder, specific language impairment, and Tourette's syndrome (Gillberg, 2010). The response options were "No," "Maybe/A Little," or "Yes." The threshold for inclusion ("optimal cutoff") for this measure was at least one 'Yes' or at least two 'Maybe / A Little' responses in total. Participants were excluded if they had (A) Nonverbal Index ≤70 on the Wechsler Intelligence Scale for Children (Fifth Edition) (Wechsler, 2014) (B) Below ESSENCE-Q-REV "optimal cutoff" for neurodevelopmental concerns (C) Caregiver(s) unable to complete intake forms (D) History of *in utero* toxin exposure (E) Gestational age < 32 weeks or intrauterine growth restriction (birth weight < 1,500 grams) (F) Hearing or visual impairment (G) Additional medical/neurologic condition, including active epilepsy, malignancy, or known brain injury/malformation (H) If they were found to have a research designation of ASD. Participants with ASD were excluded to obtain a more homogenous group so that microstructural changes on brain imaging would be reflective of sensory over-responsivity and not ASD. Participants scoring ≥15 on the Social Communication Questionnaire (Rutter et al., 2003) and above the diagnostic cut-off on the Autism Diagnostic Observation Schedule (Second Edition) (Lord et al., 2012) were considered to have a research designation of ASD.

Participants underwent direct sensory characterization through the Sensory Processing 3 Dimensions (SP3D) (Mulligan et al., 2019) scale, led by a licensed pediatric occupational therapist. Three auditory, four tactile, and three visual probes from the SP3D scale were utilized in the SOR cohort assignment process. Within each of these probes, a participant is given a score of 1 (typical), 2 (mild/moderate), or 3 (severe) in reference to the intensity of their aversive reaction. A score of 2 or 3 in any of the probes corresponds to an SOR designation in the respective domain(s), and therefore categorizes the participant into the SOR cohort. We did not exclude subjects who had other forms of sensory dysfunction like sensory under-responsivity or sensory modulation disorder and as such the non-SOR group may have subjects with these forms of sensory dysfunction.

All subjects were imaged on a single Siemens 3 Tesla (3 T) Prisma MRI scanner (Erlangen, Germany) using a 64-channel head coil. Participants were acclimated and desensitized to the MRI scanner environment (Horowitz-Kraus et al., 2016). Briefly, the child explored the scanner environment, and sat on the bed until comfortable. Head motions were minimized using foam padding on either side of the head-coil apparatus used for the scan. The child was positioned within the scanner bore and began watching a movie *via* an MRI-compatible audiovisual system, and image acquisition began. Communication was established between the child and study coordinator through headphones equipped with a built-in microphone. Verbal communication and positive reinforcement were maintained with the child throughout the scan. Scanning was terminated immediately if the child did not wish to continue. All children were awake during the entire duration of the scan.

Structural MRI of the brain was acquired with an axial 3D magnetization prepared rapid acquisition gradient-echo (MPRAGE) T1-weighted sequence. Whole brain diffusion MRI was performed at diffusion-weighting strengths (shells) of $b = 1{,}000\ s/mm^2$ (64 diffusion-encoding directions) and $2{,}500\ s/mm^2$ (96 diffusion-encoding directions), with 5 $b = 0\ s/mm^2$ volumes per shell (TE = 72.20 ms, TR = 2,420 ms, flip angle = 85 degrees, slice thickness = 2.0 mm, matrix size = 220×110, FOV = 220 mm) using single-shot spin echo echoplanar imaging with forward and reverse phase encoding. Simultaneous multiband (MB) excitation was used (MB factor = 3). The acquisition time for the $b = 1{,}000\ s/mm^2$ shell was 3 min and 23 s, and for the $b = 2{,}500\ s/mm^2$ shell was 4 min and 53 s.

The FMRIB Software Library (FSL) version 6.0.2 (Oxford, United Kingdom) was used for imaging processing and DTI parameter computation per steps previously reported (Owen et al., 2013; Chang et al., 2015; Payabvash et al., 2019). FSL's topup was used on each diffusion shell to correct for susceptibility induced distortion (Andersson et al., 2003). FSL's Eddy was used on the diffusion data to correct for motion and eddy distortions, skull stripping, outlier replacement, susceptibility-by-movement, and slice-to-volume correction. FSL's DTIFIT was used to calculate all DTI parameters: FA, radial diffusivity (RD), axial diffusivity (AD), and mean diffusivity (MD), with maps from the coregistered $b = 0\ s/mm^2$ and $b = 1{,}000\ s/mm^2$ images. Normalized multi-shell data was used to quantify NODDI parameters: NDI, orientation dispersion index (ODI), and free water fraction (FISO) with the Accelerated Microstructure Imaging *via* Convex Optimization (AMICO) Toolbox (Daducci et al., 2015).

Tract Based Spatial Statistics (TBSS) were performed on DTI and NODDI derived metrics using FSL. The Johns Hopkins University (JHU) ICBM-DTI-81 White-Matter Labeled Atlas and the JHU White-Matter Tractography Atlas, embedded in FSL, were used to extract the average DTI and NODDI values of 20 bilateral and 6 central tracts (total of 46 tracts) in automated fashion. Lateralization Index (LI) was calculated as (Right–Left)/(Right+Left) for each of the 20 bilateral tracts; thus, a left-lateralized tract had a negative LI while a right-lateralized tract had a positive LI.

All statistical analysis was performed using Stata (StataCorp. 2021. *Stata Statistical Software: Release 17*. College Station, TX: StataCorp LLC) and Matlab (Matlab, The MathWorks, Natick, MA, United States). The mean value for each parameter and 95% confidence interval was obtained for the lateralization indices of each of the bilateral tracts. Cohen's d effect sizes were obtained and a statistical significance threshold of 0.05 was used after Benjamini–Hochberg false discovery rate correction for multiple tract-wise comparisons. Two-tailed heteroscedastic t-tests were run to determine group differences in LI between SOR and non-SOR cohorts with DTI and NODDI metrics. Since this group comparison was an exploratory analysis, multiple comparison correction was not performed.

Results

Demographics

Eighty seven subjects were included in the study of which 29 were females and 58 were males; 9 of the 87 subjects were left-handed while 75 were right-handed, handedness data was not available for 3

subjects. Forty eight of the 87 children had SOR while 39 did not have SOR.

Lateralization index

DTI

Please refer to Table 1 caption for white matter tract abbreviations.

Across the full cohort, the greatest number of tracts demonstrated hemispheric lateralization for axial diffusivity (AD) with 17 of the 20 bilateral tracts being right lateralized for AD (Figure 1). CGC was strongly left lateralized, as expected from prior studies. PTR and RLIC did not show significant lateralization. For the right lateralized tracts, the Cohen's D effect sizes ranged from 0.4 to 2.5; for the left lateralized CGC, it was −1.85 (Table 1).

For fractional anisotropy (FA), most (12 of the 20) tracts were left lateralized. ALIC, ICP, SFO and UNC were right lateralized, while ACR, CGH, CP and PCR did not demonstrate any significant lateralization. The left lateralization of FA in most tracts was likely explained by the significant right lateralization of RD in these tracts, which was seen in 14 of 20 regions with Cohen's D values ranging from 0.4 to 3.4 (Table 1).

NODDI

For NDI, almost all tracts were left lateralized (18 of the 20) (Figure 2) whereas ICP was right lateralized, and ML did not show any evidence of lateralization. Cohen D effect sizes ranged from 0.5 to 2.7 (Table 1).

Most tracts were left lateralized for ODI (15 of 20 tracts). CGC, RLIC and SCR were right lateralized, whereas CST, ML, SCP and SLF were not significantly lateralized.

Lateralization effects were also seen in the free water fraction (FISO) of 16 of 20 tracts. Most tracts were right lateralized for FISO, whereas ACR, CGH, EC, ML and UNC were left lateralized.

SOR vs. non-SOR

There was no significant difference in the age, sex distribution, WISC full scale Intelligence Quotient (WISC-FSIQ) scores or the number of left versus right-handed subjects between the SOR and non-SOR groups (Table 2). Overall, there was no significant difference in age, WISC FSIQ scores or left versus right handedness between males and female subjects. Of the 20 bilateral tracts compared using the DTI metrics, the SFO was found to have increased right lateralization for FA and increased left lateralization for MD and RD ($p < 0.05$) in SOR children versus non-SOR children (Figure 3; Table 3). The ICP showed increased rightward lateralization for FA while CP showed increased right lateralization for MD and RD among SOR children.

When the males and females were analyzed separately, we found that males with SOR had increased right lateralization in the SFO for FA ($p = 0.003$) and increased left lateralization for MD ($p = 0.01$) and RD ($p < 0.001$) compared to males without SOR (Figure 4; Table 3). Females with SOR showed increased left lateralization of SCP and CGC in FA ($p < 0.05$) and increased right lateralization of CST in FA and AD and SCR in RD.

In terms of NODDI metrics, the SOR group showed decreased left lateralization of ODI in SCP compared to the non-SOR group (Figure 5). There were differences in free water fraction (FISO) with increased right lateralization for CP and reversal of lateralization for PCR and SFO (Figure 5).

When the males and females were analyzed separately, females with SOR showed a reversal of lateralization of ODI for SCP compared to females without SOR ($p < 0.001$) (Figure 6; Table 3). Males with SOR showed reversal of lateralization signal for PCR ($p < 0.01$) and SFO ($p < 0.01$) compared to males with non-SOR (Figure 6; Table 3).

Discussion

Our results agree with prior studies that demonstrate hemispheric lateralization of white matter microstructure in school-age children using conventional DTI (Trivedi et al., 2009). However, our investigation represents the most comprehensive evaluation to date of the biophysical properties that contribute to this hemispheric asymmetry of white matter microstructure in the human brain using the more advanced NODDI technique. Furthermore, we saw differences in the degree of lateralization of specific tracts for children with SOR compared to those without SOR, suggesting that this neurodevelopmental phenotype may have a "laterality signature." Lateralization is affected in association, projection and cerebellar tracts in SOR, with evidence for sexual dimorphism of the SOR trait. NODDI advances the understanding of which components of white matter microstructure contribute to hemispheric lateralization in specific tracts and how they are altered in neurodevelopmental disorders.

Hemispheric asymmetry of white matter microstructure in the human brain

For the overall cohort, most tracts were left lateralized by the FA measure. This is consistent with prior studies showing left lateralization of FA (Trivedi et al., 2009). It can be argued that this may be secondary to most people being right-handed in the population. However, when we separated the right- and left-handed individuals, there was no obvious relationship between lateralization and handedness, in agreement with prior DTI studies (Gong et al., 2005). The findings may be related to functional lateralization of the brain for e.g., speech and language processing tend to occur on the left side. Prior studies have indeed shown loss of left lateralization of FA in large association tracts in autistic adolescents compared to neurotypical children, suggesting that this may be related to impairment of social and communication function located on the left side of the brain (Lo et al., 2011).

The NODDI model allows more specificity regarding microstructural characteristics. The tracts with the greatest left lateralization of FA such as CGC and RLIC combine left lateralization of NDI with right lateralization of ODI, since this reflects higher axonal density and lower fiber orientation dispersion of the left-sided pathway, both of which contribute to more diffusion anisotropy on DTI. Likewise, the tracts with the greatest right lateralization of FA and AD such as the UNC and SFO combine the left lateralization of ODI and FISO, reflecting the higher fiber orientation dispersion on the left side as well as increased free water on the left side, leading to

TABLE 1 A and B: Cohen's *D* effect size and *p*-values (*p*-values corrected for multiple comparison) for LI of 20 bilateral tracts for DTI and NODDI metrics.

(A) DTI								
Tract	FA		AD		MD		RD	
	p-value	Cohen's *D* effect size	*p*-value	Cohen's *D* effect size	*p*-value	Cohen's *D*	*p*-value	Cohen's *D*
ACR	0.878	−0.0233	**<0.001**	0.67	**0.001**	0.512	0.527	0.103
ALIC	**<0.001**	1.01	**<0.001**	2.54	**<0.001**	1.48	0.173	0.217
CGC	**<0.001**	−3.34	**<0.001**	−1.85	**<0.001**	1.54	**<0.001**	3.38
CGH	0.161	0.228	**0.002**	0.499	0.073	0.282	0.811	−0.0364
CP	0.428	0.132	**<0.001**	1.3	**<0.001**	0.923	**0.013**	0.399
CST	**<0.001**	−0.94	**0.011**	0.398	**<0.001**	1.85	**<0.001**	1.77
EC	**<0.001**	−1.38	**<0.001**	1.73	**<0.001**	2.72	**<0.001**	2.56
FXST	**0.002**	−0.495	**<0.001**	1.54	**<0.001**	1.75	**<0.001**	1.19
ICP	**<0.001**	1.39	**0.006**	0.437	**0.002**	−0.489	**<0.001**	−1.11
ML	**<0.001**	−0.865	**0.001**	0.509	**<0.001**	1.04	**<0.001**	1.16
PCR	0.455	0.12	**<0.001**	1.11	**<0.001**	1.4	**<0.001**	0.92
PLIC	**<0.001**	−0.905	<0.001	2.13	**<0.001**	2.2	**<0.001**	1.75
PTR	**<0.001**	−0.756	0.578	0.0848	**<0.001**	0.699	**<0.001**	0.927
RLIC	**<0.001**	−2.43	0.157	0.221	**<0.001**	2.09	**<0.001**	2.94
SCP	**<0.001**	−1.18	**<0.001**	0.698	**<0.001**	1.19	**<0.001**	1.36
SCR	**<0.001**	−1.27	**0.008**	0.42	**<0.001**	1.18	**<0.001**	1.31
SFO	**<0.001**	0.69	**0.001**	0.545	0.788	0.0486	**0.037**	−0.332
SLF	**<0.001**	−1.09	**<0.001**	1.87	**<0.001**	2.6	**<0.001**	1.92
SS	**0.006**	−0.44	**<0.001**	1.42	**<0.001**	2.24	**<0.001**	1.65
UNC	**<0.001**	1.63	**<0.001**	1.48	0.851	0.0285	**<0.001**	−1.13

(B) NODDI						
Tract	NDI		ODI		FISO	
	p-value	Cohen's *D* effect size	*p*-value	Cohen's *D* effect size	*p*-value	Cohen's *D*
ACR	**<0.001**	−1.04	**<0.001**	−0.777	**<0.001**	−0.598
ALIC	**<0.001**	−1.2	**<0.001**	−2.19	**<0.001**	0.544
CGC	**<0.001**	−2.71	**<0.001**	2.5	0.725	−0.0534
CGH	**<0.001**	−1.18	**<0.001**	−0.746	**<0.001**	−0.759
CP	**0.002**	−0.488	**<0.001**	−0.876	**<0.001**	0.635
CST	**<0.001**	−0.589	0.88	−0.0231	**<0.001**	2
EC	**<0.001**	−2.22	**<0.001**	−1.53	**0.013**	−0.402
FXST	**<0.001**	−1.09	**<0.001**	−0.692	**<0.001**	0.547
ICP	**<0.001**	0.58	**<0.001**	−1.33	**0.002**	−0.513
ML	0.127	0.234	0.067	0.293	**<0.001**	1.21
PCR	**<0.001**	−1.19	**0.007**	−0.435	0.415	0.13
PLIC	**<0.001**	−1.19	**<0.001**	−0.925	**<0.001**	1.15
PTR	**0.003**	−0.466	**0.039**	−0.334	0.387	0.143
RLIC	**<0.001**	−1.16	**<0.001**	1.01	**<0.001**	0.813
SCP	**<0.001**	−0.701	0.072	−0.282	**<0.001**	0.931
SCR	**0.004**	−0.454	**0.039**	0.332	**<0.001**	0.87
SFO	**0.001**	−0.549	**<0.001**	−0.647	0.323	−0.167
SLF	**<0.001**	−1.53	0.072	−0.28	**<0.001**	0.966
SS	**<0.001**	−1.12	**<0.001**	−0.985	**0.021**	0.369
UNC	**<0.001**	−0.719	**<0.001**	−2.53	**<0.001**	−1.16

A $p < 0.05$ indicates significant lateralization of the tract. Positive effect size indicates right lateralization while negative effect size indicates left lateralization.
White matter tract abbreviations: *Commissural tracts*: (corticocortical tracts connecting left and right hemispheres): splenium (SCC), body (BCC), and genu (GCC) of the corpus callosum; *Brainstem tracts*: inferior (ICP), middle (MCP), and superior (SCP) cerebellar peduncles, pontine crossing tract (PCT), and medial lemniscus (ML); *Projection tracts*: (cortical to subcortical regions): corticospinal tract (CST), cerebral peduncle (CP), posterior thalamic radiation (PTR), internal capsule (subdivided into anterior limb (ALIC), posterior limb (PLIC), and retrolenticular (RLIC) portions), and corona radiata (subdivided into anterior (ACR), superior (SCR), and posterior (PCR) portions); *Limbic tracts*: cingulum (subdivided into cingulate (CGC) and hippocampal (CGH) portions), fornix (FX), and fornix stria terminalis (FXST); *Association tracts*: (corticocortical tracts within same hemisphere): external capsule (EC), superior fronto-occipital fasciculus (SFO), superior longitudinal fasciculus (SLF), sagittal stratum (SS), and uncinate fasciculus (UNC). The bold values indicate statistically significant *p* values ($p < 0.05$).

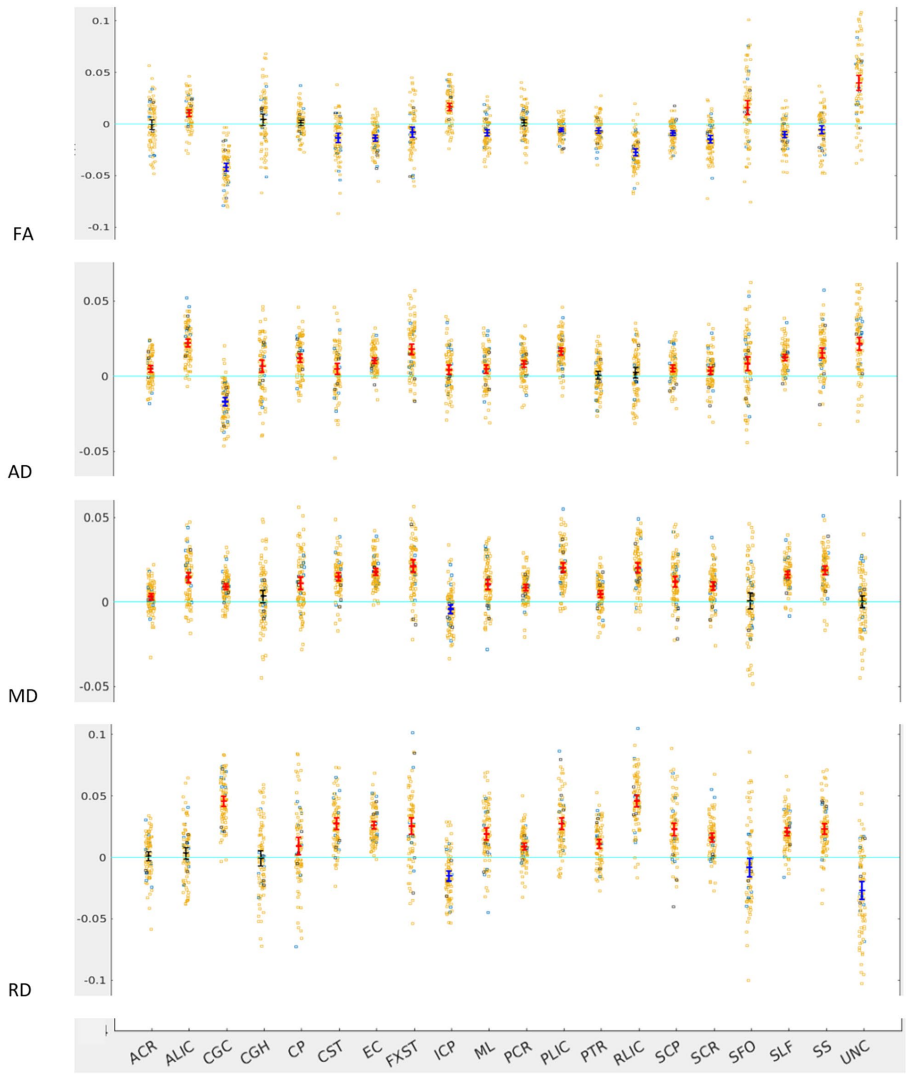

FIGURE 1
LI plotted for each of the 87 participants for the 20 bilateral tracts for DTI metrics, the mean and 95% CI are represented in the figure, 95% CI bars in red represents significant right lateralization (positive LI) of the tract while blue bar represents significant left lateralization (negative LI) of the tract. Yellow dots represent right-handed subjects (79) while blue dots represent left-handed subjects (9), subjects where handedness data was missing are plotted in black (3).

decreased diffusion anisotropy on the left side and consequent right lateralization of diffusion anisotropy in these tracts.

A majority of the tracts (ALIC, CP, CST, ML, PLIC, RLIC, SCP, SCR, SLF, and SS) that demonstrate left lateralization of FA are right lateralized on FISO. These tracts except ML also demonstrate left lateralization of NDI. These findings signify that the left lateralization of FA in these tracts is driven by the increased highly anisotropic intra-axonal water compartment and by the decreased isotropic free water fraction of the left-sided tract compared to the homologous right-sided tract. In the case of ML, there is higher axonal density on the right side as demonstrated by right lateralization of NDI; however, this is outweighed by the higher free water content on the right side leading to left lateralization of FA. Thus, NODDI analysis allows better understanding of the underlying microstructure of different tracts within the human brain and the related findings on standard DTI metrics.

Hemispheric laterality as a biomarker of sensory over-responsivity?

Our study is the first to evaluate LI in children with SOR and SPD. To our knowledge, we are also the first to characterize in detail the hemispheric lateralization of white matter microstructure using NODDI in children with neurodevelopmental concerns. By contrasting the hemispheres of a single individual, measures of lateralization solve the major problems of the large inter-individual variability of DTI and NODDI metrics as well as the variation produced by different MRI scanner hardware, software, and imaging protocols in multicenter studies and in routine clinical practice.

In terms of SPD, there was a trend toward increased lateralization in SOR children. This contrasts with decreased lateralization reported in studies of autism (Lo et al., 2011). This may be because SOR is distinct from autism (Tavassoli et al., 2018), and different forms of

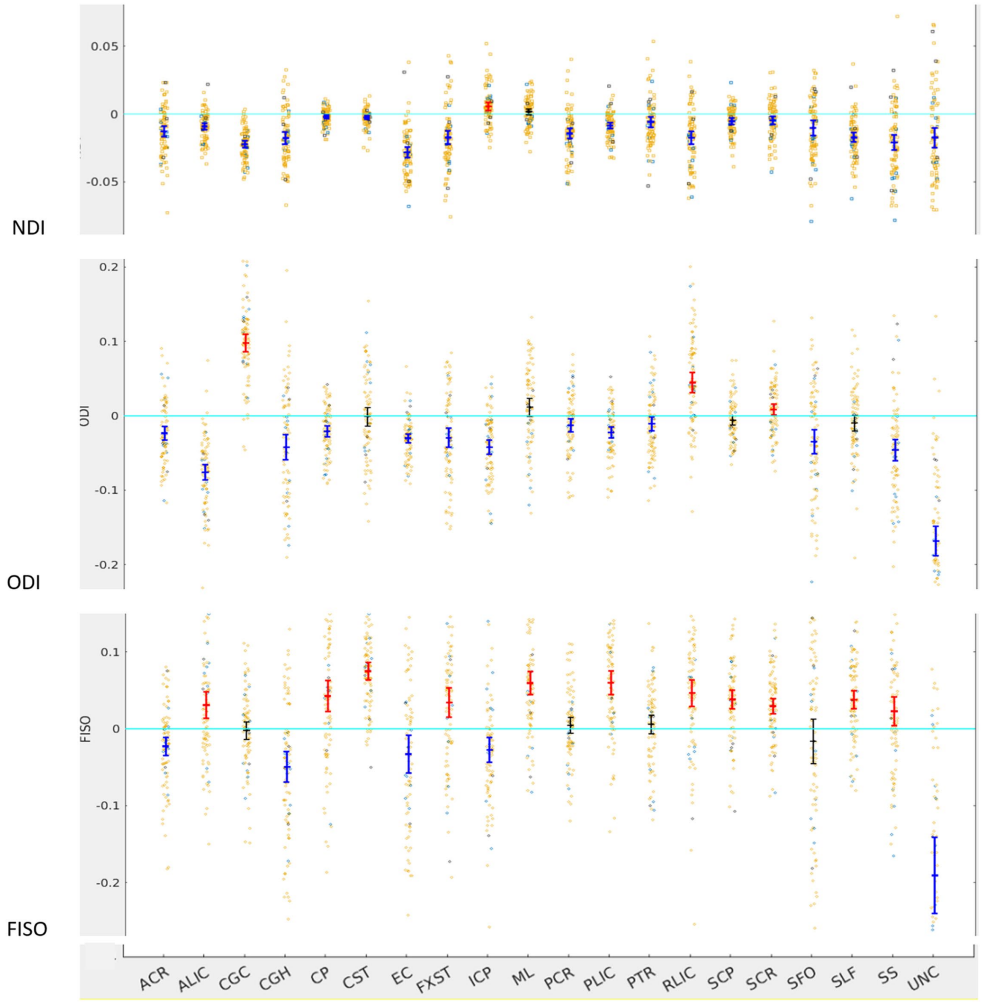

FIGURE 2
LI plotted for each of the 87 participants for the 20 bilateral tracks for DTI metrics, the mean and 95% CI are represented in the figure, 95% CI bars in red represents significant right lateralization (positive LI) of the tract while blue bar represents significant left lateralizatin (negative LI) of the tract. Yellow dots reperesent right-handed subjects (79) while blue dots represent left-handed subjects (9), subjects where handedness data was missing are plotted in black (3).

TABLE 2 Demographic characteristics of children with non-SOR and SOR, continuous variables are reported as mean±SD while categorical data is represented with absolute numbers, unpaired *t* test is used for continuous data while Pearson chi square test is used for categorical data.

	Non SOR (*N*=39)	SOR (*N*=48)	*p*-value
Age	10.3 ± 1.6	10.2 ± 1.7	0.71
Sex			
Male	27	31	
Female	12	17	0.65
Handedness			
Left	2	7	
Right	34	41	0.19
WISC full scale IQ	105.9 ± 12.9	106.1 ± 14.7	0.95

SPD might explain some of the heterogeneity seen in the findings of ASD studies (Tavassoli et al., 2018).

Association tracts like SFO were significantly more lateralized in SOR males, whereas cerebellar (SCP) and projection tracts (CST and SCR) showed altered lateralization in females. We have previously shown altered cerebellar white matter microstructure in children with SPD compared to typically developing children (Narayan et al., 2020). The current study shows alterations in lateralization of

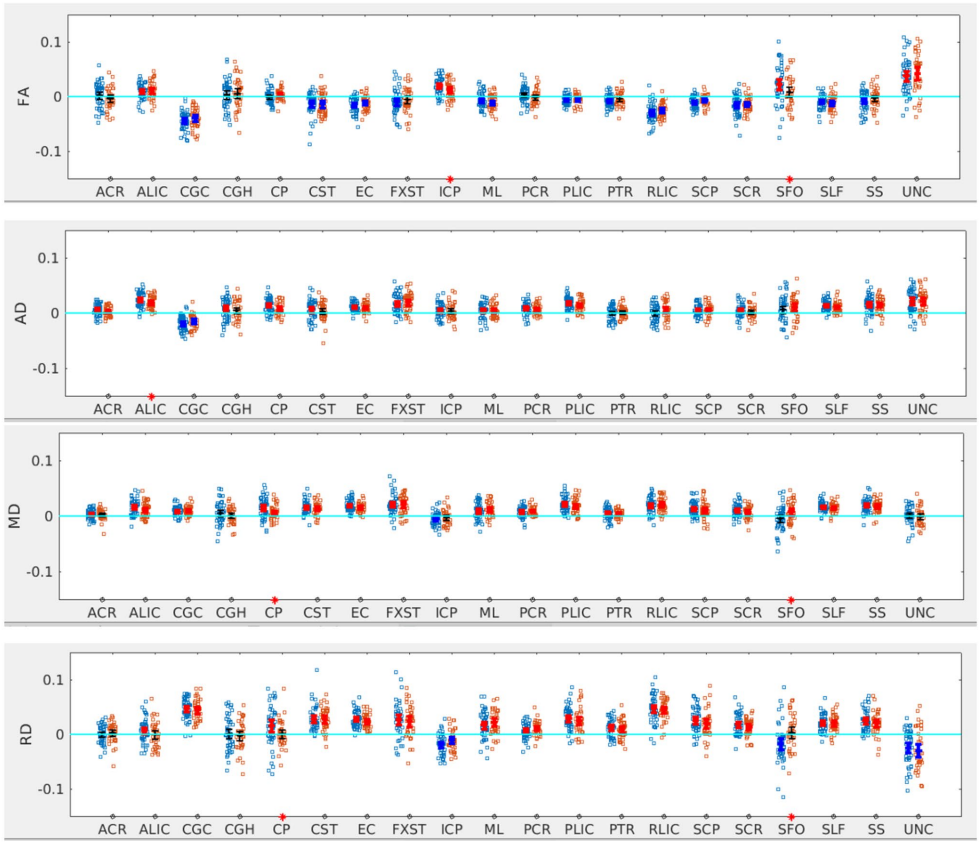

FIGURE 3
LI plotted for each of the 87 participants for the 20 bilateral tracks for DTI metrics comparing SOR (blue dots) to non-SOR (red dots) means with 95% CI are resented in the figure for SOR and Non SOR, 95% CI bars in red represents significant right lateralization (positive LI) of the tract while blue bar represents significant left lateralizatin (negative LI) of the tract. Red asterisks on the X axis represent tracts for which difference between SOR vs. non SOR was significant at $p<0.05$.

TABLE 3 *p*-values for the significant tracts when comparing SOR to non-SOR for all participants and for males and females separately (see Figures 3–6).

Metric	All participants		Males		Females	
	Tract	*p*-value	Tract	*p*-value	Tract	*p*-value
FA						
	ICP	0.03	ICP	0.02	CGC	0.04
	SFO	0.04	SFO	<0.01	CST	0.03
					SCP	0.04
AD						
	ALIC	<0.05	ALIC	0.02	CST	0.02
MD						
	CP	0.02	ALIC	0.03		
	SFO	0.02	SFO	0.01		
RD						
	CP	0.04	SFO	<0.001	SCR	<0.05
	SFO	<0.01				
ODI						
	SCP	0.02			SCP	<0.001
FISO						
	CP	<0.01	CP	<0.05	CP	<0.01
	PCR	0.03	PCR	<0.01		
	SFO	0.02	SFO	<0.01		

10.3389/fnins.2023.1088052

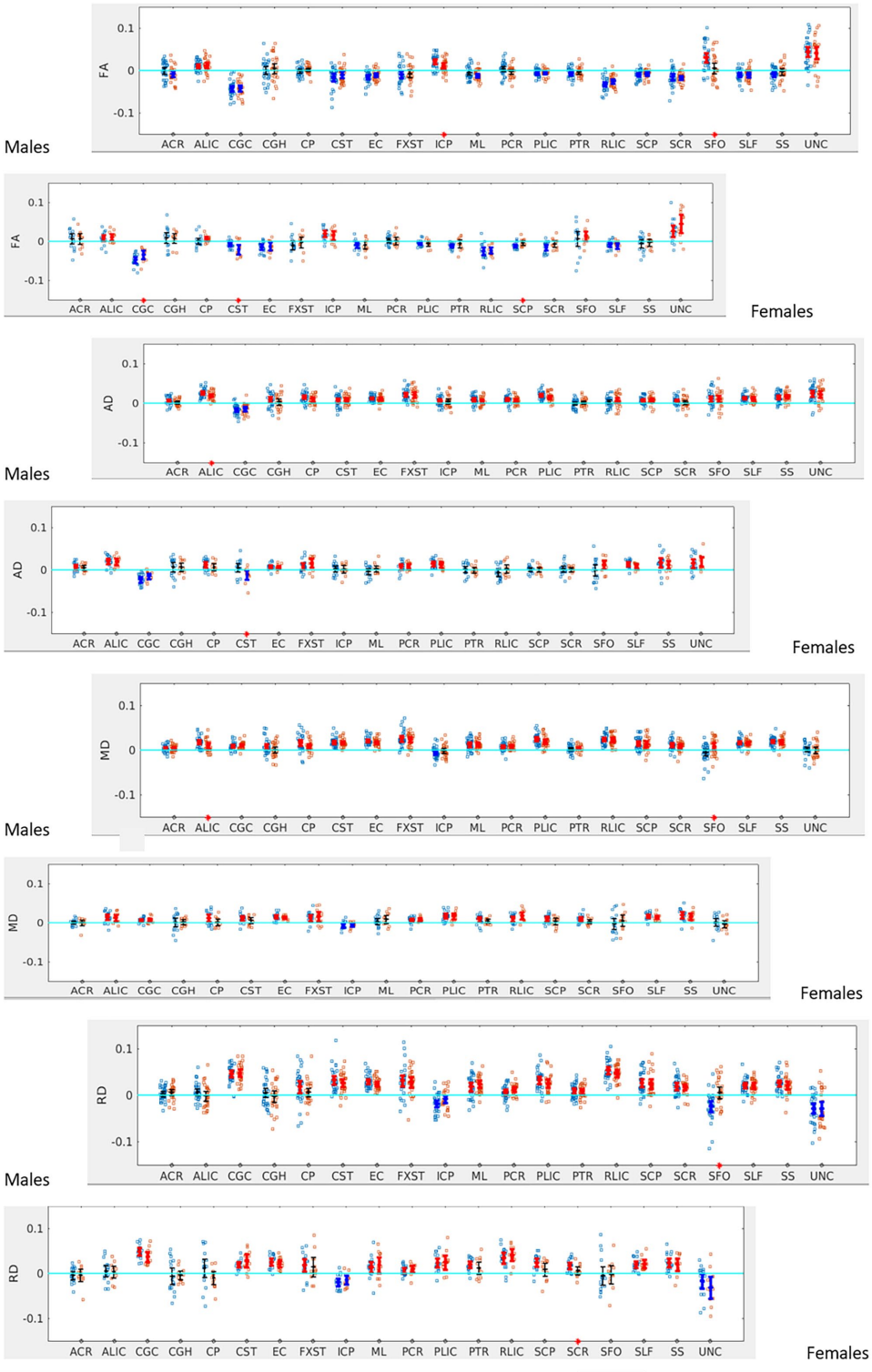

FIGURE 4
LI plotted for boys (n=58) and girls (n=29) separately for the 20 bilateral tracts for DTI metrics comparing SOR (blue dots) to non-SOR (red dots) means with 95% CI are resented in the figure for SOR and Non SOR, 95% CI bars in red represents significant right lateralization (positive LI) of the tract while blue bar represents significant left lateralizatin (negative LI) of the tract. Red asterisks on the *X* axis represent tracts for which difference between SOR vs. non SOR was significant at p<0.05.

cerebellar white matter in females with SPD. This reinforces recent studies which show the cerebellum to be lateralized and cerebral-cerebellar tract lateralization likely secondary to lateralization of brain function (Kang et al., 2015). The sex differences in the tracts affected may reflect differences in the phenotypic manifestation of SPD between males and females (Osório et al., 2021). The distinct

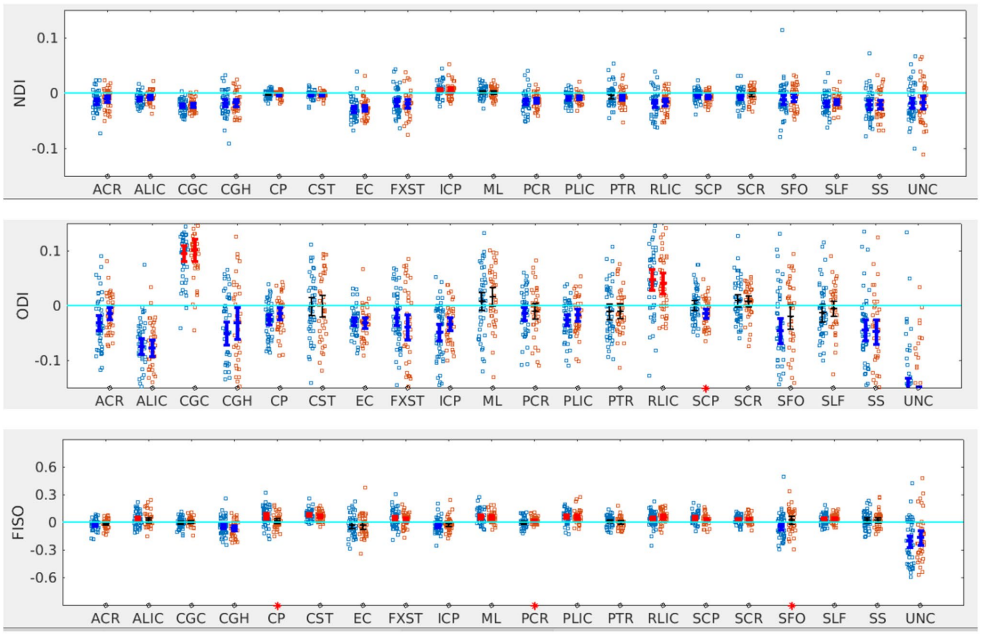

FIGURE 5
LI plotted for each of the 87 participants for the 20 bilateral tracks for NODDI metrics comparing SOR (blue dots) to non-SOR (red dots) means with 95% CI are resented in the figure for SOR and Non SOR, 95% CI bars in red represents significant right lateralization (positive LI) of the tract while blue bar represents significant left lateralizatin (negative LI) of the tract. Red asterisks on the X axis represent tracts for which difference between SOR vs. non SOR was significant at $p<0.05$.

signatures in microstructure in males versus females may be secondary to biological differences in SOR in males versus females. Prior studies have shown differences in myelination and cerebral white matter architecture between males and females (Kodiweera et al., 2016; Geeraert et al., 2019; Buyanova and Arsalidou, 2021).

We have also previously shown altered white matter microstructure in the posterior projection tracts in children with the auditory over-responsivity subtype of SOR (Tavassoli et al., 2019). It is likely that, when looking at SOR as a whole, large association tracts may be involved as these may be affected in multisensory integration in children. Our finding of changes in lateralization within the SFO is probably reflective of this.

Analysis of NODDI metrics shows a trend toward increased lateralization among the children with SOR. However, the greatest differences were seen in ODI and FISO, suggesting that differences in microstructure in SOR are likely due to altered fiber orientation dispersion and altered free water content within tracts. A study in adults with autism (Andica et al., 2021) has shown increased FISO and decreased NDI mainly in the commissural and long-range association fibers with predominant distinct sides depending on the tract involved. The study also showed higher specificity and accuracy with NODDI parameters, especially FISO, than standard DTI parameters. In our cohort with SOR, we did find differences in fiber orientation dispersion and free water fraction and there was also a difference in the ODI and FISO patterns for girls versus boys. Prior studies in adults have shown NODDI to have better sex discrimination than standard DTI metrics (Kodiweera et al., 2016). The differences in NODDI parameters are important in understanding the neurobiological basis of distinct phenotypes and further hypothesis-driven studies are warranted in this area to confirm the exploratory findings in this report on hemispheric asymmetry differences in those with SOR versus non-SOR SPD.

Limitations and future directions

A limitation of the study is that children without SOR are a heterogenous group and a large control group of typically developing children was not available for comparison. The non-SOR children may have various forms of SPD such as sensory under responsivity, sensory craving, and sensory discrimination disorder. These forms of SPD may have different patterns of microstructural changes that can be explored in larger cohorts. In addition, SOR can be divided into subtypes including auditory over-responsivity, visual over-responsivity and tactile over-responsivity as well as mixed subtypes. We did not distinguish the different subtypes in this analysis. Different subtypes may involve different tracts which are involved in the sensory pathway and may account for the differences seen in multiple tracts. These differences in different subtypes of SOR can be explored in larger cohorts. We did not account for puberty which may possibly affect the brain imaging and phenotypic results. Our cohort was aged 8–12. Even though there has been a trend toward earlier puberty in girls, given the narrow range and the young age of the study group, children in this study are less likely to have undergone puberty (Brix et al., 2019).

As mentioned in the methods section since the group comparison was an exploratory analysis multiple comparison correction wasn't performed. However, these results are hypotheses generating and can be the bases for studies in larger cohorts to investigate these differences in detail.

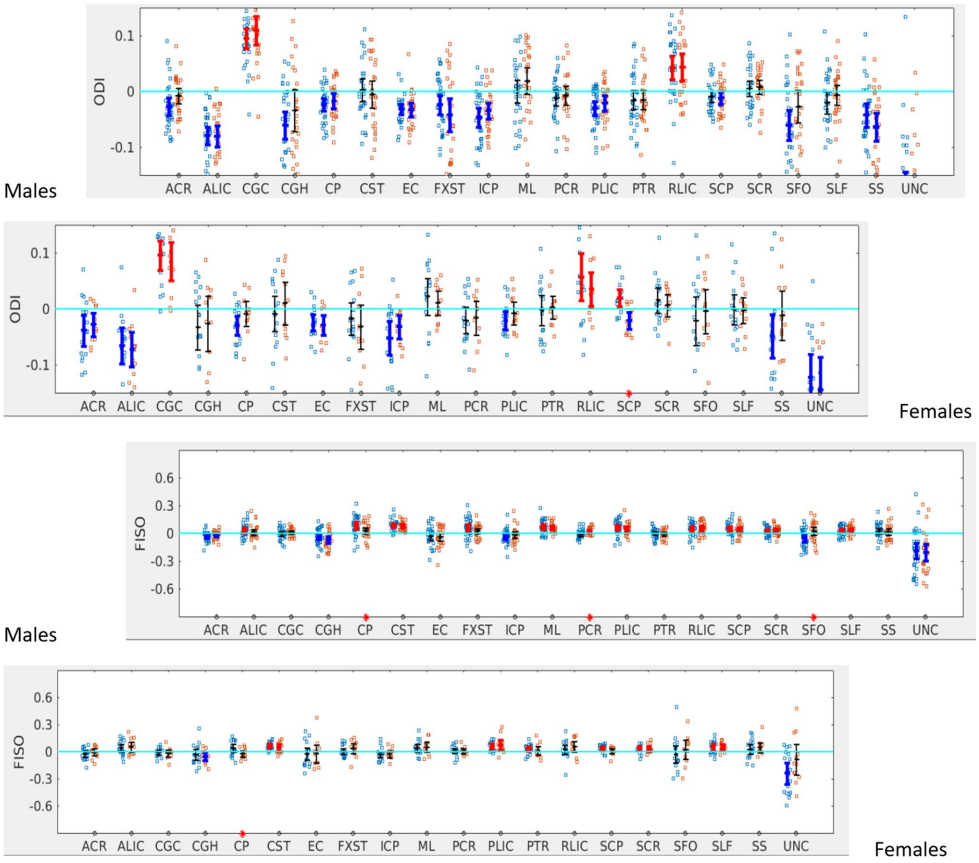

FIGURE 6
LI plotted for boys (n=58) and girls (n=29) separately for the 20 bilateral tracts for ODI and FISO comparing SOR (blue dots) to non-SOR (red dots) means with 95% CI are resented in the figure for SOR and Non SOR, 95% CI bars in red represents significant right lateralization (positive LI) of the tract while blue bar represents significant left lateralizatin (negative LI) of the tract. There were no significant differences between SOR and non-SOR NDI and hence these are not analyzed saperatly for males and females. Red asterisks on the X axis represent tracts for which difference between SOR vs. non SOR was significant at p<0.05.

Conclusion

Our study shows that advanced dMRI provides valuable insights into the neurobiological basis of sensory processing dysfunction, which is now recognized as a fundamental feature of ASD as well as a significant neurodevelopmental challenge for many children not on the autistic spectrum. SOR shows distinctive laterality differences from non-SOR SPD in white matter microstructure which differs between males and females. Assessing hemispheric asymmetry may help eliminate the variability associated with scanner hardware, software, scan protocols and also interindividual variation. Hence, dMRI measures of lateralization may potentially serve as clinically useful imaging biomarkers for neurodevelopmental disorders such as sensory processing dysfunction, including all its subtypes. Better elucidating the white matter microstructure and connectivity of those with SPD might also aid neuroscientific research on sensory processing, which is the early developing gateway into the brain, and which needs to develop normally for downstream systems such as language and attention to then develop and function properly.

Data availability statement

The datasets presented in this study can be found in online repositories. The names of the repository/repositories and accession number(s) can be found at: The raw data have been submitted to the NIMH Data Archive (NDA) for public dissemination.

Ethics statement

The studies involving human participants were reviewed and approved by UCSF Committee on Human Research institutional review board. Written informed consent to participate in this study was provided by the participants' legal guardian/next of kin.

Author contributions

SP carried out image processing, and analyses interpreted the findings, wrote, and revised the manuscript. JW-J, IB, and LC assisted in data collection, analysis, and in interpretation of findings and

revised the manuscript. ML, MR, RC, KT, and RG performed the SP3D assessments and collected and assisted in the interpretation of data, and revised the manuscript. PM and EM designed the study, interpreted findings, and contributed to the writing and revision of the manuscript. All authors contributed to the article and approved the submitted version.

Funding

The study was funded by the National Institute of Health R01 grant, award number MH116950. The research was conducted in the absence of any commercial or financial relationships that could be construed as a potential conflict of interest.

Conflict of interest

The authors declare that the research was conducted in the absence of any commercial or financial relationships that could be construed as a potential conflict of interest.

Publisher's note

References

Andersson, J. L., Skare, S., and Ashburner, J. (2003). How to correct susceptibility distortions in spin-echo echo-planar images: application to diffusion tensor imaging. *NeuroImage* 20, 870–888. doi: 10.1016/S1053-8119(03)00336-7

Andica, C., Kamagata, K., Kirino, E., Uchida, W., Irie, R., Murata, S., et al. (2021). Neurite orientation dispersion and density imaging reveals white matter microstructural alterations in adults with autism. *Mol. Autism.* 12:48. doi: 10.1186/s13229-021-00456-4

Brix, N., Ernst, A., Lauridsen, L. L. B., Parner, E., Støvring, H., Olsen, J., et al. (2019). Timing of puberty in boys and girls: a population-based study. *Paediatr. Perinat. Epidemiol.* 33, 70–78. doi: 10.1111/ppe.12507

Buyanova, I. S., and Arsalidou, M. (2021). Cerebral white matter myelination and relations to age, gender, and cognition: a selective review. *Front. Hum. Neurosci.* 15:662031. doi: 10.3389/fnhum.2021.662031

Chang, Y. S., Gratiot, M., Owen, J. P., Brandes-Aitken, A., Desai, S. S., Hill, S. S., et al. (2015). White matter microstructure is associated with auditory and tactile processing in children with and without sensory processing disorder. *Front. Neuroanat.* 9:169. doi: 10.3389/fnana.2015.00169

Chang, Y. S., Owen, J. P., Desai, S. S., Hill, S. S., Arnett, A. B., Harris, J., et al. (2014). Autism and sensory processing disorders: shared white matter disruption in sensory pathways but divergent connectivity in social-emotional pathways. *PLoS One* 9:e103038. doi: 10.1371/journal.pone.0103038

Chang, Y. S., Owen, J. P., Pojman, N. J., Thieu, T., Bukshpun, P., Wakahiro, M. L., et al. (2015). White matter changes of Neurite density and fiber orientation dispersion during human brain maturation. *PLoS One* 10:e0123656. doi: 10.1371/journal.pone.0123656

Daducci, A., Canales-Rodríguez, E. J., Zhang, H., Dyrby, T. B., Alexander, D. C., and Thiran, J. P. (2015). Accelerated microstructure imaging via convex optimization (AMICO) from diffusion MRI data. *NeuroImage* 105, 32–44. doi: 10.1016/j.neuroimage.2014.10.026

DeRosse, P., Nitzburg, G. C., Ikuta, T., Peters, B. D., Malhotra, A. K., and Szeszko, P. R. (2015). Evidence from structural and diffusion tensor imaging for frontotemporal deficits in psychometric schizotypy. *Schizophr. Bull.* 41, 104–114. doi: 10.1093/schbul/sbu150

Fletcher, P. T., Whitaker, R. T., Tao, R., Dubray, M. B., Froehlich, A., Ravichandran, C., et al. (2010). Microstructural connectivity of the arcuate fasciculus in adolescents with high-functioning autism. *NeuroImage* 51, 1117–1125. doi: 10.1016/j.neuroimage.2010.01.083

Floris, D. L., Wolfers, T., Zabihi, M., Holz, N. E., Zwiers, M. P., Charman, T., et al. (2021). Atypical brain asymmetry in autism-a candidate for clinically meaningful stratification. *Biol. Psychiatry Cogn. Neurosci. Neuroimag.* 6, 802–812. doi: 10.1016/j.bpsc.2020.08.008

Geeraert, B. L., Lebel, R. M., and Lebel, C. (2019). A multiparametric analysis of white matter maturation during late childhood and adolescence. *Hum. Brain Mapp.* 40, 4345–4356. doi: 10.1002/hbm.24706

Gillberg, C. (2010). The ESSENCE in child psychiatry: early symptomatic syndromes eliciting neurodevelopmental clinical examinations. *Res. Dev. Disabil.* 31, 1543–1551. doi: 10.1016/j.ridd.2010.06.002

Gong, G., Jiang, T., Zhu, C., Zang, Y., He, Y., Xie, S., et al. (2005). Side and handedness effects on the cingulum from diffusion tensor imaging. *Neuroreport* 16, 1701–1705. doi: 10.1097/01.wnr.0000183327.98370.6a

Gotts, S. J., Jo, H. J., Wallace, G. L., Saad, Z. S., Cox, R. W., and Martin, A. (2013). Two distinct forms of functional lateralization in the human brain. *Proc. Natl. Acad. Sci. U. S. A.* 110, E3435–E3444. doi: 10.1073/pnas.1302581110

Horowitz-Kraus, T., Buck, C., and Dorrmann, D. (2016). Altered neural circuits accompany lower performance during narrative comprehension in children with reading difficulties: an fMRI study. *Ann. Dyslexia* 66, 301–318. doi: 10.1007/s11881-016-0124-4

Kang, X., Herron, T. J., Ettlinger, M., and Woods, D. L. (2015). Hemispheric asymmetries in cortical and subcortical anatomy. *Laterality* 20, 658–684. doi: 10.1080/1357650X.2015.1032975

Kodiweera, C., Alexander, A. L., Harezlak, J., McAllister, T. W., and Wu, Y. C. (2016). Age effects and sex differences in human brain white matter of young to middle-aged adults: a DTI, NODDI, and q-space study. *NeuroImage* 128, 180–192. doi: 10.1016/j.neuroimage.2015.12.033

Lange, N., Dubray, M. B., Lee, J. E., Froimowitz, M. P., Froehlich, A., Adluru, N., et al. (2010). Atypical diffusion tensor hemispheric asymmetry in autism. *Autism Res.* 3, 350–358. doi: 10.1002/aur.162

Leisman, G., Melillo, R., Melillo, T., Machado, C., Machado-Ferrer, Y., Chinchilla, M., et al. (2022). Taking sides: asymmetries in the evolution of human brain development in better understanding autism Spectrum disorder. *Symmetry.* 14:2689. doi: 10.3390/sym14122689

Lo, Y.-C., Soong, W.-T., Gau, S. S.-F., Wu, Y.-Y., Lai, M.-C., Yeh, F.-C., et al. (2011). The loss of asymmetry and reduced interhemispheric connectivity in adolescents with autism: a study using diffusion spectrum imaging tractography. *Psychiatry Res. Neuroimaging* 192, 60–66. doi: 10.1016/j.pscychresns.2010.09.008

Lord, C. R. M., DiLavore, P. C., Risi, S., Gotham, K, and Bishop, S. *Autism diagnostic observation schedule, 2nd*. Torrence, CA: Western Psychological Services (2012).

Madsen, K. S., Jernigan, T. L., Iversen, P., Frokjaer, V. G., Mortensen, E. L., Knudsen, G. M., et al. (2012). Cortisol awakening response and negative emotionality linked to asymmetry in major limbic fibre bundle architecture. *Psychiatry Res.* 201, 63–72. doi: 10.1016/j.pscychresns.2011.07.015

Marco, E. J., Hinkley, L. B., Hill, S. S., and Nagarajan, S. S. (2011). Sensory processing in autism: a review of neurophysiologic findings. *Pediatr. Res.* 69, 48r–54r. doi: 10.1203/PDR.0b013e3182130c54

Miller, L. J., Schoen, S. A., and Nielsen, D. M. (2012). "Sensory processing disorder: implications for multisensory function" in *The new handbook of multisensory processing*. ed. B. E. Stein (Cambridge MA: MIT Press), 707–721.

Mulligan, S., Schoen, S., Miller, L., Valdez, A., Wiggins, A., Hartford, B., et al. (2019). Initial studies of validity of the sensory processing 3-dimensions scale. *Phys. Occup. Ther. Pediatr.* 39, 94–106. doi: 10.1080/01942638.2018.1434717

Narayan, A., Rowe, M. A., Palacios, E. M., Wren-Jarvis, J., Bourla, I., Gerdes, M., et al. (2020). Altered cerebellar white matter in sensory processing dysfunction is associated with impaired multisensory integration and attention. *Front. Psychol.* 11:618436. doi: 10.3389/fpsyg.2020.618436

Ocklenburg, S., Friedrich, P., Güntürkün, O., and Genç, E. (2016). Intrahemispheric white matter asymmetries: the missing link between brain structure and functional lateralization? *Rev. Neurosci.* 27, 465–480. doi: 10.1515/revneuro-2015-0052

Osório, J. M. A., Rodríguez-Herreros, B., Richetin, S., Junod, V., Romascano, D., Pittet, V., et al. (2021). Sex differences in sensory processing in children with autism spectrum disorder. *Autism Res.* 14, 2412–2423. doi: 10.1002/aur.2580

Owen, J. P., Marco, E. J., Desai, S., Fourie, E., Harris, J., Hill, S. S., et al. (2013). Abnormal white matter microstructure in children with sensory processing disorders. *Neuroimage Clin.* 2, 844–853. doi: 10.1016/j.nicl.2013.06.009

Palacios, E. M., Owen, J. P., Yuh, E. L., Wang, M. B., Vassar, M. J., Ferguson, A. R., et al. (2020). The evolution of white matter microstructural changes after mild traumatic brain injury: a longitudinal DTI and NODDI study. *Sci. Adv.* 6:eaaz6892. doi: 10.1126/sciadv.aaz6892

Park, H. J., Westin, C. F., Kubicki, M., Maier, S. E., Niznikiewicz, M., Baer, A., et al. (2004). White matter hemisphere asymmetries in healthy subjects and in schizophrenia: a diffusion tensor MRI study. *NeuroImage* 23, 213–223. doi: 10.1016/j.neuroimage.2004.04.036

Payabvash, S., Palacios, E. M., Owen, J. P., Wang, M. B., Tavassoli, T., Gerdes, M., et al. (2019). Diffusion tensor tractography in children with sensory processing disorder: potentials for devising machine learning classifiers. *Neuroimage Clin.* 23:101831. doi: 10.1016/j.nicl.2019.101831

Postema, M. C., van Rooij, D., Anagnostou, E., Arango, C., Auzias, G., Behrmann, M., et al. (2019). Altered structural brain asymmetry in autism spectrum disorder in a study of 54 datasets. *Nat. Commun.* 10:4958. doi: 10.1038/s41467-019-13005-8

Rutter, M, Bailey, A, and Lord, C *The social communication questionnaire: manual* Los Angeles: Western Psychological Services (2003).

Schmitz, J., Fraenz, C., Schlüter, C., Friedrich, P., Jung, R. E., Güntürkün, O., et al. (2019). Hemispheric asymmetries in cortical gray matter microstructure identified by neurite orientation dispersion and density imaging. *NeuroImage* 189, 667–675. doi: 10.1016/j.neuroimage.2019.01.079

Takao, H., Abe, O., Yamasue, H., Aoki, S., Sasaki, H., Kasai, K., et al. (2011). Gray and white matter asymmetries in healthy individuals aged 21-29 years: a voxel-based morphometry and diffusion tensor imaging study. *Hum. Brain Mapp.* 32, 1762–1773. doi: 10.1002/hbm.21145

Takao, H., Hayashi, N., and Ohtomo, K. (2013). White matter microstructure asymmetry: effects of volume asymmetry on fractional anisotropy asymmetry. *Neuroscience* 231, 1–12. doi: 10.1016/j.neuroscience.2012.11.038

Tavassoli, T., Brandes-Aitken, A., Chu, R., Porter, L., Schoen, S., Miller, L. J., et al. (2019). Sensory over-responsivity: parent report, direct assessment measures, and neural architecture. *Mol. Autism.* 10:4. doi: 10.1186/s13229-019-0255-7

Tavassoli, T., Miller, L. J., Schoen, S. A., Jo Brout, J., Sullivan, J., and Baron-Cohen, S. (2018). Sensory reactivity, empathizing and systemizing in autism spectrum conditions and sensory processing disorder. *Dev. Cogn. Neurosci.* 29, 72–77. doi: 10.1016/j.dcn.2017.05.005

Trivedi, R., Agarwal, S., Rathore, R. K. S., Saksena, S., Tripathi, R. P., Malik, G. K., et al. (2009). Understanding development and lateralization of major cerebral fiber bundles in pediatric population through quantitative diffusion tensor Tractography. *Pediatr. Res.* 66, 636–641. doi: 10.1203/PDR.0b013e3181bbc6b5

Wechsler, D. *Wechsler intelligence scale for children-fifth edition*. Bloomington, MN: Pearson (2014).

Xu, M., Calhoun, V., Jiang, R., Yan, W., and Sui, J. (2021). Brain imaging-based machine learning in autism spectrum disorder: methods and applications. *J. Neurosci. Methods* 361:109271. doi: 10.1016/j.jneumeth.2021.109271

Yasmin, H., Aoki, S., Abe, O., Nakata, Y., Hayashi, N., Masutani, Y., et al. (2009). Tract-specific analysis of white matter pathways in healthy subjects: a pilot study using diffusion tensor MRI. *Neuroradiology* 51, 831–840. doi: 10.1007/s00234-009-0580-1

Zhang, H., Schneider, T., Wheeler-Kingshott, C. A., and Alexander, D. C. (2012). NODDI: practical in vivo neurite orientation dispersion and density imaging of the human brain. *NeuroImage* 61, 1000–1016. doi: 10.1016/j.neuroimage.2012.03.072

frontiers | Frontiers in Neuroscience

TYPE Original Research
PUBLISHED 23 June 2023
DOI 10.3389/fnins.2023.1205489

OPEN ACCESS

EDITED BY
Jurgen Germann,
University Health Network (UHN), Canada

REVIEWED BY
Elysa Jill Marco,
Cortica Healthcare, United States
Gavin Elias,
University of Toronto, Canada

*CORRESPONDENCE
Alessandra Carta
✉ alessandra.carta@aouss.it

†These authors have contributed equally to this work

RECEIVED 13 April 2023
ACCEPTED 07 June 2023
PUBLISHED 23 June 2023

CITATION
Sotgiu MA, Lo Jacono A, Barisano G, Saderi L, Cavassa V, Montella A, Crivelli P, Carta A and Sotgiu S (2023) Brain perivascular spaces and autism: clinical and pathogenic implications from an innovative volumetric MRI study. *Front. Neurosci.* 17:1205489. doi: 10.3389/fnins.2023.1205489

Brain perivascular spaces and autism: clinical and pathogenic implications from an innovative volumetric MRI study

Maria Alessandra Sotgiu[1†], Alessandro Lo Jacono[2†], Giuseppe Barisano[3†], Laura Saderi[4], Vanna Cavassa[2], Andrea Montella[1], Paola Crivelli[5], Alessandra Carta[2*] and Stefano Sotgiu[2]

[1]Department of Biomedical Sciences, University of Sassari, Sassari, Italy, [2]Unit of Child Neuropsychiatry, Department of Medicine, Surgery and Pharmacy, University of Sassari, Sassari, Italy, [3]Department of Neurosurgery, Stanford University, Stanford, CA, United States, [4]Clinical Epidemiology and Statistics Unit, Department of Medicine, Surgery and Pharmacy, University of Sassari, Sassari, Italy, [5]Radiology Unit, Department of Medicine, Surgery and Pharmacy, University of Sassari, Sassari, Italy

Introduction: Our single-center case–control study aimed to evaluate the unclear glymphatic system alteration in autism spectrum disorder (ASD) through an innovative neuroimaging tool which allows to segment and quantify perivascular spaces in the white matter (WM-PVS) with filtering of non-structured noise and increase of the contrast-ratio between perivascular spaces and the surrounding parenchyma.

Methods: Briefly, files of 65 ASD and 71 control patients were studied. We considered: ASD type, diagnosis and severity level and comorbidities (i.e., intellectual disability, attention-deficit hyperactivity disorder, epilepsy, sleep disturbances). We also examined diagnoses other than ASD and their associated comorbidities in the control group.

Results: When males and females with ASD are included together, WM-PVS grade and WM-PVS volume do not significantly differ between the ASD group and the control group overall. We found, instead, that WM-PVS volume is significantly associated with male sex: males had higher WM-PVS volume compared to females ($p = 0.01$). WM-PVS dilation is also non-significantly associated with ASD severity and younger age (< 4 years). In ASD patients, higher WM-PVS volume was related with insomnia whereas no relation was found with epilepsy or IQ.

Discussion: We concluded that WM-PVS dilation can be a neuroimaging feature of male ASD patients, particularly the youngest and most severe ones, which may rely on male-specific risk factors acting early during neurodevelopment, such as a transient excess of extra-axial CSF volume. Our findings can corroborate the well-known strong male epidemiological preponderance of autism worldwide.

KEYWORDS

autism, glymphatic system, perivascular spaces, Virchow-Robin spaces, MRI

1. Introduction

Autism spectrum disorder (ASD) is a lifetime multifaceted neuropsychiatric disorder featured by a constellation of early-appearing social communication and interaction deficits with repetitive sensory-motor behaviours; it is also characterized by a strong prevalence of males (American Psychiatric Association, 2013; Lord et al., 2022). ASD prevalence is continuously increasing with current estimations of 1/57 children, only partly attributable to a higher public awareness and better diagnostic criteria, which generates a substantial burden on public health care (Lord et al., 2018, 2022). Three severity dimensions (level 1, 2, and 3) were added into the Diagnostic and Statistical Manual of Mental Disorders, Fifth Edition (DSM-5) to specify patient's needs and social functioning (American Psychiatric Association, 2013). It is common (about 70%) for children with ASD to have other neurodevelopmental disorders that may have similar dysregulated neurobiological pathways (Lord et al., 2022), mostly Intellectual Disability (ID; 40%), Attention Deficit Hyperactivity-impulsivity Disorder (ADHD 30%) (Lai et al., 2019; Carta et al., 2020), and Epilepsy (ranging 8 to 30%) (Lai et al., 2014), along with sleep disorders (i.e., insomnia, ranging 15%–80%) (Lai et al., 2019). The etiology of ASD is highly complex and involves interacting networks between genetic and environmental risk factors (Sanders et al., 2015; Kim et al., 2019; Willsey et al., 2022). Studies have associated over a hundred among genetic loci and prenatal environmental factors (stress, undernutrition, drugs exposure, and maternal immune activation), all contributing to increase the ASD risk in offspring (Betancur, 2011; Doi et al., 2022; Hirota and King, 2023). In recent years, the early prenatal immune-mediated hypothesis has gained credibility due to microglia activation in brain autoptic studies of individuals with ASD (reviewed in Sotgiu et al., 2020). Other neuroanatomical differences have been observed in the brains of individuals with ASD in their first years of life, such as brain volume overgrowth, cortical thickness, and increased volume of perivascular spaces (PVS), also named as Virchow-Robin spaces (Ecker et al., 2012). These spaces are located around penetrating arteries and are surrounded by astrocytic vascular endfeets that express aquaporin-4 (AQP4). AQP-4 water channels permit cerebrospinal fluid (CSF) flow into the brain through arterial PVS and then into the interstitial fluid. This mixed fluid is then carried toward venous PVS to reach meningeal lymphatic drainage and cervical lymph nodes (Iliff et al., 2012; Plog and Nedergaard, 2018; Taoka and Naganawa, 2020). This network, called the glymphatic system (GS), is central to brain homeostasis for fluid transportation and waste removal (Plog and Nedergaard, 2018; Troili et al., 2020). There is growing interest associating GS and PVS with neurological disorders, as these changes to GS could cause harmful protein build-up (Liu et al., 2020; Troili et al., 2020; Barisano et al., 2022). Some studies suggest that individuals with ASD tend to have increased levels of Aβ (Wegiel et al., 2012; Westmark, 2013; Westmark et al., 2016). Furthermore, the level of extra-axial CSF in the subarachnoid space remains abnormally high even at 3 years of age, whereas it increases from birth to 7 months and decreases between 12 to 24 months (benign external hydrocephalus) in typical development (Shen et al., 2013; Shen, 2018). Occasionally, macrocephaly caused by an excess extra-axial CSF volume may not be benign, rather suggesting a putative link between abnormal CSF circulation and the development of autism (Shen et al., 2017; Dinstein and Shelef, 2018). Being the subarachnoid space directly linked to the PVS, it is not uncommon to observe an enlargement of PVS in ASD population. A pioneering MRI study demonstrated brain PVS dilation in 7/16 ASD patients (Taber et al., 2004). Later, PVS enlargements were confirmed only in ASD with co-occurring developmental delay (Zeegers et al., 2006) and only in 20% of non-syndromic ASD patients (Boddaert et al., 2009). These tenuous associations were ascribable to the fallacy of visual assessment of visible and large-caliber PVS mainly in regions of interest. A recent study with a new diffusion tensor imaging along the perivascular spaces (DTI-ALPS) technique demonstrated that ASD patients can have a significant GS dysfunction, which is strictly related to age (Li et al., 2022). Other innovative techniques (Barisano et al., 2022) can improve the quantification of PVS and enable new clinical investigations. A novel MRI processing approach, with automated quantification of the combination of T1- and T2-weighted images and the filtering of non-structured noise, has been recently developed (Sepehrband et al., 2019) which strongly improves the contrast-ratio between PVS and the surrounding tissue, thus facilitating PVS mapping and quantification. Here, by using this innovative method, we conducted, for the first time, a single-center case–control study on PVS in children with ASD and with other neuropsychiatric disorders. Based on aforementioned studies, we hypothesized that an imbalance between the production and drainage of CSF in autism may result in an enlargement of PVS. Furthermore, individuals with ASD often experience sleep issues which, in principle, can contribute to worsen this imbalance (Xie et al., 2013).

2. Materials and methods

2.1. Participants

This study was approved by the Ethics Committee of Azienda Ospedaliero-Universitaria, Cagliari, Italy (PROT. PG/2023/5144), and all procedures were performed in accordance with the relevant guidelines and regulations. A written informed consent was obtained from parents or legal guardians of all young participants. Clinical files of children with ASD and with neuropsychiatric disorders other than autism (NP/Non-ASD group) have been retrospectively and consecutively collected at the Child Neuropsychiatry Unit, University Hospital, Sassari. To reduce the complexity of the population under study, we only included patients living and born in Sardinia between January 1st, 2010 and December 31st, 2021. To be eligible, all children, with an age ranged between 2 and 7 years, must have been previously subjected to brain MRI, in line with guidelines for assessment of comorbidity conditions in ASD (NICE—National Institute for Health and Clinical Excellence, n.d.). MRI investigations are not mandatory for individuals with ASD, but professionals in Italy, as in other countries, frequently use them as part of the diagnostic process. However, it is important to mention that MRI investigation may be necessary in children with ASD who have abnormal neurological examination, macrocephaly, dysmorphisms, headache, convulsions or EEG abnormalities. Indeed, their MRI scans reveal a greater occurrence of pathological findings (Rochat et al., 2020).

Besides, clinical files had to contain cognitive and behavioral assessments along with a complete medical review. Based on this, 81 patients with ASD and 114 patients of the NP/Non-ASD group were recruited. Out of the ASD group, 9 children were excluded due to

incomplete medical records, 4 due to poor MRI quality, and 3 due to missing MRI plane data. Out of the NP/Non-ASD group, 43 patients were excluded for several reasons: 21 had incomplete medical records, 8 missed MRI sequences, 6 had missing data on MRI planes, and 8 had inadequate quality of MRI. Thereafter, 65 ASD (83%) and 71 NP/Non-ASD (65%) individuals were included, owing to the following exclusion criteria: inadequate quality of MR imaging, missing data on MRI planes and missing MRI sequences, incomplete medical records, MRI demonstration of massive malformations or tumors, massive stroke and/or hemorrhage.

2.2. Clinical methods

Diagnoses were supported by parent interviews, direct child assessment, review of available parent (and teacher for school-age children) questionnaires, as well as available prior records. At least two evaluators were involved in the diagnostic assessments, including licensed psychologists and/or supervised medical residents in child and adolescent neuropsychiatric, post- and pre-doctoral fellows. One evaluator conducted the parent structured interview with parents for the anamnestic history as well as earlier history and current use of psychoactive medications for the ADHD. Another evaluator administered and scored the Autism Diagnostic Observation Schedule, second edition (ADOS-2).

After these assessments, child and parent evaluators shared their observations, discussed their clinical impressions, and reviewed all available clinical information. To further characterize the sample, additional parent-report measures, such as the Child Behavior Checklist (CBCL; Achenbach, 1999) the Vineland Adaptive Behavior Scale (VABS; Sparrow et al., 1984) or the Adaptive Behavior Assessment System—Second Edition (ABAS-II; Harrison and Oakland, 2015) survey interviews were collected.

The diagnostic assessment was conducted by at least one licensed neuropsychiatrician, or at least one supervised resident medical doctor, and consisted of parent interviews using the Autism Diagnostic Interview—Revised (ADI-R; Rutter et al., 2003), child testing and observations using the ADOS-2. Additional parent measures were also collected including the CBCL and the ABAS among others. For all studies, ADOS-2 and ADI-R were administered and scored during clinical assessment by clinically trained staff currently in training for research reliability. For this purpose, consensus ADOS-2 scoring was obtained with a research-reliable specialist. Based on ADOS and ADI scores, clinicians detected the three levels of patient's rehabilitation needs and performed a formal diagnosis for ASD in line with the DSM-5 criteria.

Cognitive abilities were assessed using the Wechsler Intelligence Scale for Children (WISC-IV; Wechsler, 2004) and the Wechsler preschool and primary scale of intelligence-III (WPPSI-III; Wechsler, 2002). LEITER International Performance Scale—revised (LEITER-R; Roid et al., 2013), or Raven's Coloured Progressive (CPM) were selected based on the participant age and cognitive abilities. The Standard Progressive Matrices (SPM) (Raven, 1998) or the Griffith's Mental Development Scale-Extended Revised (GMDS-ER; Luiz et al., 2006) were used when the child was likely to fail to complete any of the other cognitive scales because of the absence of language or his/her reduced attention resources. Some patients in the sample were not sufficiently collaborative and standardized tests results were considered invalid.

Detailed objective evaluation (to highlight dysmorphic traits), neurological examination (e.g., motor dyspraxia, pyramidal or extrapyramidal signs), clinical course (e.g., regression over neurodevelopmental phases) and anamnestic information (e.g., family history of ASD, other neurodevelopmental disorders, autoimmune diseases) were used to identify children with high risk for genetic mutations. Of these, those children with confirmed alterations on these clinical and genetic parameters were defined as possible syndromic ASD type. Based on these clinical selection criteria, children with high risk for syndromic ASD were screened for chromosomal heritable or *de novo* mutations, including micro- as well as macro-deletions/insertions. In detail, blood samples were collected to evaluate standard karyotype, FRAXA gene and array-CGH. In those with a previous specific familial history for chromosomal mutations, a FISH of the specific gene was requested. In our sample, we identify a total of 8 alterations: three children with heterozygous deletion at chromosome 22q11.2 on chromosomal microarray; one with 47XXY, one with 49XXXY and one with Down's syndrome at the standard varitype analyses. Finally, two kids were found with Fragile-X syndrome.

In sum, the following clinical variables were considered for the eligible children with ASD in our study:

- ASD type (essential, complex/syndromic).
- ASD diagnosis confirmed by the Autism Diagnostic Observation Schedule (ADOS-2; Lord et al., 2012).
- ASD severity level (1, 2, and 3; American Psychiatric Association, 2013).
- Composite intelligence quotient (IQ) of the Wechsler Preschool and Primary Scale of Intelligence-III (WIPPSI-3) or Wechsler Intelligence Scale for Children (WISC-IV) scales (normal >85; borderline: 84–71; mild ID: 55–70; moderate ID: 40–55; severe ID<40).
- Griffiths Mental Development Scales (GMDS) to measure the rate of development of young infants.
- Comorbidities: ADHD, ID, Epilepsy, Sleep disorder (insomnia).
- Genetic testing.
- MRI standard report (increased PVS, abnormal CSF circulation, malformation, normal) (Table 1).

In the NP/Non-ASD group, ADHD diagnosis was based on developmental history and extensive clinical examination and further supported by the ADHD parent's rated scale by Conners—CPRS (Conners et al., 1998). Epilepsy was diagnosed or excluded with wake and sleep electroencephalographic patterns along with patient's history; sleep disorders were diagnosed with parent-report sleep screening instrument designed, the Children's Sleep Habits Questionnaire (CSHQ) and wake and sleep electroencephalographic features (Owens et al., 2000). The adaptive and the cognitive profiles in the NP/Non-ASD group participants were evaluated throughout the same instruments used to test intellectual abilities in the ASD children. The following clinical variables were considered for children of the NP/Non-ASD group:

- Diagnosis other than ASD.
- Comorbidities: ADHD, ID, Epilepsy, Sleep disorder (insomnia).
- Composite IQ (as for ASD group).
- Griffiths Mental Development Scale.
- Genetic testing (when appropriate).
- MRI standard report (as above; Table 1).

TABLE 1 Demographic, clinical and descriptive MRI analyses of the total cohort, stratified between NP/Non-ASD and autism cases.

Patients		Total cohort (*n* =136)	NP/Non-ASD (*n* =72)	ASD (*n* =64)	*p*
Median (IQR) age, years		4 (2–6)	4 (2–7)	3 (2–5)	0.06
Females, *n* (%)		53 (39.0)	32 (44.4)	21 (32.8)	0.17
Complex autism (%)		–	–	54 (84.4)	–
ASD Severity *n* (%)	Mild 1	–	–	10 (15.6)	–
	Moderate 2	–	–	18 (28.1)	
	Severe 3	–	–	36 (56.3)	
IQ levels *n* (%)	Normal	19 (37.3)	11 (52.4)	8 (26.7)	0.34
	Borderline	16 (31.4)	6 (28.6)	10 (33.3)	
	Mild	7 (13.7)	1 (4.8)	6 (20.0)	
	Moderate	6 (11.8)	2 (9.5)	4 (13.3)	
	Severe	3 (5.9)	1 (4.8)	2 (6.7)	
ADHD, *n* (%)		13 (9.6)	3 (4.2)	10 (15.6)	**0.04**
Sleep disorders, *n* (%)		24 (17.7)	0 (0.0)	24 (37.5)	**<0.0001**
Epilepsy, *n* (%)		17 (12.5)	8 (11.1)	9 (14.1)	0.60
MRI findings					
PVS enlargement, *n* (%)		7 (5.1)	3 (4.2)	4 (6.3)	0.71
Abnormal size of CSF spaces, *n* (%)*		17 (12.5)	13 (18.1)	4 (6.3)	**0.04**
Gliosis, *n* (%)		27 (19.9)	14 (19.4)	13 (20.3)	0.90
Malformation, *n* (%)**		11 (8.1)	8 (11.1)	3 (4.7)	0.22
Normal, *n* (%)		62 (45.6)	31 (43.1)	31 (48.4)	0.53
Median (IQR) WM-PVS volume (n. of voxel)		545 (334.5–902.5)	532.5 (312.0–735.5)	621.5 (374–1,061)	0.07
WM-PVS grade, *n* (%)	1 (1–10)	6 (4.4)	5 (6.9)	1 (1.6)	0.10
	2 (11–20)	32 (23.5)	15 (20.8)	17 (26.6)	
	3 (21–40)	57 (41.9)	35 (48.6)	22 (34.4)	
	4 (>40)	41 (30.2)	17 (23.6)	24 (37.5)	

*Benign enlargement or restriction of ventricular size; benign enlargement of subarachnoid space; idiopathic aqueduct stenosis, megacisterna magna, Chiari I with or without syringomyelia. **Macrocephaly, microcephaly, cerebellar atrophy, abnormal septum pellucidum, abnormal corpus callosum, abnormal neuronal migration, abnormal cortical organization. Significant *p* values are in bold.

2.3. MRI processing

Standard MRI acquisition was performed, in all individuals, by using the same 1.5 Tesla Philips MRI scanner at the University Hospital in Sassari. The following sequences and planes were considered: T1-weighted spin-echo axial (TR: 357–895 ms; TE: 10–15 ms; flip angle: 69) and T2-weighted turbo spin-echo axial (TR: 4,000–7,000 ms; TE: 100 ms; flip angle: 90;) imaging with a spatial resolution of 0.8 × 0.8 × 4.4 mm^3 and 0.4 × 0.4 × 4.4 mm^3, respectively. One senior neuroradiologist (PC with 13 years of experience), blinded to clinical information, performed the MRI qualitative analysis. Special attention was given to evaluating shape/size of perivascular and subarachnoid spaces. Lateral ventricles were defined enlarged when the largest diameter perpendicular to the midline measured in axial slices on the frontal horn, body and/or the atrium was above 10 mm, whereas PVS were defined enlarged when there were at least 3 PVS whose diameter perpendicular to the PVS' main axis was above 3 mm (Boddaert et al., 2009). Gliosis was identified in T2 sequences as areas with a higher signal intensity compared with the surrounding white matter. Other MRI abnormalities, such as mega cisterna magna, idiopathic aqueduct stenosis, Chiari I with or without syringomyelia were considered, as they may indicate abnormal CSF circulation. Cerebellar atrophy, abnormal septum pellucidum, abnormal corpus callosum, neuronal migration (cortical ectopias) and cortical organization (lissencephaly or focal cortical dysplasia) were also taken into account. These classifications were made qualitatively based on the overall impression of the neuroradiologist. Macro/microcephaly was assessed clinically based on head circumference. Spatial resolution, MRI planes and sequences of the two datasets (ADS vs. NP/Non-ASD) were comparable. Subsequent MRI processing was conducted using a semi-automated quantification algorithm for PVS. A multi-modal approach enhanced the PVS visibility by combining T1 and T2 images that were adaptively filtered to remove non-structural high frequency spatial noise (Sepehrband et al., 2019; Barisano et al., 2022). A white matter mask was generated with a fast and sequence-adaptive whole-brain segmentation algorithm applied on T1 images (Puonti et al., 2016), and was subsequently eroded by 1 voxel. T2 images were then rigidly transformed to the T1 space. White matter intensity was uniformized across space using the default values of the 3dUnifize function in AFNI (Cox, 1996). In the eroded white matter mask applied on the

T2-weighted image, we calculated voxel-wise the average intensity difference between the voxel and its surrounding voxels. The intensity difference maps were reviewed blind to clinical status to the clinical and demographic information, and an intensity difference higher than 60 was used to define a voxel as a white matter PVS (WM-PVS) voxel. Since the slice thickness was larger than the PVS thickness, the number of voxels rather than the mm^3 was the adopted measurement unit for the volume of white matter and PVS. Also, as the PVS volume is highly correlated with the WM volume (Barisano et al., 2021), the PVS volume value was normalized using the amount of white matter for each individual. Since the majority of PVS studies in the literature report only the visual scores of the MRI-visible PVS (Barisano et al., 2022), in our study we included a qualitative estimate of the extent of the PVS burden. Therefore, the number of WM-PVS voxel clusters was calculated. WM-PVS voxel clusters were identified automatically in each axial slice within the eroded white matter mask: PVS voxels were considered part of the same cluster if their edges or corners touch. Finally, we recorded for each subject the highest number of WM-PVS visible in a single axial slice, and adapted a validated 5-point scale (MacLullich, 2004) to define the following WM-PVS grades (Figure 1):

- WM-PVS Grade 0: denoted 0 PVS.
- WM-PVS Grade 1: denoted for 1 to 10 PVS.
- WM-PVS Grade 2: for 11 to 20 PVS.
- WM-PVS Grade 3: for 21 to 40 PVS.
- WM-PVS Grade 4: for more than 40 PVS.

2.4. Statistical analysis

Sample characteristics were summarized with medians and interquartile ranges (IQR) for quantitative variables, and with absolute and relative (percentages) frequencies for qualitative ones. Shapiro–Wilk test was used to assess normality of data. Comparison of qualitative variables was performed with Chi Square or Fisher exact test, whereas Mann–Whitney or Kruskal-Wallis test were used for the comparison of quantitative variables between two or more groups, respectively. Spearman's correlation was performed to assess the relationship between the different MRI measurements. Statistical significance level was set at $p < 0.05$. STATA software version 17 (StataCorp, TX) was used to perform all statistical computations.

3. Results

Table 1 reported detailed demographic and clinical information between ASD cohort and NP/Non-ASD group. A total of 136 patients (61% males) were evaluated; of these, 72 (55.6% males) were cNP/Non-ASD individuals and 64 (67.2% males) children with ASD. The median age in the total cohort was 4 years (IQR: 2–6), 4 years in the NP/Non-ASD and 3 in the ASD group. Children with ASD were diagnosed with complex ASD in 84.4%, mostly with level 3 (severe autism 56.3%). Intellectual disability (from mild to severe) was found in 40% ASD and 19% NP/Non-ASD. ADHD and sleep disorders were significantly more represented within the ASD group (15.6 and 37.5%; $p = 0.04$ and < 0.0001, respectively). On the contrary, the frequency of epilepsy was equally distributed among the two groups (Table 1).

Descriptive standard MRI data indicated a significant impairment of CSF circulation within the NP/Non-ASD compared to ASD ($p = 0.04$; Table 1).

WM-PVS volume was directly related with the WM-PVS grade (Supplementary Figure S1). Median WM-PVS volume increases as WM-PVS grade increases, from 161 (IQR: 115–228) voxels in grade 1 to 1,114 (IQR: 949–1,422) voxels in grade 4.

Table 2A shows the difference of median WM-PVS volume and frequencies of WM-PVS grade according to sex in the whole cohort (ASD plus NP/Non-ASD). When males and females with ASD are included together, WM-PVS grade and WM-PVS volume do not significantly differ between the ASD group and the control group

TABLE 2 Comparison between PVS-WM volume and WM-PVS visual grades with (a) the sex of the whole cohort, (b) NP-Non-ASD versus ASD males, (c) NP-Non-ASD versus ASD females, (d) autism cases < and≥ 4 years of age, and (e) according with ASD severity.

		(a) Whole cohort		(b) Male cohort		(c) Female cohort		(d) Age of ASD cases		(e) Severity of ASD		
Groups (n. of patients)		All males (83)	All females (53)	Male NP-Non-ASD (40)	Male ASD (43)	Female NP-Non-ASD (32)	Female ASD (n = 21)	<4 years (35)	≥4 years (29)	Mild level 1 (10)	Moderate level 2 (18)	Severe level 3 (36)
Median (IQR) WM-PVS volume (n. of voxel)		596* (361–1,099)	425 (306–701)	545 (353–931.5)	705 (392–1,196)	415 (267–660.5)	425 (337–730)	795** (431–1,252)	422 (324–657)	488.5 (332–657)	417 (294–855)	751.5 (434–1,155)
WM-PVS grade *n* (%)	1 (1–10)	3 (3.6)	3 (5.7)	3 (7.5)	0 (0.0)	2 (6.3)	1 (4.8)	1 (2.9)	0 (0.0)	0 (0.0)	1 (5.6)	0 (0.0)
	2 (11–20)	19 (22.9)	13 (24.5)	7 (17.5)	12 (27.9)	8 (25.0)	5 (23.8)	6 (17.1)	11 (37.9)	3 (30.0)	6 (33.3)	8 (22.2)
	3 (21–40)	35 (42.2)	22 (41.5)	22 (55.0)	13 (30.2)	13 (40.6)	9 (42.9)	10 (28.6)	12 (41.4)	5 (50.0)	6 (33.3)	11 (30.6)
	4 (>40)	26 (31.3)	15 (28.3)	8 (20.0)	18* (41.9)	9 (28.1)	6 (28.6)	18*** (51.4)	6 (20.7)	2 (20.0)	5 (27.8)	17 (47.2)

Significant results are indicated with asterisks. WM-PVS grade 4 showed a progressive increase in frequency in relation to the progressive severity of ASD (20.0%, 27.8% and 47.2% in the mild, moderate, and severe level, respectively). *$p = 0.01$; **$p = 0.006$; ***$p = 0.03$.

overall. We found, instead, that males had higher WM-PVS volume compared to females ($p = 0.01$).

Considering the cohort of only males, children with ASD also showed a higher median WM-PVS volume (705, IQR 392–1,196) compared to males of the NP/Non-ASD group (545, IQR 353–931.5; Table 2B) and a significant difference in the WM-PVS grade, being the extreme grade (grade 4) more represented in ASD than in NP/Non-ASD males. On the contrary, no difference was found in WM-PVS volume and WM-PVS grade between female ASD and female NP/Non-ASD (Table 2C).

Stratifying children with ASD by age < and ≥ 4 years, both median WM-PVS volume and frequency of WM-PVS grade 4 were higher in younger ASD patients compared to those with 4 years or more (795, IQR: 431–1,252 vs. 422, IQR; 324–657; $p = 0.006$, and 18, 51.4% vs. 6, 20.7%; $p = 0.03$, respectively) (Table 2D and Figure 2).

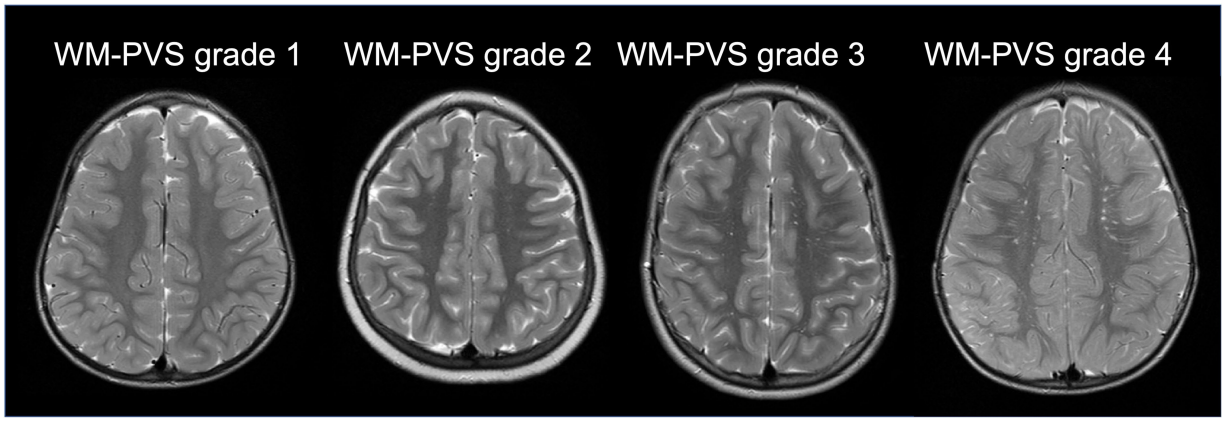

FIGURE 1
WM-PVS grades. Representative cases of the four WM-PVS grades observed in our cohort. WM-PVS on T2-weighted axial images appear as hyperintense structures in the white matter, linear or punctate depending on whether their course is parallel or perpendicular to the axial acquisition plane, respectively.

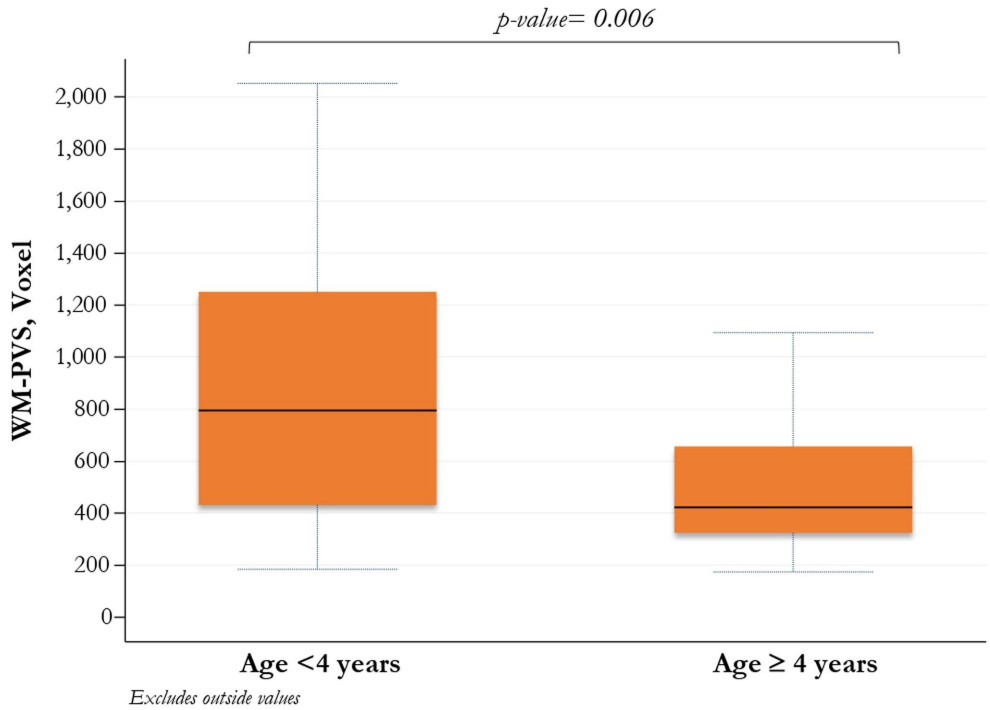

FIGURE 2
Comparison between WM-PVS volume and ASD patients (<4 years/≥ 4 years). PVS_WM enlargement is significantly more present at a younger age in ASD patients.

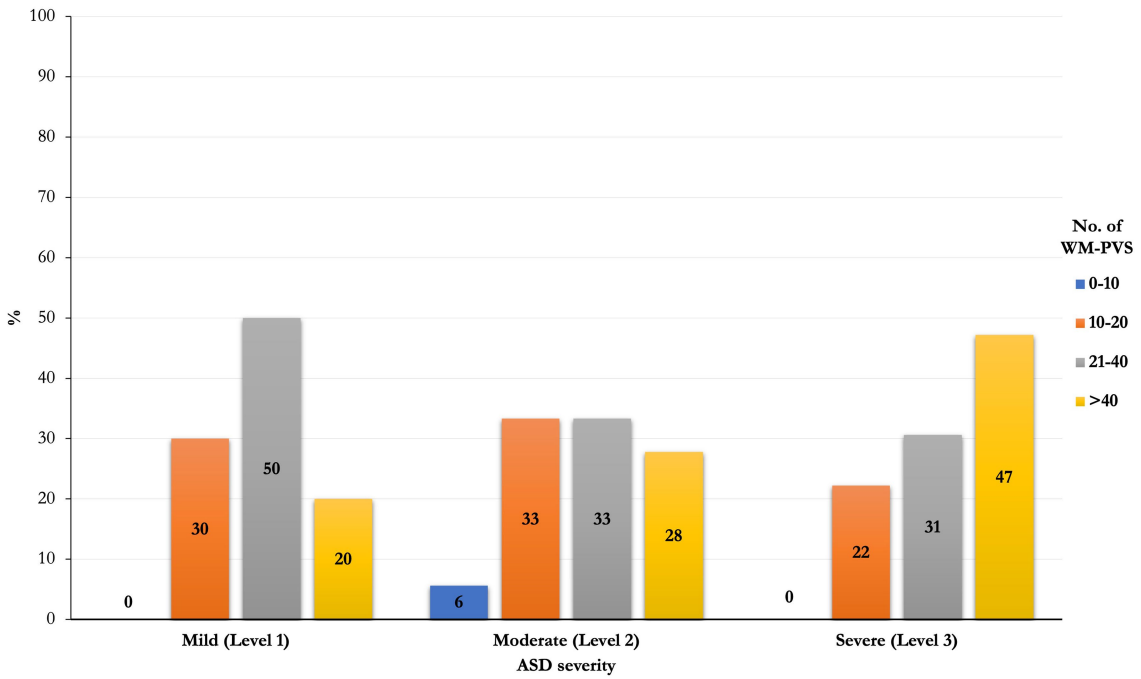

FIGURE 3
Frequencies distribution of PVS class between severity of ASD. An increasing prevalence of the number of WM-PVS more than 40 emerged as the ASD severity worsened (level 1 to level 3): only 20% of ASD patients with mild severity (level 1) had WM-PVS Grade 4, while 47% of level 3 severity ASD patients had WM-PVS Grade 4. This trend is not significant (p =0.22).

Although not significantly (p = 0.22). an increasing prevalence, of the number of WM-PVS more than 40 emerged as the ASD severity worsened: only 20% of ASD patients with mild severity (level 1) had WM-PVS Grade 4, while 47% of level 3 severity ASD patients had WM-PVS Grade 4 (Table 2E and Figure 3). Among the ASD-associated comorbidities (ADHD, Epilepsy, ID, Sleep disorders), the highest WM-PVS grade was directly related to insomnia but not to other comorbid disorders, although rating of sleep co-occurring condition in both cohorts was lower compared to the expected rate from literature.

4. Discussion

Apart from the rare monogenic ASD forms, ASD etiology and the heterogeneity of its symptoms constellation involve a complex interaction of genes, environment, epigenetic and immunological factors. None of these factors alone are enough to fully explain the causes of ASD (Kim et al., 2019; Lord et al., 2020; Trost et al., 2022). Consequently, the vast majority of autistic disorders remains of undetermined origin and attempts to discover common risk factors for all/most ASD forms seem yet destined to fail. In general, core ASD features, age at onset and subsequent clinical trajectories vary substantially from one individual to another, making it necessary to define distinct ASD subtypes (Lord et al., 2018). ASD forms can show heterogeneity at their onset being ASD occurrence classified of either an "early" or "regressive" type. In the early-onset ASD, children present with early problems in behaviour and interaction, while in the regressive pattern the loss of communication is manifested later, conventionally after having learned 5 words and used them for at least 3 months (Zwaigenbaum, 2019). Male children with regressive ASD onset can have abnormal, though transient, age-dependent brain enlargement on MRI (Nordahl et al., 2011), associated with an excess of peripheral pro-inflammatory cytokines (Ashwood et al., 2011). Interestingly, children later diagnosed with autism, have shown, on MRI, a transient excess volume of extra-axial CSF (EA-CSF) in the subarachnoid space, which did not correlate to the reduced brain parenchymal size (Shen et al., 2018). Here the CSF, that circulates in two compartments divided by a lymphatic-like membrane called SLYM (Møllgård et al., 2023), is in direct communication with PVS. PVS, typically <3 mm, are not seen on standard MRI sequences, but become visible when they are enlarged as a consequence of glymphatic flow reduction (Potter et al., 2015; Mestre et al., 2017).

In children, PVS dilation is not a common finding, with the exception of some rare genetic/metabolic diseases, such as mucopolysaccharidoses (Zafeiriou and Batzios, 2013). Some association has been initially reported in ASD (Taber et al., 2004; Zeegers et al., 2006; Boddaert et al., 2009) based on studies with traditional visual and subjective MRI measuring. A recent study with an innovative DTI-ALPS method has assessed an age-related GS dysfunction in a limited group of patients with ASD (Li et al., 2022). With our study we aimed at giving more insight into the relationship between ASD and WM-PVS by increasing the sample size (this is the largest study conducted so far) and by using a novel MRI-processing approach which ameliorates PVS mapping and quantification (Sepehrband et al., 2019; Barisano et al., 2022). Also, for the first time, we aimed at investigating the association between WM-PVS and ASD severity and associated comorbidities.

The first result of the study is that WM-PVS volume is significantly associated with the male sex. All males (both ASD and NP/Non-ASD)

are distinguished by a significantly higher WM-PVS volume compared to females, in line with previous results (Zhu et al., 2011; Barisano et al., 2021). Additionally, the highest WM-PVS grade is more frequent in male ASD patients than NP/Non-ASD children, while no differences were found in females. Results are in line with the concept that male epidemiological preponderance in autism may rely on male-specific risk mechanisms and/or female-specific protective mechanisms (Floris et al., 2021). These mechanisms can act early during neurodevelopment although age and comorbidities strongly modulate the pattern of differences later in life (Lai et al., 2017).

In our study, frequency distribution of WM-PVS grades according to different severity levels of ASD shows an increasing trend, with 80% "mild" ASD patients with less than 40 WM-PVS (WM-PVS grade 0–3) in a single MRI section and 53% "severe" ASD patients with more than 40 visible WM-PVS (WM-PVS grade 4). Consistently, patients with ASD and insomnia tend to have higher WM-PVS volume compared to ASD patients without sleep issues, although this result was not statistically significant. Previous studies reported an association between higher PVS visibility on MRI and impaired sleep quality and efficiency (Berezuk et al., 2015; Aribisala et al., 2020) and obstructive sleep apnea (Song et al., 2017). In fact, sleep has been shown to be important for a proper functioning of the glymphatic system (Hablitz and Nedergaard, 2021).

Moreover, PVS dilation is significantly associated with a younger age in ASD patients (less than 4 years in our study). This finding is of particular importance as it corroborates the aforementioned age-related GS dysfunction in patients with ASD studied with DTI-ALPS MRI (Li et al., 2022) and the transient excess volume of EA-CSF in children who have been diagnosed as ASD later in their life (Shen et al., 2018).

Finally, we found no relation between WM-PVS and epilepsy or IQ. A recent study in a large sample of healthy young adults found no association between WM-PVS and cognitive function (Barisano et al., 2021), while in pediatric idiopathic generalized epilepsy and post-traumatic epilepsy MRI-visible PVS alterations have been described (Duncan et al., 2018; Liu et al., 2020). This disagreement is possibly due to the relatively low number of patients with epilepsy (17/136) in our study, which was not specifically focused on epilepsy. ADHD alone or in comorbidity seems also not to be related to PVS enlargement, possibly because ADHD is mediated by factors unrelated to immune-mediated or PVS-related mechanisms (Sotgiu et al., 2020; Carta et al., 2022).

While in previous studies the MRI-visible PVS were typically assessed through visual rating systems which provided a qualitative estimate of the PVS burden, current neuroimaging tools allow to perform segmentation of PVS on brain MRI. This advancement, coupled with improvements in quality and spatial resolution of the MRI data, increased the sensitivity in PVS detection on MRI and is leading to the exploration of novel quantitative and morphological features of MRI-visible PVS and their use as neuroimaging biomarker for neuropsychiatric disorders.

Our study does have limitations. Anamnestic data collection might have been impaired by the retrospective nature of the study. To overcome this problem, we used a very strict selection of the patients. The ADHD rates are generally considered to be up to 50% in school-aged autistic children. With the selection criteria given the age range of our participants may be undercounting an ADHD condition and, in principle, can affect results in our non-ASD cohort. Another limitation is the use of 2D MRI data, which prevented us to compute 3D maps of WM-PVS. However, this flaw was homogeneously distributed throughout the study groups. Also, we acknowledge that, being a hospital-based study, we may have selected for more severe and complex ASD cases and could not identify matched NP/Non-ASD children without neuropsychiatric disorder, which may have biased the final outcome. However, sex male is more represented in all neurodevelopmental disorders and, in line with this naturalistic representation, it could be seen as strength of our clinical study. On the other hand, a possible bias is related to attainment bias: the sample might be skewed to the level 3 of ASD, being underpowered to detect PVS in children with mild phenotype of ASD (level 1 and 2), overcalling the relationship between volume of PVS and clinical severity. Finally, the impact of ASD at this young age grouping (<4 years) may, in theory, affect cohort assignment, particularly in the youngest group. However, no significant differences emerged in comparison groups for the age assignment criteria (0–3 or 2–4 years).

With the given limitations, we found that, compared with NP/Non-ASD, ASD male, but not female, patients present more frequently a high number of WM-PVS (WM-PVS grade 4) on MRI. WM-PVS grade 4 was also more frequently observed in ASD patients younger than 4 years of age compared with older ASD patients. Additionally, we observed a trend for a higher frequency of WM-PVS grade 4 in patients with severe forms of autism compared with milder forms, and for higher WM-PVS volume in ASD patients with sleep disturbances compared with those without. Our study may shed new light on the alleged, though formerly weak, association between ASD and GS dysfunction.

Our results suggest that PVS dilation is a neuroimaging feature of ASD in male patients and is particularly evident in younger ASD patients (< 4 years of age), corroborating the findings of early mechanisms related to the transient excess volume of EA-CSF (and PVS dilation) acting during neurodevelopment, being modulated later in life (Lai et al., 2017; Shen et al., 2018; Li et al., 2022).

We believe that PVS could serve as a biomarker for identification of early and severe forms of autism and that the impairment of GS, resulting in the enlargement of PVS, could act as a cofactor which contribute to the worsening of the ASD clinical severity. Based on our findings, volumetric and morphometric MRI studies can be included in the clinical evaluation of the patient, particularly in children with severe ASD and syndromic ASD. Currently, we are unable to forecast potential therapeutic implications of our findings, which are planned in next studies.

Data availability statement

The raw data supporting the conclusions of this article will be made available by the authors, without undue reservation.

Ethics statement

The studies involving human participants were reviewed and approved by Ethics Committee of Azienda Ospedaliero-Universitaria, Cagliari, Italy (PROT. PG/2023/5144). Written informed consent to

participate in this study was provided by the participants' legal guardian/next of kin.

Author contributions

MS, AL, GB, LS, VC, AM, PC, AC, and SS contributed to the study conception and design. Material preparation, data collection, and analysis were performed by GB, AL, LS, VC, and PC. Critical revision of the article for important intellectual content—AC and AM. The manuscript was written by AL, GB, MS, and SS. All authors contributed to the article and approved the submitted version.

Funding

This work was supported by "BANDO FONDAZIONE DI SARDEGNA 2022 E 2023—PROGETTI DI RICERCA DI BASE DIPARTIMENTALI (D.R.16/2022)" grant. The funding sources were not involved in study design, collection, analysis, interpretation of data and in the writing of the report.

Conflict of interest

The authors declare that the research was conducted in the absence of any commercial or financial relationships that could be construed as a potential conflict of interest.

Publisher's note

Supplementary material

The Supplementary material for this article can be found online at: https://www.frontiersin.org/articles/10.3389/fnins.2023.1205489/full#supplementary-material

References

Achenbach, T. M. (1999). "The child behavior checklist and related instruments" in *The use of psychological testing for treatment planning and outcomes assessment*. ed. M. E. Maruish. *2nd* ed (Mahwah, NJ: Lawrence Erlbaum Associates Publishers), 429–466.

American Psychiatric Association (2013). *Diagnostic and statistical manual of mental disorders. Fifth Edition*. Washington, DC: American Psychiatric Association.

Aribisala, B. S., Riha, R. L., Valdes Hernandez, M., Muñoz Maniega, S., Cox, S., Radakovic, R., et al. (2020). Sleep and brain morphological changes in the eighth decade of life. *Sleep Med.* 65, 152–158. doi: 10.1016/j.sleep.2019.07.015

Ashwood, P., Krakowiak, P., Hertz-Picciotto, I., Hansen, R., Pessah, I., and Van de Water, J. (2011). Elevated plasma cytokines in autism spectrum disorders provide evidence of immune dysfunction and are associated with impaired behavioral outcome. *Brain Behav. Immun.* 25, 40–45. doi: 10.1016/j.bbi.2010.08.003

Barisano, G., Lynch, K. M., Sibilia, F., Lan, H., Shih, N.-C., Sepehrband, F., et al. (2022). Imaging perivascular space structure and function using brain MRI. *NeuroImage* 257:119329. doi: 10.1016/j.neuroimage.2022.119329

Barisano, G., Sheikh-Bahaei, N., Law, M., Toga, A. W., and Sepehrband, F. (2021). Body mass index, time of day and genetics affect perivascular spaces in the white matter. *J. Cereb. Blood Flow Metab.* 41, 1563–1578. doi: 10.1177/0271678X20972856

Berezuk, C., Ramirez, J., Gao, F., Scott, C. J. M., Huroy, M., Swartz, R. H., et al. (2015). Virchow-Robin spaces: correlations with polysomnography-derived sleep parameters. *Sleep* 38, 853–858. doi: 10.5665/sleep.4726

Betancur, C. (2011). Etiological heterogeneity in autism spectrum disorders: more than 100 genetic and genomic disorders and still counting. *Brain Res.* 1380, 42–77. doi: 10.1016/j.brainres.2010.11.078

Boddaert, N., Zilbovicius, M., Philipe, A., Robel, L., Bourgeois, M., Barthélemy, C., et al. (2009). MRI findings in 77 children with non-syndromic autistic disorder. *PLoS One* 4:e4415. doi: 10.1371/journal.pone.0004415

Carta, A., Fucà, E., Guerrera, S., Napoli, E., Valeri, G., and Vicari, S. (2020). Characterization of clinical manifestations in the co-occurring phenotype of attention deficit/hyperactivity disorder and autism Spectrum disorder. *Front. Psychol.* 11:861. doi: 10.3389/fpsyg.2020.00861

Carta, A., Vainieri, I., Rommel, A.-S., Zuddas, A., Kuntsi, J., Sotgiu, S., et al. (2022). Temperament dimensions and awakening cortisol levels in attention-deficit/hyperactivity disorder. *Front. Psych.* 13:803001. doi: 10.3389/fpsyt.2022.803001

Conners, C. K., Sitarenios, G., Parker, J. D., and Epstein, J. N. (1998). The revised Conners' parent rating scale (CPRS-R): factor structure, reliability, and criterion validity. *J. Abnorm. Child Psychol.* 26, 257–268. doi: 10.1023/a:1022602400621.

Cox, R. W. (1996). AFNI: software for analysis and visualization of functional magnetic resonance neuroimages. *Comput. Biomed. Res.* 29, 162–173. doi: 10.1006/cbmr.1996.0014

Dinstein, I., and Shelef, I. (2018). Anatomical brain abnormalities and early detection of autism. *Lancet Psychiatry* 5, 857–859. doi: 10.1016/S2215-0366(18)30355-9

Doi, M., Usui, N., and Shimada, S. (2022). Prenatal environment and neurodevelopmental disorders. *Front Endocrinol (Lausanne)* 13:860110. doi: 10.3389/fendo.2022.860110

Duncan, D., Barisano, G., Cabeen, R., Sepehrband, F., Garner, R., Braimah, A., et al. (2018). Analytic tools for post-traumatic Epileptogenesis biomarker search in multimodal dataset of an animal model and human patients. *Front. Neuroinform.* 12:86. doi: 10.3389/fninf.2018.00086

Ecker, C., Suckling, J., Deoni, S. C., Lombardo, M. V., Bullmore, E. T., Baron-Cohen, S., et al. (2012). Brain anatomy and its relationship to behavior in adults with autism spectrum disorder: a multicenter magnetic resonance imaging study. *Arch. Gen. Psychiatry* 69, 195–209. doi: 10.1001/archgenpsychiatry.2011.1251

Floris, D. L., Filho, J. O. A., Lai, M.-C., Giavasis, S., Oldehinkel, M., Mennes, M., et al. (2021). Towards robust and replicable sex differences in the intrinsic brain function of autism. *Mol. Autism.* 12:19. doi: 10.1186/s13229-021-00415-z

Hablitz, L. M., and Nedergaard, M. (2021). The glymphatic system: a novel component of fundamental neurobiology. *J. Neurosci.* 41, 7698–7711. doi: 10.1523/JNEUROSCI.0619-21.2021

Harrison, P. L., and Oakland, T.. ABAS-3. Western Psychological Services Torrance (2015).

Hirota, T., and King, B. H. (2023). Autism Spectrum disorder: a review. *JAMA* 329, 157–168. doi: 10.1001/jama.2022.23661

Iliff, J. J., Wang, M., Liao, Y., Plogg, B. A., Peng, W., Gundersen, G. A., et al. (2012). A paravascular pathway facilitates CSF flow through the brain parenchyma and the clearance of interstitial solutes, including amyloid β. *Sci. Transl. Med.* 4:147ra111. doi: 10.1126/scitranslmed.3003748

Kim, J. Y., Son, M. J., Son, C. Y., Radua, J., Eisenhut, M., Gressier, F., et al. (2019). Environmental risk factors and biomarkers for autism spectrum disorder: an umbrella review of the evidence. *Lancet Psychiatry* 6, 590–600. doi: 10.1016/S2215-0366(19)30181-6

Lai, M.-C., Kassee, C., Besney, R., Bonato, S., Hull, L., Mandy, W., et al. (2019). Prevalence of co-occurring mental health diagnoses in the autism population: a systematic review and meta-analysis. *Lancet Psychiatry* 6, 819–829. doi: 10.1016/S2215-0366(19)30289-5

Lai, M.-C., Lerch, J. P., Floris, D. L., Ruigrok, A. N. V., Pohl, A., Lombardo, M. V., et al. (2017). Imaging sex/gender and autism in the brain: etiological implications: imaging sex/gender and autism in the brain. *J. Neurosci. Res.* 95, 380–397. doi: 10.1002/jnr.23948

Lai, M.-C., Lombardo, M. V., and Baron-Cohen, S. (2014). Autism. *Lancet* 383, 896–910. doi: 10.1016/S0140-6736(13)61539-1

Li, X., Ruan, C., Zibrila, A. I., Musa, M., Wu, Y., Zhang, Z., et al. (2022). Children with autism spectrum disorder present glymphatic system dysfunction evidenced by diffusion tensor imaging along the perivascular space. *Medicine* 101:e32061. doi: 10.1097/MD.0000000000032061

Liu, C., Habib, T., Salimeen, M., Pradhan, A., Singh, M., Wang, M., et al. (2020). Quantification of visible Virchow–Robin spaces for detecting the functional status of the

glymphatic system in children with newly diagnosed idiopathic generalized epilepsy. *Seizure* 78, 12–17. doi: 10.1016/j.seizure.2020.02.015

Lord, C., Brugha, T. S., Charman, T., Cusack, J., Dumas, G., Frazier, T., et al. (2020). Autism spectrum disorder. *Nat. Rev. Dis. Primers.* 6:5. doi: 10.1038/s41572-019-0138-4

Lord, C., Charman, T., Havdahl, A., Carbone, P., Anagnostou, E., Boyd, B., et al. (2022). The lancet commission on the future of care and clinical research in autism. *Lancet* 399, 271–334. doi: 10.1016/S0140-6736(21)01541-5

Lord, C., Elsabbagh, M., Baird, G., and Veenstra-Vanderweele, J. (2018). Autism spectrum disorder. *Lancet* 392, 508–520. doi: 10.1016/S0140-6736(18)31129-2

Lord, C., Rutter, M., DiLavore, P., Risi, S., Gotham, K., and Bishop, S. (2012). *Autism diagnostic observation schedule--2nd edition (ADOS-2)*. Los Angeles, CA: Western Psychological Corporation. (2012);284.

Luiz, D. M., Foxcroft, C. D., and Povey, J. L. (2006). The Griffiths scales of mental development: A factorial validity study. *South African Journal of Psychology* 36, 192–214.

MacLullich, A. M. J. (2004). Enlarged perivascular spaces are associated with cognitive function in healthy elderly men. *J. Neurol. Neurosurg. Psychiatry* 75, 1519–1523. doi: 10.1136/jnnp.2003.030858

Mestre, H., Kostrikov, S., Mehta, R. I., and Nedergaard, M. (2017). Perivascular spaces, glymphatic dysfunction, and small vessel disease. *Clin. Sci.* 131, 2257–2274. doi: 10.1042/CS20160381

Møllgård, K., Beinlich, F. R. M., Kusk, P., Miyakoshi, L. M., Delle, C., Plá, V., et al. (2023). A mesothelium divides the subarachnoid space into functional compartments. *Science* 379, 84–88. doi: 10.1126/science.adc8810

NICE—National Institute for Health and Clinical Excellence Autism—Quality standard (QS51) 2014 (n.d.). Available at: https://www.nice.org.uk/guidance/qs51.

Nordahl, C. W., Lange, N., Li, D. D., Barnett, L. A., Lee, A., Buonocore, M. H., et al. (2011). Brain enlargement is associated with regression in preschool-age boys with autism spectrum disorders. *Proc. Natl. Acad. Sci. U. S. A.* 108, 20195–20200. doi: 10.1073/pnas.1107560108

Owens, J. A., Spirito, A., and McGuinn, M. (2000). The Children's sleep habits questionnaire (CSHQ): psychometric properties of a survey instrument for school-aged children. *Sleep-New York* 23, 1043–1051. doi: 10.1093/sleep/23.8.1d

Plog, B. A., and Nedergaard, M. (2018). The Glymphatic system in central nervous system health and disease: past, present, and future. *Annu. Rev. Pathol. Mech. Dis.* 13, 379–394. doi: 10.1146/annurev-pathol-051217-111018

Potter, G. M., Chappell, F. M., Morris, Z., and Wardlaw, J. M. (2015). Cerebral perivascular spaces visible on magnetic resonance imaging: development of a qualitative rating scale and its observer reliability. *Cerebrovasc. Dis.* 39, 224–231. doi: 10.1159/000375153

Puonti, O., Iglesias, J. E., and Van Leemput, K. (2016). Fast and sequence-adaptive whole-brain segmentation using parametric Bayesian modeling. *NeuroImage* 143, 235–249. doi: 10.1016/j.neuroimage.2016.09.011

Ravens. Ravens standard progressive matrices and colored progressive matrices (Raven, Raven, & Court, J. H.) (1998).

Rochat, M. J., Distefano, G., Maffei, M., Toni, F., Posar, A., Scaduto, M. C., et al. (2020). Brain magnetic resonance findings in 117 children with autism Spectrum disorder under 5 years old. *Brain Sci.* 10:741. doi: 10.3390/brainsci10100741

Roid, G. H., Miller, L. J., Pomplun, M., and Koch, C. (2013). *Leiter international performance scale-third edition*. Los Angeles, CA: Western Psychological Services.

Rutter, M., Le Couteur, A., and Lord, C. (2003). *Autism diagnostic interview-revised*. Los Angeles, CA: Western Psychological Services.

Sanders, S. J., He, X., Willsey, A. J., Ercan-Sencicek, A. G., Samocha, K. E., Cicek, A. E., et al. (2015). Autism sequencing consortium. Insights into autism spectrum disorder genomic architecture and biology from 71 risk loci. *Neuron* 87, 1215–1233. doi: 10.1016/j.neuron.2015.09.016

Sepehrband, F., Barisano, G., Sheikh-Bahaei, N., Cabeen, R. P., Choupan, J., Law, M., et al. (2019). Image processing approaches to enhance perivascular space visibility and quantification using MRI. *Sci. Rep.* 9:12351. doi: 10.1038/s41598-019-48910-x

Shen, M. D. (2018). Cerebrospinal fluid and the early brain development of autism. *J. Neurodev. Disord.* 10:39. doi: 10.1186/s11689-018-9256-7

Shen, M. D., Kim, S. H., McKinstry, R. C., Gu, H., Hazlett, H. C., Nordahl, C. W., et al. (2017). Increased extra-axial cerebrospinal fluid in high-risk infants who later develop autism. *Biol. Psychiatry* 82, 186–193. doi: 10.1016/j.biopsych.2017.02.1095

Shen, M. D., Nordahl, C. W., Li, D. D., Lee, A., Angkustsiri, K., Emerson, R. W., et al. (2018). Extra-axial cerebrospinal fluid in high-risk and normal-risk children with autism aged 2–4 years: a case-control study. *Lancet Psychiatry* 5, 895–904. doi: 10.1016/S2215-0366(18)30294-3

Shen, M. D., Nordahl, C. W., Young, G. S., Wootton-Gorges, S. L., Lee, A., Liston, S. E., et al. (2013). Early brain enlargement and elevated extra-axial fluid in infants who develop autism spectrum disorder. *Brain* 136, 2825–2835. doi: 10.1093/brain/awt166

Song, T.-J., Park, J.-H., Choi, K. H., Chang, Y., Moon, J., Kim, J.-H., et al. (2017). Moderate-to-severe obstructive sleep apnea is associated with cerebral small vessel disease. *Sleep Med.* 30, 36–42. doi: 10.1016/j.sleep.2016.03.006

Sotgiu, S., Manca, S., Gagliano, A., Minutolo, A., Melis, M. C., Pisuttu, G., et al. (2020). Immune regulation of neurodevelopment at the mother–foetus interface: the case of autism. *Clin. Transl. Immunol.* 9:e1211. doi: 10.1002/cti2.1211

Sparrow, S. S., Balla, D. A., Cicchetti, D. V., and Harrison, P. L. Vineland adaptive behavior scales. Published online (1984). Available at: http://www.disableddaughter.com/Pearlsky_vineland.pdf.

Taber, K. H., Shaw, J. B., Loveland, K. A., Pearson, D. A., Lane, D. M., and Hayman, L. A. (2004). Accentuated Virchow-Robin spaces in the centrum Semiovale in children with autistic disorder. *J. Comput. Assist. Tomogr.* 28, 263–268. doi: 10.1097/00004728-200403000-00017

Taoka, T., and Naganawa, S. (2020). Glymphatic imaging using MRI. *J. Magn. Reson. Imaging* 51, 11–24. doi: 10.1002/jmri.26892

Troili, F., Cipollini, V., Moci, M., Morena, E., Palotai, M., Rinaldi, V., et al. (2020). Perivascular unit: this must be the place. The anatomical crossroad between the immune, vascular and nervous system. *Front. Neuroanat.* 14:17. doi: 10.3389/fnana.2020.00017

Trost, B., Thiruvahindrapuram, B., Chan, A. J. S., Engchuan, W., Higginbotham, E. J., Howe, J. L., et al. (2022). Genomic architecture of autism from comprehensive whole-genome sequence annotation. *Cells* 185, 4409–4427.e18. doi: 10.1016/j.cell.2022.10.009

Wechsler, D. (2002). *WPPSI-III: Technical and interpretative manual*. San Antonio, TX: The Psychological Corporation.

Wechsler, D. (2004). *The Wechsler intelligence scale for children, fourth edition*. London, UK: Pearson Assessment, doi: 10.53841/bpstest.2004.wisc4.

Wegiel, J., Frackowiak, J., Mazur-Kolecka, B., Schanen, N. C., Cook, E. H., Sigman, M., et al. (2012). Abnormal intracellular accumulation and extracellular Aβ deposition in idiopathic and Dup15q11.2-q13 autism spectrum disorders. *PLoS One* 7, e35414–e35417. doi: 10.1371/journal.pone.0035414

Westmark, C. J. (2013). What's hAPPening at synapses? The role of amyloid β-protein precursor and β amyloid in neurological disorders. *Mol. Psychiatry* 18, 425–434. doi: 10.1038/mp.2012.122

Westmark, C. J., Sokol, D. K., Maloney, B., and Lahiri, D. K. (2016). Novel roles of amyloid-beta precursor protein metabolites in fragile X syndrome and autism. *Mol. Psychiatry* 21, 1333–1341. doi: 10.1038/mp.2016.134

Willsey, H. R., Willsey, A. J., Wang, B., and State, M. W. (2022). Genomics, convergent neuroscience and progress in understanding autism spectrum disorder. *Nat. Rev. Neurosci.* 23, 323–341. doi: 10.1038/s41583-022-00576-7

Xie, L., Kang, H., Xu, Q., Chen, M. J., Liao, Y., Thiyagarajan, M., et al. (2013). Sleep drives metabolite clearance from the adult brain. *Science* 342, 373–377. doi: 10.1126/science.1241224

Zafeiriou, D. I., and Batzios, S. P. (2013). Brain and spinal MR imaging findings in Mucopolysaccharidoses: a review. *AJNR Am. J. Neuroradiol.* 34, 5–13. doi: 10.3174/ajnr.A2832

Zeegers, M., Van Der Grond, J., Durston, S., Nievelstein, R. J., Witkamp, T., Van Daalen, E., et al. (2006). Radiological findings in autistic and developmentally delayed children. *Brain Dev.* 28, 495–499. doi: 10.1016/j.braindev.2006.02.006

Zhu, Y.-C., Dufouil, C., Mazoyer, B., Soumaré, A., Ricolfi, F., Tzourio, C., et al. (2011). Frequency and location of dilated Virchow-Robin spaces in elderly people: a population-based 3D MR imaging study. *AJNR Am. J. Neuroradiol.* 32, 709–713. doi: 10.3174/ajnr.A2366

Zwaigenbaum, L. (2019). Perspectives on regressive onset in autism: looking forward on looking back. *Neurosci. Biobehav. Rev.* 103, 399–400. doi: 10.1016/j.neubiorev.2019.06.025

frontiers | Frontiers in Neuroscience

TYPE Original Research
PUBLISHED 03 July 2023
DOI 10.3389/fnins.2023.1148683

OPEN ACCESS

EDITED BY
Jian-Huan Chen,
Jiangnan University, China

REVIEWED BY
Sheng Zhong,
Sun Yat-sen University Cancer Center, China
Alfredo Gonzalez-Sulser,
University of Edinburgh, United Kingdom

*CORRESPONDENCE
Yann Herault
✉ herault@igbmc.fr

RECEIVED 20 January 2023
ACCEPTED 02 May 2023
PUBLISHED 03 July 2023

CITATION
Martin Lorenzo S, Muniz Moreno MDM, Atas H, Pellen M, Nalesso V, Raffelsberger W, Prevost G, Lindner L, Birling M-C, Menoret S, Tesson L, Negroni L, Concordet J-P, Anegon I and Herault Y (2023) Changes in social behavior with MAPK2 and KCTD13/CUL3 pathways alterations in two new outbred rat models for the 16p11.2 syndromes with autism spectrum disorders.
Front. Neurosci. 17:1148683.
doi: 10.3389/fnins.2023.1148683

Changes in social behavior with MAPK2 and KCTD13/CUL3 pathways alterations in two new outbred rat models for the 16p11.2 syndromes with autism spectrum disorders

Sandra Martin Lorenzo[1], Maria del Mar Muniz Moreno[1], Helin Atas[1], Marion Pellen[1], Valérie Nalesso[1], Wolfgang Raffelsberger[1], Geraldine Prevost[2], Loic Lindner[2], Marie-Christine Birling[2], Séverine Menoret[3,4], Laurent Tesson[4], Luc Negroni[1], Jean-Paul Concordet[5], Ignacio Anegon[4] and Yann Herault[1,2]*

[1]Université de Strasbourg, CNRS UMR7104, INSERM U1258, Institut de Génétique et de Biologie Moléculaire et Cellulaire, Illkirch, France, [2]Université de Strasbourg, CNRS, INSERM, CELPHEDIA-PHENOMIN, Institut Clinique de la Souris, Illkirch, France, [3]Nantes Université, CHU Nantes, INSERM, CNRS, SFR Santé, Inserm UMS 016 CNRS UMS 3556, Nantes, France, [4]INSERM, Centre de Recherche en Transplantation et Immunologie UMR1064, Nantes Université, Nantes, France, [5]MNHN, CNRS UMR 7196/INSERM U1154, Sorbonne Universités, Paris, France

Copy number variations (CNVs) of the human 16p11.2 locus are associated with several developmental/neurocognitive syndromes. Particularly, deletion and duplication of this genetic interval are found in patients with autism spectrum disorders, intellectual disability and other psychiatric traits. The high gene density associated with the region and the strong phenotypic variability of incomplete penetrance, make the study of the 16p11.2 syndromes extremely complex. To systematically study the effect of 16p11.2 CNVs and identify candidate genes and molecular mechanisms involved in the pathophysiology, mouse models were generated previously and showed learning and memory, and to some extent social deficits. To go further in understanding the social deficits caused by 16p11.2 syndromes, we engineered deletion and duplication of the homologous region to the human 16p11.2 genetic interval in two rat outbred strains, Sprague Dawley (SD) and Long Evans (LE). The 16p11.2 rat models displayed convergent defects in social behavior and in the novel object test in male carriers from both genetic backgrounds. Interestingly major pathways affecting MAPK1 and CUL3 were found altered in the rat 16p11.2 models with additional changes in males compared to females. Altogether, the consequences of the 16p11.2 genetic region dosage on social behavior are now found in three different species: humans, mice and rats. In addition, the rat models pointed to sexual dimorphism with lower severity of phenotypes in rat females compared to male mutants. This phenomenon is also observed in humans. We are convinced that the two rat models will be key to further investigating social behavior and understanding the brain mechanisms and specific brain regions that are key to controlling social behavior.

KEYWORDS

copy number variation, neurodevelopment, intellectual disability, autism spectrum disorders, rat model, social behavior, recognition memory

1. Introduction

The 16p11.2 locus is a pericentromeric region found in chromosome 16, one of the most gene-rich chromosomes in our genome, for which 10% of its sequence consists of segmental duplications (Redaelli et al., 2019). These elements give strong instability and induce the appearance of copy number variations (CNV) because of the recurrent non-allelic homologous recombination mechanism (Hastings et al., 2009). The most prevalent rearrangement, deletion and duplication are generated between two low copy repeats (LCR), named BP4 and BP5, and encompasses 600 kb. 16p11.2 CNVs are an important risk factor for neurodevelopmental disorders (Torres et al., 2016), including intellectual disability (ID; Cooper et al., 2011) and autism spectrum disorder (ASD; Marshall et al., 2008; Weiss et al., 2008; Fernandez et al., 2010; Sanders et al., 2011; Steinman et al., 2016). In addition, the deletion and duplication of 16p11.2 have been linked to epilepsy (Shinawi et al., 2010; Zufferey et al., 2012; Reinthaler et al., 2014) and attention deficit hyperactivity disorder (ADHD; Angelakos et al., 2017), whereas only the duplication has been related to schizophrenia, bipolar disorder and depression (McCarthy et al., 2009; Rees et al., 2014; Steinberg et al., 2014; Drakesmith et al., 2019).

Besides, these chromosomal rearrangements have been linked to mirrored physical phenotypic effects. The 16p11.2 deletion has been associated with the risk of diabetes-independent morbid obesity and large head circumference, while the 16p11.2 duplication has been associated with low body mass index (BMI) and small head circumference (Walters et al., 2010; Jacquemont et al., 2011; Zufferey et al., 2012; D'Angelo et al., 2016). Considering this reciprocal impact on BMI and head size, it has been suggested that changes in gene transcript levels could be responsible for the symptoms associated with these CNVs. More importantly, the severity of the developmental delay and other comorbidities vary significantly in the human population with some people having an ASD or IQ below 70 and others just below average (D'Angelo et al., 2016; Chawner et al., 2021; Benedetti et al., 2022).

Animal models have been developed and characterized to investigate the interplay between genes and proteins, the consequences on brain activity and behavior and the understanding of neurocognitive processes affected in humans. Genes of the 16p11.2 region are highly conserved on mouse chromosome 7 and several mouse models for the deletion or duplication of the 16p11.2 homologous region have been generated (Horev et al., 2011; Portmann et al., 2014; Arbogast et al., 2016; Benedetti et al., 2022). Among them, our novel 16p11.2 CNV mouse models in pure C57BL/6 N genetic background named *Del(7Sult1a1-Spn)6Yah* (noted Del/+) and *Dp(7Sult1a1-Spn)6Yah* (noted Dup/+) and investigated them focusing on behavior and metabolism (Arbogast et al., 2016). We found that *Sult1a1-Spn* CNVs affect growth, weight, adiposity, activity and memory in opposite ways. Mice carrying the deletion showed weight and adipogenesis deficits, hyperactivity with increased stereotypic behavior and novel object memory impairments. Instead, mice carrying the duplication showed weight and adipogenesis increase, hypo-activity and memory improvements. We also found that the genetic background can favor the social interaction deficits in the deletion mice model. Altogether this observation suggests that this deficit could be the consequence of the genetic context.

To generate a model presenting more suitable autistic traits, we engineered the deletion or duplication of the human homologous region 16p11.2 in the rat in two different outbred genetic backgrounds. As a model of human disease, the rat is a more sociable animal than the mouse with a large spectrum of similar and complementary behavioral assessments and the outbred genetic background, although representing a challenge, could be of interest to detect the most robust phenotypes. Rats have shown differences from mice in several models of human disease in which genetically engineered animals for the same genes have been generated. The main contribution of our research is the establishment and validation of two new 16p11.2 rat models that can be helpful to test novel pre-clinical pharmacological therapies targeting specific phenotypes and finally help to improve the lives of patients.

2. Materials and methods

2.1. Rat lines and genotyping

The 16p11.2 rearrangement, deletion and duplication, were studied in rat models engineered through CRISPR/Cas9 technology (Menoret et al., 2015) as detailed in the Supplementary material (Figure 1). Rat models were then bred and maintained in our animal facility which is accredited by the French Ministry for Superior Education and Research and the French Ministry of Agriculture (agreement #A67-218-37) following the Directive of the European Parliament: 2010/63/EU, revising/replacing Directive 86/609/EEC and the French Law (Decree n° 2013-118 01 and its supporting annexes entered into legislation on 01 February 2013) relative with the protection of animals used in scientific experimentation. All animal experiments were approved by the local ethical committees (Approval Committee: Com'Eth N°17 and French Ministry for Superior Education and Research (MESR) with approval licenses: internal numbers 2012-009 and 2014-024, and MESR: APAFIS#4789-2016040511578546) and supervised in compliance with the European Community guidelines for laboratory animal care and use and every effort was made to minimize the number of animals used and their suffering.

2.2. Behavioral analysis

To decipher more in detail alterations of specific cognitive functions and autistic traits in 16p11.2 CNVs rat models on two

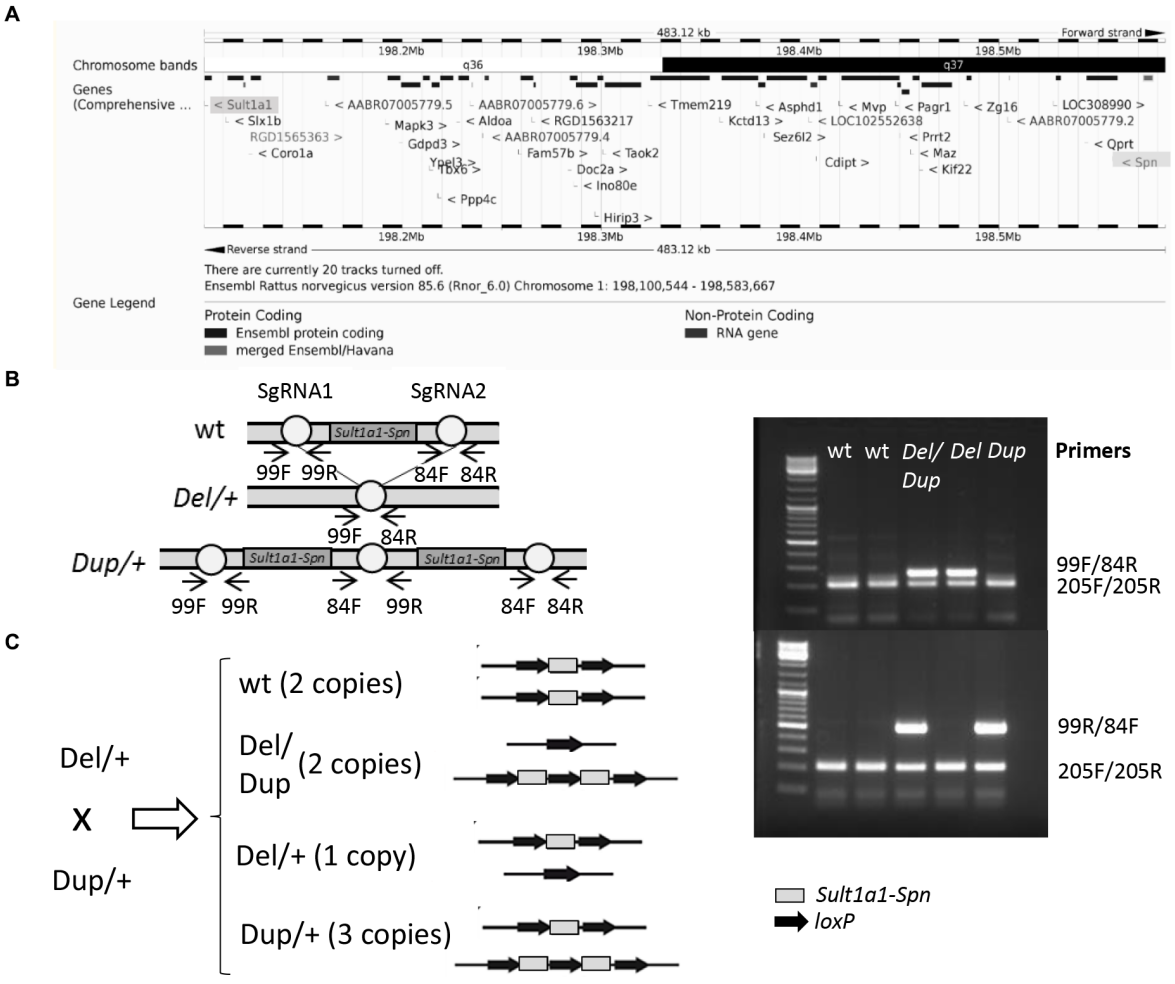

FIGURE 1
New rat SD model for the 16p11.2 syndromes. **(A)** The syntenic region 16p11.2 BP4-BP5 in the rat genome as represented in the UCSC database (Nassar et al., 2023). **(B)** Left: mutation strategy using CRISPR/Cas9 technology from the *in vitro* genome editing inside of a fertilized embryo and subsequent injection into a pseudo-pregnant female. We obtained individuals carrying the deletion and duplication of the *Sult1a1-Spn* region. Right: molecular validation. PCR-specific products for the wt (205 bp), *Del/+* (290 bp) and *Dup/+* (500 bp) alleles. **(C)** Breeding strategy for obtaining wt, *Del/+*, *Dup/+*, and *Del/Dup* littermates. **(D)** Junctions positions and details of the mutated genetic sequences for *Del* and *Dup* rat models. All genomic positions are given according to the UCSC rat genome browser (RGSC 6.0/rn6).

genetic backgrounds, Sprague–Dawley (SD) and Long Evans (LE), we evaluated several phenotypes with a validated rat phenotyping behavioral pipeline. We defined the protocol with tasks in which 16p11.2 mouse models showed robust phenotypes: alterations of exploration activity, object location and novel object recognition (NOR) memory, and social interaction. For SD 16p11.2 rat models, littermate animals from different crosses with four genotypes were used: wt, Del/+, Dup/+ and pseudo-disomic Del/Dup (Figure 1C). For LE 16p11.2 rat model, we used littermate animals from the wt and Del/+ cross to get mutant and control genotypes as littermates.

Behavioral studies were conducted in 14 to 16-week-old SD rats of both sexes separately, from 8 cohorts. Whereas LE rats were analyzed between 19 and 24 weeks old for both sexes separately, from 1 large cohort. Animals were housed in couples of 2 individuals per cage (Innocage Rat cages; 909 cm^2 of floor space; Innovive, San Diego, United States), where they had free access to water and autoclaved food (D04, Safe Diets, France). The temperature was maintained at

23°C ± 1°C and the light cycle was controlled as 12 h light and 12 h dark (light on at 7 a.m.).

On the testing days, animals were transferred to the experimental room antechambers 30 min before the start of the experiments. The body weight of the animals from the SD 16p11.2 rat models was recorded at 13 weeks old whereas the body weight of animals from LE 16p11.2 rat models was recorded at 2 weeks old, and followed at weaning and 19 weeks. All tests were scored blind to the genotype as recommended by the ARRIVE guidelines (Kilkenny et al., 2010; Karp et al., 2015). The protocols for open field, object location, object recognition memories and social interaction are described in the Supplementary material.

2.2.1. Open field

This test was used to study exploration activity. Rats were tested in an automated open field (90 × 90 × 39.5 cm) made of opaque PVC with black walls and floor (Imetronic, Pessac—France). The structure was equipped with infrared sensors for accurate location and rearing behaviors of the animal. An interface provided the formatting of signals from infrared sensors and allows communication with the computer, where the software POLY OPENFIELD v5.3.2 managed experimental data. The open field arena was divided into central and peripheral regions and was homogeneously illuminated at 15 Lux. Each animal was placed in the periphery of the open field and allowed to explore freely for 30 min. The distance traveled in the total arena and in each region of the arena, as well as, the number of rears were recorded over the test session.

2.2.2. Object location memory task

This test was based on the innate preference for the novelty showed by the rodents and it was carried out in the same open field arena as previously described. On the first day, rats were habituated to the arena for 15 min at 15 Lux. On the following day, animals were submitted to a first acquisition trial for 3 min in which they were individually placed in the presence of two identical objects A (syringe or flask for SD models and cup for LE model) located 15 cm away from one of the corners, on the northeast and northwest side of the box, respectively. In the case of the LE model, the test was refined by placing a reference band on the north wall of the open field. A 3-min retention trial (second trial) was conducted 5 min later, and then one of the familiar objects (right or left object) was displaced randomly to a novel location (B) on the south side. The exploration time of the two objects (when the animal's snout was directed toward the object at a distance ≤1 cm) was recorded during both trials. The minimum exploration time was set to 3 s, and rats that did not reach this criterion during the acquisition trial or retention trial were excluded from the study. We verified that no preference was seen during the exploration of the left and right objects. A recognition index (RI) was defined as $[(tB/(tA + tB)) \times 100]$. A RI of 50% corresponds to a chance level and a significantly higher RI reflects good recognition memory.

2.2.3. Novel object recognition memory task

This test allowed us to evaluate the ability to recognize previously encountered objects in murine models and like the Object location memory (OLM) task, this test is also based on the innate preference of rodents to explore novelty. We carried out Novel object recognition (NOR) in the same open-field arena as previously described.

Firstly, we developed the NOR test through a protocol based on the characterization of the mouse models, although we reduced the time of the trials to adapt the test to the intelligence of the rats. In the first 3 min acquisition trial, rats were presented with two identical objects A (syringe, block, bottle or flask). The animals from SD models that were evaluated in the NOR test did not belong to the same cohort as those that were analyzed in the OLM test, therefore the objects syringe and flask were never seen before the NOR test by these rats. A 3-min retention trial was conducted 3 h later. One of the two familiar objects was randomly changed for another novel object B. Test was analyzed for the OLM task.

The surprisingly good performance of the mutant individuals made us question the simplicity of this test for an intelligent animal like the rat. For this reason, we were motivated to develop a new NOR protocol.

In this case, animals from new cohorts were presented to three different objects located (A, B, C) at the northwest, northeast and southwest corner of the arena during the 3-min acquisition trial. A 3-min retention trial was conducted 3 h later. One of the three familiar objects was randomly changed for another novel object (D). The exploration time of the three objects (when the animal's snout was directed toward the object at a distance ≤1 cm) was recorded during both trials. The minimum exploration time was set to 3 s, and rats that did not reach this criterion during the acquisition trial or retention trial were excluded from the study. We verified that no particular object preference was seen during the exploration. A recognition index (RI) was defined as $[(tD/(tA + tB + tD)) \times 100]$. A RI of 33.3% corresponds to a chance level and a significantly higher RI reflects good recognition memory.

2.2.4. Social interaction task

This analysis focused on the evaluation of rat social behavior by manually scoring a battery of social interactions (Lorbach et al., 2018) among two animals of the same sex, age and genotype, housed in different cages. The test was carried out in a previously described standardized open-field arena during 10 min of video recording.

2.3. Statistical analysis

The statistical analysis of our results was carried out using standard statistical procedures operated by SigmaPlot software (Systat Software, San Jose, United States). All outliers were identified using Grubbs' test from calculator GraphPad (GraphPad Software, San Diego) or ROUT method with a Q value of 1% from GraphPad Prism 7.01 (Motulsky et al., 2006; GraphPad Software, San Diego) when data with nonlinear regression. Acquired data from the behavioral characterization of 16p11.2 rat models were analyzed using one-way ANOVA followed by Student's *t*-test and Tukey's *post hoc* test whenever data presented normal distribution and equal variance. Otherwise, we used the non-parametric Kruskal-Wallis one-way analysis of variance and the Mann–Whitney *U*-test. One sample t-test was used also to compare recognition index values to the set chance level (50%). The data to evaluate the mutant allele transmission was analyzed by a Person's Chi-squared test. Data are represented as the mean ± SEM and the statistically significant threshold was $p < 0.05$.

2.4. Transcriptomic analysis

Hippocampus from 4 Del/+ [noted as Del(16p11)], 5 Dup/+ [noted as Dup(16p11)] and 4 Del/Dup [noted as Del/Dup(16p11)] SD rats and 6 wt littermates for each, were isolated and flash frozen in liquid nitrogen. Total RNA was prepared using an RNA extraction kit (Qiagen, Venlo, Netherlands) according to the manufacturer's instructions. Samples quality was checked using an Agilent 2,100 Bioanalyzer (Agilent Technologies, Santa Clara, California, United States). All the procedures and the analysis are detailed in the Supplementary material.

The preparation of the libraries was done by using the TruSeq Stranded Total RNA Sample Preparation Guide—PN 15031048. The molecule extracted from the biological material was polyA+ RNA. The Whole genome expression sequencing was performed by the platform using Illumina Hiseq 4000 and generating single-end RNA-Seq reads of 50 bps length. The raw sequenced reads were aligned by Hisat2 against the Rno6.v96. 32,623 ENSEMBL Gene Ids were quantified aligning to the Rno6.v96 assembly. HTSeq-count was used to generate the raw counts. The downstream analyses were carried on with in-house bash scripts and R version 3.6 scripts using FCROS (Dembélé and Kastner, 2014) and DESeq2 (Love et al., 2014) packages to identify the DEGs. Raw reads and normalized counts have been deposited in GEO (Accession No. GSE225135).

We performed the functional differential analysis (Duchon et al., 2021) and grouped all the pathways into 25 functional categories (noted meta-pathways). Then, to assess the gene connectivity we build a minimum fully connected protein–protein interaction (PPI) network (noted MinPPINet) of genes known to be involved in all meta-pathways we defined as they were associated with each pathway via GO (Ashburner et al., 2000) and KEGG databases (Esling et al., 2015) and added regulatory information to build the final 16p11 dosage sensitive regulatory PPI network (noted RegPPINet). We used the betweenness centrality analysis to identify hubs, and keys for maintaining the network communication flow.

2.5. ddPCR analysis

Analyses were performed by Droplet Digital™ PCR (ddPCR™) technology. All experiments were performed following the previously published protocol (Lindner et al., 2021). Primers are described in Supplementary Table S1.

2.6. Identification of central genes linked to the behavioral phenotypes

To further study the genotype–phenotype relationship in those models we combined the behavioral results and the RNA-Seq data to identify central genes altered in the models linked to the observed phenotypes using the genotype–phenotype databases GO, KEGG and DisGeNET. For this, we combined the knowledge from the human disease database DIsGeNET and the GO genesets (see Supplementary material). Then we queried our RNA-Seq data for those genes to identify those found deregulated in the datasets. Table 1 summarized the results with the genes annotated with the expression level, regulation sense on each model, log2FC and standard deviation of the log2FC.

2.7. Proteomic analysis

Fresh entire hippocampal tissues were isolated by CO2 inhalation/dissection of naive rats and snap frozen. Then, lysed in ice-cold sonication buffer supplemented with Complete™ Protease Inhibitor Cocktail (Roche). Individual samples were disaggregated and centrifuged at 4°C for 30 min at 14000 rpm. Protein mixtures were TCA (Trichloroacetic acid/Acetone)-precipitated overnight at 4°C. Samples were then centrifuged at 14,000 rpm for 30 min at 4°C. Pellets were washed twice with 1 mL cold acetone and centrifuged at 14,000 rpm for 10 min at 4°C. Washed pellets were then urea-denatured with 8 M urea in Tris–HCl 0.1 mM, reduced with 5 mM

TABLE 1 Summary of the transcriptional analysis of the SD and LE 16p11.2 models.

Genetic background	Sprague Dawley			Long Evans		
Nb of annotated transcripts Rno6.v96	32,623					
Nb of expressed (EGs) genes	23,148					
Number of 16p11 homologous region genes [*Sult1a1-Spn*]	28					
Sexes		Male		Males	Female	Both
Genotype	Del/+	Dup/+	Del/Dup	Del/+		
Differentially expressed genes (DEG)						
Total identified by FCROS FDR < 0.05	966	1,367	1,071	1,068	1,324	1,544
Upregulated DEGs	508	719	640	613	531	737
Downregulated DEGs	458	648	431	455	793	807
Differential functional analysis (DFA)						
Number of GAGE KEGG and GOs (CC, BP, MF) terms misregulated in the model FDR < 0.1	146	68	5	248	100	31
Number of terms upregulated in the model FDR < 0.1	46	68	1	10	93	0
Number of terms downregulated in the model FDR < 0.1	100	0	4	238	7	31

TCEP for 30 min, and then alkylated with 10 mM iodoacetamide for 30 min in the dark. Both reduction and alkylation were performed at room temperature and under agitation (850 rpm). Double digestion was performed with endoproteinase Lys-C (Wako) at a ratio of 1/100 (enzyme/proteins) in 8 M urea for 4 h, followed by overnight modified trypsin digestion (Promega) at a ratio of 1/100 (enzyme/proteins) in 2 M urea. Both Lys-C and Trypsin digestions were performed at 37°C. Peptide mixtures were then desalted on a C18 spin-column and dried on Speed-Vacuum before LC-MS/MS analysis (see Supplementary material).

3. Results

3.1. General and behavioral characterization of the SD 16p11.2 rat models

The 16p11.2 region is conserved in the rat genome on chromosome 1 (Figure 1A). Using CRISPR/Cas9 we generated first the deletion and the duplication of the conserved interval containing *Sult1a1* and *Spn1* (Figures 1B,C) and we determined the precise sequence of the new borders of the deletion and duplication (Figure 1D).

To carry out the behavioral analysis of the SD 16p11.2 rat models we combined the deletion (*Del*/+) and the duplication (Dup/+) for the generation of 4 groups of genotypes: wt control, Del/Dup pseudo-disomic for the 16p11.2 conserved region, Del/+ and Dup/+ littermates (Figure 1C). Before testing, we checked the transmission of the alleles and we did not find any deviation from Mendelian rate (Supplementary Table S2). Then, we analyzed the effect of 16p11.2 CNVs on the weight of the 13 weeks old rats. We observed that male rats carrying 16p11.2 deletion showed a decrease in body weight compared to wt littermates, while males carrying 16p11.2 duplication did not show alterations compared to wt littermates (Figure 2A). The 16p11.2 rearrangements did not affect the body weight of female rats (Figure 2A).

As a first analysis for consequences of 16p11.2 CNVs in neuronal function, we measured spontaneous locomotion activity and exploratory behavior in the open field test (Supplementary Table S4). The horizontal activity was measured through total traveled distance, whereas the vertical activity was analyzed by the number of rears. As shown in Figure 2B, increased variability was observed in the distance traveled and the rearing activity. The only significant differences were found between extreme genotype male Del/+ vs. Dup/+ and between female Del/Dup vs. Dup/+ for both the distance traveled and the rearing activity in the open field.

Then, we carried out the novel object location recognition test and the novel object recognition test, common assays for assessing impaired memory in rodents. For the novel object location recognition, animals were challenged to discriminate a moved object from an unmoved object. We first evaluated the performances of males and females separately, and as no significant sex differences were noted, we combined these data across both sexes. No difference was observed between genotypes in the retention session [Kruskal-Wallis one-way analysis of variance: $H_{(3)} = 5.61$; $p = 0.132$; Supplementary Figure S1A]. We also compared the recognition index of the animals, i.e., the percentage of exploration time of the new object location, with the level of chance (50%). The new object position was always explored more than the object not moved for all the genotypes.

Following these observations, we next assessed novel object recognition from a first paradigm, based on the protocol used for the CNVs 16p11.2 *Sult1a1-Spn* mouse model. The animals should be able to differentiate an object observed previously during the acquisition phase from a novel object presented during the retention phase (Supplementary Figure S1B). All four genotypes engaged in similar levels of novelty discrimination [One way ANOVA: $F_{(3,88)} = 0.038$; $p = 0.99$]. We also compared the recognition index with the level of chance (50%). A general preference was observed for the new object compared to the familiar object. The rat 16p11.2 models displayed correct recognition memory, with an increased time of the new object exploration spent by rats compared to mice (Arbogast et al., 2016).

Thus, we used a more complex object recognition paradigm with 3 different objects (Supplementary Figure S1C). In this case, the male Del/+ carriers showed impairment in the discrimination of the novel object compared to all the other genotypes (Figure 2C). Nevertheless, no alteration was observed in the females, with all the genotypes able to discriminate the novel vs. the two familiar objects.

Finally, the last task focused on studying rat social interactions by analyzing different social behavior (Lorbach et al., 2018; Figure 2D). The Del/+ male displayed significantly increased time in solitary compared to all genotypes. In addition, 16p11.2 Del/+ was associated with the presence of more pinning, a behavior to exert dominance. Interestingly the pinning behavior was found also in the Del/Dup male animals. Furthermore, male Dup/+ showed increased agnostic behavior compared to all genotypes. Surprisingly we did not see any social phenotypes in females of the Del/+ or Dup/+ genotype.

3.2. Behavioral characterization of the LE *Del/+* 16p11.2 rat model

Elucidating the genetic mechanisms by which some CNVs influence neurodevelopment requires a rigorous quantitative analysis of the human phenotype but also the establishment of validated model systems in which the phenotypic diversity is conserved. Based on previous results obtained on a pure inbreed mouse C57BL/6JN, or on a mixed B6.C3H genetic background (Arbogast et al., 2016) and now on a rat outbred SD model, we decided to investigate if the phenotypes were robust enough, and the deficits preserved in a different background. In addition, we considered it pertinent to verify if the females were equally more resilient to the deletion of the 16p11.2 region than the males in this new genetic background. For this purpose, we engineered the deletion of the homologous region to the human 16p11.2 BP4-BP5 locus in a rat LE outbred strain and we verified the location of the specific Del interval (Supplementary Figure S2). Interestingly the transmission of the Del/+ allele was affected in females of the LE 16p11.2 model (Supplementary Table S1) while males did not show any significant change. We also evaluated the body weight of this new model for both sexes and found that the deletion of the 16p11.2 region caused a decrease in the body weight on the LE genetic background in both sexes (Figure 3A). Then, we proceeded to study the behavior using the same battery of behavioral tests (Supplementary Table S4). We analyzed the locomotion and exploratory activity of our second

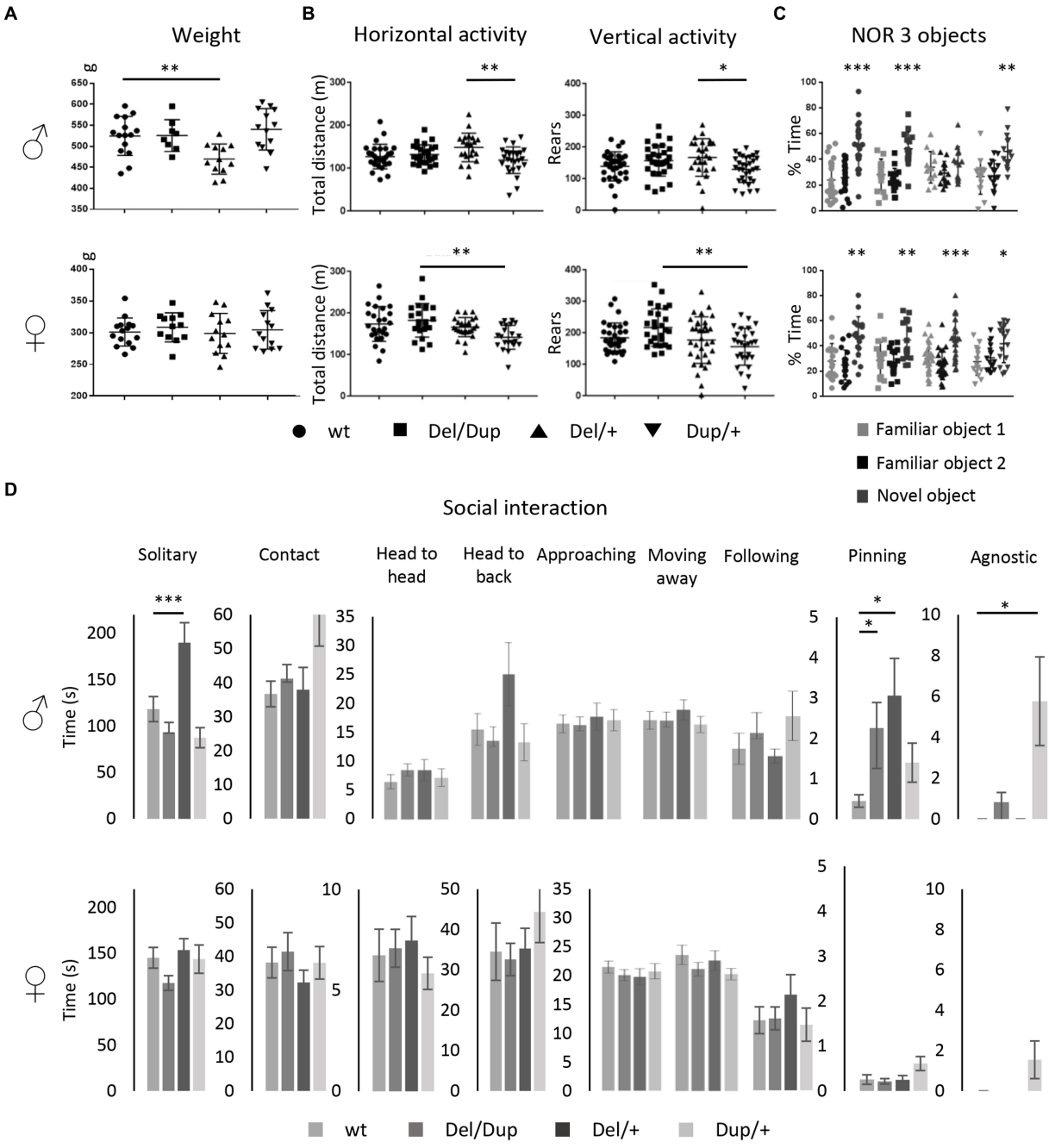

FIGURE 2
Phenotypic characterization of the 16p11.2 rat models on the SD genetic background. **(A)** Effects of *Sult1a1-Spn* rearrangements on body weight. Body Weight (g) of the 13 weeks old males [wt (n=15), *Del/Dup* (n=8), *Del/+* (n=12), and *Dup/+* (n=13)] and female rats [wt (n=15), *Del/Dup* (n=12), *Del/+* (n=13), and *Dup/+* (n=13)] from Del-Dup littermates. Only the deletion of 16p11.2 region caused reduced body weight in males [One way ANOVA between groups, $F_{(3,44)}$=6.24; p=0.001; Student t-test, *Del/+* vs. wt: $t_{(25)}$=3.39 p=0.002]. **(B)** Exploratory behavior of the rat 16p11.2 models in the open field test. Male [wt (n=28), *Del/Dup* (n=26), *Del/+* (n=21), and *Dup/+* (n=27)] and female [wt (n=25), *Del/Dup* (n=22), *Del/+* (n=26), and *Dup/+* (n=22)] rats were placed in the open field for 30min to explore the new environment. The horizontal activity was measured by the total distance traveled and vertical activity was recorded with the number of rears. Animals showed large variability and limited changes between genotypes except for *Del/+* vs. *Dup/+* male [One way ANOVA between groups, Total distance: $F_{(3,98)}$=4.33; p=0.007; Tukey's *post hoc* tests: *Del/+* vs. *Dup/+*: p=0.004; Rears: $F_{(3,117)}$=3.55; p=0.017; Tukey's *post hoc* tests: *Del/+* vs. *Dup/+*: p=0.016] and *Del/Dup* vs. *Dup/+* female [Kruskal-Wallis one-way analysis of variance, Total distance: $H_{(3)}$=14.18; p=0.003, Mann–Whitney Test: *Del/Dup* vs. *Dup/+*: p=0.002]; [One way ANOVA between groups, Rears: $F_{(3,116)}$=4.83; p=0.003; Tukey's *post hoc* tests: *Del/Dup* vs. *Dup/+*: p=0.002]. **(C)** Novel object recognition memory task of the rat 16p11.2 models after 3 h of retention with 3 objects. Male rats from different genotypes [wt (n=26), *Del/Dup* (n=16), *Del/+* (n=14) and *Dup/+* (n=16)] and female rats [wt (n=18), *Del/Dup* (n=16), *Del/+* (n=26), and *Dup/+* (n=17)] were tested for the novelty recognition. The graphs show the percentage of time spent by the animals exploring a novel object compared to the time spent exploring two familiar objects. We compared the recognition index, like the percentage of exploration time of the new object, to the level of chance (33.3%). Only the *Del/+* males showed impairment in the recognition index [One sample t-test: wt ($t_{(25)}$=4.6; p=0.0001), *Del/Dup* ($t_{(15)}$=2.82; p=0.01), *Del/+* ($t_{(13)}$=0.34; p=0.74) and *Dup/+* ($t_{(14)}$=3.58; p=0.0030)] compared to all the other genotypes in males and females. Surprisingly, no change was observed in the *Del/+* females [One sample t-test: wt ($t_{(17)}$=3.67; p=0.002), *Del/Dup* ($t_{(16)}$=3.08; p=0.01), *Del/+* ($t_{(25)}$=3.83; p=0.0008) and *Dup/+* ($t_{(16)}$=2.3; p=0.035)]. **(D)** Social interaction of the 16p11.2 rat models. Male [wt (n=15), *Del/Dup* (n=14), 16p11.2

(Continued)

FIGURE 2 (Continued)

Del/+ (n=10) and *Dup/+* (n=14)] and female [wt (n=14), 16p11.2 *Del/+* (n=15), 16p11.2 *Dup/+* (n=12) and *Del/Dup* (n=15)] rats were tested for impairment of social interaction in pairs of individuals from different home cages with the same genotype. The *Del/+* male rat showed increased solitary time [One way ANOVA between groups, Solitary behavior: $F_{(3,49)}$=9.85; p<0.001; Tukey's *post hoc* tests: *Del/+* vs. wt: p<0.001, *Del/+* vs. *Del/Dup*: p<0.001 and *Del/+* vs. *Dup/+*: p=0.005]. and pinning behavior with *Del/Dup* [Kruskal-Wallis one-way analysis of variance $H_{(3)}$=8.66; p=0.03; Mann-Whitney test: *Del/+* vs. wt: p=0.04; *Del/Dup* vs. wt: p=0.01] while Dup/+ males are more agnostic [Kruskal-Wallis one-way analysis of variance: $H_{(3)}$=13.63; p=0.003; Mann-Whitney test: *Dup/+* vs. wt: p=0.01; *Dup/+* vs. *Del/+*: p=0.02]. No altered social behavior has been detected in females (*p<0.05; **p<0.01; ***p<0.001).

model. First, we observed a reduction in the variability between the data of each individual regarding the results observed in the SD model. In addition, we detected a significant increase in horizontal activity among individuals carrying the 16p11.2 region deletion for both sexes. Finally, the Open Field test showed a significant increase in vertical activity, evaluated as the total number of rears, only in male rats. These results translate into the presence of stereotypical behaviors in this model associated with genotype and sex (Figure 3B).

Next, we performed the object location memory test (Supplementary Figure S3A; Supplementary Table S4). Our objective was to confirm, as in the case of the SD model, that the deletion of a copy of the 16p11.2 region has no impact on the object location memory in our second rat model. Considering that the 3-object discrimination protocol for the NOR test was the most appropriate, we decided to test the LE model (Supplementary Figure S3B; Figure 3C). Thus, this task showed that male mutant individuals, unlike control individuals, did not show an exploration preference for the new object. Furthermore, the object recognition index of these animals is not significantly higher than 33.3%. Instead, females carrying the 16p11.2 deletion on LE background did not develop any disorder in object recognition memory, showing a recognition index higher than the 33.3% chance level.

To get an animal model more relevant to autism with robust social behavior phenotypes shared among genetic backgrounds, we evaluated the LE model during the social interaction test (Figure 3D). Among the most interesting observations, we found that male mutant individuals spent significantly more time alone than control individuals. This phenotype was also observed in the SD 16p11.2 deletion model (Figure 2D). In addition, curiously, we discovered that these animals spent more time approaching their partner and we did not detect cases of pinning or agnostic behavior. In the case of LE females, the deletion of the 16p11.2 region had no effect on the development of social phenotypes for the evaluated events, as observed for the mutant SD females Overall the behavior results we identified were robust, as were observed similarly in the LE background to those obtained from the SD background in the 16p11.2 Del/+ model.

3.3. Expression analysis shed light on the pathways altered by a genetic dosage of the 16p11.2 homologous region

We investigated the gene expression profile of Del/+ and Dup/+ 16p11.2 male SD rat hippocampi by RNA-seq. After performing the DEA analysis using FCROS we identified 966 and 1,367 genes dysregulated (DEGs) in Del and Dup models, respectively (Table 1). Using those DEGs, we computed a PCA to assure the profile of expression of the DEGs could cluster our samples by their different gene dosage (Figure 4A). Additionally, to assure the quality of our data, we looked at the Euclidian distance between samples, calculated using the 28 genes susceptible of the dosage effect of the 16p11 region, and indeed all cluster by genotype (Figure 4B). Moreover, most of the genes of the region are following the gene dosage on the models. Looking at the FC profile across the region in the duplication, we found one gene with decreased FC expression LOC102552638, and several highly expressed genes as *Gdpd3*, two rat-specific *ABR07005778.1, AABR07005779.7*, and *Zg16*. Interestingly, in the deletion, we found 2 genes with an unpredicted increased expression, one outside of the region *RF00026,* possibly due to a bordering effect and another inside the region, *Zg16*. Overall, the gene expression dysregulation was corroborating the genetic dosage for this region in the different models (Figure 4C).

Looking at the expression of DEGs in both models, only 51% were strongly correlated to gene dosage (Figure 4D; Supplementary Table S5). Many genes of the 16p11 region (*AldoA, Mapk3, Cdipt, Coroa1, Kctd13, Ino80e, Mvp, Slx1b* and *Ppp4c*) showed a level of expression in RNA-Seq following a gene dosage effect that was confirmed by ddPCR (Supplementary Figure S4). Then, we wondered whose genome-wide DEG expression levels were positively, or negatively, correlated with the gene dosage. To answer this question, we fit a linear model considering CNVs as follows [lm(log2FC ~ CNV) == y ~ (b0 + b1*CNV)]. We found six genes of the region following a positive gene dosage effect *Aldoa, Sez6l2, Bola2, Kif22, Rad21l1, Ptx3, and Mael* with another gene, named *Chad*, out of the region, and presenting a negative correlation in the dosage model (Supplementary Table S5). Overall, 267 DEGs were commonly dysregulated in the Del/+ and Dup/+ models (19.7% shared DEGs of the total Dup/+ DEGs or 28.1% of the total Del/+ DEGs). Of those common 267 DEGS between models, 100 DEGs were downregulated in both models and 120 upregulated in both. Therefore, some functionalities should be commonly altered independently of the dosage. Nevertheless, 39 DEGs were following the region dosage effect (upregulated in the Dup/+ and downregulated in the Del/+), including the genes on the interval *Coroa1-Spn* and others like *Fam57b, Rad21l1, Mael, Ptx3* or *Rnf151,* found elsewhere in the genome, and 47 genes were altered in opposing regulatory sense. In particular, a few DEGs were following a negative dosage correlation such as *Cd8a, Evpl, Ucp3, Lipm* and *Cdh1* being upregulated in the Del/+ and downregulated in the Dup/+ (Figure 4E).

To go further, we performed the differential functional analysis (DFA) using gage (Luo et al., 2009). We found 146 and 68 pathways altered in the hippocampi of Del/+ and Dup/+ models, respectively. No downregulated pathway was found in the Dup/+ model whereas both up and downregulated pathways were found in the Del/+ hippocampi. After grouping the pathways inside of functionality-based defined meta-pathways (Duchon et al., 2021; Figure 5A; Supplementary Table S6). Although in the Dup/+ model, there were

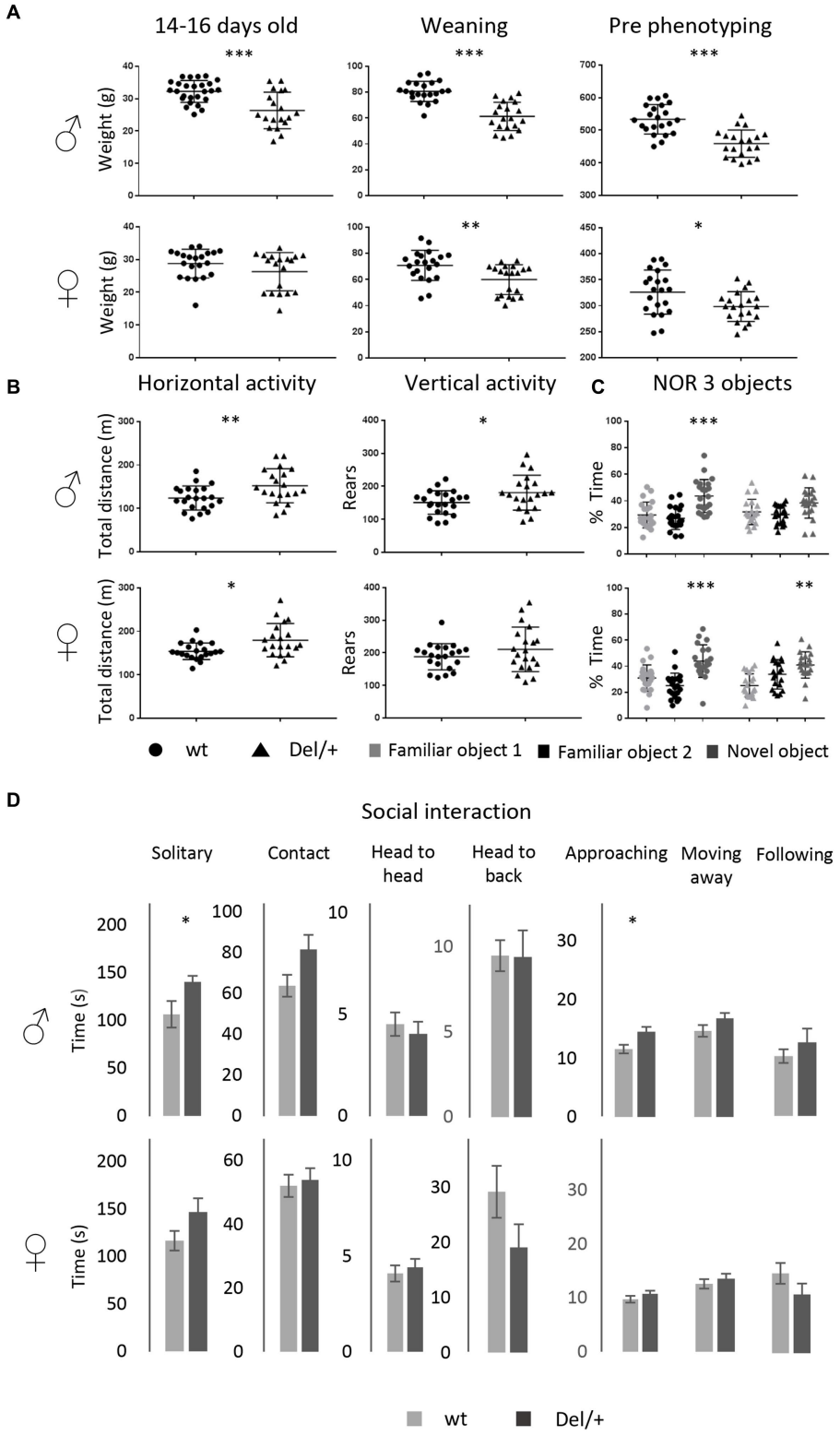

FIGURE 3
Phenotypic characterization of the 16p11.2 rat models on the LE genetic background. **(A)** Effects of *Sult1a1-Spn* deletion on body weight of LE 16p11.2 Del/+ rat model. Left: body weight (g) of the 14–16 days old males [wt (n=27) and Del/+ (n=19)] and female rats [wt (n=21) and Del/+ (n=19)]. Our observations showed a decreased body weight in Del/+ males compared to wt littermates [Student's t-test: $t_{(44)}$=3,819; p<0.001]. Central: body Weight at weaning of the males [wt (n=21) and Del/+ (n=20)] and female rats [wt (n=21) and Del/+ (n=20)] from LE Del/+ littermates. The deletion of the 16p11.2 region caused body weight decrease in male [Student's t-test $t_{(39)}$=6,550; p<0.001] and female individuals [Student's t-test $t_{(39)}$=3,036; p=0.004] compared to wt littermates. Right: body weight of 16p11.2 Del/+ male [wt (n=22) and Del/+ (n=20)] and female [wt (n=21) and Del/+ (n=20)] littermates during the first week of phenotype analysis. The male and female individuals carrying the deletion of the interest region continued to show a decrease in their body weight throughout their development [Student's t-test for males: $t_{(40)}$=5,550; p<0.001; Student's t-test for females: $t_{(39)}$=2,451;

(Continued)

FIGURE 3 (Continued)

p=0.019]. **(B)** Open Field test results illustrate the exploratory activity of the LE 16p11.2 rat model. Male [wt (n=22) and *Del/+* (n=20)] and female [wt (n=21) and Del/+ (n=20)] littermates were analyzed for horizontal and vertical activity. The 16p11.2 deletion caused increased horizontal activity in our model regardless of the sex of the animals [Student's t-test for males: $t_{(40)}$=−2,726; p=0,009; Mann–Whitney U Statistic for females: T=510,000; p=0.02]. However, the deletion of one copy of the interest region caused increased vertical activity only in male individuals [Student's t-test $t_{(40)}$=−2,174; p=0.036]. **(C)** The deletion of the 16p11.2 region causes a novel object recognition memory disorder in our rat model on LE genetic background. For the NOR test with 3 objects, the recognition index reflects the ability of rats to recognize the new object from the 2 familiar objects after a 3 h delay. Males mutant animals [wt (n=22) and Del/+ (n=20)] were impaired to recognize the new object when we compared the recognition index, like the percentage of exploration time of the new object, to the level of chance [33.3%; One sample t-test: wt ($t_{(21)}$=3.94; p=0.0008) and Del/+ ($t_{(19)}$=2.02; p=0.0569)]. However, the females of this model [wt (n=21) and Del/+ (n=20)] showed a preference for the new object that is reflected in a recognition index significantly higher than the level of chance [One sample t-test: wt ($t_{(20)}$=3.92; p=0.0008) and Del/+ ($t_{(19)}$=3.4; p=0.003)]. **(D)** Evaluation of the behavior of the LE 16p11.2 rat model in the social interaction test. The male [wt (n=11) and Del/+ (n=10)] and female [wt (n=10) and Del/+ (n=10)] of our second model were analyzed separately from the observation of different events in pairs. The Del/+ male rat showed increased solitary time [Student's t-test: $t_{(18)}$=−2,229; p=0.039] and approaching behavior [Student's t-test $t_{(19)}$=−2,679; p=0.015]. No altered social behavior has been detected in females (*p<0.05; **p<0.01; ***p<0.001).

several groups with a higher number of upregulated pathways compared to the Del/+ model, as synaptic meta-pathway, signaling or transcription and epigenomic regulation, many downregulated pathways were observed in the Del/+ model, except the "transcription and epigenomic regulation" meta-pathway not being affected. Moreover, as expected from the DEA analysis, we indeed were able to identify 23 pathways that were commonly shared and upregulated in both Del/+ and Dup/+ (Figure 5B) with most of them being related to morphogenesis with the primary cilium, and four others unrelated. Oppositely "synaptic and Synaptic: other pathways" and "metabolism" functions were more affected in the Del/+ condition, while "transcription and epigenomic regulation" or "hormone regulation" were more perturbed in the Dup/+ model (Figures 5A,C).

3.4. CUL3 and MAPK3 functional subnetworks are central to the 16p11 dosage susceptible regulatory protein–protein interaction network

Then, we built the rat 16p11 dosage susceptible regulatory protein–protein interaction network (RegPPINet; Figure 6A) using as seeds all the genes identified by gage as altered in the Del/+ and/or in the Dup/+ SD models. We aimed to gain some insights into the possible molecular mechanism altered due to the gene dosage of the region. After performing the betweenness centrality analysis and analyzing the topology of the most central network we identified 47 main hubs. Several of those hubs involved genes from the region (Figure 6A) and interestingly we identified a few central genes linked to synaptic deregulation, re-enforcing the fact that synaptic dysfunction was one of the main alterations due to the dosage change of 16p11. These most important hubs in terms of betweenness were *Chd1, Gli1, Plg, Coro1a, Epha8, Disc1, Spag6l, Cfap52 or Sema3a.* However, if we consider the most connected gene, by the sole degree of regulatory interactions, then the 16p11 dosage RegPPINet pointed to Mapk3 and Cul3 (Figures 6B,C). The first subnetwork is centered on *Mapk3* with expressed genes also found altered in both Del/+ and Dup/+ models with opposite regulatory senses (like *Cdh1* or *Mvp*). In addition, we found 3 genes on this subnetwork, *Gdnf, Gata4* and *Atp1a4* downregulated in both models and one gene *Itgb6* upregulated in both. The *Cul3* network involved several genes whose expression was found altered in both Del/+ and Dup/+ models with mirroring regulatory effects for *Kctd13, Doc2a, Kif22, Rad21l1, Ppp4c* or *Asphd1*.

3.5. Proteomics analyses further support the major relevance of 16p11 gene dosage and the central role of MAPK3 and CUL3 interactors

Then, we wondered how much of the 16p11 dosage susceptible network could be confirmed by a quantitative proteomics analysis based on the hippocampus. Seven out of the 32 proteins encoded in the 16p11.2 region, were detected and successfully quantified by mass-spectrometry in the samples analyzed. Their expression profiles showed a clear correlation with gene dose with lower expression in Del/+, intermediated expression in wt and Del/Dup genotype, and higher expression in Dup/+. Dup/Del values followed partially the wt abundance (Supplementary Figure S5). There were 3 missing measures for Bola2, and D4A9P7 in the Del/+ group, which were very likely linked to low/borderline abundance in the samples.

Interestingly, most of the genes, contributing to the functional alteration in the 16p11 dosage and the transcription network, were also detected and quantified by the proteomic technique (highlighted in yellow with an octagonal shape; Supplementary Figure S6A). We found a strong correlation between the RNA level (RNA seq count) and our proteomic quantification in wt and Del/+ individuals for all expressed genes (Supplementary Figure S6B) and DEGs (Supplementary Figure S6C). Thus, we decided to investigate the proteomics dataset on its own and search for new insights into the 16p11 syndrome alterations. We built the proteomic-specific hippocampi 16p11 MinPPINet (Supplementary Figure S7A). Very well-connected 16p11 region proteins, such as ALDOA, BOLA2, CDIPT and COROA1, unraveled the existence of two main subnetworks (Supplementary Figure S7B): the first was around MAPK3 and SRC, a proto-oncogene coding for a membrane-bound non-receptor tyrosine kinase, while the second was built around the ATP citrate lyase (ACLY). ACLY is associated through the proteasome subunit, alpha type, 4 (PSMA4), to superoxide dismutase 1 (SOD1) and CUL3 for polyubiquitination and degradation of specific protein substrates.

3.6. Sexual dysmorphism observed at the transcriptomics level in 16p11 LE deletion models

Then we wonder if the rat's genetic background can also change major transcriptomics outcomes and if any sexual dysmorphism can

10.3389/fnins.2023.1148683

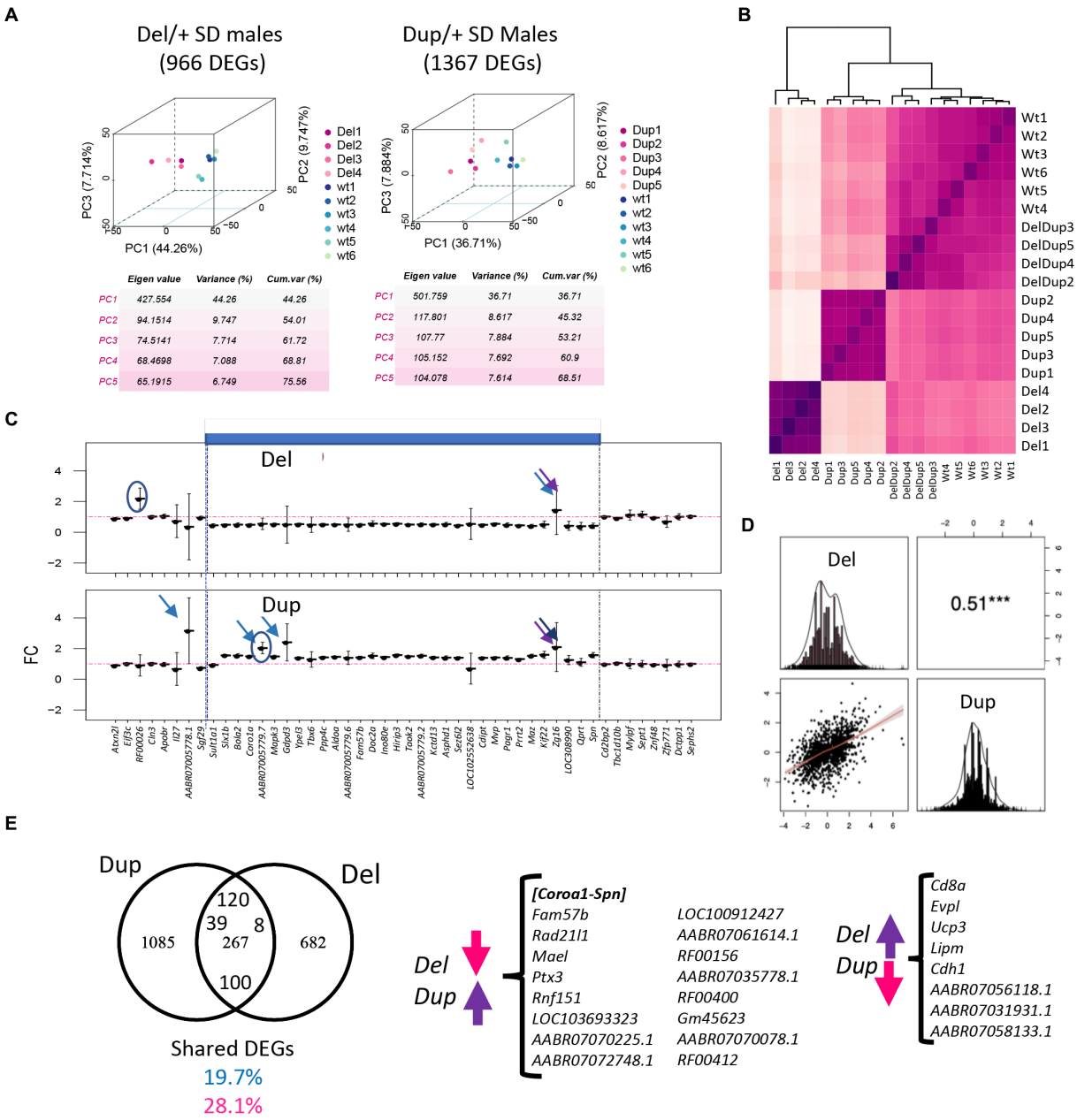

FIGURE 4
Gene expression analysis at the transcriptome and proteome level in the 16p11Del and Dup male rat hippocampi. **(A)** 3D principal component analysis (PCA) on the DEGs for each adult hippocampal sample allows for isolating the animals carrying the 16p11.2 deletion (Del/+) and the animals with the 16p11 region (Dup/+) in comparison with the wild-type littermates. From disomic (wt) adult hippocampi. **(B)** Homogeneity plot showing the gene dosage effect of the 28 genes in the 16p11.2 region and how the samples cluster by Euclidian distance. **(C)** Fold change expression levels of the genes analyzed by RNA-Seq homologous to the 16p11.2 region in rat chromosome 1 (Rno1). The genes are displayed following the order of their genomic start site coordinates. The 16p11.2 interval is indicated in blue. **(D)** Distribution and correlation diagram showing the DEGs in common between Del and Dup models and the model-specific DEGs. The shared DEGs correspond to 19.7% and 28.1% of the total DEGs identified, respectively, for the Dup and Del models. **(E)** Venn diagram showing in the left panel, the DEGs in common between the SD Del and Dup/+ models and SD male transcriptomics datasets and the background-specific DEGs. Highlighted inside the common genes those upregulated in both models, 120, downregulated in both 100 and regulated in opposing regulatory sense between Dup/+ and Del/+ models (39 upregulated in Dup/+ and 8 downregulated in Dup/+).

be detected. Thus, we isolated hippocampi from 5 females and 5 males Long Evans Del/+ and controlled wild-type littermates to carry out transcriptome analysis. The DEA analysis using FCROS identified 1,068 and 1,324 genes specifically dysregulated (DEGs) in Del/+ males and females, respectively (Table 1). Moreover, 1,544 DEGs were altered independently of the sex when we ran the analysis pooling both sexes together (Figure 7A). The computed PCA and the Euclidian distance matrix clustered the samples by their genotypes and then sex (Figure 7B). Moreover, the specific fold change of the 16p11.2 region in both males and females showed the expected downregulation in both sexes, similar to the one observed in the male SD Del/+ male model (Figure 7D). A good correlation occurred with the normalized

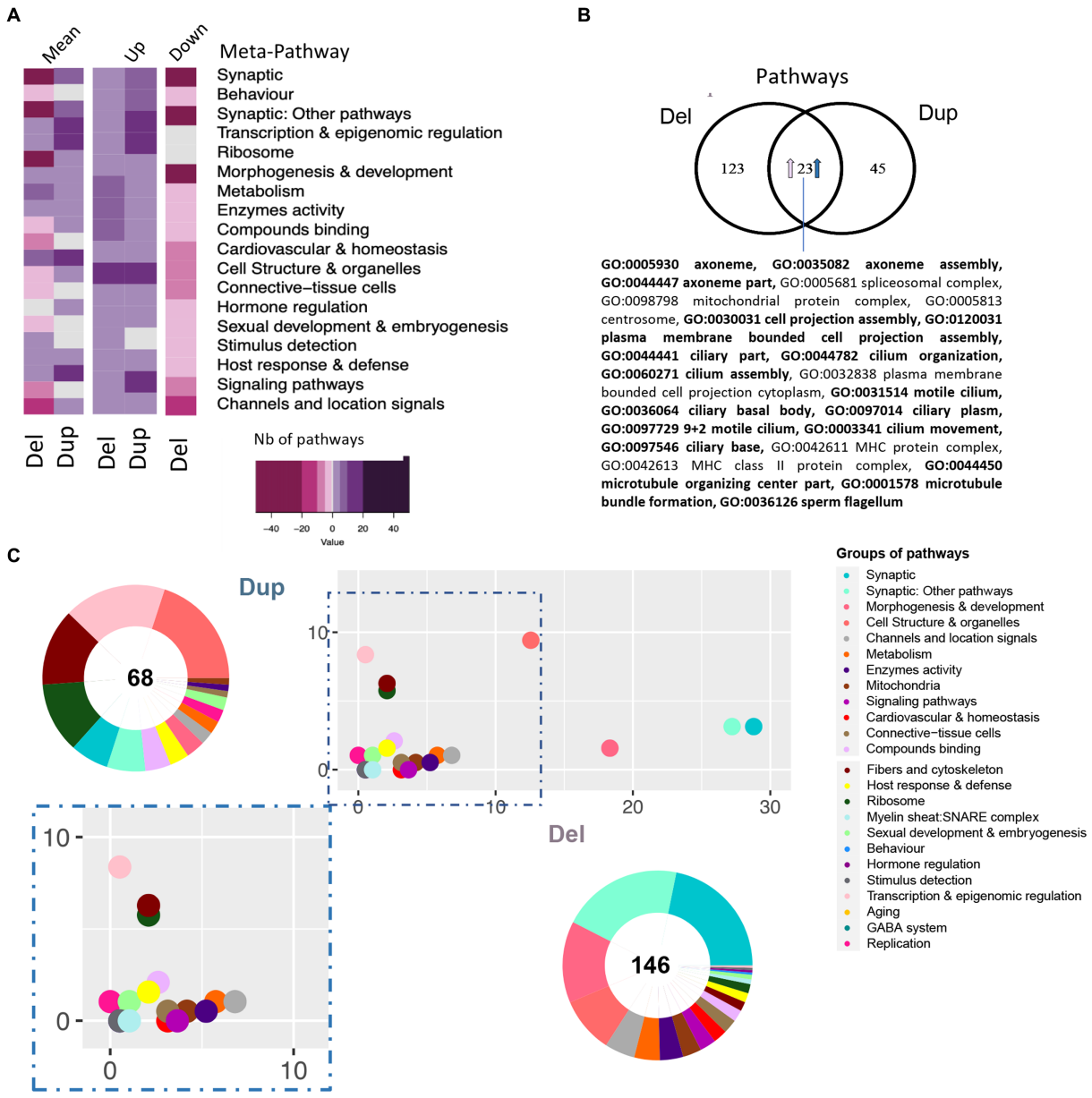

FIGURE 5
Pathway analysis of 16p11.2 SD rat Del and Dup male model based on the transcriptome of the hippocampi. **(A)** Heatmap representation of the number and regulation sense of the pathways of the Del and Dup models. Pathways identified using the GAGE R package and filtered by q-value cut-off < 0.1, were grouped in the meta-pathways shown on the ordinate. The color key represents the number of pathways within the meta-pathways 50, 20, 10, 5, 0. The minus or pink color represents downregulated pathways, the white color represents no pathway found in the meta-pathway and the purple or positive numbers stand for upregulated pathways, respectively. **(B)** Venn diagram highlighting the 23 pathways upregulated in both models and the existence of model-specific functional alteration. The percentage of shared pathways reached 33% or 15% of the total altered pathways in the Dup(16p11) and Del(16p11) models, respectively. Seventeen of those pathways are also found dysregulated in Del/Dup (in bold). **(C)** Ratio plot showing the inter-model comparison of the percentage of pathways included on each meta-pathway (group of pathways) normalized by the total number of unique pathways per meta-pathway. The x-axis and y-axis represent the SD male Del and Dup data, respectively. Outside a doughnut plot represented in the center, the number of total altered pathways found by gage analysis on each dataset and the percentage of pathways altered included on each meta-pathway is represented on the coronal area under each meta-pathway. The meta-pathways are defined in the accompanying legend.

counts of 16p11 region genes for wt and Del/+ genotypes in both LE male and female hippocampi (for wt $R^2 = 0.9996$, Del/+ $R^2 = 0.9988$) and also when comparing wt and Del/+ genotypes in males from the SD and LE genetic backgrounds (for wt $R^2 = 0.9966$, Del/+ $R^2 = 0.9987$; Supplementary Figure S8). Four genes from the region were confirmed by ddPCR to follow the dosage effect with lower expression in the Del/+ rat males and females compared to wt littermates. There was a limited number of DEGs commonly deregulated in both sexes compared to hippocampal DEGs specific for males and females and more DEGS were observed in males than in females (Figure 7C), suggesting that there was a strong influence of the sex on the genomic dysregulation induced by the deletion.

Sexual dysmorphism was also found at the level of the altered pathways. With 248 pathways altered in males and 100 identified in

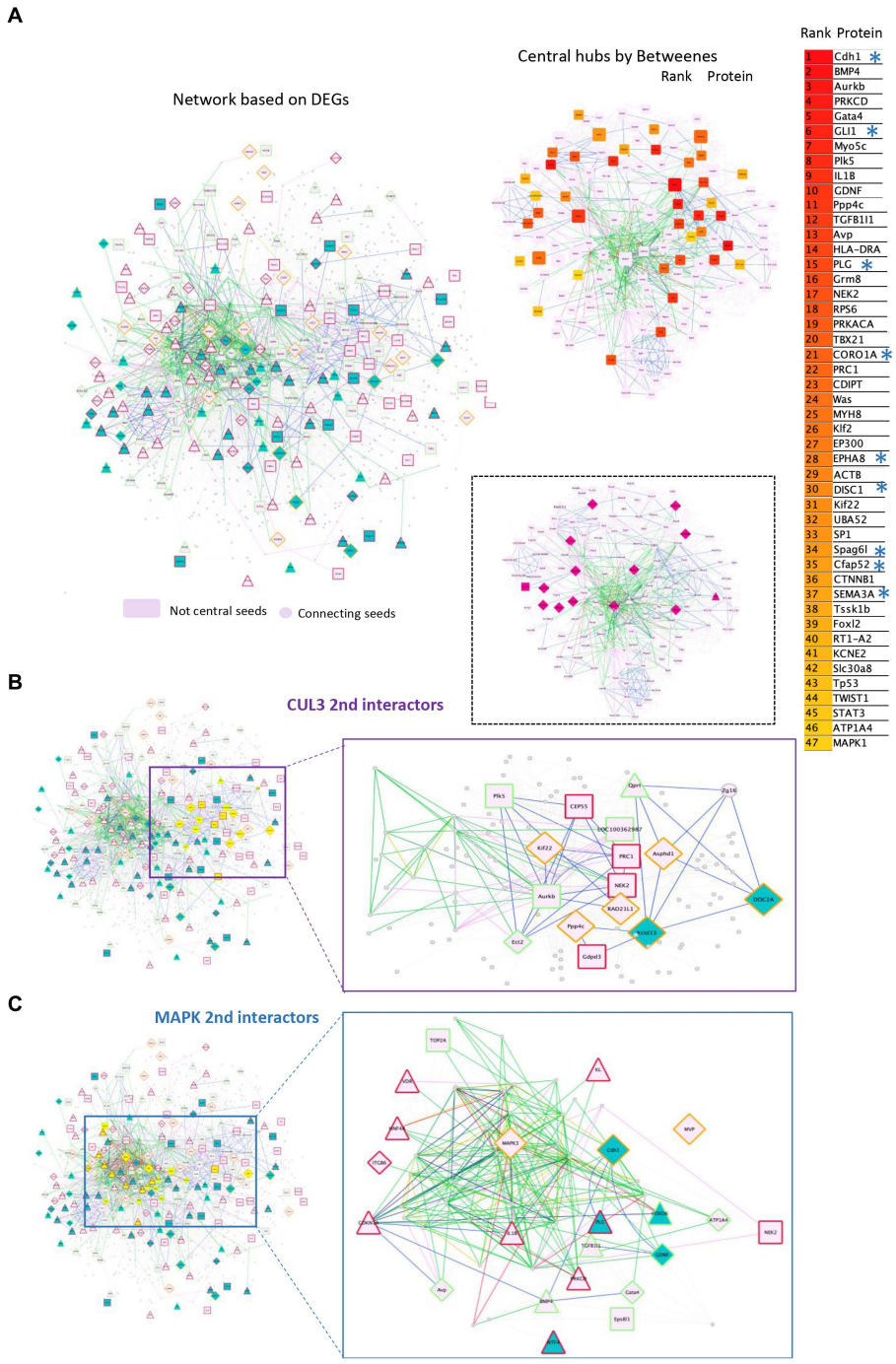

FIGURE 6
Protein–protein interaction networks altered due to the gene dosage effect based on the transcriptome analysis of the 16p11 SD rat models. **(A)** Left panel, a full rat protein–protein interaction network (RegPPINet) built using as seeds all the genes identified by gage as altered in the Del or Dup SD models visualized using the edge weighed spring embedded layout by betweenness index in Cytoscape. On the right panel, highlighting the main central nodes of the rat dosage susceptible RegPPINet network. On the bottom panel, highlight in pink the 16p11 region genes. The full RegPPINet was built by querying STRING and selecting the PPIs with a medium confidence score (CS=0.4) coming from all sources of evidence. The shapes of the nodes represent the following information: Shapes: (i) Pallid pink ellipses: represent connecting proteins added to assure the full connectivity of the network; Then the genes identified by GAGE after q-Val < 0.1 cut-offs to be contributing even slightly, to any pathway alteration and also identified in the DEA analysis by Fcros. The top 50 central genes are listed on the right side with genes known to be involved in synaptic pathways (*). **(B)** Second-level interactors of CUL3 were extracted from the main network. The left panel shows in yellow all the genes that are second-level interactors of CUL3. On the right panel, the extracted subnetwork centered around CUL3 to identify the molecular regulatory mechanisms known to exist between the interacting partners. **(C)** We extracted from the rat RegPPINet the second-level interactors of MAPK family proteins (proteins MAPK 1,3,8,9,14). Left panel, the full RegPPINet network can be observed highlighting in yellow all the genes that are second-level interactors of CUL3. On the right panel, the extracted subnetwork centered around MAPK proteins to identify the molecular regulatory mechanisms known to exist between the interacting partners. The shapes of the nodes represent the following information: Shapes: (i) Pallid pink ellipses: represent connecting proteins added to assure the full connectivity of the network; Then the genes identified by GAGE after q-Val < 0.1 cut-offs to be contributing even slightly, to any pathway

(Continued)

FIGURE 6 (Continued)

alteration and also identified in the DEA analysis by Fcros. Rectangles represent genes identified uniquely in Dup transcriptomes while triangles are for genes identified uniquely in Del transcriptomes and diamond shapes for genes identified as DEGs in both models. The edges color represent the type of interaction annotated by following the PathPPI classification (Tang et al., 2015), and ReactomeFIViz annotations as follows (i) The GErel edges indicating expression were colored in blue and repression in yellow. (ii) PPrel edges indicating activation were colored in green, inhibition in red. (iii) Interactions between proteins known to be part of complexes in violet. (iv) Predicted interactions were represented in gray including the PPI interactions identified by STRING DB (Szklarczyk et al., 2017) after merging both networks. The nodes bordering color represent If the gene was found upregulated in both models (red), downregulated in both (green) or in the mirroring regulatory sense (orange).

females, only 49 specific pathways were found deregulated in both sexes but only 2 followed the same regulatory sense (Figure 7C). We then used the classification in meta-pathways (Duchon et al., 2021) to better understand the changes associated with the deletion. Looking at the resulting component, some meta-pathway like "Synaptic," and "Synaptic: other pathways" were found downregulated in males while the resulting component was upregulated in females. Oppositely, "Behaviour," "Host & immune response," and "Morphogenesis and development" were found downregulated in males whereas those were upregulated in females (Figures 7E–F). Other meta-pathways were only found affected in Del/+ males. "Mitochondria" were only found upregulated in males while "hormone regulation" and "sexual development and embryogenesis" were downregulated only in males with no alteration in female carriers (Figures 7E–F). Overall, the alteration of pathways appeared to be more pronounced in males than in females.

Looking into the number of DEGs and pathways shared and unique in both SD and LE genetic backgrounds, we identified 182 common genes, most of them following the same regulatory sense and 48 pathways, 28 upregulated and 20 downregulated in both models (Figure 8A). Moreover, even though the number of total pathways altered in LE was higher than in SD (248 and 146 respectively) when looking at the proportion of pathways grouped on each meta-pathway considering the total number of unique pathways altered in both models only an important increase in "Cell structure" meta-pathway in LE compared to SD could be highlighted (Figure 8B). Considering the results obtained, we identified similar changes in the meta-pathways profiles pointing to the existence of a conserved and robust functional alteration profile (Figure 8C), mirrored in most of the meta-pathways in the Dup/+ model. Overall the main meta-pathways for synapse ("synaptic" and "synaptic other pathways") were commonly altered in the Del/+ models.

The few functional changes between the two genetic backgrounds were in "Apoptosis & cell death" and "post-translational modifications" which were only found affected in the LE background.

4. Discussion

In the present study, we described the first behavioral and cognitive phenotypes of 16p11.2 deletion and duplication of new rat models on SD and LE genetic backgrounds. A cognitive deficit was found in the novel object recognition memory test with 3 objects, and a defect in social interaction was observed with increased isolation behavior, a typical autistic trait, in 16p11.2 *Del*/+ males. The deletion of the *Sult1a1-Spn* region was also associated with the appearance of increased pinning events, a behavior considered an expression of dominance. In addition, this type of behavior could also be seen among pseudo-disomic *Del/Dup* carriers, suggesting a genetic construct effect not related to the dosage of genes from the region. This phenomenon may result from the new deletion allele that could alter the expression of neighboring genes. Besides, 16p11.2 duplication in males was linked to an increase in aggressiveness. These phenotypes could be associated with autistic traits and psychotic symptoms identified in patients affected by 16p11.2 rearrangements (Niarchou et al., 2019).

Interestingly in both outbred genetic backgrounds, the social and cognitive phenotypes were more noticeable in males than Del/+ females. The characterization of these models on a non-consanguineous genetic background allowed us to observe initially a large phenotypic variability compatible with the large symptomatic variability and the low penetrance of the neuropsychiatric disorders associated with CNVs 16p11.2 in humans. But it is important to emphasize that higher variability in the behavior outcome of phenotypic analysis hinders our research. We have used 8 cohorts of rats to increase the number of animals (about 20–25 animals per experiment) to be able to gather a larger part of the population. For these reasons, we consider it pertinent to analyze the robustness of the phenotypes associated with the 16p11.2 deletion (CNV that has caused a more severe phenotype in the SD model) through the new rat models with outbred genetics.

While in the SD model, the variability of behavior between individuals only allowed us to observe a trend of hyperactivity, in the new LE model we could corroborate a decrease in variability and the significant presence of hyperactivity and repetitive behaviors in males. In addition, we again detected a cognitive disorder in object recognition memory in males of the LE model, confirming the robustness of this phenotype in the 16p11.2 deletion syndrome.

Finally, when analyzing the social behavior of the LE model, we were also able to confirm the association of solitary behavior phenotype with the deletion of the genetic interval in males. Although there were direct contact events between the tested animals, these rats avoided the behavior of staying close to each other while exploring the test. This is a very common practice among rats, unlike mice tend to be more solitary, which makes rats more sociable beings and animal models most useful for the study of social disorders. In addition, curiously, we discovered that these animals spent more time approaching their test partner, which could be interpreted as cautious or scary behavior to approach an unknown animal.

In this area also, we again observed a greater sensitivity of the male sex or a greater resilience of the female sex to the deletion of the 16p11.2 region in this new genetic background. This phenomenon is also observed in humans where more males are affected by ASD than females in the population. Our observation supports the theory of Empathy-Systematization, according to which sexual psychological differences reflect a reinforcement of systematization in the male and

10.3389/fnins.2023.1148683

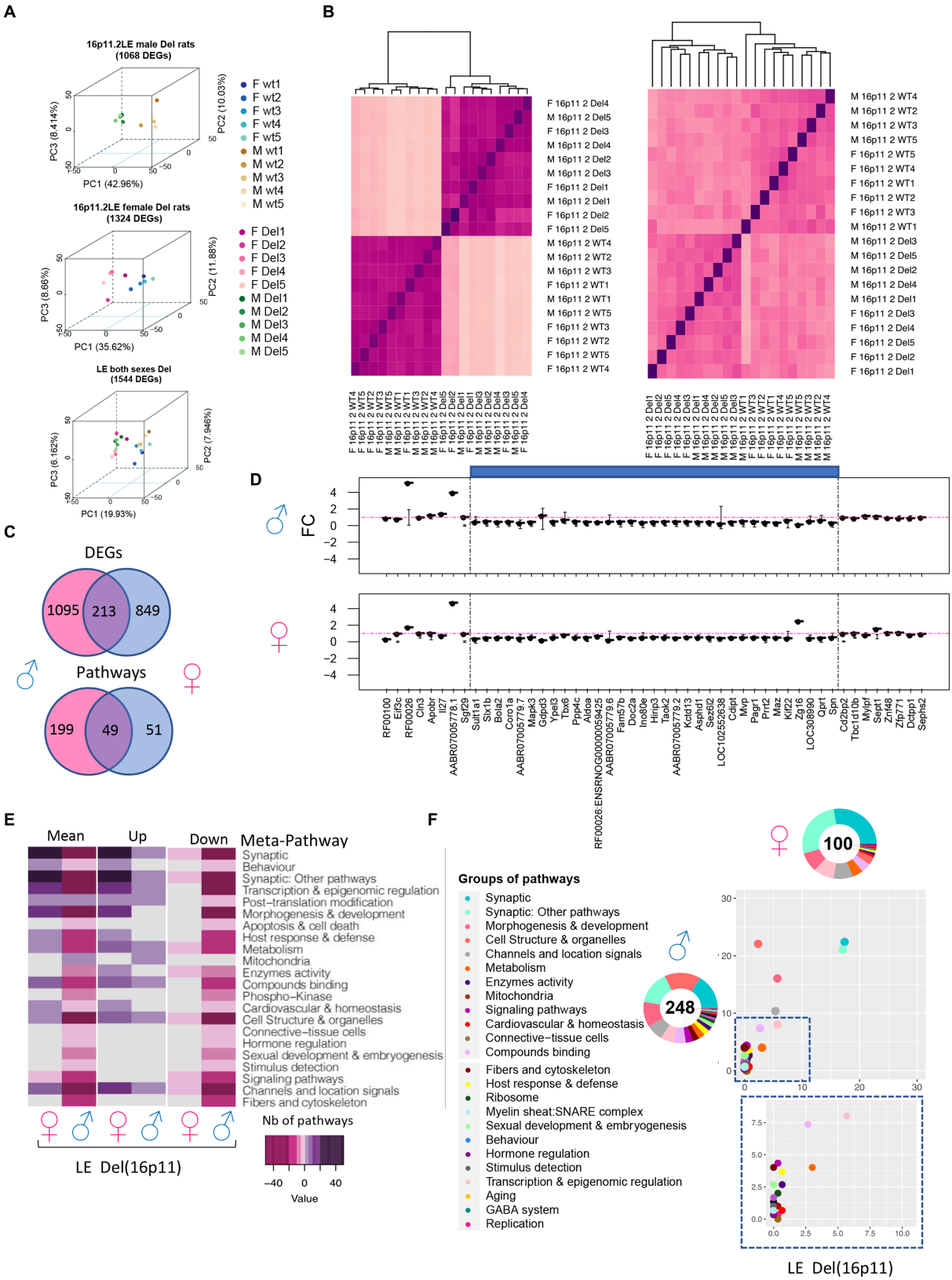

FIGURE 7
Gene expression analysis of 16p11 LE Del and control littermate (wt) male and female rats. **(A)** 3D-PCA on the DEGs for each adult hippocampal sample allows us to isolate the LE rats carrying the 16p11.2 deletion (Del) in comparison with the wild-type littermates in both sexes as shown in the upper and middle plots. As shown in the bottom plot even though there are some differences by sex the genotype effect is the major difference between the animals and its variability is explained in the first component "PC1." **(B)** Homogeneity plot showing the gene dosage effect of (left) the 28 genes in the 16p11.2 region and how the samples cluster by Euclidian distance, and (right) all DEGs identified in both male and female datasets. **(C)** Venn diagram

(Continued)

FIGURE 7 (Continued)

showing in the upper panel, the DEGs were found common between the male and female LE datasets. The shared DEGs correspond to 16.2% and 20% of the total DEGs identified, respectively, for female and males. In the bottom panel, the Venn diagram shows the pathways in common between the male and female LE datasets. The shared pathways correspond to 19.7% and 49% of the total pathways identified. **(D)** Fold change expression levels of the genes from the region homologous to 16p11.2 in Rno1. The genes are displayed following the order of their genomic start site coordinates. The deleted areas for each model appear shaded in blue. **(E)** Group of meta-pathways showing up or downregulation with a color key corresponding to the number of pathways within the meta-pathways. **(F)** Ratio plot showing the inter-model comparison of the percentage of pathways included on each meta pathway normalized by the total number of unique pathways per meta-pathway. The x-axis and y-axis represent the female and male data, respectively. Outside a doughnut plot representing in the center the number of total altered pathways found by gage analysis one each dataset and the percentage of pathways altered included on each meta-pathway is represented on the coronal area under each meta-pathway. The metapathways are defined in the legend.

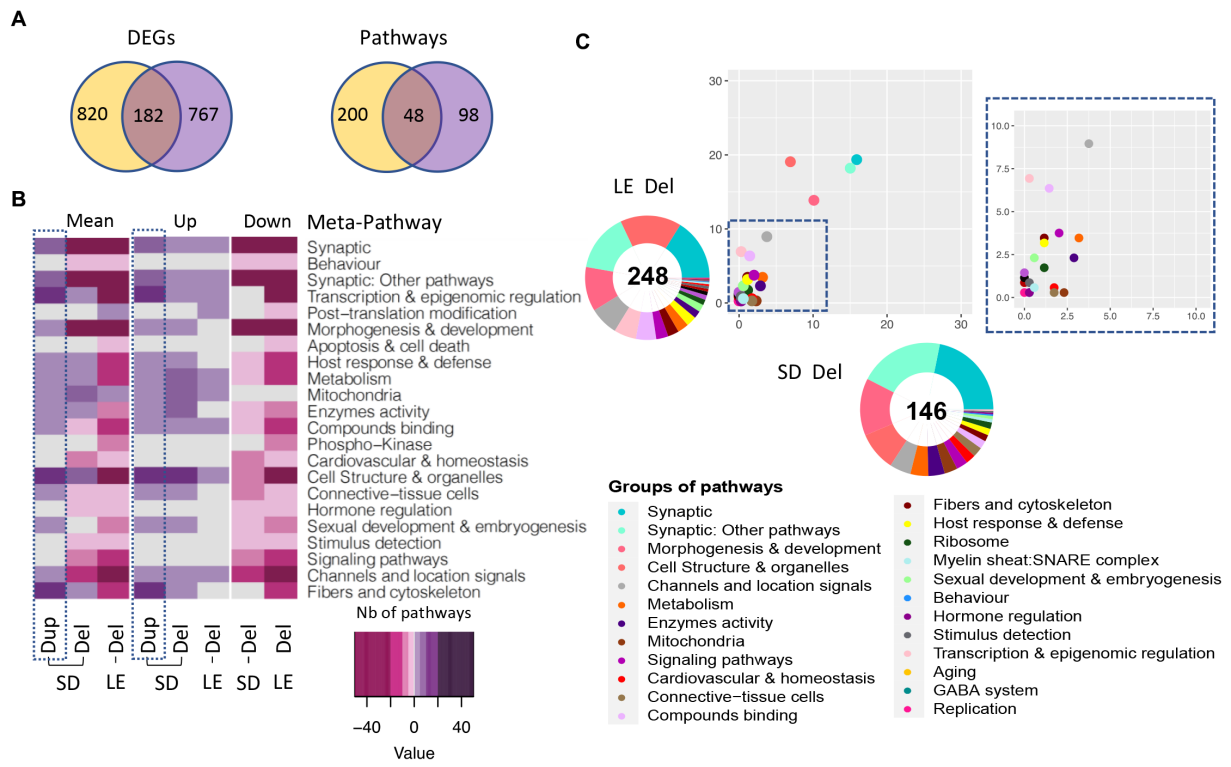

FIGURE 8
Gene expression analysis of the males LE vs. SD Del (16p11) rat models. **(A)** Venn diagram showing in the left panel, the DEGs in common between the LE and SD male transcriptomics datasets and the background-specific DEGs. The shared DEGs correspond to a 16.2 and 20% of the total DEGs identified, respectively, for the Dup and Del models. **(B)** Heatmap representation of the number and regulation sense of the pathways altered in the male rat from SD Del, SD Dup and LE Del models. **(C)** Ratio plot showing the inter-model comparison of the percentage of pathways included on each meta-pathway, normalized by the total number of unique pathways per meta-pathway. On the x-axis and y-axis represent the rat male SD Del and LE Del data, respectively. Outside a doughnut plot representing in the center the number of total altered pathways found by gage analysis for each dataset and the percentage of pathways altered included on each meta-pathway is represented on the coronal area under each meta-pathway.

a reinforcement of empathy in the female. In the context of TSA, this theory has an extension, called the "extreme male brain" according to which individuals are characterized by deficiencies in empathy with an intact or increased systematization (Baron-Cohen et al., 2005, 2011). Our data are also consistent with the proportion of identifying 16p11.2 rearrangements favorable for boys compared to girls reported in a previous study. This paper indicated a male: female ratio of 1.3:1 for the 16p11.2 deletion in autistic individuals and 1.6: 1 for the 16p11.2 deletion in patients with intellectual disability / developmental delay (Polyak et al., 2015). Further studies are needed for a better understanding of the mechanisms underlying risk and resilience to disease between the sexes.

Besides, we decided to evaluate the effect of 16p11.2 CNVs on the body weight of our rat models. Our study demonstrates that the deletion of the genetic interval causes only a significant reduction in body weight of young mutant males on SD background. However, for the LE model, we decided to measure the body weight of our animals at three different moments of their development. We were able to verify that the 16p11.2 deletion also causes a decrease in the weight of the mutant males at three ages, but the female sex seems to start with a normal body weight and suffer a significant loss throughout its development. These results are in line with the characterization of 16p11.2 mouse models (Arbogast et al., 2016). However, in our rat model, the male rats carrying 16p11.2 duplication do not show a

phenotype. On the other hand, considering the results obtained in the phenotypic study of the mouse and rat model, as opposed to the symptoms diagnosed in patients, we could hypothesize that the effect of 16p11.2 BP4-BP5 CNVs on body weight may be a specificity of the human species.

The gene expression analysis of mRNA isolated from adult rat hippocampi in SD 16p11.2 Del/+ and Dup/+ models demonstrated that 23 pathways were commonly shared and mis-regulated in both Del/+ and Dup/+. In the 16p11.2 rat models, the pathway around the primary cilium was also found altered; as described previously in mice (Migliavacca et al., 2015). Other changes found in the Del/+ pathways were mirrored to some extent in the Dup/+ but the severity of the changes varied between the two conditions. In addition, several additional pathways were different confirming diverse effects induced by the Del/+ and the Dup/+, as found in the mouse models (Arbogast et al., 2016). One of the main alterations due to the dosage change of 16p11 was linked to the synapses, with the main central genes not linked to the regions: *Chd1, Gli1, Plg, Epha8, Disc1, Spag6l, Cfap52 or Sema3a,* except *Coro1a;* Six of which, *Chd1, Gli1, Plg, Disc1, Sema3a and Coro1a,* are reported to "abnormality of the nervous systems" in the Human Phenome Ontology. Interestingly, the most connected genes highlighted the MAPK3 and CUL3 subnetworks in the 16p11.2 models. MAPK3 is a gene from the 16p11.2 interval, thus subjected to change in dosage, and involved in the 16p11.2 syndromes (Pucilowska et al., 2015, 2018) whereas CUL3 is a target of KCTD13, another gene of the 16p11.2 region, controlling the RHOA pathway perturbed in 16p11.2 models (Lin et al., 2015; Martin Lorenzo et al., 2021). Both molecular pathways were also pointed in the proteomic studies, linked, respectively, with other proteins like SRC and ACLY.

Using the analysis of both sexes in the LE 16p11.2 Del model, we identified more DEGs in the male mutant hippocampi compared to females; DEGs that were also found in the SD genetic background. Of the 248 pathways altered in the Del/+ males and 100 identified in mutant females, 49 pathways were found deregulated in both sexes. More effects were observed in males than in females in various pathways, including the synapse, the Behavior, and mitochondria. By introducing the known gene/phenotype associations, described in the DisGeNet, GO and Kegg databases, we identified *Prrt2* as a candidate gene involved in "aggressively and stereotyped behaviour" that was found upregulated in the Dup/+ model and downregulated in Del/+. We also found 4 other genes from the 16p11.2 region involved in autistic behavior (defined by increased time in isolation) downregulated in Del and upregulated in Dup/+: *Taok2, Kctd13, Sez6l2, Mapk3*. The last two are also found in the proteomics analysis as differentially quantified peptides (Eps). Similarly, we found several genes linked to increasing time in isolation only upregulated in the Del/+ model as *Glp1r, Sema3a* or *Disc1*. Next, we wondered if we could identify any gene potentially responsible for the hypoactivity phenotype observed in the Dup model and we found 9 genes: *Coro1a*, Kctd13, Sez6l2, Spn, Aldoa, Mapk3*, Cdh1, Doc2a* and *Prrt2*. Finally, we identified 4 genes, namely *Eps*, *Prrt2, Mapk3,* and *Cdh1,* linked to memory and cognition deficits observed in the Del/+ model carriers and with mirroring regulatory sense in Dup/+ individuals.

Overall, the two new rat models for the 16p11.2 syndromes described here are promising in terms of behavior alteration with more social phenotypes and similar molecular pathways, MAPK2 and KCTD13/CUL3/RHOA affected in the rat brain compared to the mouse. We already described some craniofacial changes in the SD 16p11.2 models close to the human features (Qiu et al., 2019). Nevertheless, further explorations are needed to explore the variety of phenotypes related to humans as it is currently done in the mouse. More in-depth social behavior analysis (Rusu et al., 2022) provides a more detailed description of social impairment and a strong quantitative approach is crucial to pursue if we wish 1 day to test a drug that can mitigate the social impairment observed in the 16p11.2 syndromes.

Data availability statement

The datasets presented in this study can be found in online repositories. The GEO online repositories (Accession No. GSE225135).

Ethics statement

The animal study was reviewed and approved by Com'Eth N°17.

Author contributions

YH: conceptualization. SMa, MM, and WR: data curation. MM, VN, and WR: formal analysis. YH and LN: funding acquisition. SMa, HA, MP, LL, LN, and VN: investigation. J-PC, SMe, IA, M-CB, and YH: methodology. M-CB, IA, and YH: project administration. SMe, LT, GP, IA, and WR: resources. MM and WR: software. IA, J-PC, LN, M-CB, and YH: supervision. SMe, GP, IA, M-CB, LN, WR, and YH: validation. SMa, MM, WR, and YH: visualization. SMa, MM, and YH: writing—original draft preparation. SMa, MM, HA, MP, VN, WR, GP, LL, M-CB, SMe, LT, LN, J-PC, IA, and YH: writing—review and editing. All authors contributed to the article and approved the submitted version.

Funding

This work was supported by a grant from the Simons Foundation (SFARI 548888 to YH) and by the National Centre for Scientific Research (CNRS), the French National Institute of Health and Medical Research (INSERM), the University of Strasbourg (Unistra), French government funds through the "Agence Nationale de la Recherche" in the framework of the Investissements d'Avenir program by IdEx Unistra (ANR-10-IDEX-0002), a SFRI-STRAT'US project (ANR 20-SFRI-0012), "TEFOR" "Investissements d'Avenir" (ANRIIINSB-0014), EUR IMCBio (ANR-17-EURE-0023), and INBS PHENOMIN (ANR-10-IDEX-0002-02) and also provided to the GenomEast platform, a member of the "France Génomique" consortium for the RNASeq processing (ANR-10-INBS-0009), and to the Proteomic platform of IGBMC, that was supported by an ARC foundation grant (Orbitrap) and a Canceropole Grand Est foundation grant. The funders had no role in the study design, data collection and analysis, decision to publish, or preparation of the manuscript.

Acknowledgments

We would like to thank the members of the research group, the IGBMC laboratory and of the ICS for their help in brain morphometric analysis. We extend our thanks to the animal caretakers of the ICS who are in charge of the mice's well-being.

Conflict of interest

The authors declare that the research was conducted in the absence of any commercial or financial relationships that could be construed as a potential conflict of interest.

Publisher's note

Supplementary material

The Supplementary material for this article can be found online at: https://www.frontiersin.org/articles/10.3389/fnins.2023.1148683/full#supplementary-material

References

Angelakos, C. C., Watson, A. J., O'brien, W. T., Krainock, K. S., Nickl-Jockschat, T., and Abel, T. (2017). Hyperactivity and male-specific sleep deficits in the 16p11.2 deletion mouse model of autism. *Autism Res.* 10, 572–584. doi: 10.1002/aur.1707

Arbogast, T., Ouagazzal, A.-M., Chevalier, C., Kopanitsa, M., Afinowi, N., Migliavacca, E., et al. (2016). Reciprocal effects on neurocognitive and metabolic phenotypes in mouse models of 16p11.2 deletion and duplication syndromes. *PLoS Genet.* 12:e1005709. doi: 10.1371/journal.pgen.1005709

Ashburner, M., Ball, C. A., Blake, J. A., Botstein, D., Butler, H., Cherry, J. M., et al. (2000). Gene ontology: a tool for the unification of biology. The gene ontology consortium. *Nat. Genet.* 25, 25–29. doi: 10.1038/75556

Baron-Cohen, S., Knickmeyer, R. C., and Belmonte, M. K. (2005). Sex differences in the brain: implications for explaining autism. *Science* 310, 819–823. doi: 10.1126/science.1115455

Baron-Cohen, S., Lombardo, M. V., Auyeung, B., Ashwin, E., Chakrabarti, B., and Knickmeyer, R. (2011). Why are autism spectrum conditions more prevalent in males? *PLoS Biol.* 9:e1001081. doi: 10.1371/journal.pbio.1001081

Benedetti, A., Molent, C., Barcik, W., and Papaleo, F. (2022). Social behavior in 16p11.2 and 22q11.2 copy number variations: insights from mice and humans. *Genes Brain Behav.* 21:e12787. doi: 10.1111/gbb.12787

Chawner, S., Doherty, J. L., Anney, R. J. L., Antshel, K. M., Bearden, C. E., Bernier, R., et al. (2021). A genetics-first approach to dissecting the heterogeneity of Autism: phenotypic comparison of Autism risk copy number variants. *Am. J. Psychiatry* 178, 77–86. doi: 10.1176/appi.ajp.2020.20010015

Cooper, G. M., Coe, B. P., Girirajan, S., Rosenfeld, J. A., Vu, T. H., Baker, C., et al. (2011). A copy number variation morbidity map of developmental delay. *Nat. Genet.* 43, 838–846. doi: 10.1038/ng.909

D'Angelo, D., Lebon, S., Chen, Q., Martin-Brevet, S., Snyder, L. G., Hippolyte, L., et al. (2016). Defining the effect of the 16p11.2 duplication on cognition, behavior, and medical comorbidities. *JAMA Psychiat.* 73, 20–30. doi: 10.1001/jamapsychiatry.2015.2123

Dembélé, D., and Kastner, P. (2014). Fold change rank ordering statistics: a new method for detecting differentially expressed genes. *BMC Bioinformatics* 15:14. doi: 10.1186/1471-2105-15-14

Drakesmith, M., Parker, G. D., Smith, J., Linden, S. C., Rees, E., Williams, N., et al. (2019). Genetic risk for schizophrenia and developmental delay is associated with shape and microstructure of midline white-matter structures. *Transl. Psychiatry* 9:102. doi: 10.1038/s41398-019-0440-7

Duchon, A., Del Mar Muñiz Moreno, M., Lorenzo, S. M., De Souza, M. P. S., Chevalier, C., Nalesso, V., et al. (2021). Multi-influential genetic interactions alter behaviour and cognition through six main biological cascades in down syndrome mouse models. *Hum. Mol. Genet.* 30, 771–788. doi: 10.1093/hmg/ddab012

Esling, P., Lejzerowicz, F., and Pawlowski, J. (2015). Accurate multiplexing and filtering for high-throughput amplicon-sequencing. *Nucleic Acids Res.* 43, 2513–2524. doi: 10.1093/nar/gkv107

Fernandez, B. A., Roberts, W., Chung, B., Weksberg, R., Meyn, S., Szatmari, P., et al. (2010). Phenotypic spectrum associated with de novo and inherited deletions and duplications at 16p11.2 in individuals ascertained for diagnosis of autism spectrum disorder. *J. Med. Genet.* 47, 195–203. doi: 10.1136/jmg.2009.069369

Hastings, P. J., Lupski, J. R., Rosenberg, S. M., and Ira, G. (2009). Mechanisms of change in gene copy number. *Nat. Rev. Genet.* 10, 551–564. doi: 10.1038/nrg2593

Horev, G., Ellegood, J., Lerch, J. P., Son, Y. E., Muthuswamy, L., Vogel, H., et al. (2011). Dosage-dependent phenotypes in models of 16p11.2 lesions found in autism. *Proc. Natl. Acad. Sci. U. S. A.* 108, 17076–17081. doi: 10.1073/pnas.1114042108

Jacquemont, S., Reymond, A., Zufferey, F., Harewood, L., Walters, R. G., Kutalik, Z., et al. (2011). Mirror extreme BMI phenotypes associated with gene dosage at the chromosome 16p11.2 locus. *Nature* 478, 97–102. doi: 10.1038/nature10406

Karp, N. A., Meehan, T. F., Morgan, H., Mason, J. C., Blake, A., Kurbatova, N., et al. (2015). Applying the ARRIVE guidelines to an in vivo database. *PLoS Biol.* 13:e1002151. doi: 10.1371/journal.pbio.1002151

Kilkenny, C., Browne, W. J., Cuthill, I. C., Emerson, M., and Altman, D. G. (2010). Improving bioscience research reporting: the ARRIVE guidelines for reporting animal research. *PLoS Biol.* 8:e1000412. doi: 10.1371/journal.pbio.1000412

Lin, G. N., Corominas, R., Lemmens, I., Yang, X., Tavernier, J., Hill, D. E., et al. (2015). Spatiotemporal 16p11.2 protein network implicates cortical late mid-fetal brain development and KCTD13-Cul3-RhoA pathway in psychiatric diseases. *Neuron* 85, 742–754. doi: 10.1016/j.neuron.2015.01.010

Lindner, L., Cayrou, P., Jacquot, S., Birling, M. C., Herault, Y., and Pavlovic, G. (2021). Reliable and robust droplet digital PCR (ddPCR) and RT-ddPCR protocols for mouse studies. *Methods* 191, 95–106. doi: 10.1016/j.ymeth.2020.07.004

Lorbach, M., Kyriakou, E. I., Poppe, R., Van Dam, E. A., Noldus, L. P. J. J., and Veltkamp, R. C. (2018). Learning to recognize rat social behavior: novel dataset and cross-dataset application. *J. Neurosci. Methods* 300, 166–172. doi: 10.1016/j.jneumeth.2017.05.006

Love, M. I., Huber, W., and Anders, S. (2014). Moderated estimation of fold change and dispersion for RNA-seq data with DESeq2. *Genome Biol.* 15:550. doi: 10.1186/s13059-014-0550-8

Luo, W., Friedman, M. S., Shedden, K., Hankenson, K. D., and Woolf, P. J. (2009). GAGE: generally applicable gene set enrichment for pathway analysis. *BMC Bioinformatics* 10:161. doi: 10.1186/1471-2105-10-161

Marshall, C. R., Noor, A., Vincent, J. B., Lionel, A. C., Feuk, L., Skaug, J., et al. (2008). Structural variation of chromosomes in autism spectrum disorder. *Am. J. Hum. Genet.* 82, 477–488. doi: 10.1016/j.ajhg.2007.12.009

Martin Lorenzo, S., Nalesso, V., Chevalier, C., Birling, M. C., and Herault, Y. (2021). Targeting the RHOA pathway improves learning and memory in adult Kctd13 and 16p11.2 deletion mouse models. *Mol. Autism.* 12:1. doi: 10.1186/s13229-020-00405-7

Mccarthy, S. E., Makarov, V., Kirov, G., Addington, A. M., Mcclellan, J., Yoon, S., et al. (2009). Microduplications of 16p11.2 are associated with schizophrenia. *Nat. Genet.* 41, 1223–1227. doi: 10.1038/ng.474

Menoret, S., De Cian, A., Tesson, L., Remy, S., Usal, C., Boule, J. B., et al. (2015). Homology-directed repair in rodent zygotes using Cas9 and TALEN engineered proteins. *Sci. Rep.* 5:14410. doi: 10.1038/srep14410

Migliavacca, E., Golzio, C., Maennik, K., Blumenthal, I., Oh, E. C., Harewood, L., et al. (2015). A potential contributory role for ciliary dysfunction in the 16p11.2 600 kb BP4-BP5 pathology. *Am. J. Hum. Genet.* 96, 784–796. doi: 10.1016/j.ajhg.2015.04.002

Motulsky, H. J., and Brown, R. E. (2006). Detecting outliers when fitting data with nonlinear regression - a new method based on robust nonlinear regression and the false discovery rate. *BMC Bioinformatics* 7:123.

Nassar, L. R., Barber, G. P., Benet-Pagès, A., Casper, J., Clawson, H., Diekhans, M., et al. (2023). The UCSC Genome Browser database: 2023 update. *Nucleic. Acids Res.* 51, D1188–D1195.

Niarchou, M., Chawner, S. J. R. A., Doherty, J. L., Maillard, A. M., Jacquemont, S., Chung, W. K., et al. (2019). Psychiatric disorders in children with 16p11.2 deletion and duplication. *Transl. Psychiatry* 9. doi: 10.1038/s41398-018-0339-8

Polyak, A., Rosenfeld, J. A., and Girirajan, S. (2015). An assessment of sex bias in neurodevelopmental disorders. *Genome Med.* 7:94. doi: 10.1186/s13073-015-0216-5

Portmann, T., Yang, M., Mao, R., Panagiotakos, G., Ellegood, J., Dolen, G., et al. (2014). Behavioral abnormalities and circuit defects in the basal ganglia of a mouse model of 16p11.2 deletion syndrome. *Cell Rep.* 7, 1077–1092. doi: 10.1016/j.celrep.2014.03.036

Pucilowska, J., Vithayathil, J., Pagani, M., Kelly, C., Karlo, J. C., Robol, C., et al. (2018). Pharmacological inhibition of ERK signaling rescues pathophysiology and behavioral phenotype associated with 16p11.2 chromosomal deletion in mice. *J. Neurosci.* 38, 6640–6652. doi: 10.1523/JNEUROSCI.0515-17.2018

Pucilowska, J., Vithayathil, J., Tavares, E. J., Kelly, C., Karlo, J. C., and Landreth, G. E. (2015). The 16p11.2 deletion mouse model of Autism exhibits altered cortical progenitor proliferation and brain Cytoarchitecture linked to the ERK MAPK pathway. *J. Neurosci.* 35, 3190–3200. doi: 10.1523/JNEUROSCI.4864-13.2015

Qiu, Y., Arbogast, T., Lorenzo, S. M., Li, H., Tang, S. C., Richardson, E., et al. (2019). Oligogenic effects of 16p11.2 copy-number variation on craniofacial development. *Cell Rep.* 28:3320. doi: 10.1016/j.celrep.2019.08.071

Redaelli, S., Maitz, S., Crosti, F., Sala, E., Villa, N., Spaccini, L., et al. (2019). Refining the phenotype of recurrent rearrangements of chromosome 16. *Int. J. Mol. Sci.* 20:1095. doi: 10.3390/ijms20051095

Rees, E., Walters, J. T. R., Georgieva, L., Isles, A. R., Chambert, K. D., Richards, A. L., et al. (2014). Analysis of copy number variations at 15 schizophrenia-associated loci. *Br. J. Psychiatry* 204, 108–114. doi: 10.1192/bjp.bp.113.131052

Reinthaler, E. M., Lal, D., Lebon, S., Hildebrand, M. S., Dahl, H. H., Regan, B. M., et al. (2014). 16p11.2 600 kb duplications confer risk for typical and atypical Rolandic epilepsy. *Hum. Mol. Genet.* 23, 6069–6080. doi: 10.1093/hmg/ddu306

Rusu, A., Chevalier, C., De Chaumont, F., Nalesso, V., Brault, V., Hérault, Y., et al. (2022). A 16p11.2 deletion mouse model displays quantitatively and qualitatively different behaviours in sociability and social novelty over short- and long-term observation. bioRxiv [Preprint].

Sanders, S. J., Ercan-Sencicek, A. G., Hus, V., Luo, R., Murtha, M. T., Moreno-De-Luca, D., et al. (2011). Multiple recurrent de novo CNVs, including duplications of the 7q11.23 Williams syndrome region, are strongly associated with autism. *Neuron* 70, 863–885. doi: 10.1016/j.neuron.2011.05.002

Shinawi, M., Liu, P., Kang, S.-H. L., Shen, J., Belmont, J. W., Scott, D. A., et al. (2010). Recurrent reciprocal 16p11.2 rearrangements associated with global developmental delay, behavioural problems, dysmorphism, epilepsy, and abnormal head size. *J. Med. Genet.* 47, 332–341. doi: 10.1136/jmg.2009.073015

Steinberg, S., De Jong, S., Mattheisen, M., Costas, J., Demontis, D., Jamain, S., et al. (2014). Common variant at 16p11.2 conferring risk of psychosis. *Mol. Psychiatry* 19, 108–114. doi: 10.1038/mp.2012.157

Steinman, K. J., Spence, S. J., Ramocki, M. B., Proud, M. B., Kessler, S. K., Marco, E. J., et al. (2016). 16p11.2 deletion and duplication: characterizing neurologic phenotypes in a large clinically ascertained cohort. *Am. J. Med. Genet. A* 170, 2943–2955. doi: 10.1002/ajmg.a.37820

Szklarczyk, D., Morris, J. H., Cook, H., Kuhn, M., Wyder, S., Simonovic, M., et al. (2017). The STRING database in 2017: quality-controlled protein-protein association networks, made broadly accessible. *Nucleic Acids Res.* 45, D362–D368. doi: 10.1093/nar/gkw937

Tang, H., Zhong, F., Liu, W., He, F., and Xie, H. (2015). PathPPI: an integrated dataset of human pathways and protein-protein interactions. *Sci. China Life Sci.* 58, 579–589. doi: 10.1007/s11427-014-4766-3

Torres, F., Barbosa, M., and Maciel, P. (2016). Recurrent copy number variations as risk factors for neurodevelopmental disorders: critical overview and analysis of clinical implications. *J. Med. Genet.* 53, 73–90. doi: 10.1136/jmedgenet-2015-103366

Walters, R. G., Jacquemont, S., Valsesia, A., De Smith, A. J., Martinet, D., Andersson, J., et al. (2010). A new highly penetrant form of obesity due to deletions on chromosome 16p11.2. *Nature* 463, 671–675. doi: 10.1038/nature08727

Weiss, L. A., Shen, Y., Korn, J. M., Arking, D. E., Miller, D. T., Fossdal, R., et al. (2008). Association between microdeletion and microduplication at 16p11.2 and autism. *N. Engl. J. Med.* 358, 667–675. doi: 10.1056/NEJMoa075974

Zufferey, F., Sherr, E. H., Beckmann, N. D., Hanson, E., Maillard, A. M., Hippolyte, L., et al. (2012). A 600 kb deletion syndrome at 16p11.2 leads to energy imbalance and neuropsychiatric disorders. *J. Med. Genet.* 49, 660–668. doi: 10.1136/jmedgenet-2012-101203

frontiers | Frontiers in Neuroscience

TYPE Original Research
PUBLISHED 03 August 2023
DOI 10.3389/fnins.2023.1106573

OPEN ACCESS

EDITED BY
Flavia Venetucci Gouveia,
University of Toronto, Canada

REVIEWED BY
Christopher Scott Ward,
Baylor College of Medicine, United States
Andersen Chang,
Baylor College of Medicine, United States

*CORRESPONDENCE
Brandon L. Pearson
✉ blp2125@cumc.columbia.edu

RECEIVED 23 November 2022
ACCEPTED 17 July 2023
PUBLISHED 03 August 2023

CITATION
Baker BH, Zhang S, Simon JM, McLarnan SM, Chung WK and Pearson BL (2023) Environmental carcinogens disproportionally mutate genes implicated in neurodevelopmental disorders. *Front. Neurosci.* 17:1106573. doi: 10.3389/fnins.2023.1106573

Environmental carcinogens disproportionally mutate genes implicated in neurodevelopmental disorders

Brennan H. Baker[1], Shaoyi Zhang[2], Jeremy M. Simon[3], Sarah M. McLarnan[1], Wendy K. Chung[4] and Brandon L. Pearson[1]*

[1]Department of Environmental Health Sciences, Mailman School of Public Health, Columbia University, New York, NY, United States, [2]Master of Public Health Program, Department of Epidemiology, Mailman School of Public Health, Columbia University, New York, NY, United States, [3]Department of Genetics and Neuroscience Center, University of North Carolina at Chapel Hill, Chapel Hill, NC, United States, [4]Department of Pediatrics and Medicine, Columbia University Irving Medical Center, New York, NY, United States

Introduction: *De novo* mutations contribute to a large proportion of sporadic psychiatric and developmental disorders, yet the potential role of environmental carcinogens as drivers of causal *de novo* mutations in neurodevelopmental disorders is poorly studied.

Methods: To explore environmental mutation vulnerability of disease-associated gene sets, we analyzed publicly available whole genome sequencing datasets of mutations in human induced pluripotent stem cell clonal lines exposed to 12 classes of environmental carcinogens, and human lung cancers from individuals living in highly polluted regions. We compared observed rates of exposure-induced mutations in disease-related gene sets with the expected rates of mutations based on control genes randomly sampled from the genome using exact binomial tests. To explore the role of sequence characteristics in mutation vulnerability, we modeled the effects of sequence length, gene expression, and percent GC content on mutation rates of entire genes and gene coding sequences using multivariate Quasi-Poisson regressions.

Results: We demonstrate that several mutagens, including radiation and polycyclic aromatic hydrocarbons, disproportionately mutate genes related to neurodevelopmental disorders including autism spectrum disorders, schizophrenia, and attention deficit hyperactivity disorder. Other disease genes including amyotrophic lateral sclerosis, Alzheimer's disease, congenital heart disease, orofacial clefts, and coronary artery disease were generally not mutated more than expected. Longer sequence length was more strongly associated with elevated mutations in entire genes compared with mutations in coding sequences. Increased expression was associated with decreased coding sequence mutation rate, but not with the mutability of entire genes. Increased GC content was associated with increased coding sequence mutation rates but decreased mutation rates in entire genes.

Discussion: Our findings support the possibility that neurodevelopmental disorder genetic etiology is partially driven by a contribution of environment-induced germ line and somatic mutations.

KEYWORDS

somatic mutation, mutagenesis, *de novo* mutation, carcinogen, neurodevelopmental disorders, autism

Introduction

While cancer epidemiologic studies have a long history of integrating genetic and environmental factors into disease causation (Shields and Harris, 2000), researchers, with small exception (Kinney et al., 2010; Pugsley et al., 2021), have not readily implicated environmentally-induced mutations as etiological drivers of neurodevelopmental disorders (NDD) and other diseases. *De novo* mutations contribute to a large proportion of sporadic cases of ASD, schizophrenia, and intellectual disability (De Ligt et al., 2012; Xu et al., 2012; Fromer et al., 2014; Iossifov et al., 2014), yet the underlying mutational processes have not been interrogated, or have been attributed to intrinsic mutational processes (e.g., random replication error) rather than environmental carcinogens. Similarly, environmental exposures may be responsible for a large proportion of NDD (Landrigan, 2010; Bellinger, 2012; Rauh and Margolis, 2016). While potential underlying molecular mechanisms such as epigenetics have been explored in great detail (Perera and Herbstman, 2011; Tran and Miyake, 2017; Emberti Gialloreti et al., 2019), environmentally induced mutation remains a strong yet generally untested candidate mechanism that may link environmental exposures to neurodevelopment (Kinney et al., 2010; Pugsley et al., 2021). For instance, PAHs—a class of chemicals found in tobacco smoke and air pollution—form metabolites in the body that bind with DNA and promote mutation (Whyatt et al., 1998). Consequently, PAHs are well known causes of cancer (Boffetta et al., 1997; Kriek et al., 1998; Kim et al., 2013). Epidemiologic studies have linked prenatal PAH exposure to cognitive developmental delays, reduced intelligence, and ASD (Perera et al., 2006; Edwards et al., 2010; von Ehrenstein et al., 2014; Jedrychowski et al., 2015). However, no studies have examined whether mutations in NDD genes induced by PAHs and other environmental exposures contribute to these epidemiologic associations despite evidence that NDD genes are generally longer (King et al., 2013; Sugino et al., 2014; Gabel et al., 2015) and show considerable overlap with cancer driver genes (Crawley et al., 2016; Qi et al., 2016). To test the hypothesis that NDD genes are more susceptible to mutagens than non-NDD genes, we analyzed a whole genome sequencing (WGS) dataset containing nearly 200,000 single nucleotide substitution mutations in human induced pluripotent stem cell (iPSC) clonal lines exposed to 12 classes of environmental carcinogens (Kucab et al., 2019). We assessed the susceptibility to environmental mutation of genes and disease-associated gene sets by (1) evaluating gene ontology for top mutated genes; (2) developing an online tool for assessing the propensity of 12 mutagen classes to cause mutations in gene sets associated with specific human diseases; (3) investigating gene length, expression, and GC content as potential drivers of elevated mutability using Quasi-Poisson models; and (4) testing whether specific disease-related genes are enriched for bulky DNA adduct repair.

Materials and methods

Environmental mutation vulnerability of disease genes

Analyses were performed using R (Team, 2018). We analyzed the substitution mutations from 324 iPSC subclones dosed with 79 environmental carcinogens (Kucab et al., 2019). From whole-genome-sequencing data at ~ 30-fold depth, Kucab et al. (2019) called mutations in subclones subtracting on the primary iPSC parental clone. We compared the observed rates of exposure-induced mutations in disease-related gene sets with the expected rates of mutations based on control genes randomly sampled from the genome. Disease gene sets contained 91 ASD (Abrahams et al., 2013), 104 schizophrenia (Wang et al., 2019), 25 ADHD (Demontis et al., 2019), 33 Alzheimer's (Giri et al., 2016), 18 ALS (Association T.A., 2019), 81 type 2 diabetes (Mahajan et al., 2014), 80 coronary artery disease (Nikpay et al., 2015), 96 obesity (Locke et al., 2015), 253 congenital heart disease (Jin et al., 2017), and 31 orofacial cleft genes (Beaty et al., 2016; Supplementary Table S1). Gene sets were either curated (i.e., published in review articles or curated by scientific organizations) or based on genes with significant disease-associated loci from genome wide association studies (GWAS). We included adult onset, congenital, heritable, and life-style-associated diseases to determine if our hypothesized NDD enrichment was specific. Since our analyses were restricted to just a handful of disease gene sets and results could depend on the methods of gene set curation, we created an online tool where custom gene lists can be queried using the algorithm we generated.[1] Using this tool, users may input more up-to-date gene lists. For example, our ASD list included all genes labeled as high confidence by the Simons Foundation Autism Research Initiative (SFARI) at the time of the analysis, but SFARI is constantly updating this gene list as our understanding of the genetic basis of ASD evolves.

To determine expected mutation rates, we randomly sampled 1,000 sets of 300 genes from the human genome and used the iPSC mutation dataset (Kucab et al., 2019) to calculate average rates of mutation per-gene-per-treated iPSC subclone within each exposure class. Our unit of analysis was mutations per gene, so it was not necessary to match the number of randomly sampled genes with the number of genes in each disease set. To check this assumption, we plotted the relationship between the size of randomly sampled gene sets, varying from 10 to 300 genes, with the number of mutations per subclone treated with the radiation class of chemicals. To characterize the degree to which certain disease gene sets were mutated more than expected, we compared these hypothesized expected mutation rates to the mutation rates for each disease gene set within each environmental exposure in clonal iPSC cultures (Kucab et al., 2019) using two-sided exact binomial tests. For a given chemical exposure and disease gene set, the exact binomial test null hypothesis was that the disease gene set had the same per gene mutation rate as the per gene mutation rate of the 1,000 sets of 300 genes described above. Rejection of the null hypothesis indicated that the disease gene set was mutated more or less than the mutation rate of randomly sampled genes. Single genes were allowed to contribute multiple mutations to the mutation rate numerators. Significance was assessed at alpha level 0.05 with table wide Bonferroni corrections. This analysis was repeated for mutations in entire genes as well as coding sequence (CDS) mutations determined using the Ensembl variant effect predictor (McLaren et al., 2016). Although entire genes contain introns and other non-coding sequence, a large proportion of GWAS signals map to non-coding regions (Zhang and Lupski, 2015), so variants in these loci may still contribute to disease.

For mutations in entire genes in PAH-treated iPSCs, we conducted a sensitivity analysis by calculating p-values from empirical null distributions rather than from exact binomial tests. Monte Carlo null distributions for each disease gene set were obtained by randomly sampling 1,000 sets of genes from the human genome equal to the number of genes in a given disease gene set. The total number of

1 http://environmentalmutation.com

mutations in each randomly sampled gene set was determined. Two-tailed p-values were calculated as the proportion of randomly sampled gene sets mutated more or less than the comparison disease gene set, whichever was smallest, multiplied by two.

To externally-validate this approach, we repeated the gene mutation analysis in an independent dataset of human WGS data from 14 lung cancers from individuals living in highly polluted regions (Yu et al., 2015). Because PAHs are a major component of pollution, we hypothesized that mutational patterns would be similar between these samples and the PAH-treated iPSCs.

We conducted a sensitivity analysis to explore the role of gene length in environmental mutagen vulnerability. In this analysis, a selected NDD gene list was created by combining all ASD, ADHD, and schizophrenia genes from the lists described above. We then divided the list into four separate lists based on gene length quartiles, and repeated the above analysis for mutations in entire gene bodies.

In an additional sensitivity analysis, we explored the mutational susceptibility of cancer driver genes, and genes with overlap between cancer and NDD. We utilized a list of 233 high confidence cancer genes with confidence scores ≥ 1.5 based on a scoring system developed by (Bailey et al., 2018), and a list of 14 genes that overlap between this cancer gene list and the selected NDD gene list described above.

Gene ontology

We performed gene ontology (GO) analysis on all genes which contained coding sequence (CDS) variants in PAH-treated iPSCs. GO analysis was performed using FUMA with ensembl version 92, protein coding genes set as the background, and a Bonferroni correction (Watanabe et al., 2017). In an additional sensitivity analysis, we included all genes with CDS mutations in iPSCs exposed to all environmental mutagens rather than just PAH-treated iPSCs.

Sequence characteristics and mutation vulnerability

Autism spectrum disorder-implicated NDD genes tend to be longer than other genes (King et al., 2013; Zylka et al., 2015). To visually examine if vulnerability of neurodevelopmental genes or CDS to mutagens is attributable to gene length, we plotted the distributions of entire gene and CDS lengths for our disease gene sets, along with the distributions of lengths for entire genes and CDS mutated entirely at random. Random mutations were modeled by randomly sampling (i.e., mutating) 100,000 nucleotides from all genes or all CDS in the human genome, so the probability of a sequence being mutated was entirely governed by its length.

To further explore associations of length with mutability, we modeled the effects of sequence length, expression, and percent GC content on mutation rate using multivariate Quasi-Poisson regressions, with separate models for mutations in CDS and entire genes. Gene and CDS start and stop positions were obtained from GENCODE Release 38[2] and used in conjunction with the "BSgenome.Hsapiens.UCSC.hg38" R package to calculate genomic sequence lengths (end minus start position) and GC content (proportion of sequence positions with either a G or C nucleotide). When modeling associations of sequence properties with CDS mutations, CDS lengths and GC content were computed per gene: all CDS segments within a single gene were summed as the total coding sequence length, and CDS GC content was calculated per gene rather than per individual CDS segment. Gene expression data were reads per kilobase of transcript per million mapped reads (RPKM) obtained from RNA-seq of iPSCs generated using the Sendai virus method (Churko et al., 2017), the same method used to create the iPSCs used by Kucab et al. (2019). After excluding genes with missing length, expression, or GC content data, Quasi-Poisson models included 75,756 gene and 1,852 CDS mutations. Coefficients from these models were multiplied by the interquartile range (IQR) for each variable and then exponentiated into rate ratios per IQR increase.

Local sequence and mutation vulnerability

To explore the role of local sequence context on mutability, we aligned 7-mers centered on each gene or CDS mutation identified by Kucab et al. (2019), along with 50,000 7-mers randomly sampled from the human genome. We performed this analysis for all mutations, and stratified by chemical exposure class. We also examined the role of local sequence context by generating COSMIC signatures (Tate et al., 2019) for *de novo* mutations in individuals with neuropsychiatric diseases, including 42,607 ASD cases (Feliciano et al., 2018; Zhou et al., 2021), 617 schizophrenia cases (Fromer et al., 2014), and 145 individuals with severe intellectual disability (De Ligt et al., 2012; Rauch et al., 2012).

Polycyclic aromatic hydrocarbon adduct repair associated mutation

To determine if NDD genes are linked to PAH adduct repair, we analyzed an existing genome-wide PAH adduct repair assay dataset (Li et al., 2017) to see if adducts are preferentially located in specific disease-related gene sets. Genome-wide PAH adduct repair data come from translesion excision repair-sequencing (tXR-seq) of GM12878 cells, which were grown to ~ 80% confluence before treatment with 2 μM benzo[a]pyrene diol epoxide-deoxyguanosine for 1 h at 37°C in a 5% CO_2 humidified chamber. tXR-seq captures all DNA damage, regardless of whether or not it is repaired (Li et al., 2017). We computed the average DNA damage enrichment across each gene or CDS in all 10 disease-related gene sets by inputting bigWig files from Li et al. (2017) into the deepTools2 'computeMatrix' function (Ramírez et al., 2016). By default, the 'computeMatrix' function scales input sequences to the same length. Output enrichment values from the 'computeMatrix' function are based on the units of the input bigWig files, which, in this case, were tXR-seq counts normalized for total sequencing depth on each chromosome (Li et al., 2017). We used one-way ANOVA to compare levels of DNA damage in genes, which were normally distributed, between disease gene sets, and performed pairwise contrasts with a false discovery rate correction. Kruskal–Wallis and Dunn's Test were employed for CDS DNA damage data, which were not normally distributed.

2 https://www.gencodegenes.org/human/

Results

Environmental mutation vulnerability of disease genes

There were 769 unique genes across all ten disease gene sets, and overlap between sets was minimal (Figure 1A). Among the 183,133 substitution mutations identified by Kucab et al. (2019), 92,204 occurred in known genes. Across all chemical treatments, all disease gene set genes had a combined 7,587 total mutations. Per-nucleotide mutation rates for each chemical by disease gene set combination ranged from 0 to 5.77×10^{-7}. We plotted the distributions of entire gene and CDS lengths for our disease gene sets, along with the distributions of lengths for the 1,000 sets of 300 randomly sampled gene and CDS sequences (Figures 1B,C). NDD and metabolic disease gene sets such as ASD, schizophrenia, ADHD, obesity, and type-2 diabetes contained the longest genes, while ALS genes and randomly sampled genes were the shortest (Figure 1B). On the other hand, average CDS lengths for most disease gene sets were comparable (Figure 1C).

We compared per gene mutation rates in our disease gene sets with genes randomly sampled from the human genome (1,000 sets of 300 genes). Mutations per subclone increased linearly with the number of randomly sampled genes while the number of mutations per gene per subclone remained flat (Figure 2), confirming that it was not necessary to match the number of randomly sampled genes with the number of genes in each disease set.

The most mutagenic exposures were radiation and PAHs, which induced an average of 0.066 and 0.058 substitution mutations per-gene-per-treated iPSC subclone, respectively across our 10 disease related gene sets (Figure 3A; Supplementary Table S2). ASD, ADHD, schizophrenia, obesity, and type-2 diabetes genes were mutated significantly more than expected by almost every chemical class. Congenital heart disease, oral cleft, and coronary artery disease were rarely mutated more than expected; while Alzheimer's disease genes were never mutated more than expected (Figure 3A; Supplementary Table S3). There was some evidence for ALS genes being mutated less than the expected per-gene mutation rate by aromatic amines and nitro-PAHs, although these differences were not statistically significant after Bonferroni correction. Results were similar in a sensitivity analysis calculating *p*-values from Monte Carlo empirical null distributions for PAH-treatment mutations (Supplementary Figure S1). As in the main analysis, ASD, ADHD, schizophrenia, obesity, and type-2 diabetes genes were mutated significantly more than expected.

Among the 2,061 identified coding sequence variants, these overarching patterns were not observed (Figure 3B). While there was evidence for exposure causing more coding sequence mutations than

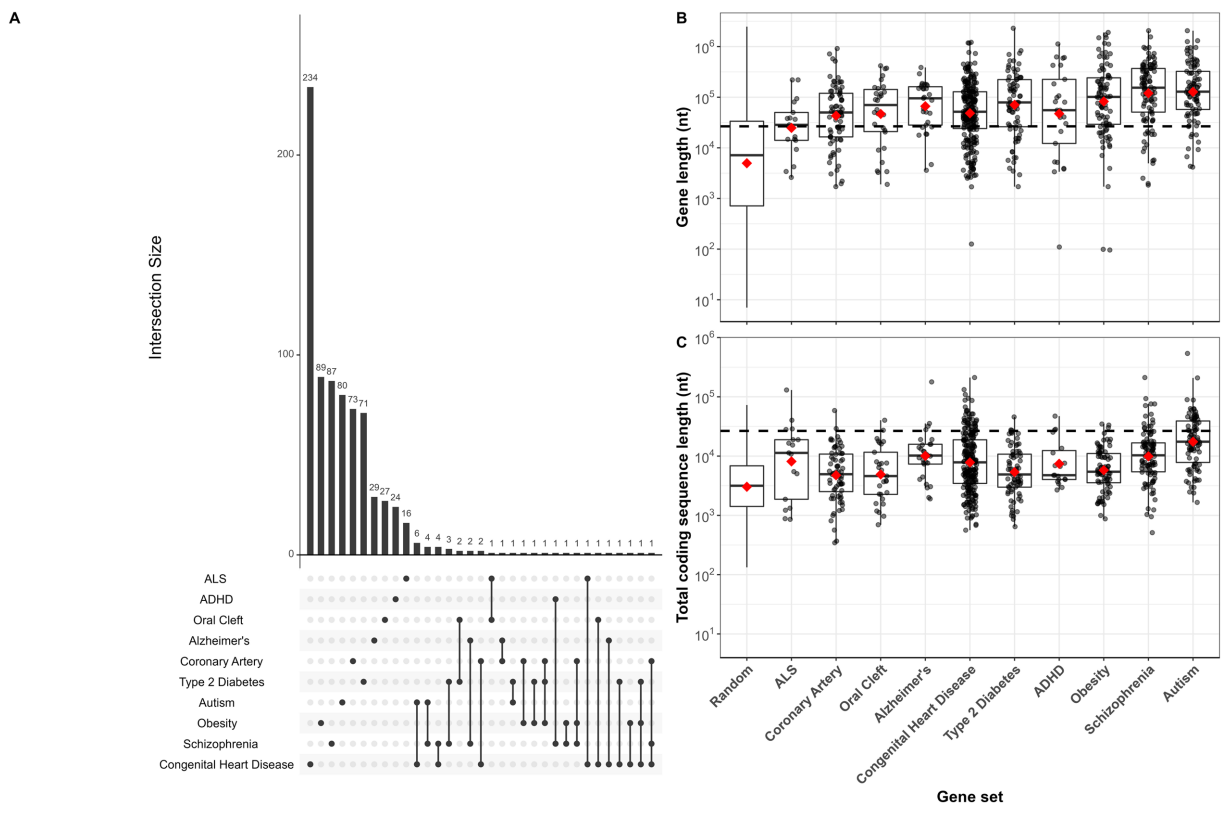

FIGURE 1
(A) Gene set intersection plot. Horizontal bars depict gene set sizes. Gene sets included in each intersection are indicated by a single or connected dot(s), and sizes of the intersections are indicated by vertical bars. For single, unconnected dots, vertical bars indicate the number of genes exclusive to that set. For example, among 253 Congenital Heart Disease genes, 6 overlapped with Autism genes, while 234 had no overlap with other gene sets. Intersections with zero overlap not shown. **(B,C)** Sequence length boxplots with median and 1.5 interquartile range (IQR) whiskers shown for each disease implicated gene set for entire genes **(B)** and coding sequence **(C)**. Red diamonds indicate mean sequence length for each set indicated on x-axis, and dashed black line across entire plot indicates mean gene length of randomly mutated genes (modeled by randomly sampling (i.e., mutating) 100,000 nucleotides from all genes or all CDS in the human genome). Gene and CDS boxplots also shown for all 300,000 randomly sampled sequences (1,000 sets of 300 genes or CDS).

expected for 9 specific exposure/disease combinations, none of them remained statistically significant following Bonferroni correction (Figure 3B).

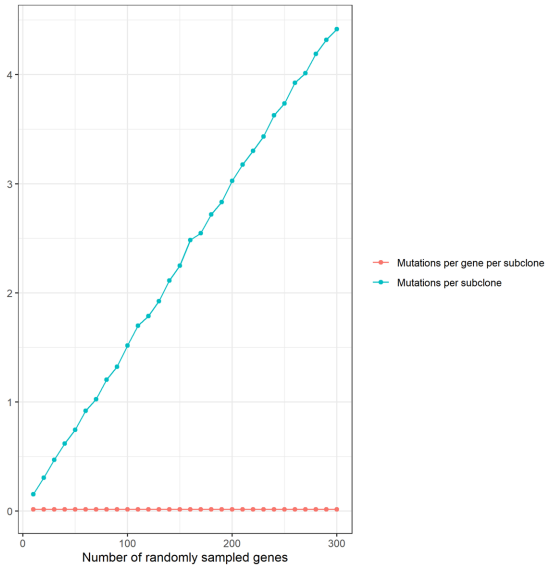

FIGURE 2
Thousand sets of genes were randomly sampled for each gene set size ranging from 10 to 300 in intervals of 10. For each random gene set size, the number of mutations in subclones treated with the radiation class of chemicals was determined. Mean mutations per subclone and mutations per gene per subclone were plotted against the random set size.

We repeated this analysis in an independent dataset of human WGS data from 14 lung cancers from individuals living in highly polluted regions. In these samples, the greatest increases in observed over expected gene mutations were in genes related to ASD, schizophrenia, and obesity (Figure 3C). However, contrasting with the mutational patterns in PAH-exposed iPSCs, ADHD genes were not mutated more than expected, and genes associated with congenital heart defects were mutated more than expected even after Bonferroni correction (Figure 3B).

Average gene lengths of disease gene sets were consistent with patterns of mutability. For instance, ASD, schizophrenia, obesity, and ADHD genes, which were on average longer than other disease-related genes, had the greatest increases in observed versus expected chemical-induced mutations, while ALS, coronary artery disease, oral cleft, and Alzheimer's disease genes, which are much shorter in length, were not mutated more than expected (*cf.* Figures 1B, 3A). Genes mutated entirely at random (modeled by randomly sampling nucleotides from the genome) were on average longer than all disease-associated genes, further indicating that gene length was a strong driver of mutability (dashed horizontal line, Figure 1B).

A sensitivity analysis stratifying NDD genes by sequence length quartiles demonstrated a strong role of sequence length in NDD gene mutability (Supplementary Figure S2). Genes in the top quartile had an average length of 678,000 nucleotides and were mutated more than the expected per-gene mutation rate by all chemical exposure classes. By contrast, the bottom quartile genes averaged 20,000 nucleotides in length and were mutated less than the expected mutation rate by several exposures (Supplementary Figure S2).

Another sensitivity analysis explored the mutability of cancer driver genes, and genes overlapping between cancer and

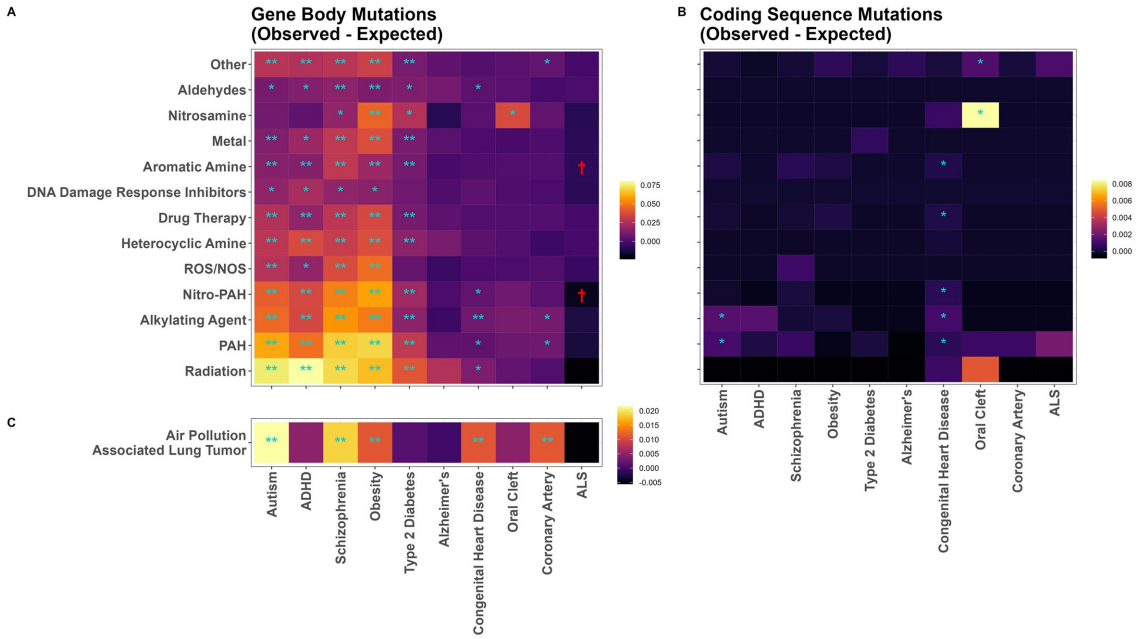

FIGURE 3
Mutation vulnerability of disease associated genes to various carcinogens. Heatmaps of observed minus expected mutations in disease gene sets for **(A)** mutations in gene body sequence following chemical treatment in iPSC, **(B)** mutations in coding sequences following chemical treatment in iPSC, and **(C)** mutations in 14 human lung cancers from individuals living in highly polluted regions. Significant levels from exact binomial tests. Higher mutation rates: *$p < 0.05$; **Bonferroni-adjusted $p < 0.05$. Lower mutation rates: †$p < 0.05$.

neurodevelopmental processes (Supplementary Figure S3). NDD genes were mutated at higher-than-expected rates by all chemical classes except for nitrosamines, while cancer driver genes were never mutated more than expected. Furthermore, genes overlapping between the NDD and cancer lists were never mutated more than expected.

Gene ontology

Gene ontology analysis on the 692 genes which contained coding sequence (CDS) variants in PAH-treated iPSCs revealed enriched gene ontologies closely related to neurodevelopment: neuron projection, neuron part, and calcium ion binding (Supplementary Table S4). Furthermore, the enriched plasma membrane term may be related to metabolic diseases including obesity and type 2 diabetes (Cheng et al., 2018). Similar results were obtained when the analysis included all 2,061 CDS mutations in iPSCs exposed to all environmental mutagens rather than just PAH-treated iPSCs. For instance, the top three gene ontology terms were neuron projection guidance, sensory organ morphogenesis, and cell morphogenesis involved in neuron differentiation (Supplementary Table S5), supporting our hypothesis that NDD genes are particularly vulnerable to environmental mutagens.

In addition to the vulnerability of NDD genes to environmental mutagens uncovered here, genes associated with obesity and type 2 diabetes were mutated by chemical treatment more than expected. We therefore hypothesized that these genes might be linked to neurodevelopmental processes. To explore this possibility, we performed GO analysis on our list of obesity- and type 2 diabetes-associated genes, but found no evidence for enrichment of NDD processes (Supplementary Table S6).

Sequence characteristics and mutation vulnerability

Quasi-Poisson regressions further supported a stronger role of sequence length in gene but not CDS mutation number. Controlling for expression and GC content, each interquartile range increase (IQR) in gene length was associated with a 1.104-fold increase in gene mutation rate (rate ratio (RR) = 1.104, 95% CI [1.102, 1.105]; Figure 4A), while an IQR-increase in CDS length was associated with a 1.050-fold increased CDS mutation rate (RR = 1.050, 95% CI [1.045, 1.055]; Figure 4D).

Quasi-Poisson regressions also showed significant effects of GC content and expression on gene and CDS mutability. Expression was not associated with mutability for genes (RR = 1.001, 95% CI [0.988, 1.014]; Figure 4B), while each IQR increase in expression was associated with a 13% decreased mutation rate for CDS (RR = 0.870,

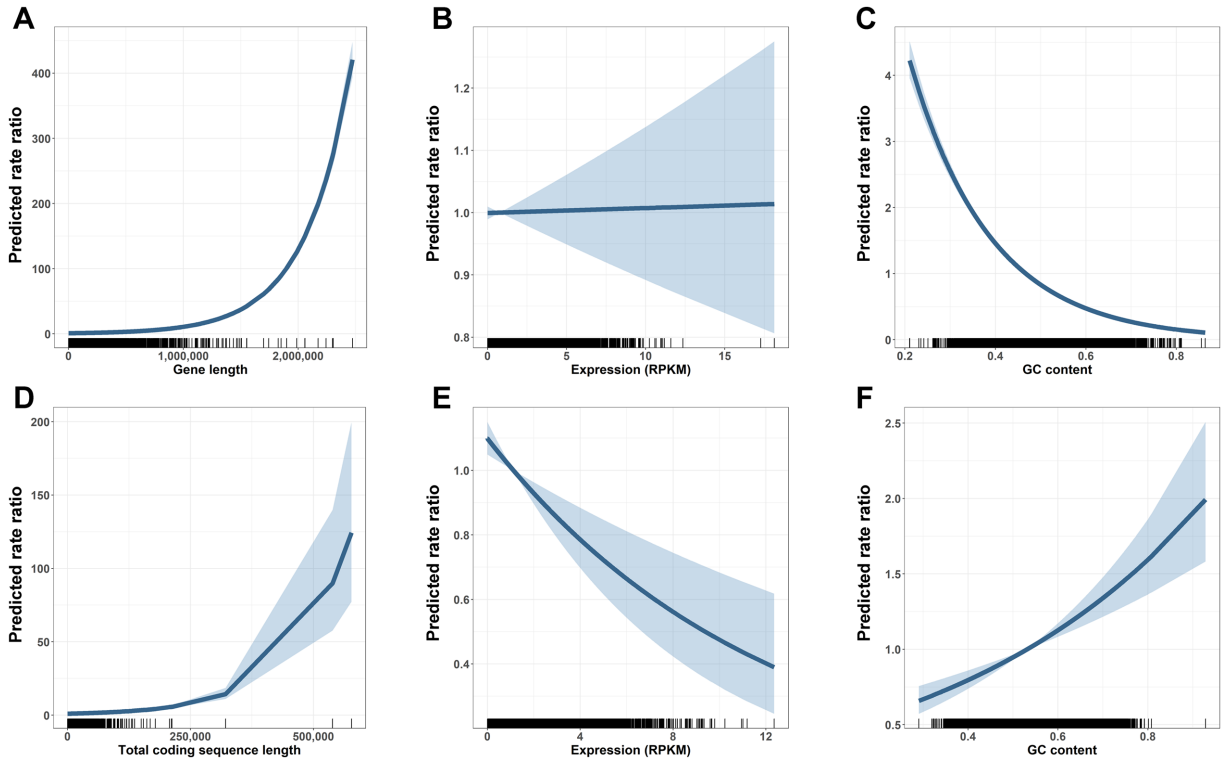

FIGURE 4
Gene length and other determinants of mutation vulnerability across gene bodies and coding sequences. Gene body Quasi-Poisson model results **(A–C)** depict centered rate ratios (lines) and 95% confidence intervals (shaded regions) at each value of *x* (i.e., panel A shows the predicted mutation rate ratio of a gene with gene length indicated on the *x*-axis versus a gene with length, expression, and GC content set to the mean). Distribution of gene characteristics shown along the x axis, with one mark per observation. Longer gene length is associated with higher mutation frequencies across carcinogen treated cells **(A)**. Expression is not associated with altered mutation risk across gene bodies **(B)**. Higher GC content is associated with decreased mutation risk across gene bodies **(C)**. Coding sequence (CDS) Quasi-Poisson model results **(D–F)** depict centered rate ratios (lines) and 95% confidence intervals (shaded regions) at each value of *x*. Distribution of CDS characteristics shown along the *x* axis, with one mark per observation. Longer coding sequence is associated with a modestly increased risk of mutation **(D)**. Higher gene expression is associated with reduced CDS mutations **(E)**. In contrast to the gene body, higher GC content is associated with increased risk of CDS mutation **(F)**.

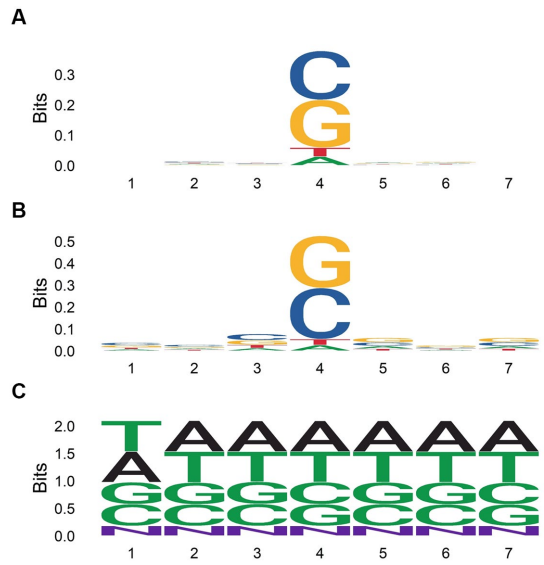

FIGURE 5
Nucleotide content of 7-mers centered on each gene body **(A)** or coding sequence **(B)** mutation among all single base substitutions identified by Kucab et al. (2019), and for 50,000 7-mers randomly sampled from the human genome **(C)**.

95% CI [0.812, 0.931]; Figure 4E). Similarly, the consequence of GC content was different for genes and CDS. Each IQR-increase in gene GC content was associated with a 0.524-fold decreased mutation rate (RR = 0.524, 95% CI [0.508, 0.539]; Figure 4C), while each IQR-increase in CDS GC content was associated with a 1.274-fold increased mutation rate (RR = 1.274, 95% CI [1.175, 1.381]; Figure 4F).

Local sequence and mutation vulnerability

We aligned 7-mers centered on each gene or CDS mutation, along with randomly sampled 7-mers from the human genome (Figure 5). Mutated regions were GC enriched, while randomly sampled 7-mers contained equal proportions of each nucleotide. G and C were more highly enriched in 7-mers centered on CDS mutations compared to 7-mers centered on gene mutations. Thus, CDS mutations may be governed more strongly by local GC content. When aligning 7-mers on each gene or CDS mutation stratified by chemical exposure, this pattern held for some but not all chemical classes (Figure 6).

In the COSMIC mutational signatures analysis, single base substitution enrichments for all neuropsychiatric cases and controls

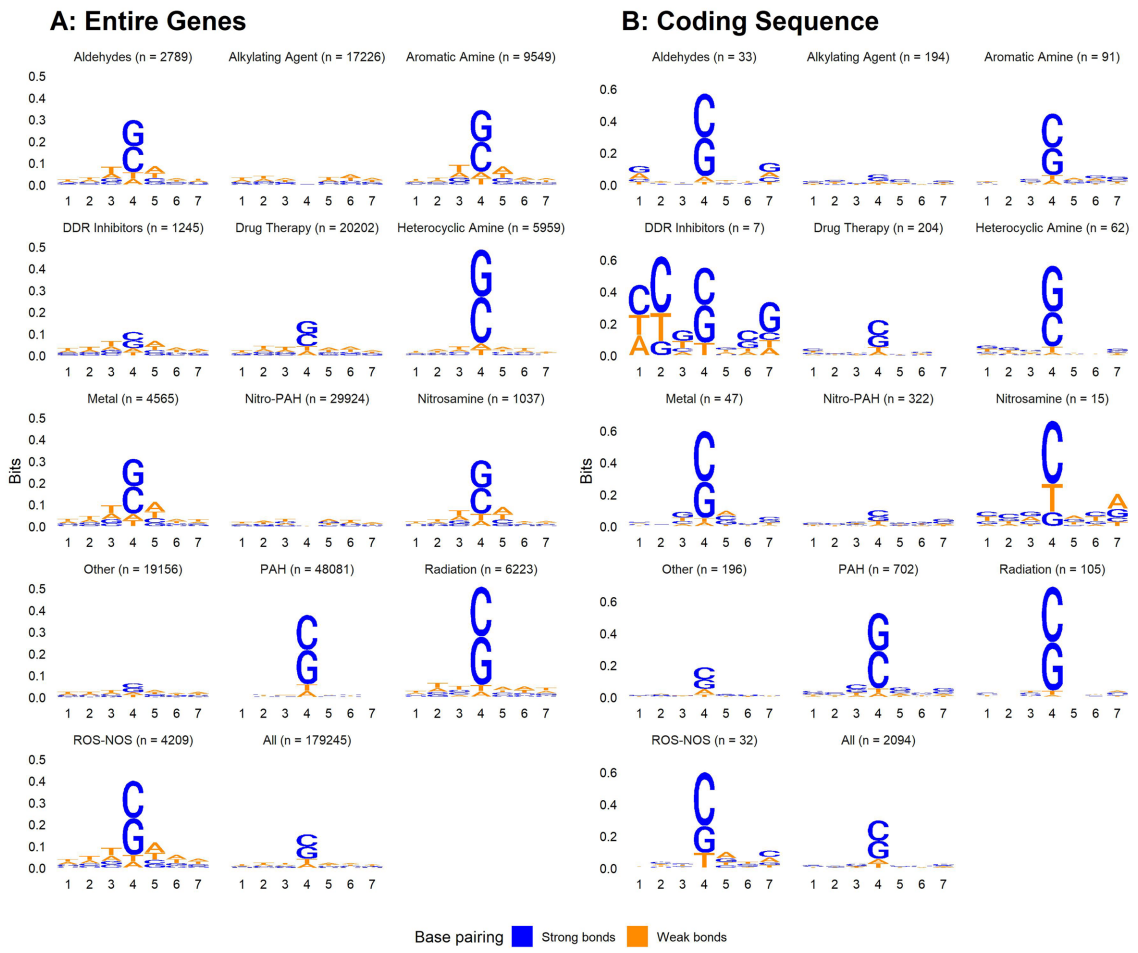

FIGURE 6
Nucleotide content of 7-mers centered on each gene body **(A)** or coding sequence **(B)** mutation among all single base substitutions identified by Kucab et al. (2019), stratified by chemical class.

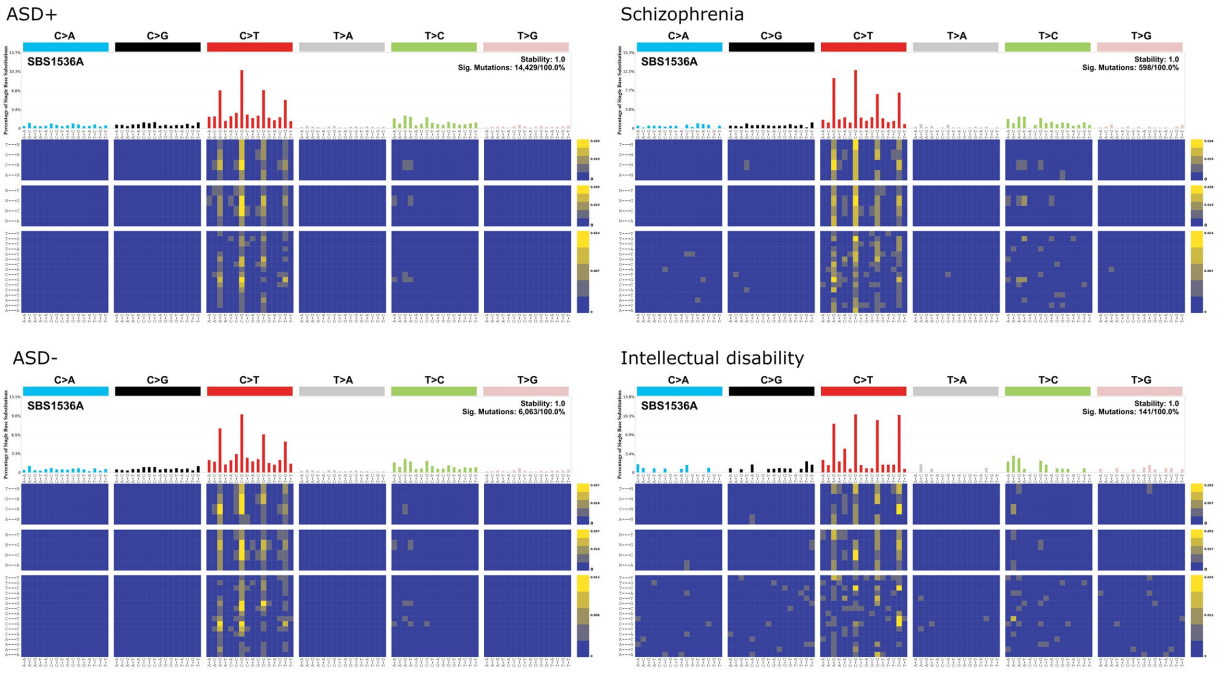

FIGURE 7
COSMIC single base substitution signatures for *de novo* mutations in individuals living with autism spectrum disorders (ASD) and their family members as controls (ASD−; Feliciano et al., 2018), schizophrenia (Fromer et al., 2014), and intellectual disability (De Ligt et al., 2012).

were clock-like/aging associated signatures (i.e., SBS1; Figure 7), which are enriched for NpCpG to NpTpG substitutions. The SBS1 signature does not resemble any of the chemical mutation signatures identified by Kucab et al. (2019). One could interpret this preliminary analysis to suggest that *de novo* mutations in ASD, schizophrenia, and intellectual disability reflect sporadic mutational processes rather than chemical-induced mutation. However, it is also possible that mutational signatures generated from iPSC cultures are not readily comparable to *in vivo* human mutational signatures. For instance, methylated CpG sequences are disproportionately targeted by environmental carcinogens such as PAHs, which form guanine adducts that induce G to T transversions at methylated CpGs (Pfeifer, 2006).

Polycyclic aromatic hydrocarbon adduct repair associated mutation

An existing genome-wide PAH adduct repair assay dataset (Li et al., 2017) was utilized to determine if NDD genes are linked to PAH adduct repair. Pairwise contrasts revealed that DNA damage following PAH treatment was significantly enriched in genes of ASD-related genes compared to genes associated with coronary artery disease, congenital heart defects, and orofacial cleft (Figures 8A, B; Supplementary Table S7). Schizophrenia genes similarly demonstrated more DNA damage compared to coronary artery disease and congenital heart defect genes (Figures 8A, B). However, this pattern of increased DNA damage in neurodevelopmental diseases was not observed for CDS. In fact, ASD and schizophrenia CDS were among the diseases with the lowest levels of DNA damage (Figures 8C, D). Although over half of the Dunn's Tests contrasts were significant (Supplementary Table S7), differences in the mean and median CDS DNA damage enrichments between diseases were minimal (Figures 8C, D).

Discussion

We have shown that environmental carcinogens may disproportionately mutate neurodevelopmental and metabolic genes. ASD, ADHD, schizophrenia, obesity, and type-2 diabetes genes were mutated significantly more than expected based on the mutation rate of randomly sampled genes, while GO analyses revealed that genes mutated by PAHs and other environmental carcinogens were overwhelmingly enriched for neurodevelopmental processes. Environmentally induced mutations may play a greater role in neurodevelopmental disease than previously assumed. Rather than attributing sporadic neurodevelopmental diseases to intrinsic mutational processes, this work suggests that some proportion of genetic neurodevelopmental disease risk may be explained by environmental mutagenesis.

Neurodevelopmental genes may be particularly sensitive to mutation because the transcriptome of neural tissues, especially neurons, is biased toward longer genes (King et al., 2013; Zylka et al., 2015). Our analyses revealed that sequence length was a strong driver of mutability, although the association between sequence length and mutability was twice as strong for genes

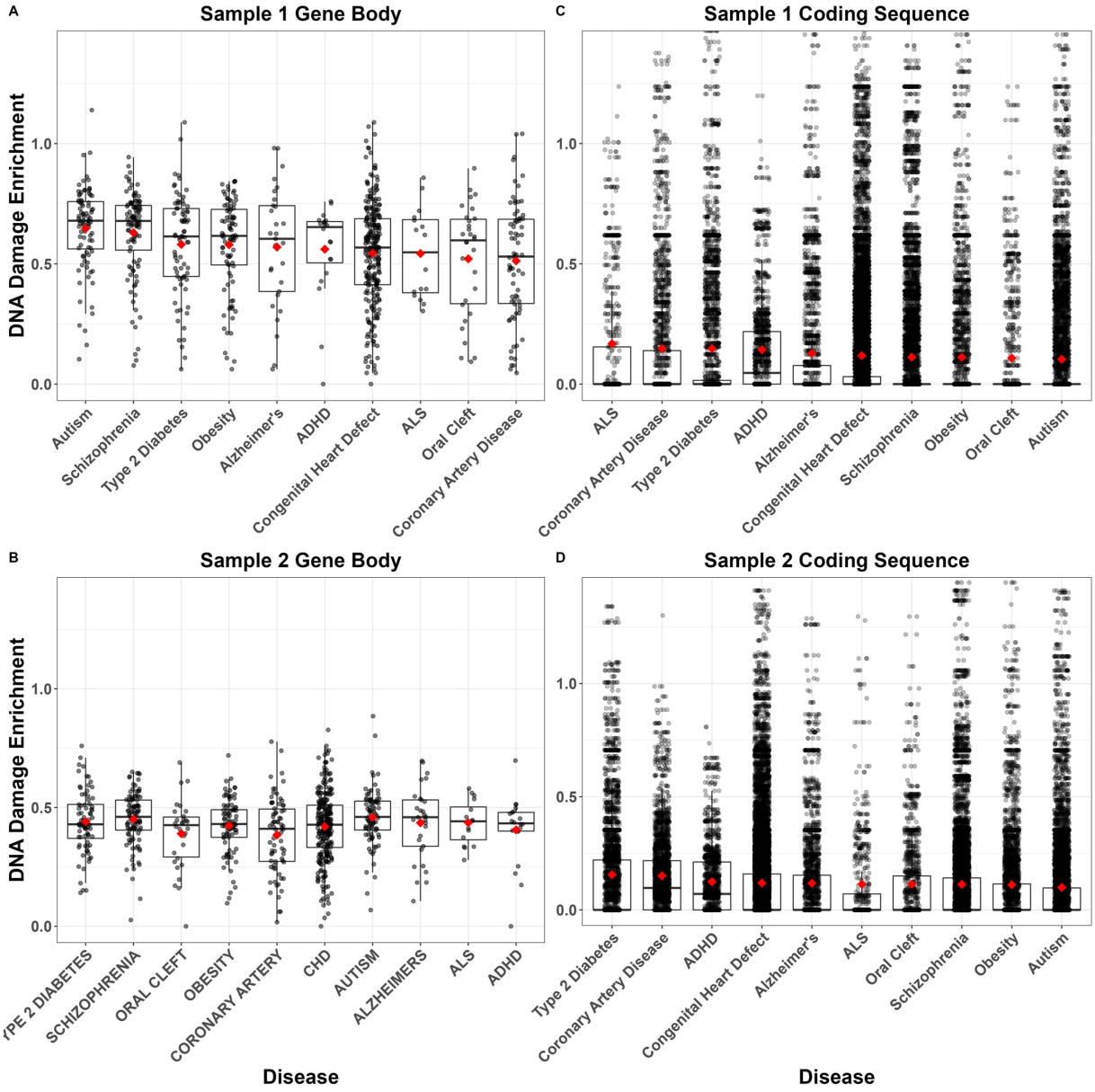

FIGURE 8
Average DNA damage enrichment following polycyclic aromatic hydrocarbon (PAH) treatment of GM12878 cells across each gene body **(A,B)** or coding sequence **(C,D)** in each of 10 disease-related gene sets. Enrichment values indicate the number of tXR-seq counts per gene/coding sequence, controlling for sequence length. Boxplots show median and interquartile range (IQR) with 1.5 IQR whiskers. Gene sets are ordered left–right within each panel from highest to lowest mean enrichment (red diamonds). Data come from two samples of treated cells from Li et al. (2017).

compared to CDS. Other factors may more strongly govern the mutability of protein coding sequences. For instance, we found that higher expression was associated with lower CDS mutation rate, while expression had no effect on the mutability of entire genes. This corroborates prior work showing that lowly expressed genes harbor more mutations (Pleasance et al., 2010), a phenomenon that might be attributable to transcription-coupled DNA repair (Fousteri and Mullenders, 2008; Hanawalt and Spivak, 2008).

Similarly, the effect of GC content was different for genes and CDS. Increased GC content was associated with fewer mutations in genes, but more mutations in CDS. These results are consistent with prior studies indicating that the effect of GC content on mutation rate varies over different genomic scales. GC content across entire genes may reflect higher order DNA structure, and increased GC content has been shown to correlate with decreased mutation rate at higher genomic scales (Wolfe et al., 1989; Hodgkinson and Eyre-Walker, 2011). CDS GC content, however, may more accurately reflect the effect of local GC content on mutability. Cytosines may experience higher mutation rates than other bases because methylated cytosines in CpG dinucleotides are vulnerable to deamination into thymidine. Furthermore, these mutations occur

at higher rates in regions with higher local GC content (Fryxell and Moon, 2005).

Our analyses of the relationship between gene characteristics and mutability show that sequence length is a strong driver, but not the only factor contributing to the elevated mutability of neurodevelopmental disease genes in this dataset. However, our models excluded several characteristics known to be associated with mutation. Studies of cancer driver genes have more comprehensively examined associations of gene characteristics with mutability (e.g., Lawrence et al., 2013; Gorlov et al., 2018). Additional gene and/or sequence characteristics examined in relation to mutability include open versus closed chromatin state (Ying et al., 2010; Schuster-Böckler and Lehner, 2012; Thurman et al., 2012), epigenetic markers (Coarfa et al., 2014), replication timing (earlier replicating regions have a lower mutation rate: Lang and Murray, 2011), di- and/or tri-nucleotide composition (Millar et al., 2002; Samocha et al., 2014), evolutionary conservation (Michaelson et al., 2012), and protein-DNA interactions identified *via* ChIP-seq (e.g., transcription factor binding) (Yang et al., 2018).

Although *de novo* mutation has previously been hypothesized as a pathway linking environmental exposures to increased NDD risk, particularly ASD (Kinney et al., 2010; Pugsley et al., 2021), this hypothesis has not been explicitly tested. For instance, epidemiologic research has linked many known carcinogens, such as air pollutants and heavy metals, with elevated ASD rates at the population level, but none of these studies include mutation data [reviewed by Pugsley et al. (2021)]. Addressing this limitation will require formal mediation analyses showing associations of environmental exposures with increased *de novo* mutation rates, which in turn result in elevated incidence of neurodevelopmental disease. We are unaware of any studies employing this type of mediation approach for environmental exposures, although the mediating role of *de novo* mutations has been investigated for paternal age (Gratten et al., 2016; Taylor et al., 2019). In the future, whole genome/exome sequencing studies of neurodevelopmental diseases such as ASD will need to collect data on environmental exposures to assess this hypothesis.

This work has several limitations. First, our findings that environmental chemicals may disproportionately mutate neurodevelopmental disease genes supports but is not an explicit test of the hypothesis described above. Second, the methods of gene set curation could bias our analyses comparing observed rates of exposure-induced mutations in disease gene sets with the mutation rate of control genes randomly sampled from the genome. To partially address this limitation, we created an online tool allowing researchers to query their own gene sets. Another limitation was our reliance on mutations called in cultured human iPSCs rather than *in vivo*. Because PAHs are a major air pollutant, we attempted to externally validate the results from PAH-exposed iPSCs by analyzing lung tumor mutations from humans living in highly polluted regions. However, future studies might better validate these results using animal models dosed with comparable levels of the environmental chemicals examined by Kucab et al. (2019). Additionally, the use of one iPSC line precludes an examination of potential genetic variability in gene-set mutation vulnerability. Future research should account for diverse genetic backgrounds in genomic instability in disease specific *de novo* mutations.

Author's note

Custom gene lists can be queried using the algorithm we generated at www.environmentalmutation.com.

Data availability statement

Publicly available datasets were analyzed in this study. This data can be found here: Data are available from the primary sources cited. The SPARK gene variants are available to approved researchers through SFARI upon review. The code generated during this study are available on GitHub at: https://github.com/brennanhilton/environmental-mutation-calculator.

Author contributions

BB, JS, WC, and BP contributed to conception and design of the study. BB and SZ performed the statistical analysis. BB wrote the first draft of the manuscript. All authors contributed to manuscript revision, read, and approved the submitted version.

Funding

This work was supported by the NIH grants: P30ES009089, R21ES032913, and R24ES029489.

Acknowledgments

The authors would like to thank to Dr. Barbara Corneo of the Columbia Stem Cell Initiative provided valuable intellectual contribution to the conception of our study.

Conflict of interest

The authors declare that the research was conducted in the absence of any commercial or financial relationships that could be construed as a potential conflict of interest.

Publisher's note

Supplementary material

The Supplementary material for this article can be found online at: https://www.frontiersin.org/articles/10.3389/fnins.2023.1106573/full#supplementary-material

References

Abrahams, B. S., Arking, D. E., Campbell, D. B., Mefford, H. C., Morrow, E. M., Weiss, L. A., et al. (2013). SFARI gene 2.0: a community-driven knowledgebase for the autism spectrum disorders (ASDs). *Mol. Autism.* 4:36. doi: 10.1186/2040-2392-4-36

Association T.A. (2019). *Genetics [online]*. Washington, DC: The ALS Association.

Bailey, M. H., Tokheim, C., Porta-Pardo, E., Sengupta, S., Bertrand, D., Weerasinghe, A., et al. (2018). Comprehensive characterization of cancer driver genes and mutations. *Cell* 173, 371–385. e318. doi: 10.1016/j.cell.2018.02.060

Beaty, T. H., Marazita, M. L., and Leslie, E. J. J. F. (2016). Genetic factors influencing risk to orofacial clefts: today's challenges and tomorrow's opportunities. *F1000Res*:5:2800. doi: 10.12688/f1000research.9503.1

Bellinger, D. C. (2012). A strategy for comparing the contributions of environmental chemicals and other risk factors to neurodevelopment of children. *Environ. Health Perspect.* 120, 501–507. doi: 10.1289/ehp.1104170

Boffetta, P., Jourenkova, N., and Gustavsson, P. (1997). Cancer risk from occupational and environmental exposure to polycyclic aromatic hydrocarbons. *Cancer Causes Control* 8, 444–472. doi: 10.1023/A:1018465507029

Cheng, M., Mei, B., Zhou, Q., Zhang, M., Huang, H., Han, L., et al. (2018). Computational analyses of obesity associated loci generated by genome-wide association studies. *PLoS One* 13:e0199987. doi: 10.1371/journal.pone.0199987

Churko, J. M., Lee, J., Ameen, M., Gu, M., Venkatasubramanian, M., Diecke, S., et al. (2017). Transcriptomic and epigenomic differences in human induced pluripotent stem cells generated from six reprogramming methods. *Nat. Biomed. Eng.* 1:826. doi: 10.1038/s41551-017-0141-6

Coarfa, C., Pichot, C. S., Jackson, A., Tandon, A., Amin, V., Raghuraman, S., et al. (2014). Analysis of interactions between the epigenome and structural mutability of the genome using Genboree workbench tools. *BMC Bioinformatics* 15, 1–12. doi: 10.1186/1471-2105-15-S7-S2

Crawley, J. N., Heyer, W.-D., and Lasalle, J. M. J. T. I. G. (2016). Autism and Cancer share risk genes, pathways, and drug targets. *Trends Genet.* 32, 139–146. doi: 10.1016/j.tig.2016.01.001

De Ligt, J., Willemsen, M. H., Van Bon, B. W., Kleefstra, T., Yntema, H. G., Kroes, T., et al. (2012). Diagnostic exome sequencing in persons with severe intellectual disability. *N. Engl. J. Med.* 367, 1921–1929. doi: 10.1056/NEJMoa1206524

Demontis, D., Walters, R. K., Martin, J., Mattheisen, M., Als, T. D., Agerbo, E., et al. (2019). Discovery of the first genome-wide significant risk loci for attention deficit/hyperactivity disorder. *Nat. Genet.* 51:63. doi: 10.1038/s41588-018-0269-7

Edwards, S. C., Jedrychowski, W., Butscher, M., Camann, D., Kieltyka, A., Mroz, E., et al. (2010). Prenatal exposure to airborne polycyclic aromatic hydrocarbons and children's intelligence at 5 years of age in a prospective cohort study in Poland. *Environ. Health Perspect.* 118, 1326–1331. doi: 10.1289/ehp.0901070

Emberti Gialloreti, L., Mazzone, L., Benvenuto, A., Fasano, A., Garcia Alcon, A., Kraneveld, A., et al. (2019). Risk and protective environmental factors associated with autism Spectrum disorder: evidence-based principles and recommendations. *J. Clin. Med.* 8:217. doi: 10.3390/jcm8020217

Feliciano, P., Daniels, A. M., Snyder, L. G., Beaumont, A., Camba, A., Esler, A., et al. (2018). SPARK: a US cohort of 50,000 families to accelerate autism research. *Signal. Synapse* 97, 488–493. doi: 10.1016/j.neuron.2018.01.015

Fousteri, M., and Mullenders, L. H. (2008). Transcription-coupled nucleotide excision repair in mammalian cells: molecular mechanisms and biological effects. *Cell Res.* 18, 73–84. doi: 10.1038/cr.2008.6

Fromer, M., Pocklington, A. J., Kavanagh, D. H., Williams, H. J., Dwyer, S., Gormley, P., et al. (2014). De novo mutations in schizophrenia implicate synaptic networks. *Nature* 506:179. doi: 10.1038/nature12929

Fryxell, K. J., and Moon, W.-J. J. M. B. (2005). CpG mutation rates in the human genome are highly dependent on local GC content. *Mol. Biol. Evol.* 22, 650–658. doi: 10.1093/molbev/msi043

Gabel, H. W., Kinde, B., Stroud, H., Gilbert, C. S., Harmin, D. A., Kastan, N. R., et al. (2015). Disruption of DNA-methylation-dependent long gene repression in Rett syndrome. *Nat. Cell Biol.* 522, 89–93. doi: 10.1038/nature14319

Giri, M., Zhang, M., and Lü, Y. (2016). Genes associated with Alzheimer's disease: an overview and current status. *Clin. Interv. Aging* 11:665. doi: 10.2147/CIA.S105769

Gorlov, I. P., Pikielny, C. W., Frost, H. R., Her, S. C., Cole, M. D., Strohbehn, S. D., et al. (2018). Gene characteristics predicting missense, nonsense and frameshift mutations in tumor samples. *BMC Bioinformatics* 19, 1–14. doi: 10.1186/s12859-018-2455-0

Gratten, J., Wray, N. R., Peyrot, W. J., Mcgrath, J. J., Visscher, P. M., and Goddard, M. E. J. N. G. (2016). Risk of psychiatric illness from advanced paternal age is not predominantly from de novo mutations. *Nature Genet.* 48, 718–724. doi: 10.1038/ng.3577

Hanawalt, P. C., and Spivak, G. (2008). Transcription-coupled DNA repair: two decades of progress and surprises. *Nat. Rev. Mol. Cell Biol.* 9, 958–970. doi: 10.1038/nrm2549

Hodgkinson, A., and Eyre-Walker, A. J. N. R. G. (2011). Variation in the mutation rate across mammalian genomes. *Nature Rev. Genet.* 12, 756–766. doi: 10.1038/nrg3098

Iossifov, I., O'roak, B. J., Sanders, S. J., Ronemus, M., Krumm, N., Levy, D., et al. (2014). The contribution of de novo coding mutations to autism spectrum disorder. *Nature* 515:216. doi: 10.1038/nature13908

Jedrychowski, W. A., Perera, F. P., Camann, D., Spengler, J., Butscher, M., Mroz, E., et al. (2015). Prenatal exposure to polycyclic aromatic hydrocarbons and cognitive dysfunction in children. *Environ. Sci. Pollut. Res.* 22, 3631–3639. doi: 10.1007/s11356-014-3627-8

Jin, S. C., Homsy, J., Zaidi, S., Lu, Q., Morton, S., Depalma, S. R., et al. (2017). Contribution of rare inherited and de novo variants in 2,871 congenital heart disease probands. *Nature Genet.* 49, 1593–1601. doi: 10.1038/ng.3970

Kim, K.-H., Jahan, S. A., Kabir, E., and Brown, R. J. (2013). A review of airborne polycyclic aromatic hydrocarbons (PAHs) and their human health effects. *Environ. Int.* 60, 71–80. doi: 10.1016/j.envint.2013.07.019

King, I. F., Yandava, C. N., Mabb, A. M., Hsiao, J. S., Huang, H.-S., Pearson, B. L., et al. (2013). Topoisomerases facilitate transcription of long genes linked to autism. *Nat. Cell Biol.* 501, 58–62. doi: 10.1038/nature12504

Kinney, D. K., Barch, D. H., Chayka, B., Napoleon, S., and Munir, K. M. J. M. H. (2010). Environmental risk factors for autism: do they help cause de novo genetic mutations that contribute to the disorder? *Med. Hypotheses* 74, 102–106. doi: 10.1016/j.mehy.2009.07.052

Kriek, E., Rojas, M., Alexandrov, K., and Bartsch, H. (1998). Polycyclic aromatic hydrocarbon-DNA adducts in humans: relevance as biomarkers for exposure and cancer risk. *Mutat. Res.* 400, 215–231. doi: 10.1016/S0027-5107(98)00065-7

Kucab, J. E., Zou, X., Morganella, S., Joel, M., Nanda, A. S., Nagy, E., et al. (2019). A compendium of mutational signatures of environmental agents. *Cells* 177:e816, 821–836.e16. doi: 10.1016/j.cell.2019.03.001

Landrigan, P. J. (2010). What causes autism? Exploring the environmental contribution. *Curr. Opin. Pediatr.* 22, 219–225. doi: 10.1097/MOP.0b013e328336eb9a

Lang, G. I., and Murray, A. W. J. G. B. (2011). Mutation rates across budding yeast chromosome VI are correlated with replication timing. *Genome Biol. Evol.* 3, 799–811. doi: 10.1093/gbe/evr054

Lawrence, M. S., Stojanov, P., Polak, P., Kryukov, G. V., Cibulskis, K., Sivachenko, A., et al. (2013). Mutational heterogeneity in cancer and the search for new cancer-associated genes. *Nat. Cell Biol.* 499, 214–218. doi: 10.1038/nature12213

Li, W., Hu, J., Adebali, O., Adar, S., Yang, Y., Chiou, Y.-Y., et al. (2017). Human genome-wide repair map of DNA damage caused by the cigarette smoke carcinogen benzo[a]pyrene. *Proc. Natl. Acad. Sci. U. S. A.* 114, 6752–6757. doi: 10.1073/pnas.1706021114

Locke, A. E., Kahali, B., Berndt, S. I., Justice, A. E., Pers, T. H., Day, F. R., et al. (2015). Genetic studies of body mass index yield new insights for obesity biology. *Nat. Cell Biol.* 518, 197–206. doi: 10.1038/nature14177

Mahajan, A., Go, M. J., Zhang, W., Below, J. E., Gaulton, K. J., Ferreira, T., et al. (2014). Genome-wide trans-ancestry meta-analysis provides insight into the genetic architecture of type 2 diabetes susceptibility. *Nature Genet.* 46, 234–244. doi: 10.1038/ng.2897

Mclaren, W., Gil, L., Hunt, S. E., Riat, H. S., Ritchie, G. R., Thormann, A., et al. (2016). The ensembl variant effect predictor. *Genome Biol.* 17:122. doi: 10.1186/s13059-016-0974-4

Michaelson, J. J., Shi, Y., Gujral, M., Zheng, H., Malhotra, D., Jin, X., et al. (2012). Whole-genome sequencing in autism identifies hot spots for De novo germline mutation. *Cell (Cambridge, MA)* 151, 1431–1442. doi: 10.1016/j.cell.2012.11.019

Millar, C. B., Guy, J., Sansom, O. J., Selfridge, J., Macdougall, E., Hendrich, B., et al. (2002). Enhanced CpG mutability and tumorigenesis in MBD4-deficient mice. *Science* 297, 403–405. doi: 10.1126/science.1073354

Nikpay, M., Goel, A., Won, H.-H., Hall, L. M., Willenborg, C., Kanoni, S., et al. (2015). A comprehensive 1000 genomes-based genome-wide association meta-analysis of coronary artery disease. *Nat. Genet.* 47:1121. doi: 10.1038/ng.3396

Perera, F., and Herbstman, J. J. R. T. (2011). Prenatal environmental exposures, epigenetics, and disease. *Reprod. Toxicol.* 31, 363–373. doi: 10.1016/j.reprotox.2010.12.055

Perera, F. P., Rauh, V., Whyatt, R. M., Tsai, W.-Y., Tang, D., Diaz, D., et al. (2006). Effect of prenatal exposure to airborne polycyclic aromatic hydrocarbons on neurodevelopment in the first 3 years of life among inner-city children. *Environ. Health Perspect.* 114, 1287–1292. doi: 10.1289/ehp.9084

Pfeifer, G. (2006). "Mutagenesis at methylated CpG sequences" in *DNA Methylation: Basic Mechanisms*. eds. W. Doerfler and P. Böhm (Berlin: Springer), 259–281.

Pleasance, E. D., Cheetham, R. K., Stephens, P. J., Mcbride, D. J., Humphray, S. J., Greenman, C. D., et al. (2010). A comprehensive catalogue of somatic mutations from a human cancer genome. *Nature* 463, 191–196. doi: 10.1038/nature08658

Pugsley, K., Scherer, S. W., Bellgrove, M. A., and Hawi, Z. J. M. P. (2021). Environmental exposures associated with elevated risk for autism spectrum disorder may augment the burden of deleterious de novo mutations among probands. *Mol. Psychiatry.* 27, 710–730. doi: 10.1038/s41380-021-01142-w

Qi, H., Dong, C., Chung, W. K., Wang, K., and Shen, Y. J. H. M. (2016). Deep genetic connection between Cancer and developmental disorders. *Hum. Mutat.* 37, 1042–1050. doi: 10.1002/humu.23040

Ramírez, F., Ryan, D. P., Grüning, B., Bhardwaj, V., Kilpert, F., Richter, A. S., et al. (2016). deepTools2: a next generation web server for deep-sequencing data analysis. *Nucleic Acids Symp. Ser.* 44, W160–W165. doi: 10.1093/nar/gkw257

Rauch, A., Wieczorek, D., Graf, E., Wieland, T., Endele, S., Schwarzmayr, T., et al. (2012). Range of genetic mutations associated with severe non-syndromic sporadic intellectual disability: an exome sequencing study. *Lancet* 380, 1674–1682. doi: 10.1016/S0140-6736(12)61480-9

Rauh, V. A., and Margolis, A. E. (2016). Research review: environmental exposures, neurodevelopment, and child mental health–new paradigms for the study of brain and behavioral effects. *J. Child Psychol. Psychiatry* 57, 775–793. doi: 10.1111/jcpp.12537

Samocha, K. E., Robinson, E. B., Sanders, S. J., Stevens, C., Sabo, A., Mcgrath, L. M., et al. (2014). A framework for the interpretation of de novo mutation in human disease. *Nat. Genet.* 46, 944–950. doi: 10.1038/ng.3050

Schuster-Böckler, B., and Lehner, B. J. N. (2012). Chromatin organization is a major influence on regional mutation rates in human cancer cells. *Nat. Cell Biol.* 488, 504–507. doi: 10.1038/nature11273

Shields, P. G., and Harris, C. C. (2000). Cancer risk and low-penetrance susceptibility genes in gene-environment interactions. *J. Clin. Oncol.* 18, 2309–2315. doi: 10.1200/JCO.2000.18.11.2309

Sugino, K., Hempel, C. M., Okaty, B. W., Arnson, H. A., Kato, S., Dani, V. S., et al. (2014). Cell-type-specific repression by methyl-CpG-binding protein 2 is biased toward long genes. *J. Neurosci.* 34, 12877–12883. doi: 10.1523/JNEUROSCI.2674-14.2014

Tate, J. G., Bamford, S., Jubb, H. C., Sondka, Z., Beare, D. M., Bindal, N., et al. (2019). COSMIC: the catalogue of somatic mutations in Cancer. *Nucleic Acids Symp. Ser.* 47, D941–D947. doi: 10.1093/nar/gky1015

Taylor, J. L., Debost, J.-C. P., Morton, S. U., Wigdor, E. M., Heyne, H. O., Lal, D., et al. (2019). Paternal-age-related de novo mutations and risk for five disorders. *Nat. Commun.* 10, 1–9. doi: 10.1038/s41467-019-11039-6

Team, R. C. (2018). *R: A Language and Environment For Statistical Computing*. Vienna, Austria: R Foundation for Statistical Computing; (*2018*).

Thurman, R. E., Rynes, E., Humbert, R., Vierstra, J., Maurano, M. T., Haugen, E., et al. (2012). The accessible chromatin landscape of the human genome. *Nat. Cell Biol.* 489, 75–82. doi: 10.1038/nature11232

Tran, N. Q. V., and Miyake, K. J. I. J. O. G. (2017). Neurodevelopmental disorders and environmental toxicants: epigenetics as an underlying mechanism. *Comp. Funct. Genom.* 2017, 1–23. doi: 10.1155/2017/7526592

Von Ehrenstein, O. S., Aralis, H., Cockburn, M., and Ritz, B. (2014). In utero exposure to toxic air pollutants and risk of childhood autism. *Epidemiology* 25, 851–858. doi: 10.1097/EDE.0000000000000150

Wang, Q., Chen, R., Cheng, F., Wei, Q., Ji, Y., Yang, H., et al. (2019). A Bayesian framework that integrates multi-omics data and gene networks predicts risk genes from schizophrenia GWAS data. *Nat. Neurosci.* 22:691. doi: 10.1038/s41593-019-0382-7

Watanabe, K., Taskesen, E., Van Bochoven, A., and Posthuma, D. (2017). Functional mapping and annotation of genetic associations with FUMA. *Nat. Commun.* 8:1826. doi: 10.1038/s41467-017-01261-5

Whyatt, R., Bell, D., Jedrychowski, W., Santella, R., Garte, S., Cosma, G., et al. (1998). Polycyclic aromatic hydrocarbon-DNA adducts in human placenta and modulation by CYP1A1 induction and genotype. *Carcinogenesis* 19, 1389–1392. doi: 10.1093/carcin/19.8.1389

Wolfe, K. H., Sharp, P. M., and Li, W.-H. J. N. (1989). Mutation rates differ among regions of the mammalian genome. *Nat. Cell Biol.* 337, 283–285. doi: 10.1038/337283a0

Xu, B., Ionita-Laza, I., Roos, J. L., Boone, B., Woodrick, S., Sun, Y., et al. (2012). De novo gene mutations highlight patterns of genetic and neural complexity in schizophrenia. *Nat. Genet.* 44:1365. doi: 10.1038/ng.2446

Yang, J., Wei, X., Tufan, T., Kuscu, C., Unlu, H., Farooq, S., et al. (2018). Recurrent mutations at estrogen receptor binding sites alter chromatin topology and distal gene expression in breast cancer. *GBC* 19, 1–15. doi: 10.1186/s13059-018-1572-4

Ying, H., Epps, J., Williams, R., and Huttley, G. J. M. B. (2010). Evidence that localized variation in primate sequence divergence arises from an influence of nucleosome placement on DNA repair. *Mol. Biol. Evol.* 27, 637–649. doi: 10.1093/molbev/msp253

Yu, X.-J., Yang, M.-J., Zhou, B., Wang, G.-Z., Huang, Y.-C., Wu, L.-C., et al. (2015). Characterization of somatic mutations in air pollution-related lung cancer. *EBioMedicine* 2, 583–590. doi: 10.1016/j.ebiom.2015.04.003

Zhang, F., and Lupski, J. R. J. H. M. G. (2015). Non-coding genetic variants in human disease. *Hum. Mol. Genet.* 24, R102–R110. doi: 10.1093/hmg/ddv259

Zhou, X., Feliciano, P., Wang, T., Shu, C., Astrovskaya, I., Hall, J., et al. (2021). Integrating de novo and inherited variants in over 42,607 autism cases identifies mutations in new moderate risk genes. *medRxiv*. doi: 10.1101/2021.10.08.21264256 [Epub ahead of preprint].

Zylka, M. J., Simon, J. M., and Philpot, B. D. J. N. (2015). Gene length matters in neurons. *Signal. Synapse* 86, 353–355. doi: 10.1016/j.neuron.2015.03.059

Frontiers in Neuroscience

Provides a holistic understanding of brain function from genes to behavior

Part of the most cited neuroscience journal series which explores the brain - from the new eras of causation and anatomical neurosciences to neuroeconomics and neuroenergetics.

Discover the latest Research Topics

See more →

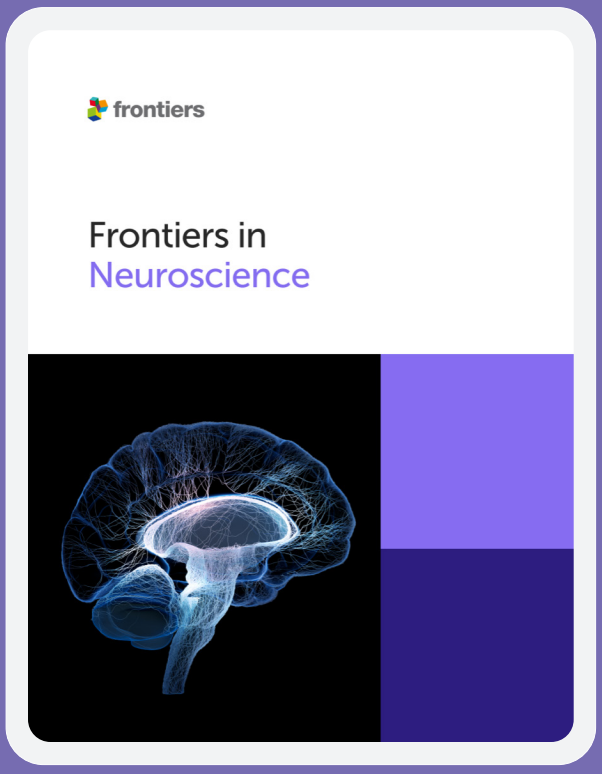

Frontiers

Avenue du Tribunal-Fédéral 34
1005 Lausanne, Switzerland
frontiersin.org

Contact us

+41 (0)21 510 17 00
frontiersin.org/about/contact